

CONFERENCE PROCEEDINGS

2017

1-22 March 2017
Melbourne, Victoria | Australia

Deep Foundations Institute
326 Lafayette Avenue
Hawthorne, New Jersey 07506 USA
Tel: 973 423 4030
Fax: 973 423 4031
staff@dfi.org
www.dfi.org

Piling and Foundation
Specialists Federation
235 Charles Street
Launceston TAS 7250 Australia
Tel: 0425 209 401
admin@pilingfederation.org.au
www.pilingfederation.org.au

Sponsored by

BAUER FOUNDATIONS AUSTRALIA

PREFACE

On behalf of the Piling and Foundation Specialist Federation (PFSF) of Australia, the Deep Foundations Institute (DFI) and the Conference Organizing Committee we welcome this inaugural joint conference. The theme selected for this conference covered piling and ground improvement works associated with building and infrastructure developments, including foundation works and retention requirements for basements to provide an all-inclusive interest within the geotechnical profession nationally and internationally. By introducing a broad range of topics the Committee hoped that all disciplines as practiced around the globe in building and infrastructure works would provide interesting, educational and thought-provoking opportunities.

The DFI has existed for over 40 years, and was created to provide a forum as an international association of contractors, engineers, manufacturers, suppliers, academics and owners in the deep foundations industry. This multidisciplinary membership fits comfortably within the aims of the PFSF, whose charter has the same ideals for its Australasian membership.

On behalf of the Conference Organizing Committee, we would like to extend our thanks and gratitude to all attendees, exhibitors, underwriters, and presenters who helped make this inaugural Conference happen, an event we hope to be the forerunner of many

We have been blessed with having our four keynote speakers of the caliber of Dan Brown (as the newly appointed President of the DFI), Harry Poulos, Chris Haberfield and Phillipe Vincent accept our invitation to attend and to share their wisdom and world-leading expertise with us. We remain indebted to these gentlemen.

Dan Brown's presentation "Challenges in the Design and Construction of Deep Foundations for Transportation Infrastructure Projects" provided us with an overview of challenges that affect design and construction and the methods that have been successfully employed on large projects.

Harry Poulos' presentation "Designing Piles for Seismic Events" provided a topic reminder for the Australasian region of approaches that designers can adopt for foundation design in seismic areas, elaborating on earthquake characteristics, design parameters and design actions induced in foundation piles, together with practical methods of design to cater for those design actions.

Chris Haberfield's topic was "Geotechnical Design Considerations for Rock Socketed Piles". Chris' work is the result of many years' experience as an academic and as a leading geotechnical consultant. Chris detailed the various influences that affect performance of socketed piles, demonstrating how an understanding of those influences can produce more confident and cost-effective pile designs.

Philippe Vincent is a leading practitioner in the field of geotechnical and environmental engineering, particularly associated with ground improvement works. His presentation "Ground Improvement by Dynamic Replacement within intertidal Mangrove Mud Environment, ICTHYS LNG, Darwin", highlighted the design philosophy, construction methods and site constraints, quality controls and results achieved for work on that major project.

This publication contains peer reviewed technical papers pertaining to the session topics selected by the Conference Organizing Committee.

Selection of papers for presentation proved a most challenging task as Reviewers were faced with a number of high quality papers, unfortunately not all of which could be fitted

into the limited conference time available. We thank all authors for their submissions and our Reviewers around the globe for their efforts in ensuring quality submissions.

Undoubtedly, without the hard work and dedication of all those involved, this Inaugural Conference would not have been possible. In particular we thank Mark Johnson, Executive Director, PFSF, for his vision of introducing the DFI to Australasia, and to Theresa Engler, DFI Executive Director, for her support in ensuring the conference would have the experience and undoubted expertise of the DFI organization.

The Conference would not have been possible without the tireless work of the Conference Organizing Committee, Session Chairs, Authors, Reviewers, Sponsors, Exhibitors, and Volunteers. As we have come to expect and appreciate, the DFI Staff has done an amazing job organizing, preparing, guiding, supporting, corralling, and gently prodding to ensure the Conference is executed flawlessly. Therefore, we would be remiss if we did not acknowledge specifically the efforts of Theresa Engler, DFI Executive Director, and Lauren Nance, DFI Senior Meetings and Events Specialist.

In closing, we would like to express our appreciation for having been provided the opportunity to be a part of the inaugural PFSF-DFI Conference 2017, Melbourne, Australia.

Program Co-Chairs
Gary Chapman (Golder Associates) Slav Tchepak (Keller)

ORGANIZING COMMITTEE

Mark Johnson, Executive Officer | *Piling and Foundation Specialists Federation*

Theresa Engler, Executive Director | *Deep Foundations Institute*

Slav Tchepak, *Keller*

Lauren Nance, Meeting & Event Manager | *Deep Foundations Institute*

TECHNICAL COMMITTEE

Slav Tchepak, Program Co-Chair | *Keller*

Gary Chapman, Program Co-Chair | *Golder Associates*

Mary Ellen Large, Technical Activities Manager | *Deep Foundations Institute*

Derek Avalle, *Keller*

Engineering Frances Badelow, *Mott*

MacDonald David Klingberg, *Golder*

Associates Robert May, *Golder*

Associates

Bruce McPherson, *Douglas Partners*

Peter Mitchell, *Aurecon*

Julian Seidel, *Foundation Specialists*

Group Pawan Sethi, *Coffey, A Tetra Tech*

Company Doug Stewart, *Golder*

Associates

Ondrej Synac, *Keller*

John Wagstaff, *Wagstaff Piling*

Nic Wharmby, *March*

Construction Patrick Wong,

PKW Solutions

CHALLENGES IN THE DESIGN AND CONSTRUCTION OF DEEP FOUNDATIONS FOR TRANSPORTATION INFRASTRUCTURE PROJECTS

Dan Brown, P.E., Ph.D., D.GE, Dan Brown and Associates, P.C.

ABSTRACT

Renewal and revitalization of transportation presents a challenge in the need for replacement, repair, and improvements of existing bridges, as well as increased construction of transit systems within existing transportation rights of way. Difficulties with conventional deep foundation systems occur because of the limited site access, adjacent structures, the need to maintain traffic, and other constraints on construction activity. Major projects are often performed in a design-build contract environment in which the schedule is aggressive, and where speed and reliability represent major considerations. Foundation designers are confronted with a need to solve problems with a construction-oriented mindset, where typical experience with lowest cost solutions may not reflect the most effective approach. This presentation presents an overview of the challenges that may affect design and construction of deep foundations in this environment and the methods that have successfully been employed on several large transportation projects in the U.S.

Keywords: site access, design-build, deep foundations, transportation, infrastructure

CONSTRUCTION METHODS AND QUALITY OUTCOMES FOR BORED CAST-IN-SITU PILES – A REVIEW OF CURRENT PRACTICE

Ben Collingwood, Foundation Specialists Group, Melbourne, Australia; +61 3 94174333, bcollingwood@foundationspecialists.com.au
Jim Slatter, Foundation Specialists Group, Brisbane, Australia; +61 7 3831 4600 jslatter@foundationspecialists.com.au

ABSTRACT

It is well known that the adoption of an appropriate construction methodology is critical to quality outcomes for bored piles (drilled shafts). Many case studies have been published documenting quality issues that have arisen due to a range of causes involving ground conditions, ground support, drilling and cleaning techniques, groundwater, concrete properties and concreting methods, amongst other things. Despite the body of published information, pile defects remain common in practice. The authors share over 40 years' experience in the Australian piling industry and have participated in many hundreds of projects involving bored piles in design, construction and testing roles. It is the authors' experience that many defects are caused by conditions or practices that are known to be problematic, but that are often not recognised or addressed at the time of the works. This paper provides an overview of industry practices and key factors relevant to quality outcomes. The authors draw upon their own construction experience, published case studies and guidelines, and observations from independent pile testing activities they have been involved in across the Australian piling industry. The intent of the paper is to provide a consolidated review of typical industry practices and to highlight key areas in which construction quality can be enhanced.

Keywords: bored pile, drilled shaft, tremie concrete, polymer slurry, bentonite slurry, pile construction

INTRODUCTION

There are many published studies of cases where bored piles have been constructed and found to have concrete defects. The authors have had personal involvement in many cases where the outcomes and learnings are not publically available. The nature and cause of defects is always dependent on site and project specific factors, and therefore methodologies and materials that produce satisfactory outcomes in certain circumstances may be problematic elsewhere.

The process of bored pile construction encompasses the following key areas:

- excavation and ground support;
- pile preparation and cleaning;
- pile reinforcement and fitments.
- concrete supply and mix performance;
- concrete placement methodology;

Each of these elements is equally important and can influence construction quality in completed piles. In the authors' experience, it is often a combination of seemingly minor issues that leads to significant defects in piles. Conversely, attention to detail in all aspects of bored pile construction is required to produce outcomes of a consistently high standard.

The intent of this paper is to provide commentary and recommendations, based on the authors' industry experience, in relation to practical aspects of bored pile construction, with the intention of alerting the reader to the range of issues that must be considered on a site by site, if not pile by pile, basis.

The majority of issues and recommendations discussed herein are known across the industry and have been discussed previously by other authors. Comprehensive guidance in relation to all aspects of bored pile construction is available in a significant body of published work, most notably FHWA GEC10 (U.S. Federal Highways Administration, 2010). However, in the authors' experience, there is a disconnection between the level of industry knowledge generally, and the way in which works are

executed at a site level. Too often fundamental errors, omissions, or misjudgements are made on site, which are indicative of a lack of understanding and/or attention to important aspects of the construction process. It is hoped that this paper will provide a readily accessible starting point for enhancing the knowledge and understanding of industry personnel who can directly influence project outcomes.

EXCAVATION AND GROUND SUPPORT

Industry practice for bored pile construction in Australia involves a broad range of construction plant and equipment to suit project scale and geotechnical conditions. Drilling plant can range in size from excavator or truck mounted drilling attachments to large scale hydraulic drilling equipment of up to around 40 tonne metre torque. Drilling is typically carried out using a combination of conventional flight augers, drilling buckets, core barrels and cleaning buckets or plates. In specialised applications, equipment such as rock rollers or percussion drills may be used to suit difficult ground conditions. This paper deals primarily with conventional drilling techniques with associated ground support, although many aspects of this paper apply to more specialised drilling techniques also.

Ground support techniques also vary considerably based on ground and ground water conditions. In stable ground conditions, no ground support may be required. Groundwater ingress into the pile shaft is the most common cause of instability in bored piles. This applies to piles in rock as well as soils, as weathered and/or fractured rock can be prone to collapse, particularly if there is a strong flow of water into the excavation. Selection of appropriate ground support, particularly for piles constructed where groundwater is present, is a critical element of successful bored pile construction.

Common ground support methods and associated causes of difficulties and defects are outlined in the following sections.

Temporary and Permanent Steel Liners

Temporary steel liners are often used to support soil strata that may otherwise be unstable. A summary of the basic forms of temporary liner use is as follows:

- Short top liners of a few metres in length to stabilise material at and near working surface level;
- Partial length temporary steel liners which extend through potentially unstable material to a depth at which the ground is self-supporting;
- Partial length temporary steel liners which extend through potentially unstable or erodible material to a depth at which water or drilling fluid is used to support the excavation sidewalls. An excess water head inside the pile may be used in some cases where the ground is not susceptible to deterioration, whereas polymer or bentonite drilling slurries are commonly used for support in materials which may otherwise degrade. Polymer slurry is often preferred in current practice due to its relative ease of preparation and maintenance in cases where ground conditions are conducive, whereas bentonite is generally used in cases where ground conditions are less stable;
- Full length temporary steel liners which are removed after concrete placement, or permanent casing which is left in place. For rock socketed piles, it is common for liners to terminate at the level of competent rock below which the socket is formed unsupported.

Proper consideration should be given to the depth and diameter of temporary steel liners and the method of installation and extraction. Liner internal diameters should typically be in the order of 50mm larger than the nominal pile diameter to allow free passage of the drilling and cleaning tools. It is undesirable to have temporary liners with voids around the outside, which can fill with water or slurry. In certain circumstances where there is insufficient fluid concrete head inside the liner when the casing is later removed or where the water is trapped, this water can flow back into the pile or mix with the concrete and cause contamination, as shown in Figure 1. It is therefore preferable to drive, vibrate or screw the casing into the ground leaving little or no external void. In all instances it is important that the pressure head inside the casing remains greater than the pressure head outside the

casing when the casing is removed. This may require the casing to be filled with water prior to extraction.

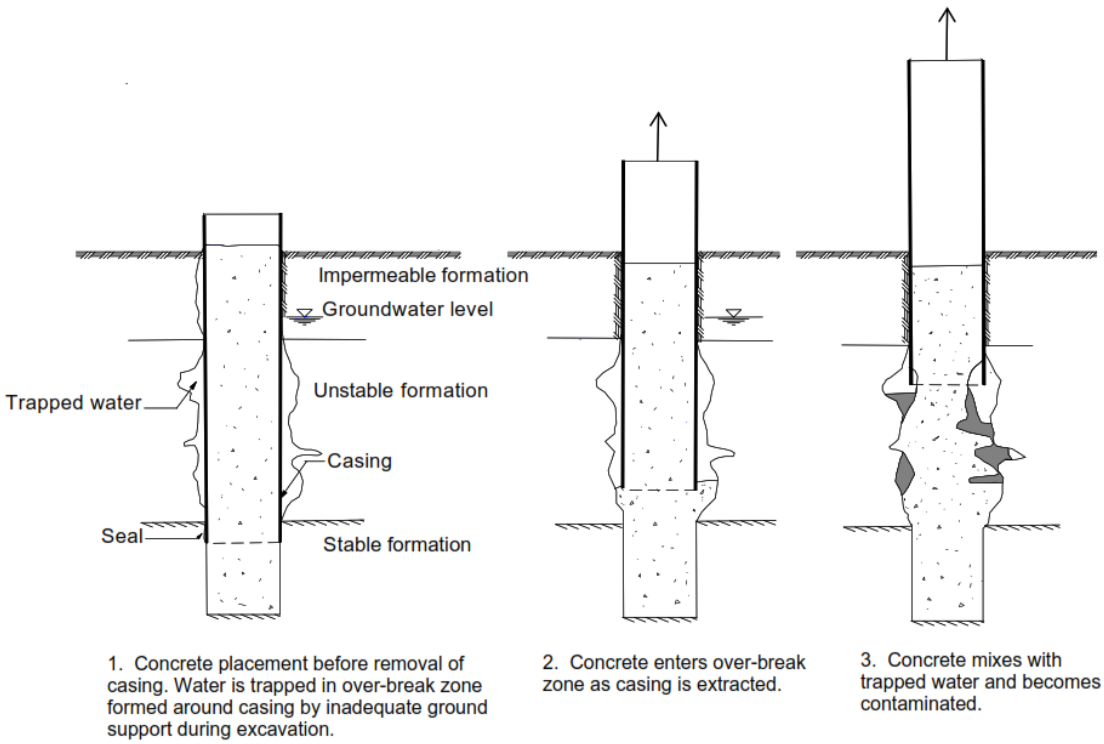


Figure 1. Defect formation due to water filled voids outside casing.

Certain specifications require permanent steel liners that extend to the top of the founding strata (e.g. Queensland Department of Transport [DTMR] Specification MRTS63, 2016); with a socket usually formed in rock below the liner. The DTMR specification requires that rock socketed piles be dewatered, where possible, for inspection and concreting. This can often lead to socket instability in weathered or fractured material. It is often difficult in practice to achieve a watertight seal at the toe of a permanent steel liner and ingress of groundwater and soil at the toe of the liner may occur where high excess external water pressure exists. Dewatering such piles to facilitate inspection increases the risk of non-conformances. Where inadequate seal is achieved and the liner cannot be installed to increased depth, or the socket is collapsible, the pile should be filled with water or drilling fluid and concreted in the wet. The use of water, rather than drilling fluid, may have some disadvantages as outlined in the following section.

The use of a permanent steel liner may also create conditions that are conducive to the occurrence of concrete bleed, which has been known to cause significant defects. Bleed effects are discussed further in later sections of this paper. Where permanent liners are adopted, a compatible bleed resistant concrete mix must be used.

Use of Water as Fluid Support in Lieu of Drilling Slurry

A common solution for piles constructed in stiff cohesive materials (or better) below the water table is to excavate and complete the pile underwater. In favourable ground conditions, side-wall stability can be achieved by filling the pile with water to a level above that of the prevailing ground water table, so as to provide excess hydrostatic pressure within the pile. Where ground permeability is sufficiently low to maintain an excess head of water within the pile, the resulting excess hydrostatic pressure can be sufficient to support the sidewalls.

However, whilst many soils can remain stable for short durations under such conditions, they often become less stable with time. Soils with low liquid limits such as clayey or silty sands, fissured clays, and some types of weathered rock can degrade rapidly when exposed to free water and sudden instability can occur. In such circumstances, sidewall collapse during drilling, cleaning, or during the process of reinforcement placement and concreting can be extremely problematic. This can often result in significant over-break, rework, and /or soil inclusions within the completed pile. Except in cases where ground stability is high, the use of water in lieu of polymer or bentonite fluid is a relatively high risk solution. In cases where ground conditions may be marginal for this support method, an alternative support method such as temporary steel liners or polymer drilling fluid should be available so that it can be rapidly implemented if required.

A significant disadvantage of the use of water in lieu of other drilling fluids is its inability to suspend sediment. The process of drilling and cleaning the pile can often result in heavily silt laden water within the pile at the time of pile preparation and concrete placement. Rapid settlement of particles within the pile can result in sedimentation at the pile base and on top of the rising column of concrete during pouring. Such sediment can remain at the base of the pile or can be left as contamination within the pile shaft if not properly displaced.

The use of water only as ground support is therefore generally only suitable in the following circumstances:

- Where an excess water pressure head of at least 1m can be maintained inside the pile for the duration of drilling, pile cleaning and preparation and concreting;
- Excavation side-walls which have a high level of stability, sufficiently low permeability to allow excess pressure head within the pile to be maintained, and where materials are not subject degradation when exposed to free water;
- Piles which can be caged and poured with minimal delay after the completion of excavation, where pour volumes are relatively modest and concrete can be placed within a time frame that does not allow significant settlement of sediment within the pile. Generally, such piles would tend to be smaller in diameter and of limited depth where reinforcing and tremie placement time is minimal.

In all cases, careful monitoring of concrete level during placement, over-pour and inspection of the condition of the top of the concrete upon completion of the pour should be conducted to check for any sidewall collapse or contamination. These measures are part of good practice for all bored piles constructed in other than dry conditions as discussed later in this paper.

Pile Construction under Polymer and Bentonite Drilling Slurry

Polymer and bentonite drilling slurries have the capacity to provide a robust and controlled method of providing ground support in unstable ground when well executed. The use of polymer based drilling fluids is relatively common in Australian industry, in lieu of more traditional bentonite drilling fluids. Polymer fluids offer the advantage of shorter preparation and mixing times, easier conditioning methods which require less plant, and often lower disposal costs.

Specifications for the use of bentonite drilling fluid have been widely published in technical documentation and specifications (e.g. FPS, 2006). Many studies have also been conducted over an extended period into the performance of bentonite slurries as ground support and their effect on pile performance (e.g. Fleming and Sliwinski, 1977; Holden, 1984; O'Neill and Reese,1988; Majano and O'Neill, 1993).

In contrast, published technical information in relation to polymer use is less common (e.g. Ata and O'Neill, 1998; Lam and Jefferis, 2015). As proprietary polymer products can vary substantially, users are largely reliant on manufacturer's guidelines in relation to product use, and their own project experience with particular products. Consequently, the following sections tend to focus more on

issues related to polymer slurry as noted, though much of the commentary is equally relevant to bentonite slurry use.

Planning and Establishment

Proposed tanks and equipment for mixing, storage, pumping and cleaning of drilling slurry, including volumetric capacity, footings and bearing requirements, require proper planning. The storage capacity of the slurry plant is relevant to the amount of polymer that contractor has in reserve during drilling. This is important to be able to progress the works, i.e. open additional holes where appropriate prior to pouring previously excavated piles, and to respond to rapid drilling fluid losses in open holes should they occur. It is generally recommended that at least 50% of the largest expected pile volume in surplus slurry should be maintained on site. This should be increased if the contractor intends to have multiple piles open at the same time, as is generally the case.

The layout of the plant should always ensure that used slurry is returned to a settlement/cleaning tank and reconditioned prior to re-use. Polymer fluid is normally circulated through settlement tanks to allow coarse particles to settle out and be removed, as a primary means of fluid reconditioning. Suitably sized settlement tanks should therefore always be incorporated. Used slurry of any type should never be pumped directly into storage tanks containing fresh or reconditioned slurry.

Pumping equipment must be appropriate for the slurry type. For polymer handling, high shear pumps should be avoided as they shear polymer strands and reduce drilling fluid effectiveness. Low shear pumps (eg. piston type) should be used for polymer slurry handling.

The proposed slurry product should be suitable for the expected site conditions, based on previous experience and the manufacturer's recommendations. Factors such as soil type, groundwater salinity or contamination, and expected head pressure differential must be considered. Generally, the suitability of polymer slurry products is more sensitive to site conditions than bentonite. There are many different polymer based products available for various applications and with differing properties. Details of the proposed mixing methodology, dosage rates and any proposed additives should be determined in advance, in consultation with manufacturers. It is common practice to use a small percentage (e.g. 0.5% by weight) of bentonite or other fine material additive in polymer slurries to control fluid loss in granular materials. The proposed polymer mix and methodology should give consideration to how fluid loss will be controlled in the event that it is higher than is desirable.

Slurry disposal at the completion of the works should be addressed well in advance. Some polymers can be broken down with the use of additives and disposed of via the sewer as trade waste (with appropriate permissions) or alternatively transported off site as liquid waste. Bentonite slurry generally requires disposal as liquid waste. The method of disposal should be confirmed at the planning stage.

Excavation Stage

Protection of adjacent piles must be considered at all stages of excavation works. Depending on near surface ground conditions, it is generally advisable to use partial length temporary steel liners to support the top of the excavation and prevent collapse due to undermining or localised surcharging of the working platform. Temporary liner lengths vary, depending on conditions and particularly near surface ground conditions. It is also necessary to ensure that sufficient spacing is maintained between open piles to prevent interaction during drilling and/or concreting. This is again dependent on ground conditions, however, a minimum of four pile diameters (centre to centre) between piles is generally a reasonable starting point. Open pile excavations should be monitored closely during drilling and concreting for signs of interaction. In the authors' experience, it would not be inconceivable that piles could interact during drilling or pouring at six pile diameters or more in unfavourable ground conditions. As a general matter of good practice, the contractor should sequence their works such that spacing between open pile excavations is maximised at all times.

Maintenance of adequate head of drilling fluid in the pile at all times is a critical aspect of successful pile construction. Slurry levels must be maintained above ground water levels at all times. There is often a significant risk of pile collapse when fluid levels inside the pile approach the level of the surrounding ground water. It is therefore recommended that, as a minimum, slurry levels be maintained 1m above ground water level and preferably in the order of 1.5m to 3m above. Maintaining excess slurry head must be balanced with the rate of drilling fluid loss and changes in the slurry level with down-hole activities.

Drilling fluid levels can rise and fall significantly due to the volume of Kelly bars and drilling tools, and particularly upon extraction of drill tools filled with spoil. Surge (or overflow) tanks, which allow polymer to overflow into an adjacent tank/vessel during drilling and flow back rapidly into the pile on extraction of the tools, should be used in all cases where groundwater is within 3m of working platform level. Whilst surge tanks are not the only way of maintaining a positive head within the pile, they provide a simple and effective solution in many circumstances and are recommended.

Drilling and cleaning tools should be designed to allow slurry flow around the tool during lowering and extraction, in order to prevent excessive piston effects which can lead to excavation instability. Venting of buckets and/or provision of an annulus around tools to allow flow of fluid past the tools is necessary. Either full size buckets with internal vents, or undersized buckets with reamers or similar can be used provided the opening through or around the tool is sufficiently large.

Controlling the rate of extraction of drill tools from the hole is particularly important. Guidelines for rates of tool extraction should be determined based on flow bypass characteristics and implementation of these guidelines should be monitored during the works. Generally, the drill string should be able to be lifted from the hole with little excess load on the winch, beyond self-weight. Any increase in load is indicative of a suction effect. Creation of suction during extraction of drill tools either due to insufficient bucket venting, or excessive extraction rate is a common cause of collapse in piles drilled under fluid.

Regular testing of the slurry should be carried out to monitor its condition. The testing regime should cover the stock of slurry in storage, as well as the condition of polymer in the pile hole immediately prior to concreting. Examples of bentonite specifications can be found in FPS (2006). Testing of polymer slurry is not as widely specified, but should normally include pH, viscosity (e.g. marsh funnel), sand content and mud density as a minimum. The proposed testing regime should be documented including testing methods, frequency and acceptance criteria for both general use and concreting. Slurry testing should be carried out routinely – preferably three checks per day per location – and recorded so that trends in slurry condition can be identified before problems occur. This is necessary to ensure slurry of good quality is in use and available in storage at all times, and that the site personnel are consistent in the way they manage the slurry. Records of all test results should be maintained so that in the event of excavation instability or other construction difficulties, a forensic review of the records can be undertaken to determine and rectify the cause of the problem.

Construction delays, open excavations

Pile excavations that are left open for extended periods of time can lead to a loss of strength and stability of soils in the vicinity of the pile. This does not only generate risks for the completion of the pile that is open, but also other piles in the vicinity that are subsequently excavated. Particularly in granular layers, significant over break in in one pile is often followed by similar difficulties in surrounding piles. In some cases this may be due to the inherent nature of the soil strata, but it is the authors' view that in many cases this is due to progressive disturbance and loosening of the soil due to construction processes.

Consideration should be given during programming and management of site activities to avoid having open excavations for extended periods of time. Ideally, piles will be concreted within 24 hours of the completion of excavation, although this is often not possible in practice.

It is critical that drilling fluid levels are maintained during any delays in construction. Positive head must be maintained at all times, including site shutdown periods. Control measures should be implemented to monitor and control slurry levels in piles left open for extended periods, such as having a reserve fluid volume that can flow into the pile or float switch arrangements.

PILE PREPARATION AND CLEANING

Following the completion of excavation, pile preparation is critical prior to reinforcement and concrete placement. This element of the construction process is often given insufficient attention in both construction planning and during site activities. Pile cleaning is a particularly important aspect of the construction process, as inadequate cleaning and slurry preparation can result in pile integrity issues and a soft base. Cleaning involves removing any sediment or loose material from the base of the pile as well as controlling sedimentation of material suspended in the polymer during the period between cleaning and completion of the concrete pour.

Sidewall Cleaning

It is good practice to roughen the sockets of high load capacity bored piles, particularly when drilled under water or fluid. Roughening is generally only practically achievable in low and medium strength rock. Bentonite slurry is known to form filter-cake on pile sidewalls, and this can occur in some rock sockets as well as permeable soil (Holden, 1984). Polymer has significantly less potential to form a filter cake than bentonite slurry. However, smearing of rock sockets during drilling can occur in some rocks. Where it can be carried out effectively, roughening of sockets is highly likely to improve the load-settlement performance of the pile and helps negate the effects of any deleterious sidewall material.

In rock socket materials which are susceptible to moisture content changes (e.g. Melbourne mudstone), it is good practice to ream socket side-walls in piles that are not poured within 24 hrs of drilling. Reaming tools need to be properly designed and methodology should be pre-planned, as it is necessary to ensure casing diameters are chosen to enable passage of the proposed reaming tools.

Base Cleaning

Base cleaning is often carried out initially using mechanical methods, i.e. cleaning buckets which are employed after the pile has been drilled to depth. Effective mechanical base cleaning requires drilling tools that form a regular flat base and compatible (i.e. identically shaped) cleaning tools that effectively remove any sediment and loose material. It is common in practice to see drilling tools which cut a tapered base being used in conjunction with flat based cleaning tools – such incompatible geometric combinations are generally ineffective and leave debris at the base of the pile. Ideally, base cleaning tools should be capable of cutting the base of the pile when used to ensure a regular clean base.

Socket formation in strong rock often requires the use of a coring bucket, which cuts an annulus into the rock before the core is broken off and removed. This can result in an irregular pile base making conventional mechanical cleaning ineffective and base cleaning in general difficult. For piles cast under water or slurry, airlifting may be able to achieve a clean base where the base is irregular in shape. However, this approach has many practical problems in achieving consistent results. Milling the base of the pile flat using a specialised rock cutting or grinding tool is generally necessary to facilitate mechanical cleaning of the base, if airlifting cannot be carried out effectively.

Airlifting is the process of sucking water or slurry along with any sediment or debris from the base of the pile. As the fluid is sucked up from the base of the pile, fresh fluid is added to the top of the pile. This process can be used to clean the base of the pile and also re-condition the slurry more broadly. In the authors' experience this process is often poorly executed in practice and the effectiveness of

airlifting in achieving a clean base is highly variable. Important factors in relation to effectiveness are as follows:

- Geometry of the airlift tube and inlet, and the pressure and flow velocity that can be generated. Various bell-mouthed and sweeper type airlifts have been tried previously with variable effectiveness. The critical factor is that the velocity of flow at the inlet must be sufficient to scour or lift material from the base. This is affected by flow volume and the area of opening between the inlet and the rock – not just the size of the tube or inlet. Hence, the height of the inlet off the base of the pile can be critical. Again, cleaning by airlifting is much more likely to be consistently effective if the base is flat and regular in geometry.
- The passage of the airlift around the base of the pile – it can be difficult to control the location of the airlift inlet well enough to achieve complete coverage of the pile base. Airlifting should always be carried out initially before the reinforcing cage has been placed. In some cases, a second airlift may be necessary to re-clean the base after placement of the cage to remove any remaining sediment and to complete final conditioning of the fluid. Airlifting inside the reinforcing cage is less effective due to the restricted movement of the equipment around the pile base.

A critical aspect of base cleaning is the methodology used to verify base cleanliness. The most common method of checking base cleanliness is the use of a weighted sounding tape. While rudimentary, the authors have found this to be a practical and effective method in the majority of cases, provided it is well executed. The weight at the end of the tape should be metal and should have a flat rather than pointed end, so that the difference between a clean base and a sediment covered base can be felt. Generally, for example, a short piece of 36mm to 40mm rebar (or similar) hanging vertically provides a sharp feeling on a clean base in a rock socket in competent material, and a dull or soft feeling on an unclean base. While it is difficult to accurately control the location of the tape, the use of a large number of sounding locations (say a minimum of one location per 250 cm^2 of base area) would be expected to provide sufficient coverage. A similar sounding method for piles founding in very dense sand has been reported by Lam et al. (2010). This incorporated a 100mm x 100mm x 20mm metal plate on a tape measure, and the use of grading system for the quality of base response.

More sophisticated commercial cameras and measurement devices are also available and can be implemented where practicable and necessary. The ability of many of these cameras to provide clear images in dirty water, polymer, or bentonite slurry is limited. More sophisticated cameras which are able to provide images via air chambers are often slow, complex to operate and expensive. Pile Dynamics, Inc. has recently developed the SQUID (Shaft Quantitative Inspection Device) which is designed to measure the thickness of soft material or debris on top of the bearing strata and the strength of the bearing layer. To the knowledge of the authors, this device has not yet been used in Australia.

Based on the authors' experience, a diligent and well executed program of sounding inspections, both before cage placement and immediately prior to pouring, would be expected to provide satisfactory outcomes in the majority of cases. In cases where pile performance is critically dependent on base response at serviceability loads, or where experience with the chosen construction methodology and/or ground conditions is limited, more sophisticated base inspection methods may be warranted. In all instances, it is recommended that the level of attention given to base cleanliness and acceptance requirements is commensurate with end bearing design requirements – in some cases, base load-settlement response will be more critical than others.

Fluid Preparation

It is necessary to condition drilling fluid prior to concrete placement to ensure adequate performance in relation to sedimentation and flow properties. Specification requirements for concreting phase are generally more onerous than for the excavation phase (FPS, 2006; U.S. Federal Highways Administration, 2010).

The conditioning of bentonite slurries is generally carried out by partially or completely replacing the slurry in the pile with fresh or recycled material from the slurry plant, which is best achieved by extracting slurry from the base of the pile and introducing clean slurry at the top of the pile until sufficient quality is achieved.

There are a number of different approaches which can be implemented in various combinations to manage sedimentation and condition of polymer slurry. These are generally as follows:

- Suspension of fines within the polymer and caging and pouring within a time frame that minimal sedimentation occurs to prevent material drop out.
- Promoting rapid settlement of suspended material from the polymer via the use of additives immediately prior to final cleaning;
- Refreshing the polymer by pumping out contaminated polymer and replacing it with fresh or reconditioned (cleaned) polymer.

The most appropriate approach for polymer slurry depends on the properties of the slurry and the particles suspended (or partially suspended) within it. For piles in which suspended particles are relatively fine and can remain in suspension for the duration of the pour, and/or pours which can be completed rapidly, the first approach given above may be adequate.

In some cases, it can be sufficient to provide for a delay of as little as 30 to 60 minutes settlement time prior to mechanical cleaning of the base, where additives are used or rapid drop out of particles occurs unaided. The effectiveness of this approach will depend on the properties of the polymer product in use and the drilling fluid generally. However, the effectiveness of this approach must not be assumed and should be verified by sampling slurry from the base of the pile and observing the settlement characteristics, as well as base inspections to confirm adequate cleanliness.

In most large and/or deep piles constructed with either bentonite or polymer slurry, air lifting or pumping of from the base of the pile prior to caging is generally necessary and would normally be considered good practice as it assists in refreshing/cleaning the slurry as well as removing base sediment.

The method of cleaning and conditioning drilling fluid should always be planned and documented in advance, and the effectiveness of the chosen method for the conditions should be verified on site and monitored on a pile by pile basis. The contractor should include slurry testing procedures and pre-pour checks in their site processes, to ensure that slurry condition is suitable for concreting. Target slurry characteristics and acceptance criteria before concrete pouring should be clearly stated.

It is the authors' view that pre-pour pile preparation is often given insufficient attention in construction planning and monitoring. A very clear, comprehensive and well defined pre-pour preparation methodology addressing the above items should be included in the construction procedure and monitored continuously on site, as it is critical that quality outcomes are achieved in relation to pile performance and integrity. A failure to adequately manage fluid properties and cleanliness can result in a range of defects including soft/contaminated pile toes, concrete inclusions and/or sand deposition around reinforcing cages.

PILE REINFORCEMENT AND FITMENTS

Pile reinforcement cage detailing is an important aspect of bored pile construction which is often overlooked. Poor cage detailing and cage placement methodology can often contribute to quality issues. The design of pile reinforcement, both generally and at splice or starter bar locations, must avoid congestion and ensure that concrete can flow adequately around the cage. A summary of commonly used bar spacing requirements are provided based on EFFC/DFI (2016) is shown in Table 1. The size of the tremie should be considered in smaller diameter piles, as this adds to the congestion

in the pile at the time of the pour. An example of the consequences of steel and tremie pipe congestion is shown in Figure 2.

A useful approach to cage splicing in multi-section cages is to reduce the cage diameter in alternating sections of the pile, so that the bars can overlap radially at the splice. As structural actions are generally greatest at the top of the pile, a small reduction (say 50mm to 70mm) in cage diameter in lower sections is usually inconsequential to structural adequacy and can significantly enhance cage placement times and concrete flow at splices.

Centralisation of the cage in the drilled hole is essential to avoid non-conformances due to out of position and/or inadequate cover in the completed pile. The common industry approach with light weight plastic roller spacers is prone to dislodgement or failure of spacers, and can often present a significant risk of cages moving to side of hole. Either concrete spacers or skid type spacers welded to cage are available and provide a more robust solution. However, skid spacers present the risk of dislodging material from the excavation sidewalls and can result in localised inclusions affecting cover concrete in some instances. In all cases, spacers should be selected in consideration of ground conditions, relevant aspects of construction methodology (e.g. whether or not temporary or permanent casing is used, cage placement method) and durability considerations. At least six to eight equally spaced cage spacers should be used at each level they are attached – the use of spacers at quarter points only is insufficient.

Table 1. Commonly used bar spacing requirements for bored piles (EFFC/DFI, 2016)

SPACING FOR BORED PILES			
LOCATION	**CLAUSE**	**VALUE**	**COMMENT**
horizontal and vertical spacing of bars	ACI336.1, 3.4.9	$\geq$ 100mm	including at laps.
	FHWA GEC10, 8.4	$\geq$ 5 in	required by many agencies, where tremie placement of concrete is anticipated
		$\geq 10\ D_G$	where D_G = maximum aggregate size; see also comment above
	EN1536, 7.5.2.5	$\geq$ 400mm	
	EN1536, 6.3.2.2	$\geq 4D_G$	where D_G = maximum aggregate size.
	EN1536, 7.5.2.6	$\geq$ 100mm	for single or bundles of longitudinal bars.
	EN1536, 7.5.2.7	$\geq$ 80mm	for lap length, provided that $D_G \leq$ 20mm (special consideration must be given to the maintenance of sufficient concrete flow, see sections 3 and 6).
	EN1536, 7.5.2.9	$\geq 1.5D_G$ and $\geq 2.0D_S$	for layers of bars, placed radially, where D_S = (steel) bar diameter.

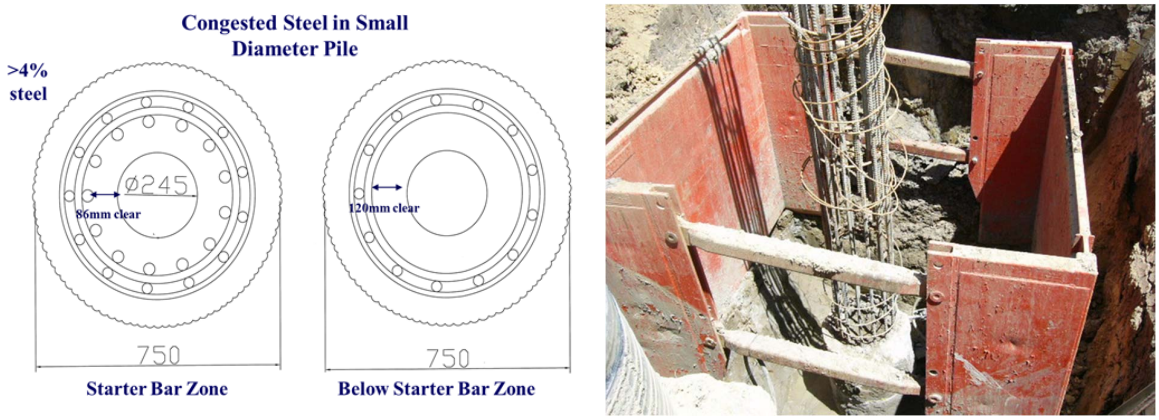


Figure 2. Steel congestion and subsequent over-trimming of contaminated zone in small diameter bored pile cast under polymer slurry.

The practice of resting cages on the base of the pile can also promote failure of the spacers, as the cage can tend to deform under its own weight and lean against the sidewalls of the excavation for support.

This increases the load on spacers, which are consequently more likely to fail. Where practicable, hanging cages marginally off the bottom of the excavation provides a more reliable method of promoting accurate cage positioning as cages tend to remain centrally located for their full depth.
Low cut-offs (i.e. significantly below working platform level) present an additional risk as the position of pile/cage often cannot be confirmed at the time of the pour. In such cases, the use of a lightweight cage extension or hanging bars up to working platform level can be used to reduce the risk of out of tolerance cages.

When placing a cage, if it does not install smoothly then all cage sections should be removed to determine the issue. Forcing the cage further into the hole via mechanical means (e.g. using an excavator) has been known to occur, which is indicative of a problem. In such circumstances there is a high potential for soil/sludge to be dislodged from the walls onto the pile base as well as cage spacers being damaged in the process, and it is unlikely that cover requirements will be achieved.

CONCRETE SUPPLY AND MIX PERFORMANCE

Defective concrete in piles are often the result of unsuitable pre-mixed concrete, either due to inappropriate mix design or failures in batching and delivery processes. Bored pile construction requires a concrete mix with suitable workability (slump and spread) and workability retention time (workability life), in order to allow successful placement. Historically, it has been common practice to use design slumps of around 180mm to 220mm, and many available specifications are based on minimum slump of this order. It is the view of the authors that these conventional mixes provide little margin for error and significantly more suitable concrete mixes are now available. Figure 3 shows one type of commonly observed defect that can results from inadequate concrete workability. It is advisable to build as much redundancy as is economically possible into mix design with respect to flow properties and workability life.

Recent advances in concrete technology and industry practice have led to the development of the industry guideline documents, "*Recommended Practice – Tremie Concrete for Deep Foundations*" (Concrete Institute of Australia, 2012) and *EFFC/DFI Best Practice Guide to Tremie Concrete for Deep Foundations* (European Federation of Foundation Contractors/Deep Foundations Institute, 2016), which provide recommendations for workability, workability life and mix constituents. The recommendations of these documents are considered to represent current best practice.

The concrete mixes recommended in these guidelines can generally be described as self-compacting or highly flowable concrete. Vicroads concrete specification (Vicroads, 2016) describes self-compacting concrete as: "*Concrete that is able to flow and consolidate under its own weight, completely fill the formwork or bore hole even in the presence of dense reinforcement, whilst maintaining homogeneity and without the need for additional compaction.*" In general terms this type of mix requires less coarse aggregate, increased sand and cementitious material, lower water-cement ratio, and higher doses super-plasticizer and viscosity modifying agents, compared to more conventional mixes.

It should be noted that highly workable concrete can be sensitive to segregation due to settlement of solid constituents. The authors' have been involved in cases where a conforming and seemingly well performing highly flowable mixes have been subject to settlement of aggregate in the upper sections of the completed pile, leaving essentially a sand-cement grout in the top few metres of the pile. It is important with these mixes to ensure that testing is frequent and accurate, and to check for settlement of aggregate in the uppermost zone of the pour. If the mix does not appear to have the correct proportion of aggregate, the pile should be over-poured until a properly proportioned mix can be seen at the top of the pile.

It is also essential in all cases to understand the workable life of the fluid concrete mix, as larger concrete pours can often take in excess of 4 hours and sometimes up to 8 hours or more. Provision should be made in the mix design to allow for difficulties and delays during the pour. As a minimum, an allowance for 50% more than the expected duration of the pour should be made in determining the

required workability life of the mix, and double the expected time is often appropriate for shorter pours.

Delays to concrete delivery and/or placement significantly increase the risk of concrete contamination. A common mechanism that can occur when delays are experienced during a pour, in conjunction with sedimentation from drilling fluid, is shown in Figure 5. During a delay, the older concrete already placed in the pile can lose workability due to a lack of agitation and at the same time settlement of sediment can occur from fluid in the pile. Upon recommencing the pour, concrete can tend to well up around the tremie pipe and flow up over the older concrete. This tends to roll sediment or contaminated concrete at the surface of the concrete into the cage and sidewalls where it can be trapped. An example of this effect from an exposed diaphragm wall panel is shown in Figure 4. To mitigate this risk, pours must be continuous and delays to concrete supply must be minimal. Poor concrete supply service should never be tolerated, and concrete suppliers should be made aware of the possible consequences of intermittent supply.



Figure 3. Example of 'matressing' effect due to weak flow through reinforcing cage due to inadequate concrete workability. (EFFC/DFI, 2016)



Figure 4. Void in diaphragm wall panel as consequence of concrete placement delays.

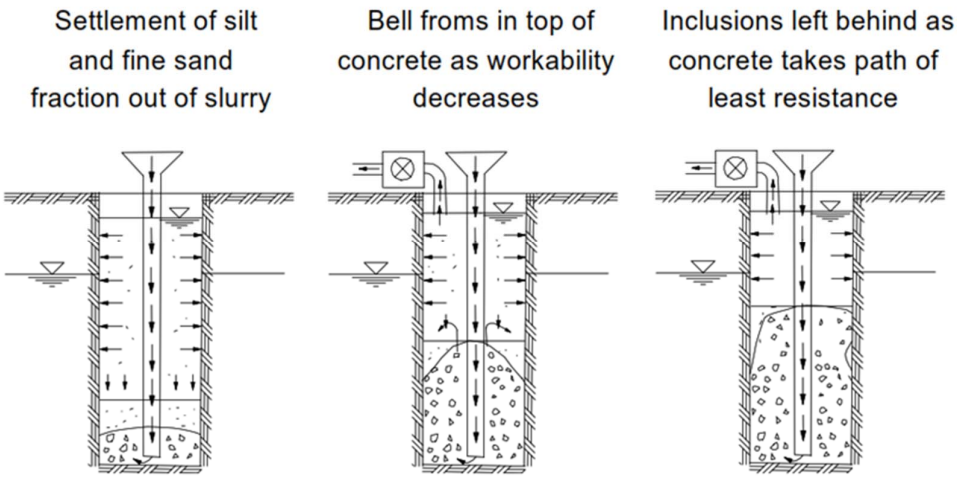


Figure 5. Common mechanism of defect formation by inclusions due to concrete placement delays.

Bored pile mixes must also be resistant to bleed, the causes of which are often not well understood in practice. The following description of concrete bleed is given by Hudson (1999): "*Bleeding, also known as water gain, is a form of segregation in which some of the water in the mix tends to rise to the surface of freshly placed concrete. This is caused by the inability of the solid constituents of the mix to hold all of the mixing water when they settle downwards*". Cast-in-situ piles are known to provide conditions which can tend to generate bleed, primarily due to the comparatively large depth of concrete and resulting pressure head that can be generated within the column of concrete. This provides a significant driving force to expel excess water from the mix. The depth of concrete in piles is significantly greater than most other concreting applications, and therefore provides both high in-situ pressures and volumetric potential for bleed.

In conditions where the excavation side walls are permeable bleed water can be lost into the surrounding ground without channelling up through the pile. However, piles cast within an impermeable liner, or low permeability soils are known to provide conditions which are conducive to bleed related problems. In such cases, the bleed water has no path to escape to other than the top of the pile or any exposed natural material.

The migration of significant quantities of free water towards the top of the pile generates defects that are generally observed to occur as follows:

- bleed tracks, both around the perimeter of the pile and within the concrete mass, often at the location of reinforcement;
- loss of cement paste and/or increased water content in distinct zones leading to runs of low strength material which are generally more prevalent towards the top of the pile where the cumulative effects of upward flow are greatest; and
- a general reduction in the overall quality of concrete in the uppermost sections of the piles which are most greatly affected by the cumulative movement of water to the surface of the pile.

Excessive bleed has often been observed by the authors to be due to the use of an inappropriate concrete mix design, and in some instances this problem has been found to be associated with the use of manufactured sand which has a tendency to hold less water than natural sand. It is advisable to avoid manufactured sand where possible concrete mix design used in bored piles.

Testing methods for the assessment of concrete bleed potential are outlined by EFFC/DFI (2016).

CONCRETE PLACEMENT METHODOLOGY

Many specifications are used in Australian industry, which address concrete placement methods (eg. QTMR, 2016; Vicroads, 2015; RMS, 2014); as well as many private sector project specific documents. Some are quite prescriptive, while others are fairly limited in terms of their requirements and provide significant flexibility for the contractor.

Concrete placement by tremie method is addressed in detail in EFFC/DFI (2016) *Best Practice Guide to Tremie Concrete for Deep Foundations*, which provides practical guidelines in relation to methods of placement as well as concrete properties.

A detailed review of common specifications and methodologies for concrete placement is beyond the scope of this paper. However, the following provides commentary in relation to critical aspects of concrete placement methodologies, in order to avoid concrete contamination in the pile.

Following the proper cleaning and preparation of the pile and any drilling fluid, the requirements for successful placement of concrete are as follows:

- A suitable tremie pipe or concrete pump system to deliver uncontaminated concrete initially to the toe of the pile, and then with sufficient vertical and horizontal control of the discharge end to maintain the outlet at the correct depth and relatively centrally within the pile. All tremie joints must be water tight incorporating suitable O-ring seals, waterproof tape, or similarly effective

seals. Where used, end closures should also be watertight. Where an open tremie or concrete pump is used, a suitable ball, sponge or vermiculite separator must be used to prevent concrete falling through water. The volume of the separator should be appropriate to ensure effectiveness, and it should be remembered that inflated balls will reduce in size under water pressure at depth.

- As a minimum, hydrostatic pressures inside and outside the pile should be balanced or excess hydrostatic pressure inside the pile should be present at the commencement of the pour. For ground stability, excess internal pressure is always recommended.
- Following the commencement of concrete flow, hydrostatic pressures in the concrete in the tremie must always exceed the external fluid pressure, otherwise fluid can permeate into the tremie and contaminate the concrete. This is illustrated in Figure 6. For tremies with end caps, the tremie must be sufficiently full, generally at least two thirds to three quarters full, before it is lifted off the base of the pile to promote flow and prevent water ingress.
- A controlled means of carefully raising the discharge end so that it always remains embedded into the concrete. At the commencement of flow, the tremie should be approximately 100mm above pile base to allow water and concrete out, but to limit the depth that the initial discharge of concrete falls through fluid and to ensure that the toe of the tremie becomes embedded in the fluid concrete as quickly as possible. The tremie must be embedded a minimum of around 2m and ideally less than around 6m into concrete at all times.
- The supply of concrete should be effectively continuous, with only nominal delays between trucks as they are repositioned for discharge.
- Concrete pours should be supervised at all times by an experienced engineer/supervisor, who should make records of the pour as it is occurring including depths to top of concrete, toe of tremie and length of tremie remaining, depth of liner and level of fluid in the pile. No tremie sections should be removed without the approval of the supervising engineer/supervisor. Depth records should be recorded at the start and finish of each truck, and before and after removal of tremie sections or movements in the depth of steel liners. It is important that allowance is made in the length of the tremie for it to be lifted to the level required for disconnecting joints to remove tremie sections, and if necessary to assist in concrete flow (noting that lifting or surging the tremie for the purposes of encouraging flow should be avoided where possible). Typically, to achieve a minimum embedment of 2m into the concrete, at least 3m to 3.5m embedment should be provided when the tremie hopper is in its normal level for concrete discharge.
- Concrete should be over poured to a level sufficient to ensure sound concrete at cut-off level and also to ensure that pore water pressures within the fluid concrete are greater than those of the external groundwater. Significant care should be taken with piles with deep cut-offs and in particular piles with cut-off levels below ground water level. In such cases it may be necessary to significantly over pour piles or leave the pile excavation filled with water or drilling fluid until the concrete has set. Pumping off of water/drilling fluid from piles with deep cut-off can lead to water ingress and associated concrete damage.
- Recovery methods to be implemented in the event that any blockages occur at commencement or at a later stage during the pour should be determined in advance. In the event that irregularities occur during the pour, it is important that there is a clearly defined course of action. In certain circumstances, piles can be successfully completed after a tremie blockage. However, appropriate recovery methods vary considerably in each instance and a discussion of this topic is outside the scope of this paper.
- The last 2m to 3m depth of drilling fluid will generally be contaminated with cement. To avoid degradation of the broader drilling fluid stock, this slurry should be pumped to specific settlement tank and reconditioned before reuse.

At all stages during the pour and upon completion, in order to prevent ingress of groundwater to the fluid concrete mix, it is necessary to maintain excess hydrostatic pressure within the pile compared to the groundwater outside the pile. If the groundwater pressure outside the pile exceeds the water pressure within the fluid concrete, water can migrate into the concrete mix before it sets. This can have the following effects:

- Loss of concrete strength due to an increase in water-cement ratio locally within affected areas the concrete;
- Piping of ground water through the pile and washout of cement paste from the fluid concrete. This effect is often evident as excess water piping (or bubbling) to the surface of the pile and can appear to be similar to bleed effects.

An example of damage caused by excess external water pressure at the time of casing extraction is shown in Figure 7.

Immediately after placement, high slump concrete (of the type used in bored pile construction under water) is essentially fluid and the pressure within the fluid concrete is generally thought to be close to hydrostatic up to a critical concrete depth (Collingwood, 2000). It is noted that the density of fluid concrete is greater than water and therefore the pressure gradient within the pile is greater than that of water if it is in the hydrostatic condition. Further, the pressure within fluid concrete is comprised of the concrete pressure head plus the head of any water that is present above the concrete.

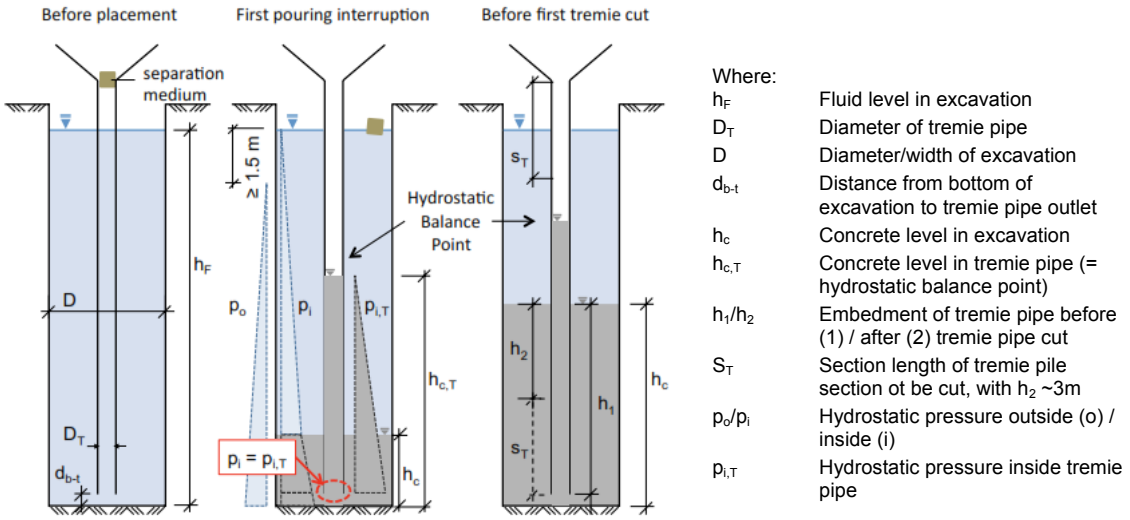


Figure 6. Pressure balance within pile during concrete placement (EFFC/DFI, 2016).



Figure 7. Concrete degradation due to excess water pressure outside of liner when extracted.

While excess internal pressures must be maintained throughout, a critical time for potential groundwater ingress to the pile is a short time after placement, when the weight of the concrete begins

to be transferred to the solid particles within the concrete matrix and the pressure of the water within the concrete mix is no longer at a maximum, but the concrete is not yet properly set. It is at this stage, in particular, that groundwater pressure differential can lead to concrete degradation, even when hydrostatic pressure balance is seemingly satisfactory.

The exact conditions which can result in defects due to this effect are not well defined or understood. The reason for this is that the fluid properties of concrete mixes and their curing rates vary substantially from project to project, along with ground water conditions. It is the authors' experience that the following conditions are more likely to lead to quality issues associated with excess external groundwater pressures:

- The use of mixes with lower concrete slumps and shorter slump life, which tend to reduce the pressures within the fluid concrete during and immediately after placement;
- Working platform levels which are close to the groundwater level, and/or concrete cut-off levels which are close to, or below ground water level, where concrete is not over-poured and left in place;
- Permeable ground conditions which allow free movement of groundwater;
- Charged (artesian) groundwater.

The above conditions tend to produce higher groundwater pressures and mobility, and lower initial pressures within the fluid concrete mix. Such conditions create a situation where concrete is more susceptible to degradation by ingress of external groundwater and should be considered in the formulation of construction methodologies.

DESIGN AND ORGANISATIONAL ISSUES

In the authors' experience, it is common for a combination of design and organisational issues to contribute to defective piles, as well as construction methodologies. Some important considerations in this regard are as follows:

- Structural details, such as reinforcing cage bar configurations and tolerance, and starter bar and splice details must consider constructability. Designers need to design and specify for ease of construction, not simply for documentation, and need to be able to respond to project requirements during construction to enhance quality outcomes. Current design approval processes, particularly on major public projects, can be problematic in this regard. Design approval processes need to be able to be fast tracked where necessary;
- Prescriptive specifications that may be inappropriate and project intransigence with regard to alterations to materials and details of construction methodology can be significantly detrimental. For example, if a conforming bored pile mix is not performing adequately on site, the mix must be altered immediately. Project approval processes can sometimes take several weeks, meaning it is not practically possible to make adjustments to concrete mix in a timely manner. Material approval processes need to be able to be fast tracked where necessary;
- Generally, a greater understanding of pile construction issues is required by designers and project superintendents. Over reliance on specifications can be detrimental, and a lack of understanding can often lead to incorrect interpretation or application. It is important that the piling contractor can respond to difficulties and challenges in the most appropriate way, with support from other project participants.

There are many examples in the authors' experience of where clients, designers, superintendents and project managers have contributed to pile quality issues through their actions (or inaction). It is important that all project participants understand and respect that bored pile construction is an often challenging operation that requires favourable circumstances in all aspects in order to produce consistent and reliable outcomes. Defective piles are not in the interest of the contractor, the designer or the owner. The best project outcomes are achieved when all parties are working together to achieve a practical, high quality outcome, and project protocols are designed to enable this to occur.

CONCLUSIONS

The process of bored pile construction has been extensively researched and documented in academic research, industry guidelines, and specifications over many years. The body of knowledge in relation to best practice construction methods is comprehensive. Australian industry has many highly experienced practitioners and organisations that are fully aware of the issues discussed herein. Yet many fundamental problems and associated quality issues are observed in industry practice.

It is the authors' observation that project personnel – those who are charged with executing and supervising work on site – often have a limited understanding of issues that are of critical importance. This indicates that the body of industry knowledge on the topic is not being effectively transferred to key operational personnel. It is the authors' hope that providing a consolidated summary of matters of importance in this paper, will assist industry in transferring an understanding and appreciation of best practice bored pile construction methodologies and common pitfalls to personnel at an operational level.

REFERENCES

Ata, A.A. and O'Neill, M.W., 1998. *Side-wall stability and side-shear resistance in bored piles constructed with high molecular weight polymer slurry*. Deep foundations on bored and auger piles, Van Impe & Haegeman (eds), Balkema, Rotterdam.

Collingwood, B. 2000. *The Effects of Construction Practices on the Performance of Rock Socketed Bored Piles*. Ph.D Disertation. Department of Civil Engineering, Monash University Clayton.

Concrete Institute of Australia (CIA), 2012. *Recommended Practice – Tremie Concrete for Deep Foundations*. Concrete Institute of Australia.

European Federation of Foundation Contractors/Deep Foundations Institute (EFFC/DFI), 2016. *EFFC/DFI Best Practice Guide to Tremie Concrete for Deep Foundations*. First Edition, 2016.

Federation of Piling Specialists (FPS). 2006. *Bentonite Support Fluids in Civil Engineering*, 2nd Edition. January, 2006.

Federal Highways Administration, 2010. *FHWA GEC10 Drilled Shafts: Construction Procedures and LRFD Design Methods.* NHI Course No. 132014, Geotechnical Engineering Circular No. 10. D.A. Brown, J.P. Turner, R.J. Castelli. Publication No. FHWA-NHI-10-016. National Highway Institute, U.S. Department of Transportation, Federal Highways Administration. Washington, D.C.

Fleming, W.G.K. and Sliwinski, Z.J., 1977. *The use and influence of bentonite on bored pile construction - CIRIA Rep PG3*, Construction Industry Research and Research Association, London, UK.

Holden, J.C., 1984. *Construction of bored piles in weathered rocks*. Research Report No. 34, Road Construction Authority of Victoria, Melbourne.

Hudson, 1999. Concrete *Workability with High Fines Content Sands*. Quarry, February, 1999.

Lam, C. and Jefferis, S., 2015. *Performance of Bored Piles Constructed Using Polymer Fluids: Lessons from European Experience*. J. Perform. Constr. Facil., 10.1061/(ASCE)CF.1943-5509.0000756, 04015024.

Lam, C., Troughton, V., Jefferis, S. and Suckling, T., 2010. *Effect of support fluids on pile performance – a field trial in east London*. Ground Engineering. October 2010.

Majano, R.E. and O'Neill, M.W., 1993. *Effect of dosage and exposure time of slurries on perimeter load transfer in bored piles*, Proc. Second Int. Geotechnical Seminar on Deep Foundations on Bored and Auger Piles. Balkema, Rotterdam, Ghent, Belgium.

New South Wales Department of Roads and Maritime Services (RMS), 2014. *QA Specification B59 – Bored and Cast-in-Place Reinforced Concrete Piles (Without Permanent Casing).* Edition 5 / Revision 0, Roads and Maritime Services. February 2014.

O'Neill, M.W. and Reese, L.C., 1988. *Drilled shafts: construction procedures and design methods - Rep. No. FHWA-H1-88-042*, Federal Highways Administration, Washington DC.

Queensland Department of Transport and Main Roads (QTMR), 2016. *Specification MRTS63 – Cast in Place Piles*. Queensland Department of Transport and Main Roads, January 2016.

Vicroads, 2015. *Vicroads Standard Specification 606 – Bored Cast-in-Place Piles (Without Permanent Casing)*. Vicroads, March, 2015.

VicRoads, 2016. *Vicroads Standard Specification 610 – Structural Concrete*. Vicroads. January 2016.

DESIGN OF A RAFT ASSISTED PILED FOUNDATION FOR A HIGH RISE PREFABRICATED HOTEL STRUCTURE IN PERTH, WA.

Lucie Spencer, Project Geotechnical Engineer, CMW Geosciences, Perth, WA, Australia.
Craig Butterworth, Director/ Principal Geotechnical Engineer, CMW Geosciences, Perth WA, Australia

ABSTRACT

This paper presents the design of a raft enhanced pile group recently constructed for a hotel development in Perth, WA. At the time of construction in 2016 the hotel was the tallest prefabricated hotel in Australia.
The structure covers the entire 12 m by 32 m development footprint, located in an inner city environment, and directly surrounded by existing structures. The small site and lack of space required innovative thinking in terms of the substructure design.
The ground conditions comprise a layer of medium dense sand underlain by variable layers of stiff clay, silts and sands. Groundwater was around 1.5 m below ground level.
The substructure design was carried out on the basis of a raft enhanced pile group. This allowed the use of much shorter piles than a conventional pile solution, thereby permitting the adoption of CFA piling techniques. This also allowed the raft thickness to be reduced to such that the substructure works were maintained above the groundwater level.
The design was carried out in general accordance with the Australian Standard AS 2159 and using conventional piled raft design techniques involving iteration between elastic soil settlement software and structural analysis software until spring reactions were obtained with convergence of the two models. Following this springs were introduced to model piles in the structure.
Due to the variable nature of the ground and resulting uncertainty in pile base capacity it was not considered appropriate to design the system as a pile assisted raft with piles loaded beyond their ultimate geotechnical design strength. As a result, all piles were designed based on a maximum load maintained within the elastic response region, with the majority of the load taken by the piles. However, the combined capacity of the raft and the piles allowed for a saving in pile lengths and numbers of around 40%, when compared to a conventional pile group designed in accordance with the Australian Standard AS 2159.
The raft slab was monitored during construction in order to check the actual displacements against the design displacements. At the end of construction, the settlements were found to be within 2 mm of the design values.

INTRODUCTION

The Wellington Street area of Perth in the CBD is undergoing recent regeneration which includes the King's Square development, Perth Arena and the Wellington Street Bus Station. The proposed hotel development is close to the recent developments on a Lot previously occupied by a low rise development. Due to the small size and constrained nature of the site, the substructure design for the tower needed to take into account available space and the impact of the works on adjacent properties. This paper presents reasoning for the choice of substructure design, details of the design methodology adopted, results from limited post construction monitoring and potential improvements that could be considered for similar future developments.

PROPOSED DEVELOPMENT

The hotel development comprises a 17 level tower structure. Aside from an isolated lift core located on one side of the floor plan, the ground floor is formed directly on the existing ground surface with no basement. The superstructure occupies the full site footprint (12m x 32m in plan), constructed using modular prefabricated units with internal non-structural walls. Figure 1 shows a photo of completed structure.



Figure 1: Photo of the Finished Structure

(photo taken by CMW staff)

Original ground levels surrounding the almost level site generally ranged from RL10.5m AHD at the northern corner to approximately RL11.5m AHD at the southern corner.

Existing single and two storey masonry buildings, located adjacent to the eastern and southern site boundary, were considerably dilapidated. The Telstra Building, supported on piles, was located on the opposite side of the narrow Shafto Lane. Figure 2 shows the site location in relation to the surrounding structures.



Figure 2: Google Image of the Site

(source https://www.google.com.au/maps/place)

The total working compression load was approximately 95MN and the worst case factored compression load was up to 151MN. Due to the location of the lift core, a significant amount of the load was eccentrically loaded to one side of the building footprint. The typical working column load was approximately 2500kN with a typical working core wall load of 700kN/m run. The average pressure under the raft was approximately 250kPa at working load and 400kPa at ultimate load. Figure 3 shows the column and wall layout at ground floor level.

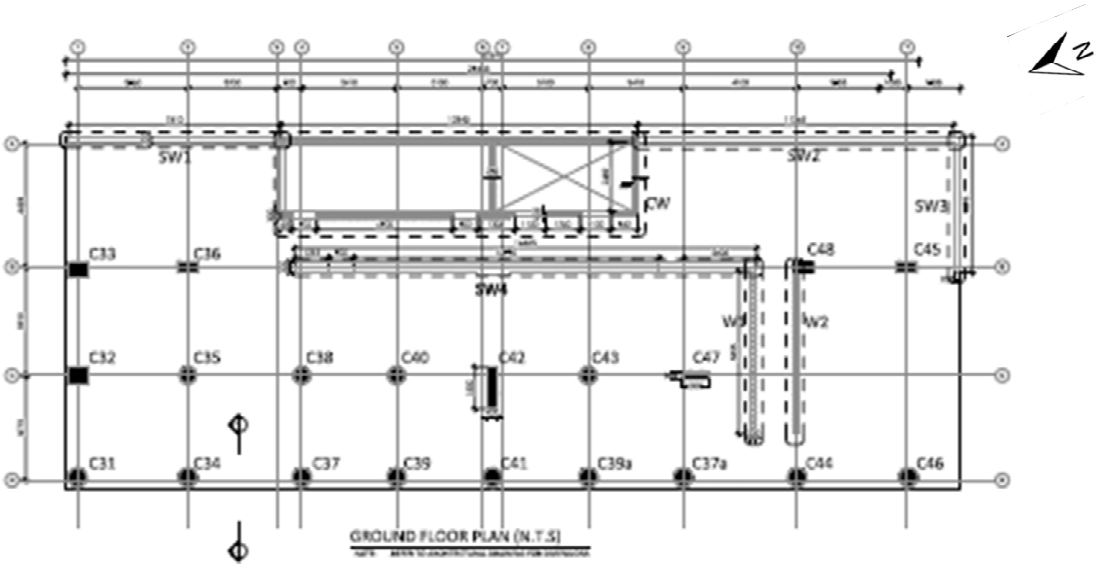


Figure 3: Ground Floor Plan- Columns and Walls Layout

SITE LAYOUT AND GEOLOGICAL CONDITIONS

The geotechnical investigation comprised three cone penetration tests (CPTs) to refusal and three hand auger boreholes to 4m below existing ground level. The geotechnical investigation layout is presented in Figure 4.

The ground water levels measured on site during the geotechnical investigation ranged from approximately RL 9.0m AHD (1.53m BGL) to around RL 9.1m AHD (1.96m BGL), with an average relative level of RL 9.0m AHD at the time of the investigation.

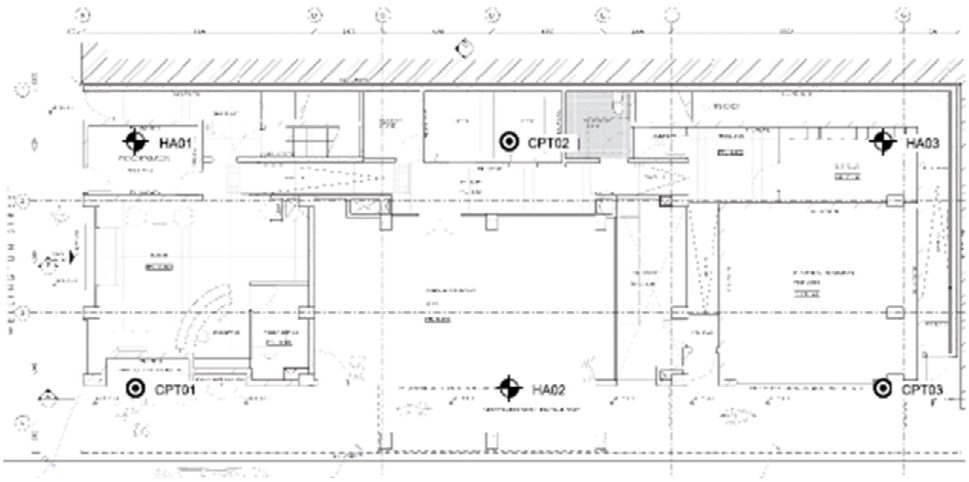


Figure 4: Geotechnical Investigation Layout on Site

Results from a typical CPT are presented in Figure 5.

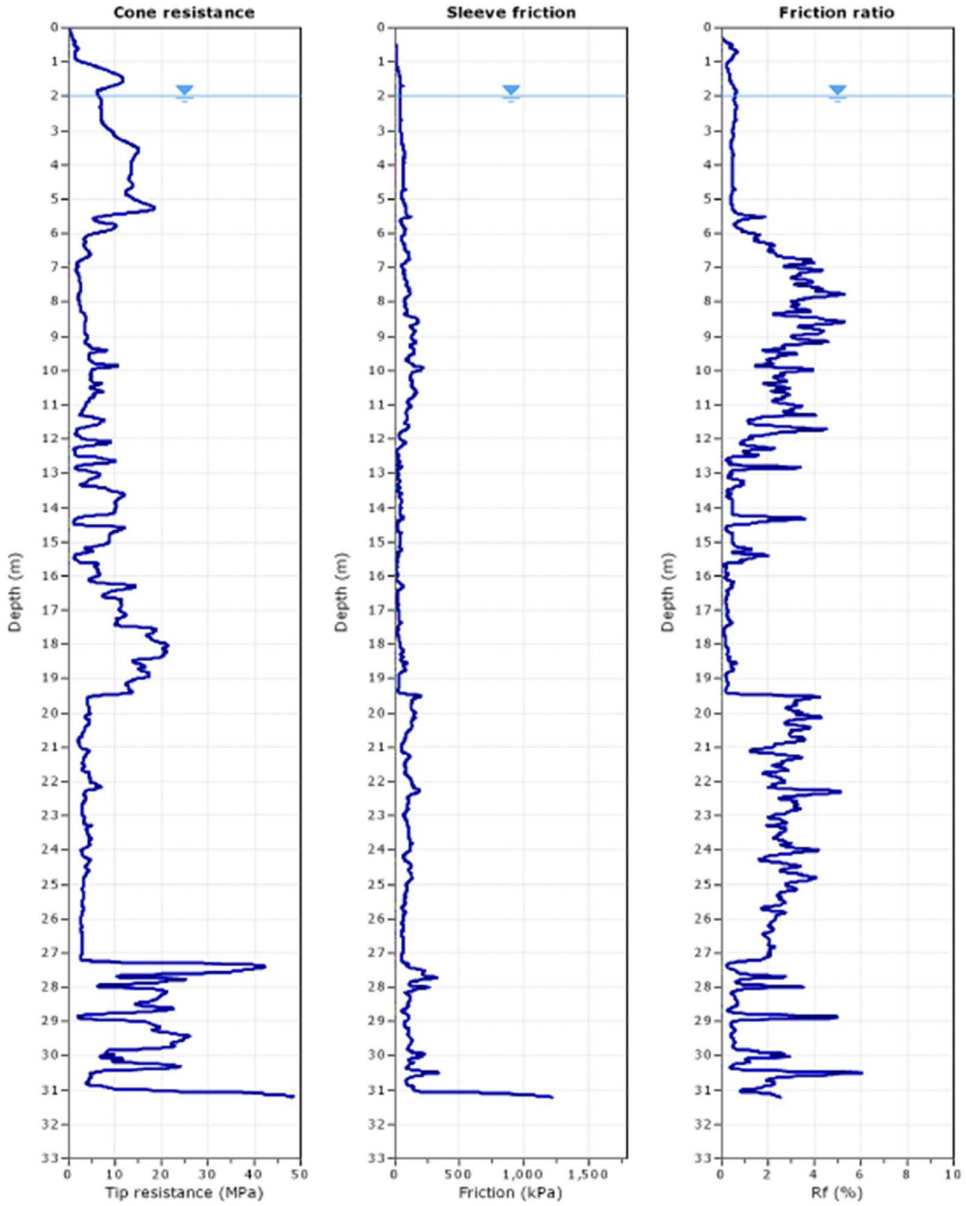


Figure 5: Typical Cone Penetration Test Results

The interpretation of ground conditions was based on the results of the geotechnical investigation as well as knowledge gained from previous projects in the area and published information (Ref. Proceedings of the Seminar on New MetroRail City Project, 2007, Tunnelling and Underground Structures).

Historical records indicated a lake, known as Lake Kingsford, in the area of the proposed hotel. The lake was later drained to form plots of land. However, no lake deposits were interpreted from the results of geotechnical investigation.

The design ground model comprised Fill over Spearwood dune sands, followed by layers of clays, silts and sands of the Guildford Formation. The Kings Park Formation bedrock was interpreted at a depth of around 31 m below ground level. The ground model adopted for the design is presented in Figure 6.

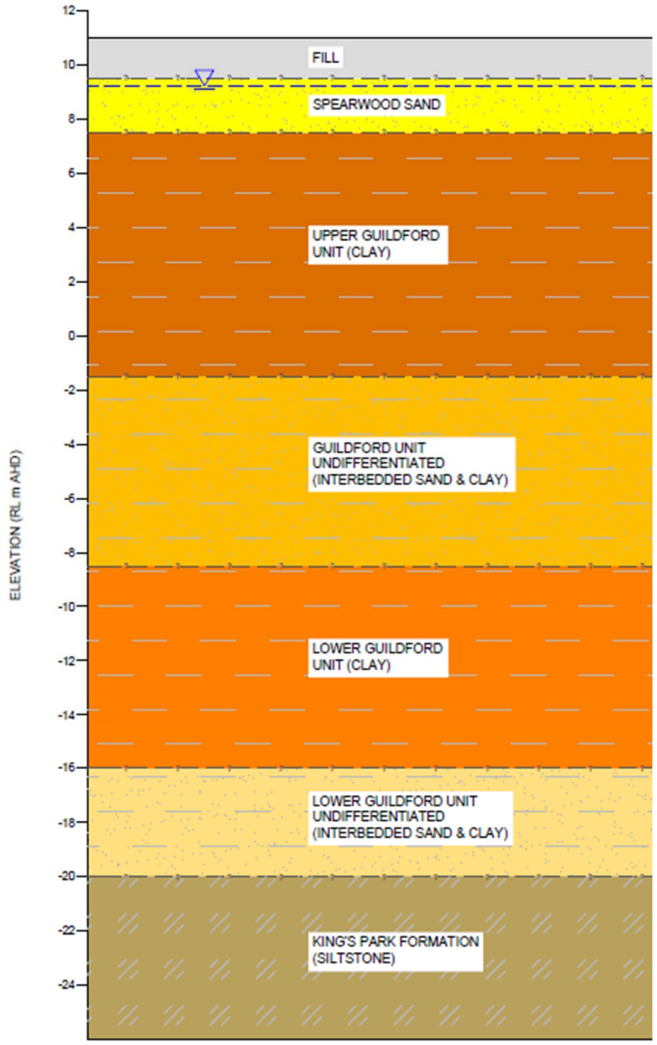


Figure 6: Ground Model

FOUNDATION DESIGN SOLUTION

Settlement criteria were developed based on consideration of the pre-fabricated nature of construction and poor condition of adjacent masonry structures. The angular distortion was limited to 1/500 between adjacent columns. Bearing in mind that columns were relatively closely spaced (approximately 4m apart) this equates to maximum allowable differential settlement of 8mm between adjacent columns. The total settlement limit was set to 25mm at ultimate load.

Comments on conventional foundation options for the development and reasons for their exclusion are presented in Table 1.

TABLE 1- Foundation Design Options Considered

Foundation Option	Details	Reason for exclusion
Single piles	Rotary bored piles formed with sockets into the underlying Kings Park Formation. Piles would need to be around 40 m in length. Bentonite or polymer required during construction.	Size of bentonite polymer plant would make site inaccessible for piling equipment without major logistical issues (moving plant around site). As a result rotary piles would be very expensive with long construction period.
Pile Groups	Groups of two to four piles per column formed using CFA piling equipment and limited to around 20 m in length, formed in sands and clays of the Guildford Formation.	Potentially inefficient design due to the requirement to offset pile caps to columns located on the site boundary. Interlayered nature of Guildford unit resulted in low end bearing component of the pile design, and associated low ultimate geotechnical design strength. Pile caps likely to become very close to each other as a result of the close spacing of columns.
Raft Foundation	Single raft foundation across full footprint of the Lot.	Offset location of the lift core and perimeter columns potentially problematic for balanced settlement across the raft.

Given the disadvantages of the various options outlined in Table 1, the adoption of a combined pile and raft was considered the most cost and programme effective solution.

Consideration was given to either a raft enhanced pile group or a pile enhanced raft, as defined in the ICE Manual of Geotechnical Engineering (Volume 2 Geotechnical Design, Construction and Verification). The differences with these two systems is explained in Figure 7, and can be broadly defined as follows:

- For a raft enhanced pile group, both the piles and the raft will work within a pseudo-elastic range behaviour. The pile group capacity is not fully mobilised at the anticipated working load. Piles are usually stiffer and attract most of the design load.
- For a pile enhanced Raft, piles are designed to mobilise all their ultimate capacity. The raft will usually carry the bulk of the design load.

Fully mobilised pile capacity was defined as the summation of individual pile capacities. Individual pile capacity was based on a settlement of approximately 10% of the pile diameter.

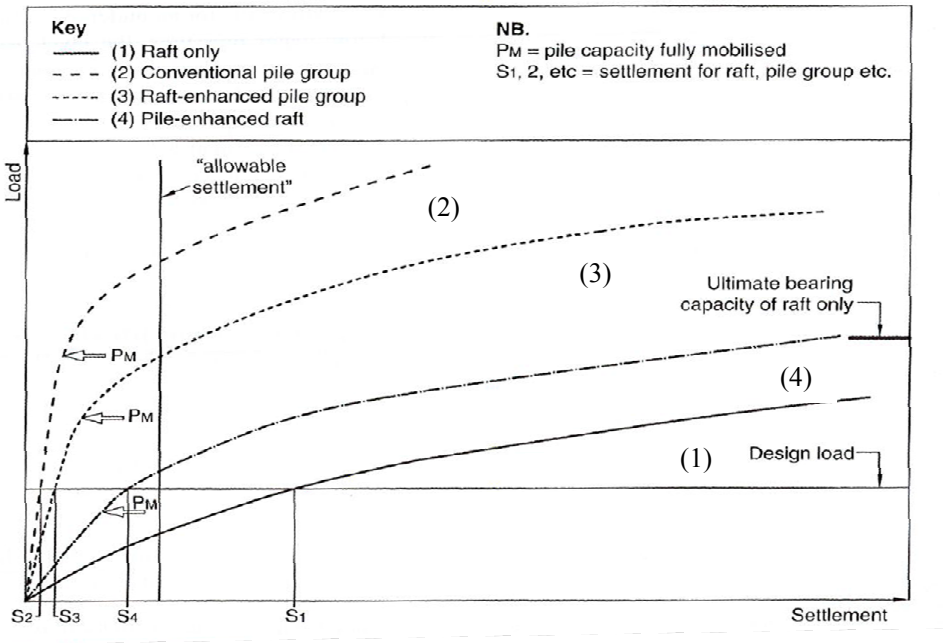


Figure 7: Design Philosophy of Raft-enhanced Pile Group

(extracted from ICE Manual of Geotechnical Engineering, 2012, Volume 2 Geotechnical Design, Construction and Verification)

Whilst consideration was given to both of the above options, the decision to adopt a raft enhanced pile group was made by the geotechnical engineers for the following reasons:

- The higher settlement associated with the pile assisted raft may have been problematic for the prefabricated nature of the structure, and insufficient programme time was available to address this with the structural engineers.
- The pile base bearing material was likely to be variable, comprising interlayered clay and sand. This is expected to result in a large variation in pile base stiffness and capacity. This variation in pile performance makes the design of the raft more complex if the piles are loaded close to or beyond the fully mobilised capacity.
- By adopting a raft enhanced pile group the raft thickness could be reduced compared to the pile assisted raft. As the groundwater was shallow, this omitted the requirement to dewater the site.

DESIGN METHODOLOGY

As the design was carried out in accordance with the Australian Standard AS2159-2009: Pile Design and Construction, the design geotechnical capacity of the overall raft enhanced pile group was designed in general accordance with Section 4.4.4 of the standard. The design geotechnical design strength of the raft and piles were calculated as shown in equation 1.

$$R_{d,g,c} = \phi_{gs} R_{d,ug,s} + \phi_g R_{d,ug,} \text{ where} \qquad (1)$$

$R_{d,g,c}$ = design geotechnical strength of combined raft and piles

ϕ_{gs} = geotechnical strength reduction factor for the shallow or raft footing (assessed to be 0.56)

$R_{d,ug,s}$ = design ultimate geotechnical strength of shallow or raft footing

ϕ_g = geotechnical strength reduction factor for piles (assessed to be 0.56)

$R_{d,ug}$ = design ultimate geotechnical strength of piles

To avoid overloading the individual piles, an additional limit was imposed on the design as shown in equation 2:

$$E_{dp} \leq 0.9R_{d,ug}, \text{ where} \quad (2)$$

E_{dp} = design loads on individual piles under ultimate limit state actions calculated from the pile/raft interaction analysis

$R_{d,ug}$ = design ultimate geotechnical strength of piles

The purpose of this additional criteria was to check that individual pile reactions were within the predicted range of elastic movements of the piles. As discussed previously, this limit was applied due to the uncertainty in pile ultimate capacity and resulting uncertainty in pile stiffness at a high percentage of the ultimate geotechnical strength.

METHOD OF ANALYSIS

RAFT DESIGN

Settlements and structural forces in the raft were calculated by iterations between geotechnical settlement software and structural analysis as described by Cracknell. P. A in the publication Design Applications for Raft Foundations (Hemsley 2000).

Settle 3D software version 3.0 (Rocscience), a three dimensional programme for analysis of vertical consolidation and settlement, was used to calculate settlement of the raft without piles and to derive appropriate spring stiffness values of the soil under the raft.

The influence of the raft stiffness on settlements and bending moments is fundamental. For a raft that is essentially rigid, the differential settlement is small but the bending moment is very high. In contrast, for a raft that is fully flexible, the differential settlement is large, and the bending moment is much lower. The stiffness of real rafts is between the two extremes and the relative soil-raft stiffness and soil structure interaction needs to be carefully considered.

The working and ultimate bearing pressures on the soil beneath the raft were initially calculated from the structural model using uniform soil springs, carried out using CSI SAFE software, and input into the geotechnical Settle 3D model. Based on these bearing pressures, settlements at ultimate and working loads were calculated using the geotechnical software Settle 3D, by Rocscience. The soil spring stiffness distribution at the underside of the raft, which is a function of the applied load, ground conditions, shape and size of the footings, was obtained from Settle 3D and supplied back to the structural CSI SAFE model. The above sequence was then repeated until the structural and geotechnical models converged with similar settlement profiles.

Three iterations between the two models were required in order to calculate the settlement profile beneath the raft to be sufficiently similar between the two models (within 10%).

The vertical soil spring stiffness (k) under the raft were determined from Settle 3D as shown in equation 3.

$$k = \frac{\sigma}{s} \qquad (3)$$

σ= pressure under the raft

s= settlement.

The final raft spring stiffness distribution plot is presented in Figure 8. As can be seen from the plot, the subgrade pressures from the structural model and the resulting spring stiffness distribution was simplified in order to speed up the input of springs into the structural model. It is recognised that this resulted in minor errors between different spring zones.

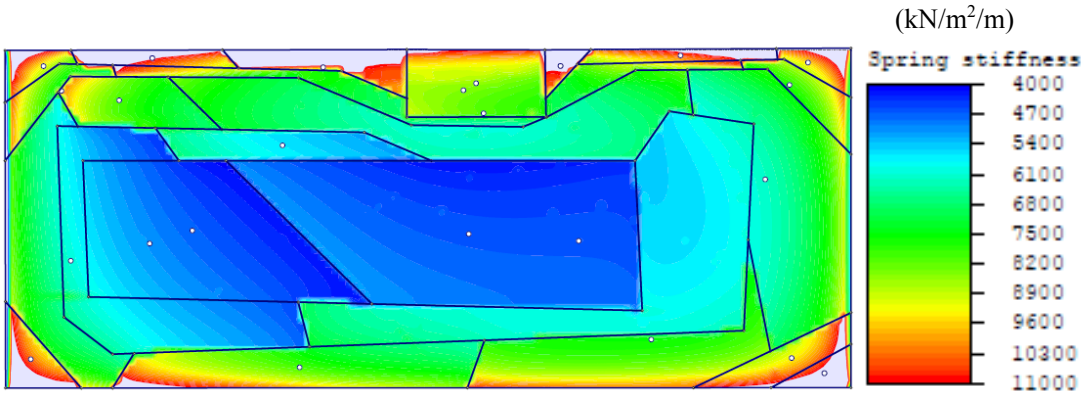


Figure 8: Spring Stiffness Distribution beneath the Raft

The maximum estimated long term settlement of between 35 mm and 75 mm under working loads was calculated based on our analysis of the raft only. Having previously assessed these settlements to be too high, the results could be used to develop the location of piles beneath the raft to control settlement and pile structural forces. Figure 9 presents the anticipated settlements of the raft only obtained from Settle 3D.

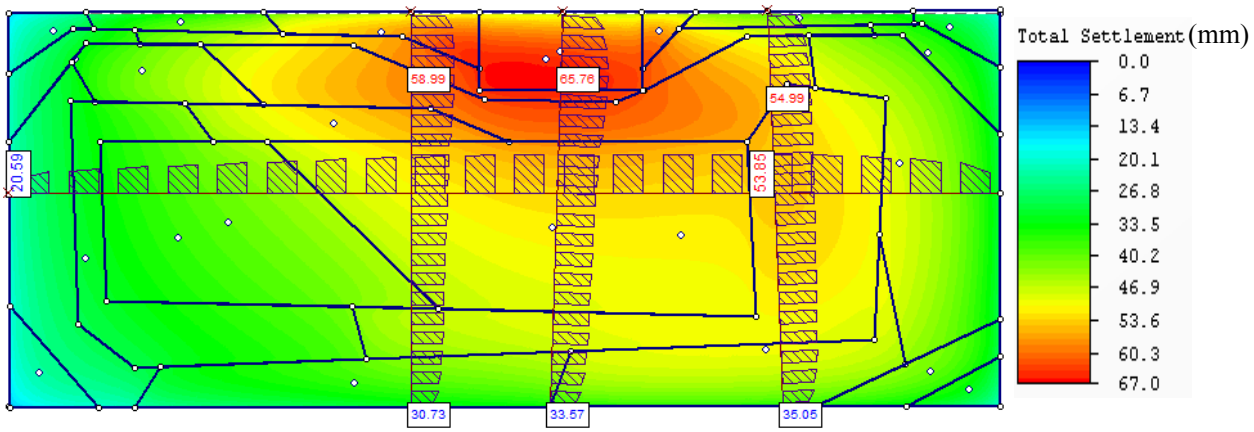


Figure 9: Settlement of the Raft Only Obtained from SETTLE 3D

The settlement of a section through the centre of the raft only was also checked using software Plaxis 2D. The Small Strain Hardening Soil model (HS small) which is an advanced model in Plaxis for the simulation of non-linear soil stiffness. In contrast to the standard linear soil stiffness models, the Hardening Soil Model also accounts for stress dependency of stiffness moduli. Table 2 summarises the soil parameters used in the model:

TABLE 2- The Hardening Soil Model Parameters for the Plaxis analysis

Unit	Description	φ' (°)	ϒ (kN/m^3)	E_{50} (MPa)	Eu_R (MPa)	G_0 (MPa)	OCR
1	Spearwood Sand	35°	18	50	150	250	1.5
2	Upper Guildford Unit (CLAY)	31°	18	25	70	121	3
3	Guildford Unit Undifferentiated (CLAY/SAND)	34°	18	100	300	300	3
4	Lower Guildford Unit (CLAY)	31°	18	25	70	250	3
KEY: E_{50} – triaxial stiffness, Eu_R – triaxial unloading stiffness, G_0 – small strain shear modulus							

The Plaxis analysis indicated lower settlements at working loads to the values calculated within the initial Settle 3D model. Whilst the secant stiffness values at a shallow depth were similar within both models, as a result of lower strains with depth, higher secant stiffness values were calculated in the Plaxis model within the deeper units. As a result, the Settle 3D model was adjusted to allow for the smaller strain stiffness values in the lower Guildford units.

PILE DESIGN

The load settlement response of the piles and the raft were considered in isolation and combined in the structural model without consideration of the group effects of the piles and the raft working together. However, in the absence of a detailed assessment, a conservative pile spring stiffness values was adopted to allow for potential interaction effects, as shown in Figure 11.

Initial pile design was carried out using correlations with CPT cone tip resistance, q_c, for the estimate of ultimate shaft friction and end-bearing. Due to the uncertainty in end-bearing materials, the design was based on the assumption that the piles were formed into either dense sand or stiff clay. The piles were then designed to reduce overall settlement of the raft whilst maintaining pile loads below the ultimate geotechnical pile capacity. The individual pile positions were optimised based on magnitude of bending moments in the raft and to control displacements of the raft.

The ultimate total geotechnical design strength ($R_{d,ug}$) of a 750mm diameter pile, founded at RL -3.4m AHD, was estimated to be between approximately 2,500 kN and 3,400kN. The ultimate shaft capacity was estimated to be approximately 1,700kN.

Details of the soil parameters used for the pile design have been summarised in Table 3.

TABLE 3- Pile Design Parameters

Soil type	Ultimate Shaft Friction (kPa)	Ultimate End Bearing (kPa)
Spearwood Sand	75	n/a
Upper Guildford Unit (CLAY)	50	n/a
Guildford Unit Undifferentiated (CLAY/SAND)	70	1800/4000

In total there were 40 No 750mm diameter piles required to control settlement of the raft and maintain pile loads within the criteria defined earlier. All piles were founded in Guildford Unit Undifferentiated with a toe level set at RL -3.4m AHD. The final pile layout is presented in Figure 10.

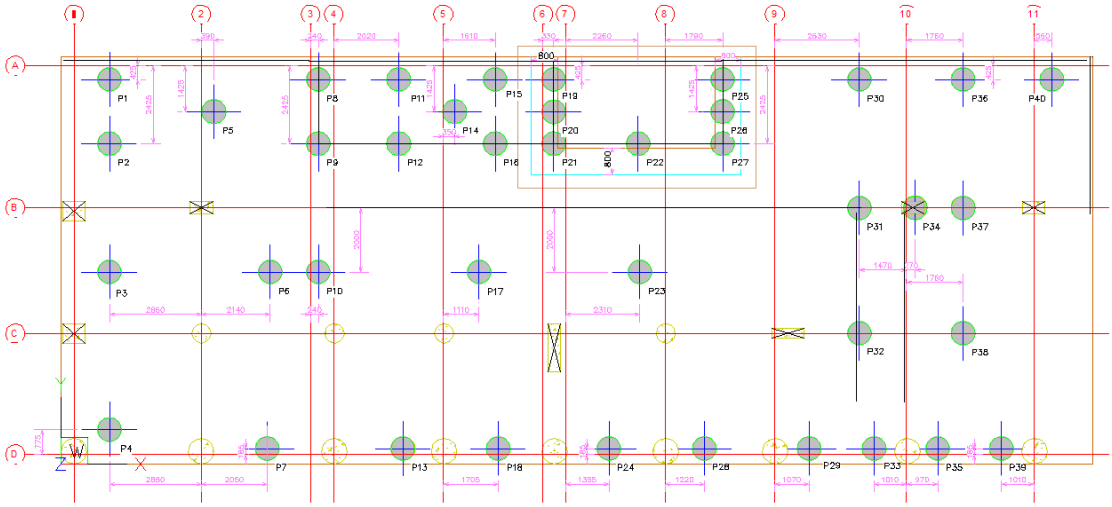


Figure 10: Final Pile Layout

The pile load settlement performance was calculated using t-z curves using Deltares D-Pile Software. An elastic spring response of around 200,000kN/m was adopted as a design value. The anticipated settlement of a single pile at maximum working load of 2,500kN is predicted to be 12mm. An estimated load displacement diagram for a single pile is presented in Figure 11. In addition, single and small groups of piles were modelled in CSI SAFE using reduced spring values to allow for local variation in ground conditions.

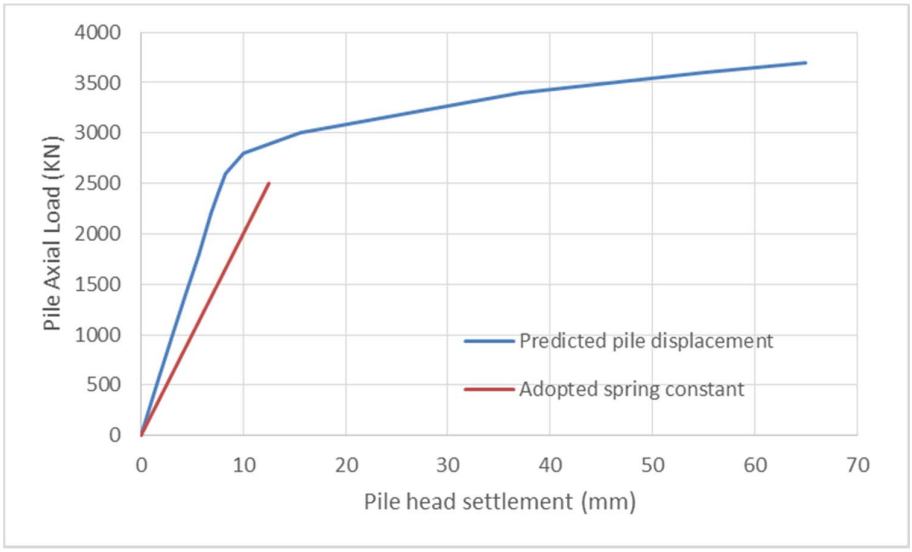


Figure 11: Estimated Load Displacement for a 750mm diameter Pile

RAFT ENHANCED PILE GROUP DESIGN

Based on equation 1 the design geotechnical strength of the combined raft and piles was calculated to be in the order of 450 MN. This well above the factored design load of 150 MN. As a result, the critical criteria for the design, as expected, is settlement performance at the working loads.

By combining the load settlement response of the raft and the piles within the structural model, the raft assisted pile group has been calculated to result in a maximum settlement of around 15 mm at Working Load. The differential settlement between adjacent columns was limited to a maximum value of 8mm.

The anticipated bearing pressures and settlement contours for the raft assisted pile group under working load obtained from the structural model CSI SAFE are presented in Figures 12 and 13 below.

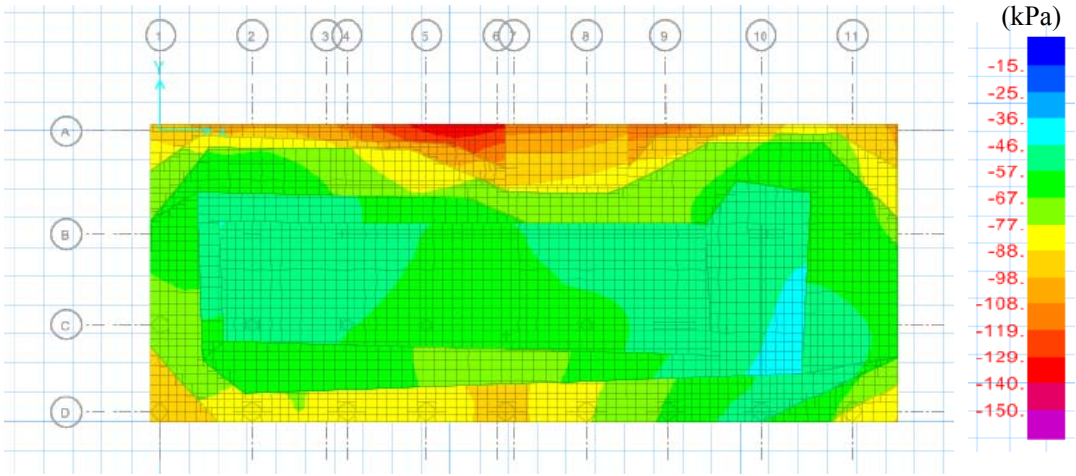


Figure 12: Bearing Pressures (kPa) under the Raft at Working Load (CSI SAFE)

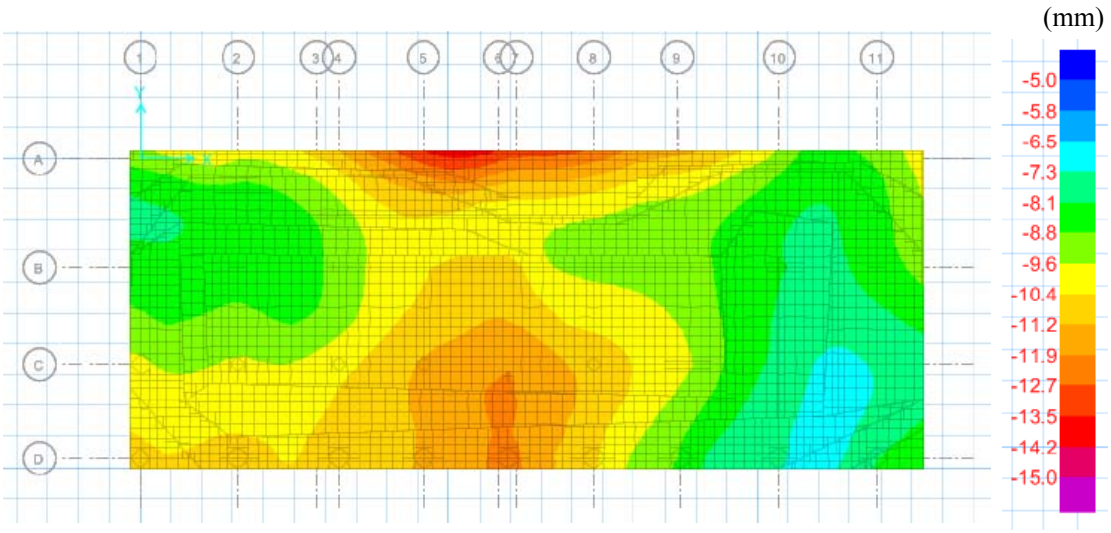


Figure 13: Settlement (mm) of Raft Assisted Pile Group at Working Load (CSI SAFE)

The individual pile loads were obtained from CSI SAFE programme based on the pile and raft subgrade spring stiffness values provided from the geotechnical model.

POST CONSTRUCTION SETTLEMENT

Settlement of the raft has been monitored at three locations during construction. One monitoring target was set up in the middle of the raft assisted pile group and two targets along the edges. Monitoring results were provided to us by the principal contractor on site, Mode Modular Construction. The location of the monitoring targets on site are presented in Table 4 and Figure 14.

Originally, we have specified monitoring of the raft slab at 7 different locations and also at different stages of construction but unfortunately readings were taken only upon completion of the whole structure at three targets.

Table 4 – Raft Monitoring Results

Station	Top of the raft level prior to construction of the structure RL (m AHD)	Top of the raft level upon completion of construction RL (m AHD)	Settlement (mm)
M3	10.594	10.584	10
M6	10.598	10.592	6
M7	10.595	10.589	6

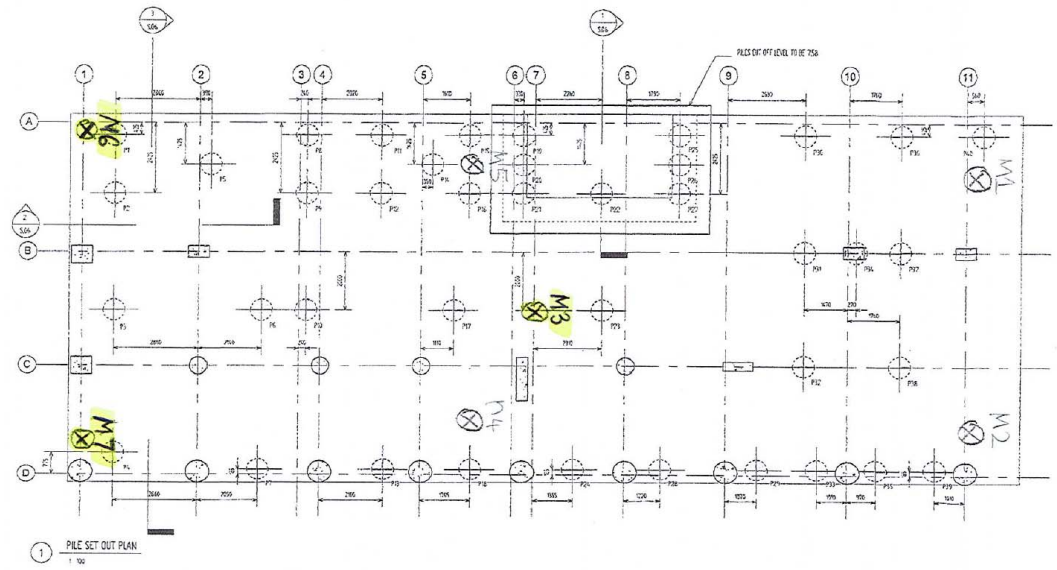


Figure 14: Location of Settlement Monitoring Targets

The measured settlement at the top of the raft slab at the end of construction was 10mm in the middle of the piled raft and 6mm at the edges of the piled raft. The measured settlement values on site correlated extremely well with the predicted design settlement values within 2mm of the actual measured piled raft displacement at given locations.

CONCLUSION

By designing the foundation as a raft enhanced pile group, we were able to provide the following significant design/construction advantages:

1. Use of short CFA piles within minimal reinforcement allowing much easier construction compared to rotary bored piles or extensive CFA pile groups.
2. A higher percentage of the ultimate geotechnical design strength of the piles could be adopted by combining the pile and raft capacity.
3. The combination of the raft and the pile group allowed greater robustness in design and no reliance on pile base capacity for control of settlements in variable soils.
4. Installation of a limited number of piles beneath the raft allowed the thickness of the raft to be significant reduced compared to a raft only solution.

By shortening the piles and changing the construction technique, we have achieved savings of approximately 40% in construction costs in addition to considerable savings on programme compared to the base design comprising conventionally designed bored piles with rock sockets.

FURTHER SAVINGS/DESIGN IMPROVEMENTS

Limited settlement monitoring results at the time of construction correlated extremely well with our predicted settlement. However, a number of iterations between the geotechnical and structural model were required in order to derive the final load settlement response. In addition, the design method did not take into account potential interaction effects between the piles and the raft foundation.

Using geotechnical finite element modelling that incorporates both structural elements and appropriate soil models, such as Plaxis 3D, it is possible to consider the full interaction between the soils and the raft without resort to manual iterations between structural and geotechnical modelling software. However, the use of a single model by the geotechnical engineer raises potential commercial issues with

regard to provision of and reliance on information if the geotechnical engineer is modelling structural performance. Whilst this should be easily managed during the design process, close collaboration between structural and geotechnical engineers is required in order to realise the efficiency of this modelling method without duplication of effort.

Following the completion of the above design, we have used Plaxis 3D to compare results. A discussion on this may be presented in a subsequent paper.

In piled raft design it is important to realistically determine the allowable settlement limit. If this limit is set too low the opportunity to use piled rafts could be lost. By increasing the allowable total settlement of the piled raft, the number of piles could have been reduced and the piles could potentially have been designed to perform within the non-linear range. Time constraints prevented us from developing the scheme further and reducing the number of piles. The uncertainty in pile toe response due to end-bearing in interbedded sands and clays also presented a challenge in the piled raft design. However, have been dealt with by establishing upper bound and lower bound pile stiffness and applying the different stiffness values to different areas of the piled raft to account for the worst case variability in the toe response. Such analysis would be particularly important for assessment of bending moments in the raft.

REFERENCES

Australian Standard AS2159- 2009 Piling- Design and Installation

Burland, J.B., 1995, Piles as Settlement Reducers, Associazione Geotecnica Italiana- 19 Convegno Nazionale de Geotecnica, Pavia 19-21 Settembre 1995

ICE Manual of Geotechnical Engineering, 2012, Volume 2 Geotechnical Design, Construction and Verification, ICE Publishing, One Great George Street, Westminster, London SW1P 3AA, UK, 1537 p.

Poulos, H.G., 2001, Piled Raft Foundations: Design and Applications, Geotechnique 51, No.2, 95-113

Proceedings of the Seminar on New MetroRail City Project, 2007, Tunnelling and Underground Structures, Organised by Australasian Tunnelling Society, Australian Geomechanics Society, Engineers Australia, 306 p.

Hemsley. J. A. (2000). Design applications of raft foundations.

Software Settle 3D 3.0, product version 3.011

Software Plaxis 2D 2010

Software CSI SAFE 2014

PERFORMANCE OF LARGE-DIAMETER BORED PILE SOCKETED IN SANDSTONE AND SILTSTONE IN THAILAND

Zaw Zaw Aye, Seafco PCL, Bangkok, Thailand, +66859091029; zawzawaye@gmail.com
Thayanan Boonyarak, Seafco PCL, Bangkok, Thailand, +66805818799; thayanan@seafco.co.th
Nutthapon Thasnanipan, Seafco PCL, Bangkok, Thailand, +66846660555; nutthapon@seafco.co.th
Sereyroath Chea, Seafco PCL, Bangkok, Thailand, +66935503967; sereyroath.chea@gmail.com

ABSTRACT

As there are only limited numbers of bored pile constructed in sandstone and siltstone in Thailand, load transfer and settlement behavior of a pile in these rocks are still not fully understood. Major factors which influence the performance of the pile in the sedimentary rock should be systematically investigated. The objective of this paper is to analyze load distribution and load-settlement behavior of bored pile in sedimentary rock. Interpreted data was obtained from instrumented load testing results of large-diameter bored piles. These piles were drilled in aeolian soil and socketed in sandstone or siltstone, having socketed length varying from 1 to 3 times the pile diameter. Factors that influenced pile settlement behavior, consisting of rock type at the pile base, socket length, at-rest earth pressure and rock conditions, were analyzed. For interpretation of results, analytical solutions were used to estimate load bearing capacity and calculate settlement of each pile. According to test results of mobilized unit skin friction in siltstone, relationship of 0.1 – 0.3 square root of the unconfined compressive strength of rock appears to reasonably capture the measured shaft friction. Note that shaft movement in siltstone layer was not fully mobilized as maximum pile head settlement was still less that 1% of the pile diameter.

Keywords: Load-settlement behavior, Load transfer mechanism, Sandstone, Siltstone

INTRODUCTION

Extensive research of bored pile construction in soft soil in Thailand and Myanmar (Boonyarak et al., 2016; Aye et al., 2015) has been carried out. However, behavior of bored pile in weak rocks such as sandstone and siltstone is still not fully understood. Unit skin friction and unit end bearing of piles in these weak rock were reported by Horvath et al. (1983) and Pells and Turner (1980), respectively. Further research is still required to minimize variation in data presented in their study.

This paper presents interpretation of load testing results of instrumented piles. These piles were excavated in aeolian deposit in the Northeast Thailand. Some piles were socketed in sandstone or siltstone. Analysis results of load-settlement, shaft shortening, pile settlement estimation, factor for calculating shaft friction and end bearing are reported. Discussion and explanation of pile behavior in sandstone and siltstone is provided.

BRIEF INFORMATION OF THE PROJECT

Project locations

The construction sites are located in Khon Kaen and Nakhorn Ratchasima Provinces in the Northeast Thailand. Bored piles in this project were designed for supporting elevated structures for railways, overpasses and U-turn bridges for vehicles. These overpasses and U-turn bridges are distributed along the existing railways with the distance of about 180 km.

Soil profiles

Soil profile obtained from six soil investigation boreholes interpreted in this paper is shown in Fig. 1. Most soils in this region are aeolian deposit consisting silt and sand at the top. Sedimentary rocks, sandstone (refer to Fig. 2a) and siltstone (see Fig. 2b), locate underneath these soils. Two groups of soil profiles are categorized by their location of investigation boreholes. Figure 1a shows soil profiles

for NBH 34, 41 and 52. At the location of NBH 34 and 52, piles were socketed in siltstone. For NBH 41, depth of siltstone was deeper than the required pile tip, thus this pile was embedded in hard clay. Piles at NBH 138, 146 and 148 were embedded in very dense sand, hard clay and siltstone, respectively as shown in Fig. 1b. High variation and discontinuity of overburden strata among NBH 138, 146 and 148 were observed due to changes in geological conditions in the past. Typical ranges of unconfined compressive strength of sandstone and siltstone in this project are 10-35 MPa and 8-30 MPa, respectively. Dip angles of both rocks are from 1 to 5 degrees.

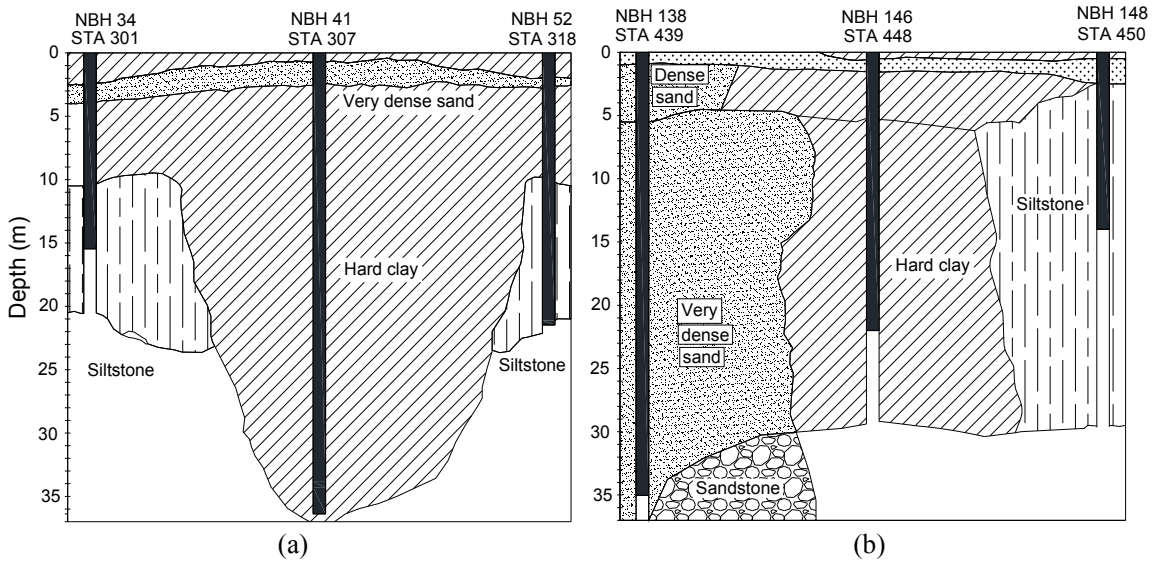


Fig. 1 Soil profile for (a) NBH 34, 41 and 52; (b) NBH 138, 146 and 148



Fig. 2 Rock samples (a) Sandstone; (b) Siltstone

Bored pile construction sequences and quality control

Typical construction sequences of bored pile in this project are shown in Fig. 3. The sequences are as follows: (a) First, pre-boring of hard soil at the surface is carried out. (b) Temporary steel casing is driven using vibro hammer to protect borehole collapse in soft soil layer (i.e., loose sand and soft clay). (c) Excavation is carried out using flight auger inside the casing or in hard clay layer. (d) Prior to

encounter unstable soil layer beneath the depth of the casing, drilling fluid (bentonite slurry) is poured into the borehole for stabilization. Drilling bucket is used for excavation under the slurry until reach sandstone or siltstone. To excavate these rocks, core barrel and bullet teeth rock auger are adopted. Slurry circulation using pump and desander is used for cleaning of slurry in the borehole. (e) Reinforcement cage is lowered into the borehole one after another. Then, concrete is placed through a tremie pipe to replace the drilling fluid until reach the pile cut-off level. (f) Finally, the temporary casing is extracted before the concrete sets.

For quality control, deviation and inclination of the borehole are controlled to be within 75 mm at ground level and 1:100, respectively. The methods for controlling deviation and inclination of borehole are conventional survey technique and drilling monitor apparatus. To ensure the quality of the drilling fluid, recommended range of bentonite properties and testing method is given in Table 1. Prior to reinforcement cage lowering, rock samples at the pile base are indentified and sediment measurement using sounding by measuring tape is carried out. Concrete slump and setting time for wet-process bored pile in this project are 150-200 mm and 4-6 hours, respectively.

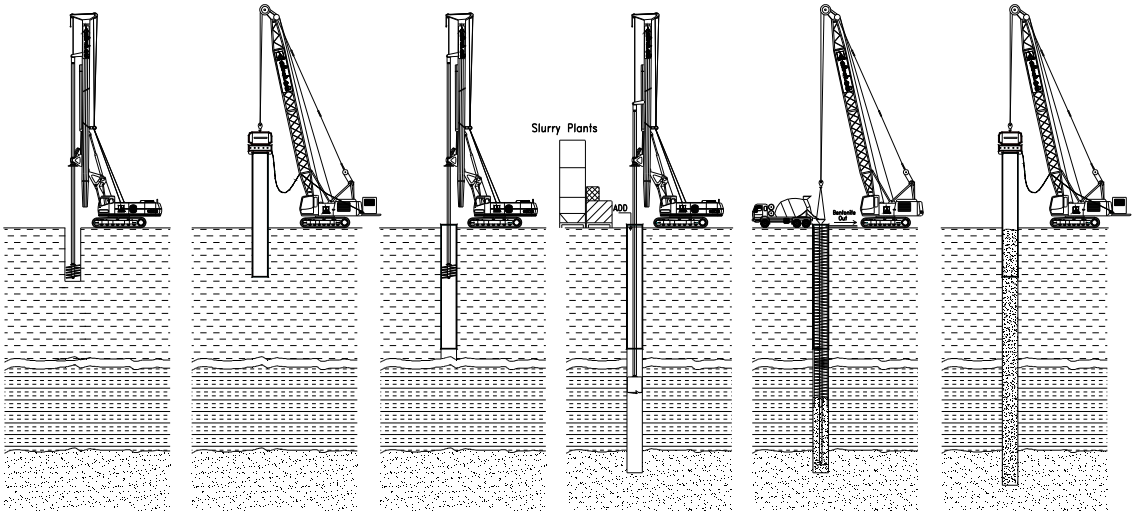


Fig. 3 Typical construction sequences for bored pile

Table 1. Properties of bentonite specified for the project

Item	Value		Test Method
	During excavation	During concreting	
Density	1.03 - 1.15 g/ml	1.03 - 1.10 g/ml	Mud density balance
Viscosity	30-80 sec/quart	30-60 sec/quart	Marsh cone
pH	8 -12	8 -12	pH indicator
Sand Content	Less than 4%	Less than 2%	Sand screen

Note: A quart is equal to 946 ml

LOAD TESTING AND DATA ANALYSIS

Static pile load test and instrumentation

Axial compression static load tests according to ASTM D1143 standard were carried out on non-working piles along the route of the project. Four anchor piles for each test pile were used as a reaction system. Maintained loading procedures up to 2.5 times the design working load were adopted. Total seven instrument pile load tests are reported in this paper. Test piles diameters are 1.2 m and 1.5 m with pile tip ranging from 14.0 m to 36.3 m. Majority of the piles were embedded in either siltstone or

sandstone. In the area where these stone are relatively deep, piles were embedded in very dense sand or hard clay. Table 2 summarizes details of test piles reported in this paper.

In each test pile, total twelve numbers of vibrating wire strain gages were installed, having two strain gages each in six different depths. The first set of strain gages (installed within 1 m below the pile cap) was used for calibration against the applied loading. The last set of strain gage was installed at a distance of 1 m above the pile base. The remaining strain gages were generally located at the strata boundaries or at the mid-points in thick strata layers. Five rod extensometers were embedded in each instrumented test pile with the same tip as each strain gage (except the first layer of strain gage).

Table 2. Details of test piles

Pile location	D (m)	Pile tip (m)	Safe working load (kN)	Socket length (m)	Soil/rock type at pile tip	δ (mm)	δ_s (mm)	δ_t (mm)
NBH034	1.2	15.5	7,000	5.0	Siltstone	8.11	5.52	2.59
NBH041	1.2	36.3	7,000	-	Clay	11.02	8.23	2.79
NBH052	1.2	21.3	7,000	8.3	Siltstone	7.17	5.64	1.53
NBH138	1.2	35.0	7,000	-	Sand	9.94	7.18	2.76
NBH146	1.2	22.0	6,500	-	Clay	5.74	5.12	0.62
NBH148	1.2	14.0	7,500	9.0	Siltstone	5.65	4.57	1.08
NBH148	1.5	14.3	10,000	9.3	Siltstone	8.43	5.10	3.33

Note: D = Pile diameter
δ = Measured settlement at pile head
δ_s = Measured pile shortening
$\delta_t = \delta - \delta_s$ = Toe settlement

Back-analysis using conventional equations

To obtain parameters for design for pile capacity and settlement, conventional equations were adopted. For shaft friction in soils, α and β methods proposed by Tomlinson (1995) were used for fine-grained soil and coarse-grained soil, respectively. In rock layers, relationship between unconfined compressive strength of rock and pile resistance proposed by Horvath et al (1983) was employed for back-analysis. To calculate settlement of pile, an equation proposed by Tomlinson (1995) was selected. The selection criteria were based on the finding reported by Boonyarak et al. (2016) that analytical equations provide reasonable results for pile with settlement less than 2% of the pile diameter.

INTERPRETATION OF RESULTS

Load-settlement relationship

Load-settlement curves from every pile load testing are shown in Fig. 4a. At safe working load (SWL, refer to Table 2), settlement of each pile was ranging from 2-3 mm. These settlements were significantly less than 10 mm, recommended by Eurocode 7 (1997). To compare load-settlement behavior among all piles, with different safe working loads, the applied load was normalized with safe working load and settlement was normalized by its diameter as shown in Fig. 4b. At maximum test load of 2.5 times the safe working load, settlements of all piles were still less than 1% of the pile diameter (D). Ng et al. (2001) reported that toe settlement at failure load is estimated to be 4.5%D. It suggests that all piles reported in this paper were still not fully mobilized at maximum test load. Thus, back-analyzed friction and end bearing should be larger than those the reported value in this paper.

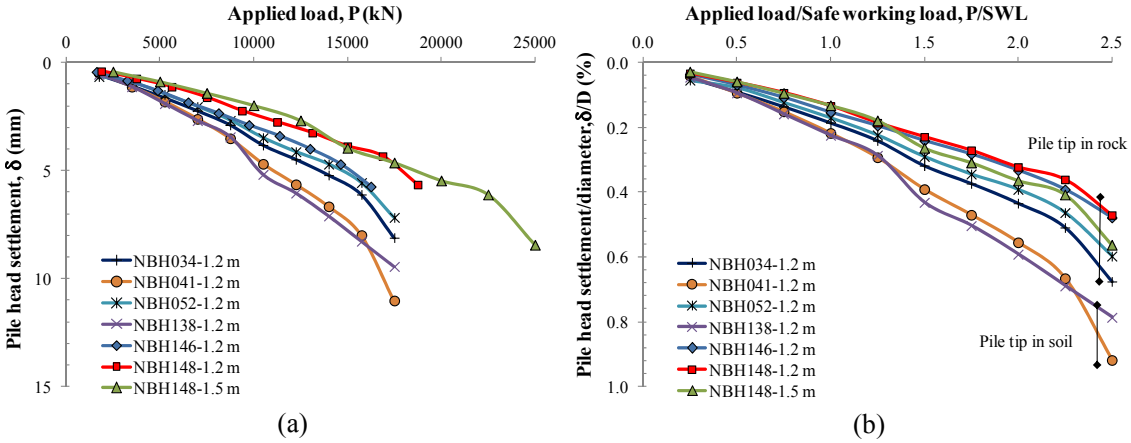


Fig. 4 (a) Load-settlement curves from all tests; (b) Normalized load-settlement curves

Shaft shortening of pile

Comparison between measured shortening of pile using rod extensometer and interpreted shortening from Hooke's law is shown in Fig. 5. Shortening of piles having tips in soil (hard clay or very dense sand) were about half of the interpreted shortening (0.5PL/AE). For piles with tip in siltstone, shortening of each pile was between 0.75PL/AE and PL/AE. This is because stiffness in rock layer is significantly larger than those in soil, causing smaller toe settlement in the former than the latter. Proportion of shaft shortening and total settlement at pile head of all piles is ranging from 0.7 to 0.8.

Calculation of pile settlement

To calculate pile settlement, Equation 1 proposed by Tomlinson (1995) is adopted.

$$\delta = \frac{(W_s+2W_b)L}{2A_sE_p} + \frac{\pi W_b B(1-\nu^2)I_p}{4A_bE_s} \qquad [1]$$

In this equation, the first and second terms refer to elastic shortening of the pile and settlement of soil at pile base, respectively. The modulus of elasticity of clay, sand and rock were 800 C_u, 2000N and 500 UCS, respectively. The value C_u, N and UCS are undrained shear strength, standard penetration test results (SPT-N) and unconfined compressive strength, respectively. The modulus of elasticity of pile (E_p) was assumed to be 33 GPa.

Figure 6 shows comparison between measured and computed pile settlement normalized by its diameter. From the comparison, calculated settlement for pile in soil reasonably agrees with the measured results. However, for pile embedded in siltstone, substantial difference between measured and calculated results is observed. A possible reason for this discrepancy is variation in rock quality causing inaccuracy of estimation of elastic modulus of rock at pile base.

BACK ANALYSIS OF DESIGN PARAMETER

Mobilized skin friction

Data from strain gages were analyzed to obtain unit skin friction in each layer of soil or rock. Table 3 shows ranges of back-analyzed skin friction for each soil type.

Table 3. Ranges of mobilized unit skin friction from each type of soil

Soil type or rock type	Unit skin friction (kN/m^2)
Stiff clay	25 - 70
Hard clay	120 - 250
Very dense sand	50 - 300
Completely decomposed siltstone	280 - 360
Moderately to slightly weathered siltstone	400 – 1,000

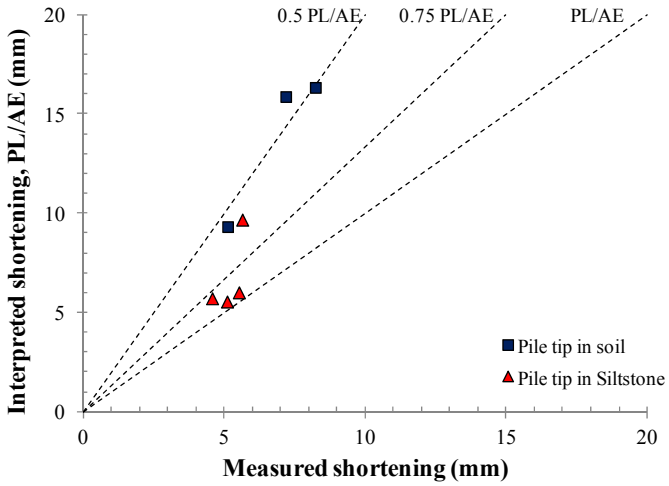


Fig. 5 Shortening of test piles

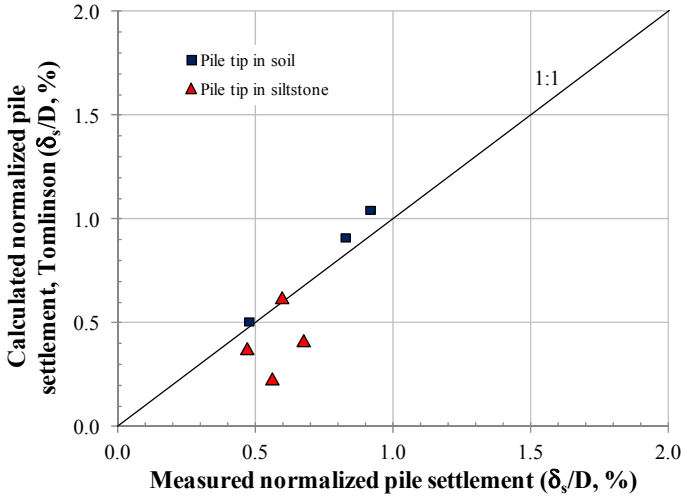


Fig. 6 Comparison between measured and calculated pile settlement

Adhesion factor in fine grained soil

Figure 7 shows back-analyzed adhesion factor (α) and undrained shear strength (C_u) of silt and clay. The undrained shear strength was obtained from semi-empirical relationship between standard penetration test (SPT-N), using C_u = 6.25N (Terzaghi, 1943). Three approaches from literature and code of practice were used to estimate adhesion factor and compared with the measured results. It can be seen that the estimation from the three methods still give a reasonable estimation of α for most

results. Note that some back-analyzed data are substantially larger than those from the three approaches. Those data were obtained from highly weathered siltstone that cannot be collected during sampling. Thus, friction of this highly weathered siltstone can be significantly larger than adhesion factors for clay in the literature. Note that highly weathered siltstone described in this paper is characterized as more than half of the rock sample decomposed to soil.

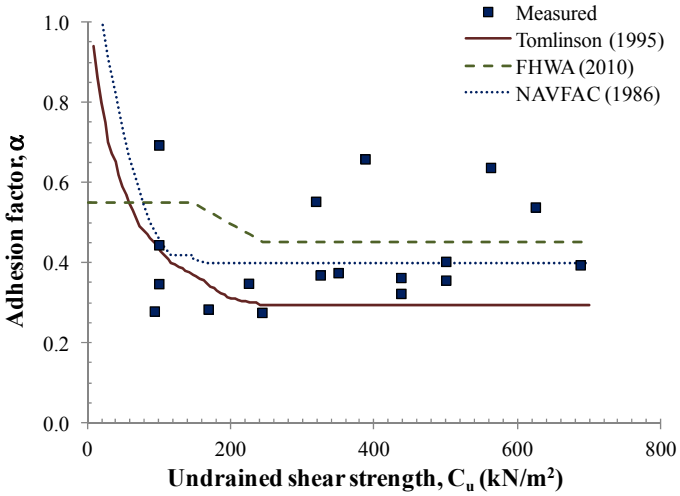


Fig. 7 Back-analyzed adhesion factor in fine grained soil

Friction factor in coarse-grained soil

Relationship between back-analyzed friction factor in coarse-grained soil (β) and internal friction angle of soil is shown in Fig. 8. Angle of internal friction was obtained from semi-empirical relationship from SPT-N (Peck et al., 1974). To back-analyze the parameter friction factor from literature are used for comparison. In normally consolidated soil, β factor is assumed to be $K_s \tan \delta$. Earth pressure coefficient (K_s) was assumed to be 0.70 and angle of pile/soil friction (δ/ϕ') of 0.75 Kullhawy, 1984) was adopted. It can be seen that using K_s of 0.7 and δ/ϕ' of 0.75 significantly underestimated some back-analyzed friction factors. A possible reason to the observation is the sand at the site may be in highly over-consolidated state due to change in stress history. This change in stress history is likely to be caused by changing in sea level in the past. To take the effect of overconsolidation ratio into account, coefficient of earth pressure simplified from Schmidt (1966) expressed as $K_{0,OC} = (1\text{-}\sin \phi')(OCR^{\sin \phi'})$ is adopted. In this figure, overconsolidation ratio of 5 and 10 are shown for comparison. According to the back-analyzed data, relatively large friction factor can be reasonably estimated using OCR of 10.

Mobilized shaft friction in rock

Figure 9 shows mobilized unit shaft friction in siltstone layer. Relationship between unconfined compressive strength of rock (UCS) and unit friction from 0.1 to 0.3 square root of UCS are used for comparison. Horvath et al. (1983) reported that fully mobilized friction in rock were from 0.2 to 0.3 square root of UCS. In this paper, mobilized unit skin friction can be estimated by 0.1 square root UCS line. One of possible reasons to this observation was shaft movement in siltstone layer was not fully mobilized as maximum pile head settlement was still less that 1% of the pile diameter (refer to Fig. 4). This small shaft movement resulted in relatively small shaft friction in rock layer compared with those in the literature.

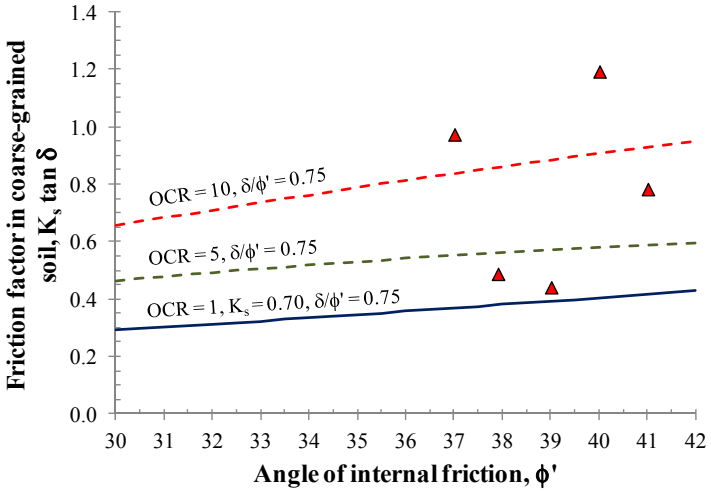


Fig. 8 Back-analyzed friction factor in sand

End bearing in soil and rock

In Fig. 10a, maximum pile toe settlement to pile diameter and mobilized end bearing is shown. All piles reported in this paper settled less than 1% of the pile diameter. According to Ng et al. (2001), toe movement up to 4.5% of pile diameter is required to substantially mobilize end bearing. Thus, end bearing parameter (N_q) was not analyzed in this study for pile in soil. It is as expected that end bearing for piles in siltstone were clearly larger than those in soil, even they were not fully mobilized. The maximum mobilized end bearing in soil and siltstone in this study were 400 kN/m^2 and 5,400 kN/m^2, respectively, still less than estimated end bearing in the design of 5,500 kN/m^2 and 10,000 kN/m^2, respectively.

To further analyze end bearing parameter in rock, mobilized end bearing is normalized with its unconfined compressive strength as shown in Fig. 10b. The normalized end bearing is compared with relationship of rock strength reported by Pells and Turner (1980). In their study, maximum base pressures are reported at normalized toe settlement of 1% and 2% the pile diameter. For comparison, it is assumed that the relationship is linear up to 1% of normalized toe movement. For data in this paper, normalized end bearing were between 0.1UCS and 0.3UCS. Strength of rock can be varied from very weak rock to strong rock. Note that end bearing of pile was not fully mobilized so that actual back-analyzed strength is expected to be larger than the reported data.

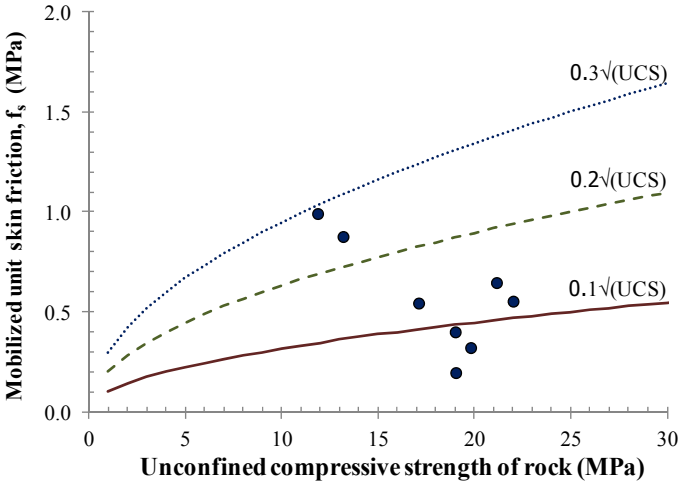


Fig. 9 Unit skin friction in rock

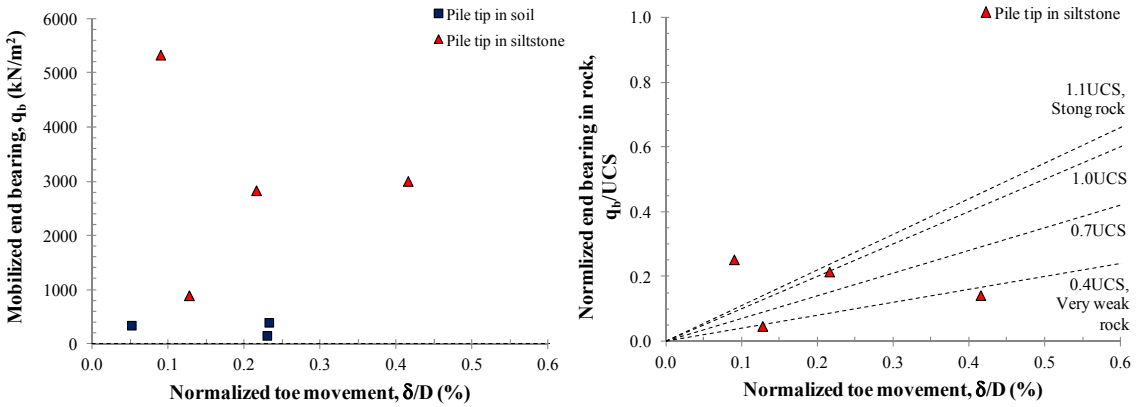


Fig. 10 (a) Mobilized in bearing in soil and rock; (b) Normalized end bearing in siltstone

SUMMARY AND CONCLUSIONS

Interpreted results from instrumented static pile load tests are reported in this paper. Bored piles were constructed using rotary drilling and socketed into sandstone and siltstone in the Northeast Thailand. Unit skin friction and end bearing of soil and siltstone were back-analyzed and compared with those reported in the literature. According to the measured data and back-analysis, following conclusions may be drawn:

- Shaft shortening of piles with tip embedded in sand or clay was about half of the interpreted elastic shortening (i.e. 0.5PL/AE). For piles having tip in siltstone, shaft shortening was between ¾ and 1 of the interpreted elastic shortening (i.e., 0.75 to 1 PL/AE). This is because stiffness in rock layer is significantly larger than those in soil, causing smaller toe settlement in the former than the latter. Proportion of shaft shortening and total settlement at pile head for all piles is ranging from 0.7 to 0.8.
- Settlement of pile embedded in soil can be reasonably calculated using analytical solution. However, for pile embedded in siltstone, discrepancy between measured and calculated results occurs. A possible reason for this observation is variation in condition of rock or degree of weathering causing inaccuracy in estimation of elastic modulus of rock at pile base.
- The estimation of friction in clay using three methods proposed in codes of practice and literature provides a reasonable result for most results. However, data from highly weathered siltstone was significantly larger than adhesion factors in the literature. This is because effect of stress history on strength of soil.
- For friction factor in sand, taken effects of overconsolidation ratio into account improves the estimation of back-analyzed friction. For sand near surface, soil with normally to slightly over-consolidated condition is suitable to back-analyze the data. For very dense sand or sand at larger depth, sand with high overconsolidation ratio (i.e., about 10) reasonably capture the measured results. This is because changes in stress history of soil formation at the site.
- To estimate mobilized unit skin friction in siltstone, relationship of 0.1-0.3 square root of unconfined compressive strength appears to reasonably capture the result. However, this value is substantially smaller than those reported in the literature. One of possible reasons to this observation was shaft movement in siltstone layer was not fully mobilized as maximum pile head settlement was still less that 1% of the pile diameter.

REFERENCES

ASTM D 1143. 1994. Standard test method for piles under static axial compressive load, West Conshohoken, P.A., USA

Aye, Z. Z., Boonyarak, T., Maung, A. W., Thasnanipan, N. and Prongmanee, N. (2015). Back-analysis

of design parameters for bored pile in Yangon. International Conference in Soft Ground Engineering, Singapore (ICSGE), pp 563-570

Boonyarak, T., Aye, Z. Z., Thasnanipan, N., Supawo, S. and Chea, S. 2016. Settlement prediction of large-diameter bored pile in Bangkok soils. Proceeding of the Sixth International Conference on Geotechnique, Construction Materials and Environment (GEOMATE 2016), 14-16 November 2016, Bangkok, Thailand. Paper in CD

EN1997. 1997. Eurocode 7: Geotechnical design. Part 1: General rules [Authority: The European Union Per Regulation 305/2011, Directive 98/34/EC, Directive 2004/18/EC]

FHWA (U.S. Department of Transportation Federal Highway Administration). 2010. Drilled Shafts: Construction Procedures and LRFD Design Methods. National Highway Institute

Horvath, R. G., Kenney, T. C. and Kozicki, P. 1983. Method of improving the performance of drilled piers in weak rock. Canadian Geotechnical Journal, 20, 758-772

Kullhawy, F. H. 1984. Limiting tip and side resistance, fact or fallacy, Proc. Symposium on Analysis and Design of Pile Foundations, American Society of Civil Engineers, San Francisco, 80-98

NAVFAC (Naval Facilities Engineering Commands). 1986. Design Manual 7.02 Foundations and Earth Structures. Alexandria, Virginia

Ng, C., Yau, T., Li, J., and Tang, W. 2001. New Failure Load Criterion for Large Diameter Bored Piles in Weathered Geomaterials. J. Geotech. Geoenviron. Eng., 10.1061/(ASCE)1090-0241(2001)127:6(488), 488-498.

Peck, R. B., Hansons, W. E., and Thornburn, T. H. 1974. Foundation Engineering. New York: John Wiley & Sons

Pells, P. J. N. and Turner, R. M. 1980. End-bearing on rock with particular reference to sandstone. Proceeding of International Conference on Structural Foundation on rock. Sydney, Australia, pp 181-190

Schmidt, B. 1966. Discussion of earth pressures at rest related to stress history. Canadian Geotechnical Journal, 3, 239–242

Terzaghi, K. 1943. Theoretical Soil Mechanics. Wiley & Sons, New Jersey.

Tomlinson M.J.,1995. Pile foundation, The carrying capacity of piles and pile groups, Foundation design & Construction 6th edition, pp. 265-316.

PILE FOUNDATION SOLUTIONS IN THE DEEP QUATERNARY SEDIMENTS OF BOTANY BAY

Paul A. O'Brien, Geotechnical Engineer, Golder Associates Pty Ltd, Sydney, NSW, Australia,
Thomas G. Cuniowski, Geotechnical Engineer, Golder Associates Pty Ltd, Sydney, NSW, Australia
Gary A. Chapman, Senior Principal Geotechnical Engineer, Golder Associates Pty Ltd, Melbourne, VIC, Australia

1 ABSTRACT

The new Amcor B9 paper mill in Botany, NSW, Australia, involved the design and construction of a new paper mill founded within the Botany Basin Sediments. There were numerous design and construction challenges to address, including tight settlement tolerances for the paper machine footings (6 mm total and 1/2000 mm differential limits), high variable and cyclic loads, deep (>25 m) bedrock and uncontrolled fill material across the site. The mill structure design incorporated a deep driven precast and CFA piled foundation solution, with a comprehensive swathe of testing to validate pile capacity and expected settlements. The pile design for the mill structure included the installation of approximately 1000 piles, with pile testing comprising dynamic testing and a static load test on precast piles. With consideration of Sydney's increasing demand for development space in relative close proximity to the city's CBD, industrial areas in the Botany Bay area are likely to make way for heavy or complex commercial and residential structures. Therefore, a better understanding of the engineering behaviour of sediments underlying these areas would allow for efficient foundation solutions. This paper presents a discussion on effective foundation testing techniques and the effects that the behaviour and characteristics of the Botany Bay sediments impose on deep piled solutions.

Keywords: pile design, pile testing, pile capacity, settlement sensitive, cemented sands, pile relaxation

2 PROJECT DETAILS

2.1 New paper mill

The project involved the construction of the largest recycled paper machine in Australia. The paper machine is 330 m (1080 ft) long, 22 m (72 ft) high, and capable of producing 1.6 km (1 mile) of paper per minute. Construction commenced in early 2011 and new paper mill officially opened in early 2013. The early works contract was awarded to Baulderstone Construction Pty. Ltd. (Lend Lease Corp. Ltd.), with the D&C contract awarded to a consortium headed by Leighton Contractors Pty. Ltd. (CPB Contractors Pty. Ltd.), which included Golder Associates Pty. Ltd. as the geotechnical designer and reviewer.

2.2 Site history and effect on local topography

The site has been used as a paper mill since 1902, and as such, has layers of uncontrolled fill and buried objects within the upper fill materials associated with historical industrial use. The fill material generally comprised of loose and very loose sands, with isolated pockets of cohesive materials, peats, pulped paper and general construction waste. In addition, during construction, underground storage tanks were identified at depth, indicating the historical extent of filling across the site was extensive. The presence of this generally uncontrolled fill was a factor for determining that the most cost effective foundation solution for the paper mill was piled foundations, to bypass these materials.

3 GEOLOGICAL SETTING

3.1 Regional geology

The site is underlain with quaternary aged sediments of generally marine, alluvial and aeolian origin (1:100,000 Sydney Geological Series Sheet), locally known as Botany Sands. Hatley (2004) eloquently encapsulated numerous texts and has presented a summary of the geology of the Botany Basin, which comprises four units, as outlined in Table 1.

Table 1: Generalised geology of the Botany Basin

Soil Unit	Thickness range	Description
Upper Unit	0-20 m *(0-66')*	Most commonly encountered in close proximity to Botany Bay itself. A heterogeneous mix of fine to medium grained loose sand, with interbedded clays, silts and peats. Generally aeolian and estuarine deposits of the Holocene period.
Third Unit	0-30 m *(0-98')*	Deposited over the clays and sands of the underlying *Second Unit*. Generally a clean, fine to medium grained, cemented quartz sands. Generally aeolian, littoral dune or beach deposits of the late Pleistocene period. The unit also comprises thin, intermittently persistent clays and organic peat layers.
Second Unit	0-15 m *(0-49')*	Deposited over the sands, clays and gravels of the underlying *Basal Unit*. Generally comprises fluvial and marine deposits of fine to medium grained, clay rich quartz sands, and estuarine and lagoonal clay and peat deposits of the middle Pleistocene period. Clean, fine to coarse grained quartz sands are also present in areas of channel fill
Basal Unit	0-30 m *(0-98')*	Deposited over the underlying Hawkesbury sandstone unit. Generally comprises fluvial and aeolian deposits of clean, medium to coarse grained sands with gravel lenses and marine deposits of sands. Also comprises thin, peaty estuarine muds and organic clay layers.

The 'Third Unit' sands, with an average thickness of 15 m (49 ft) across the Botany Basin area, are of interest from an engineering and construction perspective. Firstly, they are generally at the depth where pile foundations are likely to be founded (and where excavations are likely to extend to) for future constructions. Secondly, the cemented layers/crusts (formed by evaporation of mineral rich groundwater [McNally and Branagan, 1998]) which can be metres thick, have favourable engineering properties and generally high bearing capacities. There are various texts available that discuss the geological and hydrogeological properties of these sediments, but little literature on their engineering properties.

3.2 Results from geotechnical investigations

Prior to foundation design, Golder Associates carried out geotechnical investigations across the site comprising boreholes in 2006, and cone penetrometer tests (CPTs) in 2008. Results of the geotechnical investigations are summarised in Table 2, with a cross section across the alignment of the paper mill shown in Figure 1.

Table 2: Site specific geotechnical design units

Design Unit	Depth to base range	Description	CPT q_c range (average)	SPT N range (average)	Youngs Modulus (MPa)
Unit 1: Fill	4 to 6.5 m *(13' to 22')*	Fill, VL-L sands, clays and peats, pulped paper, rubble	0 to 3 (1) MPa *0 to 435 (145) psi*	2 to 9 [7]	2 to 5 (3)
Unit 2: MD-D sands	6 to 8 m *(20' to 40')*	Sands, inferred to be the *Upper Unit*	15 to 30 (20) MPa *2175 to 4350 (2900) psi*	22 to 30 [26]	30 to 50 (40)
Unit 3: VD sands	N/A[(1)] *(N/A[(1)])*	Sands, inferred to be the *Third Unit*, with peat and clay zones	30 to >70[(2)] (45) MPa *4350 to >10000[(2)] (6500) psi*	37 to >58[(3)] [>52[(3)]]	200 to 300 (250)

1) Geotechnical investigations were not carried out to depths greater than 28 metres, and the base of the Unit 3 material was not identified. Bedrock was also not encountered on site..
2) Practical CPT refusal when q_c > 70 MPa (10000 psi).
3) Practical SPT refusal when hammer double bouncing and/or operator decision.

The depth of the Unit 3 material was reasonably consistent across the footprint of the paper mill, and CPT/SPT results generally showed that this material extended to depths of up to 24 m (79 ft) below existing ground surface levels. Negative pore pressures, indicating that dilatancy was occurring, were observed during CPTu testing in this material.

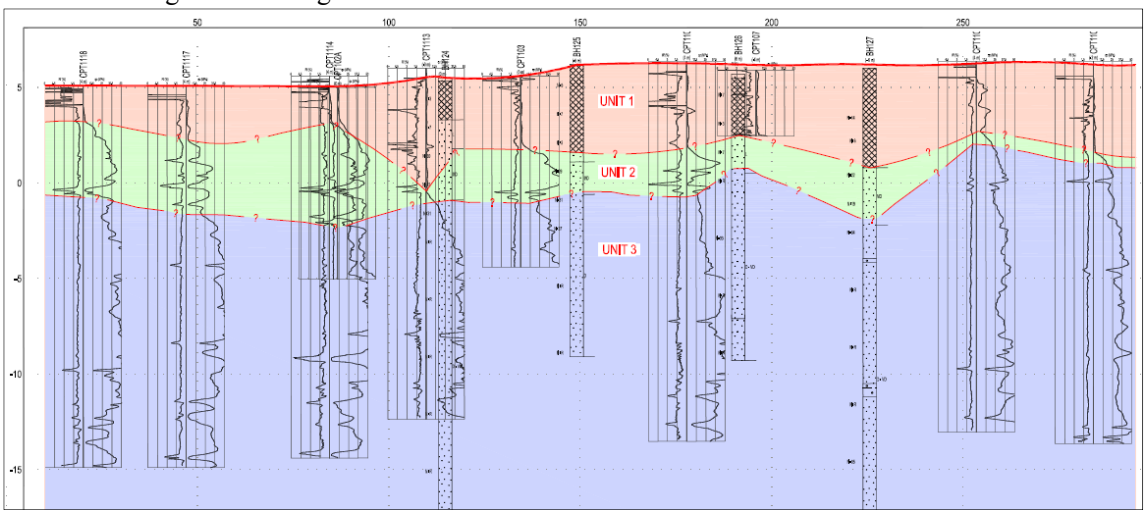


Figure 1: Cross section across paper mill alignment

4 PAPER MILL FOUNDATION

The building housing the mill and the machine itself was founded on approximately 1000 piles. The large and heavy machinery produces high frequency and cyclic forces including variable cantilever loads, requiring a robust foundation solution. Ongoing operation of the paper machine requires a rigid foundation, where small differential settlements can impact the highly sensitive machinery, possibly causing unsatisfactory paper production. The adopted foundation solution would also need to be validated to ensure that the cyclic load patterns (between 50 RPM and 550 RPM) did not coincide with the natural frequencies of foundations.

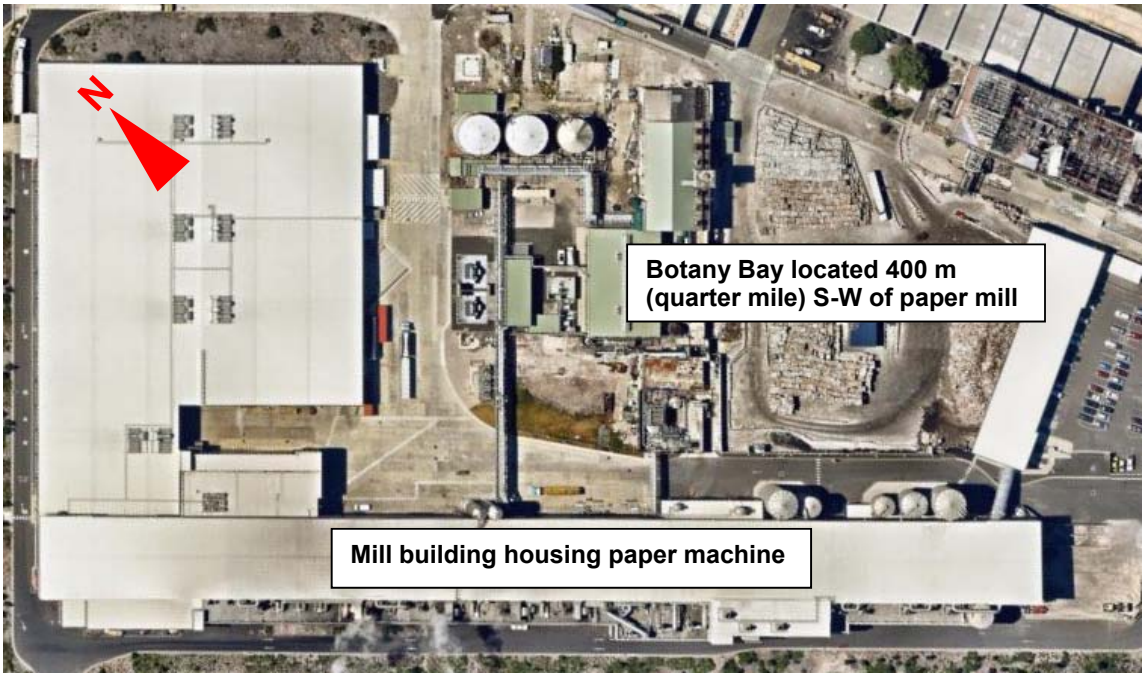


Figure 2: Plan view of project site

4.1 Settlement tolerances and adopted foundation solution

Strict settlement (<6 mm [<1/4 in.] total) and differential settlement tolerances (<0.5 mm/m [<0.02 in./ft] between adjacent foundations) were stipulated by the paper machine manufacturer to provide sufficient support for the sensitive machine. Theoretical differential settlement calculations were assessed to not provide sufficient confidence considering the tight machine limits. A stringent footing design and thorough testing regime before and during construction was stipulated to provide confidence in and to check on settlement predictions.

Pile foundations were chosen to provide the necessary settlement control for the paper machine. A driven reinforced concrete pile option was adopted to support the bulk of the paper machine, due to the ability for driven precast piles to provide adequate and economic installation and testing while validating pile integrity and capacity. Some CFA piles were also installed to provide additional uplift support associated with the cantilever loads imposed by the machine. The piles were designed to be founded in the sands of the *Third Unit*.

4.2 Pile installation

All piles were installed under a Golder geotechnical engineer's supervision, to record blow counts and penetration depths, and provide advice on suitable driving stresses, founding levels, further driving and pile testing requirements. The following data was recorded and/or carried out during construction:

- Set, hammer drop height and Temporary Compression (TC) recorded periodically during pile drive and at End Of Drive (EOD).
- High strain dynamic load testing using Pile Drive Analyser (PDA) during pile driving, including Case Pile Wave Analysis Program (CAPWAP) analysis.
- Re-strike (RST) high strain dynamic tests to assess pile set-up or relaxation (including PDA/CAPWAP analysis on selected piles)
- Static load test.

Piles were installed to practical refusal, typically nominated as a set of approximately 3 mm/blow or less. Restrike tests were carried out on all piles approximately 14 days or more after EOD. Real time pile capacity checks were undertaken during installation, using the Hiley Formulae to calculate field capacity estimates for all piles (calculated from the EOD and RST data). PDA and CAPWAP analysis was selected for approximately 10 % of piles or for piles where unusual drive or set up behaviour was observed (i.e. inferred structural damage). A static load test was performed on a single driven pile in order to simulate the expected load sequence on the pile during machine construction and operation sequence to confirm pile top load settlement performance.

4.3 Pile testing

The Hiley Formulae (Hiley) has been used around the world for decades, and is often considered the most comprehensive dynamic formula for calculating field capacity of driven piles (Rauf, 2012). Hiley takes into account the hammer weight and drop height, and quantifies the loss of transferred energy due to the compression of the pile and soil. Because of its relatively simple calculation technique, Hiley was chosen as a technique for estimating field capacities for all driven piles installed for the mill building and machine in combination with calibration to dynamic pile test results. Individual pile capacities were assessed, and the following Modified Hiley Formula was adopted to calculate the ultimate bearing capacity (R_u):

$$R_u = \frac{WgH}{s + {}^{tc}/_{2}} \qquad [1]$$

where: W is the mass of the pile hammer (kg), g is the gravitational constant (9.81 m/s^2), H is the free fall height of the hammer (metres), s is the final set of the pile (mm per blow) and tc is the temporary compression of the pile measured on final blow.

PDA testing was undertaken on approximately 10% of the total installed piles, particularly focusing on the piles supporting the paper machine. PDA testing is a widely used and accepted test to assess pile integrity and capacity. Due to the geological setting and stringent design requirements, PDA was considered to be an economical test method due to its ability to carry out testing in conjunction with pile installation, while providing real time data on pile and soil responses to maximise drive efficiency and minimise likelihood of pile damage. PDA also provides the ability to conduct refinement of field capacity data in for form of a CAPWAP analysis, which provides an accurate capacity estimate by calculating pile and soil variables, forces and motions from one-dimensional wave propagation theory and simple integration.

Due to the strict differential settlement limits specified for the machine foundations, a static load test was also carried out. This was undertaken to observe the settlement and elastic behaviour of the pile foundation under expected load and geological conditions, in order to provide additional confidence with regard to the differential settlement predicted using theoretical methods. The pile chosen for the static load test was part of a pile group supporting columns having the largest difference in cantilever design loads to replicate the 'worst case' of differential settlement that the machine would impose on the foundations.

4.4 Capacity and Settlement Validation

Cost and time constraints prohibited the carrying out PDA and CAPWAP analysis on all production piles of the paper machine. For the paper mill, a combination of dynamic pile driving formulae, PDA/CAPWAP and a single static load test was considered the optimum approach for pile capacity and settlement validation. Pile capacity estimates developed from dynamic pile driving formula (such as the Modified Hiley used in this case) historically are known to over or under predict pile capacity (Likins et al., 2012). This is due to formula assumptions, such as assuming static and dynamic behaviour of the pile are the same and that the pile acts as a rigid body that when struck, with instantaneous compression of the entire pile. To validate pile capacity for all piles, the Hiley capacity estimates were compared with the CAPWAP estimates for the PDA tested piles (Figure 3).

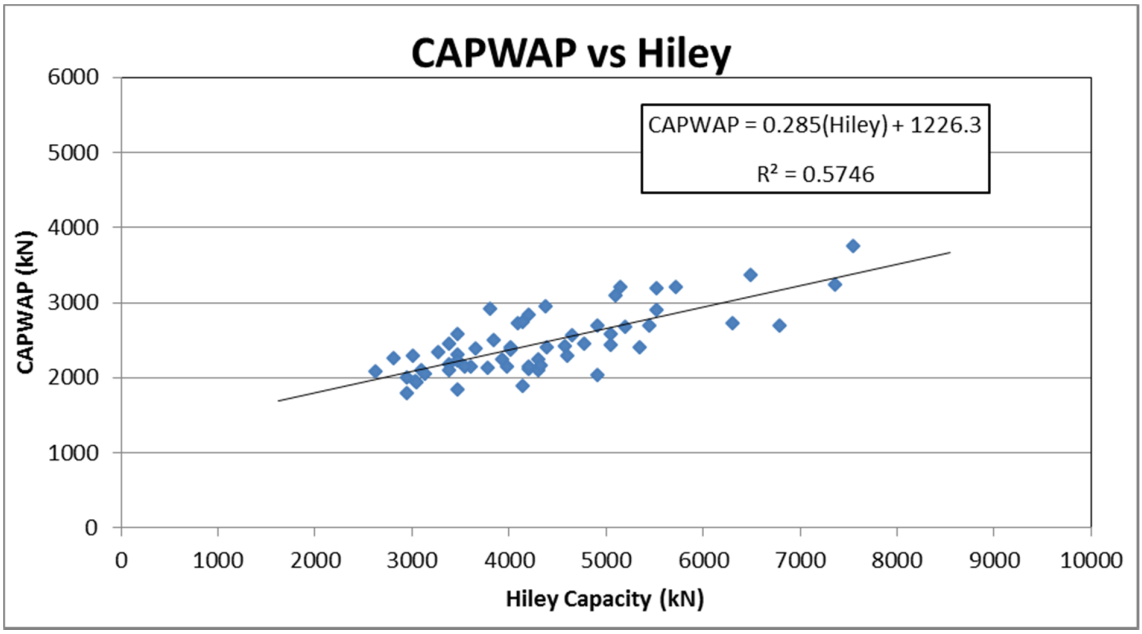


Figure 3: CAPWAP and Hiley Comparison

A linear regression model with all available PDA data assessed the correlation between CAPWAP and Hiley in order to adjust capacity estimates carried out using Hiley on piles with no PDA testing. The

correlation coefficient R^2 (indicates proportion variance in CAPWAP prediction from Hiley) was used to adopt an appropriate Factor of Safety (FoS) to provide confidence when comparing estimated pile capacities and required design ultimate pile loads.

Pile settlement validation compared the static load test settlement results with estimated theoretical settlement calculations. PDA testing and CAPWAP analysis was done on the test pile before and after the execution of the static load test to also allow for a comparison between static and dynamic testing results. The static load test subjected a single pile to the axial loads (dead, live and cantilever) expected to be imposed on the pile from the construction and operation of the paper machine. Pile head deflections were measured using both dial gauges and precise level (accurate to 0.1 mm [0.004 in.]) during the load cycle to observe total and residual movement of the pile head and to assess elastic behaviour. The load displacement data plotted in Figure 4 show that the test pile generally behaved in a linear elastic manner. Pile stiffness was calculated from the static load test, with group settlements then calculated using the commercially available program PIGLET, and compared with design limits.

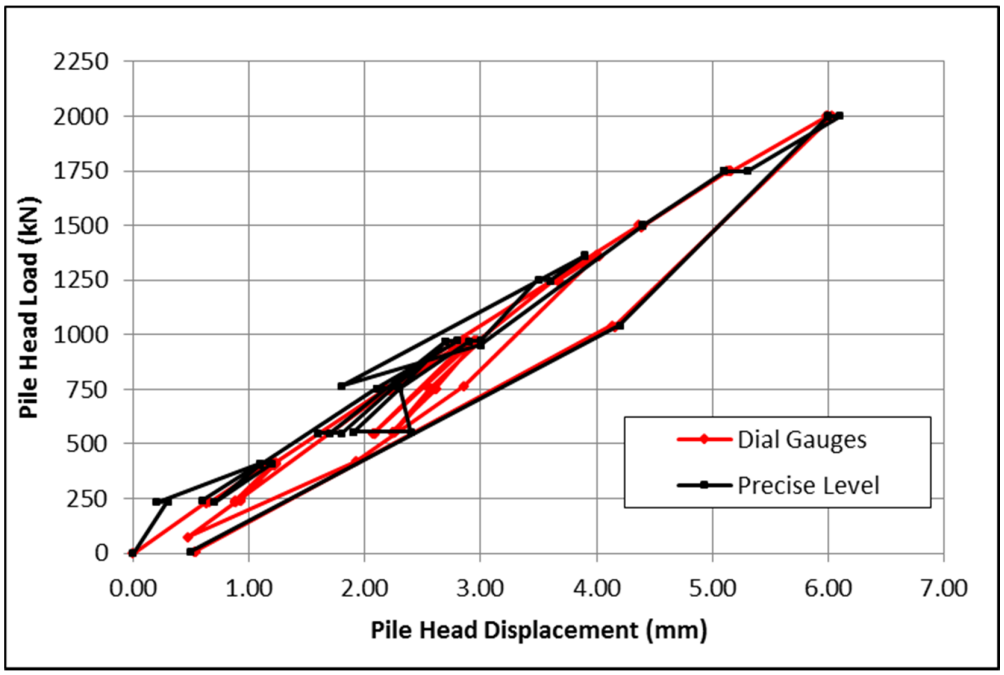


Figure 4: Static Load Test Results

5 DISCUSSION

5.1 Temporary strength gain and pile relaxation

Pile driving in dense and very dense sands located below the water table is known to cause dilatancy, which leads to the generation of negative pore pressures which in turn temporarily increases effective stresses. Dilatancy during pile driving has been observed and reported on previously by Chow et. al. (1998) and Seidel et. al. (1992), however, is often not considered during foundation design. The cause and amount of dilation is a factor of the soil density, mineralogy and speed of densification (will effects the time allowed for negative pore pressures to dissipate). Dilation of the soil during pile driving needs to be considered during design and construction, and piling contractors should be made aware of the phenomenon so as not to create future bearing and settlement issues due to insufficiently driven piles.

The time taken for excess pore pressures to dissipate at the base of the pile, and the subsequent decrease in effective stress and potential partial reduction of end bearing is a function of the aforementioned factors, as well as depth of groundwater and the soil's hydraulic conductivity. The likelihood of dilatancy occurring during pile driving can often be predicted where negative pore pressures are generated during CPTu investigations. Dissipation testing when negative pore pressure is observed

during CPT testing is useful in providing an indication of the required time for pile driving induced pore pressures to dissipate, however, the authors are not aware of any correlations available in the Botany Bay sands.

Significant pile relaxation was observed across the site during pile installation. During the early stages of pile installation, restrike tests were conducted at varying periods after initial EOD (end of drive refusal) to observe relaxation. This trial showed many piles showing a significant increase in set (decrease in estimated capacity), often not stabilising until up to 2 weeks after driving to initial refusal, enabling pile re-drive up to an additional 2.5 m (8 ft) depth. This unusually long period of pore pressure dissipation was inferred to be a result of a combination of the geology (very dense sands with intermittent clay/peat layers), likely group effects related to piles being installed in close proximity (<1 m [3 ft] apart) and tidal influences.

5.2 Comparison between Dynamic and Static Test Results

Figure 5 presents a comparison of the pile head load displacement curves obtained from the static load test and those calculated from a CAPWAP analysis carried out before and after the static load test. These results show a close agreement between top load-settlement estimated by CAPWAP to that observed during the static load test. The settlement estimates obtained from dynamic testing of the piles supporting the paper mill were considered likely to accurately predict actual settlement observations in that geological setting, and added confidence that the dynamic pile test methods are likely to accurately predict static load capacity estimates.

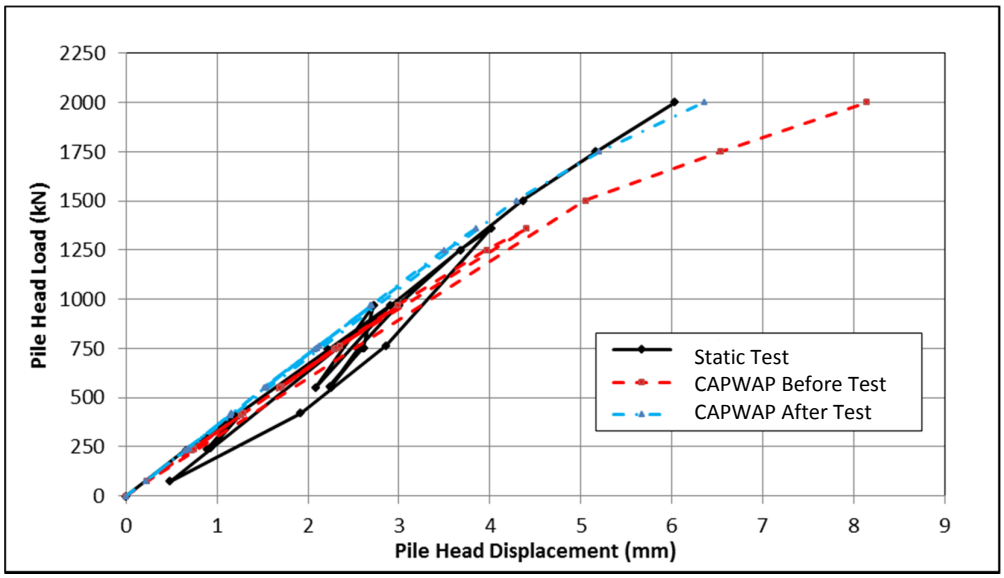


Figure 5: Comparison of Static and Dynamic Test Results

5.3 Assessing CAPWAP results and Botany Bay geology

PDA and CAPWAP tested piles that were located close to a CPT or borehole are presented in Table 3, with CPT q_c versus depth plot and a borehole summary shown in Figure 6. As can be seen from the results of CAPWAP, there is variation between shaft resistance and base resistance across these piles, even where piles have similar founding depths and have the same cross sectional area. To understand this, it should be noted that there are isolated and laterally discontinuous peat and clay layers, located at various depths, as illustrated in Figure 6. CPT 1113 and BH124 were located approximately 10 m (33 ft) apart, however, the clay zone at 12.1 m (40 ft) depth encountered in BH124 was not identified in CPT1113. However, both the borehole and CPT identified a minor peat zone at approximately 14 m (46 ft) depth.

Table 3: Selected CAPWAP results

Pile number	Embedment (m)	Pile size (mm)	PDA pile resistance (shaft, base) (kN)	CAPWAP/Hiley ratio
116	11.6	350	2731 (1085, 1646)	0.67
119	11.2	300	3781 (1940, 1841)	0.72
121A	9.1	275	2125 (586, 1539)	0.56
122	11.6	275	2050 (1255, 795)	0.64
124A	11.6	350	2914 (1429, 1485)	0.77
124B	9.7	350	2945 (1004, 1941)	0.67
129A	11.5	275	2184 (1305, 879)	0.65

The presence of the clay and peat layers are likely to have led to reduced capacities in some piles. It is likely then that the variations between CAPWAP capacities at similar depths are influenced by:

- The presence of isolated and laterally discontinuous peat and clay zones being located within 2 x pile diameters of the pile founding levels of certain piles.
- The thickness of, and penetration into, the cemented sand zones at the base of the pile.
- The localised composition and thickness of the fill materials at individual pile positions.
- The presence of thicker clay and peat layers at greater depths, which create a smearing effect that reduces the shaft resistance in some piles.

In addition there were a number of dewatering activities being carried out on site during and after the installation of the piles. During dewatering, numerous ground monitoring wells were monitored to assess the drawdown effects of these activities. In all wells, the groundwater drawdown was slower and less pronounced that finite element models predicted. Therefore, the dissipation of negative pore pressures were reduced, increasing temporary strength gain and influencing the Hiley EOD capacity estimations. No dissipation testing was carried out in the dense sands in this area during geotechnical investigations.

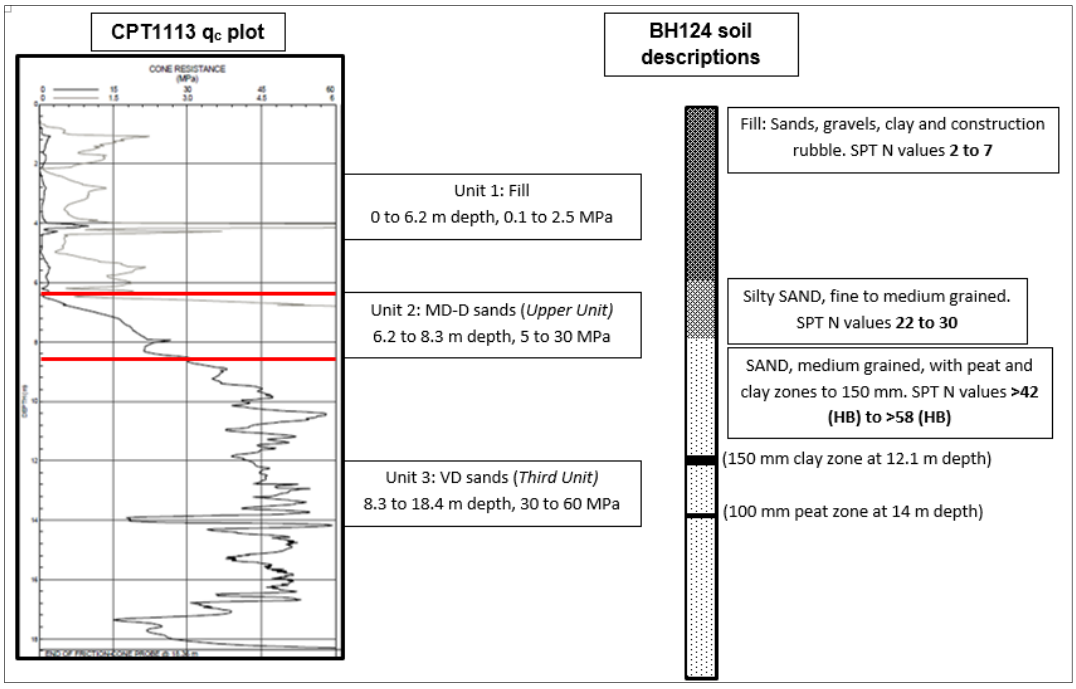


Figure 6: Summarised investigation information around test piles of interest

5.4 Impacts on future foundation designs in the Botany Bay area

It is likely that due to the increased urban spread occurring in Sydney and its close proximity to the CBD, the Botany Bay area will be slowly converted from mainly industrial and commercial land, to medium and high density commercial/residential. It is unlikely that these future constructions will have the stringent settlement requirements or require the level of pile design analysis that was required for this project. Future construction may rely on conservative and empirical design calculations and correlations. The results of the pile testing carried out in this area show that significant load can be carried on piles founded on the very dense *Third Unit* botany sands, however a careful approach to settlement and capacity validation must be undertaken due to the presence of isolated and discontinuous clay and peat zones. For future design where pile foundations are being considered, it would be beneficial to carry out preliminary pile trials to refine design parameters and assumptions, which would lead to significant cost savings if compared to relying on empirical and generalised pile analysis and design.

6 CONSTRUCTION CHALLENGES AND CONSIDERATIONS

6.1 Pile installation induced vibrations and post installation vibrations and excavations

Due to the loose, granular nature of the upper fill materials and marine sediments, the possibility of pile installation induced settlements was considered. The site was located close to settlement sensitive infrastructure, such as roads, services and heritage structures. Therefore, settlement and vibration monitoring was recommended, and was carried out during the pile installation. During installation, no settlement inferred to be associated with the pile installations was observed on site. This is likely due to the method of installation relying on impact driving rather than vibratory driving.

Post pile installation, a sheetpile wall was installed 0.5 m (< 2 ft.) from a pile and pile cap at the eastern end of the mill building. The sheetpile wall was installed to facilitate the construction of a large storage pit, the purpose of which was to hold reject and pulped paper material. 2-D PLAXIS models were created to simulate excavation and vibration, and to ascertain the optimum embedment depth and stiffness of the sheetpiles. Modelling indicated 7 m (22 ft.) long, GU7N-D sheetpiles, with 3.5 m (11.5 ft.) embedment below excavation would provide the required stiffness and displacement control.

The GU7N-D sheetpiles were also able to be installed by a low-vibration piling rig. Vibrations during installation were required to not exceed a Peak Particle Velocity of 20 mm/sec, to reduce the likelihood and proliferation of vibration induced densification of the sand and subsequent settlement (Gaba et al. 2003). Vibration and displacement monitoring devices were installed on the existing housing facility before sheetpile installation, with results showing movement and vibration limits were not exceeded.

6.2 Post installation dewatering

The Botany Bay area has a relatively shallow groundwater table. Temporary dewatering, required for the construction of three underground storage tanks, occurred after piled foundations had been installed and construction commenced. These tanks were located close to settlement sensitive infrastructure. Even small dewatering induced settlements under the piles could have detrimental effects on their long term performance, possibly causing structural re-distribution of loads.

2D-PLAXIS models were created to simulate dewatering effects on the piles, with horizontal proliferation of water draw-down and associated settlements analysed. Isolated clay zones and tidal recharge effects (Somerville 2005) were included in the models, to predict settlements. Additionally, groundwater and settlement monitoring were carried out record settlements and drawdown. From these results, it was clear that the proximity to the ocean and associated tidal movements increased groundwater recharge rates, thereby reducing dewatering induced settlements.

It is important to note two things in regards to tidal movements and their effects on dewatering in the Botany Bay area of Sydney. First, the associated recharge needs to be considered during the design and

analysis of dewatering pumps, wells and spear-points, to ensure sufficient drawdown is achieved to allow for a dry excavation. Second, dewatering associated flowing sands, an important consideration in the Botany Bay sands, needs to be analysed to ensure safe excavations and subsidence are avoided.

6.3 Ground improvement

The paper and equipment storage building immediately north of the paper mill machine, did not have the same high cyclic loads as the paper mill. Settlement limits however, were still stringent (<15 mm [<3/5 in.] total). Preliminary investigations indicated that the stratigraphy consisted mainly of granular construction rubble, overlying loose sands, overlying dense to very dense sands. Therefore, shallow foundations following ground improvement was chosen as the foundation solution for this building.

High energy impaction compaction (HEIC), considered a practical and cost effective solution, was the chosen ground improvement method. During HEIC, an area at the southern section of the storage facility showed poor ground improvement results, with subsequent investigations (CPTs/GPR) identifying isolated and one extensive non-granular layer, inferred to be either cohesive materials, pulped paper or organic material. A 3 m (10 ft.) high preload with settlement plates was installed and left in place and monitored for 2 months, to reduce settlement and to compare the actual settlement with predictions.

The results of settlement data indicated that the non-granular layers were likely to be over-consolidated firm to stiff clay, not pulped paper or organic material (Cuniowski, 2016). This is due to the settlement results indicating primarily consolidation, with little to no secondary consolidation observed. The settlement behaviour of pulped paper would mimic very soft soils or organic matter, *ie* normally consolidated with high secondary consolidation factors (0.03 to 0.06). The rationale being pulped paper and organic material would experience primary and secondary consolidation, as well as degradation (and decomposition), which is time dependant not stress dependant.

Therefore, where ground improvement is required for future projects in the Botany Bay area, thorough geotechnical investigations are recommended. This will help identify the stratigraphy, and occurrence and characteristics of any poor ground materials, and help assess whether granular or cohesive ground improvement techniques, or a combination of both, are most suitable for the site and project in question.

7 SUMMARY AND CONCLUSIONS

In summary:

- The Hiley formula typically over-estimated the pile capacity across the site, but provided an accurate estimate after comparison and adjustment using PDA analysis. The partial cementation of the sands has created a crust on which the piles achieved practical refusal. Underneath the cemented crust, is generally un-cemented (but still very dense) sands and sometimes peat and clay zones. The PDA correlated Hiley formula results proved to be a useful tool for controlling pile installation on site. The overestimation by Hiley was likely due to inherent assumptions in the Hiley formula.
- Due to the minor silt content and isolated (but sometimes laterally continuous) cohesive zones, the hydraulic conductivity of the very dense Botany Bay sands is lower than a clean sand. It is therefore likely that the time for pile relaxation and negative pore water pressure dissipation to occur will take longer than when compared to a clean sand. Additional time (minimum of 2 weeks) should be planned for, when carrying out re-driving and re-strike tests in the dense and very dense Botany sands to include for this effect. CPT dissipation tests carried out during initial geotechnical investigations would also allow for a better estimate of this effect.
- Pile testing shows that even with small section piles, significant load capacity is possible when piles are founded in and within the very dense, cemented sands of the *Third Unit* of the Botany Bay geology. Testing also showed that settlement of the piles found in this material under load could be regulated to achieve small tolerances, and that complex future structures (sensitive structures, high-rise, heavily loaded foundations) can be successfully constructed in the

geological setting provided the appropriate level of testing is carried out during both planning and construction.

To conclude:

- Comprehensive but suitable geotechnical investigations and preliminary pile testing during the planning and design phase can lead to significant design and construction costs savings and efficiencies for future constructions in the Botany Bay area.
- Carrying out sufficient and sophisticated pile testing in conjunction with numerical modelling during construction, will allow for design assumptions and inputs to be verified and refined to meet stringent design constraints in the challenging geological conditions of Botany Bay.

8 ACKNOWLEDGEMENTS

The authors would like to thank the wider project team including the client Amcor Ltd, the principal contractor Leighton Contractors Pty Ltd, pile installation contractors Wagstaff Piling and the structural engineers at Klopfer Dobos Pty Ltd. Secondly, the authors would like to thank their senior colleagues at Golder Associates for allowing two young engineers to work on a technically challenging and rewarding project and for their assistance in the development this paper. Finally, the authors would like to thank their families for their encouragement and support in writing this paper.

9 REFERENCES

1:100,000 Sydney Geological Series Sheet 9130, NSW Department of Industry; Resources and Energy

Chow, F.C., Jardine, R.J., Brucy, F. and Nauray, J.F. (1998). "The Effects of Time on the Capacity of Pipe Piles in Dense Marine Sand." Journal of Geotechnical and Geoenvironmental Engineering, ASCE, vol. 124, no. 3, pp. 254-264, March 1998.

Cuniowski, T.G. (2016). "Geotechnical design challenges associated with construction of the new AMCOR paper mill in Botany, NSW." Proceedings of the 11th Australian and New Zeaand Young Geotechnical Professionals Conference, NZGS, pp. 116-121, October 2016.

Gaba, A. R., Simpson, B., Powrie, W and Beadman, D. R (2003). "Embedded retaining walls – guidance for economic design." CIRIA C580, London, 390pp.

Hatley, R. K. (2004). "Hydrogeology of the Botany Basin." Australian Geomechanics, 39 (3), 73-90.

Likins, G., Fellenius, B., and Holtz, R. (2012). "Pile Driving Formulas: Past and Present. Full-Scale Testing and Foundation Design." Geocongress 2012, ASCE, March 2012.

McNally, G.K. and Branagan, D.F. (1998). "An overview of the Engineering Geology of the Botany Basin." Geol Soc Australia, Collected Studies in Engineering Geology, Hydrogeology and Environmental Geology, Fourth Series: Environmental Geology of the Botany Basin, McNally, G.H. and Jankowski, J.

Rauf, A. (2012). "Estimation of Pile Capacity by Optimising Dynamic Pile Driving Formulae". University of Waterloo, Ontario, Canada.

Seidel, J. P., Anderson, G. D. and Morrison, N. J. (1992). "The Effects of Pile Relaxation on Toe Capacity and Stiffness. Application of Stress-Wave Theory to Piles." F. B. J. Barends (ed.), Balkema, Rotterdam, 1992.

Somerville, S. H. (2005). "Control of groundwater for temporary works". CIRIA Report 113, London, 87pp.

THE APPLICATION OF RAPID LOAD TESTING IN SINGAPORE

Soon-Hoe Chew, National University of Singapore, Singapore, ceecsh@nus.edu.sg
Peter Middendorp, Allnamics, The Hague, The Netherlands, middendorp@allnamics.eu
Joost Bakker – Allnamics, The Hague, The Netherlands, bakker@allnamics.eu
Gilbert Chuah – Allnamics International (S) Pte Ltd, Singapore, gilbert@allnamics.asia

ABSTRACT

The Rapid Load Testing (RLT) of foundation piles has been applied worldwide since 1984. Several International and national codes are available, such as the Japanese Code of Practice (2002), ASTM D7383-2010, German recommendation on Piling (2012) and Eurocode (2015). RLT methods like Statnamic and StatRapid are gaining popularity in Asia, Europe and North America. For checking the performance of piles, they are more economical, faster and environmentally friendly than Static Load Testing (SLT), while yielding good correlations with SLT results through an objective analysis method. To date (October 2016) hundreds of piles have been successfully tested by RLT method in Singapore. A number of these RLT tests were coupled with static load testing correlation tests, some of them with instrumentation for shaft load transferred. Examples of some correlation results for foundations installed in various geological formations in Singapore are presented in the paper. The findings from these results indicate that loading rate effects are negligible for Rapid Load Test results when foundations are socketed in competent non-cohesive soil layers and derive most of their capacity from these soil layers.

Keywords: rapid load testing, static load testing, comparison, loading rate effects, cast in situ piles.

INTRODUCTION

Rapid Load Testing (RLT), by which a quasi-static load is applied to a foundation pile, is used increasingly as an alternative to Static Load Testing (SLT) for cast in-situ piles, such as drilled shafts or bored piles. It is recognized nowadays that the determination of the pile capacity with Dynamic Load Testing (DLT) through signal matching techniques such as CAPWAP, TNOWAVE and AllWave-DLT, yield a wide spread of results for cast in-situ piles (Stahlmann et. al, 2012), making it practically very difficult, if not impossible to calibrate the DLT results with SLT results. This spread is due to the empirical and subjective assumptions that are used to interpret the test data, especially for cast in-situ piles (Holeyman et al. 2001, Viana da Fonseca in 2008, Herten et al, 2013). This is further complicated by the inhomogeneity of the concrete and variable cross-sections over the pile length for the cast in-situ piles.



Fig. 1. Rapid Load Testing systems (RLT). Statnamic (STN) with launching a reaction mass, StatRapid (RLT) by dropping a weight on rubber cushioning

Rapid Load Test (RLT) analysis results are unique and person independent as long as the analysis is performed in accordance with a guideline (such as the Dutch guidelines issued by CUR in 2010 and implemented in the Eurocode EN ISO 22477-10,). The analysis technique is

simple and straightforward, and signal matching is not required. RLT results can be easily checked by engineers without special expertise in RLT.

The principle of RLT can be defined as follows: the duration of the impact load is chosen such that the whole pile moves in a narrow velocity range and thus the pile - soil interaction can be considered as quasi-static at a moment that the pile velocity is zero (at moment maximum displacement). As a consequence, the pile and soil interaction can be modelled as a single mass-spring-damper system, and stress wave phenomena do not have to be considered. Longer piles need longer load durations to generate quasi-static behaviour. The two common loading mechanisms for RLT are the combustion gas pressure test apparatus (e.g. Statnamic Method), and the cushioned drop mass test apparatus (e.g. StatRapid Method). For drop mass systems the RLT load duration is controlled by the mass and spring combination. The RLT peak load is controlled by the drop height of the mass. With RLT the pile shaft is only under compression and therefore tension forces that could damage the concrete will not occur. RLT methods have been applied worldwide since 1984 (Gonin et al., 1984) and several International and national codes are available, such as the Japanese Code of Practice (2002), ASTM D7383-2010, Eurocode EN ISO 22477-10, German recommendation on Piling (2012) and the aforementioned CUR guideline (2010). To date (2016) RLT devices are available with maximum test loads ranging from 0.1 MN till 65MN

RLT methods like Statnamic (STN) and StatRapid (STR) (Figure 1) are also gaining popularity in Asia (2015 Chew et al.), as they are more economical than SLT, while yielding good correlations with SLT results through objective analysis methods. The most widely applied analysis technique for non-cohesive soils is the Unloading Point Method (UPM) 1992 (Middendorp et al.), while for cohesive soils the Sheffield method (SHM) is applied, which is not further discussed in this paper, but is clearly described by Brown and Powell (2013).
The Unloading Point Method is based on the principle that at time of maximum displacement ($t_{u,max}$) the pile velocity is zero and therefore damping force component is zero. So at time $t_{u,max}$ the static resistance F_{static} equals the measured rapid test load (F_{RLT}) minus the inertia force component (pile mass times acceleration):

$$F_{static} = F_{RLT} - M_{pile}.a. \qquad (1)$$

These parameters are all measured and are thus known quantities. So F_{static} and the corresponding displacement at time $t_{u,max}$ is an accurate data point on the equivalent static load testing curve, with additional loading cycles yielding additional points.

For a single cycle test the RLT derived static load-settlement behaviour is fit by a hyperbolic curve, based on one UPM point and the derived initial pile stiffness at the start of RLT loading. For multiple cycle testing, a best fit hyperbolic curve through successive UPM points will give the RLT derived static load-settlement behaviour. The hyperbola approach allows a straightforward method for the calibration of RLT with SLT results.

For comparison between RLT and SLT conducted on the same piles, care has to be taken as one of the methods is loading on the virgin pile (called “virgin loading cycle”), while the other method will be loaded onto the pre-loaded pile (called “subsequent loading cycle” pile). The start for the “subsequent loading cycle” should correspond with the final permanent residual settlement of the previous “virgin loading cycle”. Correlations with SLT will give proper results when these loading cycle permanent settlements are taken into account.

COMPARISON OF RLT WITH SLT

A prescribed correlation factor can be applied to correct for the loading rate dependency of soils. This correlation factor can also be obtained from site specific correlation tests between RLT and SLT. When

loading rate dependency is not known, SLT (using Maintained Load Test) can be performed to calibrate with RLT, and to derive the loading rate factor. However, this would require similar pile and soil conditions for both testing methods. It is to be noted that a pile which is load tested for the first time (i.e. virgin loading cycle) will generally have a softer response than a pile that has been preloaded (i.e. subsequent loading cycle). Therefore if SLT and RLT are executed on the same pile, the test that is performed first will reflect a softer response and the test performed later will show a stiffer response. Hence, the sequence of the tests performed has to be taken into account, and correlation be made on the load equals to the past maximum load level at the end of the first test method. On the other hand, when RLT and SLT are performed on two separate neighbouring piles, both RLT and SLT results show very similar virgin loading cycle responses when soil and pile conditions are similar and consistent. For split up of toe resistance and shaft friction additional embedded instrumentation is required for RLT similar as for SLT.

RAPID LOAD TESTING IN EUROPE, SINGAPORE AND MALAYSIA

RLT has been applied in Europe since 1990 in the Netherlands, UK, Germany and Belgium and hundreds of piles have been tested since. RLT was first introduced in Malaysia and Singapore some 20 years ago (Chow et al., 1998). Over 1000 RLT via Statnamic tests have been performed very successfully, in which over 100 SLT-RLT correlation tests were conducting using Statnamic method. To date (October 2016) hundreds of piles have been tested by RLT via StatRapid method in Singapore and Malaysia in which several tens of SLT-RLT correlation tests were correlated with StatRapid method. A number of SLT correlation tests were conducted with strain gauges installed along the shaft for load transfer determination. The results of these correlations show that for Singaporean soil and pile conditions, results from the UPM interpretation method of RLT results give a good approximation to results from SLT, even without the application of any correlation factors for loading rate effects. This is observed when piles are socketed into strong and competent material (with SPT N-values from 30 to 100) where majority of the pile capacity is derived from non-cohesive soil layers and the pile load-settlement behavior is still mostly elastic. This observation is also in-line with the correlation factor recommendations per Eurocode EN ISO 22477-10 recommending a correlation factor of 0.94 for piles installed in sand. Note that this correlation factor of 0.94 is with reference to the pile loaded close to the real ultimate static capacity of piles, where the settlement is significant. In cases where the load level is still within the initial elastic range, the settlement is still small and the correlation factor is close to 1.0.

CASE STUDY OF RLT-SLT CORRELATION TEST USING STATRAPID

Traditionally SLTs are used predominantly for pile design and proof load test regimes in Singapore and Malaysia. As part of the national productivity improvement drive, the authorities have allowed the use of RLTs for the replacement of SLTs as long as the correlation factors for the piles installed in similar soil can be established. These correlation factors are established with the conduct of a correlation test; usually by comparing load settlement results from SLT against RLT on the same pile or for neighbouring piles with the same geological formation. This paper discusses 3 case studies of which different sequences of testing were conducted:

(a) SLT first followed by RLT,

(b) RLT first followed by SLT,

(c) SLT and RLT applied on two separate neighbouring piles.

SLT followed by RLT (RLT by StatRapid Method)

A construction site for private development at 27 Tampines St 92 was secured for the research of the use of RLT (StatRapid method). This is labeled as “Tampines Project”. The SLT on Pile No. ULT-1 was conducted from 20/08/2013 to 23/08/2013 for up to 300% of the working load. This bored pile has

a diameter of 600mm and is 24.0m long with a design working load of 2.12MN. It was found that the settlement at 1.0 times working load is 3.7mm; the settlement at 2.0 times working load is 8.3mm and the settlement at 3.0 times working load is 15.7mm. The permanent settlement upon unloading at the end of the 3rd cycle was found to be 4.5mm.

The summary of load-settlement results from the SLT are presented in Figure 2.

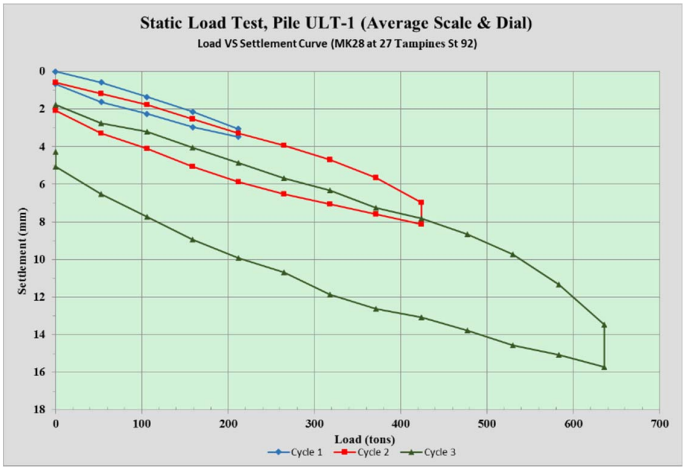


Fig. 2. Load-settlement results from ULT-1 by SLT (Tampines Project)

A multi-cycle StatRapid load test was conducted subsequently on ULT-1 on 2 September 2013 to determine the equivalent static load-displacement behavior of the pile. The RLT was performed with 4 load cycles up to around 3 times working load. A maximum StatRapid load of 7.0MN was applied to ULT-1 during the load test. The deployed drop weight and height as well as the spring system were based on predictions generated with the AllWave-RLT software, and these predictions were validated during the actual test. The summary of load- displacement plots for all RLT cycles are shown in Figure 3. The with UPM derived static load settlement results are presented in Figure 4.

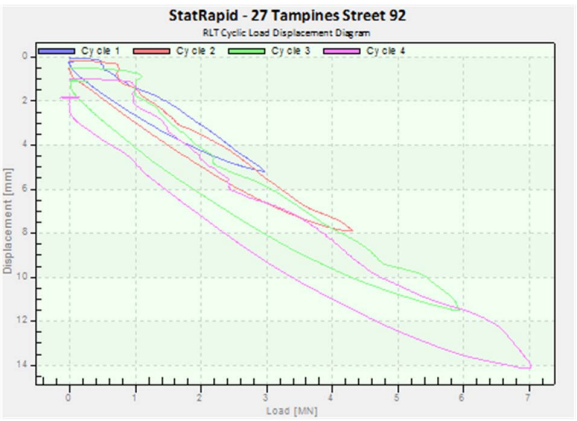


Fig 3. Load-settlement results RLT on ULT-1 (Tampines Project)

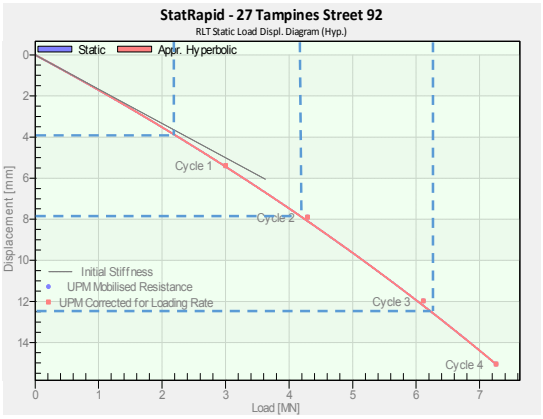


Fig 4. Equivalent static load-settlement results from RLT by UPM

It can be found that the settlement from RLT **at** 1.0 times working load is 4.0mm; the settlement at 2.0 times working load is 8.0mm, and the settlement at 3.0 times working load is 12.4mm. As RLT was conducted after the SLT with pile permanent residual settlement of 4.5mm, the RLT loading cycles should continue as "subsequent loading cycle", and the comparison should be made after taking into account the permanent residual settlement. The summary of the RLT results as "virgin loading cycle" and as "subsequent loading cycle" are shown in Table 1.

Table 1. Tampines Project ULT-1: Comparison of SLT and RLT (StatRapid)

Times of Working Load	Applied Load [A]	Settlement from Static Load Test using Kentledge method [B]		Settlement from StatRapid Method - As "virgin loading cycle" (mm) [D]	Settlement from StatRapid Method – taking into account residual settlement (mm) [E = D+C]
		Settlement (mm) [B]	Residual Settlement (mm) [C]		
1	2.1 MN	3.7	-	4.0	-
2	4.2 MN	8.3	-	8.0	-
3	6.3 MN	15.7	4.5	12.4	16.9

The simplified soil profile is shown in Figure 5. It is noted that majority of the pile is installed in hard sandy soil with N > 12, with more than half of the length in N > 50. The RLT load-settlement curves showing the unloading point very close to the maximum StatRapid load.

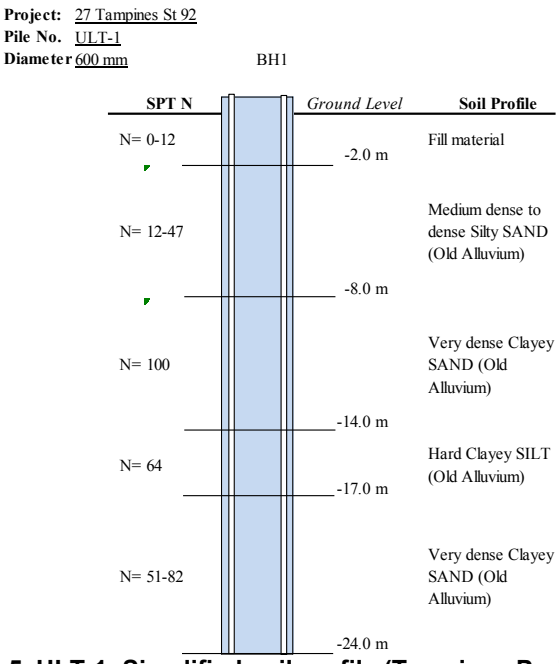


Fig 5. ULT-1: Simplified soil profile (Tampines Project)

The SLT and RLT results gave the settlement value of 15.7mm and 16.9mm respectively at 3.0 times of working load. It is clear that the RLT (StatRapid) results correlate well with the static load test results (SLT) without the use of a loading rate factor for this site after accounting for the residual settlement from the previous loading from the SLT.

RLT (StatRapid method) followed by SLT

A correlation test between SLT and RLT (StatRapid) was conducted at 6 Derbyshire Road, a private high rise residential development project. This is labeled as "Derbyshire Road Project". The authorities requested for StatRapid load test to be conducted first, so as to have a Class A prediction results as comparison with SLT load settlement results to be obtained later.

The RLT was conducted on Pile No. P41 for up to 200% WL on the 16th of July 2015. This bored pile has a diameter of 1000mm and is 48.6m long with a design working load of 5.57MN. From the RLT load test, it was found that the settlement at 1.0 times working load is 7.0mm and the settlement at 2.0 times working load is 16.0mm. The cumulative permanent residual settlement upon RLT loading and unloading was found to be 2.5mm. The summary of the RLT load cycles, corresponding UPM results and simplified soil profile of P-41 are presented in Figures 6, 7 and 8 respectively.

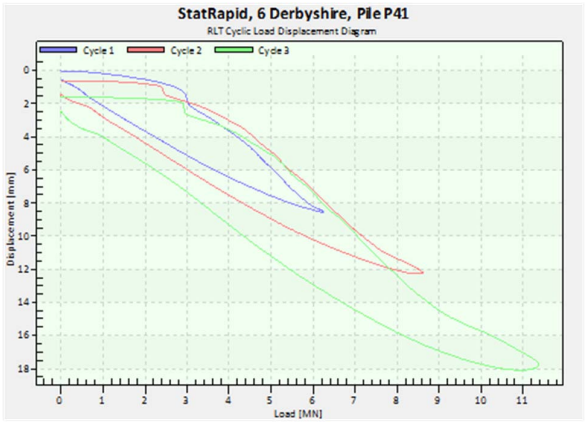


Fig 6. Load-settlement results from P-41 by RLT (Derbyshire Road Project)

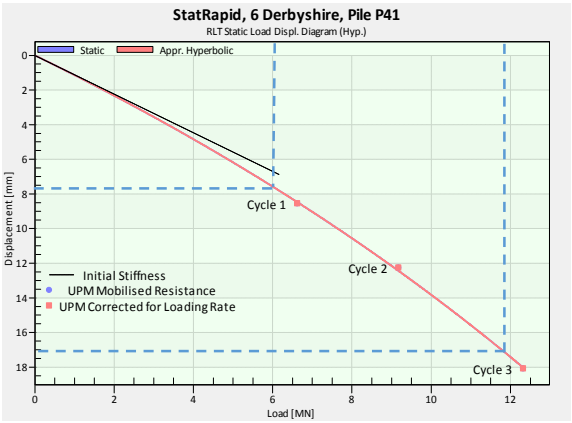


Fig 7. Equivalent static load-settlement results from RLT by UPM

Project: 6 Derbyshire Road
Pile No. P-41
Diameter: 1000 mm BH6

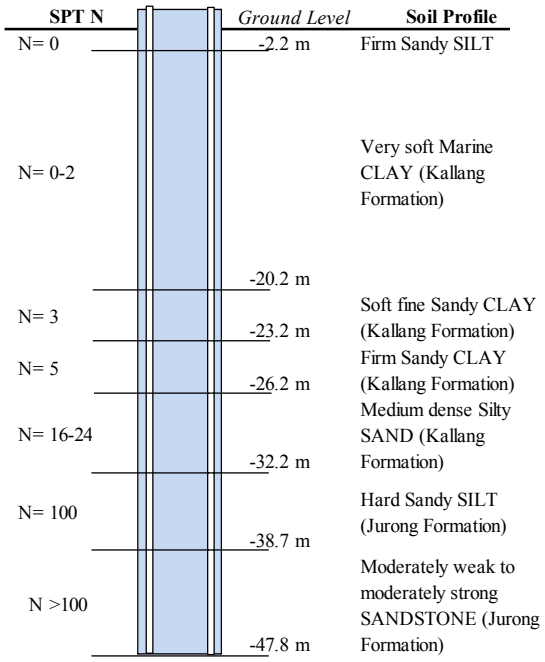


Figure 8. P-41: Simplified soil profile (Derbyshire Road Project)

The StatRapid final report was submitted to the client on the 24th July 2015 and the SLT was allowed to commence after this date. The SLT on Pile No. P-41 was conducted from 24th August 2015 to 28th August 2015 for up to 200% of the working load. It was found that the settlement at 1.0 times working load is 6.5mm; the settlement at 2.0 times working load is 13.5mm. The permanent settlement upon

unloading was found to be 1.5mm. The summary of load settlement results from the SLT are presented in Figure 9.

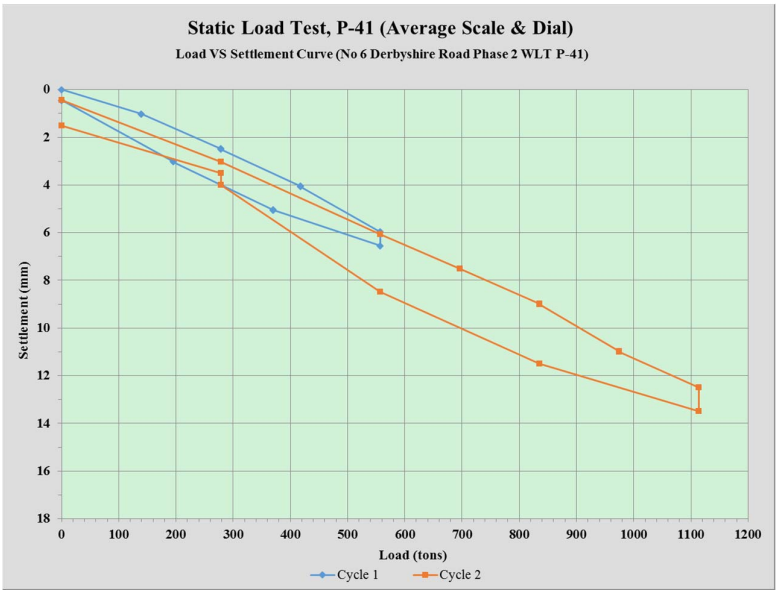


Fig 9. Load-settlement results from P-41 by SLT (Derbyshire Road Project)

As SLT was conducted after the RLT with pile permanent residual settlement, the SLT loading cycles should continue as "subsequent loading cycle". The summary of the SLT results as "virgin loading cycle" and as "subsequent loading cycle" are shown in Table 2.

Table 2: 6 Derbyshire Road P-41: Comparison of RLT and SLT

Load Cycle	Applied Load [A]	Settlement from StatRapid Method [B]		Settlement from Static Load Test using Kentledge method - As "virgin loading cycle" [C]	Settlement from Static load test - taking into account residual settlement (mm) [D = C+B]
		Settlement (mm)	Residual Settlement (mm)		
1	1.0xWL (5.57MN)	7.0	-	6.5	-
2	2.0xWL (11.14MN)	16.0	2.5	13.5	16.0

For this project, both SLT and RLT results gave the settlement of 16.0mm at 2.0 times the working load. Thus, it is clear that the RLT results correlate perfectly with the SLT results without the use of a loading rate factor for this site after accounting for the residual settlement from the previous loading method.

Thus, it can be concluded from this project that for piles installed in soft clay followed by hard sandy material, most of the shaft friction and end bearing were derived predominantly from the sandy material. Hence, effects of loading rate effects appear to be negligible.

SLT and RLT on two separate neighbouring piles with the same soil profile

A StatRapid load test was performed on a bored pile at Henderson Road, for the construction of high-rise residential project. This is labelled as "Henderson Road Project". A correlation exercise was

conducted on the RLT (StatRapid) results against two SLT conducted earlier on two separate neighbouring piles installed in similar soil profiles.

The RLT load test was conducted on Pile No. P-37 for up to 200% WL on the 16th of July 2015. This bored pile has a diameter of 1300mm and is 29.4m long with a design working load of 9.75MN. From the RLT load test, it was found that the settlement at 1.0 times working load is 1.6mm and the settlement at 2.0 times working load is 5.2mm. The cumulative permanent residual settlement upon RLT loading and unloading was found to be 2.5mm. The summary of the RLT load cycles, and corresponding UPM results of P-37 are presented in Figures 10 and 11 respectively.

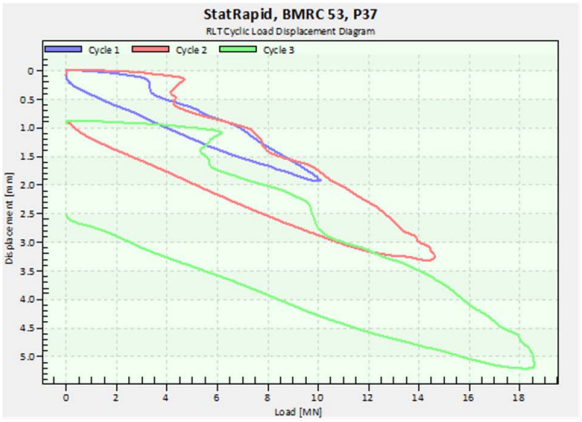


Fig 10. Load-settlement results from P-37 by RLT (Henderson Road Project)

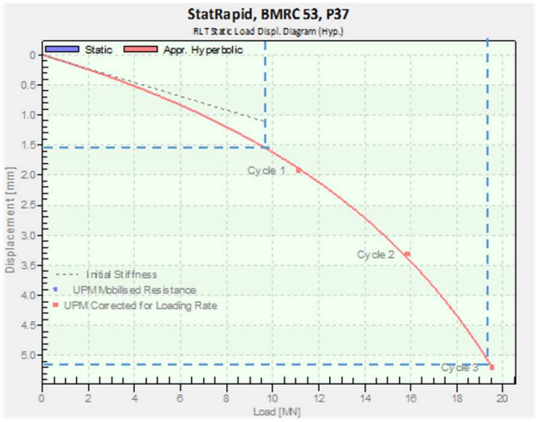


Fig 11. Equivalent static load-settlement results from RLT by UPM

The correlation review exercise was performed on the 12th August 2014 on piles iULT-4 and iULT-5 which were installed into similar soil profiles. The soil profiles of P-37, iULT-4 and iULT-5 are presented in Figure 12.

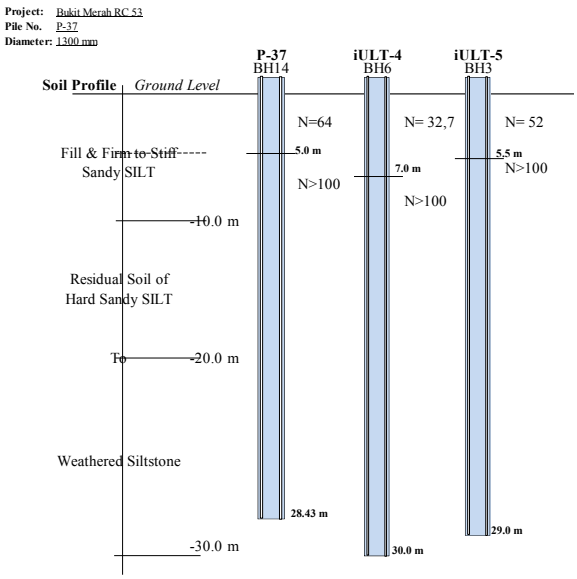


Figure 12. P-37, iULT-4 & iULT-5: Simplified soil profile (Henderson Road Project)

The comparison of the load-settlement behaviour of these three piles, with different pile diameters, has to be done on settlement normalised by the pile diameter. The summary of the settlement over pile diameter, at 1.0 time and 2.0 times working load, for these three piles are given in Table 3.

Table 3: Henderson Road Project: Comparison of P-37 (RLT) and iULT-4/5 (SLT)

Pile Ref.	Method of Testing	Pile Diameter [mm]	Settlement / Pile Diameter @ 1.0xWL [%]	Settlement / Pile Diameter @ 2.0xWL [%]	Simplified Soil Profile Description (Pile penetration into)
P-37	RLT	1300	0.13	0.40	~5m of N=20-70, and 23.4m of N=100
iULT-4	SLT	1500	0.17	0.37	~7m of N=20-70, and 23.0m of N=100
iULT-5	SLT	1500	0.12	0.30	~5.5m of N=20-70, and 23.5m of N=100

It was revealed that the soil profile for P-37 based on nearest BH of BH14 is indeed very much similar to that of BH6 (near to iULT4) and BH3 (near to iULT5). They are having the same pattern of soil profile with almost the same thickness of socketing N>100 material (about 23 m). Hence, these three piles (P-37, iULT4 and iULT5) are having very similar normalised settlement at 1.0xWL and 2.0xWL. This indicates that the pile load-settlement behaviour by RLT and SLT are very well correlated, after normalising the results to take into account different pile diameters. Hence, pile P-37 can be considered as "correlating very well" with static pile load test iULT4 and iULT5.

Thus, it can be concluded that for piles installed in pre-dominantly sandy material (where most of the shaft friction and end bearing derives from this material), effects of loading rate effects appear to be negligible.

CONCLUSIONS

The Rapid Load Testing (RLT) method including Statnamic and StatRapid have gained popularity in Europe and Asia because of the consistent and user independent results that correlate well with static load testing (SLT) results, the economic advantages, the reduction in testing time and the limited space requirements.

The interpretation method for RLT based on the Unloading Point Method (UPM) is a simple interpretation method, yielding a unique user independent result for the prediction of the equivalent static load-settlement behavior of a foundation pile.

A number of correlation tests between SLT and RLT have been performed for a variety of soil types. Some correlation tests were conducted on single pile with SLT loading first followed by RLT, while other tests were performed with RLT first followed by SLT. There are also correlation test conducted on two separate neighbouring piles using SLT and RLT respectively.

Most of the piles in Singapore are designed to have piles socketed into dense sandy soil or very stiff residual soil or rock with SPT higher than 100 and the settlement criteria for these pile are very stringent. As a results, piles are designed with much higher factor of safety in terms of bearing capacity.

Hence, the loading rate effect is negligible in this situation, even when the soil profile contains deposits of soft clay. Due to the relatively low pile velocities, the Unloading Method (UPM) can therefore be applied without a loading rate correlation factors.

Care has to be taken when comparing the settlement behavior of piles loaded as "virgin load cycle" and that loaded as "subsequent loading cycle". The settlement of "subsequent loading cycle" should take into account the final permanent residual settlement of the previous "virgin loading cycle".

A number of correlation tests were conducted in Singapore at three different sites with different soil profiles. The results showed that RLT results correlate very well with SLT results, after taking into account the loading sequence, and the settlement normalized by the pile diameter. All these piles derived their capacity predominantly from sandy material; hence no loading rate factors had to be used in these cases.

REFERENCES

Brown, M.J. & Powell, J.J.M. 2013. Comparison of rapid load test analysis techniques in clay soils. ASCE Journal of Geotechnical & Geoenvironmental Engineering **139**, 152-161.

Chew, S.H., Middendorp, P., Bakker, J., Chuah, G., 2015, Recent advances of rapid load testing in Asia and Europe, Proceedings of the XVI European Conference on Soil Mechanics and Geotechnical Engineering (ECSMGE)XVI ECSMGE 2015.

Chow, Y.K.,Chew, S.H.,Chow,W.M. Chuah, L.S. 1998. Case Histories of Statnamic Pile Load Test. Thirteenth Southeast Asian Geotechnical Conference,Tapei, Taiwan.pp 479-484

Deutsche Gesellschaft für Geotechnik, 2012. Recommendations on Piling. (EA-Pfähle), ISBN 978-3-433-03018-9, 221-224, Ernst & Sohn. Germany.

Gonin, H., Coelus, G., Leonard. 1984. M.S.M. Theory and performance of a new dynamic method of pile testing, Proceedings of the Second International Conference on the Application of Stress Waves on Piles, Stockholm, Balkema Rotterdam, NL

Herten, M., Baeßler, M., Niederleithinger, E., Georgi, S. 2013. Evaluation of Dynamic Load Testing on bored piles. (Bewertung dynamischer Pfahlprobebelastungenan Bohrpfählen), Pfahl-Symposium, Braunschweig, 2013.

Holscher, P, Tol A.F. van & Brown, M.J. 2010. European standard and guidelines for rapid load testing on piles. In DFI and EFFC pp. 1-8 Deep Foundation Institute.London, UK

Middendorp, P.; Bermingham, P. And Kuiper, B. (1992). Statnamic load testing of foundation piles, Proc. 4th Int. Conf. Appl. Stress-Wave Theory to Piles, The Hague, Rotterdam, Balkema.

ISO/DIS 22477-10:2015. Geotechnical investigation and testing - Testing of geotechnical Structures - Part 10: Testing of piles: rapid load testing.

Rapid Load Testing on Piles, Interpretation Guideline, 2010. Cur publication 230, CUR Commission H410, CRC Press, ISBN: 978-0-415-69520-6, the Netherlands, 2010

Stahlmann, J., Fischer,J., Middendorp, P. 2012. Rapid Load Test and Dynamic Load Test - A comparison (Rapid-Load-Tests und dynamische Pfahlprobebelastungen – Ein Vergleich). Baugrundtagung 2012, German Geotechnical Society.

Viana da Fonseca, Santos, A.J.A. 2008. International Prediction Event, Behaviour of CFA, Driven and Bored Piles in Residual Soil Experimental Site – ISC, 2,September 2008 / 240x170 / 688 pages ISBN: 978-972-752-104-3 ISBN: 978-989-95625-1, 2008

GROUND IMPROVEMENT BY DYNAMIC REPLACEMENT WITHIN INTERTIDAL MANGROVE MUD ENVIRONMENT, ICHTHYS LNG, DARWIN

D. MITCHELL, Deputy Director, John Holland Territoria Civil, Darwin, NT, Australia, Daniel.Mitchell@jhg.com.au

P. VINCENT, Managing Director, Menard Oceania, Sydney, NSW, Australia, pvincent@menard.com.au

J. RACINAIS, Technical Manager, Menard, France, jerome.racinais@menard-mail.com

ABSTRACT

In September 2011, Menard Oceania (MO) was engaged by Mac Mahon John Holland Joint Venture (MJHJV) to provide ground improvement solution for the $34bn Ichthys LNG development. With close to 400,000m2 of mangrove swampland set to be reclaimed and improved, this project was a great opportunity to showcase the technical, commercial and environmental benefits that Dynamic Replacement (DR) ground Improvement technique can provide. The ground improvement works involved complete design and construction for the Ichthys LNG site located at Blaydin Point on a low lying peninsula in Darwin Harbour. Dynamic replacement and stone columns technique were selected to treat intertidal mangrove mud to achieve required bearing strength, stability and limit settlement to an acceptable levels. The site is underlain by a 3m to 5m thick layer of highly organic mangrove muds with very soft shear strength ranging from 0kPa to 12kPa at depth. The site is exposed to daily sea water level tidal variations of up to 8m, which created significant constructability constraints and slope instability risks. This paper presents the design philosophy, the process involved in the selection of the construction methods, the site constraints encountered during the works and a review of the results achieved, quality control and post constructions performance.

Keywords: Ground improvement, dynamic replacement, maritime environment, mangrove muds, pressuremeter tests

INTRODUCTION

Inpex Browse, Ltd (Inpex) and its partner Total are developing the Ichthys gas field to pipe gas to onshore facilities at Blaydin Point on the south side of East Arm in Darwin Harbour. The proposed LNG plant consists of gas receiving facilities, 2 x 4.2Mtpa nominal capacity LNG trains, LPG and condensate production facilities, product storage and export facilities, a module offload facility (MOF), a flare pad (FP) and associated off plot facilities.

The proposed on-shore facilities are located on extremely soft intertidal mangrove muds, therefore an appropriate ground improvement was required to achieve required strength and stability of site works and limit long term settlement to an acceptable level.

Various ground improvement techniques were studied to select the most suitable for the ground conditions and site constraints encountered at the Blaydin point site. Dynamic replacement technique was selected for onshore section to improve soft mangrove mud to depths of 5.5m and Stone Columns (SC) technique was selected for MOF off-shore section to improve intertidal deposits to a depth of 2.5m.

This paper presents DR design and construction works performed between December 2012 and August 2013 at Flare Pad Area.

SITE LOCATION

The proposed onshore gas plant site is at Blaydin Point which is on the peninsula of Darwin Harbour. The Blaydin Point peninsula covers an area of about 200ha and is vacant Crown land. The north, east and west boundaries of the site are surrounded by water. The southern boundary extends to the junction of the site access road with sealed road to Wickham Point.

The Flare Pad is a discrete area located to the west of the Plant Site and linked by an earth fill causeway. The flare pad consists of an earth and rock filled pad with surface dimensions of approximately 165m x 577m and connected to the plant site by a causeway. The flare pad area (including flare causeway), is raised above the mudflats by 3.0m to 4.0m to a maximum finished level of +6.2 m Australian Height Datum (AHD) at the pad centre with appropriate grading to pad perimeter for stormwater drainage.

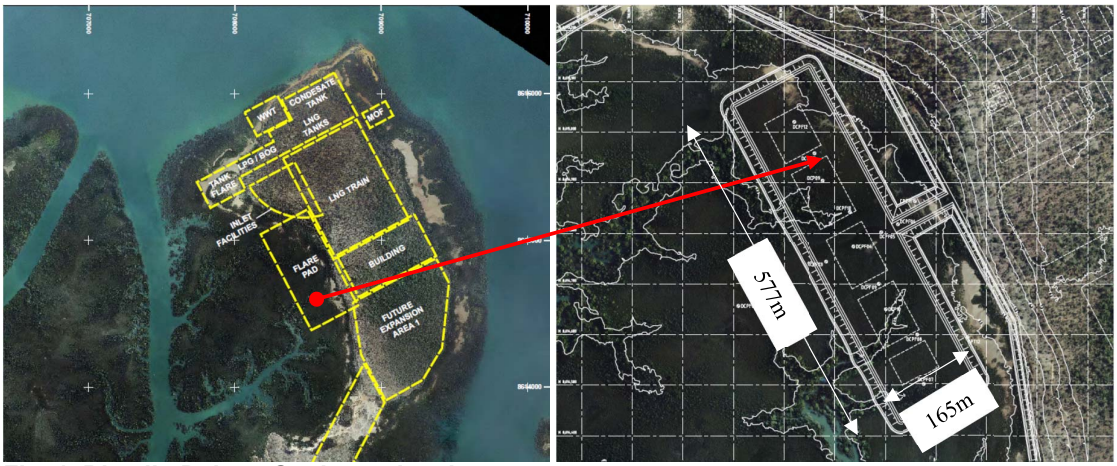


Fig. 1. Blaydin Point – Onshore plant layout

PROJECT REQUIREMENTS

Ground treatment was designed to improve existing soft marine clay or mud soils such that improved ground may safely and effectively support the defined loads while achieving the specified design criteria for bearing capacity, stability and settlement over the design life of 28years.

General Loading

Ground improvement works were designed to achieve bearing capacity and specific performance criteria under 2.0m to 4.0m of imported fill, construction loading of 20kPa applied up the platform edge and 50kPa applied to 10m of the platform edge. Permanent load of 6kPa was applied to within 10m of the embankment edge. Figure 2 shows the typical loading conditions to be assumed at design stage within the Flare Pad footprint.

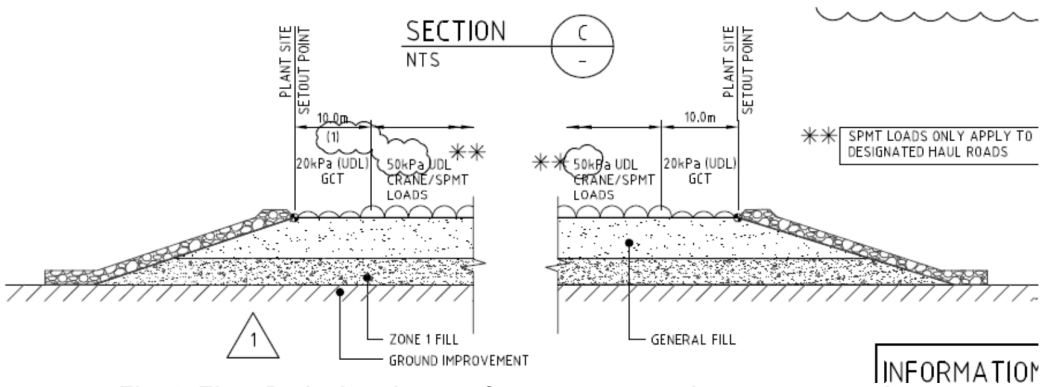


Fig. 2. Flare Pad – Load cases for temporary and permanent works

The flare pad also supports settlement sensitive structures like prefabricated pipe racks with pad footings and ground flares which each were surrounded by an enclosure fence approximately 20 metres in height supported on wide strip footings.

Design loads between 44kPa to 50kPa were applied at the base of the footings, approximately 1.0m below the finished ground surface. A loading of 47kPa for the ground flare enclosure fence was applied to 9.0m wide strip footings, approximately 2.2m below the finished ground level.

Allowable Ground Movements

The maximum ground movements for the finished surface in general plant areas over a 28 years design life was limited to those given in Table 1.

Table 1. Maximum ground movements.

Parameter measured at any point on the finished Plant ground surface	Design limit
Vertical Settlement - Non Settlement Sensitive areas (mm)	50
Vertical Settlement - Settlement Sensitive areas (mm)	40
Horizontal displacement (mm)	20
Differential settlement (-)	1:500 over a 25m chord

Environmental requirements

The Ichthys LNG project has very strict environmental control requirements and selected ground improvement method were required to minimise environmental impacts, including the impact on mangroves, preventing Potential Acid Sulphate Soils (PASS) disturbance, appropriately managing PASS and Acid Sulphate Soils (ASS), minimising turbidity, minimising waste production, discharges and dust generation.

TECHNIQUE DESCRIPTION

Dynamic Replacement (DR) method is a technique for improvement of highly compressible, organic and weak soils (Wong, 2004). During the works, the tamping energy drives granular fill material down into the compressible soils to form a large diameter soil reinforcement pillar, with a diameter of 2-3.5m. Stone pillars are formed by placing a blanket of granular fill material over the area to be improved, and then driven into the soil below by repeated tamping.

DR pillars are formed through a succession of tamping and back-filling sequences. DR pillars are formed by dropping a 20-25 tonnes weight pounder from a height of 10m-20m. This technique can deliver replacement ratios of up to 25%. A typical construction sequence is shown in Figure 3.

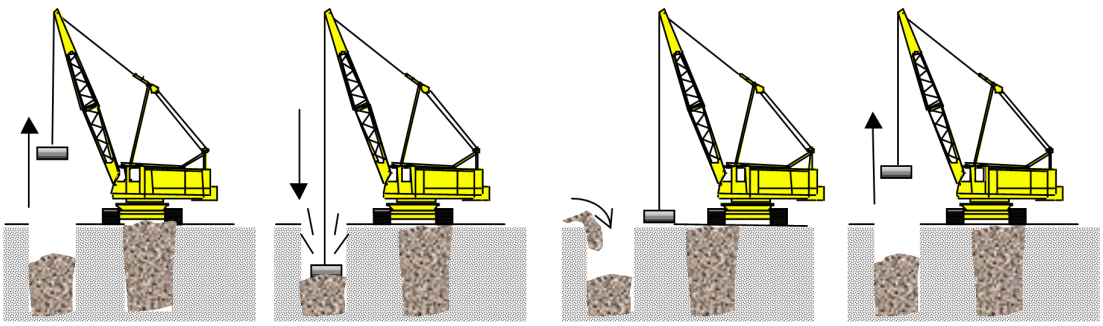


Fig. 3. Dynamic Replacement – Schematic of typical DR works sequence

Material used to form DR pillars was sourced from local quarry. DR material was specified as formed using granular fill with aggregate up to 500mm of nominal size with fines content less than 10% and free from organic inclusions. Aggregate size between 400mm to 500mm in size was restricted to within 5%. Photo of the supplied material is shown in Fig. 4.



Fig. 4. Blasted rock used for DR works and working platform

Table 2 shows design parameters adopted during design based on proposed quarry shot rock material.

Table 2. DR pillar parameters adopted to design.

Parameter	Pillar value
Uncompacted density γ (t/m3)	1.4 to 1.7
Natural friction of angle ϕ (degs)	35
Compacted friction of angle ϕ (degs)	42
Young modulus E (MPa)	40

The proposed parameters have been adopted based on past experience working with similar rock material within soft mud environment. These values have been verified by in-situ testing during an extensive calibration prior to production works commencement. DR pillar Young's modulus has been confirmed by PMT testing performed in the centre of the pillar. Internal friction of angle has been confirmed by measuring natural slope angle of the DR material stockpile. The measured stockpile slope angle varied between 36 and 38degress, hence satisfied design requirements.

GROUND CONDITIONS

Site Geology

The review of Darwin Regional geological sheet indicates that this area in underlain by Quaternary age marine alluvium overlying Early Proterozoic rocks of Finnis River Group, Burrell Creek Formation. Quaternary age deposits consist of intertidal marine muds, clays and silts, within a mangrove environment. Early Proterozoic rocks consist of shale, siltstone, phyllite and fine to very coarse sandstone.

The Flare Pad site is located on a low lying peninsula orientated north to south, which protrudes into Darwin Harbour. The coastline of the peninsula is fringed by tidal mud flats and mangroves. Immediately adjacent to the shore the mangrove area is sandy. Seaward from sandy mangrove areas, muddy mangrove areas and intertidal channels dominate. Vegetation is generally dense woodland fringed by densely vegetated mangroves, approximately 4m tall.



Fig. 5. Flare Pad area – Site conditions before clearing works

Geotechnical Parameters

An extensive geotechnical field investigation has been carried out by Inpex in three (3) phases. The scope of investigation undertaken included Cone Penetrometer Testing (CPT), Standard Penetration Test (SPT), Dynamic Cone Penetration (DCP), shear vane testing (SV) and geotechnical drilling to provide a general understanding of subsurface materials has been developed.

Based on the data gathered during 3 phases of the field investigation and subsequent laboratory testing, the ground profile has been found to comprise 2m to 6m of mangrove deposits, underlain by a 1m to 2m thick discontinuous lateritic horizon. The intertidal soils comprise very soft clays with extremely low bearing capacity and present a high acid sulphate soil risk. Underlying lateritic horizons comprise gravels, sands which are loose to medium dense. Fig. 6 presents typical geotechnical cross section through the pad.

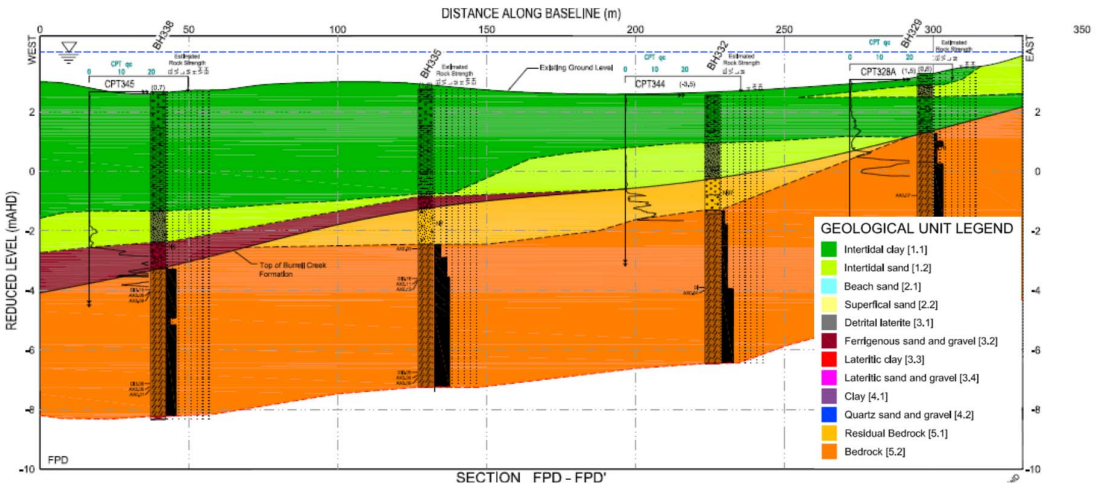


Fig. 6. Flare Pad – Geotechnical cross section in east to west direction

Interpretation of geotechnical investigation factual data has been performed using geotechnical correlations published in naval facilities engineering command design manual (1986). In addition, a parametric study of the geotechnical parameters has been carried out to derive the best fit parameters for intertidal muds. The results of this assessment is summarised in Table 3.

Table 3. Soil parameters adopted for Flare Pad site.

Parameter	Flare Pad
Moisture content W_n (%)	100-140
Liquid Limit W_L (%)	100
Unit Weight γ (kN/m3)	14
Vertical Permeability k_v (m/s)	$1.5x10^{-8}$
Compression Index C_{ce} (-)	0.329
Recompression Index C_{re} (-)	0.033
Creep Index C_{ae} (-)	0.011
Void Ratio e_0 (-)	3.5
Undrained Shear Strength s_u (kPa)	5 to 12
Layer thickness h (m)	2 to 5.5

GROUND IMPROVEMENT DESIGN

Settlement calculations

DR ground improvement was performed using two-dimensional finite element method (FEM) program PLAXIS v10. FEM was used to study short and long term settlement of improved mud/intertidal deposits beneath proposed embankment pad. The aim of the design was to estimate the required DR replacement ratio "a" to limit total settlements to levels in line with those prescribed in the performance specification.

The principle of axis-symmetrical FEM models centred on a DR pillar is to consider a given grid of pillars with a uniform load. The symmetrical properties show that it is equivalent to study just one pillar in a square mesh of same size on which equivalent portion of the load is applied (Priebe, 1995). It is although equivalent to study the problem for a pillar in a square or in a circle of same area. Then, thanks to the rotation symmetry, the problem is equivalent to a 2D model as shown on the following figure, where we chose R so that the following equation is met.

$$\pi R^2 = a^2 \qquad [1]$$

Where: R = 2D axi-symmerty model radius, a = square grid of pillars.

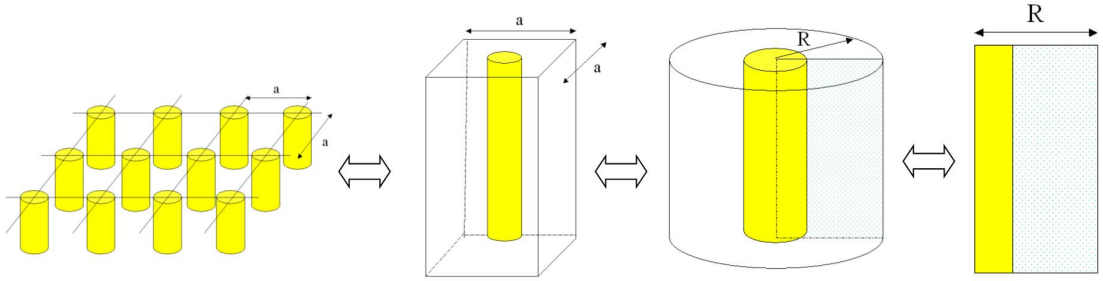


Fig. 7. DR square spacing representation in FEM axi-symmetrical analysis

The calculations for general plant area are carried out for each site investigation point (65 No.). The detailed design calculation at each location are performed in order to estimate settlement across Flare Pad area and verify differential settlement.

Based on the performed analysis, ground improvement using 2.5m diameter pillars at 5.0m x 5.0m was considered appropriate to support the pad during construction and for permanent case.

Figure 8 shows outcome of performed settlement analysis versus time. It has been estimated that for general area (non-sensitive) settlement during construction works will be between 200mm to 350mm.

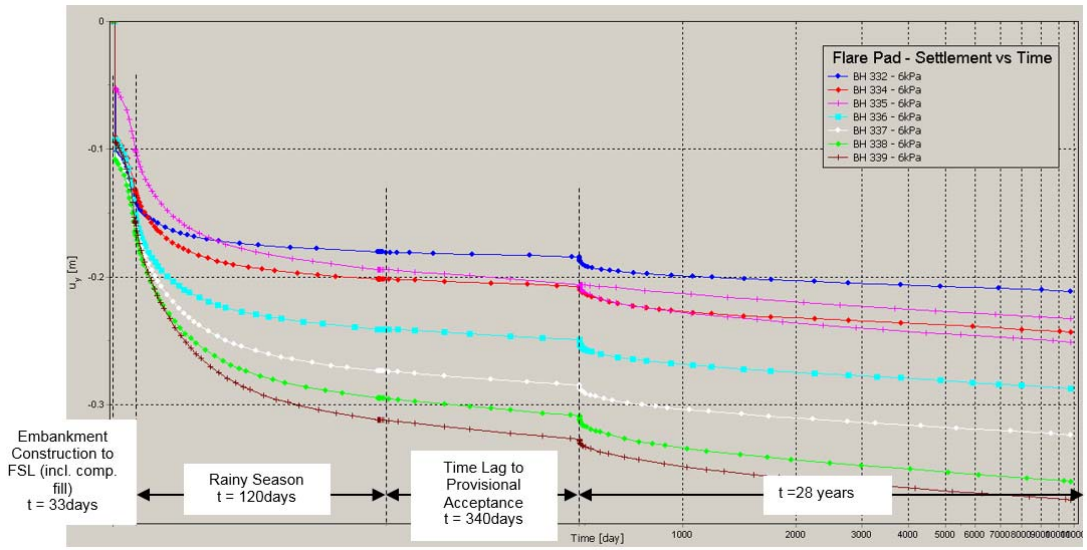


Fig. 8. Settlement vs time curves in logarithmic scale

The typical ground improvement arrangement for sensitive structures (pipe racks and ground enclosure) was unable to meet the tighter performance requirements. In order to meet long term settlement targets, a pre-loading surcharge of 1.0m thickness above final design level was proposed over the improved zone for a period of 4 months. Monitoring data yielded satisfactory ground movement in line with design predictions and following the 4 months of surcharging pre-load was removed and areas released for follow on works.

Slope stability calculations

The slope stability analyses carried out by MO validated that minimum required factors of safety against stability failure of all temporary, permanent and final constructed slopes and batters were satisfied. All possible tidal ranges have been considered, including highest (at +3.995m AHD) and lowest (at -4.105m AHD) astronomical tide, storm water levels for 1 in 100 years (at +4.90m AHD), 1 in 1000 years (at +6.00m AHD) and 1 in 10 000 years (+7.00m AHD) surge as well as rapid drawdown case for low tide with full effect of residual pore water pressures within embankments taken into account. Minimum safety factors prescribed for the design of the ground improvement works are presented in Table 4.

Table 4. Minimum required Factor of Safety against stability failure

Description of analyzed slope stability conditions	Minimum Factor of Safety against stability failure
Long term (drained)	1.5
Short term (undrained)	1.3
Earthquake	1.2

Storm surge – long term stability (drained)	1.2
Storm surge – short term stability (undrained)	1.1

Slope stability calculations, were carried out using commercially available Slope W software and using the Morgenstern-Price method. For DR treated soil layers an equivalent parameters method (Barksdale and Bachus, 1983) was adopted and the various parameters estimated accordingly.

The ground stress was measured at the middle of each treated layer in the local axi-symmetrical model. A typical value of coefficient "m" for DR works to assess slope stability was taken as m = a, for stability calculation under the embankment slope and m = 40% to 60% for stability calculation under the full weight of the embankment.

Based on the FEM axi-symmetrical analysis a value of m = 50% was derived and adopted in the slope stability assessment. The load transfer ratio coefficient "m" was reduced to m = a, under the outward 2/3 of the embankment slope length to take into account reduced effective overburden pressure and lack of confinement pressure from adjacent pillars.

Table 5. DR equivalent parameters within intertidal mud

DR – replacement conditions "a"	Equivalent unit weight	Equivalent cohesion (kPa)	Equivalent internal friction of angle (degs)
DR a = 20% (short term)	15	4.0	10.2
DR a = 25% (short term)	15.25	3.75	12.7
DR a = 20% (long term)	16	0	30
DR a = 25% (long term)	15	0	31
DR a = m (long term)	15	0	35

Figure 9 shows a typical results of the slope stability analyses around perimeter of the FP.

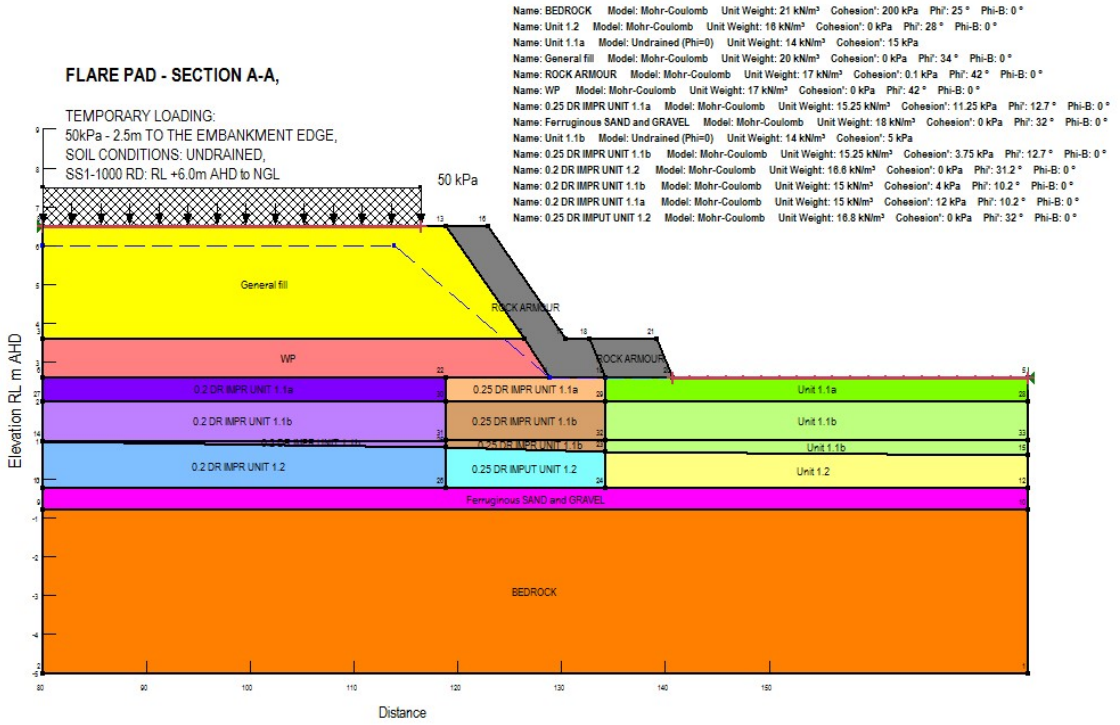


Fig. 9. Slope stability analysis using Slope W

As anticipated, the lowest factors of safety were calculated for short term (undrained) conditions for rapid drawdown cases and earthquake conditions for highest astronomical tide scenario.

CONSTRUCTION WORKS

Working platform construction

A working platform for construction works was required to support the 120t DC cranes used for ground improvement works as well as general construction loading of 10kPa for earth moving plant 20t to 30t excavators and dozers as well as 40t Moxy's.

In addition, placement of the platform and subsequently DR pillar installation was required to minimize environmental impact such as mud heave and potential disturbance on PASS soils.

Due to very soft strength of underlying mud (less than 15kPa), BRE 470 (2004) recommendations for working platform design for tracked plant could not be used. In order to safely design the working platform, FEM method of calculation was utilised with target factors of safety of 1.2. A minimum working platform thickness of 1.6m was found to be satisfactory to support construction plant.

The results of the stability assessment along the periphery of the platform indicated that a stability berm was required as well as working exclusions zones. Figure 10 highlights the working platform restrictions, in particular, placement in 1.0m thick layers only with a leading stability berm of 10m in length and associated plant exclusions.

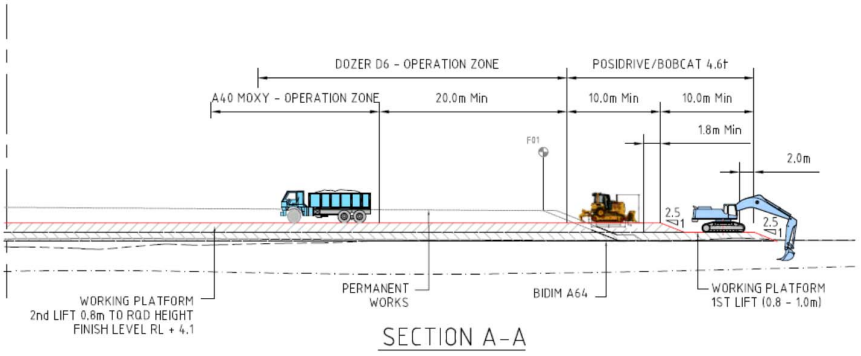


Fig. 10. Flare Pad – Working platform placement and plant restrictions

The creation of the peripheral stability berm was also providing a barrier preventing the outward movement of mud during placement of the inner platform materials thereby minimizing effects on surrounding mangrove vegetation. Based on results from the FEM analysis the required length of the leading berm was confirmed to be 10m in order to limit mud wave effect to less than 100mm within 10m of the working platform.

The additional function of the stability berm was to create confinement to DR installation. During DR works material that is pushed into the incompressible ground induces heave and lateral movement. The function of the 10m leading berm was to counterbalance soft mud waving and to prevent exposure of ASS/PASS soils.

Tidal influence

The Blaydin point is exposed to extreme tidal sea level variations. The highest astronomical tide and lowest astronomical tide based on the Australian Bureau of Methodology (www.bom.gov.au) for the

port of Darwin are +3.995m and -4.105m AHD respectively. Storm surge may cause considerably higher and lower levels, however these were not used in the design for temporary works.

MJHJV requirement was to construct a platform that would allow works to be carried out between highest astronomical tide (HAT) and lowest astronomical tide (LAT). To safely support construction plant the platform was required to be elevated 0.5m above HAT water level and minimum of 1.0m above to allow DR penetration. Elevating platform by 1.0m above HAT would have significantly increased the working platform cost, therefore platform elevation at +4.5m AHD (0.5m above HAT) was adopted during construction works. DR works during such extreme conditions were suspended. HAT tide occurs twice per month and only last a few hours, therefore it had a limited impact on the progression of the works.

Figure 11 shows typical tide level distribution for Ichthys site.

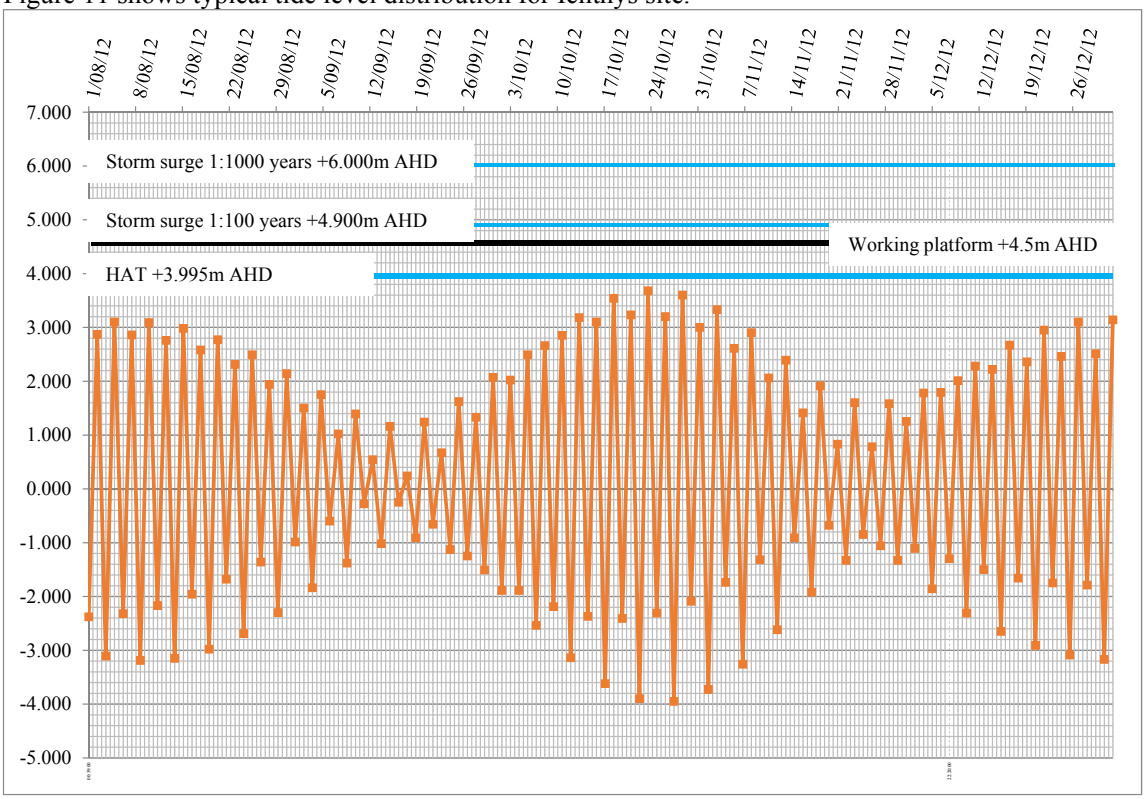


Fig. 11. Tide levels development in one month (October 2012)

Raising the platform too high was also posing a risk to the viability of the technique (penetration depth < 7.0m), reduction in productivity and a significant increase in required energy to penetrate through thicker platform.

The existing ground levels across the flare pad area varies between RL +2.0 to +2.5m AHD. Accounting for min 1.6m thick platform due to bearing requirement and/or 0.5m above HAT, the working platform thickness varied between 2.0m and 2.5m. These values were in the upper end of DR applicability.

During the production works it was discovered that two deep, but narrow creeks were fringing the Flare pad area with base at RL -0.5m AHD. Platform thickness in these areas was significantly increased from a nominal 2.0m to 5.0m.

To overcome this issue the construction methodology had to be amended. Pre-excavation down to platform base was required, followed by formation of the pillar to the required depth and closure of the pillar with pre-excavated material volume.

Environmental consideration

During the DR works in-situ material is displaced laterally while pillar is formed. In the pad centre the soil will move following the path of least resistance hence toward the ground surface, this material displacement generates platform heaving.

In order to assess the amount of heave generated during the performance of a DR pillar, Heave and Penetration Tests (HPT) was performed during the calibration works (Hamidi, 2014).

The tests indicated that after initial compaction of the working platform, the volume of heave increased fairly linearly and corresponded to approximately 60-70% of the incorporated material bulk volume. The graphic showing the measured heave volume vs material volume is presented in Fig. 12.

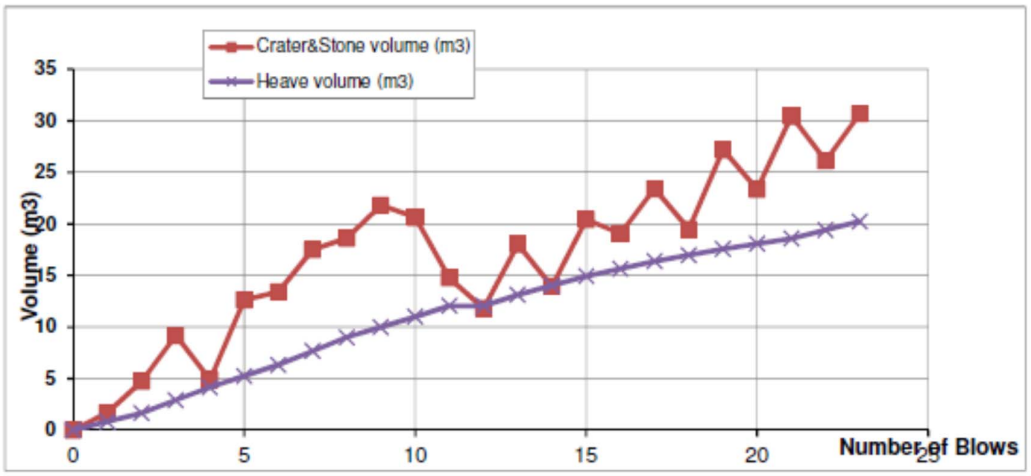


Fig. 12. Heave and penetration (HTP) test results

Following the HPT test completion the pillar was then checked to validate the diameter achieved using Down the Hole Hammer (DTH) drilling at its perimeter at 3 locations separated by 120 degrees to intercept rock fill. DTH drilling was also carried out in the middle of the DR print to verify the achieved depth. Based on tests performed a heave-height correlation was estimated.

$$H_H = \frac{65\% \cdot V_{bulk}}{S^2 - 0.25\pi D^2} = 32mm/m^3 \cdot V_{bulk} \qquad [2]$$

Where s = spacing of DR pillars (here 5m), D = DR pillar diameter, V_{bulk} = volume of backfill material.

The information derived from the HPT testing also allowed to estimate the required volume of rock to form DR pillar before excessive heave could be created.

During the extensive trial campaign, it was discovered that during DR penetration and under certain circumstances, uneven heave could be generated. This was posing an increased risk of resurgence and therefore exposure of ASS/PASS soils. It was found that such disturbance could be managed during the works as soon as particular ground behaviours were observed. The behaviour and proposed procedures covered scenarios where mud entered the crater below platform level, when mud started to punch through weaker points of the working platform and when mud punched through the working platform and became exposed. Figures 13 and 14 present typical trigger points observed and mud management procedures.

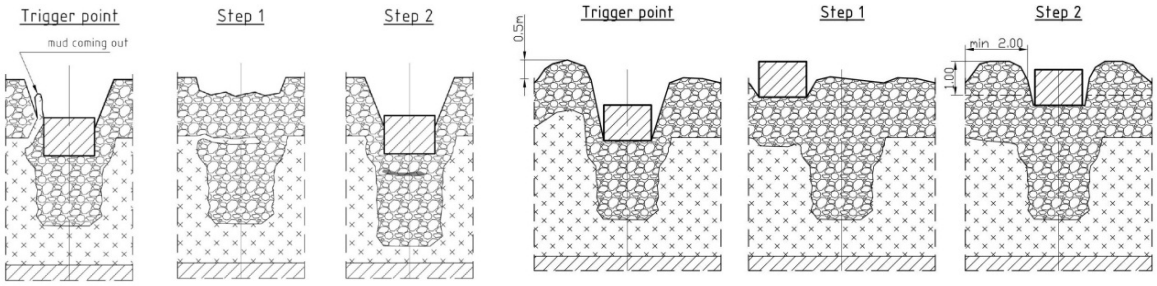


Fig. 13. Mud exposure control measure 1 and 2

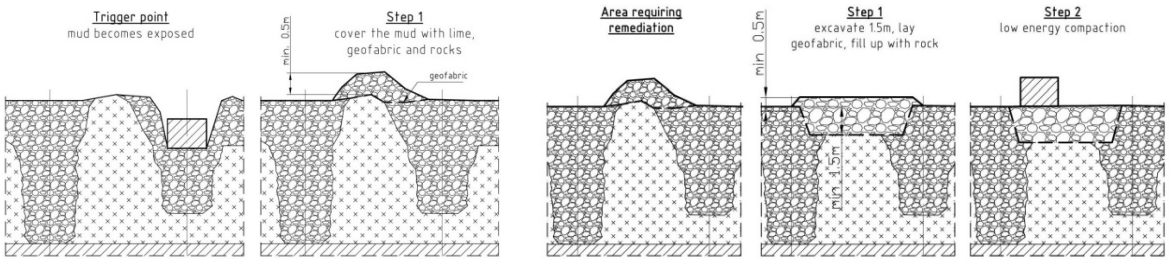


Fig. 14. Mud exposure control measure 3

TESTING AND MONITORING RESULTS

Ground improvement works testing

An extensive verification regime was adopted to confirm that the executed DR works will perform as per design expectations. **Table 6** presents the summarized ground improvement works verification program adopted for the Ichthys site.

Table 6. Testing regime adopted for Flare Pad site.

Test	Purpose	Frequency	Tested
DTH drilling	Pillar depth	-	182
DTH drilling	Pillar diameter	1 / 20,000 m^2	51
PMT	Pillar stiffness and depth	1 / 20,000 m^2	37
Heave and Penetration Test	To establish number and sequence of pounder drops to existing ground conditions	2 No	3
Plate Load Test	Pillar stiffness	2 No	11
General Fill Heave	To monitor platform movement around its periphery	Daily	Daily
QA from installation	To monitor stone usage and return pillar depth	Weekly	Weekly

Figure 15 photos of DTH drilling (left) and PMT testing performed on DR pillars.



Fig. 15. DR Testing – DTH drilling (left) and PMT testing (right) in progress

Testing results confirmed that DR pillars were installed to competent layer and achieved diameter in excess of 2.5m with an average across the site of 2.7m in diameter.

Instrumentation and monitoring

MJHJV carried out platform settlement and lateral movement monitoring over the period of the ground improvement works and post construction to the end of the Performance Guarantee (PG) period. The monitoring was required to confirm that design assumptions were met and that actual ground movements were within the levels predicted during the design phase.

Instrumentation consisted of installation and monitoring of Inclinometers (IN), Settlement Markers (SM); Settlement Plates (SP); Hydrostatic Profile Gauges (HPG) and Vibrating Wire Piezometers (VWP) spread over FP area as presented in Fig. 16.

.

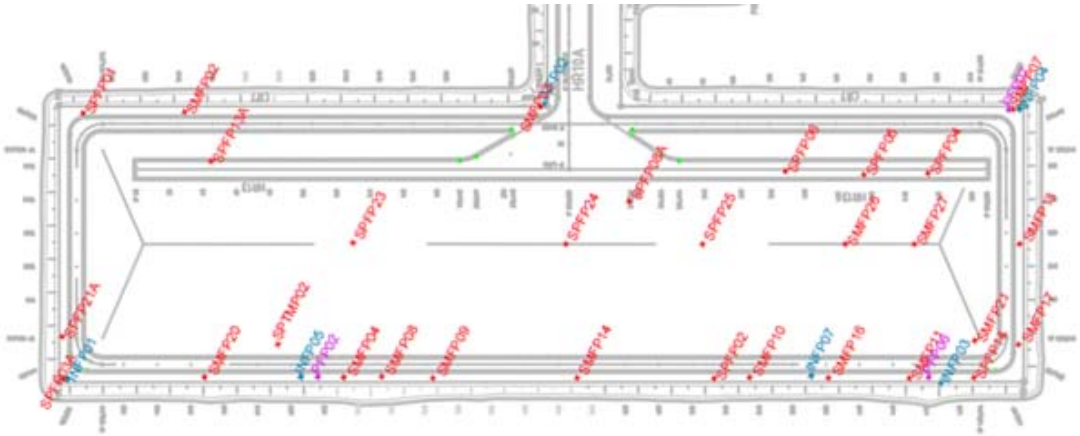


Fig. 16. Flare Pad – Instruments location for long term monitoring

Installation of monitoring points was not possible during the ground improvement works and prior to the placement of the embankment fill due to plant and equipment proposed to be used and the inability to obtain base readings, and sight lines during such works.

After discussion with all stakeholders, it was decided that the most reasonable action would be to monitor stone consumption during the works. The stone volume consumption would be used to indicate

to the design team presence of adverse ground conditions. The following indicators were set in instrumentation and testing plan (ITP).

- Stone consumption exceed 60% of theoretical quantities of stone or depth on any one column,
- Weekly average exceed 10% of theoretical quantities of stone or depth on any one column.

Following construction works, a three years post construction monitoring program was put in place in order to monitor settlement and to demonstrate that settlement predictions will continue to be met throughout the design life. The results of the monitoring are presented in Fig. 17.

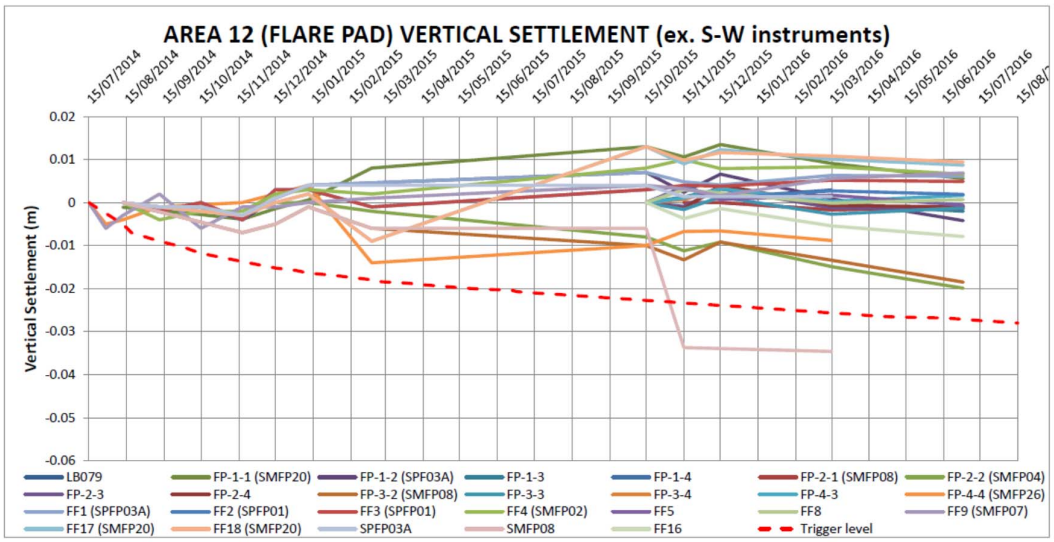


Fig. 17. Flare Pad – Results of long term settlement monitoring

The results show that settlement is well within design predictions represented by the red dashed line. Some of the points are showing slight heaving, they were located within areas previously surcharged and therefore experienced a level of rebound.

Lateral movement has been monitored using inclinometers installed as a minimum 1m away from the pad edge. The results in Fig. 18 show that deformation was within surveying tolerance and well within 20mm design limit.

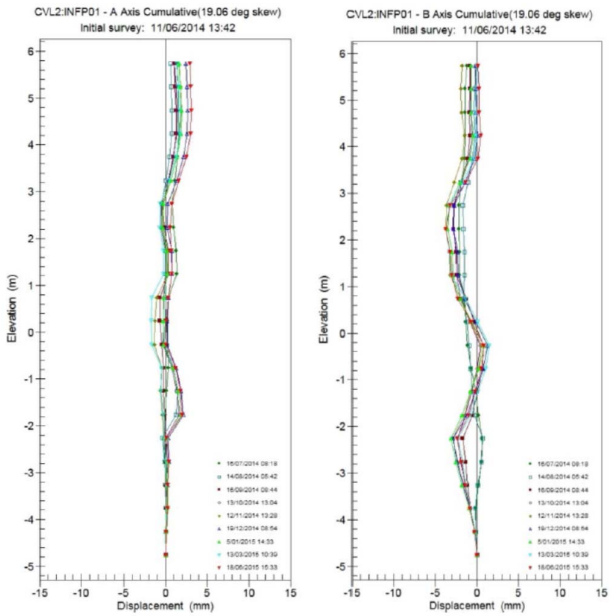


Fig. 18. Flare Pad – Inclinometer IN-01 results of long term horizontal movement monitoring

CONCLUSIONS

Dynamic replacement works was successfully completed in August 2012 after 12 months of construction works, with a treatment of approximately 350 000m2 of mangrove mud areas. During the DR works 330 000m3 of stone material have been used to form pillars and 340 000 blows performed to install pillars to competent substratum. The maximum depth of pillar confirmed by drilling was 7.8m which is the deepest recorded pillar executed by Menard in Australia.

The DR method of ground improvement created environmental and economic benefits because the excavation and replacement of ASS/PASS materials was avoided and in-situ disturbance minimized. Amongst other ground improvement techniques considered at the time (Deep Soil Mixing, Rigid inclusions), DR methodology is by far the fastest to implement, further the absence of requirement to use cementitious imported materials means that it is also the least generative of CO2 emissions.

The monitoring results two years following completion of the DR works have demonstrated the efficiency of the proposed concept and high quality of implementation achieved on site.



Fig. 19. Ichthys Site – Aerial photos taken in July 2012 (left) and July 2014 (right)

REFERENCES

Barksdale R.D., and Bachus R.C. (1983). Design and construction of stone columns. Federal Highway Administration Office of Engineering and Highway Operations, Volume I and II, Washington, DC.

BRE 470 (2004). Working platforms for tracked plant: good practice guide to the design, installation, maintenance and repair of ground-supported working platforms.

Hamidi B. (2014). Distinguished Ground Improvement Projects by Dynamic Compaction or Dynamic Replacement. Thesis for Degree of Doctor of Philosophy of Curtin University.

Naval Facilities Engineering Command. 1986. Soil mechanics – design manual 7.01.

Nyland G.W. and Gerner P.R. 1984. Engineering geology and foundation conditions in Darwin.

Plaxis version 2010. Finite element method software intended for 2D engineering, design and analysis of soil and rock.

Priebe H. 1995. The Design of vibro replacement.

Slope W version 2012. Limit equilibrium software for range of stability problems.

Wong P.K. and Lacazadieu M. 2004. Dynamic Replacement Ground Improvement – Field Performance versus Design Predictions for the Alexandria City Centre Project in Egypt.

Wong P.K. 2004. Ground improvement case studies – chemical lime piles and dynamic replacement.

MONITORING OF AN EMBANKMENT PROJECT USING RIGID INCLUSIONS AND VACUUM CONSOLIDATION DURING AND AFTER CONSTRUCTION

Stephen Buttling, National Geotechnical Consulting, Brisbane, Queensland, Australia. 0477 717 570
stephen.buttling@ngconsult.com.au
Zhong Rui, University of Wollongong, Wollongong, New South Wales, Australia. 0450 785 689
rzhong@uow.edu.au

ABSTRACT

A single unit gas fired power station was being built on the edge of the Gulf of Thailand in 2001. The soil conditions consisted of very soft to soft Holocene Marine Clay, and the site was part of a coast line which had been subsiding below high water mark for some time. In order to provide access around the power station a road system in a figure-of-eight formation was required, and this also needed to be above the design flood level, allowing for future settlement. A ground improvement scheme was proposed and constructed, which consisted of two spacings of prefabricated vertical drains (PVD) over two depth ranges, vacuum consolidation and pre-loading, and rigid inclusions.

During the construction phase, the vacuum consolidation was applied for 202 to 221 days in different zones, and monitoring allowed a prediction that the future settlement, including secondary consolidation over a period of 25 years, would be within the range of 175 to 355 mm, which met the contract requirement of less than 400 mm.

The power plant was completed and became operational in 2003. Monitoring of the road levels continued, as did the settlement, and in early 2010 the total settlement since the end of vacuum consolidation had reached about 800 mm. The monitoring data both during the ground treatment and for the following 7 years is presented and analysed. This is supported by numerical analysis using 3D finite element methods which shows good agreement with the measured data, and allows a preliminary explanation as to why the predictions were so far out.

Keywords: Embankments, Field testing and monitoring, Geotechnical engineering

BACKGROUND

After a period of bidding and negotiation, the Eastern Power and Electric Co Ltd (EPEC), an Independent Power Producer, entered into an agreement with the Electricity Generating Authority of Thailand (EGAT) in November 1997 to sell them power. In 1999 an Engineering, Procurement and Construction (EPC) contract and an Operation and Maintenance contract were signed with a supplier to provide a gas-fired (with oil as a back-up fuel) 350 MW combined cycle power plant in Bang Bo, Samut Prakarn Province, east of Bangkok. The site of the plant at Bang Bo is located immediately to the east of the Samut Prakarn Wastewater Treatment Plant, adjacent to the Gulf of Thailand (see Figure 1) in an area of very soft to soft marine clay (Bangkok clay) having low shear strength and potential for excessive settlement. The site layout comprises the main Power Plant components of generating block, cooling towers, fuel unloading area and storage tanks, switchyard and administration block, separated by access roads.

The major components of the plant were to be founded on driven precast spun concrete piles. Subsequent to technical and commercial proposals submitted in March 1999, the EPC contractor entered into a subcontract with Menard Soltraitement (Menard) on 3rd December 1999 to carry out supplementary ground investigation and detailed design of ground improvement to the very soft to soft marine clay. The requirement was to enable the soft clay to support the access roads without excessive settlement and with an acceptable factor of safety against slip circle failure. “Pre-engineering” carried out by Menard established that, between September and December 1999, the access roads had been covered with a layer of fill comprising boulders, cobbles, gravel and sand, that

was proven to be between 1.6 and 3.5 m in thickness. This had induced settlement, caused lateral displacement, and reduced the shear strength of the marine clay.



Fig. 1. Aerial view of the power plant looking south towards the Gulf of Thailand

Figure 1 shows how close the site is to the Gulf of Thailand, which is clearly visible in the top of the photograph. As a result, the protection of the site against ingress of the sea was of paramount importance. Predicted tide level information at Bang Pakong was available from the Royal Thai Navy for 2010. When this was converted to Mean Sea Level based on Chart Datum being – 1.9 m MSL, the data is as shown in Table 1.

Table 1. Relationship between levels to Chart Datum and Mean Sea Level

Water depths	Royal Thai Navy	Bang Pakong
High High Water 2010	3.40	+1.5m
Mean water depth/Mean sea level 2010	1.90	0.0m
Low Low Water 2010	-0.11	-2.01m

Since this data refers only to predicted tides for 2010, the Highest Astronomical Tide (HAT) at the project site of +1.9 m MSL as assumed in the design stage seems reasonable. Noting the soft and compressible nature of the soil, the EPC contract required that an allowance of 400 mm be made for future settlement, including secondary consolidation or creep, during the life of the plant, which was 20 years from the start of operation. To this was added an allowance of 500mm for freeboard, which gave a design level for the roads of +2.8 m MSL. The main objective of the ground improvement was therefore to control future settlement to be less than 400 mm in 25 years from the end of treatment, including secondary consolidation.

SOIL INVESTIGATION

A basic soil investigation was carried out for the EPC contractor, comprising 5 boreholes to a depth of 60 m and 1 borehole to a depth of 35 m below ground level, with Standard Penetration Testing (SPT)

at 1.5 m vertical intervals, or Shelby tube undisturbed sampling where appropriate. In addition, field vane shear tests were carried out at 4 locations to depths of about 24 m with a Geonor Vane, 2 mechanical CPT tests were carried out to depths of 25 m, and 2 CPTu (piezocone) tests were carried out also to depths of 25 m. Of these both of the CPTu tests, and the 35 m deep borehole, were located along the access road into the site from the main road, rather than within the site itself.

From the soil samples obtained the following identification tests were carried out:

- Soil classification
- Moisture content
- Atterberg limits
- Sieve analysis
- Wet and dry density
- Specific gravity

In addition, some of the samples recovered from the SPT split spoon were subjected to unconfined compression tests, while the Shelby tube samples were used for Unconsolidated Undrained (UU) Triaxial tests or oedometer one-dimensional consolidation tests.

Following the award of the ground improvement sub-contract, further soil investigation was carried out. This comprised 39 CPT tests, of which 9 were CPTu tests, and 10 dissipation tests, all carried out by Fugro, and 6 boreholes with 10 field vane shear tests, and extensive laboratory testing, carried out by Geo-Technology Consultants (GTC). In addition, GTC provided a 2-page memorandum summarising recommended design parameters based both on the results of the site-specific testing and their considerable experience in the area on other projects.

Figure 2 shows some of the results from the two investigations, where it can be seen that the Atterberg limit profile is typical for a very soft to soft marine clay, with moisture content close to or above the Liquid Limit for the upper 15 m; weight density showing very little scatter and a small rate of increase with depth; and the undrained shear strength from CPT and field vane shear testing showing little scatter but with results well below the normally consolidated clay line based on $s_u = 0.23\sigma'_v kPa$.

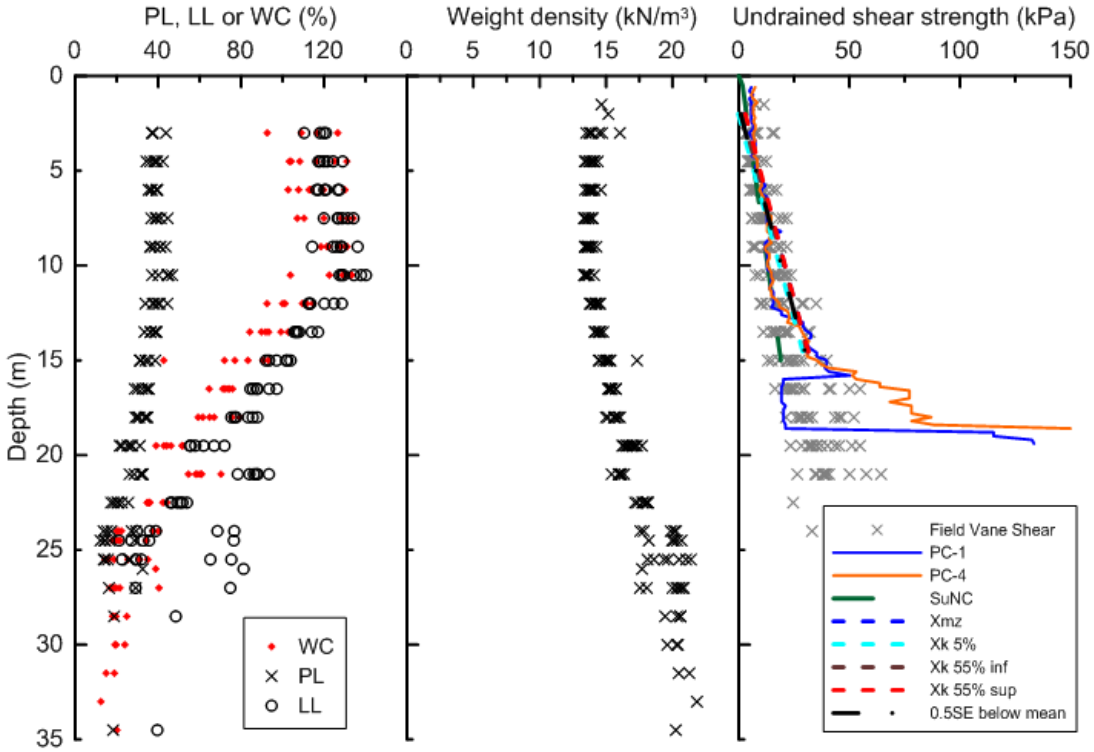


Fig. 2. Basic soil parameters from both investigations

DESIGN PARAMETERS

The design parameters used in the initial design are summarised in Table 2. There is the potential for confusion here because of different nomenclature used in different parts of the world. For example, in some places C_c is used for the Compression Index, C_r is used for recompression or C_{ur} is used for unload/reload, whereas in other places C_r is used for the Compression Ratio, defined as the Compression Index divided by $(1+e_0)$. That is true in this case, and it then becomes unclear whether the C_α values for secondary consolidation have also been divided by $(1+e_0)$.

Table 2. Design parameters used in initial ground improvement design

Layer	Thickness (m)	Weight density (kN/m^3)	Moisture content (%)	e_0	C_c	C_r	C_α	s_u (kPa)	c_v (m^2/yr)	c_h (m^2/yr)
1	5	14	125	3.4	1.41	0.32	0.005	4	0.8	0.8
2	5	14	120	3.4	1.41	0.32	0.005	8	0.7	1.5
3	5	14	92	3.01	1.28	0.32	0.004	17	0.8	1.5
4	5	16	80	2.17	1.01	0.32	0.004	26	0.9	1.5
5	4	16	55	1.44	0.78	0.32	0.004	33	0.9	1.5

GROUND IMPROVEMENT DESIGN

The ground improvement design has been described in detail in a paper by Masse et al (2002). This showed that, with the need to raise the site roads to +2.8 m MSL there was a requirement to place about 1.33 m of fill, plus another 3m to make up for expected settlement. The amount of fill posed major problems of embankment stability in the short term, and hence vacuum consolidation was used to (i) accelerate the consolidation process in conjunction with vertical drains, and (ii) achieve the required increase in undrained shear strength to permit the final embankments to have the required factor of safety of 1.5 against global instability.

The key features of the design centred around two aspects:

1. The significant amount of settlement expected due to the embankment loading, which was about 3 m in total;
2. The very low undrained shear strength of the upper layers of clay.

As a result, there were two distinct aspects to the ground improvement. These were:

1. The use of wick drains to shorten the drainage path length and hence the consolidation time, with load being applied through both vacuum consolidation and surcharging. This involved cylindrical vacuum drains, 10 m long and 50 mm in diameter on a square grid at 1 drain per 2 m^2, and also conventional prefabricated vertical drains about 100 x 5 mm, 20 m long and also on a square grid at 1 drain per 2 m^2 in the same pan area. This meant that there was one drain per 1 m^2 in the upper 10 m and 1 drain per 2 m^2 in the lower 10 m.
2. The use of the vacuum consolidation to increase the undrained shear strength of the very soft clay, and also the installation of Controlled Modulus Columns (CMC) to a depth of 10 m as rigid inclusions to increase the stiffness of the upper soil layers.

The procedure adopted for the first part of the design involved an iterative process to determine the 100% primary consolidation settlement, because of the need to allow for fill becoming submerged during the ground improvement work. This was illustrated as follows:

$$\Delta\sigma'_z = \gamma \cdot H_{fill} + \sigma_0 + \gamma' \cdot \Delta H_{primatysettlement}$$

$$\Delta H_{primarysettlement} = \frac{C_c}{1+e_0} \cdot H \cdot log\left(\frac{\sigma_0 + \Delta\sigma'_z}{\sigma_0}\right)$$

Through this procedure, plus the allowance for 25 years of secondary consolidation, the design settlement target to be achieved before stopping the vacuum consolidation was determined. The exact way in which the magnitude of the secondary consolidation was determined is not clear, but both the original design repost and the paper published by Masse et al (2002) state that the target was 160 mm. It is perhaps worthy of note that, when determining the target settlement to be achieved during the ground improvement period, the 400 mm of settlement allowed during the 25 year life was deducted from the predicted primary and secondary consolidation.

CONSTRUCTION WORK

The ground improvement work took approximately 1 year, from September 2000 to September 2001. The site was divided into 4 blocks, defined as Blocks 1, 2 and 3 and the Access Road, totalling about 10,000 m^2. The construction involved the following main steps:

1. Placement of sand blanket
2. Installation of vertical cylindrical vacuum pipes and band-shaped PVD
3. Installation of horizontal drains and connections
4. Placement of additional sand blanket and primary fill embankment
5. Excavation and sealing of peripheral trenches
6. Laying and sealing HDPE membrane
7. Connecting vacuum pumps to horizontal drains through membrane
8. Applying vacuum for three weeks
9. Placing secondary fill embankment
10. Continue vacuum while monitoring settlement, excess pore pressure, and lateral displacement

For Block 1, the vacuum was started on 23 December 2000, with fill being placed from 3 January to 30 March 2001, reaching a total height of 4.35 m. The vacuum consolidation period was expected to be about 4 – 5 months.

MONITORING DURING CONSTRUCTION

Extensive reports were submitted by Menard explaining the pre-existing situation, the design parameters, the design method, and what the future performance would be. A summary of the monitoring results is shown in Fig. 3. They also submitted reports showing that the treatment, especially the vacuum treatment, had been successful, that design targets had been met, and that the vacuum treatment could be ceased. The treatment was stopped in the 4 areas, Blocks 1, 2 and 3 and the Access Road, between 5 July and 20 August 2001. At that time the predicted future movement, including an estimated 160 mm of secondary consolidation, ranged between 95 and 355 mm.

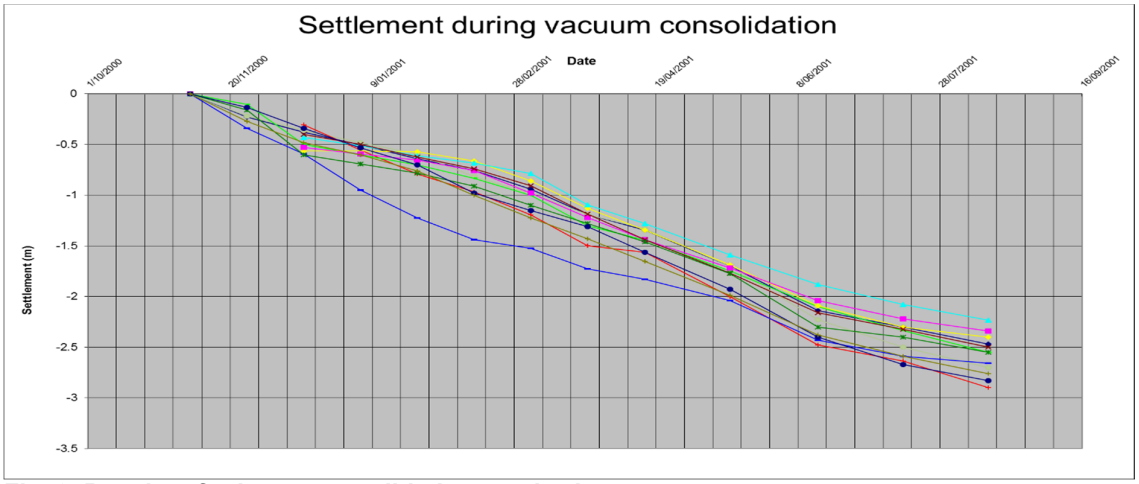


Fig. 3. Results of primary consolidation monitoring

MONITORING AFTER CONSTRUCTION

As a result of the reports submitted which suggested that future settlement would be well within the 400 mm allowed by the contract, and the confidence gained from the back-analysis using settlement data obtained during the 4 to 5 months of vacuum consolidation, the vacuum was turned off and the blocks handed over for subsequent placement of road pavements, kerbs and drainage. These were completed and the power station was opened in March 2003.

What is unusual about this ground improvement site is that post-treatment settlement monitoring commenced in May 2002, soon after the pavements had been constructed, and continued until March 2010, as shown in Fig. 4. During this time two survey companies were employed, and remedial works were carried out to pavements and kerbs, involving changes in levelling datum. Nevertheless, about 32 points around the road network were surveyed on a regular basis and the trend is clear. Based on all credible data over the period from May 2002 until March 2010, the average settlement increased from 2.86 to 3.52 m, which was nearly 1 m since the end of vacuum consolidation. Clearly this figure was well in excess of both the predicted post-treatment settlement, and the allowable figure of 400 mm. The result was that parts of the site became flooded at high tides, and the access road was in danger of going under water regularly.

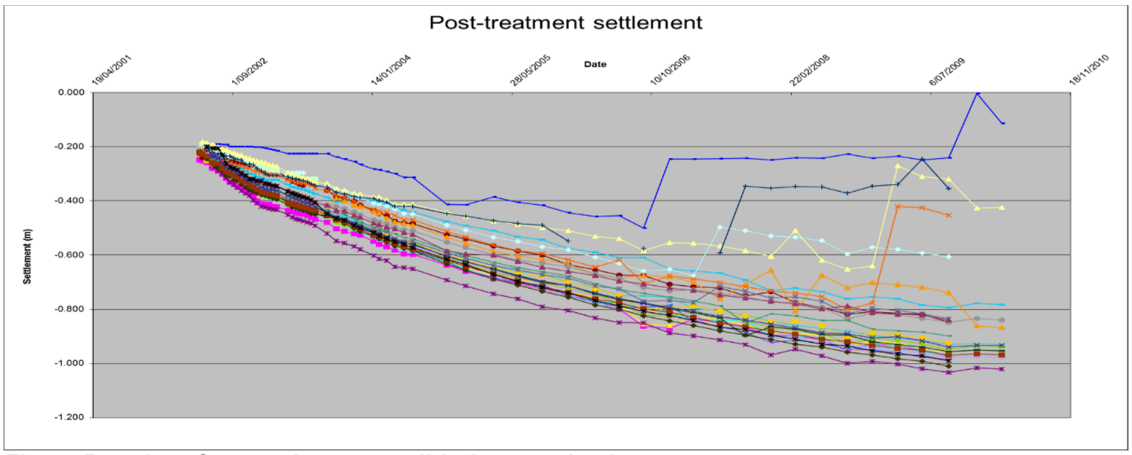


Fig. 4. Results of secondary consolidation monitoring

As a result, in early 2010 the EPC Contractor commissioned a report by an independent geotechnical consultant, who concluded that, although general surface subsidence in the area could not be ruled out as a contributing factor, it was necessary to remediate the roads in order to maintain the flood resistance of the site. After extensive analyses and discussions, it was agreed that removal of the pavement and the top layer of fill, followed by replacement with lightweight fill, would be the most cost effective method. A scheme was devised using lightweight concrete blocks, which were stacked in place by hand, as they were easy to handle and not subject to deterioration as a result of fuel oil spillage.

BACK ANALYSIS

Hand calculations

The monitoring data provided two sets of settlement records, one being rapid consolidation during the primary treatment phase with vacuum and surcharge, and the other being the post-treatment surveys comprising mainly secondary consolidation. It was necessary to manually connect the two since they had been recorded based on different benchmarks.

Figure 3 shows the settlement of 12 monitoring points during the vacuum consolidation. They are seen to be generally consistent with each other, apart from the initial rate of consolidation of Point 105 shown by the blue line, with a final range of between 2200 and 2900 mm.

Figure 4 shows the post-treatment settlement data for all 31 points monitored over a period of more than 7 years. Apart from 5 points which have apparent shifts, probably as a result of work done on the road or kerbs, the data is very consistent. The top two curves are slightly anomalous as they appear to show little settlement after December 2006, but the remainder show a consistent downward trend, even after they have been shifted. The range of settlement over the 7 year period is from about 600 to 800 mm.

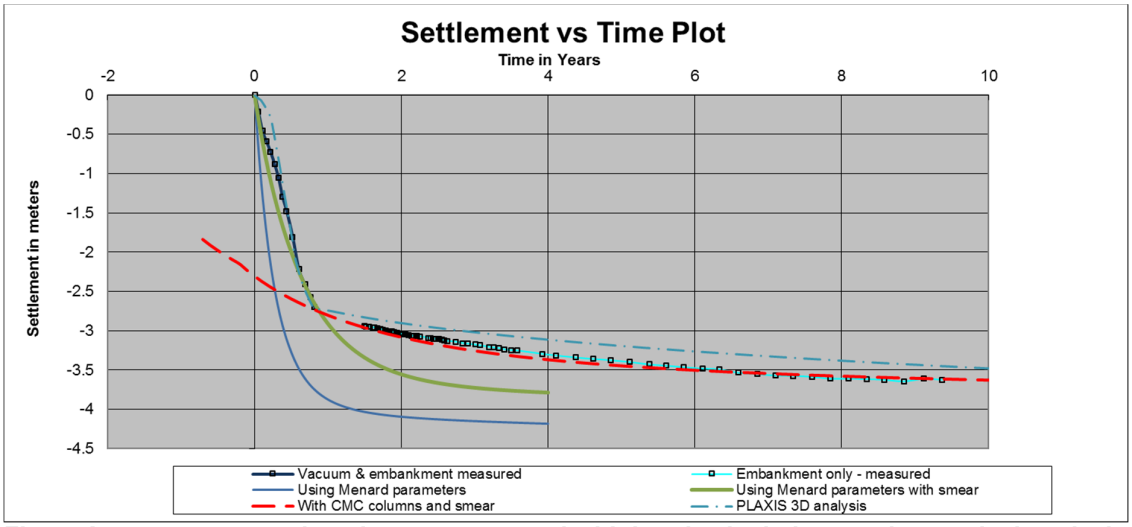


Fig. 5. Average measured settlement compared with hand calculations and numerical analysis

Figure 5 shows the average of the data in Fig. 3 and in Fig. 4 plotted as small black squares, with the post-treatment settlement data adjusted by 2.75 m. This seems to give a reasonable overall settlement/time curve. Plotted on the same chart are the settlement under vacuum consolidation based on the Menard parameters, including c_h = 1.5 m^2/yr, as well as a line using the same parameters but taking account of smear using Hansbo (1981), which seems to give a much better fit with the data. The ratios k_{h0}/k_{s0} = 4, and r_s/r_w = 4 were used. Also plotted is a line representing the post-treatment settlement with the CMC Columns, where the wick drain consolidation in the top 10 m has been replaced by an equivalent drained modulus to incorporate the effects of the rigid inclusions. These two curves appear to give a reasonable representation of the short term and long term behaviours.

Numerical modelling

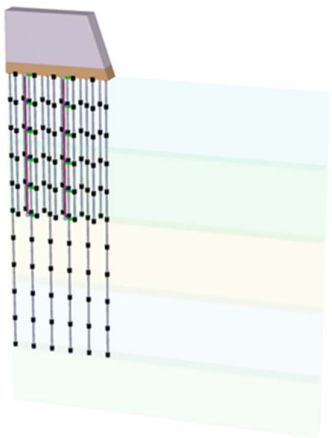
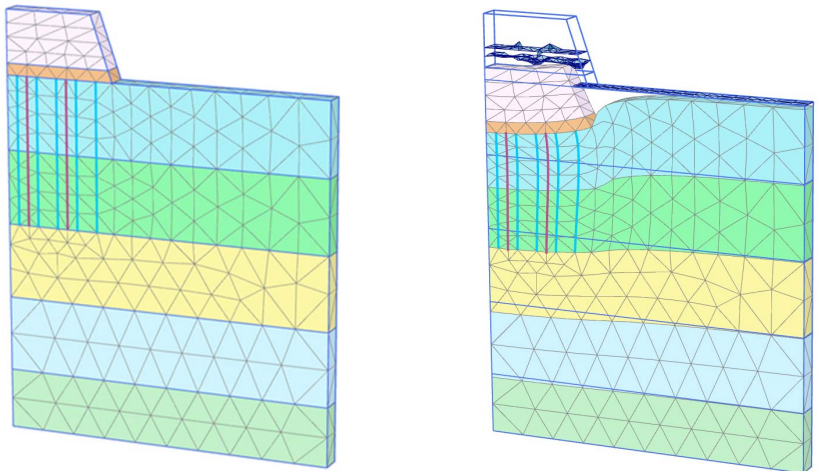


Fig. 6. Geometry of wick drains and rigid inclusions in 3D FE model

A 3D finite element model was developed using PLAXIS 3D, simulating the performance of a typical cross section in Block 2. The soil profile includes five layers with basic properties already given in

Table 2, and the Soft Soil Creep model is used for the constitutive model of the soils. The ground water table is located at the ground surface. The structural elements are shown in Fig. 6.

The symmetrical geometry of the embankment allows the model to be reduced to a half model on one side of the centreline and a slice in the longitudinal direction. The total thickness of the soil layers is 24 m and the width of model is 22.5m, which is three times the half width of the embankment. A sand blanket of 0.8 m thickness was placed on top of the ground surface and an embankment was raised to a thickness of 3.55 m, while the half width of the top surface of the embankment is 6 m. The wick drains and vacuum transmission pipes have been modelled as designed, with a square pattern with spacing of 1.414 m, and installed to depths of 20 m and 10 m, respectively. Hence, the density of the drains is 1 per m^2 between depth 0 and 10 m, and 1 per $2m^2$ between 10 m and 20 m. The CMC columns were installed in a square pattern with 1 per 8 m^2 and to a depth of 10 m. The vacuum transmission pipes and wick drains were modelled using line drain elements and the CMC columns were modelled using embedded beam elements. A total of 4312 soil elements (10-node tetrahedral element) and 6883 nodes were generated. The mesh before loading is shown in Fig. 7(a).



(a) before deformation (b) after deformation

Fig. 7. 3D FE mesh: (a) as modelled, and (b) deformed after 3900 days

According to the recorded loading history, a total of seven stages were applied, including (1) installation of drains (from 13th Sep to 13th Oct 2000), (2) placement of sand blanket (13th Oct to 3rd Dec 2000), (3) application of vacuum preloading (2nd Dec 2000 to 3rd Jan 2001), (4) application of fill surcharge while maintaining the vacuum (3rd Jan to 30th Mar 2001), (5) Consolidation under full fill surcharge and vacuum (30th Mar to 5th July 2001), (6) switching off vacuum and installing CMC columns (5th July to 4th Aug 2001), and (7) further consolidation and creep (4th Aug 2001 to 4th Aug 2011).

Soil properties

As mentioned above, the basic parameters of the soil layers, including unit weight γ, compression index C_c, swelling index C_r, initial void ratio e_0, and undrained shear strength s_u, are shown in Table 2. The s_u value of the top layer was adjusted to 8 kPa in order to avoid failure under the embankment load. The creep parameter C_α was estimated as $C_\alpha = 0.05\ C_c$, which is the highest value in the range recommended by GTC.

Permeability

The soil permeability parameters (e.g. k_h) were determined with the compression index C_c, coefficient of consolidation (e.g. c_h) and initial stress and void ratio of the soil layer. PLAXIS 3D adopts a relationship between void ratio and permeability as shown in Equation (1).

$$\log(k) = \log(k_0) + {}^{(e - e_0)}\Big/_{C_k} \qquad (1)$$

For this analysis, the permeability change index C_k is assumed to be $C_k = C_c$, so that a constant coefficient of consolidation can be obtained, which is consistent with the values given in Table 2. When $C_k = C_c$, the initial permeability can be determined by:

$$k_{h0} = \frac{c_h \gamma_w C_c}{\log(1+e_0)\sigma'_{v0}} \quad (2)$$

where e_0 and σ'_{v0} are the initial void ratio and effective vertical stress of the soil layer.

Consideration of smear zone

Based on the consolidation theory of Hansbo (1981), an equivalent permeability for each layer, for capturing the smear effect, can be determined as:

$$\bar{k}_{h0} = k_{h0} \frac{\ln\left(\frac{r_e}{r_w}\right) - \frac{3}{4}}{\ln\left(\frac{r_e}{r_s}\right) + \frac{k_{h0}}{k_{s0}} \ln\left(\frac{r_s}{r_w}\right) - \frac{3}{4}} \quad (3)$$

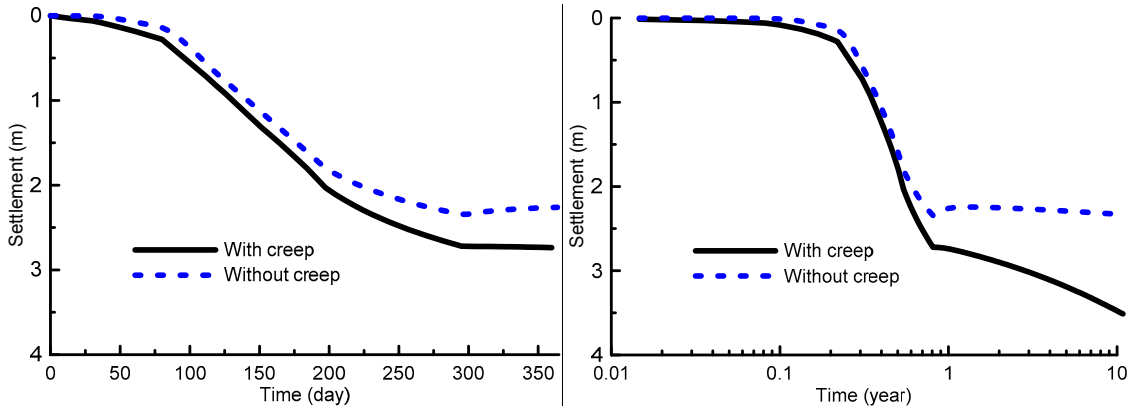
where r_e is the total radius of influence of the drain, r_s is the radius of smear zone, r_w is the equivalent radius of the drain, and k_{s0} is the permeability inside the smear zone. For this case study, it is assumed that $k_{h0}/k_{s0} = 4$, and $r_s/r_w = 4$. Table 3 gives the permeability parameters determined for each layer:

Table 3. Permeability parameters determined for each layer

Layer	Vertical permeability, k_{v0} (m/day)	Horizontal permeability, k_{h0} (m/day)	Equivalent horizontal permeability addressing smear, $\bar{k}_{h0}$ (m/day)
1	2.86×10^{-4}	2.86×10^{-4}	9.94×10^{-5}
2	8.33×10^{-5}	1.79×10^{-4}	6.21×10^{-5}
3	5.69×10^{-5}	1.07×10^{-4}	3.94×10^{-5}
4	4.27×10^{-5}	7.12×10^{-5}	2.63×10^{-5}
5	3.16×10^{-5}	5.27×10^{-5}	N/A

Results of analyses

The deformed mesh is shown in Fig. 7(b), indicating how the embankment settled about 3.6 m, and also bulged outwards near the toe. The settlement history at the centreline is shown in Fig. 8, and also compared with the measurements in Figure 5.



(a) 1st year (b) 10 years

Fig. 8 Settlement history at the centreline: (a) within the first year, and (b) within 10 years

Figure 8(a) gives the settlement results within the first year since the commencement of construction, while Fig. 8(b) shows the long-term settlement development within 10 years in logarithmic scale. It

can be seen from the plot that, apart from the real case with creep, another case considering no creep (by setting C_α to a very small value) was calculated and compared with the former. It can be observed that the effect of creep took place right from the beginning, which is consistent to 'Hypothesis B' (Leroueil 2006, Ladd et al. 1997, and Jamiolkowski et al. 1985). At the end of the first year, the creep model gave a settlement of 2.8 m while the non-creep model gave only 2.4 m. After the first year, the settlement under creep model kept increasing up to 3.5 m at 10 years, while it remained almost constant under non-creep model.

CONCLUSIONS

1. This project has provided a rare opportunity to back analyse consolidation settlement data, not only during ground improvement but for a considerable period afterwards, during the all important period of secondary consolidation.
2. The settlements have been significant, totalling over 3.5 m.
3. Some topping up of pavement levels with asphaltic concrete occurred, with consequent small increases in vertical stress at the base of the embankment, but the effects of these were negligible in relation to the overall settlement.
4. The settlement data, back analysis and numerical modelling seem to confirm that the primary consolidation had been achieved by the time the vacuum was turned off.
5. The secondary consolidation seems to have been seriously underestimated, with the result that post-construction settlements exceeded predictions by a significant margin.
6. The 3D numerical modelling confirms that the creep characteristics of the soil have played a key role in increasing the settlement after the primary consolidation. For such high creep soft soils, the underestimation of the secondary compression index C_α may cause a significant underestimation of the long-term settlement development.

ACKNOWLEDGEMENTS

The authors gratefully acknowledge the permission of Eastern Power & Electric Company to publish this paper and the data it contains, and the valuable contribution this is expected to make of the understanding of soft soil behaviour.

REFERENCES

Hansbo, S (1981). Consolidation of fine-grained soils by pre-fabricated drains. Proceedings of the 10th International Conference on Soil Mechanics and Foundation Engineering, Stockholm, 677-692.

Jamiolkowski, M., Ladd, C.C., Germaine, J.T. and Lancellotta, R. (1985). New developments in field and laboratory testing of soils. Proceedings of the 11th International Conference on Soil Mechanics and Foundation Engineering, San Francisco, Vol. 1, pp. 57-153.

Ladd, C.C., Foott, R., Ishihara, K., Schlosser, F. and Poulos, H.G. (1977). Stress-deformation and strength characteristics. State-of-the-Art Report, Proceedings of the 9th International Conference on Soil Mechanics and Foundation Engineering, Tokyo, Vol. 2, pp. 421-494.

Leroueil, S. (2006). The isotache approach. Where are we 50 years after its development by Professor Šuklje? 2006 Prof. Šuklje's Memorial Lecture, Université Laval, Ste-Foy, Québec, Canada.

Masse, F., Yee, K., Jullienne, D. and Varaksin, S. (2002). Successful application of the vacuum consolidation method on Bangkok clay to road embankment. Proceedings of IES Conference on Case Studies in Geotechnical Engineering, Nanyang Technological University, Singapore, July, pp. 33 - 44.

PLAXIS 3D Anniversary Edition. (2015).

DESIGN, CONSTRUCTION, AND LONG-TERM MONITORING OF A PILE-SUPPORTED LNG TANK IN SAVANNAH, GEORGIA

Guoming Lin, Ph.D., G.E., D.GE[1]
Cheng Lin, Ph.D., P.E[2]

ABSTRACT

This paper presents a case history for the design, construction and long-term performance monitoring of a driven prestressed concrete (PSC) piled foundation supporting a large liquefied natural gas (LNG) tank in Savannah, Georgia, USA. Following a geotechnical investigation, a design stage pile test program was performed with three objectives: to study the densification effect from pile driving on the liquefaction resistance, to test axial and lateral pile capacities, and pile behavior under lateral loads. The test program comprised five piles driven on a test pad constructed adjacent to the tank foundation. Cone penetration testing (CPT) was performed before and after pile installation to test soil densification effects from the pile driving and liquefaction potential was re-evaluated based on the soil densities after pile installation. The axial load tests involved static load testing, high strain dynamic testing, and Statnamic testing. This paper presents the findings of the densification effects, compares results from different axial testing methods and discusses the procedures to use the load test results in the pile design. The paper also comments on the construction issues and presents performance data with 10 years of monitoring.

Key Words: PSC Piles, LNG, Tanks, Settlement, Densification, Liquefaction

1. Introduction

The project site is located at the Kinder Morgan's Elba Island LNG Terminal on the Savannah River which is three miles downstream of the downtown Savannah, Georgia. This LNG terminal was initially developed in the 1970s as an LNG import terminal. The facility includes five LNG storage tanks with two larger tanks which were constructed in 2003 and 2006, respectively. The terminal is currently being converted into a liquefaction and export facility. This paper discusses pile foundations for Tank D4 which is a double walled insulated steel tank built to hold one million barrels of LNG in 2003. This tank has an outer tank diameter of 258 feet, an inner diameter of 252 feet, and liquid height of 113 feet. A number of geotechnical challenges were present in the foundation design and construction.

- The site is a typical coastal deposit site featuring a thick layer of very soft under-consolidated clay (up to 40 feet in thickness);
- The bedrock is a couple of thousand feet deep;
- There is a sand layer that is liquefiable under a high seismic design category (0.5% possibility of exceedance in 50 years).

Considering the above mentioned soil conditions, the tank foundation was designed to consist of 1600 square prestressed concrete piles with pile tip embedded to the very stiff to hard silt and/or clay layer named the Marl formation. The design and construction required permits from the Federal Energy Regulatory Commission (FERC) and the tank was monitored and inspected periodically in accordance with FERC requirements. This paper overviews the complete engineering process for an LNG tank foundation from

[1] Senior Principal and Senor Consultant, Terracon Consultants, 2201 Rowland Avenue, Savannah, GA 31404 USA
[2] Assistant Professor, University of Victoria, PO Box 1700 STN CSC, Victoria BC V8W 2Y2 Canada.

site subsurface exploration, foundation design and testing, foundation construction, to foundation performance monitoring. Some lessons learned from this project are also discussed.

2. Subsurface Conditions

The in-situ soil testing was conducted within the footprint of Tank D4 and consisted of 12 standard penetration test (SPT) borings, six cone penetration test (CPT) soundings, five dilatometer tests (DMT) soundings, and two geophysical surveys using seismic CPTs. One SPT boring at the center of the tank was drilled to 382 feet below existing grades. Based on the subsurface exploration results, the subsurface conditions for the tank site are relatively uniform and are summarized in Table 1. The groundwater table was at depths of 5 to 8 feet below the existing grade during exploration.

Table 1. Generalized subsurface stratigraphy in Tank D-4 Area

Layer No.	Soil Type	Elevation (ft, MLW*)	Thickness (ft)	SPT N (blow/ft)	CPT q_c* (tsf)	DMT E_D* (tsf)	Relative Density or Consistency
1	Hydraulic Fill/Surface Crust	11 to 7	4	4 to 22	10 to 15	30 to 80	firm to very stiff
2	Soft Clay (CH)	7 to -25	32	WOH* to 8	1 to 30	10 to 30	very soft to soft
3	Sand (SP)	-25 to -40	15	11 to 36	100 to 200	400 to 700	medium dense to dense
4	Silty Clay (Marl)	-40 to -95	55	9 to 44	30 to 80	200 to 400	stiff to hard
5	Clayey Sand (SC)	-95 to -105	10	30 to >50	N/A*	N/A	Very Dense
6	Silty Sand (SM)	-105 to -140	35	>50	N/A	N/A	Very Dense
7	Limestone	-140 to <-370	>230	>50	N/A	N/A	

*MLW=mean low water; WOH=weight of hammer q_c= uncorrected CPT tip resistance; E_D= DMT modulus; N/A= not applicable.

The above subsurface conditions present a multitude of challenges to foundation design and construction. Soils in Layers 1 and 2 are under-consolidated soft clays, undergoing subsidence under their own weight. These weak upper soils require the use of deep foundations for all structures and settling soils exert downdrag loads to pile foundations. The facility was designed to survive the Safe Shutdown Earthquake (SSE) event which was defined as ground motions having a mean recurrence interval of 10,000 years (this requirement was revised to a 5,000-year event in the subsequent versions by FERC). The stringent seismic design requirements caused liquefaction risk for the medium dense sand Layer 3. The weak upper soils were suspected to cause low lateral capacities for the piles and the number of piles and pile cap connection requirement is governed by the lateral loads associated with SSE event.

3. Foundation Design and Testing

3.1. Preliminary Foundation Design

The initial foundation design was developed based on the foregoing subsurface conditions and by evaluating different foundation options (including shallow and deep foundations). In this design, square prestressed concrete (PSC) piles were used for the tank foundation considering the following merits of PSC piles:

- Commonly used in local area with ample design and construction experience;
- Relatively reliable compared with bored piles;
- Resistance to corrosion in high sulfate soils compared with steel piles;
- Densification of sands by pile driving to increase liquefaction resistance;
- Considerable gain of pile axial capacity with time.

The pile length was mainly governed by the axial loads while the pile size was primarily controlled by the lateral load requirements. The pile settlement was not explicitly calculated but it was checked after capacities were evaluated by requiring the minimum embedment to the bearing layer (i.e. the Marl formation). This approach is largely based on the local experience with projects along the Savannah River. Due to the space limit, this paper only discusses the design and testing of pile axial capacities.

3.1.2 Pile compression and tension capacities

According to the structural engineers, the required axial compression capacity of each pile was 100 tons. The following approaches were used to estimate the axial capacities of driven piles 1) estimating adhesion values between pile and soil based on the soil strength from laboratory and field testing, 2) previous experience with pile load tests along the Savannah River, and 3) calculation of pile capacity using a computer program based on LCPC method (Bustamante and Giasenelli 1982) using CPT data.

Regardless of the approach used, the total capacity will be largely dependent on the value of adhesion between the pile and Marl formation (Layer 4) as the Marl is the pile bearing layer in the Savannah area. An adhesion value of 2.5 kips per square foot (ksf) and unit end bearing value of 50 ksf in the marl was used in estimating allowable axial capacities. These values were largely empirical and were obtained based on the tank foundations built in the 1970s and load test data, mainly from PDA tests, on piles along the Savannah River. Moreover, the downdrag force was computed for the soft clay (Layer 2) and above considering the significant difference in soil strength between Layers 2 and 3.

The allowable compression capacities are calculated using the following equation and with a factor of safety of 2.

$$R_a = \frac{R_p + R_b}{FoS} - R_n \qquad (1)$$

where R_a is the allowable compression capacity; R_p is the positive side resistance to piles contributing from Layers 3 and 4; R_b is the end bearing contributing from Layer 4; R_n is downward load calculated based on the negative skin friction from Layers 1 and 2; and FoS is a factor of safety.

The allowable tension capacities (R_t) are calculated by Eq. (2) and with a factor of safety of 2. A discount of 2/3 is factored to the total side resistance considering that the side resistance in tension is lower than in compression.

$$R_t = \frac{2}{3}\frac{R_p + R_n}{FoS} \quad (2)$$

Table 2 summarizes the allowable axial capacities for 18-inch square PSC piles that were calculated with LCPC method for soils above Marl (i.e. Layers 1, 2, and 3) and empirical values of adhesion (2.5 ksf) and unit end bearing (50 ksf) for piles in Marl (i.e. Layer 4). Table 2 also presents ultimate compression capacity for the design of load frame, jack, and load cell in the load test program. For an allowable compression capacity of 100 tons, the pile embedment should be 67 feet or tip elevation -55 feet MLW.

Table 2. Calculated pile axial capacities for 18-inch square PSC piles*

Pile embedment/tip elevation (ft)	R_{p1}* (ton)	R_{p2}* (ton)	R_n (ton)	R_b (ton)	R_a (ton)	R_t (ton)	R_u* (ton)
60/-48	74	60	20	56	75	51	154
70/-58	74	135	20	56	113	76	229
80/-68	74	210	20	56	150	101	304
90/-78	74	285	20	56	188	126	379
100/-88	74	360	20	56	225	151	454

*This calculation was based on the existing grade of 11.6 ft MLW; R_p=R_{p1}+R_{p2}; R_{p1}=positive soil resistance from Layer 3 (sand); R_{p2}=positive soil resistance from Layer 4 (marl); R_u= ultimate compression capacity, equal to R_p+R_n+R_b, which is calculated for the design of maximum load of jack and load cell in the pile load test program.

3.2. Pile Test Program

To verify and refine the preliminary pile design, a pile test program was proposed specifically to achieve the following three objectives:

- To test pile constructability at the project site;
- To study the densification effect from the pile driving by re-evaluating the liquefaction potential after pile driving;
- To test the axial pile capacity for use in the determination of the design pile length;
- To test the lateral behavior of the piles for use in pile cap and connection design, particularly the pile behavior under cyclic lateral loads (not presented in this paper).

The test was performed on a test pad of 40 square feet constructed outside the tank foundation by placing and compacting four feet of fill over the existing ground which resulted in a new ground elevation of 14.6 feet MLW. The pile test program incorporated a total of five piles (in Table 3) driven in a group as shown in Fig. 1. The pile lengths for test piles were in the range of 65 to 85 feet (corresponding to pile tip elevations

of -50 to -65 feet MLW) covering the calculated minimum pile embedment of 67 feet (or -55 feet MLW of pile tip elevation). The actual pile embedment and pile tip elevation during the construction are presented in Table 4. The test piles include two instrumented 18-inch square PSC piles, two 18-inch square piles without instrumentation and one 17.7-inch diameter prestressed cylindrical spun-cast concrete (ICP) pile. The two square piles without instrumentation were termed "dummy" piles as they were installed to form a pile group similar to that of production in order to evaluate the densification effect associated with pile driving.

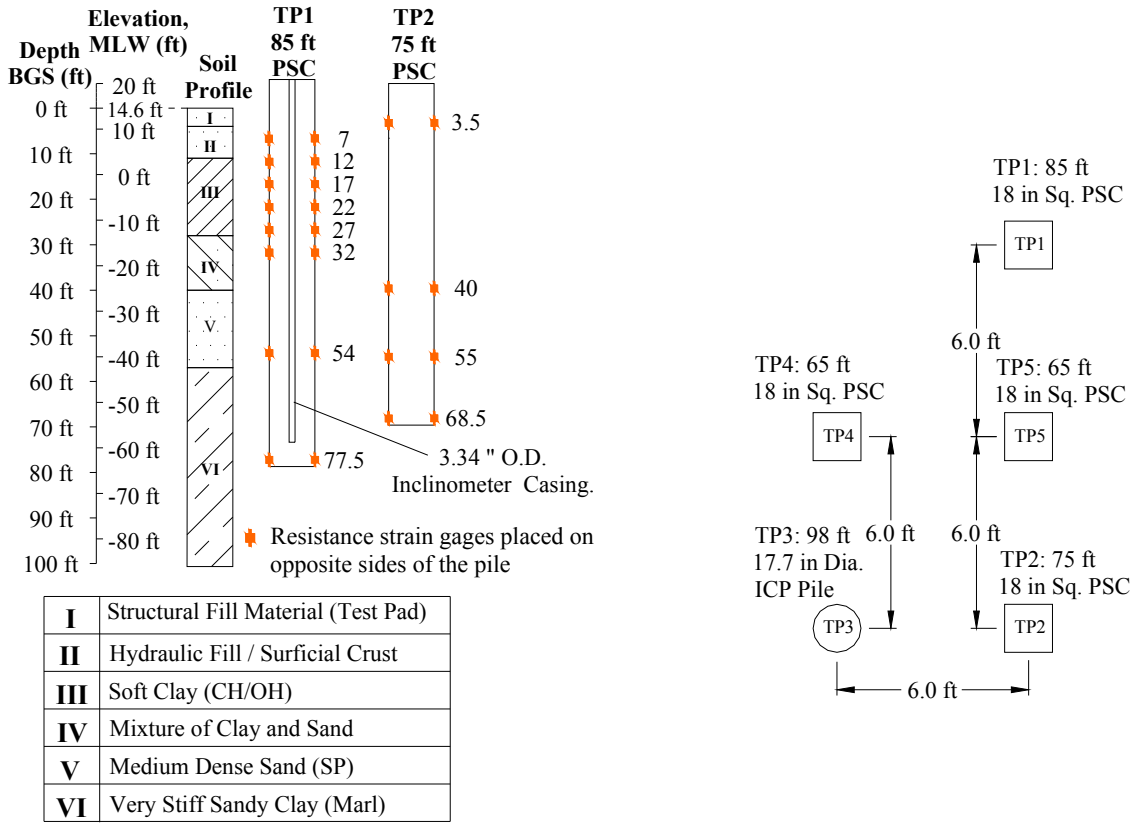
Table 3. Test pile details

Test Pile	Pile Length and Type	PDA during Initial Driving	PDA Restrike	Statnamic Testing	Static Compression Test	Lateral Load Test
TP1	85 ft 18-in sq PSC	2002-9-12	9-16	9-18	--	9-26
TP2	75-ft 18_in sq PSC	2002-9-12	9-16	9-18	9-24	9-26
TP3	98-ft 17.7-in dia ICP	2002-9-12	9-16	9-18	--	--
TP4	65-ft 18-in sq PSC	--	--	--	--	--
TP5	65-ft 18-in sq PSC	2002-9-12	9-16	--	--	--

Table 4. Summary of test pile driving conditions

Driving Information	TP1 (18" PSC)	TP2 (18" sq PSC)	TP3 (17.7" ICP)	TP4 * (18" PSC)	TP5* (18" PSC)
Initial pile length (ft)	85	75	2 x 49	65	65
Depth placed in pilot hole (ft)	37	32	18	25	25
Embedment length (ft)	79	70	85	65	65
Final tip elevation (ft, MWL)	-64.1	-55.0	-69.8	-50.4	-50.4
Maximum blow count/depth	67 bpf /57 ft	78 bpf /56 ft	53 bpf/58 ft	59 bpf/60 ft	73 bpf/58 ft
Total hammer time (minutes)	51	36	45	28	18

* Piles TP4 and TP5 were initially driven to 3 to 4 feet above final tip elevations and then driven flush to the grade after removal of the template and following the PDA restrike tests.



I	Structural Fill Material (Test Pad)
II	Hydraulic Fill / Surficial Crust
III	Soft Clay (CH/OH)
IV	Mixture of Clay and Sand
V	Medium Dense Sand (SP)
VI	Very Stiff Sandy Clay (Marl)

Fig.1. Test pile layout and Instrumentation

3.2.1 Pile construction observations

An APE D36-32 single acting open-end diesel hammer was used to drive all five test piles. This hammer has a ram weight of 7.94 kips and maximum rated energy of 83.33 kip-feet. The hammer was handled with a 3900 Manitowoc 100-ton crane with a swing lead. The pile cushion consisted of an oak hardwood between 2 pieces of 2-in thick plywood for a total cushion thickness of 6-in. During the test pile installation process, the hammer and crane appeared to be in satisfactory condition.

Prior to installing test piles, pilot holes were created with a vibratory hammer and 14-inch H-pile with steel plates welded to the web. The purpose of pile hole probing was to maintain the plumbness of the test piles during installation. All the test piles were driven from the test pad grade of approximately 14.6 feet MLW. Pilot holes were extended to depths of 25 to 35 feet below the pad grade. Each pile was placed in the pilot hole under self-weight to depths of between 18 and 37 feet. In order to reduce disturbance to the subsurface and help maintain vertical alignment of the pile, each pile was placed in its pilot hole prior to vibrating the remaining pilot holes.

The driving conditions were similar for all four 18-inch square PSC piles. The 18-inch square PSC piles required blow counts of around 30 blows per foot (BPF) but not greater than 50 BPF within the first 45 feet of driving. The hardest driving occurred in the sand layer (Layer 3) between depths of approximately 47 to 60 feet BGS. Blow counts were typically in excess of 50 BPF and occasionally greater than 70 BPF in this depth range. Driving became easier beneath this dense sand layer. At depths greater than 60 feet BGS, the blow counts were generally around 40 BPF. During pilot hole probing and subsequent driving, the ground subsided around each pile to form a cone-shaped depression of approximately 4 to 5 feet in diameter

and 3 to 4 feet in depth. The depression formed because the soils below the upper hard crust were very weak. The contractor backfilled the depression and tampered the fill in lifts after pile driving and prior to testing.

3.2.2 Effect of soil densification from pile driving on liquefaction resistance

The liquefaction analyses based on SPT, CPT and shear wave velocity indicated that localized zones within the sand layer are liquefiable during an SSE event. The pile test program was designed to test the densification from the pile driving and to re-evaluate liquefaction resistance based on the soil density after pile driving.

The test piles were installed on a 6 by 6 feet square pattern that reflects the pile layout for the tank. This pattern represents a densification zone bounded by the four piles. CPT soundings were performed at the center of the square (C1) formed by four piles TP2, TP3, TP4, and TP5 and at the midpoint of the edge between TP2 and TP3 (C2) before and after pile driving. The improvement of CPT tip resistance can be used to characterize the improvement of soil density. The increase of CPT tip resistance (q_c) at C1 due to pile driving is presented in Fig. 2.

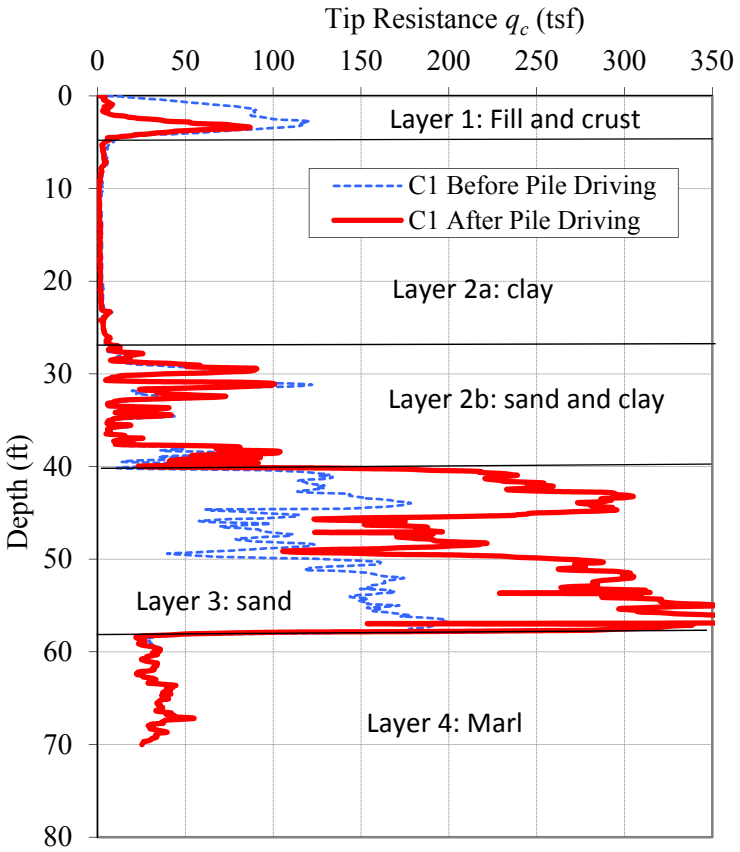


Fig. 2. The CPT tip resistance (C1) before and after pile driving

From Fig. 2, the density of the sands within Layer 3 has been drastically increased as a result of the pile installation process. The percentage of q_c increased was 96.7% at C1 and 70.5% at C2, respectively. Along with the densification from pile driving, piles driven in a closely spaced pattern can serve to confine the soils between the piles resulting in an additional increase in tip resistance. Based on the direct correlation between q_c and relative density (Dr) (Larson, 1995), the average Dr of the sand layer (Layer 3) increased from 66% to 89% at C1 compared with 66% to 81% at C2. It is reasonable that the C2 improvement index

and relative density were lower than C1 as C2 was on the edge of the pile test pattern and was only bounded by two piles. Some reduction in tip resistance was observed in the soft layers located above Layer 2, which can most likely be attributed to disturbance effects caused by the use of a vibratory hammer to create the pilot holes during driving.

The post-densification analysis indicated that sandy soils of Layer 3 have been densified to a point of being not liquefiable during the SSE event (i.e. 10,000-year recurrence).

3.2.4 Axial load test results

The pile load tests consisted of dynamic compression test using pile dynamic analyzer (PDA), statnamic testing, static compression, and reciprocal lateral load testing; the tests were performed at different times to investigate the potential set up effects of piles after installation. For the static load test, the 500-ton hydraulic jack and load cell were used which was approximately 2.5 times the calculated R_u at 67 feet of pile embedment in Table 2.

The compressive load test results are summarized in Table 6. For the static load test, the compression capacity was determined using Davisson method (Davisson 1972). Fig. 3 shows the measured load and settlement curve and the determination of ultimate compression capacity of piles.

Table 6. Compressive loads measured at different testing times

Pile No.	Type	Axial Load Test Results (kips)			
		EOD*	4DR*	6D STN*	12D SLT*
TP1	18-in sq PPC	370	640	890	
TP2	18-in sq PPC	376	629	743	847
TP3	17.7 in dia. ICP	246	642	857	
TP4	18-in sq PPC			Not Tested	
TP5	18-in sq PPC	398	458		

* EOD = End Of Driving (Dynamic); 4DR = 4 Day Restrike (Dynamic); 6D STN = 6 Day statnamic test; 12D SLT = 12 Day Static Load Test

The load-settlement curve for TP2 (in Fig. 3) indicates a plugging type failure with an ultimate capacity of 847 kips. The test results for other piles from dynamic and Statnamic testing are summarized in Table 6. The pile capacity increase over time (the setup effect) was evaluated by comparing the pile capacities from the initial driving to four-day restrike testing and six-day Statnamic testing and 12-day static load testing. TP2 indicated 2.25 time increase from the initial driving to the 12-day static load testing. However, a close examination of the pile test results indicated the test piles did not fail during the PDA restrike and statnamic testing as pile displacements were relatively small. As such, the Statnamic and PDA restrike tests served to verify the static load test results. But the ultimate pile capacities were not determined by these two test methods as the pile capacities were not fully mobilized.

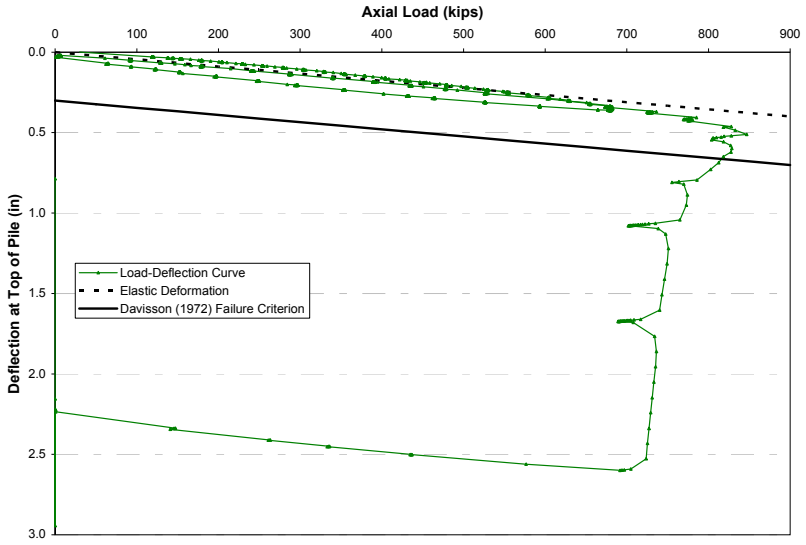


Fig. 3. Static Load Test Results of TP2

The production piles were designed based on the unit side friction (fs) and end bearing (qt) derived from the strain gage data from the statnamic and static load tests. The derived fs and qt values are summarized in Table 7. Overall, the values which were derived from this pile test program were generally larger than those used in the preliminary design. In the preliminary design, the required pile tip elevation was -55 feet MLW which was calculated before test pad was constructed. With the additional four-foot, structural fill the downdrag load would increase therefore an additional two-foot embedment was required; this resulted in a pile tip elevation of -57 feet MLW. Using the parameters derived from the pile load test, the same pile tip was obtained. This comparison indicates the overall allowable compression capacity of the pile was agreeable between preliminary design calculation and the pile load tests although distributions of fs and qt from both were different.

In the final design, the lower portion of Layer 2 (i.e. Layer 2b in Table 7) was considered as a positive resistance to the pile. As such, the negative skin friction layers were limited to the upper portion of Layer 2 (i.e. Layer 2a) and above. Such a consideration was due to 1) relatively high CPT tip resistance in Layer 2b (q_c > 30 tsf) compared with Layer 2a (q_c = 2 to 4 tsf), and 2) the observed considerable increase of CPT tip resistance in Layer 2b (by approximately 22%) but no change in Layer 2a by pile driving. Overall, after the pile load test, the pile length was shortened by approximately seven feet, leading to a substantial savings of material and construction cost.

Table 7. Derived parameters for pile design

Soil Stratum	Depth (ft)	Elevation (ft, MLW)	f_s* for preliminary design (ksf)	f_s for final design (ksf)
Structural fill	0 to 4	14.6 to 10.6	1.3	0.65
Layers 1 and 2a: (existing fill/soft clay)	4 to 28	10.6 to -13.4	0.1	0.48
Layer 2b (sand and clay mixture)	28 to 40	-13.4 to -25.4	0.41	1.53
Layer 3 (sand)	40 to 57	-25.4 to -42.4	2.2	1.74

Layer 4 (marl)	57 to 105	-42.5 to -90	2.5	3.2
Layer 4 (marl)	Unit end bearing (ksf)		50	50

*f_s=unit side friction; for preliminary design, fs for soils above Layer 4 was calculated using LCPC method and that for Layer 4 was empirical value as discussed previously. ** this value was not derived from the load test but obtained directly from preliminary design.

For the pile group, the group efficiency of 1.0 was conservatively chosen on account of the clay layer and above having negative downdrag effect and densification effect in the sand layer. The final design for the pile group is shown in Fig. 4. The pile center to center spacing was four times pile side width. The total pile number was designed to be 1600 considering the lateral loads at an SSE event. The pile length as discussed previously was determined by the design compressive load of 100 tons and the parameters in Table 7. The pile settlement was anticipated to be insignificant when the allowable compression capacity was satisfied and the piles had been extended more than five feet into the Marl.

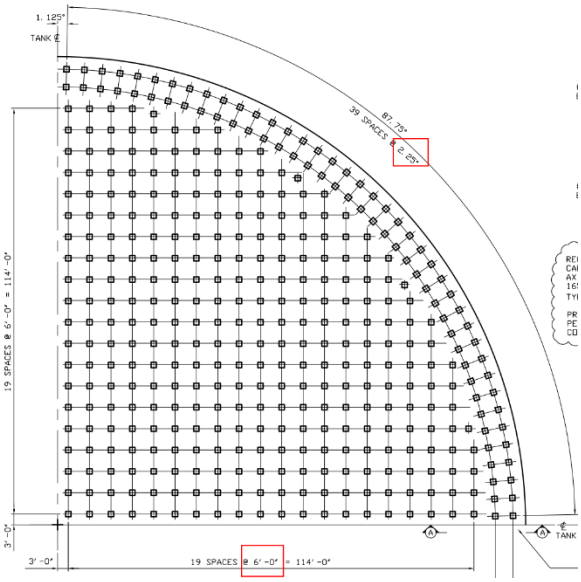


Fig. 4. A quadrant layout of pile foundation

4. Pile foundation construction

The pile driving was started with a sequence to install piles around the perimeter of the tank foundation. The confinement caused by the perimeter piles caused additional densification of the sand layer. However, as the pile driving progressed from the edge towards the center of the tank, the pile driving became increasingly more difficult because the sands became too dense. About half way into the pile construction, the pile could not be driven even with the use of larger hammers and the casting of tension bar sleeves in the pile top would not allow the piles to be cut off. Finally, predrilling had to be performed on every third or fourth pile to remove the column of soil to the sand layer in order to continue the pile driving. The problem should have been avoided by starting the pile driving from the center of the tank.

5. Long-term monitoring of foundation performance

After completion of the tank construction and prior to placing the tank into service, a hydro test was performed by filling the tank with water and monitoring the foundation settlement. The tank settled less

than 0.25 inch which was below the allowable limit of 1 inch. After being placed into the service, the tank was inspected periodically and monitored for settlements. Fig. 4 shows the measured settlement over the last ten years at four cardinal points (points 59 to 62). The average settlements were approximately 1.6 inches which were developed mainly in the first year of operation; after that, the tank gradually rebounded, in particular since 2013. By plotting the settlement trend and LNG loads on the foundation in Fig. 5, it clearly shows that the decrease of tank settlement was associated with the reduced LNG loads. In recent years, the LNG tank was almost empty. As such the tank rebounded most significantly in this period with a total rebounding of 0.3 inches.

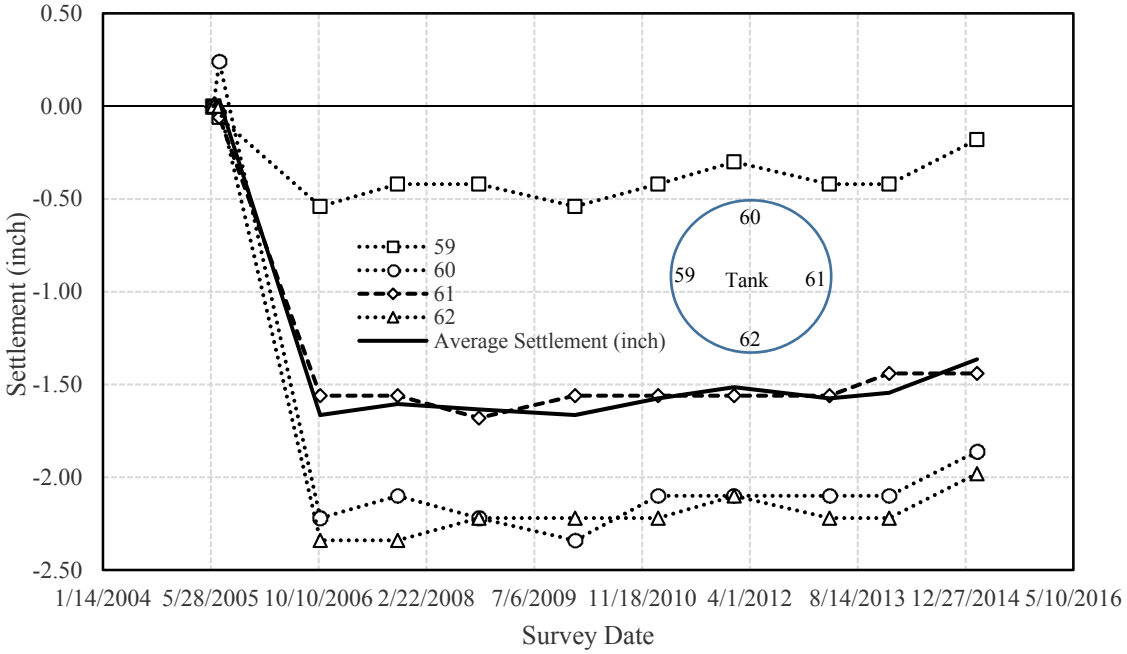


Fig. 5. Long-term monitoring of tank settlement

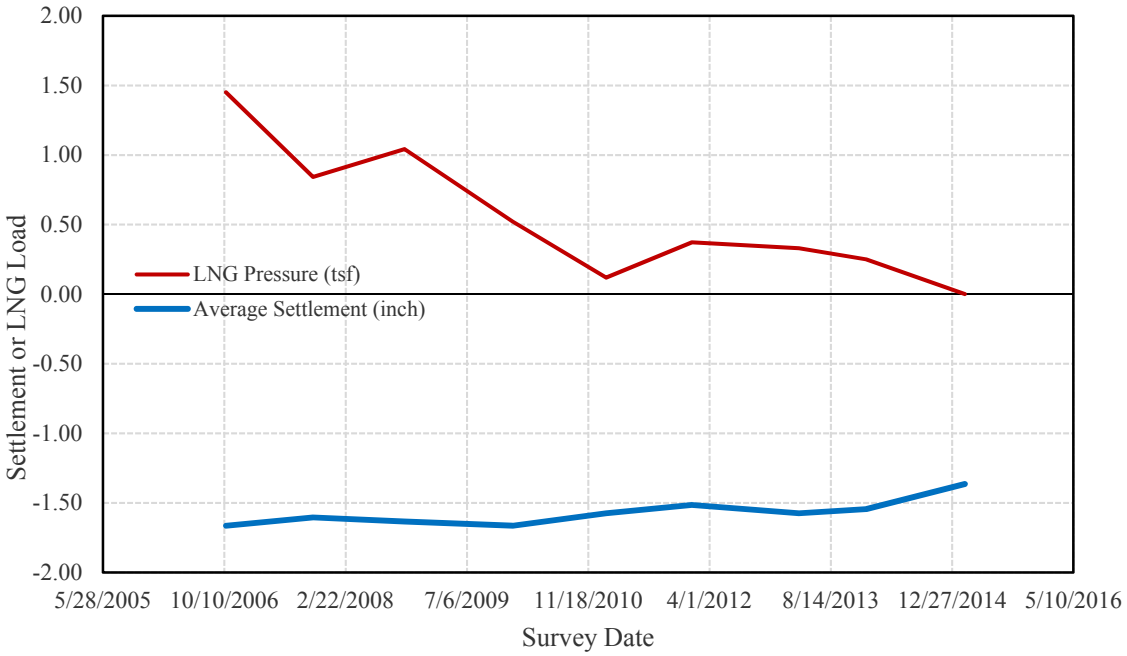


Fig. 6. Variations of tank settlement and loads

Conclusions

Based on the general overview of the subsurface exploration, foundation design and testing, foundation construction and post-construction monitoring for an LNG tank supported by 1,600 18-inch square PSC piles, the following findings and lessons learned were obtained:

1. The project site was underlain by a thick layer of soft under-consolidated clay which would cause downdrag load to the pile. The design considered this downdrag as a load and thus a factor of safety was not applied to it in calculating allowable compression capacity of the pile. The marl formation is a competent bearing layer for piles in the Savannah area, which was verified by the findings of both pile test program and the long-term foundation settlement monitoring.
2. The design practice for pile capacity estimation that employed LCPC method for soils above marl and empirical values in marl appeared reasonable compared with the pile load test results.
3. The densification effect by pile driving was remarkable in layers of sand (Layer 3) and the sand and clay mixture (Layer 2b). The increase of CPT tip resistance in both layers due to pile driving was 97% and 22%, respectively. After considering this densification effect, the liquefaction potential in the sand at a 10,000-year return period of earthquake became insignificant.
4. The test piles all experienced abrupt plunging failure in the static load test. The time-dependent pile capacity gain was significant with the 12-day capacity increase by 125% and 7-day capacity increase by 98%.
5. An important lesson was learned from the foundation construction. The pile installation sequence from tank perimeter toward the center should be avoided as the pile driving at the perimeter would densify soils inside and thus cause the hard driving inside. A reasonable sequence would be the installation of piles at the center and then outward.
6. The short-term hydro test presented considerably different results than the long-term monitoring. The former measured a negligent settlement (less than 0.25 inch) while the latter showed over one inch of settlement (i.e. 1.6 inches). Although the design practice using allowable capacity approach

and minimum embedment into marl has proven successful in the local area, the settlement calculation is still warranted, in particular for a large group of piles.

References

Davisson, M.T. (1972). "High Capacity Piles," *Proc. Soil Mechanics Lecture Series on Innovations in Foundation Construction*, American Society of Civil Engineers, ASCE, Illinois Section, Chicago.

Lin, G., Casey, T.J., Yang, W., 2004. Effect of Post Driven Pile Soil Densification on Liquefaction Resistance. SDEE

Tan, Yong, and Guoming Lin. "Comprehensive load test on prestressed concrete piles in alluvial clays and marl in Savannah, Georgia." *Journal of Performance of Constructed Facilities* 28, no. 1 (2011): 178-190.

QUALITY CONTROL AND TESTING OF JET GROUTING AND ITS INTERPRETATION IN RELATION TO THE CHRISTCHURCH TOWN HALL RESTORATION PROJECT.

Paul Marsden, Keller Geotechnique, United Kingdom, +44 2476 511266,
paul.marsden@keller.co.uk
David Chadwick, Keller Ground Engineering, Australia, +61 28 866 1155
d.chadwick@kellerge.com.au
Mathias Delapille, Keller Ground Engineering, Australia, +61 28 866 1155
m.delapille@kellerge.com.au
Chris Hughes, Brian Perry Civil, New Zealand, +64 3 363 1729
chrishu@fcc.co.nz

ABSTRACT

Following damage caused by the 2011 Christchurch earthquakes, the NZ$127.5million Christchurch Town Hall Restoration project is due for completion in 2018. The building is undergoing extensive repairs and a strengthening regime to meet New Zealand's New Building Standard. One major aspect of the project is the stabilisation of the soil directly beneath the building using interconnected jet-grouting columns installed a cellular configuration, the purpose of this being to decrease the likelihood and severity of foundation movements caused by earthquake-induced soil liquefaction and lateral spreading. The soils encountered on the site ranged from cobbles and gravels through to sandy silts with a significant quantity of timber and rootlets. This wide variation of soil types presented a number of challenges with regard to effective and consistent treatment by jet grouting. The paper presents an overview of the quality assurance practices and also the testing regime adopted on this project.

Keywords: liquefaction, lateral spreading, jet grouting, quality control, testing regime.

INTRODUCTION

Most of the deformation experienced by the Christchurch Town Hall structure over the course of the Canterbury earthquakes was caused by movement of the underlying ground. Two primary mechanisms of ground deformation were observed:

- Liquefaction of the soils underlying the building foundation
- Lateral spread of surface soils towards the free face at the river edge which runs 20 metres from the building. This mechanism also resulted in additional vertical settlement of the building foundations.

The overall foundation design philosophy adopted by the project team for the Christchurch Town Hall Conservation Project has been to improve the ground directly beneath the structure to mitigate against these two mechanisms of ground movement. Additionally, a robust raft slab is proposed to distribute the foundation loading more evenly and increase the ability of the structure to resist lateral stretch of the underlying ground.

The ground improvement system proposed by the Client's geotechnical consultants, Tonkin &Taylor, comprised a cellular arrangement of interlocking jet grout columns, this arrangement would effectively encapsulate the soil within the cells preventing lateral spread.

In total 1,097 interlocking jet grout columns, extending over the entire floor plan of the structure, were required to satisfy the design requirements.

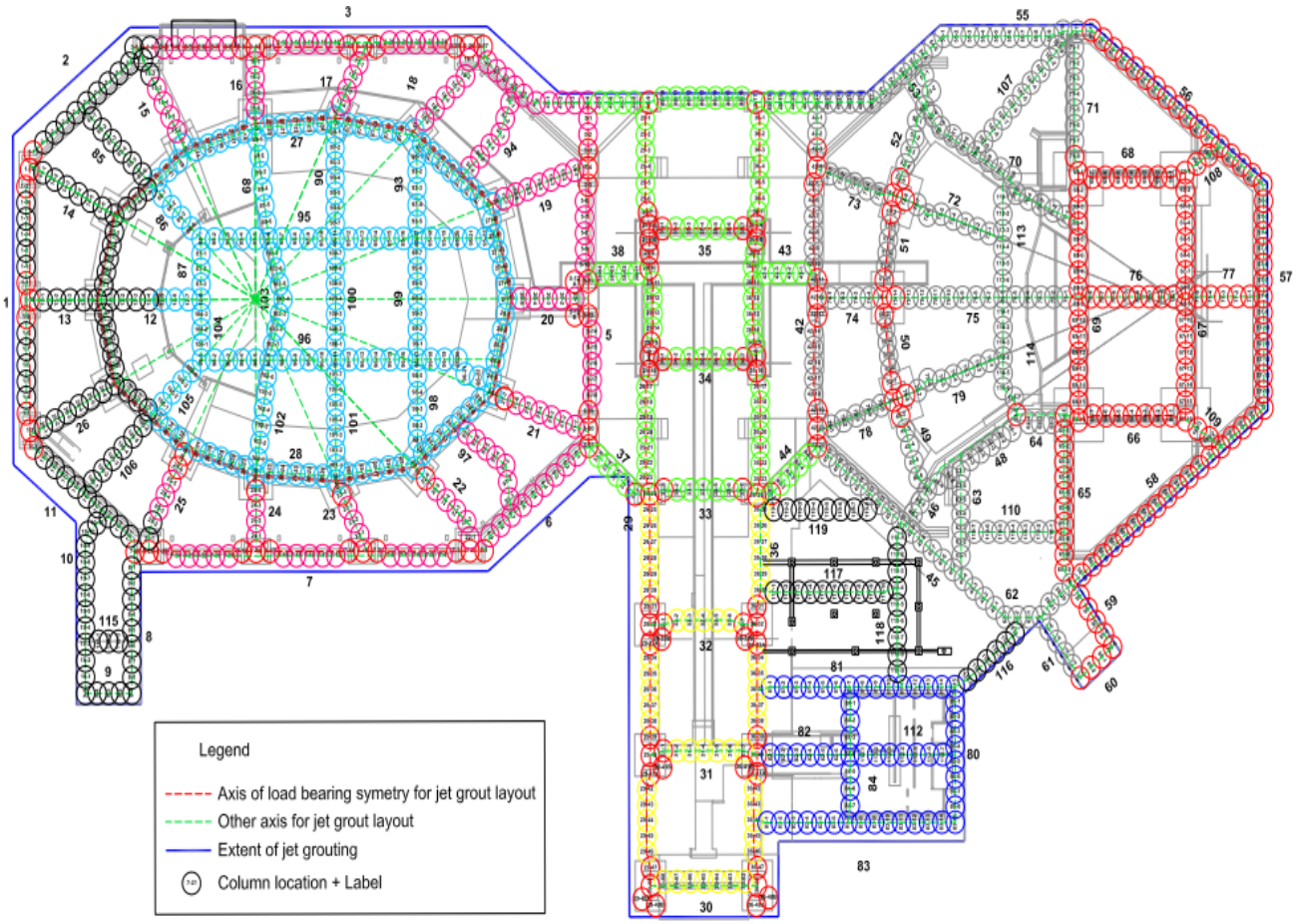


Figure 1 - Plan showing the cellular grid of jet grout columns

A comprehensive quality control, testing and inspection programme was implemented to ensure that the works achieved the design requirements in relation to column dimensions, strength and continuity of the jet grout column grid system. The testing regime, which ranged from conventionally specified methods to more direct observational techniques and the interpretation of the output from these, is also presented. Advantages and disadvantages of these options are reviewed in terms of the standards applied to quality control testing of jet grout works.

SOIL CONDITIONS

The Town Hall is underlain by post-glacial fluvial channel and overbank sediments consisting of gravel, sand and silt. A near surface layer of fill is underlain by non-plastic silt and sandy silt with lenses of silty sand and gravel, regarded as the main zone of potential liquefaction. At approximately 6 metres depth, the soil consists principally of interbedded sands and sandy gravel. The soils also contain partially mineralized roots and wood. This wide variation of soil types presented a number of challenges with regard to effective and consistent treatment by jet grouting.

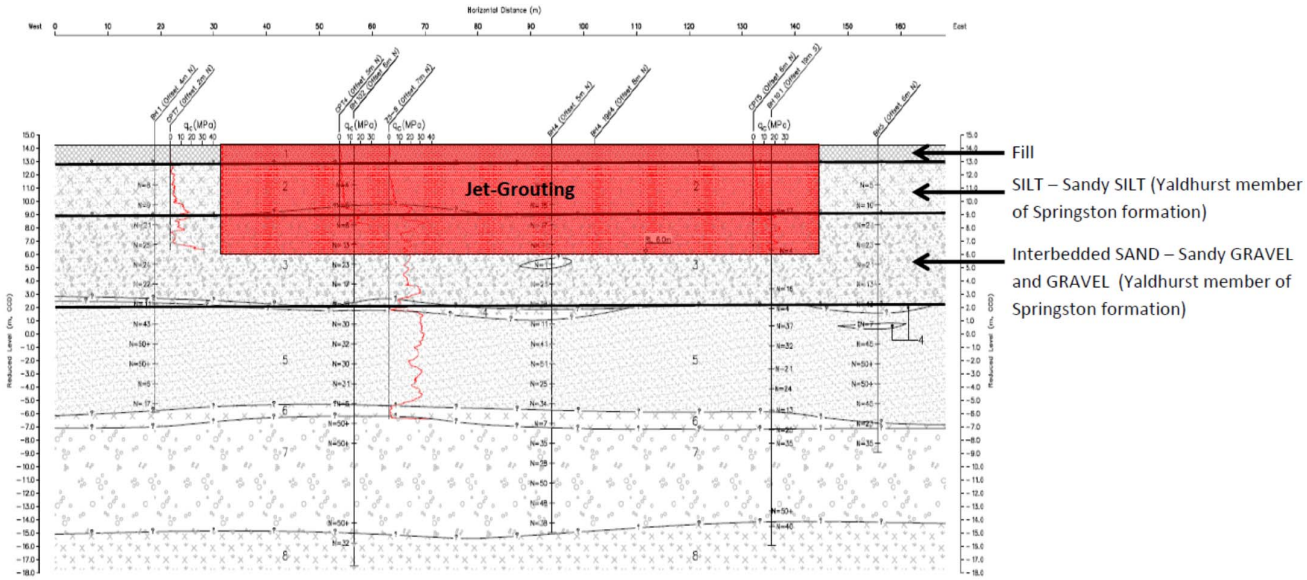


Figure 2 - Typical geological cross-section

PROJECT REQUIREMENTS & JET GROUTING TRIAL

The project Specification was based on the America Society of Civil Engineers (ASCE) Jet Grouting Guide Specification. Comments on the ASCE Specification, by the 2008 ASCE Committee on Grouting - Jet Grouting Task Force, revision 8, 01/05/2009, provided useful guidance when planning the inspection and testing and also in the review of the results. The geotechnical consultant Tonkin & Taylor also acknowledged the variability of the ground conditions, including wood and rootlets, and made provision in the Specification and overall ground treatment design for untreated zones of limited extent within the grouted mass. This practical approach is particularly important where intact sections of wood remain within the grouted matrix or where large pieces of wood cause shadowing of the adjacent soils and localised zones of untreated material



Figure 3 – Pieces of wood were vacated from the jet grout columns during installation.

The design required columns to be formed at 1.5m centres with a target diameter of 2m. To ensure interlock between adjacent columns and therefore continuity of treated material, the columns were required to overlap by 25% of the column diameter at the top reducing to 10% of the diameter at the base, to allow for drilling deviation.

A jet grouting trial, involving the installation of three pairs of columns, was conducted in order to determine the optimum jet grout parameters to suit the local soil conditions and hence be used in the production works. The column diameter was measured using two principle methods:

- Excavation of the completed columns allowing physical measurement and assessment of the jet grouted material;
- Observation of tell-tales or “radius tubes” installed within boreholes at varying radii from the centre of the column. Scouring of the painted surface of the steel tubes indicated contact by the grout jet and therefore the column diameter.

Samples of the completed column were recovered by rotary coring, logged and sent for UCS testing.



Figure 4 - Jet grout rig drilling installing the “radius tubes”.



Figure 5 – Left: Trial columns with painted circles showing the 2m target diameter. Right: The scoured "radius tubes"

For both the trial and production works, regular measurement of density, viscosity, bleed and Unconfined Compressive Strength (UCS) were used to verify the quality and consistency of the grout used. UCS cylinders were taken at a frequency of 1 set of 3 cylinders for each setup every day (2 setups in total). Density, viscosity and bleed was measured at a frequency of 3 tests per day per setup (2 setups in total).

The density and UCS of the jet grout spoil was also tested to observe the properties of the jet grouted soil, the frequency of testing was equivalent to that undertaken for the neat grout. The jet grout parameters, including grout flow rate, pressure, lift speed and rotation were measured by the rig instrumentation in real time and a graphical record produced.

TESTING OF THE JET GROUT COLUMNS

Testing of the completed jet grout columns was required to verify that the design and specification requirements were met. Rotary coring was undertaken to confirm column diameter, interlock between adjacent columns, continuity of treatment and strength of the treated material. The cores were logged and assessed by the percentage recovery, the dimensions of untreated zones and UCS testing of sections of core. It proved difficult to consistently achieve the specified 85% core recovery. To maximise core recovery and the quality of the core, different coring contractors and methods were employed and the most successful selected. Where anomalies such as zones of "soil-like" material were observed in the core, it was necessary to do further investigation to determine whether they indicated untreated soil or grouted material that had been reworked by the coring process. Several methods were used, including borehole camera surveys to inspect the bore holes.

Limitations of assessing the quality of the jet-grouting through core recovery

Generally, the camera surveys showed intact grouted material in the borehole. However two scenarios were encountered.

1) Where sands and gravel had been jet grouted, this material had the appearance of concrete (Figure 6). The very strong matrix of grout allowed a high core recovery. When the recovery

was not satisfactory, commonly due to the coring process, the camera survey confirmed the continuity and quality of the jet grouted material.



Figure 6 - Grouted sand and gravel in the wall of the core hole

2) Where a weaker matrix of grouted silt occurred, the core recovery was not sufficient to draw conclusions on the quality of the jet grouting. Borehole camera surveys were used to demonstrate an irregular surface within a competent grouted matrix. This irregular surface was created by the dislodging of pieces of gravel which were then gripped by the core barrel. Consequently, and through the rotating force of the core barrel, the pieces of gravel scoured the weak grouted matrix resulting in poor core recovery. (Figure 7).

This clearly emphasised the fact that assessing the quality of the jet grouting through the core recovery alone could be misleading. Typically when coring through a strong competent matrix the recovery was very high and further investigation was not necessarily required. However, when coring was employed through weaker grout matrices the recovery was poorer and led to doubt on the quality of the jet-grouting. The use of the borehole camera proved to be very useful in providing a continuous visual record and helped to dispel any uncertainty.



Figure 7 - Intact material within an irregular eroded surface

Limitations of the coring method to assess anomalies within the jet-grouting

Some anomalies were noted in the cores, including sections of what appeared to be loose grey "soil" containing angular gravel sized pieces of cemented jet grouted material. A high pH indicated the presence of cement within much of this material. Inspection of the borehole walls at the same depth identified a grouted mass with small soil inclusions. The combination of hard and relatively soft material proved difficult to core and occasionally broke up into the re-worked material observed.

Another anomaly was what initially appeared to be "clean washed" gravel. This was not entirely unexpected as similar gravel had been observed on previous projects including the Victoria Station Upgrade in London, where upon excavation, the jet grout columns had been seen to be fully grouted. The conclusion had been that the hard gravel pieces had rotated and ground up the relatively weak matrix allowing it to be washed away by the drill flush during coring. Close inspection of the gravel particles showed small patches of grouted matrix adhered to some of the surfaces. The drill returns collected showed fragments of grouted material and a high pH, indicative of cement. The camera surveys also demonstrated grouted material in the borehole wall.

Sampling tube

A further alternative to coring was the use of sample tubes. The tubes were pushed into freshly constructed columns and extracted the following day, once an initial grout set had occurred, to provide

a 100mm diameter continuous sample. This method was not appropriate for every location and soil horizon, as the tubes could not be pushed through significant obstructions such as large pieces of wood or gravely soils. Physical constraints such as limited headroom and subsurface structures also prevented the use of this method.

The sampling tubes did however provide good quality samples for inspection and UCS testing in the finer grained soils. The samples showed greater continuity of the grouted material than the core samples, as the sampling method did not significantly disturb or erode the sampled material. This avoided the need for additional methods of verification. Sections of core could be sent for UCS testing or cut longitudinally for inspection and logging (Figure 8).



Figure 8 - Jet grouted material recovered from a sampling tube

UCS testing of Jet Grout Spoil

Jet grout spoil was routinely collected during the works and used to form samples for UCS testing. This proved a simple and inexpensive method of obtaining representative samples. The method was expanded to provide samples at multiple elevations in several selected jet grout columns. The spoil UCS results fell within the range of data from the UCS testing of cores. As predicted, the spoil UCS results were generally at the lower end of the strength range as the relatively dense cement and larger soil particles tended to stay in the column, with a greater proportion of finer and lighter materials expelled as spoil. The spoil UCS was useful to verify the lower bound strength, proving it to be in excess of the required minimum of 2MPa at 28 days.

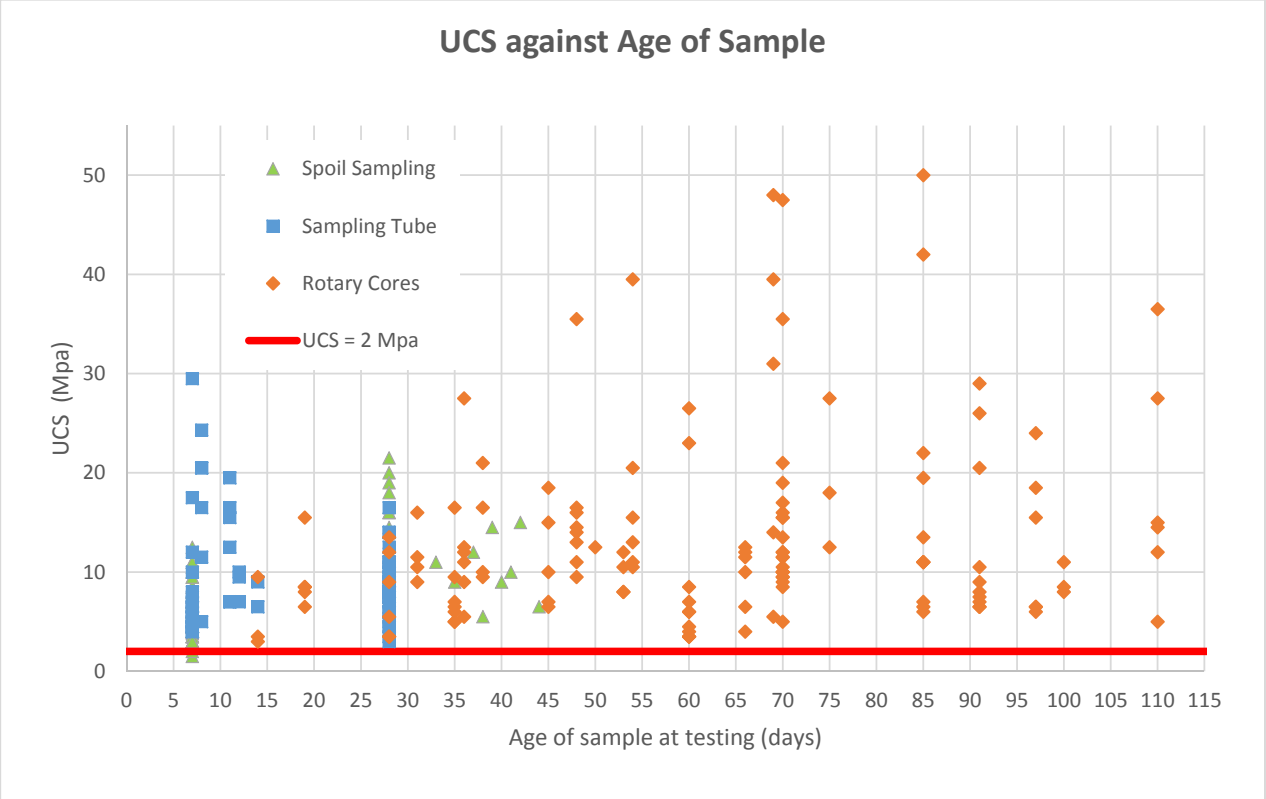


Figure 10 - UCS against age of sample

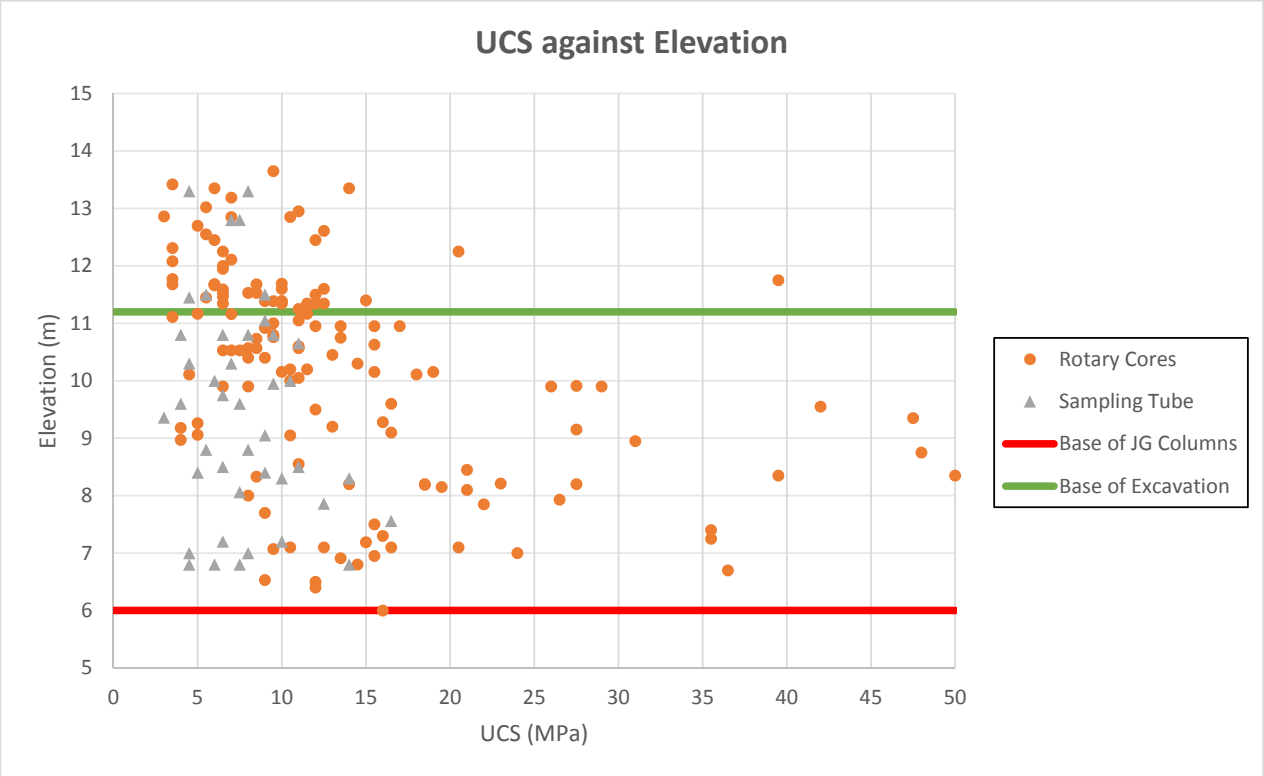


Figure 9 - UCS against Elevation

MACRO-SCALE AND MICRO-SCALE

As the works progressed, jet grout columns were exposed in the excavations for the new foundations, this enabled further verification of the column diameters and gave an opportunity to observe the internal structure of the columns. Small inclusions of intact cohesive soil were observed and described as “a soil aggregate in a grouted matrix”. On the macro scale of a 2m diameter jet grout column the grouted mass was relatively homogeneous and the soil inclusions were isolated and insignificant. However, in the relatively small diameter of a core, such inclusions may be interpreted erroneously as an untreated zone or allow the core to break up into sections of reworked material.



Figure 11 - Left: An exposed jet grout column approximately 2m wide. Right: Similar material in a sub 100mm diameter core.

CONCLUSION

The range of sampling, testing and evaluation methods adopted for the Christchurch Town Hall project provided a robust and comprehensive means to determine the effectiveness of the jet grout treatment on what was a challenging site with variable ground conditions.

The relative success of the primary investigation method, rotary coring, focussed attention on any anomalies observed. It prompted additional inspection to be undertaken and the use of alternative testing methods to verify that the soil had been cemented by jet grouting and that the anomalies were therefore the result of disturbance and modification during the coring process. The success of coring on past projects has been variable. On some projects it has provided satisfactory samples, on others the cores were clearly not representative of the grouted mass and therefore were discounted in favour of alternative inspection and testing methods.

When planning the sampling, testing and evaluation regime on future projects, a broad range of methods applicable to the individual site conditions should be considered, particularly where gravels, cobbles or boulders are present in a relatively weak grouted matrix. The comments on the American Society of Civil Engineers Jet Grouting Guide Specification, by the 2008 ASCE Committee on Grouting, provide useful guidance when planning the inspection and testing and also in the review of the results.

The risk of modification of the sample by the sampling technique should be considered. The use of the complementary and alternative techniques described above, may assist in this regard. No one technique may be suitable for all soil conditions on a site. Coring may be the most practical means of sampling one soil type, whilst another horizon may require a different technique for sampling or verification.

The Christchurch Town Hall project provided a useful opportunity to assess the relative merits of different sampling and verification methods and the additional experience and data gained, will prove invaluable for future projects.



Figure 12 - The jet grout columns exposed during excavation, with the target diameter shown in yellow painted circles.

ACKNOWLEDGEMENTS

The Authors wish to acknowledge the Client, Christchurch City Council, the Main Contractor and KGE – BPC JV's Client, Hawkins Construction; and the Client's geotechnical consultants, Tonkin & Taylor. The authors are appreciative of permission to include information, data and figures in this paper. All un-referenced figures are by Keller Ground Engineering.

REFERENCES

Tonkin & Taylor Ltd. Christchurch Town Hall Conservation Project - Technical Specification for Soil Stabilisation by Jet Grouting V1.6, Wigram, Christchurch, 2015.

Tonkin & Taylor Ltd. Christchurch Town Hall Conservation Project - Design Features Report For Overall Geotechnical Design, Wigram, Christchurch, 2014.

Tonkin & Taylor Ltd. Christchurch Town Hall Conservation Project - Geotechnical Factual Report, Wigram, Christchurch, 2014.

Keller Holding GmbH Christchurch Town Hall - Layout Design for Jet Grouting, Revision 7, Offenbach am Main, May 2016

Geo-Institute of ASCE Grouting Committee, Jet Grouting Task Force, Jet Grouting Guideline, June 2009

DESIGN, CONSTRUCTION AND DESIGN VALIDATION THROUGH HIGH STRENGTH TESTING (PDA) OF CFA AND DD FOUNDATIONS

Stefano Pirrello, Keller Foundations, Sydney, Australia, +61 0421 000 127,
stefano.pirrello@keller.com.au

Sydney's booming real estate market has pushed property developers to invest in historically "no-go" areas, which were previously too expensive to develop. These areas are usually near rivers where the sites are underlain by deep alluvial and estuarine sediments. In these ground conditions conventional bored pile techniques are often not competitive. Contiguous Flight Auger (CFA) and Drilled Displacement Piles (DD) techniques are on the other hand suitable for these ground conditions. This paper deals with the design and construction challenges encountered with these piling techniques for a series of high-rise towers in Sydney's West. The advantages of DD over CFA piles such as reduced overall spoil with substantial cost savings and achievable rock sockets in medium strength bedrock are discussed. Design validation through interpretation of real-time data from the piling rigs' on-board computer data, and low and high strain pile dynamic testing (PDA) is discussed. Testing data is presented as CAPWAP (Case Pile Wave Analysis Program) analyses for different concrete grades.

Keywords: Design of Pile foundations, CFA, DD, PDA, CAPWAP

INTRODUCTION

The booming real estate market in Sydney has pushed property developers in investing in historically "no-go" areas, which were previously too expensive to develop. These areas are usually near rivers where the sites are underlain by deep alluvial and estuarine sediments. In these ground conditions conventional bored pile techniques are often not competitive. Contiguous Flight Auger (CFA) and Drilled Displacement (DD) Pile techniques are on the other hand suitable for these ground conditions and were utilised using concrete injection methods. This paper deals with the design and construction challenges encountered with these piling techniques for a series of high-rise towers in Sydney's West.

GEOLOGY & GEOTECHNICAL CHARACTERIZATION OF THE SITE

The Sydney 1:100 000 Geological Series Sheet shows that the site is underlain by man-placed filling and alluvial/estuarine sediment. The sediment comprises silty to peaty sand, silt and clay. Shell layers are also expected to be present within the soil profile. The Prospect/Parramatta River 1:2500 Acid Sulphate Soil Risk Map shows the site as 'Disturbed Terrain' in which soil investigations are required to assess acid sulphate soil potential. Several Cone Penetration Tests and Boreholes were carried out during the geotechnical investigation. All boreholes were extended to bedrock and NMLC-sized diamond core drilling was used to obtain 50mm continuous core of the rock, enabling unconfined compression strength testing to be carried out on selected samples. A summary of the ground conditions encountered on this site and inferred from the CPTs can be described as follows:

- FILL (Unit A) – concrete, bitumen, sand, gravel and clayey filling to depths between 0.3m to 1.8m;
- ALLUVIUM (Units B and C) – clayey and sandy soils to depths of between 16m and 23m. The soils became firm to stiff (clays) and dense to medium dense (sands) with depth. Occasionally soft and loose layers were also encountered;
- SANDSTONE BEDROCK (Unit D) – encountered from depths of between 16m and 23m. The bedrock had typically a weathered layer low strength (LS, defined as having typical ucs values of 2 to 6MPa) up to 1m thick over medium strength (MS, ucs = 6 to 20MPa) to high strength to the base of the cores at 22m to about 30m.

Stiff clay/dense sand (i.e. Unit C) variability can be appreciated on the two cross sections of the site given in Figure 2 and Figure 3, below. The locations of the cross-sections along with the borehole locations are shown in Figure 1.

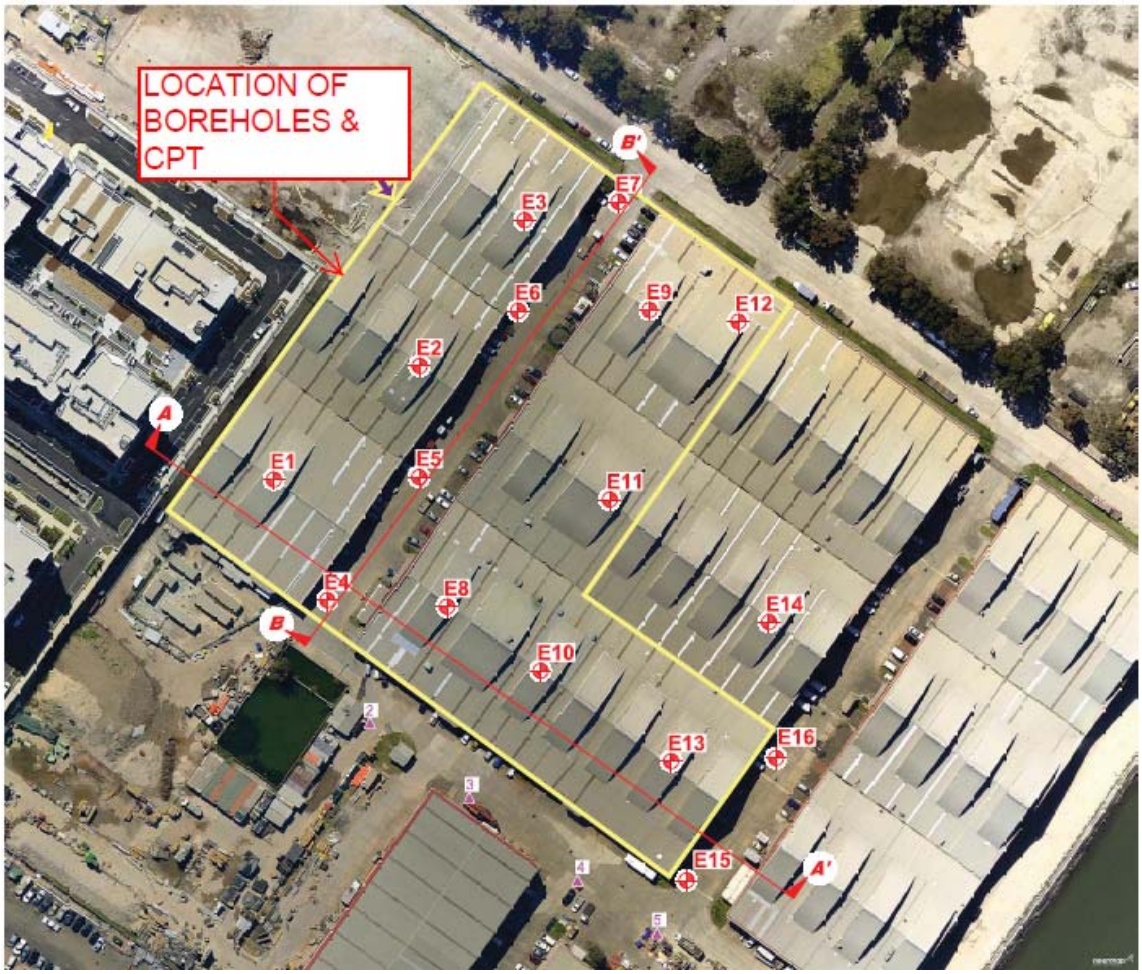


Fig. 1. Test Location

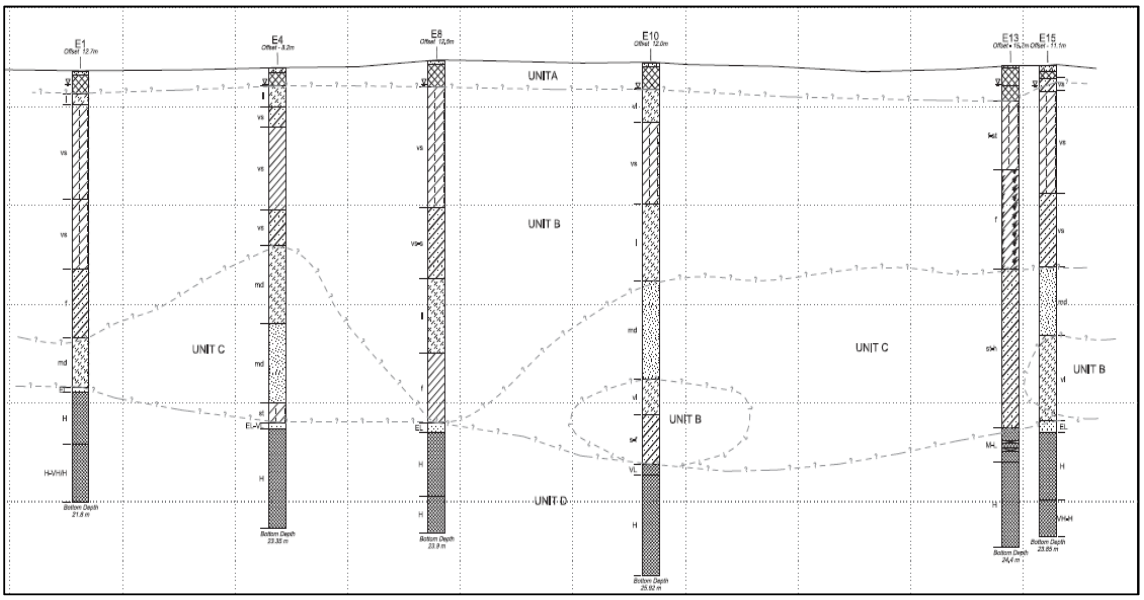


Fig. 2. Cross-section A-A'

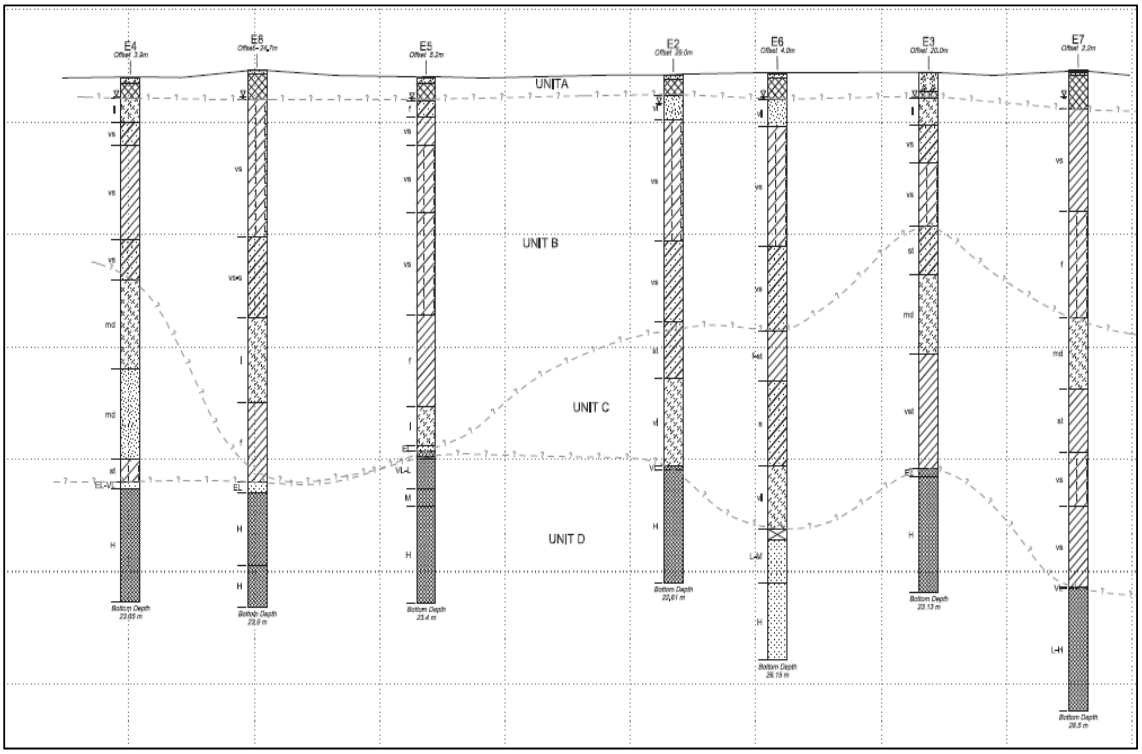


Fig. 3. Cross-section B-B'

PRACTICAL CONSIDERATIONS ON THE PILE TYPES ADOPTED FOR THIS SITE

CFA piles are a non-displacement form of cast in situ piles. Theoretically the volume of spoil coincides with the volume of the auger. DD piles on the other hand seek to laterally displace the soil and consequentially improve the latter, with the advantage of having virtually no spoil. Figure 4 below shows schematically the conceptual difference between CFA and DD penetration. A summary of the most popular displacement heads is presented in Figure 5.

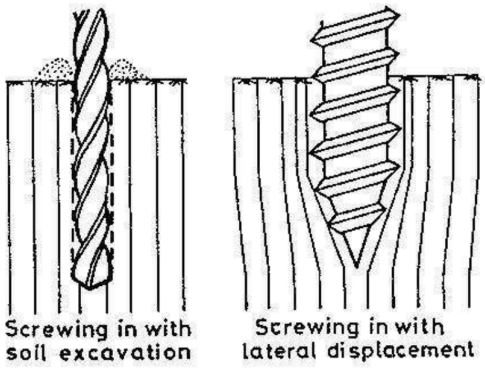


Fig. 4. Wood drill vs wood screw analogy (after Van Impe, 1988)

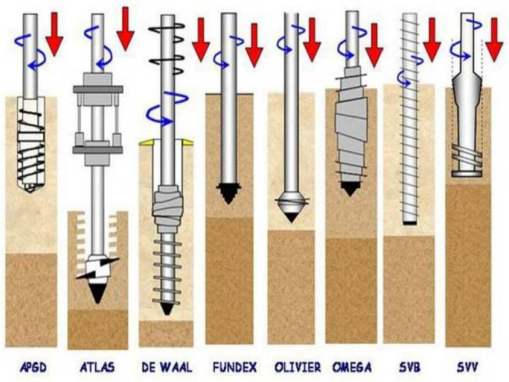


Fig. 5. Most popular full displacement augers (after Prezzi and Basu 2005)

A detailed explanation of these two piling system is outside the scope of this paper with the focus being the advantages and disadvantages of the respective pile types. CFA piles can be used in most soil conditions. Modern piling rigs have sufficient power and torque that can deliver a reasonably high production rate while achieving considerable depths with rock socket lengths often sufficient to satisfy design requirements. On the other hand DD piles have the limitation of not being able to displace the

soil when the soils are too stiff/hard or too dense. DD augers can be successfully employed when there is limited thickness of stiff soil over bedrock. For this project a stiff clay contour map was developed for this site, aiding with the assessment of identifying areas where one piling technology could be used over the other. This assessment was carried out using the available geotechnical data presented in Figures 2 and Figure 3. The results of the inferred Unit C contour map is presented in Figure 6 below.

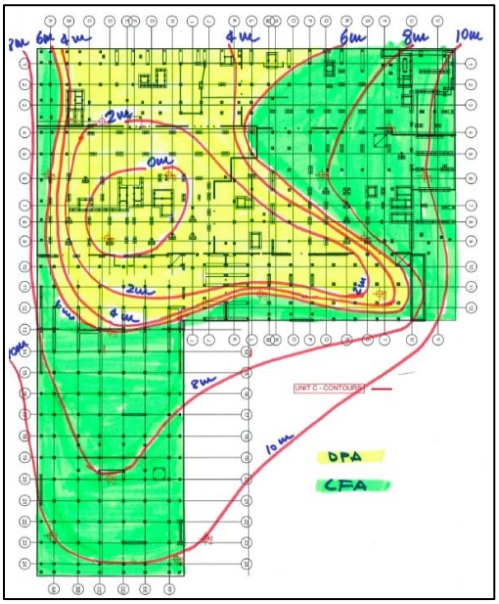


Fig. 6. Unit C - Contour Map

As can be seen from the contour map shown above, the area with no or little stiff clay (zero metre contour line) is limited to a small area compared to the overall site area. If traditional DD heads presented in Figure 5 were used, this would result in CFA Piles being used for 80% of the project piles because the DD piles could not achieve the required socket lengths in the rock. The high costs of spoil removal resulting from a predominantly CFA solution on this project would have a detrimental effect on project costs. As a consequence every effort was made to reduce the volume of spoil generated by piling. A displacement auger capable of drilling through thicker layers of stiff clay and founding in the rock, extend the chances of its applications within this site. Figure 7 shows the modified DD head custom made for this site.



Fig. 7. Keller's modified DD head.

The DD head adopted was a hybrid of the Omega and De Waal heads, utilizing an "Omega-type" head with a 3m to 6m auger extension. This guaranteed extending the application of the DD piles within layers up to 6m of Unit C, while still delivering the required designed minimum pile sockets of up to 1m length in the MS Sydney Sandstone.

PILE DESIGN & SETTLEMENT PREDICTION

The pile design was carried out in accordance with limit state procedures as outlined in the Australian Standard AS2159-2009, which requires piles to fulfil both serviceability and strength requirements. The geotechnical reduction factor adopted for low and high redundancy piles was 0.65 and 0.71 respectively. The foundation design for this project comprised the design and construction of over 800 piles, the final scheme comprising 55% CFA piles and 45% DD. Pile diameters comprised 600mm and 750mm, with all piles being socketed up to 1m into MS Sandstone to meet design requirements. The proposed development extends to an area greater than 24 football fields. Different design zones were developed, targeting any significant variability of the soil and bedrock profile. Differences such as thicknesses of soft soil (i.e. Unit B), Unit C, and levels of the MS Sandstone had to be assessed and considered in the design. A typical geotechnical soil profile for this site is presented in Table 1.

Table 1. Typical Soil Profile and Geotechnical Parameters

Unit	Thickness (m)	Base of unit RL m AHD	Ultimate Shaft Adhesion (kPa)*	Ultimate End-Bearing (kPa)*
B	10	-8	15	-
C	8	-16	40	-
D(LS Sandstone)	2	-18	120	-
D (MS Sandstone)	N.A.	N.A.	450	30000

Note: (*) LS and MS sandstone parameters were based on Pells (1998)

As all piles were founded in bedrock any potential ground improvement in the case of the DD piles was ignored, so technically these piles were designed as CFA piles. Structural capacity of the piles was dictated by Clause 5.3.4 AS2159-2009, which states that for partially reinforced piles the maximum structural load allowed is essentially $0.3f'_cA_g$. Table 2 shows the maximum design loads for 600mm and 750mm piles.

Table 2. Maximum Structural design load for partially reinforced piles on this site

Diameter (mm)	f'c (MPa)	Eds(kN)*	Ed*(kN)
600	65	4075	5500
750	65	6370	7550

Note:
Eds = serviceability load
Ed = Factored design load
(*)Eds ≈ Ed/1.35

Negative skin friction, assessed to be 20kPa, resulting from the consolidation of the compressible layer, Unit B, provided an additional load to be considered for both the structural pile design and for serviceability assessment. Pile settlement predictions under ultimate and working load were assessed with aid of the commercial program RATZ, written and developed by Randolph (1994). Table 3 provides the settlement estimates, including both pile shortening and negative skin friction effects, for the piles loaded in accordance with Table 2.

Table 3. Settlement prediction under serviceability load

Diameter (mm)	f'c (MPa)	Eds(kN)*	δ (mm)
600	65	4075	9
750	65	6370	12

CONSTRUCTION ASPECTS AND QA

Two major construction aspects were concerning the designers while opting for the revised DD head. These were:

1. The uncertainties related to the performance of this new auger drilled through an unusually thicker Unit C layer. In particular, in case of slow penetration, a combined effect of a prolonged penetration and high torque could lead to the "*side loading" (also known as "flighting" or "soil decompression")* effect for the non-cohesive component of Unit C. This would make the soil surrounding the auger collapse onto the auger.
2. Consideration was also given to the potential within Unit C layer of built up pore pressures due to the displacement effect within the clay potentially causing squeezing of newly formed adjacent pile shafts.

The CFA and DD piling rigs were all equipped with on-board computers (PL3000) which allow the site personnel and the designer access to continuous monitoring of the all aspects of pile construction in real time. This information includes:

- Boring rate (m/min);
- Penetration rate(mm/rev);
- Extraction rate (m/min);
- Torque (% of maximum);
- Concrete pressure (bar);
- Concrete oversupply (% above theoretical) and Ideal pile shape

The penetration rates and torque from the PL3000 records served to provide confirmation of rock head levels and socket lengths. The analysis of the above information, along with the validation of the rationalised design profile assumed, provided the designers with the confidence required for successful penetration of the Unit C layer in a timely manner.

EFFECTS OF DD INSTALLATION

The opportunity was taken to carry out an additional geotechnical investigation involving CPTu probes aimed to assess pore pressure prior and after installation of DD piles. The CPTu's were carried out prior and after construction of piles. The results showed that the water pressure rarely increased due to the installation process and where increases occurred, those increases were modest and always less than the concrete pressure during which the piles were built. Figure 8, shows the CPTu testing arrangement prior to and after installation of the piles.

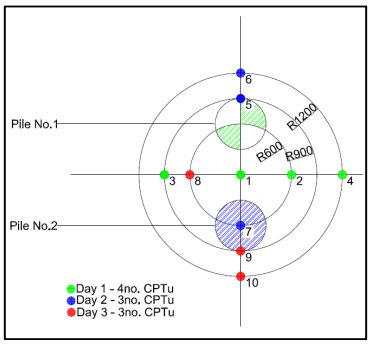


Fig. 8. Keller's CPTu test rational.

CPTu tests were positioned at concentric distances of 1d, 2d and 3d from the middle of the twin pile configuration. The testing sequence was carried out as follow:

- Day 1 – #4 CPTu test were carried out (i.e. 1 to 4) prior installation of the first pile (i.e. green pile);
- Day 2 - #3 CPTu were carried out (i.e. 5 to 7). Then the second pile (i.e. blue pile) was installed;
- Day 3 - # CPTu were carried out (i.e.8 to 10).

Typical results of CPTu tests carried out are prior and after installation are given in Figure 9.

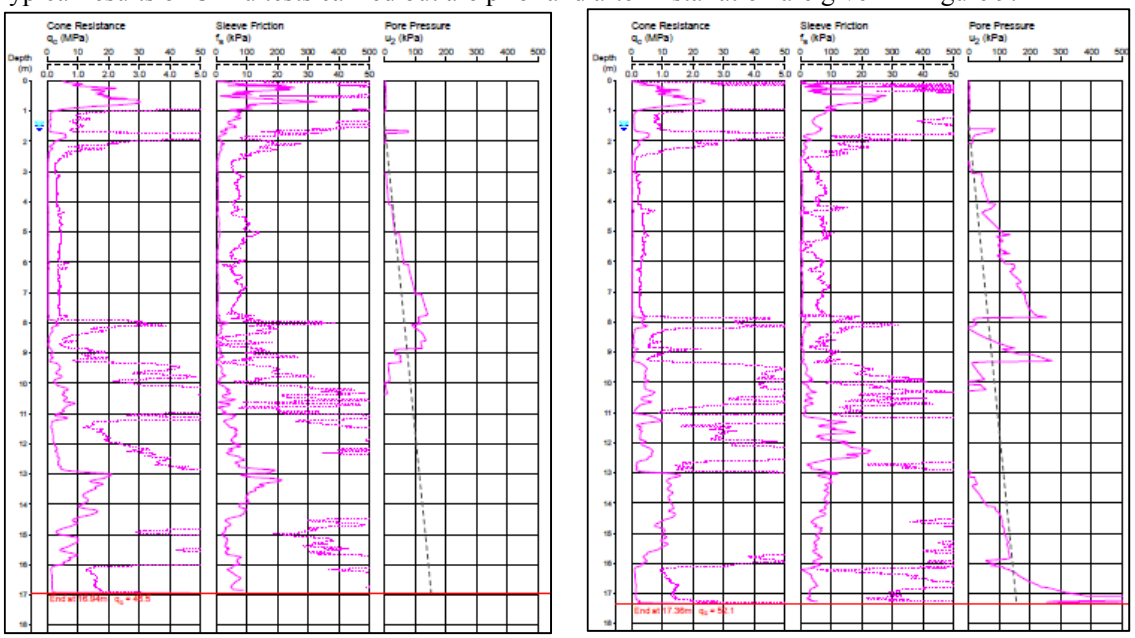


Fig. 9. Typical CPTu results. From left to right CPTu1 and CPTu7

The increase of pore pressure after installation can be appreciated in CPTu7 at 8m and 9.5m depth. However, this increase is still less than the concrete head pressure and therefore the integrity of the newly formed pile shafts is not a concern. An increase in pore pressure greater than the concrete head pressure would be a potential indicator of damage to the pile e.g. pile "necking" at the depths where the pore pressures exceeded concrete pressures.

PILE TESTING

Dynamic pile testing was carried out on 18 Piles, of which 7 of the more heavily loaded piles are presented. Dynamic pile testing is widely accepted in the Australian piling industry as an alternative to conventional static tests. The test is regarded as being sufficiently accurate but at a much lower cost than alternative load tests and regarded as an excellent tool for assessing pile performances economically. The total number of tests performed represented 2.3% of the total number of piles installed, but this was considered satisfactory given previous extensive experience from adjacent sites, supplemented by data from the PL3000 monitoring that confirmed socket length requirements. Unit pile loads and settlement criteria were satisfied in accordance with AS2159-2009. Settlement due to negative skin friction was also considered in accordance with clause 4.6.3 of AS2159-2009.

All piles tested were production piles socketed into the sandstone bedrock. A potential disadvantage of dynamic testing of reasonably highly loaded piles is that the hammer drop height must be sufficient to deliver enough energy on the pile to mobilise and prove the required pile resistance whilst not damaging the pile. None of the piles were damaged during the tests as the developed stresses within the piles due to the dynamic impact were continuously monitored. Test signals were recorded on site by means of PDA monitoring and testing devices. "Table 4", reports the test results. Pile test analyses were carried

with CAPWAP, from which the interpreted load displacement curves at construction stage are given in Figure 10 and Figure 11.

Table 4. Summary of dynamic pile loading test results

Pile ID	Pile dia (mm)	Installed depth (m)	Ed/φ_g	Mobilised End Bearing (kN)	δ Mobilised Resistance (mm)
242	600	21.5	6600	8250	22
167	600	22.0	7909	7985	21
211	600	21.4	3365	6295	15
203	600	21.0	3365	9226	22
248	600	21.5	6600	5548	16
126	750	23.3	11574	18000	28
232	750	23.3	9474	6678	21

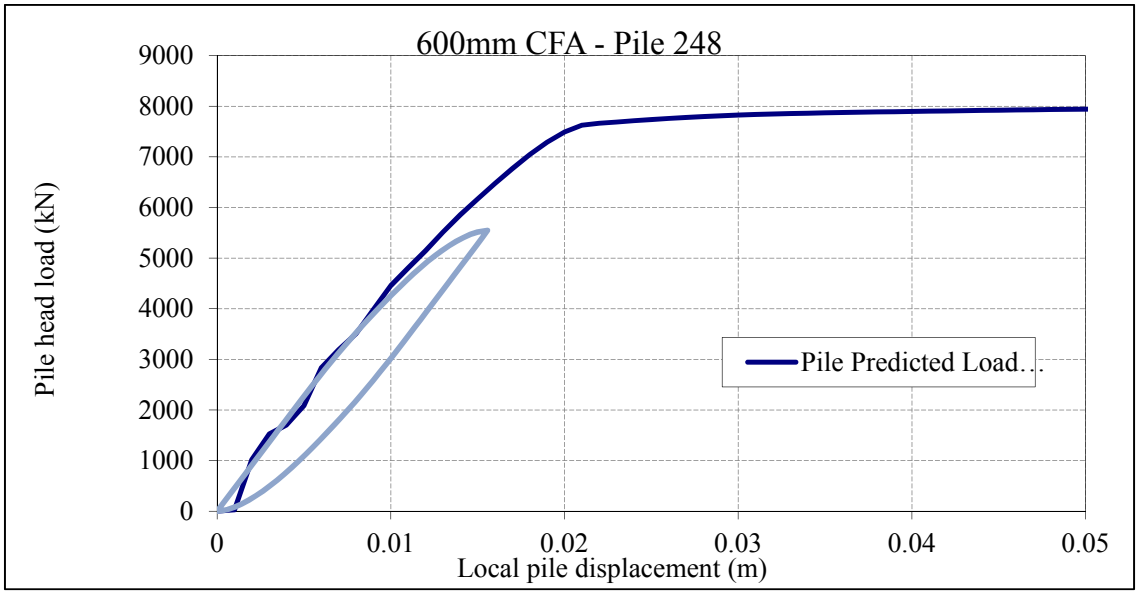


Fig. 10. Pile 248 - Predicted vs Tested Load/ Settlement Curve.

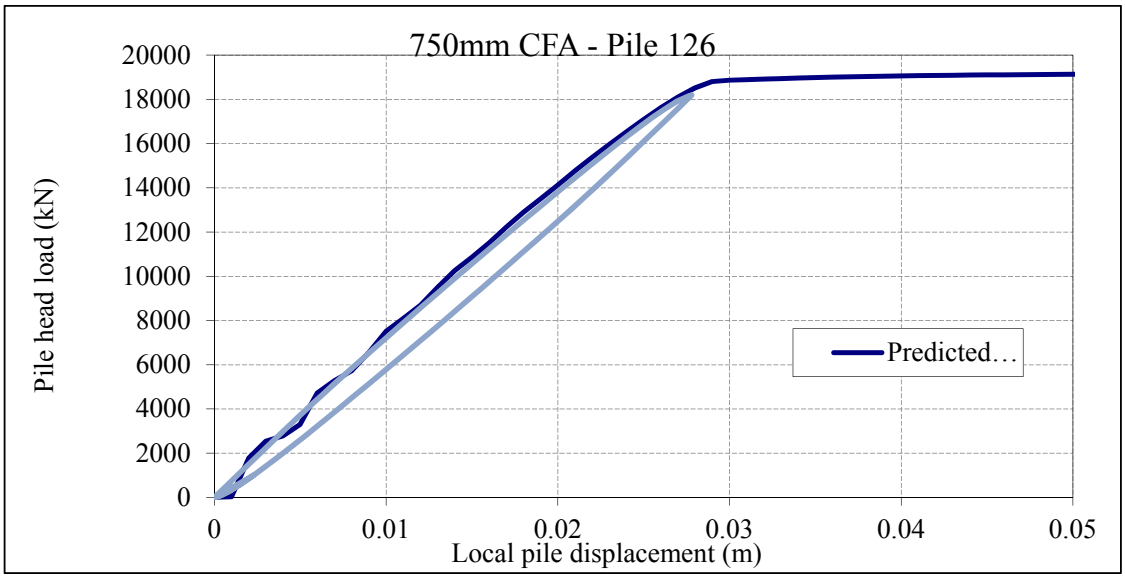


Fig. 11. Pile 126 - Predicted vs Tested Load/ Settlement Curve.

Figure 10 and Figure 11 show that in both piles #126 and #248 the pile capacity was not fully mobilised. This pile response is typical of a pile socketed in bedrock where a lot of energy is required to induce the deflection required to fully mobilise all of the socket resistance, particularly end bearing.

SUMMARY AND CONCLUSION

Technical differences between CFA and DD piles were briefly discussed. The main focus of this paper is to explain the rationale of selecting one method over the other and its application and limitations within different ground conditions.

DD pile augers were adopted to offset construction limitations so they could be employed in stiff soil layers. The quality control during construction was also discussed focusing on two major aspects such as “side loading” and “pore pressure increase”. Design load settlement predictions were validated by means of comparison with PDA testing carried out on the same piles.

The work was completed on time and on budget.

ACKNOWLEDGEMENTS

The author would like to thank all colleagues involved in the project from conception to delivery. A special mention goes to the construction team on delivering a state of the art product, which enabled designers to push the design envelope.

REFERNCES

Australian Standard, AS2159-2009. Piling- Design and installation.

Brown, D.A, 2005. Practical considerations in the selection and use of continuous flight auger and drilling displacement piles. American Society of Civil Engineers, ASCE J. Geotechnical special publication No.132, pp.1-11.

Larish, M.D, Williams, D.J., Slatter, J.W., 2012. Load capacity of auger displacement piles. International conference on ground improvement and ground control (ICGI 2012).

Larish, M.D, Arnold, M., Uhlig, M., Schwiteilo, E., Williams, D.J., 2013. Stress and displacement monitoring of auger displacement piles. Proceedings of Pile, June 2-4, Vol. 1, pp. 1-12.

Larish, M.D, Nacke, E., Arnold, M., Scheuermann, A., 2014. Simulation of auger displacement installation. International Journal of Geotechnical Engineering, Vol. 8, pp. 458-462.

Pells, P.J.N, Dougals, D.J. Rodway, B., Thorne, C., McMahon, B.K., 1978. Design loadings for foundations on shale and sandstone in the Sydney region. Australian Geomechanics J. Vol.G8, pp. 31-39.

Pells, P.J.N., 1998. State of practice for design of socketed piles in rock. Proceedings of the 8th A.N.Z. Conference on Geomechanics, Hobart, pp. 307-326.

Randolph, M.F., 1994. RATZ load transfer analysis of axially loaded piles, program manual.

Slatter, .J, 2006. Recent developments in continuous flight auger (CFA) and cast-*in-situ* displacement screw piling in Melbourne. Australian Geomechanics J. Vol. 41, No. 3, pp. 17-24.

Van Impe, W.F., 1988. Considerations on auger pile design. Proc. of 1st 2nd Int. Conference on Deep Foundations on Bored and Augered Piles, Ghent, Balkema.

Van Impe, W.F., 1994. Influence of screw pile installation parameters on the overall pile behaviour. Workshop 'Piled Foundations: Full Scale Investigations, Analysis and Design', Naples.

CENTRIFUGE MODELLING OF DISPLACEMENT PILES AND INSTALLATION EFFECTS

L. King, Monash University, Clayton, Victoria, Australia, louis.king@monash.edu
A. Bouazza, Monash University, Clayton, Victoria, Australia, malek.bouazza@monash.edu
J. Gniel, Golder Associates, Richmond, Victoria, Australia, jgniel@golder.com.au
C. Gaudin, Centre for Offshore Foundation Systems, University of Western Australia, Perth, Australia, christophe.gaudin@uwa.edu.au
C. O'Loughlin, Centre for Offshore Foundation Systems, University of Western Australia, Perth, Australia, conleth.oloughlin@uwa.edu.au

ABSTRACT

This paper presents some recent advancements in centrifuge modelling, which enable the installation of displacement piles to be performed in-flight while measuring ground responses. Details and results are provided from a series of experiments where 21 full-displacement piles were installed into a sample of consolidated kaolin clay at 40g. The piles were pushed into the sample at a constant rate of penetration, with installation reaction loads and pore pressures measured. Insight into the installation effects of the full-displacement piles was obtained by undertaking in-situ testing pre- and post-installation of piles. The findings show that centrifuge testing has the potential to play an important role in furthering the current understanding of displacement pile behaviour and installation effects.

INTRODUCTION

Displacement piles and displacement ground improvement columns cause soil to undergo significant distortion and shearing during installation, which alters the soil properties. It is essential to consider these changes in soil properties to estimate the behaviour of pile foundations with higher degree of accuracy. However, the installation effects of displacement piles are widely considered as one of the most difficult geotechnical mechanisms to model, both analytically and numerically, and experimental data is needed to advance the current state of knowledge.

Theories, analytical and semi-analytical, have been developed to describe the displacement pile installation process. Randolph et al. (1979) applied the cylindrical Cavity Expansion Method (CEM) to model the installation of a displacement pile in a fine grained cohesive soil. However, cylindrical CEM only considers the field variables in radial coordinates, and hence the soil-pile interface can only be modelled as a frictionless material. Baligh (1985) introduced the Strain Path Method (SPM), which assumes soil flows around the tip of a displacement pile. SPM was shown to model the stress and strain fields, particularly within close proximity to the pile, more accurately compared to the cylindrical CEM. While these methods account for the installation effects of a displacement pile and can be used to estimate a resulting ultimate bearing capacity, they are unable to describe the load-settlement behaviour of such piles. With the added complexity of group effects, existing analytical methods do not provide a means to accurately calculate the ground response to the installation of a group of displacement piles in a cohesive soil.

The advancement of computational power, numerical techniques and constitutive models has improved the accuracy of numerical analysis, particularly in regard to modelling pile installation. However, even with advanced techniques, Finite Element Method (FEM) suffers a number of disadvantages due to the large deformations, which results in mesh distortion and tangling. Mesh-free methods such as Discrete Element Method (DEM), Smoothed Particle Hydrodynamics (SPH) and Material Point Method (MPM) are the next generation of computational techniques that are able to deal with large deformation problems. However, these advanced techniques are computationally expensive, complex and yet to be incorporated into commercial packages. Such methods are considered to still be in the development stage and are yet to provide a complete solution to pile installation problems.

While full-scale trials and case studies are an ideal method to provide insight into displacement pile installation effects, they can be costly, time consuming and difficult to instrument. Physical modelling at enhanced gravitational fields provides an alternative to full-scale trials, where engineering stresses are maintained through scaling laws (Garnier et al. 2007). These scaling laws are favourable when investigating the time-dependent behaviour of cohesive soils, since a 1/N scale model subjected to an N x g acceleration field will undergo consolidation at a rate of N^2 times faster than the prototype. For the testing of pile installation effects in cohesive soils, centrifuge modelling allows the dissipation of excess pore water pressures and the pile load-settlement behaviour to be captured over much shorter timeframes than the prototype.

As part of a broader research topic studying piled embankments, 45 displacement piles were installed into a sample of consolidated kaolin clay, 21 of which were jacked into the sample at 40 g. The testing was undertaken at the University of Western Australia (UWA) centrifuge facility. An Accutronic Model 661 beam centrifuge which has a 40 g-tonnes capacity and a platform radius of 1.8 m was used for this test. The Model 661 platform supports a 'strongbox' with the internal dimensions of 650 mm long, 390 mm wide and 325 mm in height. Details of the facility have been provided by Randolph et al. (1991).

This paper provides an outline of the physical modelling techniques and equipment that have been developed, and how they may provide useful information for conventional and innovative foundation systems. Specifics of a recent research project are provided as an example of current practice.

CENTRIFUGE MODELLING TECHNIQUES FOR INSTALLATION OF DISPLACEMENT PILES

Modelling installation effects within a centrifuge requires the soil properties and installation process to be accurately replicated, the structural and ground responses to be monitored and the material properties to be precisely characterised. Over recent decades the physical modelling community has made substantial advancements that enabled each of these key aspects to be performed. The following section provides background to some techniques and technologies that are available as well as details from a recent project, referred to as the piled embankment model tests.

Material preparation

Soils may be reconstituted in the strongbox using a number of processes. Clayey soils are typically prepared as a slurry under vacuum, with a moisture content close to twice the liquid limit. The slurry is then slowly poured into the strongbox and put under a press or consolidated within the centrifuge to achieve the desired strength profile. Soils from a specific site or location may also be reconstituted to accurately model the prototype. The properties of the prepared sample can be confirmed prior to installing piles by undertaking in-situ testing.

As part of the piled embankment model tests, a commercially available kaolin was used to model natural clay. Dry kaolin clay powder was mixed with water under a vacuum to form a slurry with a moisture content of 120 %. A 10 mm layer of sand was placed at the base of the strongbox prior to the placement of kaolin to provide a free drainage layer. The first layer of kaolin was placed under a press with a uniformly applied load of 100 kN (394 kPa) for two weeks, at which point axial displacements of the press had ceased. A second layer of kaolin slurry, prepared in the same manner as the previous layer, was then poured slowly into the strongbox. The sample was then consolidated in-flight for over 3 days at 60 g. The intention of the two layers of kaolin was to model an upper very soft clay layer and a deeper firm clay layer, which the piles were founded in (Fig. 1).

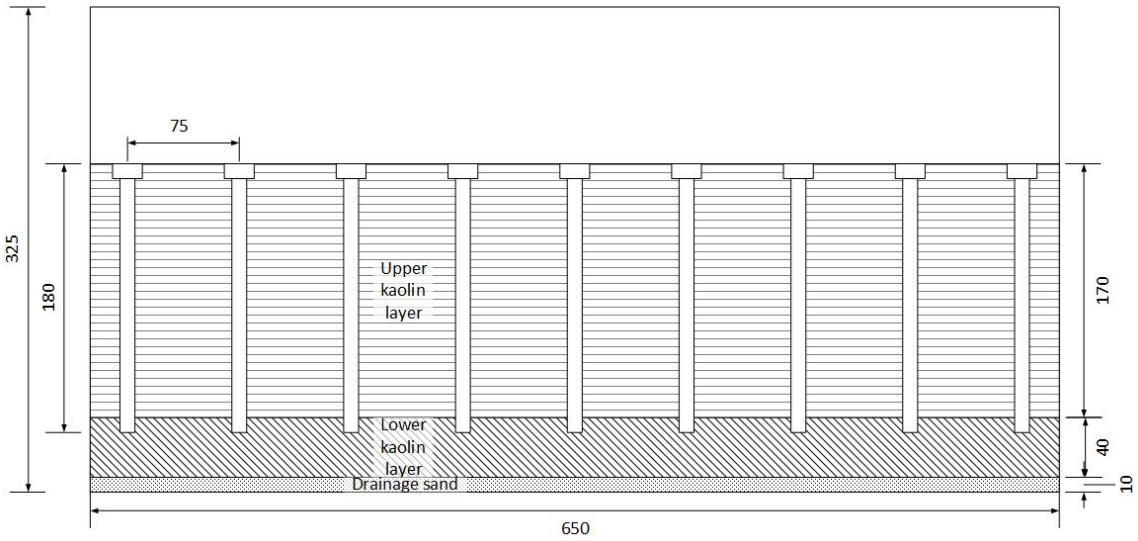


Fig. 1. Cross section (lengthways) through the piled embankment model (dimensions in millimetres)

Pile installation

In-flight actuators allow a range of processes to be carried out during a centrifuge test, including pile installation. Multi-axis actuators and control systems, such as the Package Actuator Control System (PACS) that has been developed at the University of Western Australia (De Catania et al. 2010), provide centrifuge users with the ability to undertake complex motion and load sequences.

The installation of a jacked pile in-flight may be replicated by pushing a prefabricated model pile into the soil sample using an actuator at a constant rate of penetration. The installation reaction loads are measured by an internal actuator load cell or by attaching a load cell between the pile head and actuator connection. This also provides an indication of the initial undrained ultimate bearing capacity of the pile, prior to any consolidation and pile set-up occurring.

More complex installation techniques may be modelled with the use of advanced actuators and control systems. Vibration displacement piles have been modelled by superimposing a sinusoidal motion over the constant penetration rate described above, a technique possible with the PACS. This method was described by Henke and Bienen (2014), however it was noted that the speed of vibration was too slow due to actuator limitations. The installation of driven piles has been performed in-flight with the use of miniature pile driving actuators, which simply allows a mass to free-fall under the enhanced gravitational field to scale the hammer energy appropriately (De Nicola and Randolph 1994).

Ground improvement installation techniques can also be modelled in-flight using specifically developed tools. Weber et al. (2006) described a method that simulated the installation of a dry, bottom-feed stone column. A hollow tube, which prevents soil from initially entering it, is inserted into a consolidated kaolin clay in-flight. Sand fills the hollow tube, which is then extracted. Upon extraction the tube is reinserted in a stepwise manner to compact the stone column.

For the piled embankment model tests, piles were jacked into the prepared kaolin sample at a constant rate of 1 mm/s, which is equivalent to an installation velocity of 4 cm/s in prototype scale. To reduce the effects of boundary conditions on the instrumented piles, a perimeter row of piles was installed with no instrumentation. Due to the limitations of the actuator system, these perimeter piles had to be installed at 1g. After the 1 g installation was complete, the remaining piles were jacked into the sample at 40 g (Fig. 2).

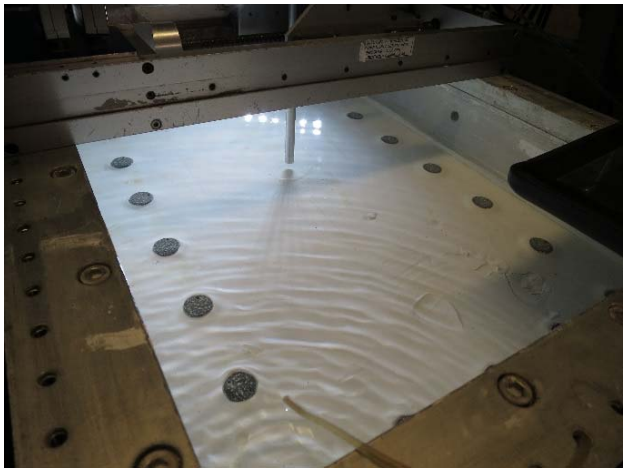
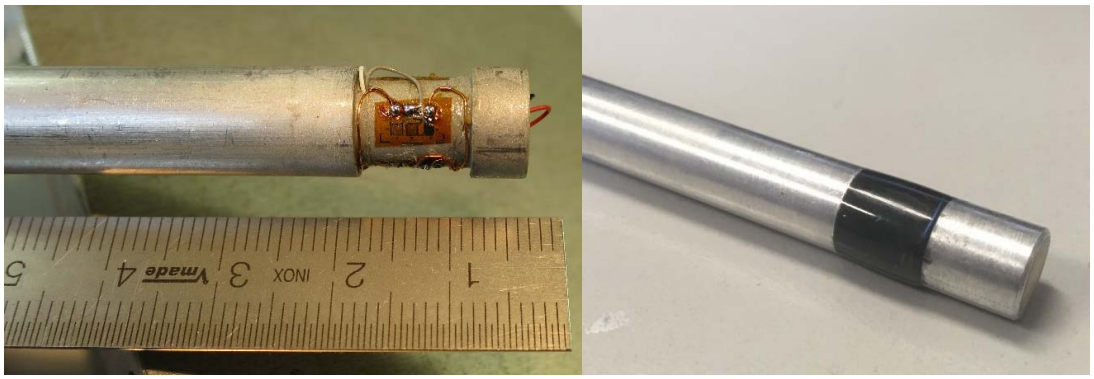


Fig. 2. Pile being jacked into a sample of kaolin clay in-flight

Instrumentation

Pile loads are commonly measured using strain gauges carefully attached to the pile shaft, which measure a change in resistance that is calibrated to provide an axial load within the pile shaft. These strain gauges, when used in quarter and half bridge arrangements, should be selected based on the model pile material to ensure the appropriate thermal resistance is applied. The instrumented area of the pile shaft should also be designed to ensure microstrains within the working limits of the strain gauge are achieved under the expected pile loads. By instrumenting the pile with load cells at multiple locations along the pile shaft, the load distribution with depth can be estimated.

The model piles for this project comprised 10 mm diameter hollow aluminium tubing, with a 1.6 mm wall thickness, which was locally thinned to 0.5 mm wall thickness at the strain gauge locations (Fig. 3) to ensure optimal strain (300 – 1000 microstrain) was achieved under the expected pile loads. During the early stages of model construction, each load comprised 2 opposite 90 degree tee rosettes connected to form a bridge. When calibrating these load cells it was found that the arrangement produced poor repeatability due to slightly non-axial loading conditions. To reduce the error that was experienced with the first strain gauge arrangement, the final model comprised 2 bridges at each load cell, which when positioned around the pile shaft was able to average the strains. This arrangement achieved accurate calibrations.

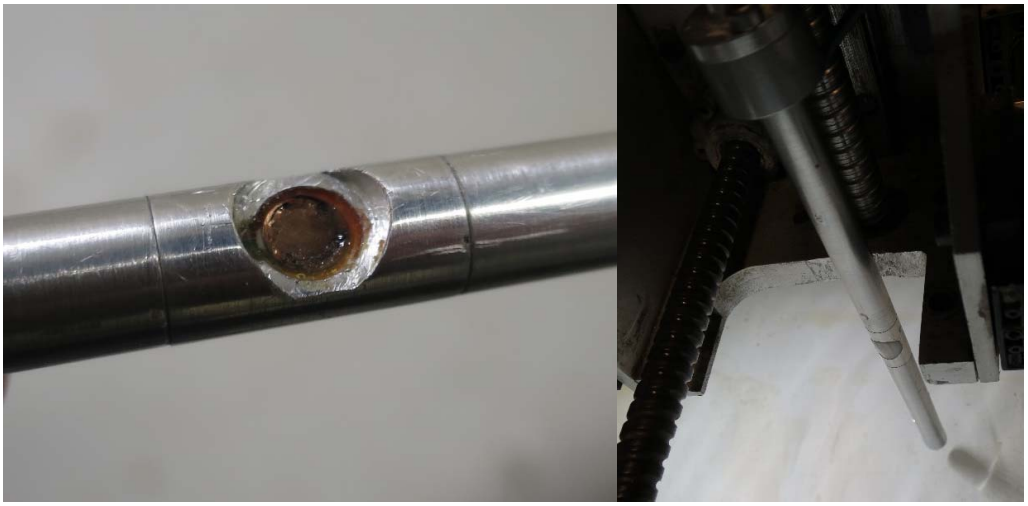


(a) (b)

Fig. 3. Pile load cell: (a) strain gauges attached to pile shaft; and (b) finished pile load cell with epoxy resin covering the strain gauges

It is widely acknowledged (Dunnicliff 1988; Weiler and Kulhawy 1982) that it is difficult to measure soil stress with great accuracy. Further challenges arise when measuring stresses at small scales, due to the reduced sensing area (diaphragm). Zhu et al. (2009) highlighted the cell action errors that can be expected from a range of commonly used miniature pressure sensors. To account for such errors, complex calibrations must be undertaken, which may only reduce the error to within a tolerable limit. Due to these limitations, soil stresses were not measured within the piled embankment model tests.

A more common application for these miniature pressure sensors is the measurement of pore pressures. Porous filters are placed over the pressure sensor, as shown in Fig. 4, which prevents any soil coming into contact with the diaphragm, and enables contact between water and diaphragm. This was the technique used to instrument piles within the piled embankment model tests, where pore pressure transducers were constructed at the mid-point of the pile shafts.



(a) (b)

Fig. 4. Model pile instrumented with pore pressure transducer: (a) pressure sensor at the mid-point of a pile shaft; and (b) pile with porous stone being jacked into kaolin sample in-flight

Displacement fields are measurable through several types of instrumentation. Laser displacement transducers are able to measure surface movements with high accuracy and sampling rates, which enable measurements like heave during pile installation to be measured. Alternatively linearly varying differential transformers (LVDTs) may be used to measure displacements of a structure, which requires the LVDT to maintain a point of contact and can impose undesirable actions. However, these methods do not provide a reliable means to measure displacements within a soil mass. An alternative to physical measuring devices is the technique of particle image velocimetry (PIV). PIV uses digital photographs and image correlation techniques to determine displacement vectors. White et al. (2003) developed software specifically to measure soil deformation within centrifuge models. In regard to pile installation, half model piles can be installed into a soil sample behind a Perspex window. Digital photographs are recorded looking through the window at time intervals throughout the test, and by implementing techniques such as PIV, displacement vectors are derived. This technique has not been used in the current piled embankment model tests, however ongoing research is planning to do such experiments.

Material characterisation

A range of in-situ tests can be implemented in-flight to accurately measure soil properties. Small scale piezocones (CPT) are commonly used, particularly in sands, to determine a range of properties. Since centrifuge modelling often tests soft and very soft clays, full-flow penetrometers (T-bar and piezoballs) have been increasingly used instead of piezocones due to their larger probe area (Fig. 5). These penetrometers develop a “flow-round” mechanism, which allows a more robust theoretical solution to be developed to relate shear strength and net penetration resistance (Einav and Randolph 2005).

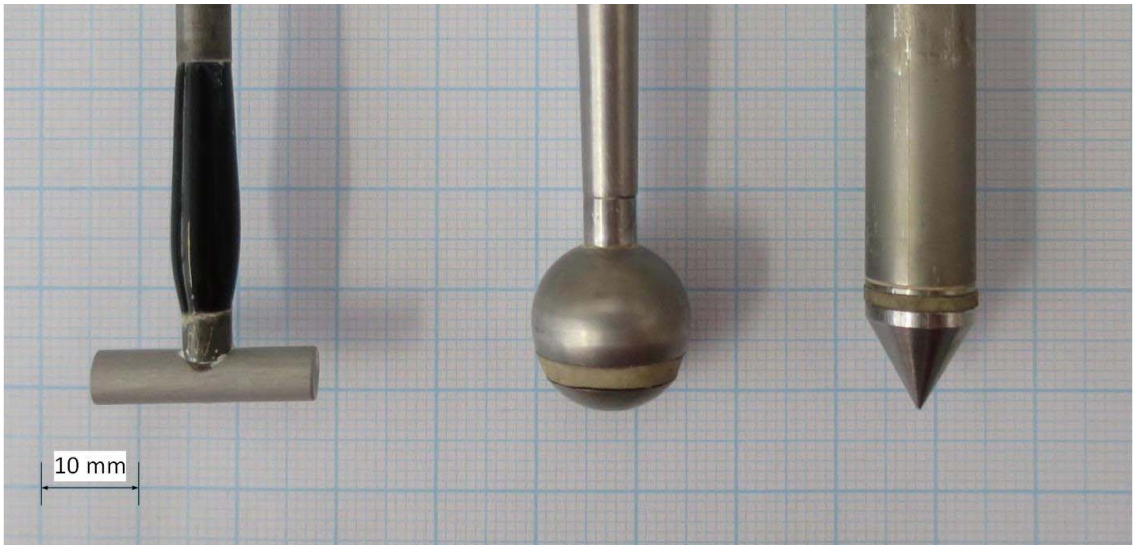


Fig. 5. Penetrometers commonly used in centrifuge modelling; from left to right, T-bar, piezoball and piezocone

These in-situ tests are able to be conducted prior to the installation of piles, to determine the initial soil properties. Subsequent testing may then be undertaken at various time intervals after the installation of piles to monitor the change in soil properties, or observe the dissipation of pore water pressures. This is a significant advantage of centrifuge modelling over field case studies, with in-situ testing rarely undertaken after the installation of piles as part of case studies.

RESULTS FROM PILED EMBANKMENT MODEL TESTS

A group of 45 displacement model piles were installed into consolidated kaolin clay, 21 of which were installed at 40 g. Pore pressures and pile installation loads were recorded, with T-bar penetrometer tests undertaken before and after the installation of piles. The model piles consisted of 10 mm diameter shafts installed on a 75 mm centre to centre grid, with 20 mm diameter enlarged heads. This resulted in a relatively low replacement ratio in regard to pile shaft (rather than enlarged head) of approximately 1.4 %, however, such replacement ratios are common for embankments supported on piles and ground improvement columns. The intention of the instrumentation and testing during the pile installation phase was to investigate whether such a low replacement ratio would significantly change the soil properties and affect the performance of the pile group.

T-bar penetrometer tests were performed after the kaolin clay had consolidated and prior to pile installation (TB02, TB03 and TB04), shown in Fig. 6a. After all 45 piles had been installed and pore pressures had been allowed to dissipate for 14 hours at 40 g, TB05 was undertaken. As can be seen in Fig. 6a, no strength increase was evident from the results of TB05.

Pile installation reactions were monitored, some of which are shown in Fig. 6b. The pile names are presented as the order they were installed, and their grid reference. For example, 5. G2 indicates the 5th pile installed at 40 g, in column G, row 2. The selected piles shown in Fig. 6b provide a spread of piles across the model area, with piles installed at the beginning and end of the installation phase. Again, while increases in pore pressures were recorded, no noticeable increase in pile installation reaction was observed.

A typical design assumption for designing embankments supported on displacement piles or columns, is to assume no strength increase results from the pile/column installation process. The results from these centrifuge experiments justify this design assumption for the pile arrangement and subsoil conditions tested.

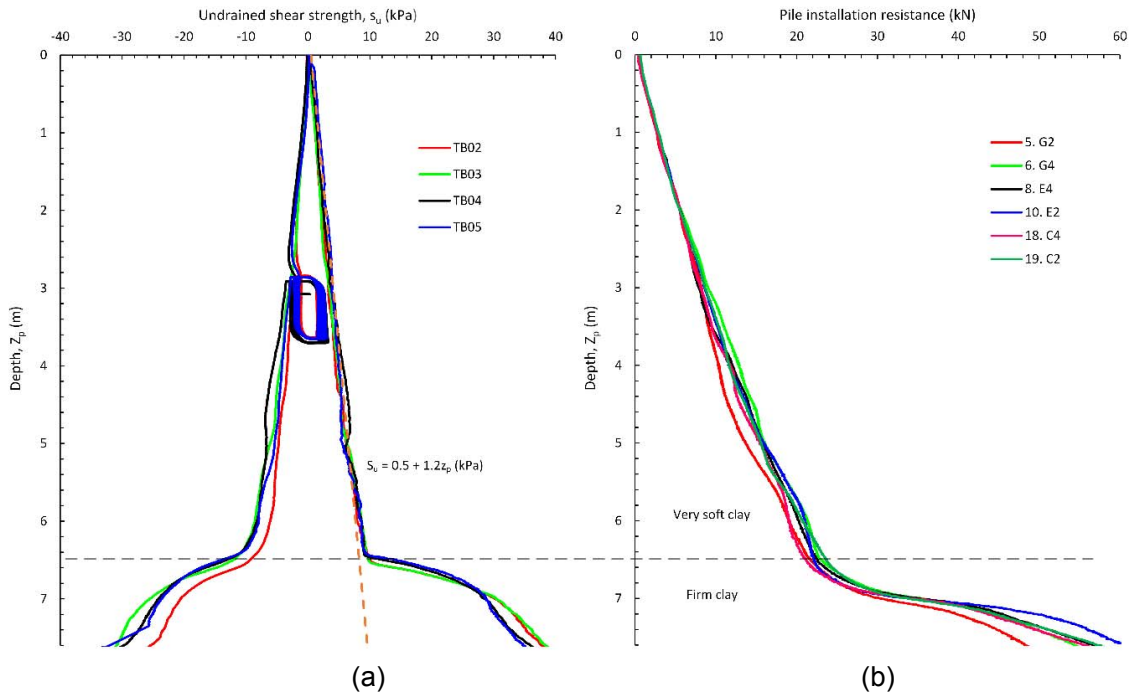


Fig. 6. (a) Undrained shear strength; and (b) pile installation resistance, plotted against depth (in prototype scale)

CONCLUSIONS

It has been shown that centrifuge modelling has the ability to replicate the installation of displacement piles and measure ground responses. Centrifuge model testing has been undertaken, where 45 displacement piles were installed into a sample of consolidated kaolin clay. Reaction loads and pore pressures were measured, as well as in-situ testing undertaken before and after piles were installed. For the materials and arrangement used, no significant strength increase resulted from the installation of piles. Experimental data from centrifuge modelling, such as the results presented, can assist in developing tools and techniques to quantify the behaviour of displacement piles.

REFERENCES

Baligh, M.M. (1985). Strain path method. Journal of Geotechnical Engineering, 111(9), pp. 1108-1136.

De Catania, S., Breen, J., Gaudin, C., and White, D.J. (2010). Development of a multiple axis actuator control system. Proceedings of the 7th International Conference on Physical Modelling in Geotechnics, Zurich, Switzerland, June 28 - July 1, pp. 325-330.

De Nicola, A., and Randolph, M.F. (1994). Development of a miniature pile driving actuator. Proceedings of the International Conference Centrifuge, Singapore, August 31 - September 2, pp. 473-478.

Dunnicliff, J. (1988). Geotechnical instrumentation for monitoring field performance, John Wiley & Sons, New York, pp. 165.

Einav, I., and Randolph, M.F. (2005). Combining upper bound and strain path methods for evaluating penetration resistance. International Journal for Numerical Methods in Engineering, 63(14), pp. 1991-2016.

Garnier, J., Gaudin, C., Springman, S.M., Culligan, P.J., Goodings, D.J., Konig, D., Kutter, B.L., Phillips, R., Randolph, M.F., and Thorel, L. (2007). Catalogue of scaling laws and similitude questions

in geotechnical centrifuge modelling. International Journal of Physical Modelling in Geotechnics, 7(3), pp. 1-23.

Henke, S., and Bienen, B. (2014). Investigation of the influence of the installation method on the soil plugging behaviour of a tubular pile. Proceedings of the 8th International Conference on Physical Modelling in Geotechnics, Perth, Australia, January 14 - 17, pp. 681-687.

Randolph, M.F., Carter, J., and Wroth, C. (1979). Driven piles in clay—the effects of installation and subsequent consolidation. Geotechnique, 29(4), pp. 361-393.

Randolph, M.F., Jewell, R.J., Stone, K.J.L., and Brown, T.A. (1991). Establishing a new centrifuge facility. Proceedings of the International Conference on Centrifuge Modelling, Colorado, June 13 - 14, pp. 3-9.

Weber, T.M., Laue, J., and Springman, S.M. (2006). Centrifuge modelling of sand compaction piles in soft clay under embankment load. Proceedings of the 6th International Conference on Physical Modelling in Geotechnics, Hong Kong, August 4 - 6, pp. 603-608.

Weiler, W.A., and Kulhawy, F.H. (1982). Factors affecting stress cell measurements in soil. Journal of the Geotechnical Engineering Division, 108(12), pp. 1529-1548.

White, D.J., Take, W.A., and Bolton, M.D. (2003). Soil deformation measurement using particle image velocimetry (PIV) and photogrammetry. Geotechnique, 53(7), pp. 619-632.

Zhu, B., Jardine, R.J., and Foray, P. (2009). The use of miniature soil stress measuring cells in laboratory applications involving stress reversals. Soils and Foundations, 49(5), pp. 675-688.

ANALYSIS OF SOIL AND STRUCTURAL THERMAL RESPONSE OF A FIELD SCALE GEOTHERMAL ENERGY PILE

Mohammed Faizal
Department of Civil Engineering, Monash University, Melbourne, Victoria, Australia.
Phone: +61 3 9905 8901, Email: mohammed.faizal@monash.edu

Abdelmalek Bouazza
Department of Civil Engineering, Monash University, Melbourne, Victoria, Australia.
Phone: +61 3 9905 4956, Email: malek.bouazza@monash.edu

ABSTRACT

The operation of ground source heat pumps combined with foundation piles can have an effect on the thermal behaviour of the pile and the surrounding soil. This paper presents the effects of continuous heating, continuous cooling, and alternate heating and cooling operations on ground and pile temperatures as well as the thermo-mechanical behaviour of a field scale energy pile. The effect of pile operation on the ground temperatures is highest near the pile and reduces with increasing radial distance. The results of the present studies generally showed that the thermal elasticity of the pile is not affected.

KEYWORDS

Geothermal energy pile; continuous operation; alternate heating/cooling; thermo-mechanical response

INTRODUCTION

Geothermal energy piles are foundation piles used as underground heat exchangers to maintain thermal comfort in buildings, via the use of ground source heat pumps (GSHPs). Ground source heat pumps are more economical and environmental friendly compared to conventional heat pumps. Energy piles can be combined with supplemental surface heaters or coolers, known as hybrid systems, for forcefully recharging the ground during non-operational times of the GSHP. Alternative heating and cooling of the GSHP improves geothermal energy usage and alleviates heat build-up in the ground and provides a balance of ground temperatures around the heat exchanger (Jalaluddin and Miyara, 2012).

The temperatures induced in the piles during GSHP operation can lead to a complex response of thermal strains and stresses in the pile concrete. An assessment of the thermo-mechanical response of energy piles for various thermal loads may assist engineers in the design process. Furthermore, an assessment of ground temperatures will also highlight any potential thermal interactions with other energy piles in actual building operations.

At present, the thermal strain and stress distribution in field scale energy piles has mostly been studied for continuous operation (Laloui et al., 2006; Bourne-Webb et al., 2009; McCartney and Murphy, 2012; Akrouch et al., 2014; Mimouni, 2014; Murphy and McCartney, 2014; Murphy et al., 2014; Wang et al., 2015). These studies have contributed considerably to the understanding of the axial thermal strain and stress distributions in the piles and have shown that pile thermal behaviour is mostly thermo-elastic without inducing major structural concerns.

The present paper adds to the current knowledge by assessing the pile thermo-mechanical and ground thermal response for continuous and alternating thermal loads of a field scale energy pile. The operation modes studied are 24 hours continuous cooling (Faizal et al., 2015), 24 hours continuous heating, (Wang et al., 2015) and alternate heating and cooling operation (Faizal and Bouazza, 2016). The forced ground thermal recharging is done during the non-operating times of the cooling unit, simulating a solar hybrid GSHP system for a scheduled intermittent mode of operation.

PILE INSTRUMENTATION AND EXPERIMENTAL PROCEDURE

The experiments for this paper were conducted on a field scale energy pile located at Monash University, Australia. The operating modes studied in this paper are 24 hours continuous heating (24H) (Wang et al., 2015), 24 hours continuous cooling (24C) (Faizal et al., 2015), and 16 hours daily cooling followed by 8 hours of daily heating (16C8H) (Faizal and Bouazza, 2016). Only 552 hours (23 days) of operational data are assessed for each operating mode.

A United Refrigeration chiller with a tank volume of approximately 35 litres was used to circulate cold water and a GeoCube TRT unit with a tank volume of approximately 4 litres was used to circulate hot water in the pile, at flowrates of 15 litre/min and 13.5 litre/min, respectively. The water temperature in the chiller and heater tanks of the 16C8H mode were manually controlled using bypass valves, before the water was released into the pile for the 16C8H mode (Fig. 1).

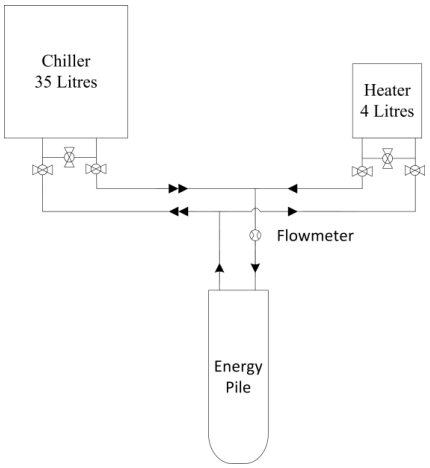


Fig. 1. Chiller and heater connection to the pile.

The hot water in the pipe loops from the heating cycles of the 16C8H mode mixed with the cold water and increased its temperatures in the cooling cycle. Also, the elevated temperatures of the ground from the heating cycle contributed to the increase of the cold water temperature in the chiller tank during the cooling cycle. This change in temperatures is expected practically in alternating heating/cooling applications of hybrid GSHP systems (Dai et al., 2015). The flow in the pile was stopped multiple times by shutting the inlet and outlet valves of the cooling/heating unit and using bypass valves to control the water temperature before releasing it into the pile. Hence, the effective cooling and heating periods in the 16C8H mode are approximately 15.5 hours and 7.5 hours, respectively.

Figure 2 shows a schematic of the instrumented pile used for this study. The bored pile (0.6 m diameter with a drill depth of 16.1 m) installed in December 2010, was specifically designed to study the changes in the pile shaft capacity after thermal loading (Wang et al., 2015), and thus is slightly different from a conventional pile. There were two Osterberg-Cell (O–Cell) load testing systems installed in the pile at approximately 10 m and 14 m below ground level, dividing the pile into three sections: the 10 m upper section, the 4 m middle section, and the lower 1 m section. Three standard HDPE pipe loops, with outer diameter of 25 mm and inner diameter of 20 mm were attached to the reinforcement pile cage. The pipes were installed 50 mm from the edge of the pile and to the top of the lower O-Cell (LOC), to a depth of 14.2 m. The spacing between the loops was about 175 mm. The top end of the pile was not restrained and the pile head was exposed to the atmosphere.

Embedment and sister bar vibrating wire strain gauges were installed at different depths along the axis of the pile. Type K thermocouples recorded atmospheric temperatures, inlet and outlet water temperatures at the pile head, and ground temperatures at eight depths in two boreholes located at radial distances of R = 0.5 m and R = 2 m from the pile edge. Thermocouple data were logged using Pico

Technology's USB-TC08 data logger. Data from strain gauges were logged using DataTaker's DT80G and CEM20 data loggers. The soil profile at the test site consisted of sands and fine to coarse to very dense clayey sands (Brighton group material), summarized in Fig. 2.

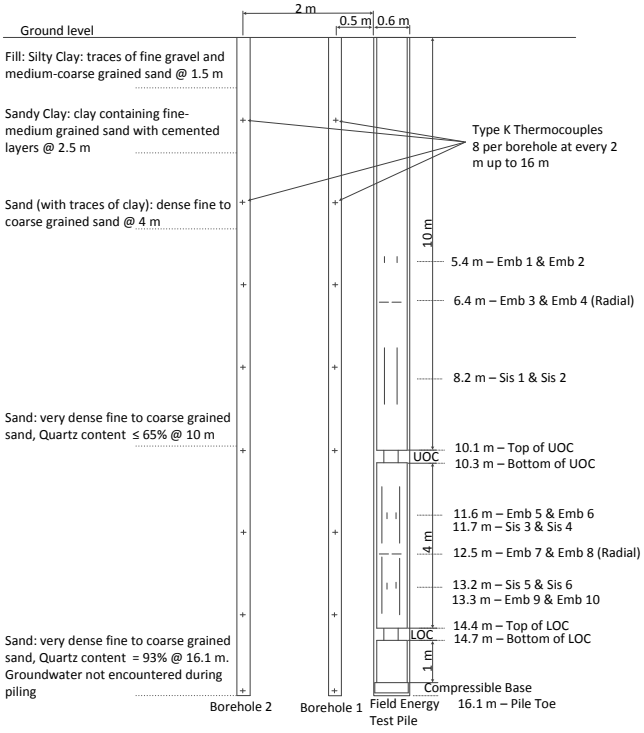


Fig. 2. Schematic of the instrumented energy pile (LOC: lower O-cell, UOC: upper O-cell, Emb: embedment strain gauges, Sis: sister bar strain gauges) (modified from (Wang et al., 2015).

The thermal strains, ε_T, induced in the concrete were calculated as:

$$\varepsilon_T = \left(f_i^2 - f_o^2\right)GB + (T_i - T_o)\alpha_s \quad (1)$$

where f_i is the resonant frequencies of the strain gauges at time i, f_o is the reference resonant frequency, GB is the calibration factor (G is gauge factor and B is batch factor), T_i is the temperature of the strain gauges at time i, T_o is the reference temperature, and α_s is the thermal expansion of the steel wire.

The free or unrestrained thermal strains ε_T, of each gauge were calculated as (Murphy and McCartney, 2014; Murphy et al., 2014):

$$\varepsilon_{T,free} = \alpha_c \Delta T \quad (2)$$

where α_c is the coefficient of linear thermal expansion of concrete and ΔT is the change in temperature of concrete. The thermal expansion coefficient of concrete depends on the constituents of the mix, and can be as high as 14.5 με /°C, while that of steel reinforcements ranges from 11.9 to 13 με /°C (McCartney et al., 2010; Stewart and McCartney, 2014). Thermally induced stresses,σ_T, were calculated from the difference between the measured thermal strains and the free thermal strains from the gauges as (Murphy and McCartney, 2014; Murphy et al., 2014):

$$\sigma_T = E\left(\varepsilon_{T,free} - \varepsilon_T\right) \quad (3)$$

where E is the Young's modulus of the pile concrete (taken as 30 GPa). In the present study, cooling is taken as compressive, giving negative thermal strains.

RESULTS AND DISCUSSIONS

The ground temperature below the surface varies with air temperature up to given depths, after which an almost constant temperature is maintained throughout the year. Fig. 3 shows the ground temperature variation with increasing depth recorded at the test site for the year 2013. The temperature becomes almost constant with values of 16 –18 °C after 8 m depth (Faizal et al., 2016). These constant ground temperatures can be used as a heat source or sink for the GSHP.

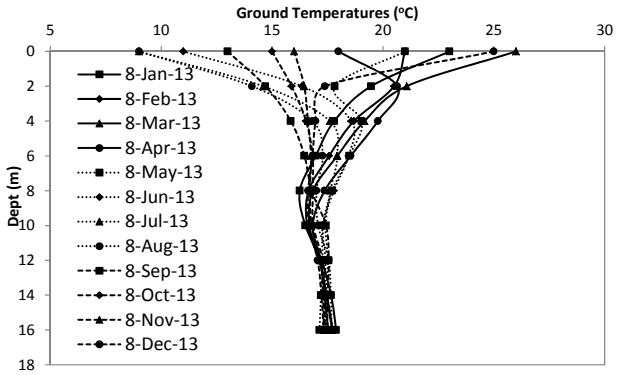


Fig. 3. Ground temperature variations with depth for year 2013 measured at the energy pile test site at Monash University (Clayton Campus), Melbourne.

Figure 4 shows the inlet water temperatures of the 24H, 24C, and the 16C8H mode. The water temperatures for the 16C8H mode are presented after the target inlet temperatures were achieved using the bypass valves, as discussed in section 2. The lowest inlet water temperatures achieved in the 24C and 24H modes were approximately 5°C. The highest inlet water temperature in the 24H mode was 45°C. The lowest initial inlet cold water temperature achieved in the 16C8H mode for the cooling cycle was approximately 16°C. The minimum inlet cold water temperatures achieved at end of cooling was approximately 7°C.

The inlet hot water temperature for the heating cycle in the 16C8H mode was initially between 30°C – 33°C and increased as high as 55°C. The hot water temperature in the 16C8H mode was maximised to study extreme operating conditions, while hot water temperature in an actual solar hybrid system will reduce and stabilize at a lower value with operation time (Dai et al., 2015). Control strategies are normally used to activate forced ground thermal recharging in actual GSHP hybrid systems (Yavuzturk and Spitler, 2000).

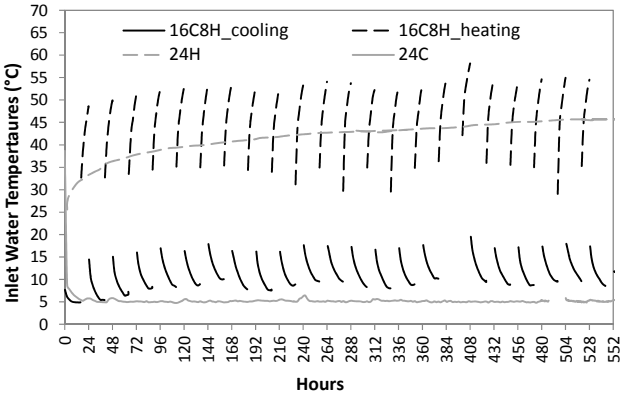


Fig. 4. Inlet water temperatures.

Fig 5 shows the ground temperatures at radial distances R = 0.5 m and R = 2 m from the pile edge, for depth, d = 12 m. The effect of pile thermal loading on ground temperatures was much higher at R =

0.5 m than R = 2 m for all modes. The ground temperature amplitudes at R = 0.5 m were also observed to be much higher in the 16C8H mode, but became negligible at R = 2 m.

The low ground temperature changes at R = 2 m leads to the conclusion that continuous and alternating pile thermal loads with high pile temperatures may not activate potential thermal interactions with other piles at 2 m or larger spacing in actual building operations.

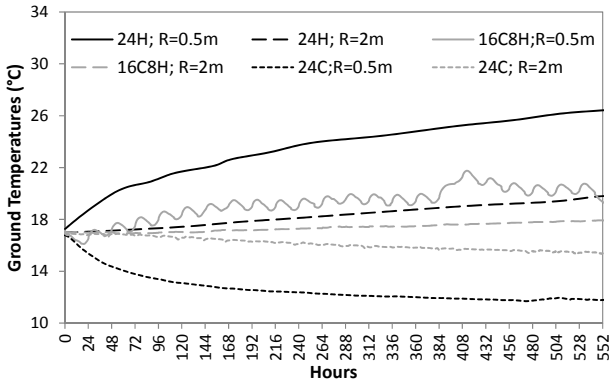


Fig. 5. Transient ground temperatures at R = 0.5 m and R = 2 m for d = 12 m.

Fig 6a, 6b, and 6c show the axial thermal strains with recovery after end of experiments for 24H, 24C, and 16C8H modes, respectively. The axial thermal strains after completion of experiments generally recover to within 20 με higher than the undisturbed strains. This indicates that the energy pile operation for continuous and alternating thermal loads is of a thermo-elastic nature.

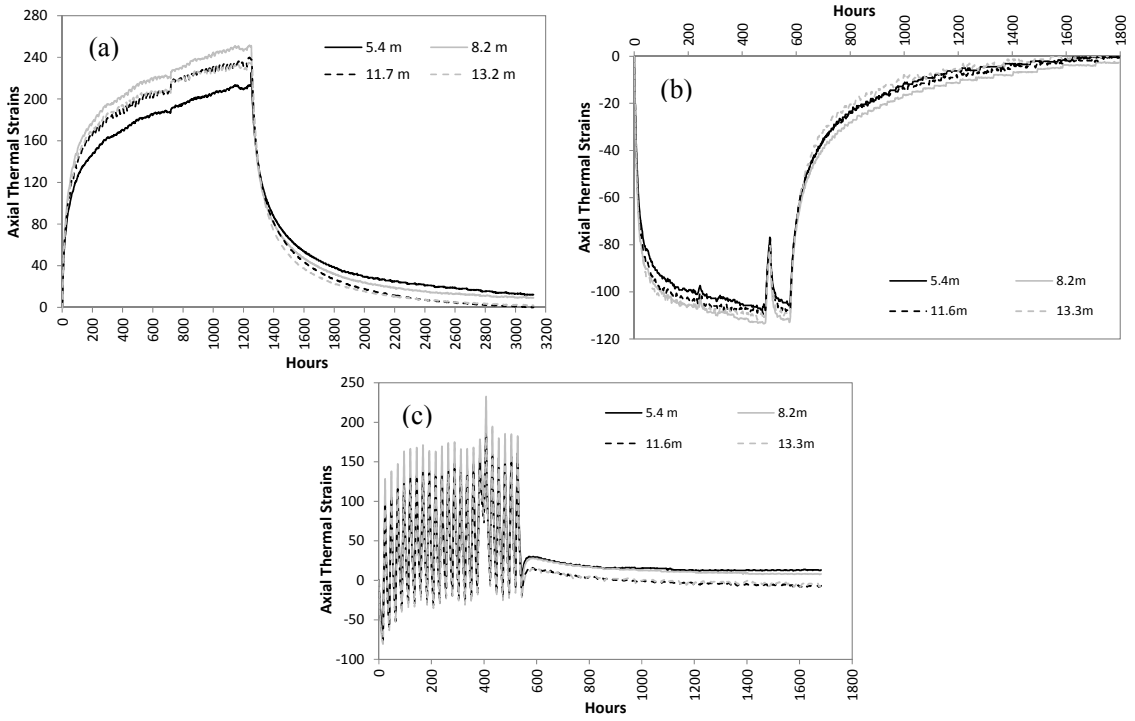


Fig 6. Transient axial thermal strains for all operating modes a) 24H (Wang et al., 2015) b) 24C (Faizal et al., 2016) c) 8C16H (Faizal and Bouazza, 2016)

Figs 7a, 7b, and 7c compare the transient pile temperatures, axial thermal strains and stresses, respectively, for all modes at d = 5.4 m. The average values of these quantities are also shown for the

16C8H mode. There was chiller operational failure due to electrical issues for approximately 15 hours at 385 hours of operation which resulted in additional heating at 408 hours in the 16C8H mode.

Due to alternate heating and cooling of the pile in the 16C8H mode, the changes in pile temperatures are cyclic, which in turn leads to cyclic changes in thermal strains and stresses. The transient thermal stresses in the 16C8H mode were observed to cycle between negative and positive values as a result of alternating pile temperatures. With operation time, the thermal strains and stresses return to similar peak values between consecutive days at end of cooling and recovery, respectively, for the 16C8H mode.

The change in transient pile temperatures, thermal strains and stresses is initially higher for all modes due to high initial thermal gradient between inlet water and ground and pile and reduces with operation time. This indicates that the thermo-mechanical response of the pile reaches steady state with the surrounding soil with operation time and that the soil-structure interaction did not limit the thermal elasticity of the pile for daily thermal loads. Hence, no substantial thermally induced deformations would occur in the pile and surrounding soil as a result of continuous and alternating thermal loads in the energy pile.

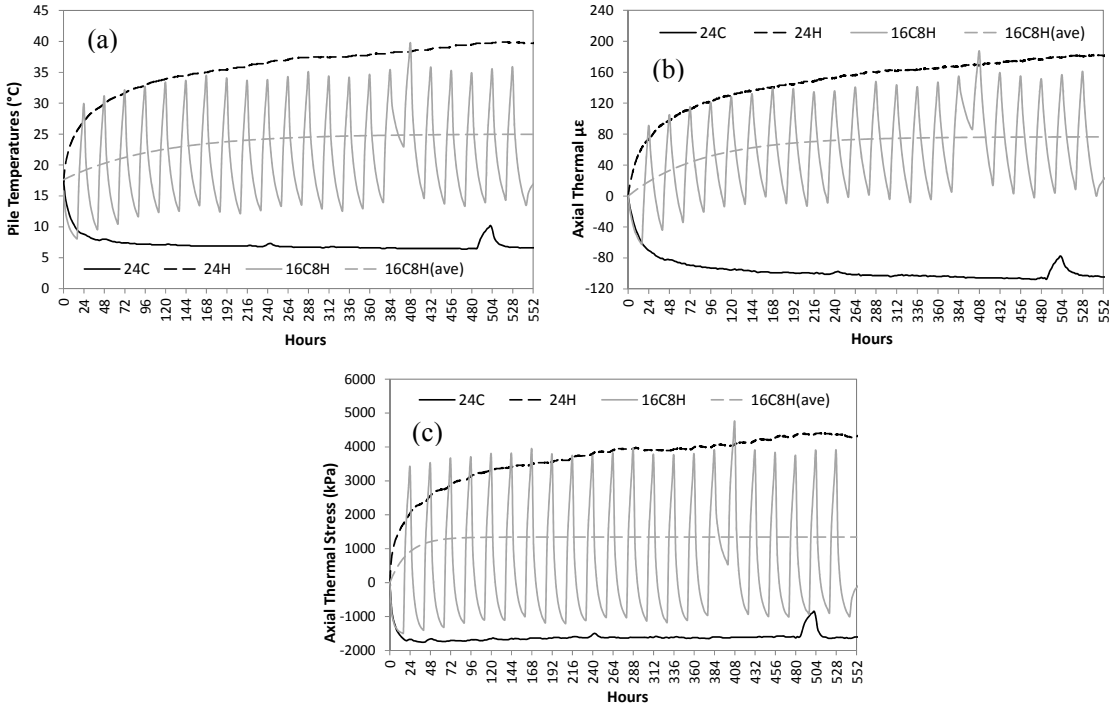


Fig. 7. Transient thermo-mechanical response of the pile at d = 5.4 m a) pile temperatures b) axial thermal strains c) axial thermal stresses.

A comparison of the thermal strains and stresses against pile temperatures is shown in Fig.s 8a and 8b, respectively (data due to chiller failure in 16C8H mode is not considered). A cyclic response of thermal strains and stresses is seen for the 16C8H modes due to cyclic changes of the pile temperature.

Higher ranges of pile temperatures are observed to lead to higher thermal strains and stresses. The thermal strains and stresses increase (almost linearly) with increasing pile temperatures. However, as discussed for Figs. 6 and 7, the thermal elasticity of the pile did not seem to be affected for all operating modes and hence no significant thermal deformations are expected in the pile for continuous and alternating thermal loads.

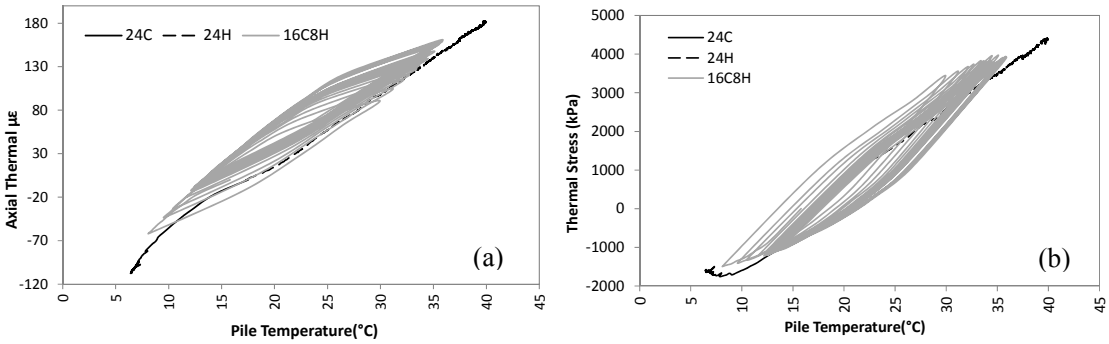


Fig. 8. a) Thermal strains against pile temperatures b) thermal stresses against pile temperatures.

Figs 9a, 9b and 9c show the average pile temperatures and average thermal strains and stresses against depth, respectively, at 360 hours of operation. The trends in thermal strains and stresses against depth are slightly different from previously studied field scale energy piles (Laloui et al., 2006; Bourne-Webb et al., 2009; Akrouch et al., 2014; McCartney and Murphy, 2012; Murphy and McCartney, 2014; Murphy et al., 2014) due to the presence of O – Cells in the pile. The lowest thermal strains (and thus the largest thermal stresses) were observed at 5.4 m depth in Fig. 9b for all modes indicating that the largest constraint was at this location along the length of the pile. The thermal strains at 8.2 m depth are less restrained (and thus lower thermal stresses) due to the low resistance provided by the top of the upper O – Cell.

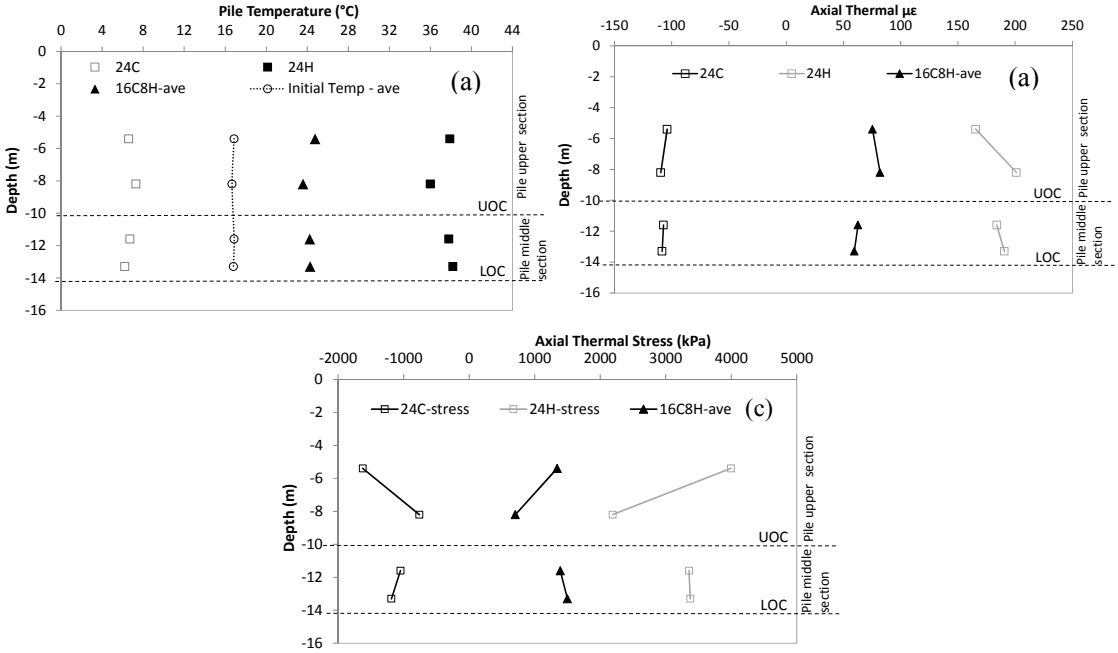


Fig. 9. a) Pile temperatures against depth b) axial thermal strains against depth and c) axial thermal stresses against depth.

Fig 9a compares the pile temperatures for all modes against the undisturbed pile temperatures. The change in temperatures compared to undisturbed pile temperatures, ΔT, at d = 5.4 m were -10.9 °C for the 24C mode, 20.6 °C for the 24H mode, and 8.9 °C for the 16C8H mode (average pile temperatures are considered for the 16C8H mode).

Differences in ΔT values in Fig. 9a lead to differences in thermal strains and stresses between all operating modes at all depths as shown in Figs 9b and 9c, respectively. Higher changes in pile temperatures induce higher thermal strains and stresses compared to initial undisturbed conditions, for a given depth. For largest ΔT = 20.6 °C at d = 5.4 m, the maximum thermal stress was 4 MPa

Fig 10 further shows the thermal stresses plotted against change in pile temperatures combined from all operating modes (for all depths) for 360 hours of operation. The thermal stresses induced in the pile are observed to increase linearly with increasing change in pile temperatures for all depths. The highest rate of change of thermal stresses with change in temperatures, *m*, was obtained at d = 5.4 m with a value of 175 kPa/°C. Murphy et al. (2014) had assessed rates of 210 to 260 kPa/°C for USAFA foundations, 104 kPa/°C from Laloui et al.(Laloui et al., 2006) and 192 kPa/°C from Bourne-Webb et al.(Bourne-Webb et al., 2009). The differences in rates in all these results is possibly due to the differences in the thermal coefficient of expansion of concrete used to calculate the thermal stresses.

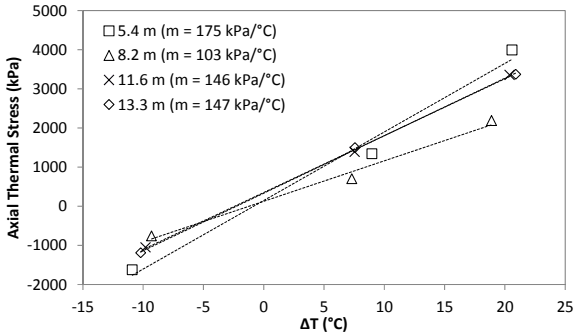


Fig. 10. Rates of change of axial thermal stresses against change in pile temperatures.

CONCLUDING REMARKS

Results from tests on a field-scale energy pile for continuous cooling and heating, and alternate heating and cooling of the pile showed that the effect of pile operation on ground temperatures reduces with increasing radial distance. Higher pile temperatures induced higher thermal stresses in the pile at all depths. The thermal strains recovered to within 20 με after completion of experiments for all modes. The continuous cooling and heating as well as alternating and cooling operations do not seem to affect the elastic response of the pile in the current soil profile. The rate of change of thermal stress with change in pile temperatures compiled from all operating modes was found to be 175 kPa/°C

ACKNOWLEDGEMENTS

The geothermal energy pile installation was funded by the Victorian Government Sustainability Fund (2009–2012), Vibropile Pty. Ltd., Golder Associates Pty. Ltd., and GeoExchange Australia Pty. Ltd. (Project No. 4678). This research project is supported under the Australian Research Council's Linkage Projects funding scheme (project number LP120200613). Their support is gratefully acknowledged.

REFERENCES

Akrouch, G., Sánchez, M., Briaud, J.-L., 2014. Thermo-mechanical behavior of energy piles in high plasticity clays. Acta Geotechnica 9 (3), 399-412.

Bourne-Webb, P.J., Amatya, B., Soga, K., Amis, T., Davidson, C., Payne, P., 2009. Energy pile test at Lambeth College, London: geotechnical and thermodynamic aspects of pile response to heat cycles. Geotechnique 59 (3), 237-248.

Dai, L., Li, S., DuanMu, L., Li, X., Shang, Y., Dong, M., 2015. Experimental performance analysis of a solar assisted ground source heat pump system under different heating operation modes. Applied Thermal Engineering 75 (0), 325-333.

Faizal, M., Bouazza, A., 2016. Field investigations of the thermo-mechanical behaviour of an energy pile with natural and forced ground thermal recharge.

Faizal, M., Bouazza, A., Singh, R.M., 2015. An experimental investigation of the influence of intermittent and continuous operating modes on the thermal behaviour of a full scale geothermal energy pile.

Faizal, M., Bouazza, A., Singh, R.M., 2016. Heat transfer enhancement of geothermal energy piles. Renewable and Sustainable Energy Reviews 57, 16-33.

Jalaluddin, Miyara, A., 2012. Thermal performance investigation of several types of vertical ground heat exchangers with different operation mode. Applied Thermal Engineering 33–34 (0), 167-174.

Laloui, L., Nuth, M., Vulliet, L., 2006. Experimental and numerical investigations of the behaviour of a heat exchanger pile. International Journal for Numerical and Analytical Methods in Geomechanics 30 (8), 763-781.

McCartney, J.S., Murphy, K.D., 2012. Strain distributions in full-scale energy foundations. DFI Journal: The Journal of the Deep Foundations Institute 6 (2), 26-38.

McCartney, J.S., Rosenberg, J.E., Sultanova, A., 2010. Engineering performance of thermo-active foundations, GeoTrends, pp. 27-42.

Mimouni, T., 2014. Thermomechanical characterization of energy geostructures with emphasis on energy piles. École Polytechnique Fédérale de Lausanne.

Murphy, K.D., McCartney, J., 2014. Seasonal response of energy foundations during building operation. Geotechnical and Geological Engineering, 1-14.

Murphy, K.D., McCartney, J.S., Henry, K.S., 2014. Evaluation of thermo-mechanical and thermal behavior of full-scale energy foundations. Acta Geotechnica, 1-17.

Stewart, M.A., McCartney, J.S., 2014. Centrifuge modeling of soil-structure interaction in energy foundations. Journal of Geotechnical and Geoenvironmental Engineering 140 (4), 04013044.

Wang, B., Bouazza, A., Singh, R., Haberfield, C., Barry-Macaulay, D., Baycan, S., 2015. Posttemperature effects on shaft capacity of a full-scale geothermal energy pile. Journal of Geotechnical and Geoenvironmental Engineering 0 (0), 04014125.

Yavuzturk, C., Spitler, J.D., 2000. Comparative study of operating and control strategies for hybrid ground-source heat pump systems using a short time step simulation model. ASHRAE Transactions 106, 192.

LATERAL RESPONSE OF POLE ON ENGINEERED DRIVEN TIMBER PILE FOOTING AT ARARAT WINDFARM TERMINAL STATION

Frank Albrecht, Albrecht Engineering, frank@albrechteng.com.au
Brian McCarthy, Meyer Timber, Australia, brianm@meyertimber.com.au

ABSTRACT

The Ararat Terminal Station (ARTS) is located 190km to the north-west of Melbourne, approximately 1.7km to the north of Elmhurst Township in the Pyrenees region of western Victoria, Australia. The site occupies an area of approximately 7.2 hectare of farmland. The electricity generated by the Ararat Wind Farm is directed to the ARTS terminal station before being connected to the grid. The ARTS structural design includes more than 180 steel yard support structures, three 25m-tall gantry 'A' frames, three modular control room buildings, a precast transformer bund, precast fire wall structures and related foundation design. Innovative driven engineered glue laminated timber (glulam) piles in a cruciform shape were used to reduce the foundation construction time, cost and the amount of concrete used in the project. It is the first time that engineered timber piles made from farmed Australian pine trees have been used in a large-scale environmentally-friendly project.

Durability of the timber was achieved by H5 treatment and the use of reinforced concrete pile caps to protect the cruciform timber piles at the ground line. A pile-driving sequence was developed based on field trials. The lateral load capacities of the piles were estimated using engineering principles and from full-scale tests in the field. This paper provides an overview of details of engineered timber cruciform piles, durability of timber piles, design information, pile construction procedures, pile-driving procedures, the testing protocol, test results and validation. The test results were compared with predictions from several methods. In addition, potential future applications of similar systems in other infrastructure projects, and opportunities for future improvements are discussed.

The structural aspects of this project were presented in a previous paper at the World Conference on Timber Engineering in Vienna in August 2016. See http://wcte2016.conf.tuwien.ac.at/home/ for further information.

Keywords: Glulam Timber Piles, Engineered Timber, Cruciform Timber and Driven Timber Piles

DESIGNING PILES FOR SEISMIC EVENTS

H G Poulos, Coffey Services Australia & University of Sydney

ABSTRACT

This paper sets out a simplified approach by which the practical foundation designer can undertake the relevant calculations to satisfy the requirements for deep foundation design in seismic areas. The following matters are dealt with:

a. Design issues that should be addressed;
b. Pile design for axial loading, including the possible effects of liquefaction;
c. Pile design for lateral loading where liquefaction does not occur;
d. Pile design for lateral loading where liquefaction does occur;
e. Measures to mitigate against liquefaction effects.

The paper is a modified version of a paper presented in 2013 to the 19th NZGS Geotechnical Symposium, Queenstown, New Zealand.

Keywords: buckling; design; earthquakes; lateral response; liquefaction; pile; remedial methods

1. INTRODUCTION

Consideration of the effects of earthquakes and seismic loadings is an increasingly important aspect of modern foundation design, and most contemporary standards have a mandatory requirement for such consideration. For example, the Australian Piling Code, AS 2159-2009, states that "a pile shall be designed for adequate strength, stiffness and ductility under load combinations including earthquake design actions". However, the methods by which such considerations can be undertaken are generally not set out in the standards, and many approaches have been utilized, ranging from very simplistic methods to extremely complex computer analyses. Accordingly, there appears to be scope for an approach that is soundly based but which is neither too simplistic nor too complex.

Poulos (1989) has suggested that there are three categories of analysis and design, as follows:

1. Category 1: empirical methods.
2. Category 2: simplified but soundly-based methods.
3. Category 3: more comprehensive methods that are soundly-based, and site-specific.

The objective of this paper is to set out a systematic but simplified approach which falls into Category 2 above, and by which the foundation designer can undertake the relevant analyses to satisfy the foundation design requirements for seismic regions. Emphasis is placed on methods that do not require "black box" software or which employ complex soil models in which the physical meaning of the parameters is unclear.

2. DESIGN ISSUES

In addition to the conventional design issues of axial load capacity, settlement, structural adequacy and durability under static imposed loadings, the design of deep foundations in seismic areas requires consideration of the following factors:

1. The effects of earthquake excitation on the axial load capacity of the foundation system;
2. The effects of earthquake excitation on the lateral response and the structural integrity of the foundation system.

In both cases, the possible loss of soil support during the earthquake due to liquefaction or partial loss of soil strength must be considered. Both the geotechnical and the structural strength of the foundations can be compromised by the earthquake effects, and so each has to be examined in turn.

For assessment of the response of the foundation during a seismic event, it is also necessary to estimate the stiffness and damping of the foundation system, since the foundation response can influence the natural period of the supported structure.

3. EFFECTS OF EARTHQUAKES ON FOUNDATION SOILS

Soil deposits at a site subjected to an earthquake may experience the following effects:

- Increases in pore pressure within the soils;
- Time-dependent vertical ground movements during and after the earthquake;
- Time-dependent lateral ground movements during the earthquake.

In foundation design, consideration must therefore be given to possible reductions in soil strength arising from the build-up of excess pore pressures during and after the earthquake. In extreme cases, the generation of pore pressures may lead to liquefaction in relatively loose sandy and silty soils.

As a consequence of the earthquake-induced ground movements, piles and other deep foundations will be subjected to two sources of additional lateral loading:

a. Inertial loadings – these are forces that are induced in the piles because of the accelerations generated within the structure by the earthquake. Consideration is generally confined to lateral inertial forces and moments, which are assumed to be applied at the pile heads.
b. Kinematic loadings – these are forces and bending moments that are induced in the piles because of the ground movements that results from the earthquake. Such movements will interact with the piles and because of the difference in stiffness of the piles and the moving soil, there will be lateral stresses developed between the pile and the soil, resulting in the development of shear forces and bending moments in the piles. These actions will be time-dependent and need to be considered in the structural design of the piles.

Thus, in addition to the usual design considerations for static loading, the above factors of strength reduction, inertial loadings, and kinematic loadings, need to be incorporated into the design process.

When considering both the strength and stiffness of soils, consideration should also be given to the effects of the high rate of loading that occur during a seismic event. Such loading rate effects tend to increase both the strength and stiffness of soils, especially clay soils.

Appropriate assessment of the geotechnical parameters is a critical component of geotechnical design for seismic actions, as it is for other types of imposed loadings. This issue is however outside the scope of the present paper, and reference should be made to references such as Kramer (1996) who discusses such issues as the effects of strain, cyclic loading and loading rate effects.

3.1 Earthquake Characteristics Required for Foundation Design

Seismic design of foundations requires information on a number of characteristics of the anticipated earthquakes at the site, including the following:

- Earthquake size or magnitude;
- Seismicity rate;
- Maximum bedrock acceleration, and it attenuation with distance from the causative fault;
- The duration;
- The predominant period;
- Representative time-acceleration relationships at bedrock level.

More details of these and other earthquake characteristics can be found in Kramer (1996). However, interaction with seismologists is highly desirable in making the above assessments for a specific site or area.

4. PILE DESIGN FOR AXIAL LOADING

4.1 Without Liquefaction

In soils that are assessed to be non-liquefiable, the conventional methods may be adopted to assess the ultimate shaft friction and end bearing capacity of the piles, including the possible effects of group action.

Only limited attention has been paid to the axial response of piles during and after an earthquake. Poulos (1993) has provided an example of a pile in clay subjected to earthquake action. The generation of excess pore pressures, and the consequent loss of strength of the clay, has been incorporated into the analysis. The main conclusions drawn from this study are as follows:

1. Earthquakes with a Richter Magnitude in excess of about 6 have the potential to generate significant excess pore pressures in the clay, causing subsequent consolidation settlement.
2. The rate of development of these settlements is similar to that obtained from Terzaghi's consolidation theory, using the coefficient of consolidation for the soil in an over-consolidated state.
3. Piles in clay may be subjected to a short-term loss of axial capacity due to the "softening" of the surrounding soil arising from pore pressure build-up.
4. Piles may also experience a long-term increase in settlement and axial force, due to the ground settlements induced by the earthquake.

4.2 Effects of Liquefaction

If liquefaction is assessed to be likely to occur within soils supporting a piled foundation, some of the issues that require consideration are as follows:

(a) Seismic excitation will cause settlements as well as lateral ground movements and thus there will be a tendency for the development of negative skin friction on those parts of the pile which tend to settle less than the soil.
(b) There will tend to be a substantial reduction in effective stress in the soil due to the generation of excess pore pressures, and this will lead to a reduction in the lateral effective

stress between the pile and the soil, and a consequent reduction in the ultimate shaft friction. This will reduce the axial capacity of the pile and the factor of safety against geotechnical pile failure. This reduction of capacity is however temporary and the initial shaft resistance should be largely re-instated after the excess pore pressures have dissipated.

To avoid temporary failure, a check should be made of the ultimate axial capacity of the pile, excluding any resistance from the liquefiable layers. Ideally, this reduced capacity should exceed the design axial load that is likely to be applied to the pile during the earthquake by a suitable factor of safety, for example, 1.25.

An additional mode of failure, buckling of the pile, may be initiated. This matter is discussed further below.

4.3 Pile Buckling

Bhattacharya and Bolton (2004) have identified another mechanism of axial failure of piles in liquefiable soils, namely buckling under axial loading due to loss of lateral support. This mechanism is generally overlooked in design, yet can be an important contributor to foundation failure. They emphasize that buckling of a pile is an unstable and destructive failure mechanism, whereas pile bending is a more stable mechanism. Pile buckling is a possible mechanism if the following conditions exist:

- The pile is end bearing and socketed into rock;
- The pile is carrying a relatively large axial load compared to the Euler buckling load of an equivalent column.

Madabhushi and May (2009) recommend that the pile design process should incorporate the following considerations:

- The ratio of the axial load to the Euler buckling load should be limited to about 1/5 to provide a safety margin on buckling;

- The slenderness ratio of the piles, SR = $L/(I/A)^{0.5}$ (where L=effective pile length within the liquefiable layer, I = minimum moment of inertia, A = pile cross-sectional area), in the buckling zone should be no greater than 50 to avoid buckling instability.

The Euler buckling load P_E can be estimated as follows:

$$P_E = \pi^2 EI/L_e^2 \qquad (1)$$

where EI=flexural rigidity of the pile
L_e = equivalent length of pile.

The equivalent length L_e depends on the end conditions of the pile. For the extreme case of a pile head that is unrestrained against both translation and rotation, but with a fixed base, $L_e = 2L_o$, where L_o = length of pile in liquefied soil, while for a pile head that is restrained against rotation, $L_e = L_o$. Alternatively, estimates of the pile buckling load can be made using the results summarised by Poulos and Davis (1980).

5. PILE DESIGN FOR LATERAL LOADING – NO LIQUEFACTION

5.1 Assessment of Inertial Loadings

For geotechnical analysis, the inertial forces imposed on the foundation system by the structure are usually obtained by the structural designers. Broadly, the maximum lateral force on the structure is generally estimated by multiplying the mass of the structure by the peak spectral

acceleration, a_{smax}. a_{smax} can be obtained most readily via the use of code-specified values for bedrock acceleration and then applying site factors to obtain surface acceleration. For a piled foundation, the lateral inertial force can be estimated as $P.a_{smax}/g$ where P = axial force on pile, and g = gravitational acceleration.

Rather than simply adopting a code-specified site factor, a site response analysis using representative earthquake records at "bedrock" level (e.g. where $v_s > 750$m/s) may be carried out to assess the ground response. From this analysis, response spectra can be obtained for the acceleration versus time history at an appropriate depth in the layer, e.g. at about 1/2 to 2/3 of the pile length, to reflect the effect of the structure being founded on a pile foundation system.

If an elastic analysis is applied to the pile and a linearly varying Young's modulus with depth is assumed to apply within the soil, then the maximum bending moment due to inertial loading, M_{imax}, can be estimated approximately from the following expression given by Randolph (1981):

(a) For a free-head pile:

$$M_{imax} = 0.1 H_i L_c / \rho_c \quad (2)$$

(b) For a fixed head pile: (fixing moment at the pile head):

$$M_{imax} = -0.1875\ H_i\ L_c\ /(\rho_c)^{0.5} \quad (3)$$

where H_i = inertial force on pile

L_c = effective pile length = $d(E_p/G_c)^{2/7}$ (4)

G_c = average shear modulus of soil over a depth equal to the effective length of the pile

ρ_c = ratio of soil modulus at a depth of ¼ of effective length to that at a depth of ½ of the effective pile length.

5.2 Assessment of Kinematic Loading Effects

To estimate the possible additional bending moments and shears in the piles arising from the kinematic ground movements during and after a seismic event, there are at least two design approaches that may be adopted:

a. A simple approach employing the results of analyses reported by Nikolaou et al (2001), among others
b. A more detailed approach involving the use of a pseudo-static analysis in which the results of a site response analysis are combined with a pile-soil interaction analysis (e.g. Cubrinovski and Ishihara, 2004, Tabesh & Poulos, 2001).

5.2.1 Simplified Analysis Method for Kinematic Moments in Pile

A convenient design approach for estimating the maximum moment induced in a pile by kinematic bending has been provided by Nikolaou et al (2001). They found that the induced moments were a maximum at interfaces between layers of different stiffness and then undertook a series of analyses to compute the bending moment at the interface between two layers (see Figure 1). They recognised that a distinction must be made between the maximum bending moment under steady state harmonic motion and the bending moment that would be developed under transient excitation, such as during an earthquake. The latter would generally be smaller than the steady state value, which would only be developed after a very large number of cycles. This distinction was also emphasized by Sica et al (2011) and Figure 2 shows, diagrammatically, the relationship between the bending moment and the frequency ratio (ratio of the predominant frequency of the earthquake to the natural frequency of the subsoil.

The following approximate relationship was developed for the peak bending moment, M_{pk}, during the transient phase of seismic excitation:

$$M_{pk} = \eta . M_{res} \quad (5)$$

where M_{res} = bending moment developed under resonant conditions
η= reduction factor to allow for non-resonant conditions.

From the results of a frequency domain analysis, Nikolaou et al developed the following fitted formula for M_{res}:

$$M_{res} = 0.042\ \tau_c\ d^3\ (L/d)^{0.30}\ (E_p/E_1)^{0.65}\ (v_{s2}/v_{s1})^{0.50} \quad (6)$$

$$\text{with} \quad \tau_c = a_s\ \rho_1\ h_1 \quad (7)$$

where d = pile diameter
L= pile length
E_p = Young's modulus of pile
E_1 = Young's modulus of upper layer
v_{s1} = average shear wave velocity in upper layer
v_{s2} = average shear wave velocity in lower layer
a_s = peak ground surface acceleration
ρ_1 = mass density of upper layer
h_1 = thickness of upper layer.

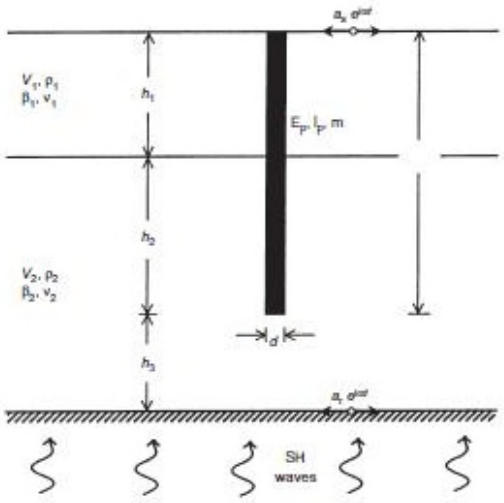


Figure 1 Model adopted by Nikolau et al (2001) for kinematic moments in pile

In the original paper, Nikolaou et al give the following expressions for the reduction factor η:

Case 1: For resonant conditions in which the fundamental period of the deposit lies within the range of predominant periods of the excitation:

$$\eta = 0.04N_c + 0.23 \quad (8)$$

Case 2: For non-resonant conditions where the fundamental period of the deposit lies outside the range of predominant periods of the excitation:

$$\eta = 0.015N_c + 0.17 \approx 0.2 \quad (9)$$

where N_c = effective number of cycles within the earthquake record.

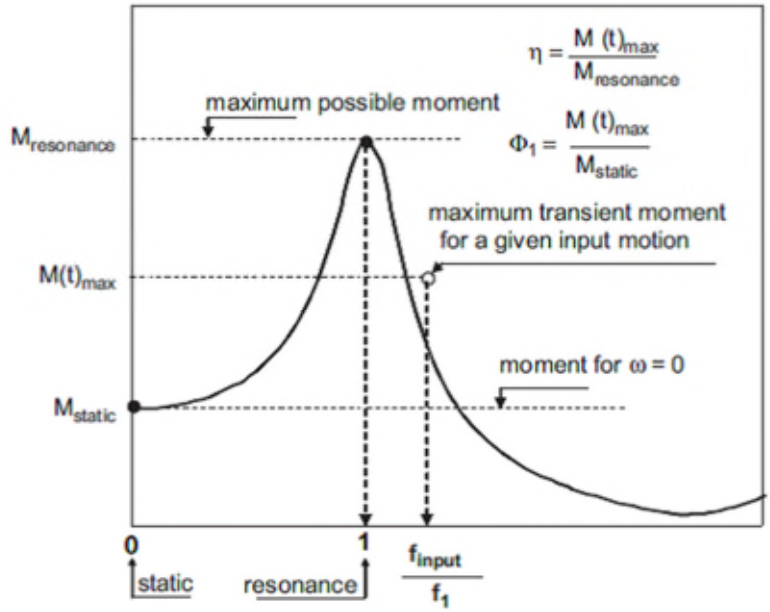


Figure 2 Relationship between pile bending moment and frequency ratio (Sica et al, 2011)

Subsequently, Sica et al (2011) have suggested the following alternative expression for the average value of η based on a series of parametric analyses:

$$\eta = 0.68(f_{input}/f_1)^{-1.5} \quad (10)$$

where f_{input} = predominant frequency of earthquake
f_1 = natural frequency of soil profile.

The above expression holds for $(f_{input}/f_1) \geq 1.5$, but for frequency ratios less than 1.5, $\eta = 0.37$, with a standard deviation of 0.17.

The value of f_{input} can be obtained from the input earthquake record, but can also be estimated (very approximately) as the inverse of the predominant period. The value of the natural period of the soil deposit, f_1, can be obtained from the following expression:

$$f_1 = v_{sav}/4H \quad (11)$$

where H = thickness of soil profile
v_{sav} = average shear wave velocity of soil profile.

5.2.3 Pseudostatic Analysis for Pile Response

Tabesh and Poulos (2001) have proposed a pseudostatic approach for estimating the maximum response of a pile during an earthquake. The approach involves the following steps:

1 A free field site response analysis is carried out to obtain the time history of surface motion and the maximum horizontal displacement of the soil along the length of the pile. In general,

a one-dimensional analysis can be employed, using commercially available codes such as SHAKE or DEEPSOIL, or else custom codes such as ERLS (Poulos, 1991).

2 The surface motion obtained in the above step is used in a spectral analysis of a single degree of freedom system whose natural period is equal to that of the supported structure. The spectral acceleration a_{spec} is thus obtained.

3 A static analysis of the pile is carried out in which the pile is subjected simultaneously to the application of the following loadings:

   (i) A lateral force at the pile head equal to a_{spec}.P, where P = vertical load acting on pile head;

   (ii) The maximum ground movements along the pile length, as obtained from Step 1.

The analysis will give the maximum moment and shear force developed in the pile by the simultaneous application of the inertial and kinematic loadings.

5.3 Combined Inertial and Kinematic Effects

The approach employed by Tabesh and Poulos (2001) may be conservative as the analysis implicitly assumes that both the inertial and kinematic loadings are in phase. However, they have found that this approach gives reasonable agreement with the results of a more complete dynamic analysis, although it does tend to be conservative, and also good agreement is found when applied to a case history in Japan.

A modification has been suggested by Tokimatsu et al (2005), using the following approach to deal with combined inertial and kinematic loadings:

- If the natural period of the superstructure is less than that of the ground, the kinematic force tends to be in phase with the inertial force, increasing the stress in the piles. The maximum pile stress occurs when both the inertial force and the ground displacements take the peak values and act in the same direction. In this case, the maximum moment is the sum of the values for inertial and kinematic effects.
- If the natural period of the superstructure is greater than that of the ground, the kinematic force tends to be out of phase with the inertial force. This restrains the pile force, rather than increasing it. The maximum pile stress tends to occur when both inertial force and ground displacement do not become maxima at the same time. In this case, the maximum moment is the square root of the sum of the squares of the moments due to each effect.

The moments via this approach have been found to be in good agreement with model tests, both with and without the effects of liquefaction.

5.4 Design Charts

Using the pseudostatic approach, Tabesh and Poulos (2007) produced some simple design charts for piles within a uniform soil profile. Figure 3 shows the problem addressed and Figure 4 gives examples of these charts for the case of a 20m long pile with a vertical load corresponding to a factor of safety of 2.5 against geotechnical failure. These charts are meant to provide only a very preliminary estimate of lateral pile response.

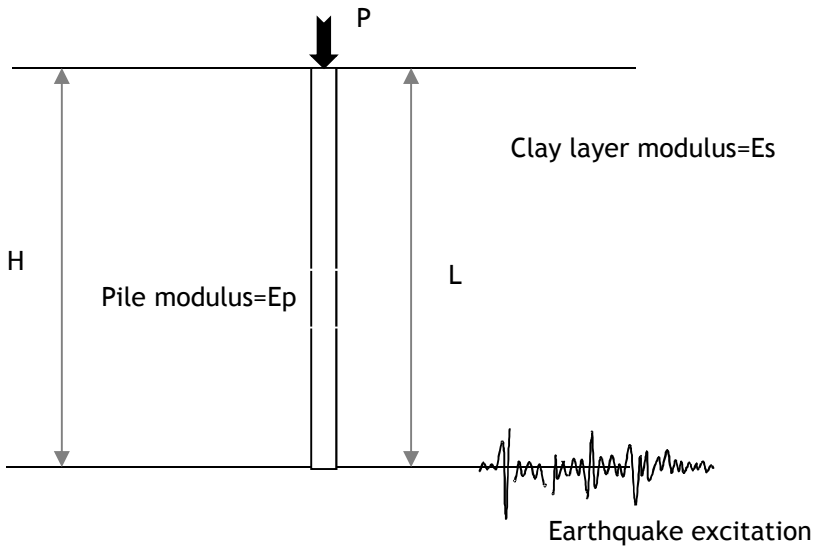


Figure 3 Problem considered for design charts

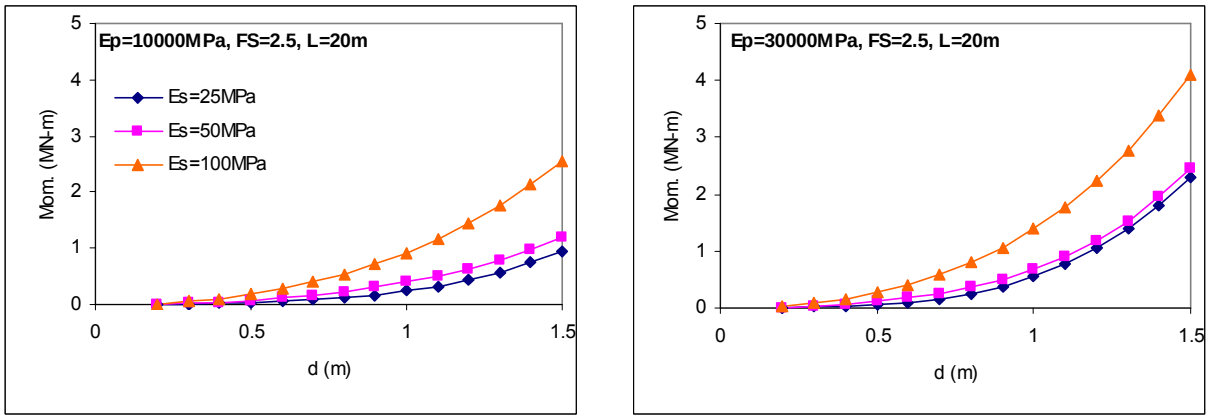


Figure 4 Typical design charts for maximum moment in 20m long pile (Tabesh & Poulos, 2007).

6. PILE DESIGN FOR LATERAL LOADING – INCLUDING LIQUEFACTION

6.1 Introduction

Soil liquefaction during a seismic event results in almost a complete loss of strength and stiffness in the liquefied soil, and consequent large lateral ground movements. The consequences of liquefaction on pile foundations can be very significant and can result in failure of the piles, as evidenced by many case histories during the 1995 Kobe earthquake (e.g. Ishihara and Cubrinovski, 1998) and the 2010-2011 events in Christchurch (e.g. Cubrinovski, 2013). A rational analysis of the behaviour of a pile in a liquefiable soil during and after an earthquake needs to take account of the effects of liquefaction on the soil properties, the natural period of the ground and the ground movements.

6.2 Simplified Analysis Based on Soil Stiffness Reduction

A procedure that has been employed in Japan to allow for the effects of liquefaction is to reduce the soil parameters by a factor which depends on the following factors:

i. The factor of safety against liquefaction, F_L;

ii. The depth below the ground surface;
iii. The original SPT (N) value of the soil.

An example of values of a reduction factor (r_k) for the modulus of subgrade reaction (k) for building foundation design in Japan is shown in Table 1 (JGS, 1998). This approach is very simplified, and considers only the effects of inertial loading. It does not incorporate the effects of kinematic loading.

Table 1 Reduction factor for modulus of subgrade reaction – building foundations (JGS, 1998)

Factor of Safety Against Liquefaction, F_L	**Depth z below ground surface (m)**	**Reduction factor r_k, applied to modulus of subgrade reaction k**			
		N≤8	**8<N≤14**	**14<N≤20**	**N>20**
≤0.5	0≤z≤10	0	0	0.05	0.1
	10<z≤20	0	0.05	0.1	0.2
0.5<FL≤0.75	0≤z≤10	0	0.05	0.1	0.2
	10<z≤20	0.05	0.1	0.2	0.5
0.75<FL≤1.0	0≤z≤10	0.05	0.1	0.2	0.5
	10<z≤20	0.1	0.2	0.5	1.0

6.3 Simplified Approach Based on Parametric Analyses

Valsamis et al (2012) have carried out an extensive set of parametric analyses and developed simplified expressions for lateral pile response in a laterally spreading soil profile. Three cases have been considered, as illustrated in Figure 5, and are as follows:

1. Case a: a 2-layer soil profile where a thick liquefiable layer overlies a non-liquefiable layer, and the pile head is unrestrained.
2. Case b: a 2-layer soil profile, as in Case a, but with the pile head restrained from both translation and rotation.
3. Case c: a 3-layer soil profile, where the liquefiable layer lies between two non-liquefiable layers, an overlying crust, and a lower continuous layer. The pile head is restrained from rotation but can translate freely.

The following expressions were derived for the maximum pile deflection, δ_{pile}:

Case a: $\delta_{pile} = \min[1.22\delta_{gr}, 29b^{1.44}.\delta_{gr}^{0.28}.J^{0.72}]$ (12)

Case b: $\delta_{pile} = \min[0.15\delta_{gr}, 0.12b^{0.74}.\delta_{gr}^{0.26}.J^{0.74}]$ (13)

Case c: $\delta_{pile} = 1.22\delta_{gr}$ (14)

where δ_{gr} = ground surface movement (m)
$J = H^6_{liq}.d/EI$
E = pile modulus (kPa)
I = pile moment of inertia (m^4)
H_{liq} = depth of liquefied soil (m)
d = pile diameter (m)
b = parameter related to corrected SPT value $(N_1)_{60,cs}$ and derived from Figure 6.

The maximum bending moment, M_{max}, is approximated by the following expressions:

Case a: $M_{max} = 2.2EI.\delta_{pile}/H^2_{liq}$ (15)

Case b: $M_{max} = 18EI.\delta_{pile}/H^2_{liq}$ (16)

Case c: $M_{max} = 17(EI.\delta_{pile}/H^2_{liq})^{0.65}$ (17)

In all cases, it is very important to use the correct units indicated above.

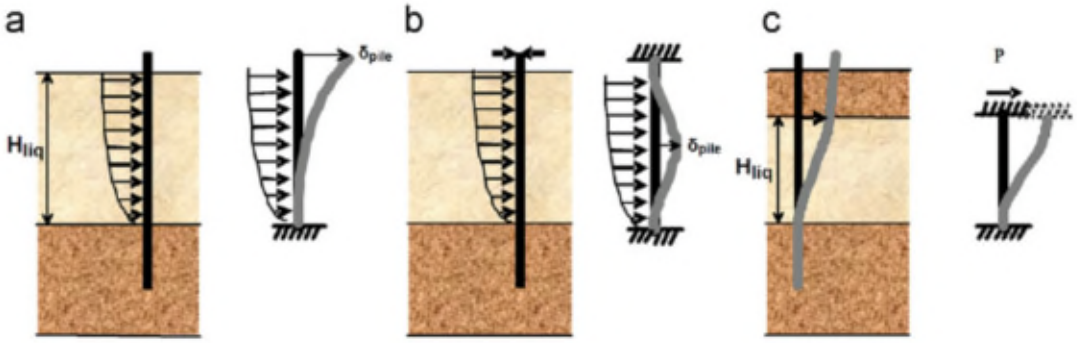


Figure 5 The design cases considered by Valsamis et al (2012)

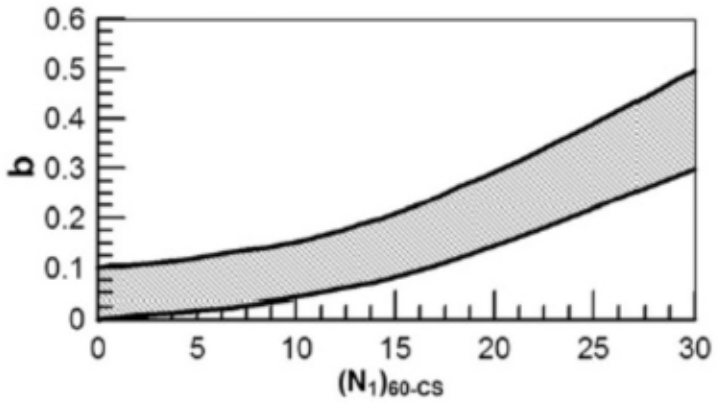


Figure 6 Parameter "b" related to corrected SPT value (Valsamis et al, 2012)

A practical difficulty with the above procedure is that the ground surface movement of a liquefied layer, $\delta_{gr,}$ is very difficult to estimate, and the computed responses depend greatly on this value.

6.4 Modified Approach Using Nikolau et al (2001)

6.4.1 Procedure

Use can be made of the equations developed by Nikolau et al (2001) to develop a simpler approach in which the amount of computational effort is relatively limited. This approach involves the following steps:

1. Estimate the reduction in shear modulus via the approach suggested by Ishihara and Cubrinovski (1998), in which the post-liquefaction shear modulus, G_{pl}, is given by:

$$G_{pl} = \beta\, G \quad (18)$$

where β = reduction factor;

G = shear modulus prior to liquefaction.

2. Estimate the bending moment for resonant conditions via equations 6-11. The shear wave velocity in the (upper) liquefied layer is now $v_{s1\text{-}liq} = v_{s1}\sqrt{\beta}$ where v_{s1} is the original shear wave velocity of the layer.

3. Estimate the modified natural frequency of the liquefied layer from equation 11, using the reduced shear wave velocity $v_{s1\text{-}liq}$.

4. Compute the correction factor η from either equations 8 and 9, or equation 10.

5. Compute the bending moment from equation 5.

6.4.2 Modulus Reduction Factor β

A key parameter choice is the value of the modulus reduction factor β. Cubrinovski (2006) suggests that β values range between 0.02 and 0.10 for cyclic liquefaction, and 0.001 to 0.02 for lateral spreading.

An alternative approach to estimating β is to relate it to the factor of safety against liquefaction F_L, or perhaps more logically, to the liquefaction potential index LPI, which is defined as follows:

$$LPI = \int F(z)\, w(z)\, dz \qquad (19)$$

where $F(z) = 1\text{-}F_L$ when $F_L<0.95$, and F_L = factor of safety against liquefaction
$F(z) = 2x10^{-6} \exp(-18.427F_L)$ when $0.95<F_L<1.2$
$F(z)= 0$ when $F_L \geq 0$
$W(z) = 10\text{-}0.5z$
z = depth below surface in metres.

The integration in equation 19 is carried out from the surface to a depth of 20m. Table 2 summarises the general levels of risk based on LPI.

To do this, use can be made of the recommendations shown in Table 1, from which ranges of values of LPI can be obtained from the range of values of F_L given in that table for the upper 10m of the profile and profile from 10 to 20m depth. Figure 7 shows the values of the modulus reduction factor β can be plotted against the derived average values of LPI, and from this plot, an empirical relationship can be drawn as follows:

$$\beta = \beta_{lim} + e^{b.LPI}(1\text{-}\beta_{lim}) \qquad (20)$$

where β_{lim} = lower limit value of β
b = index derived from fitting through the points in Figure 7, and found to be approximately -0.20
LPI = liquefaction potential index.

This relationship is also shown in Figure 7 for b = -0.2 and β_{lim} = 0.01, and shows reasonable agreement with the points derived from Table 1, despite the considerable scatter.

An alternative approach is suggested by Miwa et al (2006), in which the reduction in shear wave velocity is related to the factor of safety against liquefaction initiation. In addition, the damping ratio of a liquefied deposit is taken to be between 20 and 30%.

Table 2: Liquefaction Risk Based on Liquefaction Potential Index, LPI

LPI	Liquefaction Risk
0	Non-liquefiable
0-2	Low
2-5	Moderate
5-15	High
>15	Very high

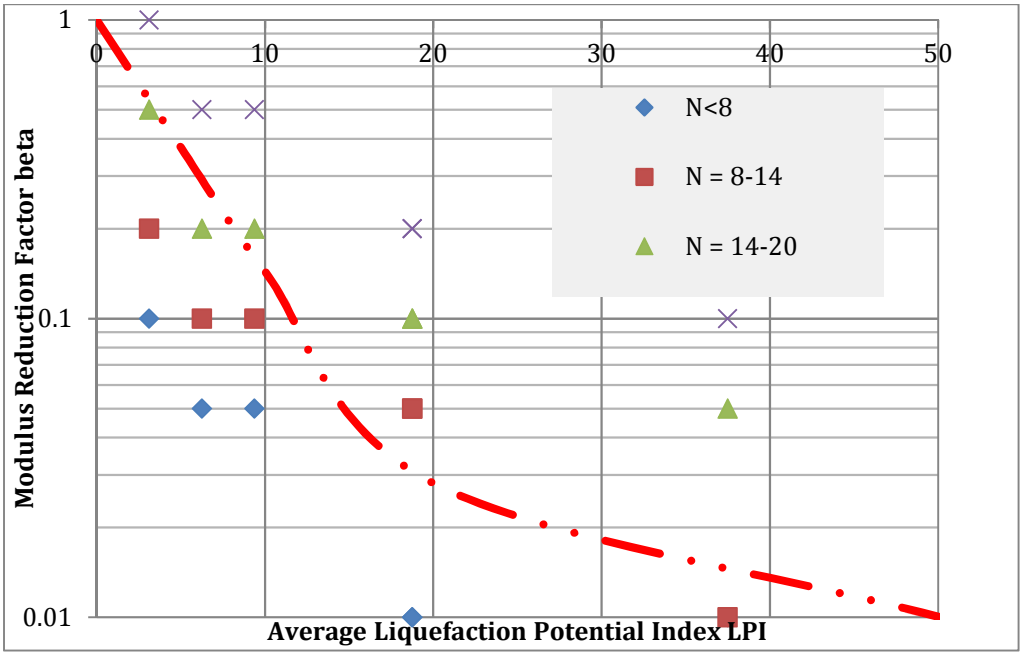


Figure 7 Relationship between modulus reduction factor b and liquefaction potential index LPI

6.4.2 Upper Limit to Kinematic Bending Moment

There will be an upper limit to the kinematic bending moment, which will occur if the layer has completely liquefied and flows past the pile. In this case (assuming that the applied pressure from the liquefied layer acts in the same direction along the whole layer), the limiting kinematic bending moment, M_{klim}, will be given by the following approximate expression):

$$M_{klim} = n.s_{u\text{-}Liq}.d\ h_1(h_1+dh) \qquad (21)$$

where n = undrained shear strength multiplier for limiting lateral pile-soil pressure

$s_{u\text{-}Liq}$.= shear strength of liquefied soil

d = pile diameter

h_1 = thickness of liquefied layer

dh = additional distance within underlying layer at which the maximum moment occurs (typically expected to be 0.5d-1d).

Data presented by Cubrinovski et al (2009) indicate that the parameter n in equation 21 may be about 9 (i.e. 4.5 times the Rankine passive pressure).

6.4.3 Estimation of Inertial Bending Moment in Pile

In cases where complete liquefaction of the upper layer occurs, with resultant lateral spreading of the liquefied soil, it has been suggested by Klimis et al (2004) that inertial effects can be neglected. However, the analyses and comparisons carried out by Liyanapathirana and Poulos (2005) indicate that inertial effects can be present and should be considered.

Following the recommendations of Liyanapathirana and Poulos (2005), the inertial force H_i can be estimated as follows:

$$H_i = a_s . P \tag{22}$$

where a_s = peak ground acceleration;
P = vertical load acting on pile.

Assuming (albeit boldly) that an elastic analysis can be applied to a pile in a liquefied layer, and that a constant Young's modulus applies to the liquefied layer, the maximum bending moment due to inertial loading, M_{imax}, can be estimated from the following expression derived from Randolph (1981):

(a) For a free-head pile:

$$M_{imax} = 0.1 H_i (L_c + h_1) \tag{23}$$

(b) *For a fixed head pile*: Fixing moment at the pile head):

$$M_{imax} = -0.1875\ H_i (L_c + h_1) \tag{24}$$

where H_i = inertial force on pile
h_1 = depth of liquefied soil
L_c = critical pile length in the non-liquefied soil, and approximated as:
$L_c = d(E_2/G_{red})^{2/7}$
G_{red} = shear modulus of the non-liquefied layer.

6.4.4 Effect of Near-Surface Crust above Liquefiable Layer

In cases where a stiffer (and non-liquefiable) crust may exist above the liquefiable layer, account needs to be taken of the effect of the stiffness of this crust on the behaviour of the pile under inertial loading, and its effect on the limiting bending moment that can be imposed on the pile.

An approximate, but conservative, allowance for the stiffness of the crust may be made by using a weighted average Young's modulus, E_{cl}, of the crust and the liquefiable layer, as follows:

$$E_{cl} = (E_c . h_c + E_l . h_l)/(h_c + h_l) \tag{25}$$

where E_c = Young's modulus of crust
h_l = thickness of crust
E_l = Young's modulus of liquefiable layer
h_l = thickness of liquefiable layer.

The maximum inertial bending moment can then be obtained from equation (23) for a free-head pile, or equation (24) for a fixed head pile.

To obtain the maximum kinematic bending moment at the interface between the liquefiable and non-liquefiable layers, the crust should not influence this value, and the simplified approach may again be used, using as before, the modulus of the liquefiable layer G_{pl} (equation 18).
When estimating the limiting bending moment that can be imposed on the pile, an additional shear force, H_{cr} and moment M_{cr} will be applied to the pile by the crust. These can be estimated as follows:

$$H_{cr} = h_{cr}.\ p_{ucr}.d \tag{26}$$

$$M_{cr} = H_{cr}\ (h_1+0.5h_{cr} + L_c) \tag{27}$$

where h_{cr} = thickness of non-liquefied crust
p_{ucr} = ultimate lateral crust-pile pressure, and which can be estimated as approximately 4.5 times the Rankine passive pressure exerted by the crust.
d = pile diameter
h_1 = thickness of liquefied layer (below crust)
L_c = critical pile length in the non –liquefied soil layer (see equation 24).

The combination of inertial and kinematic effects can then be considered as per the recommendations of Tokimatsu et al (2005) in Section 5.3.

6.5 Pseudostatic Analyses

6.5.1 Cubrinovski et al (2009).

The model developed by Cubrinovski et al(2009) is shown in Figure 8. The soil profile contains three components:

- A surface layer or crust which does not liquefy;
- A liquefiable layer;
- An underlying base layer that does not liquefy.

Each layer is characterised by a stiffness (expressed in terms of a modulus of subgrade reaction) and a limiting pile-soil pressure. The pile is analysed as a beam-spring model, and non-linear behaviour of the pile, as well as the soil, can be incorporated into the analysis by use of a finite element approach. Account is taken of both inertial and kinematic loadings.

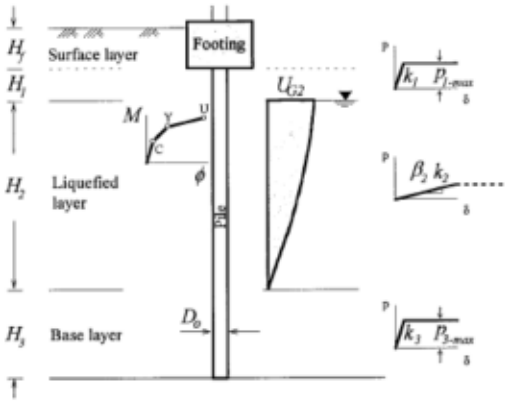


Figure 8 Model for pile in liquefied soil (Cubrinovski et al, 2009)

6.4.2 Liyanapathirana and Poulos (2005)

For piles in soils subject to liquefaction, Liyanapathirana and Poulos (2005) have developed an extension of the approach used by Tabesh and Poulos (2001) for piles in non-liquefiable soils. Account has been taken of the degradation of shear modulus of the soil that occurs with the generation of pore water pressure in the soil. The shear modulus of the soil is assumed to vary with the effective stress level of the soil as shown below:

$$G_s = G_0\left((1+2Ko)\sigma v'/\ pa\right)^{0.5} MPa \tag{28}$$

where $\sigma v'$ is the effective stress level of the soil, K_0 is the coefficient of earth pressure at rest, pa is atmospheric pressure, and G_0 is a constant which varies with the relative density, D_r, of the soil.

Although spectral acceleration has been used by Tabesh and Poulos (2001), it has been found that the inertial force at the pile head calculated using the spectral acceleration may overestimate the pile response when the surrounding soil starts to liquefy. Hence, the maximum acceleration at the ground surface, rather than the spectral acceleration, has been used to calculate the inertial force at the pile head.

The calculation steps involved in this approach can be summarised as below:

1. First, a free-field site response analysis is performed by taking into account the pore pressure generation and dissipation in the soil deposit due to the earthquake loading (Liyanapathirana and Poulos, 2002). From this analysis, the maximum ground surface acceleration, maximum ground displacement along the length of the pile, the minimum shear modulus and the effective stress level attained during the seismic activity can be obtained.
2. The superstructure is modelled as a concentrated mass at the pile head. Generally the superstructures supported by pile foundations are multi-degree-of-freedom systems but in the design of pile foundations, the superstructure is reduced to a single mass at the pile head to simplify the analysis.
3. The lateral force to be applied at the pile head is the cap-mass (vertical load divided by g), multiplied by the maximum ground surface acceleration obtained from the ground response analysis.
4. The pile-soil interaction is modelled using the spring coefficients calculated from elastic theory, based on the minimum shear modulus of the soil deposit at each depth, at any time, given by the free-field site response analysis (Step 1).
5. A non-linear static load analysis is carried out to obtain the profile of maximum pile displacement, bending moment and shear force along the length of the pile by applying the lateral forces calculated in Steps 3 and 4, and the soil movement profile calculated in Step 1, simultaneously to the pile.

This approach has been verified by comparison with the results of centrifuge tests (Wilson et al, 1999; Abdoun et al, 1997).

Comparisons have also been made with the field measurements made in the piles at the Pier 211 in Uozakihama Island after the Hyogoken-Nambu earthquake which occurred on 17th January 1995. Piles at bridge Pier 211 have a diameter of 1.5 m, and Figure 9 shows the crack distributions observed in piles after the earthquake. Ishihara and Cubrinovski (1998) have simulated this case, using their approach, and Liyanapathirana and Poulos (2005) also analysed it using their pseudostatic approach. The water table was 2.0 m below the ground surface and the upper 20 m of this site consisted of Masado sand with an initial shear modulus of 57.8 MN/m^2 and density of 2000 kg/m^3. Soil liquefaction was observed in the Masado sand layer below the water table only. Therefore only the top 20 m layer was analysed using the effective stress method incorporating

pore pressure generation and dissipation. After liquefaction, the effective stress level in the soil was reduced to a minimum of 2% of the initial effective overburden pressure. For this analysis the cyclic shear strength curve for the Masado sand given by Ishihara (1997) was used. It was assumed that the base rock had a density of 2200 kg/m^3 and a shear modulus of 75 GN/m^2.

Figure 9 shows the maximum bending moment profile along the pile obtained from the pseudostatic approach of Liyanapathirana and Poulos (2005), and also that calculated by Ishihara and Cubrinovski (1998). The lower end of the RC pile was assumed to be fixed while the pile head was assumed to be fixed to the footing but free to move in the horizontal direction. The predictions made by the pseudostatic approach agree reasonably well with the results given by Ishihara and Cubrinovski (1998). The yield moment for these piles is about 5 MNm. The computed maximum bending moment profile exceeds the yield moment near the pile head and in the vicinity of the boundary between the liquefied and non-liquefied layers. This is consistent with the location of cracks observed after the earthquake shown in Figure 9.

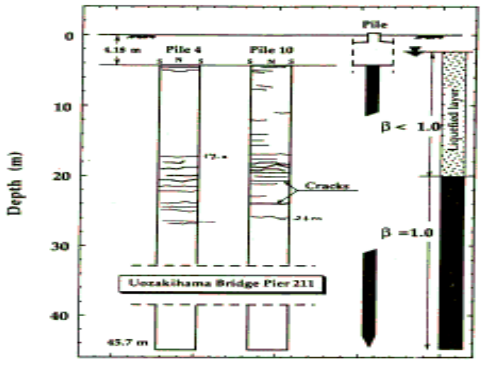


Figure 8. Cracks observed in the piles at bridge pier 211 in Uozakihama Island (Ishihara and Cubrinovski, 1998).

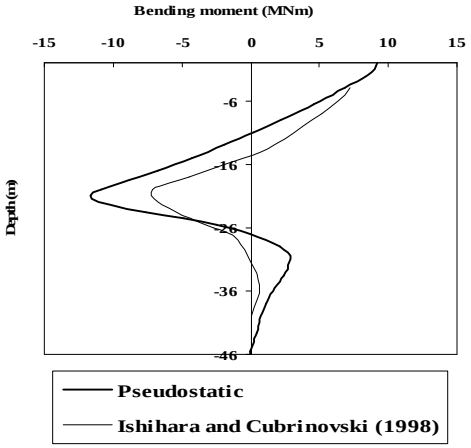


Figure 9 Cracks observed in piles at the bridge pier 211 in Uozakihama Island (Ishihara and Cubrinovski, 1998) and (b) Bending moment of the pile at Bridge Pier 211 in Uozakihama Island calculated from the pseudostatic approach and Ishihara and Cubrinovski (1998) results (β=0.01).

6.6 Example of Simplified Approach

To illustrate the application of the simplified approach, the above case of the bridge pile BP211 that was damaged in the 1995 Kobe earthquake (Ishihara and Cubrinovski, 1998) will be considered. The pile is one of a group of 22 bored piles, 1.5m in diameter, and is 41.5m long below the pile cap. The liquefiable layer is a reclaimed deposit 16m thick (below the pile cap) and has an average SPT-N value of about 10. The underlying layers consist of strata of sandy silt, with gravel, with SPT-N values ranging between about 10 and 50, with an average value of about 25. The average vertical load on a pile is 2.94 MN. A Young's modulus of the pile of 30000MPa will be assumed.

Using the relationship between shear wave velocity and SPT-N suggested by Imai and Tonouchi (1982), the shear wave velocity of the upper and lower layers is 173 and 234 m/s respectively, and the consequent small-strain shear moduli are 53.7 MPa and 103.9 MPa. Minimum and maximum damping ratios of 0.025 and 0.26 have been assumed for the strata at the site.
The earthquake characteristics at the site have not been documented, but based on other available information, it is assumed that the peak bedrock acceleration is 0.45g and that the predominant period of the earthquake is 1s.
Assuming that the piles have a fixed head, the inertial and kinematic maximum bending moments can be estimated for two cases:

- During the cyclic loading stage and prior to liquefaction;
- After liquefaction of the upper layer has developed.

(a) Cyclic Loading Phase

For the first case, the first step is to assess the amplification of ground motion, and based on the above assumptions, the natural period of the site is about 0.79s. Using, as an approximation, the classical expression for amplification of uniform harmonic motion, the ratio of predominant period to natural period is about 1.27, and for a damping ratio of 0.025, the amplification factor is found to be 2.64. Thus, the peak ground surface acceleration is estimated to be 0.45*2.64 = 1.188g. Using the small-strain modulus values, the following maximum moments are computed:

Inertial: -7.65 MNm (using equation 24)
Kinematic: 3.10 MNm (using the method of Nikolau et al, 2001, equations 5 to 9).

(b) Post-liquefaction phase

The small-strain modulus is used for the lower non-liquefiable layer, but a degraded modulus is used for the liquefied layer. To obtain this degraded modulus, given that liquefaction did indeed occur, a Liquefaction Potential Index, LPI, of 50 can be used. From equation 20, the reduction factor β is 0.01 (the limiting value assumed). The corresponding value of shear modulus is 0.54 MPa. The site period now becomes 1.10s, while the damping ratio has increased to its assumed maximum value of 0.26. Accordingly, the amplification factor from the classical dynamic theory decreases from 2.64 (for no shear modulus degradation) to 1.64 (for LPI=50), and the peak ground acceleration is then 0.45*1.64 = 0.738g.

From the expressions for inertial and kinematic bending moments (equations 24 and 5 to 9), the following values are obtained:

- Inertial moment (at pile head): -11.96 MNm
- Kinematic moment: 121.1 MNm.

However, a check needs to be made with the limiting kinematic bending moment that can occur when the liquefied layer flows past the pile. Adopting an undrained shear strength of 3 kPa for the liquefied soil, the limiting bending moment is found, from equation 27, to be 12.3 MNm. It is clear that the assumption of elastic behaviour in the Nikolau et al method (giving a huge kinematic moment of 121.1 MNm) is not valid in this case.

The values obtained from this simple analysis compare reasonable well those reported by Liyanapathirana and Poulos (2005) (approximately -9 MNm at the pile head and about 12 MNm at the base of the liquefied layer). Ishihara and Cubrinovski (1998) incorporated pile cracking into their analysis, and their computed maximum moments of about 7MNm reflect the occurrence of pile cracking, which limited the moment that could be induced in the piles. Figure 9 shows details of two piles that were excavated and shows the cracks in the piles at or near these two locations.

Most importantly, the simplified analysis indicates that large moments would have been generated at both the pile head and at the interface between the liquefied and non-liquefied layer.

6.7 Group Effects

Under inertial loading, it is now well-recognised that group effects are detrimental in that they tend to reduce the stiffness of piles within the group and decrease the overall group capacity. Methods of dealing with these effects are given by Poulos and Davis (1980) and Fleming et al (2009).

Under kinematic loading, group effects however tend to be beneficial, due to the "shielding" action of the piles. In particular, inner piles within a group tend to be subjected to smaller forces and moments developed by ground movements than outer piles, and all piles in the group tend to experience less effect than a single isolated pile. As a consequence, the consideration of a single isolated pile will generally be conservative when considering kinematic effects.

Towhata (2008) has presented an approximate approach for estimating the reduction in lateral earth pressure on a pile due to soil movement or flow past a group of piles. This reduction can be expressed in terms of two components:

1) A "shadow factor" which reduces the "downstream" pressure by a factor of 0.8 for each successive row of piles;
2) A spacing factor, α_p, which can be expressed as follows:

(i) For a non-liquefied layer:

$$\alpha_p = (0.877(1-\eta)f) / (0.877\eta + 0.123) + 1.0 \quad (29)$$

where $f = 1.0$ when $h_l/d \leq 3.8$
$f = 14[1/(h_l/d)^2] + 0.03$ when $h_l/d > 3.8$
h_l = depth of flowing soil
d = pile diameter
η = ratio of pile diameter to pile spacing (d/s).

(ii) For a liquefied layer:

$$\alpha_p = 1 / (0.599\eta + 0.401) \quad (30)$$

For practical use, it is convenient to derive a group reduction factor for the pressure developed by moving soil. If, from a practical viewpoint, s/d = 20 is considered as being sufficiently widely-spaced to represent a single pile, then the Group Reduction Factor for Pressure, RFp, can be defined as:

$$RFp = \alpha_p / \alpha_p \ (s/d=20) \quad (31)$$

Figures 10 and 11 plot the resulting values of RFp for the non-liquefied and liquefied soil cases. The beneficial effects of group action can clearly be seen from these figures. For the non-liquefied case, the effects of grouping become increasingly beneficial as the ratio h_l/d decreases, i.e. as the thickness of the moving soil decreases relative to the pile diameter.

When both inertial and kinematic effects are present, the group effects may tend to counteract each other.

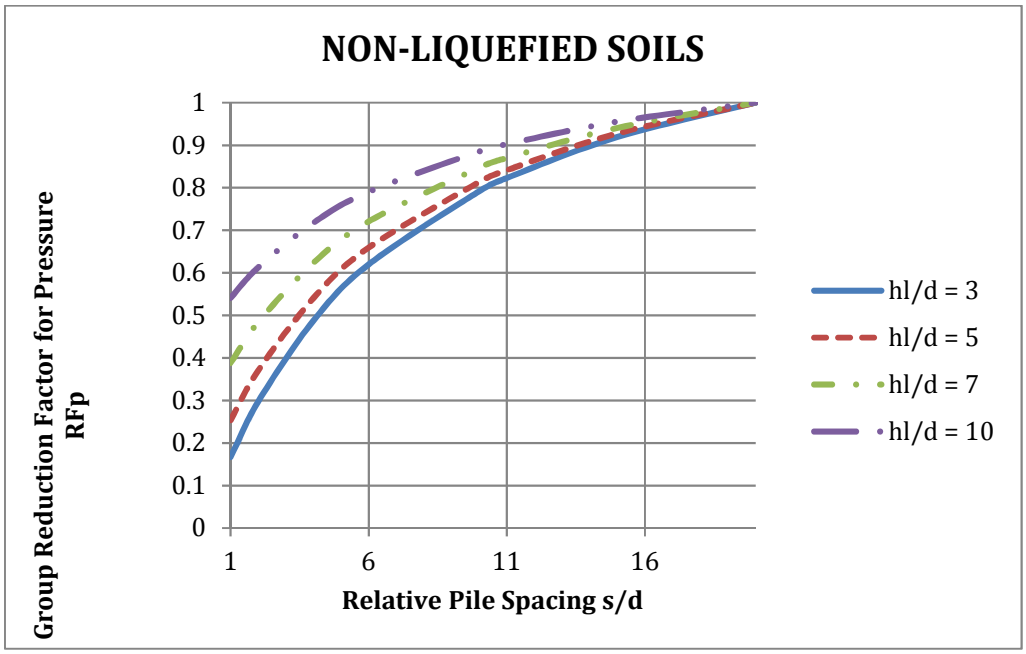


Figure 10 Group reduction factor for lateral pile-soil pressure – non-liquefied soil

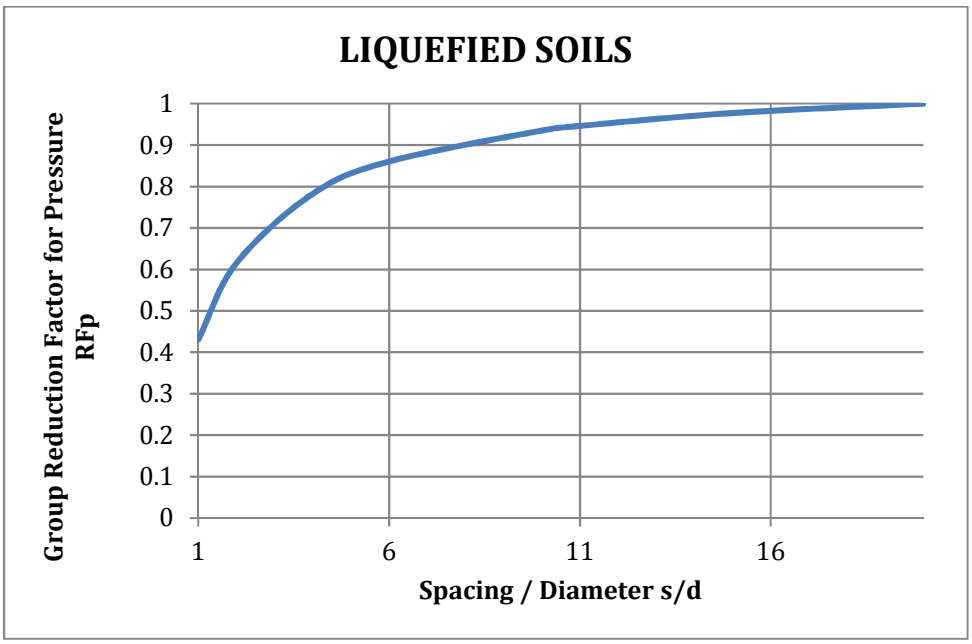


Figure 11 Group reduction factor for lateral pile-soil pressure – liquefied soil

7 FOUNDATION STIFFNESS AND DAMPING

Piles will experience vertical and horizontal movements during an earthquake due to the inertial loadings imposed by the supported structure. These movements will generally be dynamic in nature and therefore it is necessary to consider the pile head stiffnesses under dynamic loading, and the damping that will be generated by the dissipation of energy away from the piles into the surrounding soil (the radiation damping). Knowledge of foundation stiffness and damping is also required to assess the effects of structure-foundation interaction on the natural period and damping of a structure.

Theoretical solutions for the axial and lateral stiffnesses of a single pile have been provided by Novak (1987) among others. Convenient approximate solutions have been given by Gazetas (1991) for various simplified soil profiles.

In contrast to static loading, where the interaction factors between piles decrease with increasing distance between the interacting piles, the dynamic interaction factors can either increase or decrease, depending on the frequency of the loading and the spacing between the piles. It is possible that the interaction factors can be negative under some circumstances, so that group effects may possible lead to an increase in stiffness of the piles within a group, as compared with the case of static loading, where group effects generally reduce the stiffness of piles in the group. For practical design, it may often be more convenient to simplify the group as an equivalent pier, and then to use the corresponding solutions for stiffness and damping as given by Gazetas (1991).

8 MITIGATION OF LIQUEFACTION EFFECTS

8.1 Categories of Mitigation Measures

Conventional remedial measures to mitigate the effects of liquefaction can be divided into three broad categories (JGS, 1998):

- Treatment of the liquefiable soil to strengthen it;
- Treatment of the soil to accelerate the dissipation of seismically-induced excess pore pressures;
- Measures to reduce liquefaction-induced damage to the structure or facility.

8.2 Conventional Measures to Strengthen the Liquefiable Soil

An extensive discussion of measures that can be used to strengthen liquefaction-susceptible soils is given in JGS (1998). Some of the more common measures are as follows:

- Soil densification, by a variety of means, e.g. vibroflotation, blasting;
- Insertion of stiffer columns;
- Provision of drainage via stone columns.

A major limitation of all of these methods is that they cannot be used to remediate sites on which structures or facilities already exist. A number of the methods for soil densification may also not be feasible if the site is within a commercial or residential area, because of the noise and vibrations involved.

Methods involving the insertion of stiffer columns can be effective and generally involve less noise and vibration than conventional methods of densification.

8.3 Conventional Measures to Accelerate Excess Pore Pressure Dissipation

The use of stone columns or gravel drains to accelerate pore pressure drainage was developed by Seed and Booker (1977) and has been used successfully in a number of cases. In the design of stone columns for liquefaction mitigation, it is common to specify a limiting maximum pore pressure ratio (excess pore pressure divided by vertical effective stress), and this is often taken as 50%. The required length of the columns will depend on the depth of the liquefiable layer, while the required spacing of the columns will depend on the following factors:

1. The specified maximum pore pressure ratio;
2. The permeability and compressibility of the liquefiable layer;
3. The earthquake duration;
4. The equivalent number of cycles of loading from the earthquake;
5. The number of cycles to cause liquefaction;
6. The column diameter;
7. The finite permeability of the column and the effects of well resistance.

8.4 Mitigation Measures for Pile Foundations

Sato et al (2004) have suggested various countermeasures for pile foundations subjected to lateral flow of liquefiable soils. Three of these measures are illustrated in Figure 12.

The “drain piles” method aims to prevent the liquefaction of the lower layers while reducing the stiffness of the stiffer crust above the liquefiable layers. The drain piles should extend only about half-way into the upper crust, and the permeability of the drain piles should be greater than that of the liquefiable layers so that the excess pore pressures that are generated are transmitted to the upper layer. In the “earth retaining wall” method, an earth retaining wall is constructed in front of the pile foundation, to block the lateral flow. The “streamlined shield block” method involves the casting of an angled face on the upstream side of the pile cap. This angled face is meant to disperse the flowing soil and reduce its effect on the foundation.

Centrifuge tests were carried out by Sato et al (2004) to examine the effectiveness of the above countermeasures. Figure 13 summarises the test results and indicates that the “streamlined shield block” method is very effective in reducing the residual lateral displacement, and also the bending strain in the piles. It has the advantage of not requiring any ground improvement.

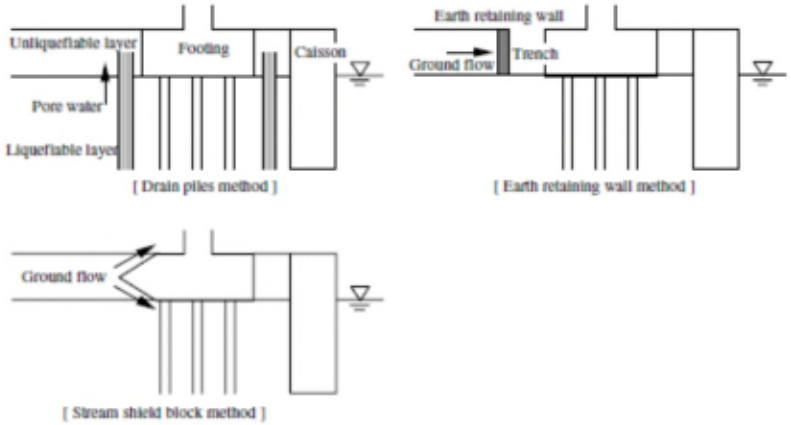


Figure 12 Countermeasures for lateral ground flow (Sato et al, 2004)

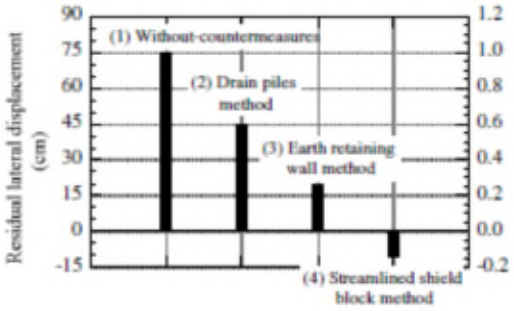


Figure 13 Measured residual lateral movements for various countermeasures (Sato et al, 2004)

8.5 Some Innovative Methods for Liquefaction Risk Mitigation

There are a number of recent innovative methods that have been explored for reducing the risk of liquefaction, several of which have the potential to be used for sites on which structures or facilities exist. A brief review of some of these methods is given below.

8.5.1 Passive Remediation via Infusion of Colloidal Silica

Colloidal silica is a dispersion of silica particles in water. With about 5% weight of silica, a colloidal silica aqueous dispersion has density and viscosity values that are similar to water, and this dispersion becomes a permanent gel abruptly after a period of time, generally a few months at most. Colloidal silica is non-toxic, biologically and chemically inert, and relatively durable. The influence of the gel is to reduce the strains in the treated soil developed by cyclic loading, and to reduce the soil permeability.

Figure 14 shows results of cyclic triaxial tests on Monterey sand, both untreated, and treated with 10% colloidal silica. The increased resistance to liquefaction is very clearly demonstrated in this figure.

Gallagher et al (2007) have described field tests to assess the performance of a dilute colloidal silica stabilizer in reducing the settlement of liquefiable soils. Slow injection methods were used to treat a 2m thick layer of liquefiable sand, using eight injection wells around the perimeter of a 9m diameter test area. The gel times ranged between 10 and 30 days. A subsequent blasting test revealed that the settlement of the treated soil was only about 60% that of an adjacent untreated area. Interestingly, there appeared to be no significant increase in the CPT resistance or the shear wave velocity, and the mechanism of improvement was considered to be due to the development of cohesion within the treated soil due to the formation of interparticle siloxane bonds.

Gallagher and Lin (2009) demonstrated that colloidal silica could be successfully delivered through 0.9m diameter columns packed with loose sand. The main factors influencing the transport of the stabilizer were the viscosity of the colloidal silica stabilizer, the hydraulic gradient, and the hydraulic conductivity of the liquefiable soil.

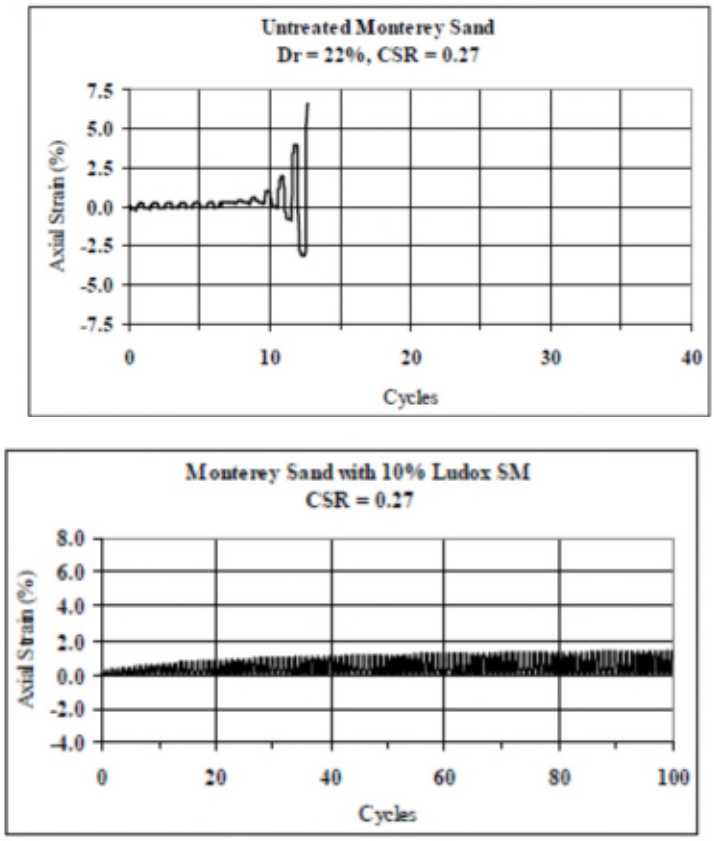


Figure 14 Comparison between cyclic behaviour of untreated sand and sand treated with 10% colloidal silica (Gallagher 2000).

8.4.2 Biogeochemical Remediation

Over the past decade, new biogeochemical techniques have been explored for the improvement of ground properties. DeJong et al (2011) summarise some of these techniques, and at least two of these have the potential to improve the liquefaction resistance of soils. The first of these involves the use of microbes to induce calcite precipitation between soil particles. The second involves the use of microbes to generate small gas bubbles within the soil and thus increase the resistance to liquefaction.

Microbially Induced Calcite Precipitation (MICP) occurs through a variety of microbiological processes, such as urea hydrolysis and denitrification. The process of calcite precipitation appears to have been discussed initially by van Meurs et al (2006), using the terms “smart soils” and “biogrout”. In Biogrout, specific bacteria create a reaction which results in the precipitation of calcium carbonate in the form of crystalline calcite on the surface of the sandy particles (see Figure 15). When this reaction occurs under the right conditions, crystals are formed between two adjacent particles, producing a connection between them. This connection increases the strength and stiffness of the soil. The longer the nutrients, bacteria and reactants are present, the thicker the layer of mineralization. An important characteristic of this process of cementation is that the permeability of the porous material only reduces slightly. The biomineralization process progresses slowly in natural circumstances, but the rate of mineralization can be enhanced by stimulating the conditions.
Test data presented by Meurs et al indicated that the strength of a treated sand could be increased by a factor of almost 5, while the stiffness was increased by a factor of 3.

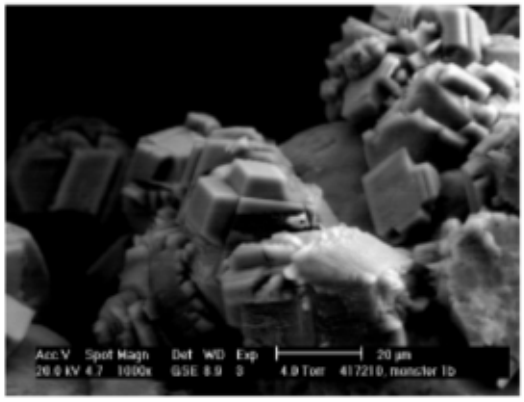


Figure 15 Scanning electron micrograph showing the mineralization of calcite onto sand grains.

DeJong et al (2010) provide a more detailed description of the process of calcite precipitation and its consequences on the geotechnical properties of the treated soil. Significant increases can be obtained in both strength and stiffness, and the volumetric behaviour can be altered from contractive to dilative, thus improving the resistance to liquefaction.

DeJong et al (2011) point out that there are a number of major challenges in implementing MICP technology. One is related to upscaling to a field scale, with issues related to cost, the stimulation of native biota, the uniformity of treatment, and the management of potentially harmful by-products. Another issue relates to the alternatives of employing bio-stimulation of native bacteria species, or the augmentation of a specific species of bacteria for a treatment zone. They suggest that bio-stimulation may be the preferred approach. A further issue may be the longevity of the treated soils, which is related to the pH of the groundwater. Tests suggest that MICP products will remain stable provided that the pH remains above 6.3.

With respect to the second technique involving microbial gas generation, Chu et al (2011) discuss some types of microorganisms that may contribute to biogas effects. This latter approach, sometimes referred to as the "Induced Partial Saturation" technique, involves the injection of non-hazardous chemicals into the ground to create gas bubbles and hence to reduce saturation. This in turn reduces the potential for liquefaction. This again has the potential to be used to improve liquefaction resistance below existing structures and buildings.

Further information on bio- and chemo-mechanical processes in soils is provided in Geotechnique (2013).

9. CONCLUSIONS

This paper has provided a review of practical methods of assessing the effects of seismic events on the behaviour of piles, and thereby, a means of designing the piles to resist seismically-induced actions. Consideration has been given to both axial and lateral effects on piles, and for cases involving no liquefaction and also where liquefaction is assessed to occur.

In cases where liquefaction may occur, consideration needs to be given to the following issues:

1. Temporary loss of axial load capacity;
2. The possibility of axial buckling of the pile;
3. Bending moments and shears developed in the pile due to both inertial and kinematic loadings;

4. The possible beneficial effects of group action in reducing kinematically-induced bending moments.

It has been demonstrated that bending moments are likely to be a maximum at or near soil layer interfaces where there is a significant difference in the stiffness of the layers. An important case is at the junction between liquefied and non-liquefied layers. A further consequence of this behaviour is that large bending moments may occur well below the pile head, where it has been customary in the past to reduce or eliminate reinforcement in concrete piles because the moments due to inertial loads have become small. Unfortunately, in cases of earthquake loading, the kinematically-induced moments may be substantial at depth if the soil is layered and the stiffness of adjacent layers differs markedly.

There are a number of methods available for mitigating the effects of liquefaction. While some of the more traditional methods may be suitable for green-field sites, they may not be feasible for existing sites. In such cases, some of the more recent innovative methods involving bio-geo-chemical processes hold considerable promise, provided that they can be demonstrated to be economically feasible at field scale.

REFERENCES

Abdoun, T., Dobry, R. and O'Rouke, T.D. (1997). "Centrifuge and Numerical Modelling of Soil-Pile Interaction During Earthquake Induced Soil Liquefaction and Lateral Spreading." *Observation and Modelling in Numerical Analysis and Model Tests in Dynamic Soil-Structure Interaction Problems – Proceedings of Sessions held in conjunction with Geo-Logan '97*, Logan Utah, 76-90.

Bhattacharya, S. and Bolton. M. (2004). Errors in design leading to pile failures during seismic liquefaction. *Proc. 5th Int. Conf. Case Histories in Geot. Eng.*, New York, Paper No. 12A-12.

Chu, J., Ivanov, V., He, J., Naemi, M., Li, B. and Stabnikov, V. (2011). Development of microbial geotechnology in Singapore. *Proc. Geo-Frontiers 2011 Conf., ASCE Conf. Proc.* Doi:10.1061/41165:397-416.

Cubrinovski, M. (2013). Liquefaction-Induced Damage in the 2010-2011 Christchurch (New Zealand) Earthquakes. *Paper EQ-1, 7th Int. Conf. Case Histories in Geot. Eng., Chicago*, CD Volume, ISBN #1-887009-17-5.

Cubrinovski, M. and Ishihara, K. (2004) Simplified Method for Analysis of Piles Undergoing Lateral Spreading in Liquefied Soils. *Soils and Foundations* 44(5): 119-133.

Cubrinovski, M., Ishihara, K. and Poulos, H.G. (2009). Pseudo-static Analysis of Piles Subjected to Lateral Spreading. *Bull. New Zealand Soc. Earthqu. Eng*., 42(1): 28-38.

DeJong, J.T., Mortensen, B.M., Martinez, B.C. and Nelson, D.C. (2010). Bio-remediated soil improvement. *Ecological Engineering*, 36: 197-210.

DeJong, J. T., Mortensen, B., Soga, K. and Kavazanjian, E. (2011). Harnessing in-situ biogeochemical systems for "natural" ground improvement. *Geo-Strata, ASCE* GeoInstitute, July/August 2011, 36-39.

Gallagher, P.M., Conlee, C.T. and Rollins, K.M. (2007). "Full-scale field testing of colloidal silica grouting for mitigation of liquefaction risk". *J. Geotech. & Geoenv. Eng., ASCE*, 133(2): 186-196.

Gallagher, P.M. and Lin, Y. (2009). Colloidal silica transport through liquefiable porous media. *J. Geotech. & Geoenv. Eng., ASCE*, 135(11): 1702-1712.

Gazetas, G. (1991). "Foundation vibrations". Chapter 15 of Foundation Engineering Handbook, 2nd Ed., Edited H.S. Fang, Chapman and Hall, New York, 563-593.

Geotechnique (2013). Symposium in Print. Bio- and Chemo-Mechanicsl Processes in Geotechnical Engineering". *Geotechnique,* 53(3).

Imai and Tonouchi (1982). Correlation of N-value with s-wave velocity and shear modulus, *Proc. 2nd European Symp. on Penetration Testing*, 67-72.

Ishihara, K. and Cubrinovski, M. (1998). Performance of large-diameter piles subjected to lateral spreading of liquefied soils. *Keynote lecture, Proc. 13th Southeast Asian Geotech. Conf.,* Taipei, 2: 13-26.

Ishihara, K. (1997). Geotechnical aspects of the 1995 Kobe earthquake. *Terzaghi Oration, Proc. 14th Int. Conf. Soil Mechs. Foundn. Eng*., Hamburg, 4: 2047-2073.

JGS (1998). *Remedial measures against liquefaction.* Ed. Japanese Geotechnical Society (JGS). Balkema, Rotterdam.

Klimis, N., Anastasiadis, A., Gazetas, G. and Apostolou, M. (2004). "Liquefaction risk assessment and design of pile foundations for highway bridge". *Proc. 13th World Conf. Earthquake Eng.*, Vancouver, Canada, Paper No. 2973.

Kramer, S.L. (1996). *Geotechnical Earthquake Engineering*. Prentice Hall, New Jersey.

Liyanapathirana, S. and Poulos, H.G. (2002). Numerical simulation of soil liquefaction due to earthquake loading. *Soil Dynamics and Earthquake Eng*., 22: 511-523.

Liyanapathirana, S. and Poulos, H.G. (2005). Pseudostatic approach for seismic analysis of piles in liquefying soil. *Jnl. Geot. & Geoenv. Eng., ASCE,* 131(12): 1480-1487.

Madhabhushi, S.P.G. and May, R. (2009). *Pile foundations*. Chapter 9 of Seismic Design of Buildings to Eurocode 8, A.Y. Elghazouli (Ed), Spon Press, London.

Mina, S. and Ikeda, T. (2006). Shear modulus and strain of liquefied ground and their app;lication to evaluation of the response of foundation structures. Struct. Eng./Earthquake Eng, 23(1): 167s-179s.

Nikolaou S., Mylonakis G., Gazetas G. and Tazoh T. (2001) Kinematic Pile Bending during Earthquakes: Analysis and Field Measurements. *Geotechnique,* 51, 425−440.

Novak, M. (1987). State of the art in analysis and design of machine foundations". *Soil Structure Interaction,* Elsevier/CML Publ, New York, 171-192.

Poulos, H.G. (1989). Pile Behaviour – Theory and Application. *29th Rankine Lecture, Geotechnique,* 39(3): 365-415.

Poulos, H.G. (1991). *ERLS User's Manual.* Coffey Partners International, Sydney.

Poulos, H.G. (1993). Effect of earthquakes on settlements and axial pile response in clays. Aust. *Civil Eng. Transactions, IEAust,* Vol. CE35(1): 43-48.

Poulos, H.G. and Davis, E.H. (1980). *Pile foundation analysis and design*. John Wiley, New York.

Randolph, M.F. (1981). The response of flexible piles to lateral loading. *Geotechnique*, 31(2): 247-259.

Sato, K., Higuchi, S. and Matsuda, T. (2004). A study of the effect of countermeasures for pile foundation under lateral flow caused by ground liquefaction. *Proc. 13th World Conf. Earthquake Eng.*, Vancouver, Paper No. 452.

Seed, H.B. and Booker, J.R. (1977). Stabilization of potentially liquefiable sand deposits. *Jnl. Geot. Eng., ASCE,* 103(GT7): 757-768.

Sica S., Mylonakis G., Simonelli A.L. (2011) Transient kinematic pile bending in two layer soils. *Soil Dynamics and Earthquake Engineering* , Vol. 31, pp. 891-905.

Tabesh, A. and Poulos, H.G. (2001). Pseudostatic approach for seismic analysis of single piles. *Jnl. Geot. & Geoenv. Eng., ASCE*, 127(9): 757-765.

Tabesh, A. and Poulos, H.G. (2007). Design Charts for Seismic Analysis of Single Piles in Clay. *Proc. ICE, Geotechnical Engineering*, 160(GE2): 85-96.

Tokimatsu, K., Suzuki, H. & Sato, M. (2005). Effects of inertial and kinematic interaction on seismic behaviour of pile with embedded foundation. *Soil Dynamics and Earthquake Engineering*, 25(753-762).

Towhata, I. (2008). *Geotechnical Earthquake Engineering*. Springer, Berlin.

Wilson, D.W., Boulanger, R.W. and Kutter, B.L. (1999). Lateral Resistance of Piles in Liquefying Sand. *Geotechnical Special Publication No. 88,* pp. 165-179.

van Meurs, G., van der Zon, W., Lambert, J., van Ree, D., Whiffin, V. and Molendijk, W. (2006). The challenge to adapt soil properties. Proc. 5 ICEG: Environ. Geotechnics: Opportunities, Challenges and Responsibilities for Env. Geotechnics, 2: 1192-1199.

Valsamis A., Bouckovalas G., Chaloulos Y. (2012. "Parametric analysis of single pile response in laterally spreading ground". *Soil Dynamics and Earthquake Engineering*, Vol. 34, pp. 99-100.

ARTIFICIAL GROUND FREEZING – A TYPICAL APPLICATION FOR THE UNDERPASS OF AN EXISTING METRO STATION IN ROME

Bruno Vingiani, Trevi S.p.A., Cesena, Italy, +39 0547 319147, bvingiani@trevispa.com
Alessandro Bertero, Trevi S.p.A., Cesena, Italy, +39 0547 319413, abertero@trevispa.com

ABSTRACT

The use of Artificial Ground Freezing (AGF) for temporary soil strengthening and seepage control is an effective alternative to grouting when dealing with soils whose degree of finesses would imply the use of highly expensive chemical grouts. However, compared to grouting, the application of this improvement technique usually needs a more accurate preliminary soil investigation campaign and a design assisted by specific calculation software. Besides a general description of the main features of this technique, the paper will describe a recent application of AGF carried out in Rome to underpass an existing metro station.

Keywords: ground, freezing, metro, station, tunnel

INTRODUCTION

Natural ground freezing occurs seasonally or permanently (permafrost) in some areas of the globe close to the poles and can negatively affect the engineering performance of underground structures. On the other hand, Artificial Ground Freezing (AGF) is man-made controllable freezing process that can be used in foundation engineering to temporarily strengthen the ground and create a barrier to the passage of groundwater. During the process, the heat is extracted from the soil in a cylindrical shape around a number of freezing pipes installed into the ground. This action produces columns of frozen soil, which expand gradually till they merge and create continuous frozen wall. The thickness of this barrier can be regulated according to the specific project requirements. Nowadays, AGF technique is applied to a wide range of foundation engineering problems where soil stability and groundwater flows are an issue (Pimentel et al. 2011, Haß and Schäfers, 2013). Typical applications include the temporary stabilization and waterproof of the ground around the excavation profile of mined tunnels until the construction of the final lining (Figure 1).

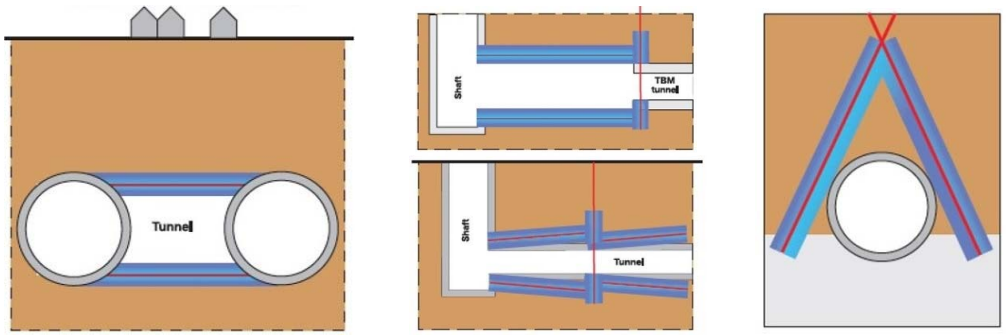


Fig. 1. Typical applications of AGF in tunnelling works

The case history described in this paper deals with a recent application of AGF carried out during the construction of metro Line "C" in Rome. Specifically, this technique has been applied to allow the construction of two single-track mined tunnels running underneath an existing metro station belonging to Line "A". In that case, the AGF has been evaluated by the Designers as the only possible solution for improving the mechanical and hydraulic characteristics of the concerned soils without causing disorders to the regular operations of the overlaying station.

BRIEF HISTORY OF AGF

The idea of AGF was conceived in France, but the first industrial application, dated 1862, was carried out in South Wales (UK) for the stabilization of a mine shaft (Schmidt, 1895). In 1883, the system was patented by German mining engineer F. H. Poetsch, and sometimes also referred as Poetsch Process.

The patented method involved the installation into the ground of an outer pipe and a concentric inner pipe. The chilled coolant (calcium chloride brine) is pumped inside the inner pipe and comes back through the outer pipe in a continuous circulation process, where the return fluid, after the exchange of calories, is re-cooled by a refrigeration plant.

A major innovation on the AGF technique occurred in France in 1962, when, for the first time, liquid nitrogen was used as coolant fluid instead of chilled calcium chloride. This innovation allowed for much faster ground freezing at lower temperatures. In this case, the liquid nitrogen, after circulating through the pipes, is released to the atmosphere in form of gas (Sanger and Sayles, 1979).

APPLICABILITY AND DESIGN REQUIREMENTS

The main advantage of AGF is that, provided that the soil is under the water table and the velocity (if any) of the groundwater is lower that certain limits, its applicability extends to any type of soil (Figure 2).

Obviously, considering the high costs involved in its use, the practical applicability of AGF is actually limited to the cases where:

- the use of soil permeation grouting techniques is unfeasible or uneconomic;
- the achievement of a perfect imperviousness of the soil is considered mandatory;
- a homogeneity of the treatment and a UCS of the concerned soil incompatible with other soil improvement methods is required (Figure 3).

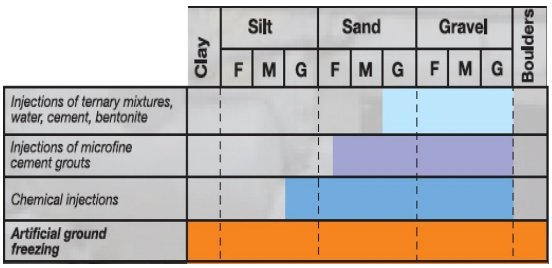


Fig. 2. Applicability of AGF compared to grouting

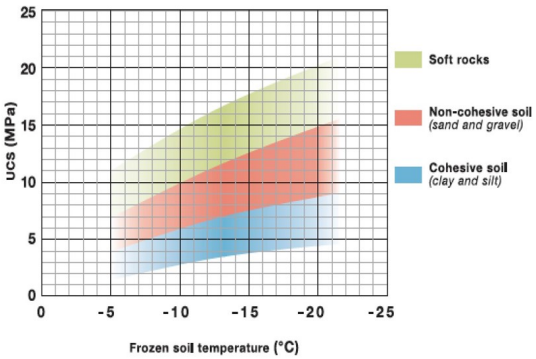


Fig. 3. Range of UCS achievable with AGF

As additional advantages of AGF, compared to other soil improvement methods, we can also mention its environmental compatibility (i.e. no material is injected into the soil and the coolant fluids are never in direct contact with the surrounding ground) and the possibility to intervene on possible defects of the ice wall before starting the excavation under its protection. In fact, the formation of the ice wall is comprehensively controlled in real-time by a specific monitoring system.

The design of AGF intervention usually needs a comprehensive soil investigation and specific laboratory tests on natural and artificially frozen soil samples. These investigations are intended to assess physical and thermal conductivity properties of the soils to be treated, as well as salinity, temperature and velocity of the groundwater (Figure 4-5).

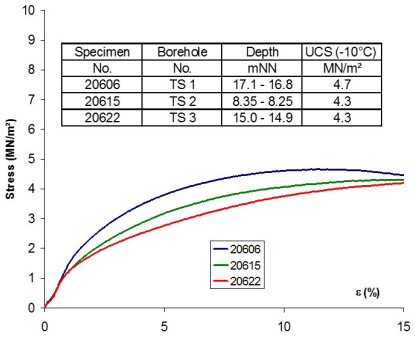


Fig. 4. UCS test on undisturbed soil samples

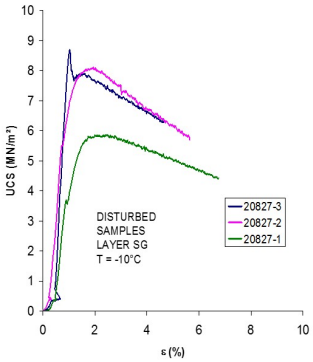


Fig. 5. UCS test on frozen (-10 °C) soil samples

The results of the soil investigation and laboratory tests are then used to run specific thermal analysis software, which allow the definition of the best freezing pipes pattern and the duration of freezing process to achieve the designated thickness of the frozen wall. The requirement of using specific and powerful software is given by the complex and mutually interacting thermal, hydraulic and mechanical mechanisms which develop during freezing and thawing processes.

For example, phase changes of the pore water caused by temperature variation can modify the pore water pressure in the soil, which, in turn, can induce mechanical deformations. At the same time, any changes in the hydraulic and mechanical features affect the thermal process by advection and changes of ice and water contents.

Since, at the end of freezing pipes installation phase, the as-built position of the latter will obviously not match perfectly to the design positions, a second and comparative thermal analysis is usually carried out once all the freezing pipes are in place (Figure 6-7).

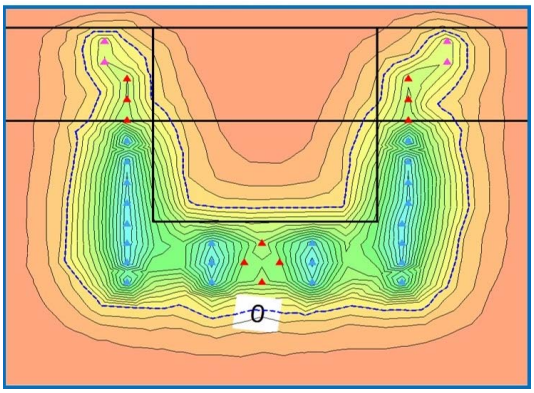


Fig. 6. Development of the frozen wall with time (designed freezing pipes position)

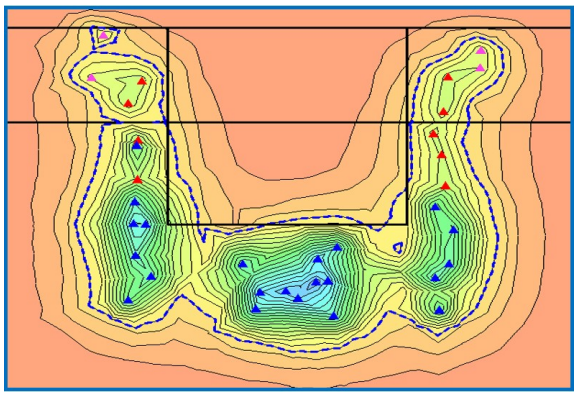


Fig. 7. Development of the frozen wall with time (as-built freezing pipes position)

In the absence of water currents, the extent of the frozen soil zone depends primarily on the frozen thermal conductivity. This parameter may vary by a factor of 4 or 5, with lower values related to silt and clays and higher values relate to rocks. Groundwater velocities higher than 3 m/day may cause problems to the formation of the frozen wall. For water flows in the range of 2-3 m/day, a reduced spacing of the freezing pipes may be sufficient to overcome the problem. On the contrary, for water flows exceeding 3 m/day, the permeability of the soil formation must be preliminary reduced by grouting. Also soil water content and salinity plays an important role in the achievement of a good result of any AGF intervention. In fact, while the first will influence the final UCS of the frozen wall, the second will have a direct impact on the freezing time required to achieve the designated thickness of the wall itself.

OTHER SPECIFIC REQUIREMENTS

Excessive deviations of the freezing pipes may lead to inhomogeneity of the treatment and an increase in the duration of freezing with related additional costs. This is why, for drilling lengths exceeding 30-40 m, the only measure of the actual position of the borehole in the space is not usually sufficient, and the use of a system able to correct such deviations while drilling should be always considered.

Trevi Directional Drilling Technology (TDDT) has been developed on the basis of the well-known Horizontal Directional Drilling (HDD) technology, used since long time to lay cables and/or pipes underneath water streams, roads, railways, buildings, etc. without digging.

The system includes a number of devices that enable to drill small diameter boreholes (50-200 mm) of considerable length (up to 200 m) with extraordinary accuracy. Drilling can be either rectilinear or curvilinear, with a radius of curvature depending on the diameter of the borehole and the stiffness of rods and casings used. TDDT system allows a real-time measurement of the position in the space of the borehole and, if deviations exceed the designated tolerances, a correction of the drilling. In the magnetic guidance system (Figure 8), the drill bit position is determined by means of a magnetic sensor located at the bottom of the drilling rods. Measurement accuracy ranges between 50 and 200 mm, according to the distance between the sensor and a reference electric field generated by two wires inserted in a specific borehole. In case directional corrections are required, the latter are performed by means of asymmetric or bevelled drill bits of different shape according to the nature of the involved soils.

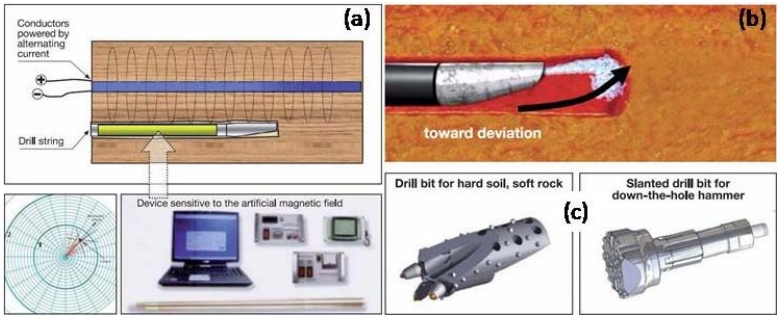


Fig. 8. TDDT system: (a) magnetic guidance system, (b) correction principle, (c) different types of directional drill bits

Such kind of measurements and controls allows for a 3D representation of the actual position of the freezing pipes, thus enabling a better interpretation of the temperature data and the development of the frozen wall (Figure 9-10).

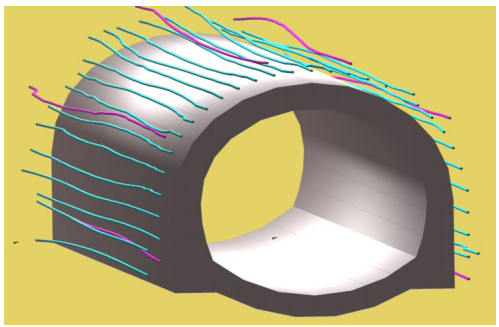


Fig. 9. 3D representation of freezing pipes

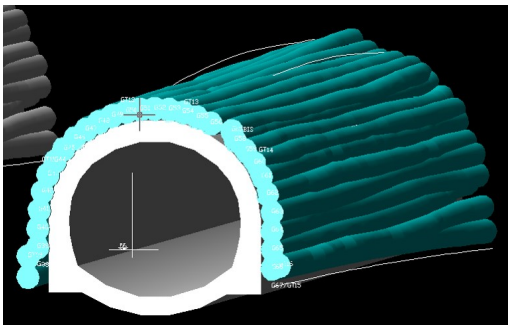


Fig. 10. 3D representation of frozen wall

Water change of state from liquid to solid and vice versa induced by freezing and thawing processes generates volume variations. These volume variations produce deformations to the surrounding

ground, thus affecting possible structures and utilities located in proximity of the area of intervention. Therefore, any AGF intervention should be always integrated by a comprehensive and automatic monitoring system able to detect and measure in real-time such deformations.

AGF TECHNIQUES

An AGF intervention can be carried out by means of two different techniques. With the first one, known as "closed circuit" or "indirect" method, the chilled coolant (a calcium chloride brine) is pumped into the freezing pipes at a temperature of -30/-35 °C. As heat is extracted from the ground, the fluid gets warmer and returns to the refrigeration plant to be re-cooled and re-circulated into the pipes in a continuous process (Figure 11).

With the second one, known as "open circuit" or "direct" method, the cooling fluid (compressed nitrogen in a liquid state) is introduced into the freezing pipes at a temperature of around -196 °C and, after circulation into the pipes, is left to evaporate in the atmosphere (Figure 12).

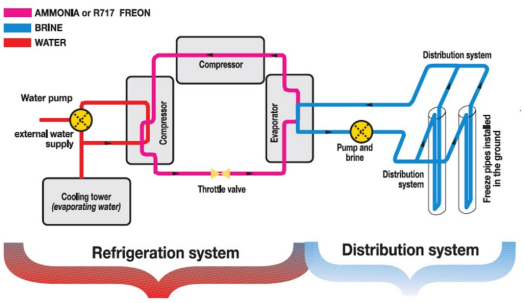


Fig. 11. Scheme of a "closed circuit" AGF plant

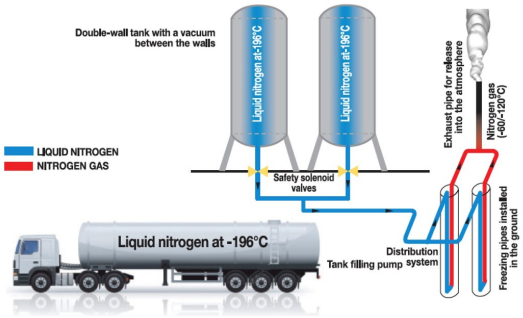


Fig. 12. Scheme of a "open circuit" AGF plant

The choice between the two methods depends on economic and logistic factors, as well as on the time required to freeze the soil. In fact, although the "closed circuit" method is generally more economical compared to the "open circuit" method, the latter can ensure a much quicker formation of the frozen wall and requires a much simpler and faster set-up of the plant.

A combination of the two methods (known as "mixed system") is also possible and sometimes adopted. In this case, while the "open circuit" method is used during the freezing phase (to reduce the time to produce the frozen wall), the "closed circuit" is used during the maintenance period, where less cooling energy is required to maintain the soil at a temperature around -2 °C.

NEW METRO LINE "C" OF ROME

The current underground metro network of Rome consists of only two lines, Line "A" and Line "B", which intersect in correspondence of the main railway station of the city, "Centrale Termini". Line "B" dates back to the Thirties and was built by cut-and-cover method, whereas Line "A", completed in the Seventies, was manly performed by TBM shields.

The new Line "C" will run northwest to southeast across the city centre, for a total length of around 25 km and 30 new stations (Figure 13). The whole project has been divided in seven sections, where only one outer section will be constructed in elevation, while all the others will be totally underground and will consist of two 6.7 m dia. parallel single-track tunnels performed by EPB shields.

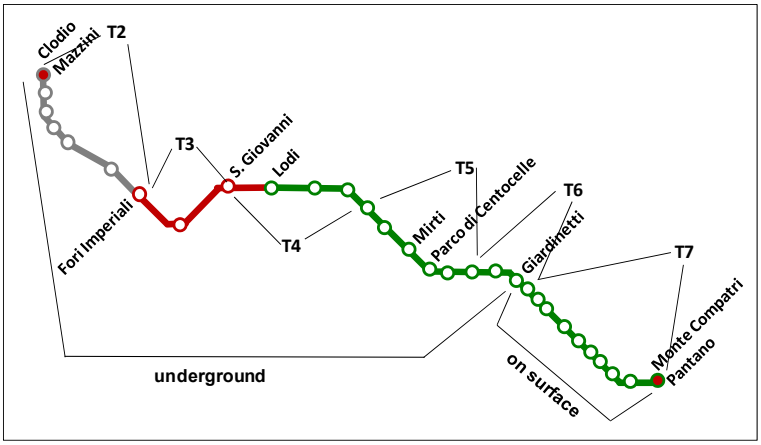


Fig. 13. New metro Line "C" of Rome

The soil profile along the central section of Line "C" is illustrated in Figure 14. From deeper to shallower strata, we encounter a base layer made of stiff over-consolidated silty clay from the Pliocene (Apl) underlying layers of sand and gravel (SG), clayey silts/sandy silts (St and Ar) and sand (Tb). A layer of made ground (R) of variable thickness covers the whole area. The ground water table is almost everywhere nearly hydrostatic with a hydraulic head at about 10 m above sea level. In the area of "San Giovanni" and "Amba Aradam" stations, the hydraulic head in the made ground is higher than in the underlying sands and gravel (SG) and there is a downward steady seepage through the finer grained soils (LSO and Ar) present above the sands and gravels.

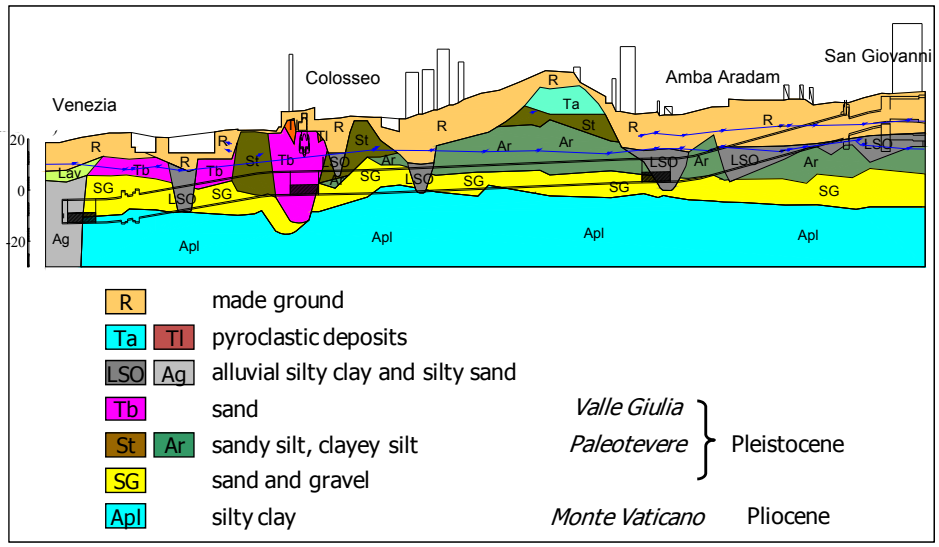


Fig. 14. Soil profile along the central section of new metro Line "C" of Rome

DESIGN ISSUES AT "SAN GIOVANNI" STATION

In correspondence of "San Giovanni" square, the new Line "C" crosses, almost perpendicularly and at a deeper depth the existing "San Giovanni" station of Line "A". In order to allow the interchange between the two lines, a new underground station has been constructed in adjacency of the existing one (Figure 15). This new station reaches a depth of 30 m below the ground and has been excavated under the protection of 55 m deep diaphragm walls.

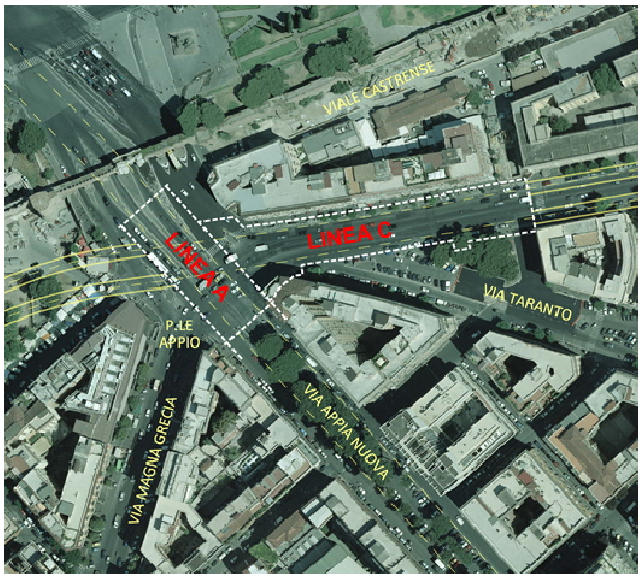


Fig. 15. Intersection of Line "C" and Line "A" in correspondence of "San Giovanni" square

Due to the presence of the bored piles on which the existing station was founded, the possibility to underpass the existing station by EPB shields was excluded and a mined excavation of the two tunnels under the protection of AGF walls was selected by the Designer as the best solution for improving mechanical and hydraulic characteristics of the concerned soils without generating disorders to the regular operations of the overlaying Line "A".

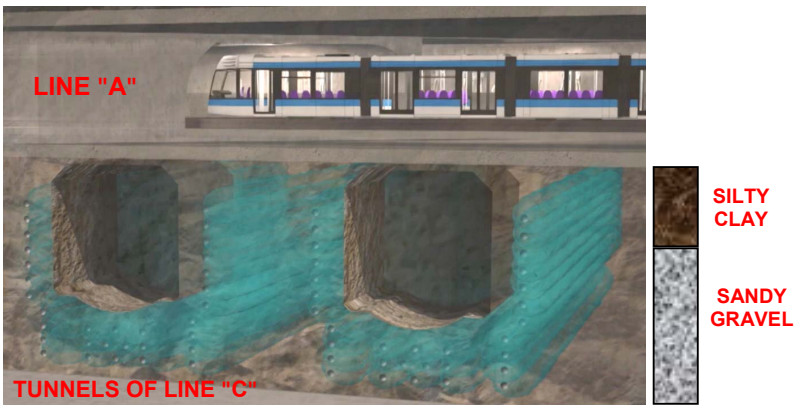


Fig. 16. Schematic of the solution adopted to underpass the existing "San Giovanni" station of Line "A"

This solution presented several technical challenges, mainly due to the limited working areas available (which required specific drilling rigs), the presence of the above-mentioned foundation piles (which were interfering with the regular pattern of the freezing pipes) and the heterogeneity of the soils to be treated (i.e. silty clay overlaying sandy gravel).

Before installing the freezing pipes, cement and chemical grouting was performed to consolidate the excavation front and to homogenize the soil. Freezing pipes and temperature sensor boreholes had an average length of 40 m and were installed working at two different levels from inside the new "San Giovanni" station (Figure 17-18).

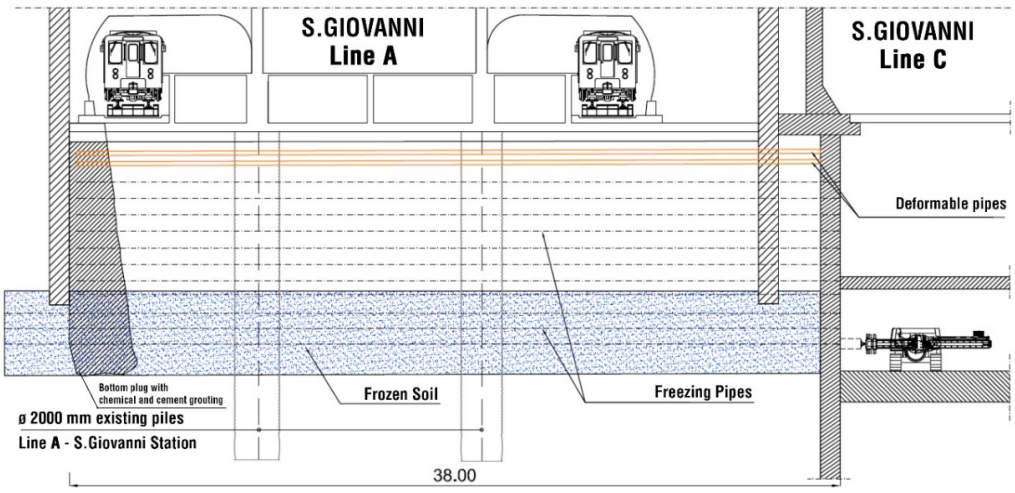


Fig. 17. AGF intervention at "San Giovanni" station – Transversal section (1)

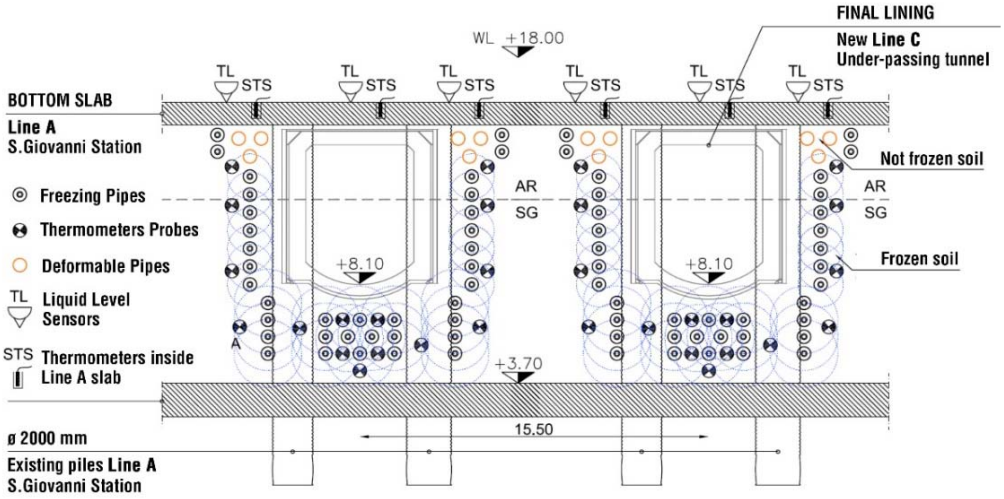


Fig. 18. AGF intervention at "San Giovanni" station – Transversal section (2)

To limit the deformations induced by the freezing process to the bottom slab of the overlaying Line "A", deformable PVC pipes were installed in the area between the slab and the top of the frozen walls.

To reduce the freezing time, the "open circuit" method was implemented at the beginning, while the "closed circuit" method was used for maintaining the frozen wall during tunnel excavation and final lining operations.

Once the ice wall was created, the diaphragm walls of the new and the existing "San Giovanni" stations were cut by diamond wire (Figure 19) and the tunnels were excavated with a temporary support consisting of steel ribs and sprayed concrete (Figure 20).

Before proceeding with the final lining, the entire tunnel profile was coated with a waterproofing membrane (Figure 21). As last operation, the foundation piles interfering with the section of the tunnels were cut by diamond wire and finally removed (Figure 22).



Fig. 19. Diaphragm wall cutting by diamond wire



Fig. 20. Temporary support by steel ribs and sprayed concrete



Fig. 21. Waterproofing and final lining



Fig. 22. Removal of the interfering piles

Due to the complexity and sensitivity of the intervention, different monitoring systems were used at site to guarantee a comprehensive and fast alert on the response of the ground and the overlaying slab of Line "A" during freezing and maintenance periods. In particular, the main structures of the existing station (i.e. diaphragm walls, pillars, slabs and rail tracks) and the diaphragm walls of the new station were monitored by (*i*) three alignments of liquid level settlement cells and electric level sensors, (*ii*) a set of thermometers implanted into bottom slab, (*iii*) a network of surveying prisms. Figure 23 shows the location in plan of the instrumentation implemented at the level of the bottom slab of Line "A".

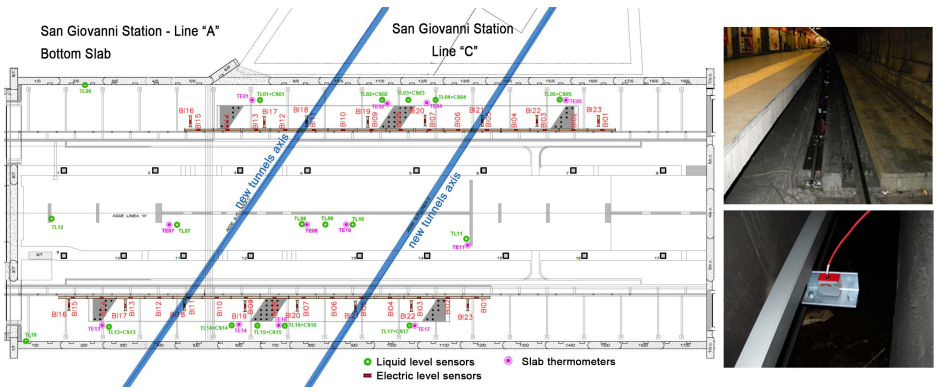


Fig. 23. Location in plan of the monitoring system implemented at the level of the bottom slab

In addition to the above-mentioned instrumentation, a set of temperature sensors was installed in specific boreholes to monitor the temperature of the ground around the freezing pipes. In selecting the position of these sensors, particular care was paid to the areas between the existing foundation piles, where the spacing of the freezing pipes was more than 3.5 m. Figure 24 shows the heaves recorded along two alignments of liquid level settlement cells located on the bottom slab of the existing station at different stages of the freezing process. For a better understanding, it has to be underlined that some initial values are not nil because some heaves ad been already generated by preliminary grouting operations.

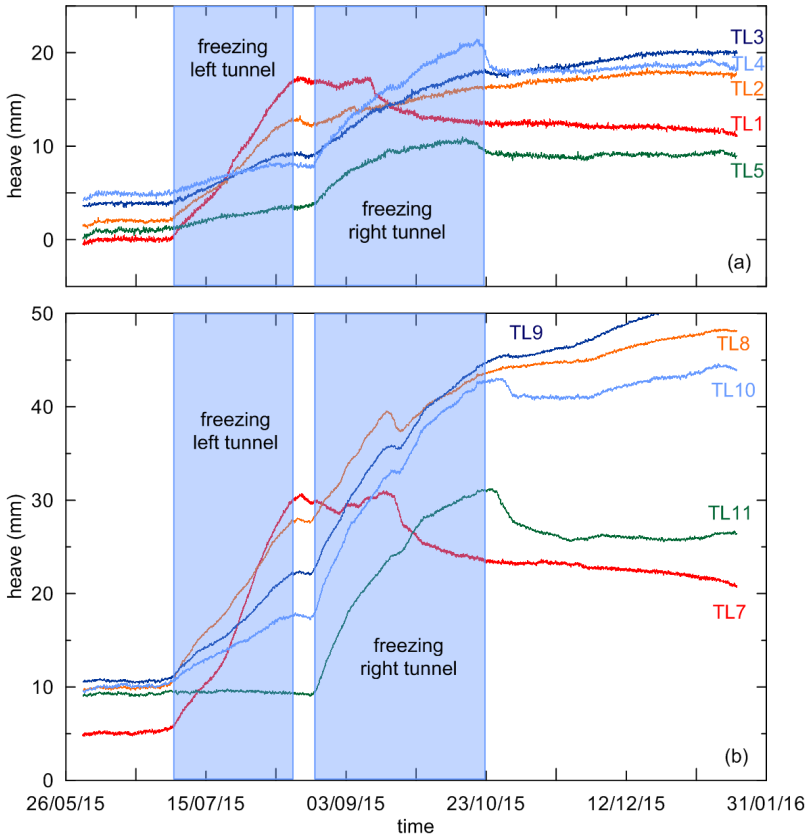


Fig. 24. Heaves recorded along two alignments of liquid level settlement cells located on the bottom slab

The direct correlation between recorded deformations and freezing activities is even more clear from Figure 25, where the heaves on the slab of the existing station are represented: (*i*) at the end of preliminary grouting activities, (*ii*) at the end of the freezing phase on the left tunnel (*iii*) at the end of the freezing phase on the right tunnel and excavation of the left tunnel.

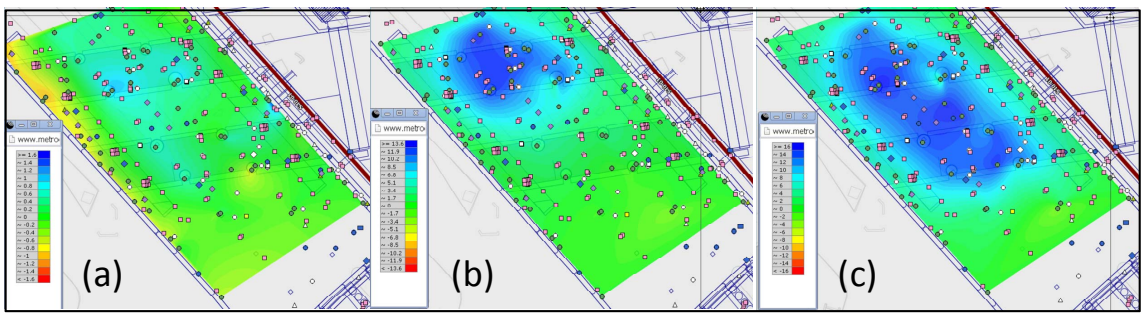


Fig. 25. Heaves recorded along two alignments of liquid level settlement cells located on the slab

CONCLUSIONS

Nowadays, AGF technique is applied to a wide range of foundation engineering problems where soil stability and groundwater flows are an issue. Tunneling in difficult soils is one typical situation where AGF can show its full potentiality. The experiences gained during the implementation of the AGF intervention at “San Giovanni” metro station in Rome, demonstrate that also in very difficult logistic and geotechnical conditions this technique can be safe and effective.

REFERENCES

Bertero A., Cribari F., Tanzi A., Fancello S., Gondolini T., Giannelli, F, Lodico M., D’Angelo M., Romani E. (2016). Metro Rome line “C” - Artificial Ground Freezing application for the underpass of the existing metro station San Giovanni - line “A”. ITA-AITES WTC 2016, April 22-28, S. Francisco, USA.

Viggiani G.M.B., Casini F., Bertero A., Cribari F., Romani E., (2016). Artificial Ground Freezing: case studies, technological development, and fundamental research. XXIV Edition Turin Geotechnical Conference, February 25-26, Turin, Italy.

Haß H., Schäfers P. (2013). Application of ground freezing for underground construction in soft ground. In Geotechnical Aspects of Underground Construction in Soft Ground. Proceedings 5th Int. Symp. TC28. Amsterdam, the Netherlands, 15-17 June 2005, CRC Press, 405-413

Pimentel E., Papakonstantinou S., Anagnostou G. (2012). Numerical interpretation of temperature distributions from three ground freezing applications in urban tunneling. Tunnelling and Underground Space Technology, 28: 57–69.

Shuster, J.A. (1982). Engineering quality assurance for construction ground freezing. In Ground Freezing 1980: Developments in Geotechnical Engineering, ed. P.E. Frivik, N. Janbu, R. Saetersdal, and L.I. Finborud. Amsterdam, Elsevier, vol. 28, pp. 333–47.

RESONANCE PILE DRIVING WITH ZERO GROUND VIBRATION

AUTHORS: Mathew Janes, M.E.Sc., P.Eng., Resonance Technology International Inc. Mark Johnson, Austral Piling

Abstract: The Resonator RD 260 Resonant Pile Driver delivers ground disturbance free, high production pile driving. The Resonator has recently been used on numerous production pile driving sites in the Netherlands and Melbourne, Australia to drive piles in sensitive areas where conventional pile drivers could not be used. Two case histories are provide in this paper which demonstrate the features and benefits of Resonant pile installation.. In the Netherlands the Resonator RD 260 was used at the Vopak Oil Storage facility in the Port of Rotterdam to install pipe and sheet pile within an active pumping gallery. The site demanded vibration free pile installation to construct a cofferdam within sensitive, highly valued assets. Access was an issue and schedule demands were stringent as shutdown windows were narrow. The RD 260 provided ground disturbance free piling immediately adjacent to fragile structures. At Vopak the only site access was using a large crane positioned over 40 m from the location of pile driving. Driving was conducted amongst 900 mm dia pipes carrying heated crude oil.

In Melbourne the RD 260 was used to drive GU 18 sheet piling adjacent to light rail easements. The project was the first of many grade separations being constructed within Melbourne urban areas to lower the light rail and provide quieter rapid transit. The original trial used an RGT MR105 series vibrator but noise and vibration criteria were exceeded. The RD 260 was brought in for a trial and performed with high production and produced negligible ground vibration. Up to 17 sheet piles 14 m in length were driven in a 2.5 hour window during the trial.

Introduction

The Resonant Pile Driving method is gaining acceptance around the world as a new method to rapidly drive piles free of ground borne vibrations. The high frequency vibrator resonates the pile, essentially turning the pile into a spring, to excite the toe of the pile with high accelerations and low amplitude. High acceleration with low amplitude generates high penetration rates but the high frequency stress waves are quickly dissipated in the soil. Typically ground borne vibrations are measured at below 1 mm/sec within 1 to 5 m of the pile. The Resonant method can drive a pile next to a glass of wine, without spilling, as has been demonstrated on numerous piling sites.

How Does Resonance Work?

The Resonant method uses a hydraulic piston - cylinder geometry to generate high magnitude, high frequency oscillating force. This is a very different mechanism than the eccentric mass technology used in conventional and variable moment vibrators.

A unique valve geometry achieves the high frequency flow switching necessary to oscillate the hydraulic piston at up to 180 Hz (10800 VPM). The valve is controlled electronically for maximum accuracy of the desired frequency. The volume of hydraulic oil delivered through the valve to the piston (flow rate) determines the amplitude while the hydraulic pressure determines the peak force.

The main advantage of the Resonant piston-cylinder method is that it allows the vibration frequency to be tuned to the natural frequency of the pile, which excites the pile like a spring. Exciting the pile

like an axial spring allows the storage (build up) and release of vast amounts of energy. In this way the pile is brought to a high acceleration state that penetrates through the soil. The challenge is to continuously tune the vibration frequency to the natural frequency of the pile as it is being driven into the ground. A computer algorithm has been developed for the Resonant Driver which automatically performs this tuning function. Through tuning to the Resonant frequency of the pile the maximum driving efficiency and maximum force at the pile tip is achieved.

Vopak Oil Storage Facility Rotterdam

At the Vopak oil storage and transfer facility in Rotterdam, NL a pipe and valve gallery required upgrading and expansion. A cofferdam was required to permit excavation and the installation of pipe piles and caps to support new structures. Typically pile driving, using either impact or vibratory methods, is not permitted at Vopak, due to the sensitive nature of the pipe valves and galleries. Poor access and difficult terrain generated by steep oil spill containment berms prevented the use of conventional or even small equipment from accessing and working at the site. The proven performance of the Resonator in similar soils convinced the owner to entertain use of the Resonator RD 260 Driver. The RD 260 was suspended from a 200 tonne crane positioned on an access road over 35 m from the location of the sheet pile wall and pipe piles. AZ 18 x 700 sheet piles 12 and 16 m in length and 323 mm od x 12.7 mm wall open ended pipe piles 24 and 28 m in length were to be driven.



Figure 1. Vopak Facility Site plan

The site is adjacent to the Maas River (Rhine) in the Port of Rotterdam. The soils consist of alluvial deposits typical of mature deltaic structures. A typical CPT plot is provided in Figure 3 which shows sands and sandy silts with interbeds of clayey silts and silts. The soils are generally weak with Qc values generally between 10 to 20 MPa with peaks of 25 to 30 MPa. Friction values range between 100 kPa to 250 kPa with Rf % of 1 to 2 % and highs of 3 to 4%.

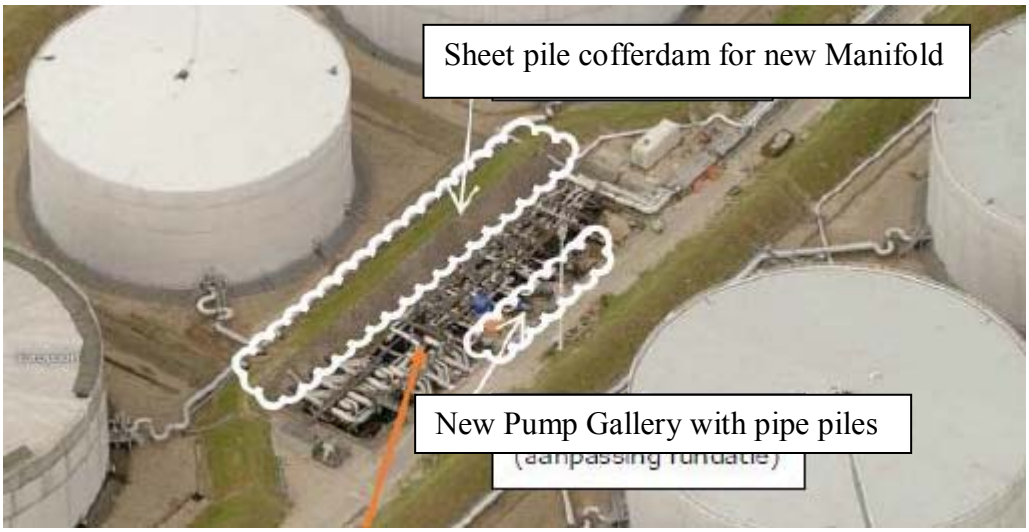


Figure 2 Site plan showing Pipe Gallery and Cofferdam location

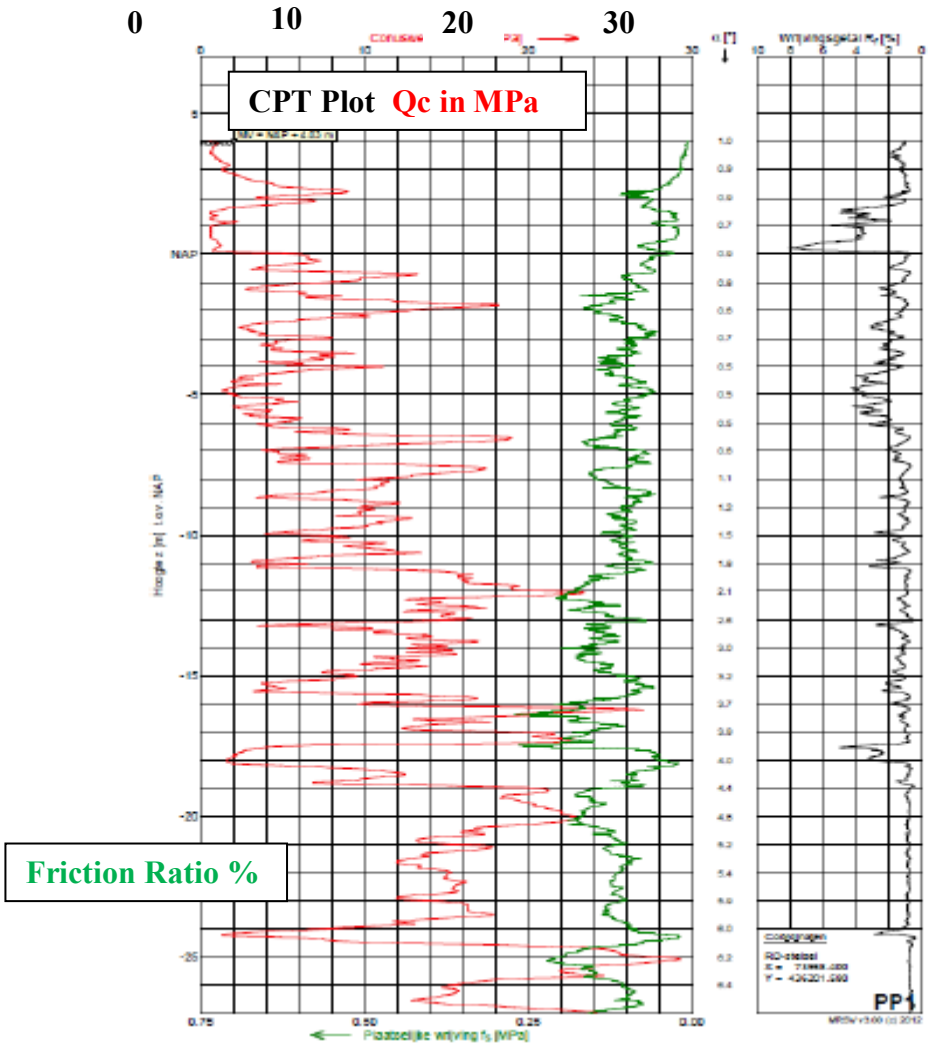


Figure 3. Typical CPT at the Vopak site, Port of Rotterdam.

Sheet piling operations began in January of 2016 with de Koning BV foundation contractors, NL. Sheet piles varying in length between 12 and 16 m were driven immediately adjacent to live pipes and valves that continued to carry heated crude and refined oils. Ground and pipe / valve monitoring was conducted throughout driving and established ground vibrations of less than 1.5 mm/sec and structure vibrations of less than 1 mm/sec. The owner specified vibrations were not to exceed 5 mm/sec.

The AZ 18 x 700 sheet piles drove easily in the 12 m lengths. Threading, plumbing, driving and completion of sheets were straightforward with driving times of less than 5 minutes common. However, the same sheet in 16 m lengths, and often immediately adjacent to easily driven 12 m sheet piles, proved to drive easily or with great difficulty. Some sheets required up to 45 minutes to drive due to, what appeared to be, clutch friction or difficulty in controlling the spreading of the sheet pile tips (when driven in pairs). Single sheets often proved to be no easier to drive. The clamping system used a single clamp situated over the clutch of the sheet pile pair and thus drove the sheet some distance from central axis and centre of mass of the sheet pile pair. When driving single sheets the clamp was placed on the centre of the sheet web and thus would be at or close to the centre of stiffness and centre of mass of the sheet.

It was determined that the cause of the difficulty in advancing the sheet is related to the off axis resonance modes of the sheet piles, both in bending and in torsion. When excited in the bending mode the sheet had a tendency to flex and form traveling or standing waves, or suffer from high amplitude 'flange flapping' where the flanges of the sheet would move laterally at high frequency and amplitude. These motions robbed energy from the driving process, increased clutch friction and increased soil damping during the driving process.

The 323 mm dia pipe piles were driven open end to working capacities of 700 to 900 kN. The pipes were driven to depths of 24 m and 28 m. The Resonator required 20 to 28 minutes to drive the pipe. Ground vibration monitoring proved peak particle velocities of about 1 mm/sec at 3 to 5 m.

This proved to be the first time the Vopak site permitted any form of pile driving within the active facility. The project proved to be a success for both the owner and the contractor as great savings were realized through the use of large, remotely based equipment that could reach into the pipe gallery and suspend the driver. Similar upgrades have been conducted at the Vopak facility since the first project was completed.

Overall the driving experiences at Vopak and similar sites indicate that a combination of axial and off axial resonant modes may coincide or be close enough in frequency to cause multiple vibration modes during driving of certain sheet sections and lengths. Typically a lighter sheet section will be more susceptible to off axis motion at lower off axis resonant modes, with more harmonic multiples, within the range of driving frequency. Should off axis resonance occur it can hamper the driving process with increased resistance (due to clutch friction and off axis vibration amplitude) and a loss of driving energy as the undesired, off axis modes and flange flapping modes absorb energy. The diagrams below in Figure 4 render a typical sheet pile in axial and off axial resonance.

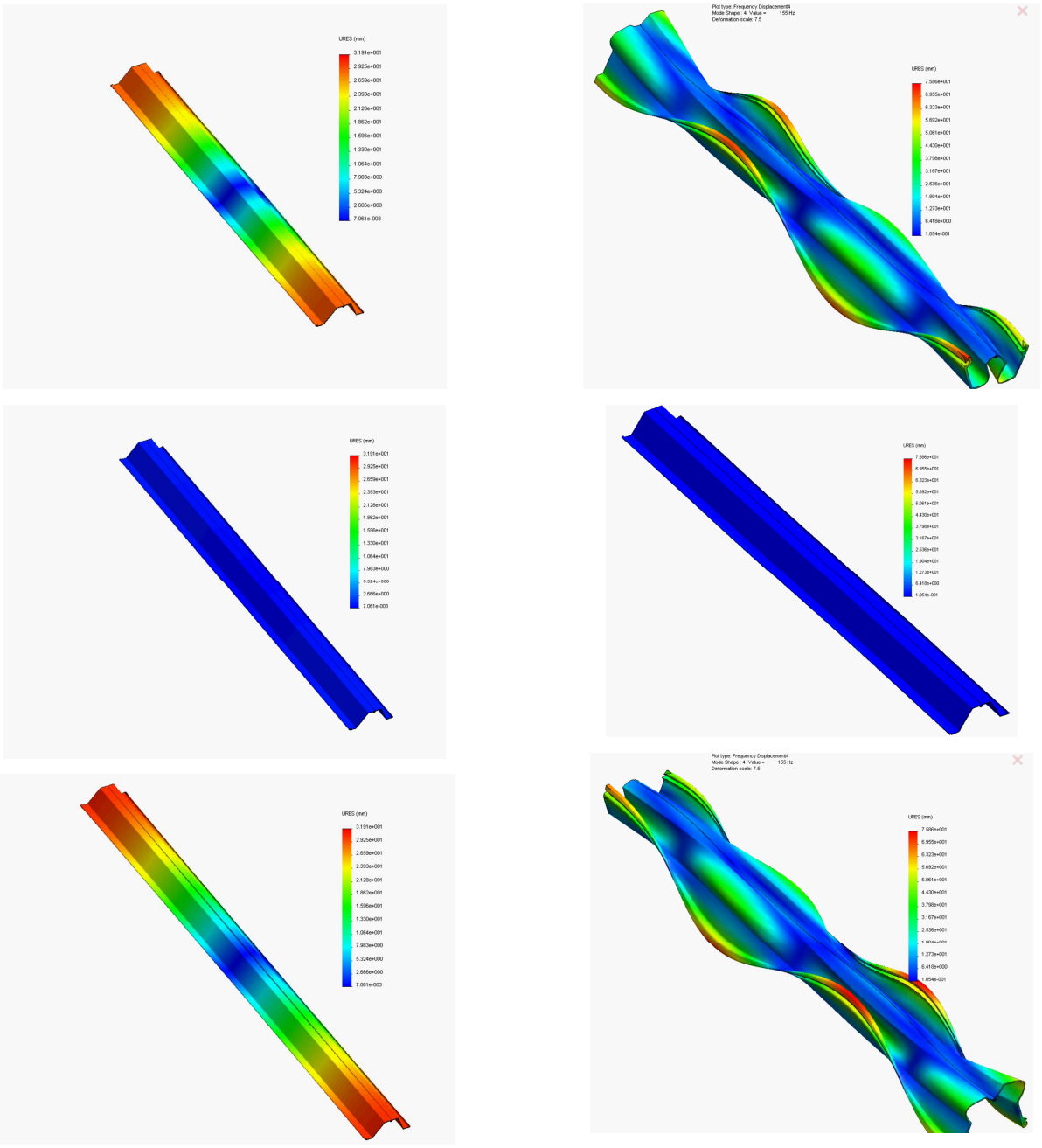


Figure 4. Axial Resonance and Off axial Resonance

Melbourne Cross Links Grade Separation Bentleigh & McKinnon Rds

Melbourne is undergoing a major grade separation as part of a cross town light rail upgrade. The existing, at surface light rail commuter service is to be lowered below existing grade within excavated trenches to decrease noise and improve traffic congestion through removal of over one hundred level crossings. A test program was conducted using a standard Bauer RGT rig with an MR105V high frequency vibratory driver. The ground at Bentleigh consists of very hard dry clays and clayey sands and thus pre-boring was required to achieve penetration. Various pre boring geometries and depths were used for the test program and the sheets were successfully driven to depth (14 to 16 m), however, noise and vibration restrictions were exceeded using the RGT system. Following the test program a change was proposed to more expensive and time consuming drilled methods of shoring construction. An additional test program was proposed using the RD 260 Resonator technology. Similar pre-boring was conducted and the sheets were driven to grade at similar or higher production using the RD 260 than with the MR 105V. The RD 260 produced a fraction (1/30th) of the ground vibration. Noise was lower with the RD 260 as well and met the required specification.

The Bentleigh site soils are represented by the borehole below in Figure 5. Soils consist of very dense sands and very dense clayey sands with SPT blow counts exceeding 60 bl/300 mm and typically in the 100 to 125 range. The formations were very dry with ground water emerging only during the wet season at depths of 8 to 10 m.

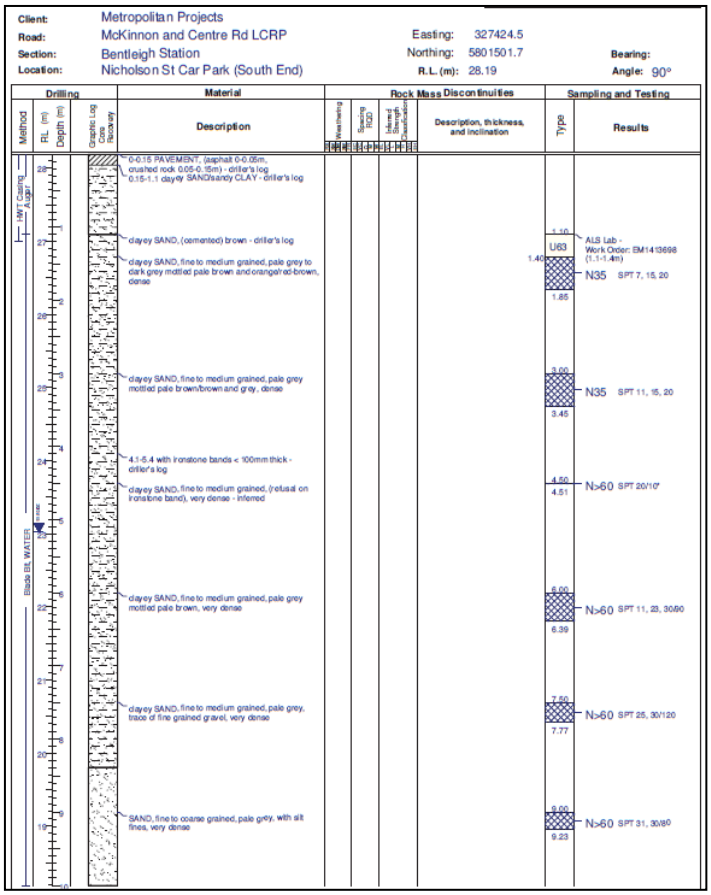


Figure 5. Bentliegh & McKinnon Road typical Borehole

The grade separations consisted of bringing the trains 6 to 8 m below ground at stations and major crossings. Long stretches of track where the trains run at high speeds were left at grade. Thus, the trenches consisted of gradual slopes into and out of the rail stations and crossing depressions. Sheet pile walls were constructed to permit excavation and placement of lowered concrete base slabs and walls supported by cast in place struts. The working easements were restricted and ran adjacent to



Figure 6. ABI base machine and Resonator RD 260 on narrow corridor site.

heavily travelled train and road corridors. Residential communities surrounded the construction with houses typically as little as 12 – 15 m from the piling work. Noise and vibration mitigation were mandatory. A program of pre-drilling followed by sheet pile driving was conductd on several sites simultaneously. Noise and vibration monitoring was conducted throughout the work.

The contractor purcashed a total of 3 RD 260 units which were mounted on Eurostyle base machines manufactured by Liebherr, ABI and Bauer. A total of over 8 months of piling was required to complete the work. GU 18 and PU32 sheet piles were driven in

lengths varying from 6 m to 18.5 m. Driving times varied as soil conditions changed across the site with some regions experiencing very hard soils (>150 bl/300mm) which required additional pre-boring. Productions as high as 28 to 34 sheet piles per day were recorded.



Figure 7. Resonator RD 260 driving GU 18 Piles

Noise

Noise monitoring was conducted for both the RGT and the Resonant sheet pile driving at the Bentleigh site in similar soils and under similar driving conditions (sheet type, length and driving time). Figure 8 indicates the measured results for noise and a regression analysis predicting noise closer to and further away from the source for each of the RGT and the Resonator. The data shows the Resonator (red

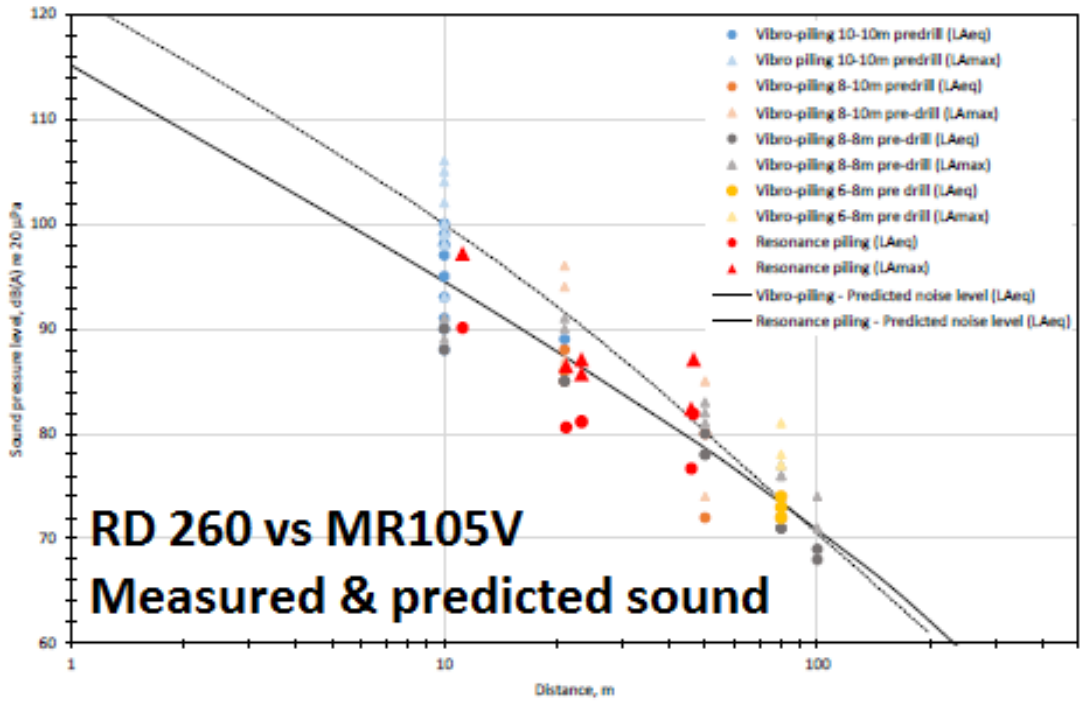


Figure 8 Measured and predicted noise levels for RD 260 and MR105V

dots) is on the order of 6 to 10 dBA lower than the RGT MR 105V hammer. The measured sound pressure indicates the Resonator achieved noise levels of 90 dBA at 12 m and 80 dBA at a distance of 20 m. This is in keeping with measurements made in Canada and Europe under similar conditions. Pipe and HP piles are significantly quieter than sheet piles as the sheet piles are very flexible and become 'loud speakers' under off axis resonant modes. Concrete piles are typically very quiet and will easily pass residential noise requirements.

Vibration

Vibration monitoring was conducted throughout the Bentleigh and McKinnon Road grade separation projects. Measured ground vibration for the RD 260 during the pile test program and throughout production driving was a maximum of 1 mm / sec at 10m. Spectral density analysis indicated the majority of the ground borne energy is at the driving frequency, which, with the Resonator is typicallhy higher than 100 Hz. Thus the motion is at a high frequency and as a result the actual ground displacement amplitudes and energy are very low. Ground motion within a range of 1 to 5 m of the pile remains at just 1 to 1.5 mm / sec. During the RGT test program measurements indicated ground vibrations as high as 30 mm/sec at 10 m from the pile. Comparative test data is shown in Figure 9 below. Thus the RD 260 Resonator produces on the order of 1/30 the vibration of a conventional vibrator and is essentially un-noticed by a human.

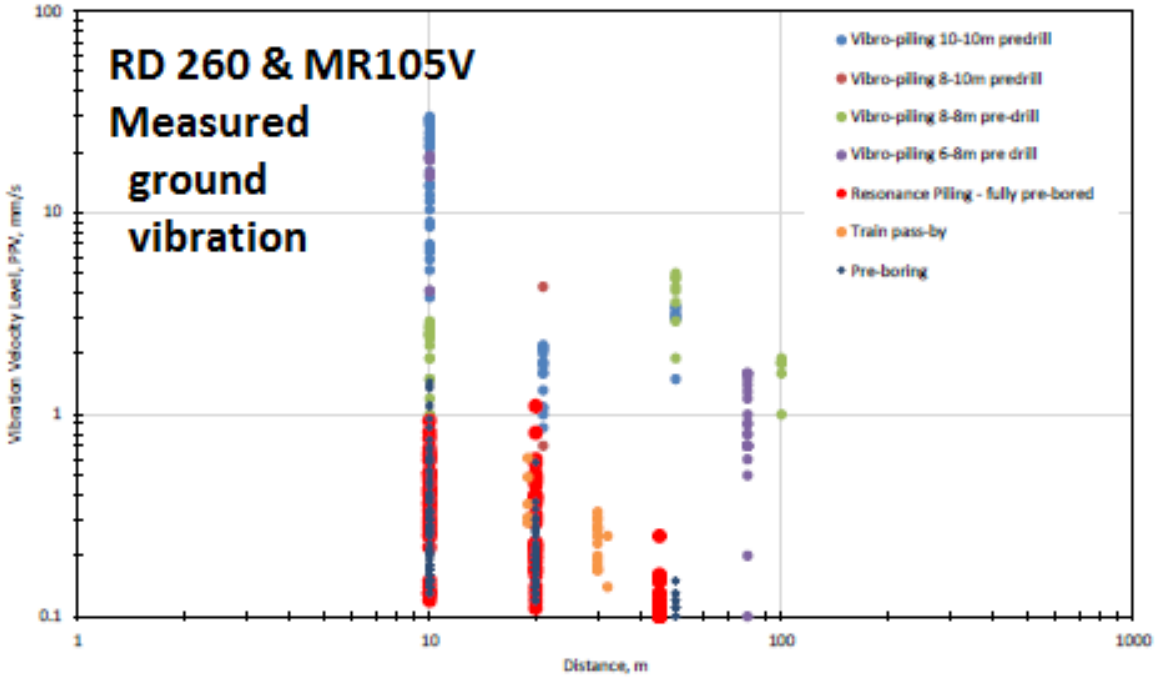


Figure 9. Measured ground vibration for RD 260 and MR105V

Conclusion

Resonant Pile driving has proven to provide rapid pile installation with negligible ground borne vibrations and negligible settlement of nearby soils or structures. High frequency vibrations cause liquefaction of the soil adjacent to the pile and high pile accelerations which push through the soil cleanly, leaving the soil undisturbed. Vibration and optical survey monitoring during Resonant driving of piles indicates little to no disturbance occurs. Noise levels are typically less than that of conventional pile driving but may be affected by off axis vibration modes and are noisier for lighter sheet piles. Pile drivability is high for heavier Z sheet or U section sheet piles where higher stiffness and pile clamp positioning closer to the centre of stiffness and centre of mass reduce off axis vibration modes. Sheet, pipe and HP piles have been successfully driven to high capacities in a variety of soils.

LEVEL CROSSING REMOVAL PROJECT – PACKAGE 1

David Chong, Douglas Partners, Melbourne, Victoria, Australia, 0421 499 456,
david.chong@douglaspartners.com.au
Chris Crowe, Douglas Partners, Melbourne, Victoria, Australia, 0421 588 786,
chris.crowe@douglaspartners.com.au
Andrew Middleton, Douglas Partners, Brisbane, Queensland, Australia, 0421 583 241,
Andrew.Middleton@douglaspartners.com.au
Mick Stadter, Douglas Partners, Brisbane, Queensland, Australia, 0409 242 497
Mick.Stadter@douglaspartners.com.au

ABSTRACT The Level Crossing Removal Project – Package 1 is part of the Victorian Governments commitment to remove 50 of the most dangerous and congested level crossings across Melbourne. This involved removing three crossings on the Frankston Line in the south east suburbs of Melbourne. The works involved replacing approximately 2.5km of at grade track with three rail cuttings up to 8 m deep at each of the bridges that replace the level crossings. The cuttings are retained by piled retaining walls and during the main construction occupation approximately 250,000 cubic metres of soil was removed. The project has presented significant geotechnical challenges due to the location in residential suburbs and tight rail corridor and rail occupation timeframe. These challenges included temporary and permanent wall stability, foundations, earthworks and dewatering. As a result, careful design and innovative construction techniques have been necessary to limit impacts on the community and meet the project timeline.

INTRODUCTION

The Level Crossing Removal Project – Package 1 is part of the Victorian Governments commitment to remove 50 of the most dangerous and congested level crossings across Melbourne. This involved removing three crossings on the Frankston Line where it crosses North Road in Ormond, McKinnon Road in McKinnon and Centre Road in Bentleigh.

The project involved replacing approximately 2.5km of at grade track with three rail cuttings up to 8 m deep at each of the bridges that replace the level crossings. The cuttings will accommodate three lines of rail tracks with the cuttings up to 25 m wide. The cuttings are retained by piled retaining walls and during the main construction occupation approximately 250,000 cubic metres of soil has been removed.

The project presented significant challenges due to the location in residential suburbs and tight rail corridor and rail occupation timeframe. As a result, careful design and innovative construction techniques have been necessary to limit impacts on the community. The geotechnical challenges generally fell into one of three areas, earthworks, structures and groundwater.

The primary earthworks challenge for the project was moving the 250,000 cubic metres of soil in a 10 day window, however, from a geotechnical viewpoint, obtaining a stable subgrade on which to operate the necessary construction plant in a short time frame with constrained site access and time to import materials was the key. Whilst closely watching the performance of the dewatering system, a range of contingency plans were developed to cope with any difficulties.

The structures comprised three bridges, stations, base slab and around 4 km of piled retaining wall. The piles included driven steel sheet piles and Continuous Flight Auger (CFA) piles. At the base of each cutting was a centrally located sump structure up to 4 m with temporary sheet pile retention. Geotechnical challenges included addressing issues with temporary and permanent stability of the walls, particularly as the lead time for the sheets required locking in the design at a very early stage. Pile driving involved the use of some innovative techniques to minimize vibrations. A structural base slab with screw pile system were adopted for two of the three cuttings that extend below the groundwater table to resist the long term hydrostatic uplift pressure and cyclic loading from trains.

Construction dewatering was also a major issue with two of the three cuttings extending below the water in a silty sand aquifer and the possibility of significantly impacting on the wall stability and construction earthworks. Silty sands are difficult to dewater at the best of times, but with the space and time constraints, an innovative horizontal directional drilling system was adopted for well installation.

PROJECT SETTING

The project was located in the south east of Melbourne and the approximate project extent is shown in Figure 1. The project area is predominantly a residential area, with shopping strips located along each of the three roads where the level crossings were removed.



Figure 1 – Project Location

The geological maps of the area indicate the underlying geology to be Tertiary age sands and clays of the Brighton Group, with occasional overlying Quaternary age sand dune and swamp deposits. Deeper investigation indicated that the Brighton Group soils were about 15-20m thick and were underlain by silts and clays of the Newport Formation which were in turn underlain by the Silurian age siltstone which forms the regional basement at depths of around 30-40m below ground level.

RETAINING WALLS

The walls comprised a combination of soldier pile walls and driven steel sheet pile walls. The soldier piles were typically used for walls located above the groundwater table and in areas that need to support vertical loads (i.e. concourse/stations, bridges). However, for majority of the walls, driven sheet piles were used due to access constraints, with the boundaries and, in some cases, buildings of the adjacent residential properties as little as 1-2 m from the back of the wall..

For sections of wall where there were limited access due to close proximity to site boundaries (in some instances about 1 m), the sheet piles were installed by a specially imported piling machine, the ‘Giken Silent Piler’ (Figure 2). The machine, about the size of a small car, is lifted and mounted onto a section of existing sheet pile wall with the machine protruding less than 1 m on either side of the

wall. The only other machinery required for the sheet pile installation is a telescopic crane or similar to lift the new sheet into 'Giken' head unit. The 'Giken' unit uses the existing sheet piles as reaction to push the new sheet pile into the ground. Where harder ground is encountered, the machine has a drill bit which can penetrate the ground ahead of the sheet piles. As such the installation process produced much less vibration or noise than conventional sheet piling. This environmental advantage enabled the 'Giken' to work through day and night without causing nuisance to the neighbours.



Figure 2 : Giken Silent Piler Used For Sheet Pile Installation

For soldier pile walls, continuous flight auger (CFA) piles were considered more suitable than conventional open hole piles due the saturated sandy material across the site. The CFA pile diameters that ranged from 600 mm to 1200 mm with centre to centre pile spacings of between 1.2 times to 3 times the pile diameter. The soldier piles were installed by standard track mounted CFA piling rigs.

For the North Road rail cutting that is above groundwater table, soldier pile walls were adopted for retention. The walls were predominantly cantilevered with the exception to a short section supported by permanent precast concrete props and another section of wall supported by the concourse decking.

For the McKinnon and Bentleigh rail cuttings up to 5 m below the groundwater table, driven steel sheet pile walls were adopted for majority of the retaining. For the sections of walls at the bridges and concourses that required to support vertical loading, CFA soldier pile walls were adopted. In these instances the centre to centre pile spacings were typically between 1.2 times to 1.5 times the pile diameter to limit the width of exposed saturated faces between the piles.

For the McKinnon and Bentleigh cuttings the structural base slab would act as a permanent prop for the walls. However as the construction of the base slab required the full depth of excavation to be undertaken, temporary restraints in the form of post-tensioned ground anchors or steel props were needed for some of the walls, predominantly sheet pile walls, to ensure stability during the construction phase. Permanent post-tensioned ground anchors were also adopted for some sections of the sheet pile walls to limit long term wall deflection. The temporary props comprised high load capacity hydraulic steel strut together with bracing along the walls (Figure 3). More than twenty-five struts were used for temporary retention with some of the struts fitted with load cells providing real time strut loads.

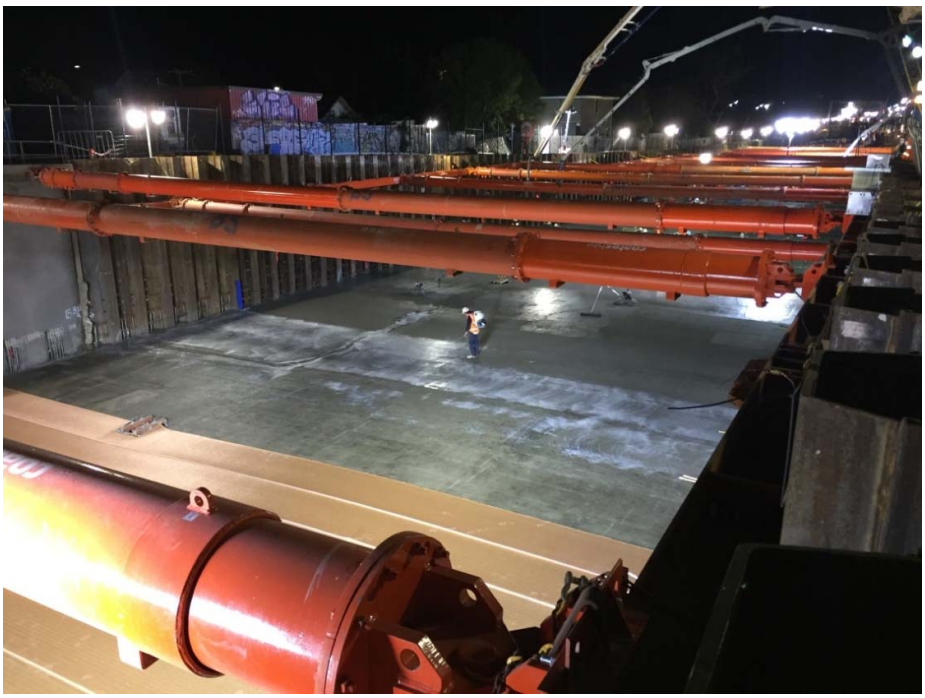


Figure 3 : High Load Capacity Hydraulic Steel Struts

A series of inclinometers were installed behind the walls to monitor ground movements during and after the construction process. A displacement vs depth plot of one of the inclinometers is shown in Figure 4.

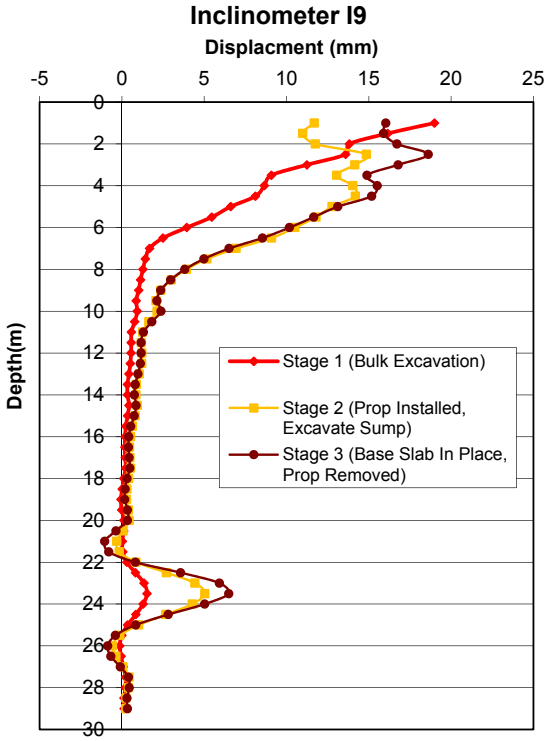


Figure 4 : Inclinometer Plot

The inclinometer is located behind the retaining wall in the McKinnon Road rail cutting where the sump structure is located. For clarity the plot has been simplified to three stages representing: Stage 1 – during bulk excavation, Stage 2 – bulk excavation completed, temporary prop installed, sump excavation commenced, and Stage 3 – base slab installed, temporary prop removed.

The deflected shapes of the three stages were in general agreement with the construction activities. Stage 1 shows maximum deflection at the top which corresponds to a cantilever wall behavior during bulk excavation prior to propping. In Stage 2, the deflection at the top reduced as a result of prop installation, but with increased movement at the bulk excavation level of 8 m due to sump excavation. In Stage 3, the deflection at the top increased again as the prop has been removed and no further deflection observed at bulk excavation level due to the installed base slab.

DEWATERING & SUBGRADE

From the very early stages of the project, it was apparent that if the rail line was to be taken under the roads, it would be necessary to excavate below the water table. This presented a number of challenges for various aspects for the design and construction of the project. Would the cuttings be drained or tanked for the permanent case? Would dewatering be needed outside the walls as well as inside? Would there be impacts on surrounding properties due to the dewatering? Perhaps, most critically, what dewatering systems could be installed and how effective would they be? On top of this, given the volumes of soil that would need to be removed, how would the dewatered soil stand up as a subgrade for hauling out?

For the two sections of cuttings, Bentleigh and McKinnon, that needed dewatering, the presence of the east-west running roads crossing the north-south running railway line, any dewatering system would effectively be split into six separate zones, which would likely need separate power supplies and discharge points. This would be further complicated by the limited corridor width, with as little as 1-2 m between the back of the cutting retaining walls and the property boundaries. Initially, conventional dewatering techniques, either deep wells or a spear/well point system, were assessed for their suitability for the project.

During the earlier stages of the project, deep wells with submersible pumps were raised as a potential solution for dewatering the rail corridor. The advantage of a deep well pumping system would have been that wells could have been located outside the cutting, with greater well spacing, and possibly located on only one side of the cutting. This solution would therefore require less surface works than other traditional dewatering systems. Initial designs were prepared and a number of trial wells were conducted. The trial wells immediately identified a problem with the proposed approach. Test pumping from the deep wells showed that the transmissivity of the aquifer was not sufficient for the proposed system. Whilst permeability testing, in the form of slug tests had been carried out in the investigation carried out in advance of design and construction, the specific storage values necessary to determine transmissivity were not investigated. Furthermore, the most permeable sands occurred in the middle of the soil profile, whereas the well screens needed to be located at or below the base of the aquifer. As a result, it was determined that the spacing of deeper wells was reduced to a point where the quantity of wells and pumps required became excessive and impractical. A positive finding from the test pumping was that the volume of water that would need to be disposed by a dewatering system would likely be significantly less than previously estimated.

Following the pumping trial, the well point option was revisited, but remained impractical. With the excavation level needing to be around 8 m below ground level and water levels in the well points needing to be another metre or two below subgrade level to ensure that the centre of the cutting could be drained, the required well point suction exceeded not just the practical limit, but was also close to the theoretical limit. At the theoretical limit, the pressure in the wells is low enough to cause the water to boil at ambient temperatures. To overcome this would have required a two stage pumping system or buried headworks, but the tight earthworks program meant that these were not viable or

practical options. As a result of this assessment, the decision was made to adopt an innovative option, horizontal directionally drilled (HDD) wells.

HDD wells have not been widely used in construction dewatering for a number of reasons, including drilling costs, difficulties in creating an effective filterpack and development of the well to remove drilling fluids. The filter issues arise due to the inability to place a sand or gravel filter pack around the pipe and the need to use large slots/ drilled holes in the pipe to avoid the effects of healing during pulling of the pipe. HDD did, however, offer the major benefit of minimal surface works. This significantly reduced the interaction with the many and varied works taking place during the rail occupation and allowed the creation of a continuous well along the entire excavation.

The selected system comprised four bores, each approximately 650m long, which were drilled from a point mid-way between Bentleigh and McKinnon, two headed north, one on the uptick side and the other on the down track side of the cutting and a further two headed south, again one on each side of the cutting. A twin pipe system was installed in each bore. A coarsely drilled outer pipe of 250 mm diameter was selected to address the pulling forces and soil pressures, whilst inside this, a more finely drilled 160mm diameter pipe wrapped in a woven geotextile filter fabric was installed. While the drilling was in process, a number of operational issues still needed addressing. Perhaps the most salient issue was the identification of the most practical way to pump water from the HDD wells, considering pump redundancy in the event of the migration of fine sediment. This had been a relatively simple issue on one of DP's previous uses of this technique at Watawala in Sri Lanka (Chandler & Broise, 2000). There, the HDD wells were installed to dewater a slope and could be drained by gravity. For this LCRP project, active pumping would be required and after some unsuccessful trials at sump construction, submersible pumps were sourced which were lowered down either end of the HDD bores.

In addition to the active dewatering, contingency plans were also developed to address failures of the dewatering system. With the fixed occupation duration, there was no scope to give advanced dewatering extra time if it hadn't worked as efficiently as planned. Removing any remaining free water from the excavation would be addressed by slotted pipes (agi drains) and the contingency for subgrade improvement was to bridge the weak material with crushed rock, geotextile filter fabric and a geogrid. Low bearing pressure tracked plant was also made available should ground conditions be unsuitable for normal wheeled dump trucks.

Overall performance of the dewatering system was variable. At Bentleigh, the HDD wells managed to achieve dewatering levels (Figure 5 shows the water levels in monitoring wells outside the retaining walls) which allowed construction to proceed unhindered, using conventional excavators, dozers and wheeled dump trucks, which can be seen in Figure 6. The drawdown of groundwater and the volume of water pumped by the HDD wells were commensurate with numerical groundwater modelling completed by Douglas Partners, which shows that when the bores were able to be operated effectively, they were a critical part of the dewatering success.

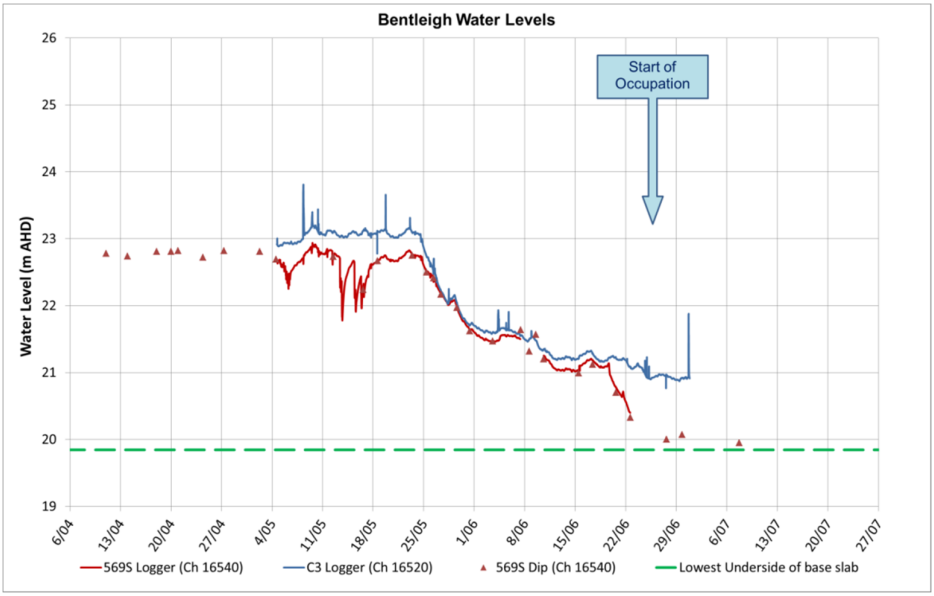


Figure 5 – Groundwater Levels at Bentleigh

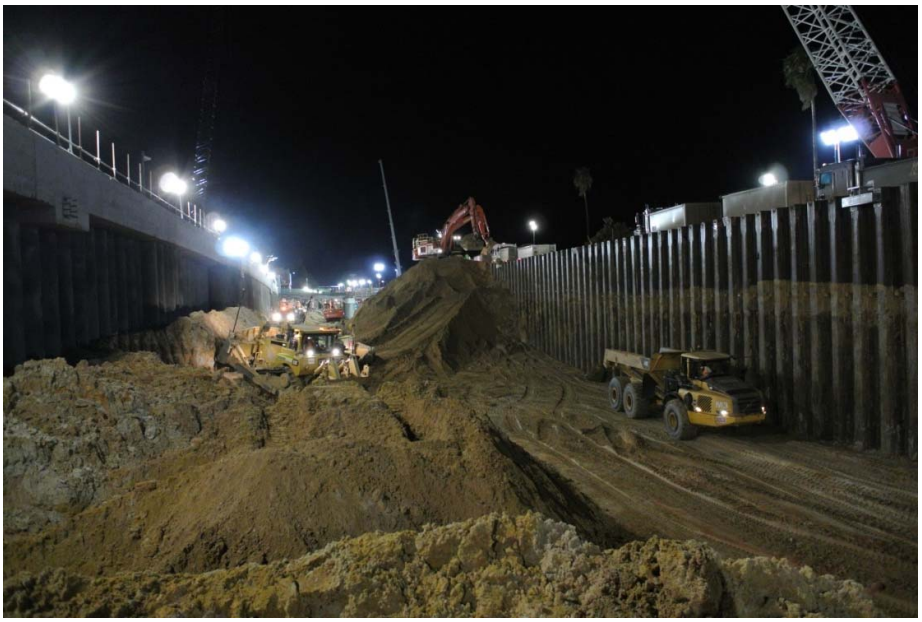


Figure 6 – Excavation at Bentleigh

At McKinnon, the HDD dewatering system performance was not as good. At the start of the occupation, water levels in the monitoring wells were still above the final subgrade level. As a result, as excavation progressed, saturated soil was encountered and the contingency measures were needed. The dewatering problems at McKinnon appear to have been associated with silting of the well, particularly the down track well which may have been compromised by the sump construction trials. . Visible inspection of the ground at McKinnon was consistent with the presence of silty fine sand, which did not drain freely. Whilst the ground was soft and spongy to walk on, there was generally no water running out of the excavated material. A typical view of the subgrade conditions is shown in Figure 7. In the end, the contingency plans together with some additional sump pumping allowed the earthworks to be completed without any significant delays.



Figure 7 – Excavation conditions at McKinnon.

SCREW PILES

In two areas of the project the base slab was located several metres below the design permanent water table. A permanent drained structure could not be considered and measures to resist hydrostatic uplift on the base slab were required. Because of the site constraints, the measures to be employed could not practically be commenced until the rail shut period. Key aspects of risk in selecting a method included the tight time, constrained rail shut period, limited work areas, lead times on materials, and measures that could be installed, tested and remediated quickly. Several options were considered and screw piles were ultimately adopted to best meet the project constraints.

The screw piles were required to perform acceptably both in compression (ie piled raft) under low groundwater levels, or under high groundwater levels with sustained tension and cyclic reduction and recovery of load due to passage of trains. A key performance criterion was limiting the long term upwards deflection of the pile heads to less than 40mm because of rail clearance requirements.



Figure 8 – Screw Pile Installation

A number of papers (eg Abdelghany et al 2010) have been published on the behaviour on helical screw piles under cyclic loads, although these primarily relate to compression and lateral loading. Abdelghany et al indicates the pile capacity degraded and deflections increased under cyclic loadings, but that after 15 cycles minimal further degradation occurred. This is similar to other published results for other pile types with reduction represented in a hyperbolic form with most movements occurring in the first 10 cycles (eg Poulos 1989, Li et al 2012).

Further to the cyclic degradation, there is an additional issue that the uplift resistance relies on ground that has been partially disturbed by the installation of the pile itself.

These issues were recognised during design and an additional reduction factor was incorporated to allow for capacity reduction and to control deflections due to degradation of cyclic uplift loading.

To confirm the assumptions made, pile testing was undertaken by the piling subcontractor on three test piles. These details of these piles are:

1. 700mm diameter helix, 6m deep, serviceability uplift load (SUL) 680kN;
2. 600mm diameter helix, 8m deep, SUL 683kN: and
3. 450mm diameter, 6m deep, SUL 496kN.

The test piles were installed into medium dense to dense sands, with predrilling through upper very stiff and hard clays layers to reduce installation torque to levels management for the equipment and the piles. Following static load tests to confirm pile performance, 20 cycles of uplift load equal to the serviceability loads indicated above were applied to the piles. The deflection at the toe of the pile was measured., along with those at the head (which incorporated elastic extension of the pile shaft, head frame and reaction piles deflections). The results of the deflections at the pile head itself tests are shown below in Figure 9.

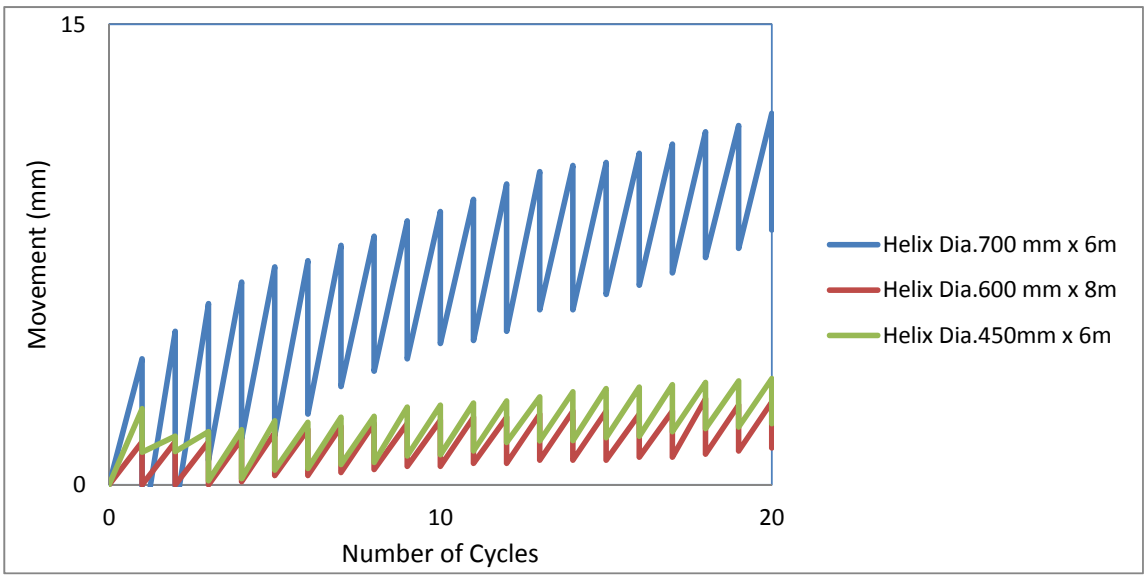


Figure 9 – Pile load test results

The results in Fig 2 indicate:

- the accumulated deflections of the pile head followed a roughly hyperbolic form, with most movements complete within 15 cycles, comparable to previous published results;
- the deflection of the pile under each load cycle was approximately 0.5% of pile helix diameter, which is consistent with the reduction factors applied in design.

SUMMARY AND CONCLUSIONS

The adoption of sheetpiles and the use of innovative piling equipment allowed the construction of retaining walls within the limited space and without undue disturbance ot the predominalty residential neighbourhood.

Douglas Partners understands that HDD for dewatering to this scale has not been implemented within Australia for construction purposes. Groundwater responses at Bentleigh were commensurate with the predicted model results for the formation, and therefore the technology should be considered as a viable future alternative, specifically in highly urbanised areas where surface access is limited, traditional dewatering approaches are not suitable, or project timeframes are compressed.

Key learnings from the adoption of HDD for advanced dewatering in Melbourne relate to the installation of filter product which is matched to the aquifer formation, the use of drilling fluids which can be broken down rapidly during well development, in well groundwater pressure monitoring (specifically for the identification of minimal available drawdown), and early identification of the lead times required by advanced dewatering.

Screw piles were designed to resist hydrostatic uplift on the base slab, with additional reduction factors to allow for cyclic degradation and installation disturbance effects. Three test screw piles of differing combinations of size and depth were installed and tested to confirm performance under cyclic uplift loading conditions. The piles were subjected to 20 cycles of uplift. The results of pile head deflection testing indicate that the accumulated movement of the piles were mostly complete within 15 cycles and followed a roughly hyperbolic form. The results also indicated that the pile head deflection under each load was approximately 0.5% of pile helix, consistent with the reduction factors in design.

ACKNOWLEDGEMENTS

The authors acknowledge the support and permission of Level Crossing Removal Authority and the project alliance team comprising The Roads Corporation, Public Transport Victoria, Metro Trains Melbourne Pty Ltd, John Holland Pty Ltd and Kellogg Brown & Root Pty Ltd. Acknowledgement is also made to SFL Piletech Pty Ltd for use of the pile testing data reported in this paper.

REFERENCES

K R Chandler & M Y Broise, 2000. Remediation of the Watawala Landslide, Sri Lanka.
8th International Symposium on Landslides, Cardiff, U.K.

Abdelghany, Y., M.Hesham El Naggar, 2010. Monotonic and cyclic behaviour of Helical Screw Piles under Axial and Lateral Loading. International Conference on Recent Advances in Geotechnical Earthquake engineering and Soil Dynamics, Paper 8

Poulos, H.G, 1989. Cyclic axial loading analysis of piles in sand. Journal of Geotechnical Engineering, 115(6), 836-852

Li, Z., Bolton, M.D. and Haigh, S.K., 2012. Cyclic axial behaviour of piles and pile groups in sand. Canadian Geotechnical Journal 49, 1074-1087

VALUE ENGINEERING THROUGH SYSTEMATIC SITE INVESTIGATION AND DESIGN OPTIMIZATION – A CASE STUDY

Dr. Manish Tiwari, Principal Geotechnical Engineer, Mott MacDonald Australia, Melbourne, Victoria, Australia, +61457070680, manish.tiwari@mottmac.com
Frances Badelow, Technical Director, Mott MacDonald Australia, Sydney, NSW, Australia, +61400463545, frances.badelow@mottmac.com
Dr. Lu Yitan, Senior Geotechnical Engineer, Mott MacDonald Singapore, +6568052837, lu.yitan@mottmac.com

ABSTRACT

Large 'design and construct' projects often present significant geotechnical risks. However, these also present significant opportunities for value engineering in design. These opportunities can be realised through systematic site investigation and close collaboration with the Contractor to dovetail the design solutions to suit construction methods. This paper presents a case study of a large infrastructure project in Singapore which involved design optimization of an earth retention system for a deep excavation in a constrained urban environment. The project also required installation of over one thousand bored piles in highly variable ground conditions - identified as a key risk. Systematic site investigation was undertaken to develop a reliable ground model. A detailed value engineering exercise identified opportunities for design optimization by changing the retention systems and construction sequence in some segments. An innovative low cost ground improvement method was used in some areas to reduce the forces on the retention system. An extensive instrumentation and monitoring plan was implemented for verification of design and to mitigate the remaining risks. This paper includes the lessons learnt on this challenging project, which are relevant to a wide range of construction projects.

Keywords: Fissure grouting, SPT, ERSS, site investigation, retaining wall, ground improvement

INTRODUCTION

Singapore has been rapidly expanding its underground Mass Rapid Transit (MRT) network over the past two decades. The Thomson-East Coast Line (TEL) forms part of this expansion and is 43 km long and fully underground comprising 31 stations. This paper describes the value engineering and design optimizations undertaken during detailed design of the earth retaining and support structures (ERSS) for one of the underground stations along TEL. The station, currently under construction, is up to 24m deep and 350m long. The edge of the station excavation is less than 10m away from the existing MRT viaduct. The proposed station is surrounded by high-rise residential and commercial structures, some within 2m of the excavation.

Land Transport Authority (LTA) of Singapore imposes stringent technical and contractual requirements on MRT construction works to ensure high quality and safety standards. These include minimum requirements for embedment of retaining walls, groundwater control, additional site investigation, instrumentation and monitoring, and compliance to LTA's Civil Design Criteria (CDC). Any deviations from the minimum requirements can only be approved by LTA after detailed calculations, analysis and field testing are completed and additional monitoring and control measures are proposed.

INVESTIGATION AND DESIGN METHODOLOGY

At the start of the project a review was undertaken of the available site investigation information from tender design stage and key ground risks were identified. Concept ERSS options were prepared and a

safety in design workshop was convened to assess potential risks with various options. The workshop also identified various constructability issues. Design of ERSS was undertaken by dividing the station footprint into 18 zones based on different structural configurations, excavation depths of permanent station and entrance structures and the Contractor's proposed construction staging and excavation sequence. Although the high number of design zones led to an increase in design time, it also created opportunities to optimize the design in several zones.

Before commencing the design, a detailed design basis report was prepared to ensure that methodology of design analysis and calculations complied with LTA CDC as well as widely accepted international guidelines (e.g. CIRIA C580) for deep excavation design. The design basis report was discussed and agreed with the independent checker and LTA and formed the basis of all design calculations.

PROJECT REQUIREMENTS

Some of the key requirements of the project are listed below.

1. Minimum retaining wall toe embedment below the final excavation level (FEL) of 13m in residual soils or 6m in Class 4 rock (highly weathered) or 1m in Class 3 rock (moderately weathered) or better. Rock was classified from Class 1 (fresh, intact) to Class 6 (residual soil).
2. Water tightness of retaining walls up to 10m below the FEL.
3. Rock fissure grouting below the toe of retaining walls around station perimeter up to 10m below FEL or to a depth where permeability of rock is less than 5×10^{-8} m/s.
4. Maximum groundwater drawdown of 2.5m during station excavation.
5. Ensure negligible damage to all the structures surrounding the excavation and movement limits on critical structures, e.g. less than 15mm movement of existing MRT viaduct.
6. Allowance for future basement excavation (13m deep) adjacent to the station over 150m length.
7. Diversion of existing major roads comprising 3 lane dual carriageway over the station footprint.

Some of the technical requirements above were considered too onerous and technically unnecessary. Value engineering and design optimization were undertaken with respect to several of these requirements as discussed in this paper.

GROUND CONDITIONS

The existing ground level across the station footprint varied between 20 to 24m above the mean sea level. The ground generally comprised of up to 3m of fill, underlain by firm to hard residual soils of Bukit Timah Formation between 4 to 52m thick. This formation is classified into 6 classes from GVI (completely weathered, residual soil) to GI (fresh, intact rock). The depth of bedrock (Class GIV (highly weathered) to GI) varied between 7m to 60m below ground surface. Up to 6m thickness of soft alluvial deposits were sandwiched between the fill and residual soils at some locations. At the start of the detailed design, a number of boreholes (with Standard Penetration Tests, SPT) and probe holes (without SPT) were available. A typical geological section along the east wall is shown in Fig. 1. The following risks were identified from longitudinal geological sections along the station perimeter.

- Rock levels were highly variable. GIV rock was locally present in a few boreholes, however its lateral extent was unknown. Hence the assessment of retaining wall toe embedment was difficult.
- There were large gaps in available SPT data along the length of retaining wall as these were not undertaken in probe holes. Since a number of soil parameters (such as undrained shear strength and stiffness) are related to SPT-N values, these could not be assessed with confidence.

- Limited borehole permeability test data were available. Hence the required extent of fissure grouting below the toe of retaining wall could not be readily established.

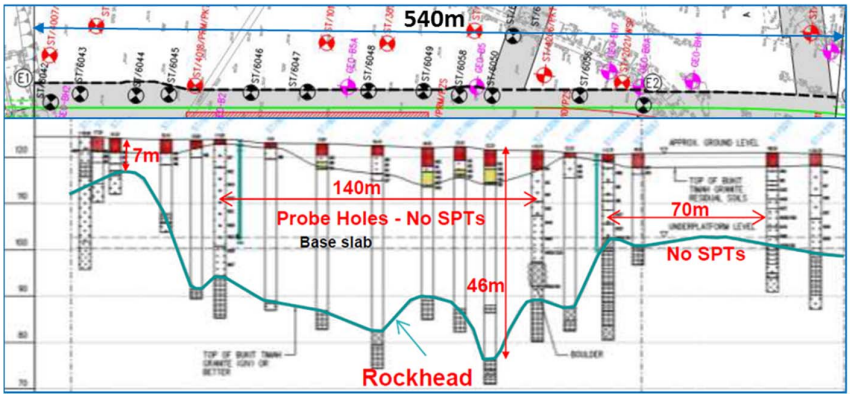


Fig. 1. Geological section along eastern retaining wall

ADDITIONAL SITE INVESTIGATION

An extensive additional site investigation (SI) was planned comprising over 120 boreholes to better understand the ground risks. The Contractor agreed to invest in the extensive SI considering the potential for risk mitigation and opportunities for value engineering during design and construction. Specifications for the SI were developed with the objective of reducing the uncertainty in rock levels, assessing the strength of soils reliably and reducing fissure grouting zones. The key specifications are summarised as follows.

- Boreholes at 10m intervals along the perimeter of the station to estimate the strength profile of soils, and to establish the depth and the class of rock. Borehole permeability tests were undertaken.
- SPTs at 1.5m vertical intervals in all boreholes to provide statistical confidence in SPT-N values when correlating with soil parameters.
- Boreholes extended to at least 13m below the proposed FEL of the station where rock was not encountered.
- Boreholes to 3m below FEL where GIII rock was encountered above the formation level.
- For the boreholes in which permeability tests were undertaken in the rock mass, boreholes extended to 10m below the FEL, regardless of the rock level.
- Where rock was above or within 10m below the FEL, borehole permeability tests were undertaken using a single packer as the borehole was progressed. Tests were undertaken over 5m vertical segments starting at 1m below the top of rock using single packer. LTA's specification required permeability tests in 10m vertical segments, however, it was considered that this might incorrectly identify a high permeability zone of 10m thickness even if the actual high permeability stratum contributing to most of the flow was of limited thickness in the segment. 5m vertical segments could better identify localised zones of high permeability rock.
- Point Load and UCS tests undertaken on rock samples to assess excavatability and rippability.

DESIGN METHODOLOGY

Excavation analysis was carried out using Finite Element (FE) Analysis software (Plaxis). Both soil and rocks were modelled as Mohr-Coulomb material. Design parameters were obtained from a

Geotechnical Interpretative Baseline Report (GIBR) prepared by LTA's consultant at the pre-tender design stage. Drained parameters were used for all soils and rocks, except alluvial clays, as the temporary excavation will be open for up to 5 years. Both seepage and hydrostatic groundwater conditions were considered as separate cases and the retention system was designed to withstand forces in both conditions.

VALUE ENGINEERING OUTCOMES

Over the course of detailed design, several value engineering opportunities were identified. Some of these were based on the additional SI data while the rest were based on a constructability assessment and construction program review. Some of the key value engineering outcomes are discussed below and resulted in significant cost and time saving for the project.

(a) Advance Confirmation of Pile Toe Levels

Bukit Timah Granite rock is known to have a highly variable weathering profile. As the design of the secant bored pile (SBP) retaining wall required a minimum embedment in rock, variability of rock posed significant challenges for fabrication of rebar cage for over 1200 bored piles (1200mm and 1600mm diameter). Additional boreholes helped in assessing the rock level and provided a reasonable degree of confidence. Rebar cages were prefabricated off-site with the cage length based on the rock levels assessed from the additional boreholes, with an additional 300mm allowance to account for sloping rock. A typical retaining wall shop drawing is shown in Fig. 2. In about 95% of the piles, the rock was encountered within 300mm of the estimated level.

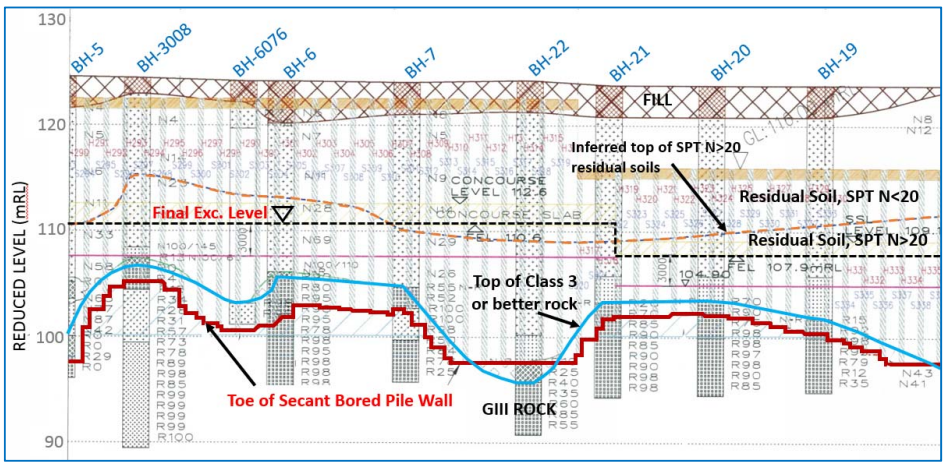


Fig. 2. Confirmation of retaining wall toe levels in variable rock profile

(b) Rock Cuts in Shallow Rock

The additional SI revealed the presence of high strength rock at shallow depths (between 7 to 15m below ground surface) in some areas of the station. In these areas, the retention system was changed to short SBP walls with a berm and vertical cut in rock below the pile toe to FEL. Fig. 3 shows a typical cross-section through one such area. This option resulted in significant cost saving as piling in hard rock was very slow at a rate of about 200 to 400mm per hour. In addition to the reduction in steel and concrete, each linear metre reduction in pile length saved two to three hours of construction time per pile. Several hundred hours of piling were saved as pile lengths were reduced by 10 to 12m over a significant length of wall. Rapid retaining wall installation also resulted in advancing the start of excavation. Although the need for rock support using shotcrete and rock bolts added to the cost of

excavation, this was far outweighed by the savings from the reduced piling works and advancement of excavation program.

(c) Optimum Estimate of Soil Stiffness

During the initial finite element analysis of the construction sequence of the station, it was observed that the ground stiffness (E') design values had significant impact on the observed retaining wall forces (bending moment and shear forces), wall deflections and strut forces. These E' values were selected using a correlation with SPT-N values, where E'=2N (MPa). In several of the additional SI boreholes, soil layers with high SPT-N values (>50 or >100) were identified in several zones. This allowed increased soil stiffness values to be adopted in these zones to optimize the design and resulted in significant reduction in pile reinforcement and strut sizes. A comparison of predicted and observed strut forces and wall deflections (see Figs. 12, 13 and Table 1) during construction showed that the monitored values were generally smaller than the predicted values for the optimized design solutions.

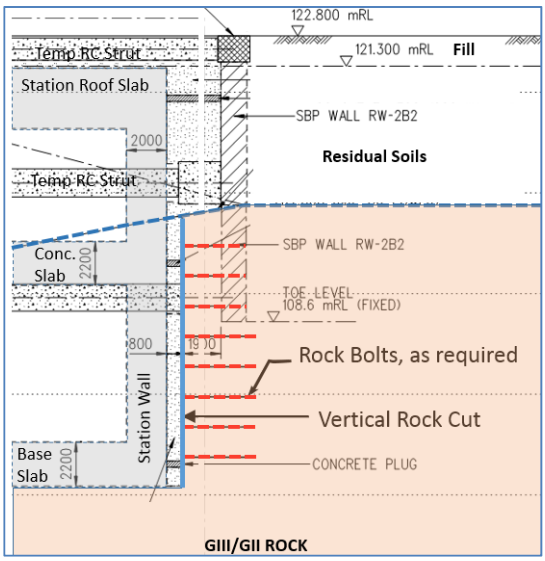


Fig. 3. A typical section utilising short SBP and rock cut

(d) Reduction in Fissure Grouting

For control of groundwater inflow into the excavation and associated drawdown, it was a technical requirement in project specifications (PS) that fissure grouting be undertaken in rock below the toe of retaining wall if it is embedded less than 10m below the formation level and the permeability of rock is higher than $5x10^{-8}$ m/s. A typical geological section with measured permeability values is shown in Fig. 4. Permeability test results indicated that for over 80% length of the wall, the rock mass had a permeability less than $5x10^{-8}$ m/s.

Furthermore, in some higher permeability (> $5x10^{-8}$ m/s) zones of highly fractured rocks, the Contractor decided to extend the retaining wall to 10m below formation level to provide a physical cut-off, which was cheaper than engaging a ground improvement subcontractor to perform fissure grouting. A novel scheme was proposed to extend the retaining wall pile lengths without steel reinforcement through fractured rock since a much shallower toe embedment was sufficient to achieve wall stability and deflection limits. Significant savings were achieved by eliminating about 90% of the required fissure grouting based on results of borehole permeability tests and extension of retaining walls.

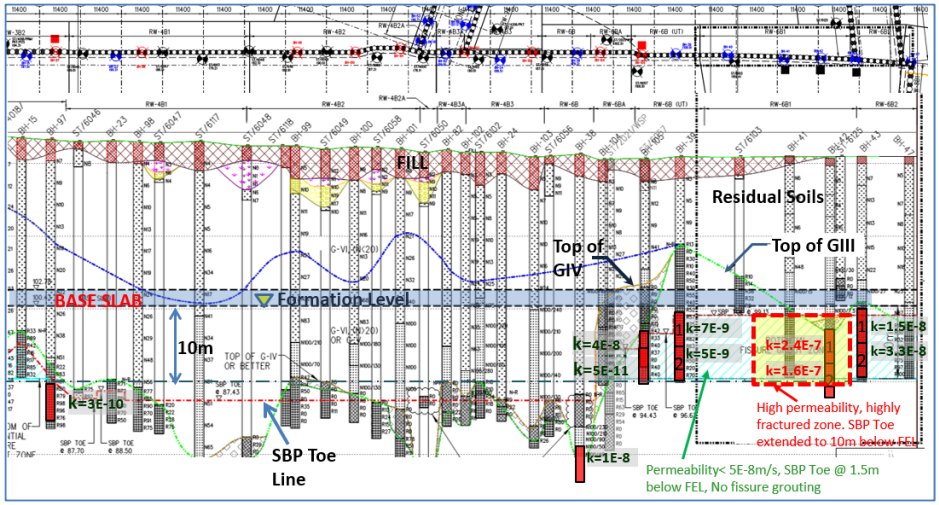


Fig. 4. Reduction of fissure grouting through permeability tests and extension of wall toe

(e) Ground Improvement using LSS Piles

A number of locations required ground improvement in soft soils to provide excavation stability and meet the retaining wall deflection limits. The Contractor proposed to use overlapping unreinforced bored piles cast with Liquefied Stabilised Soil (LSS) to improve the soil (see Fig. 5 for typical section), which was effectively ground replacement. The FE analysis showed that a LSS mix which could attain a UCS value of 1MPa at 28 days was sufficient to meet the design requirements. Since the Contractor owned the piling rigs, it was significantly cheaper to use this method than engaging a specialist ground improvement contractor. The method was more reliable in achieving the desired improved soil strength as sampling and laboratory testing for strength was undertaken for each batch of LSS.

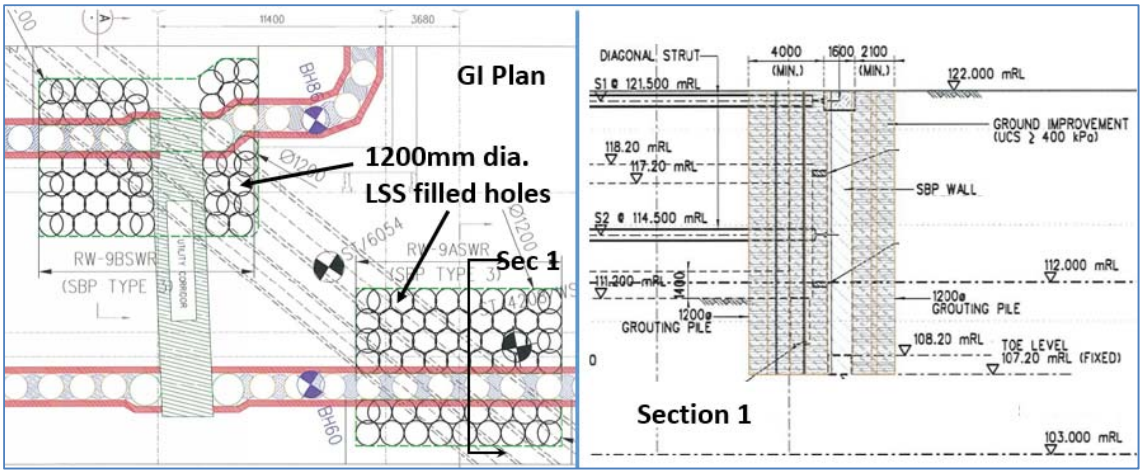


Fig. 5. Example of LSS piles for ground improvement

(f) Soft Piles with Low Strength Concrete

The PS required use of the same grade of concrete (C40) for soft and hard piles in SBP retaining wall. However, the Contractor proposed the use of C7 (f_{ck}=7MPa) concrete for soft piles instead of C40 concrete (see Fig. 6). If C40 concrete was used for soft piles, it would be difficult and time consuming to cut through them to cast hard piles after more than a few days. Furthermore, hard piles tend to deviate

towards softer ground and create verticality issues. It was shown through simple plane stress FEA that the soil arches around soft piles and the earth pressure is transferred to hard piles, therefore the soft piles act as lagging and control groundwater inflow rather than load carrying. LTA accepted the change, which resulted in significant cost reduction of the soft piles and provided flexibility in the timing of installation of hard piles. Soft piles could be installed months in advance of hard pile installation. There were concerns around segregation of aggregates in the 7MPa concrete mix due to high water cement ratio. These were alleviated by advance mix design and laboratory testing by the concrete supplier.

(g) Semi Top-Down Construction in Selected Areas

In some areas of the station, diversion of existing roads on top of the station during construction was required. The tender design had proposed to use a steel traffic deck. It was proposed that the station roof slab be cast in a top-down sequence, backfill placed to its final configuration and traffic diverted onto the backfill area, thus replacing the steel deck. A typical cross-section of the scheme is shown in Fig. 7. The roof slab provided lateral support to the SBP wall. Excavation below the slab then proceeded to the FEL with steel struts supporting the walls, i.e. a bottom-up sequence similar to the rest of the station. This construction sequence was referred to as a semi top-down sequence. The use of semi top-down sequence enabled removal of one level of steel struts and the steel traffic deck, thus leading to significant savings.

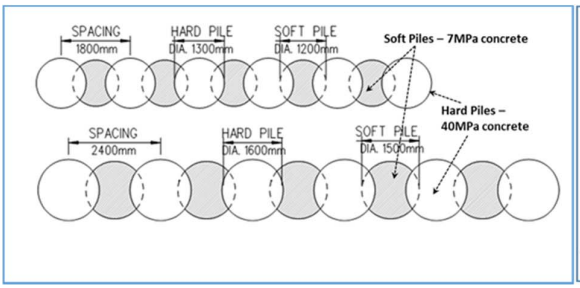


Fig. 6. Use of C7 concrete for soft piles

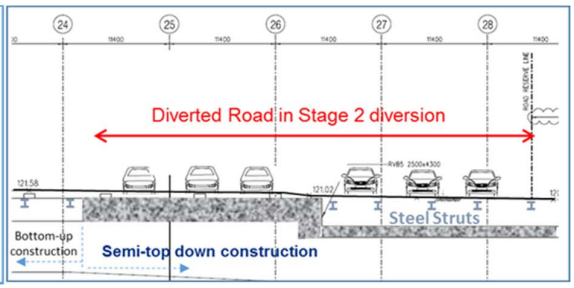


Fig. 7. Semi top-town construction to enable traffic diversion

DESIGN OPTIMIZATIONS

(a) Lower Short Term Cracked Modulus of Retaining Wall

The use of a cracked section for the flexural stiffness (EI) of concrete retaining walls is recommended in CIRIA Report C580. The use of 0.7EI for short term and 0.5EI for long term flexural stiffness of cracked section is generally applicable to diaphragm walls, but is also widely considered to be the representative flexural stiffness for bored pile walls in Singapore. A more sensible approach to quantify the short term cracked section stiffness is to perform wall section force/moment equilibrium calculations, and to assess the uncracked concrete section by considering the tension failure strain of concrete to be about 0.01%. With several rounds of iteration, the range of working stress bending moment was predicted for a range of anticipated reinforcement ratios. The calculation illustrated in Fig. 8 demonstrates that the appropriate short term cracked section flexural stiffness is 0.4EI to 0.6EI. For the final design of the retention system 0.5EI was adopted for short term stiffness during construction as the retaining wall was for temporary use. Use of 0.5EI instead of 0.7EI resulted in larger wall deflection (due to softer wall) but lower (up to 20%) bending moments and shear forces. This resulted in a reduction in steel reinforcement in the retaining walls as well as in the required strutting system, and hence significant cost savings.

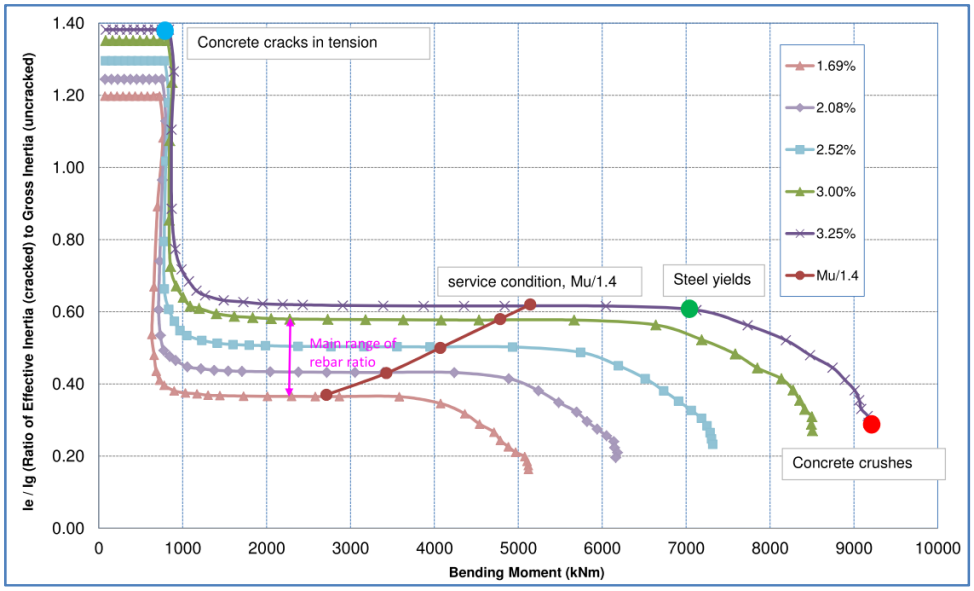


Fig. 8. Relative short term cracked stiffness of 1300mm diameter secant piles and effective modulus

(b) Cantilever CBP Wall with Ground Improvement

One of the entrances to the station connected to an existing bus interchange which was about 8m below ground, under an existing raised MRT station. The designer for permanent works had proposed to build a counterfort retaining wall, which required a temporary contiguous micropile retaining wall and underpinning of two piers of the existing station. Strategically placed additional boreholes revealed the presence of relatively shallow rock at 6 to 9m below ground surface. An alternative retention system using a combination of a CBP wall (up to 8m cantilever) and an L-shape reinforced concrete retaining wall. The original and alternative proposals are schematically shown in Figs. 9 and 10. FE analysis showed that if a ground improvement block formed by LSS piles was placed behind the CBP wall, it would reduce the earth pressures on the CBP wall and limit the deformation of ground and surrounding structures to acceptable limits.

The revised retaining wall scheme resulted in the removal of complicated temporary works (steel struts) required to support the temporary micropile retaining wall to facilitate construction of the counterfort. It also eliminated the need for underpinning the existing piers and resulted in a safer and more cost-effective design.

(c) Reinforced Concrete (RC) Struts to Replace Steel Struts

At one end of the station, which was within 8m of an existing MRT viaduct pier, a stringent ground movement limit of 15mm at the viaduct pier had to be met for the 22m deep station excavation. The initial FEA suggested that the use of steel struts as temporary support would require a large number of struts (5 levels at 4m spacing) to meet the ground movement requirements. The Contractor needed a 10m x 6m construction opening between the struts for transport of material from the excavation. To overcome these issues, it was proposed to use cast-in-situ RC struts rather than steel struts, which could be installed at a greater spacing (12 to 14m) and required only 3 levels of struts. These also required a lesser number of kingposts for vertical support compared to the steel strutting system. RC concrete struts were up to 1.5m x 1m in size together with RC walers of 1.5m x 1.5m. Significant savings were achieved by adopting RC struts, the location of which is shown in Fig.11.

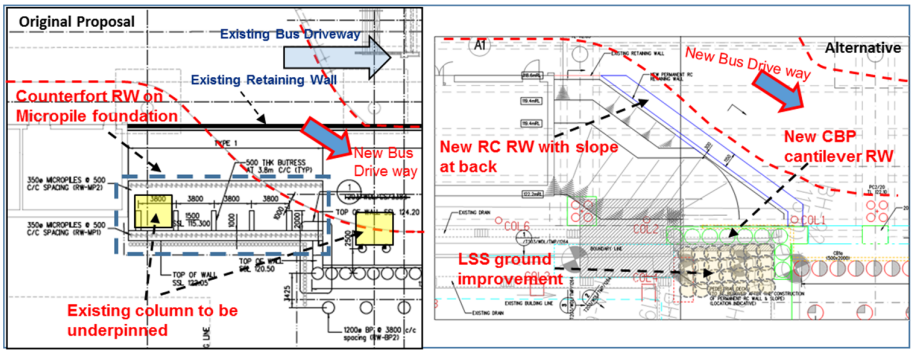


Fig. 9. Original vs. alternative retaining wall scheme (Plan)

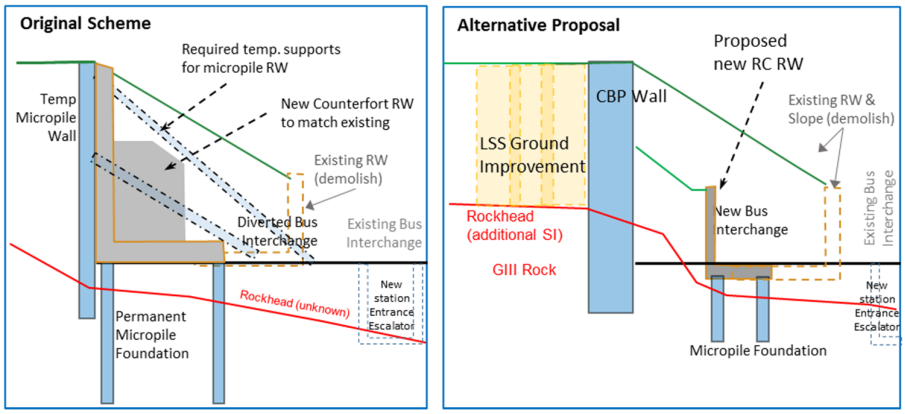


Fig. 10. Original vs. alternative retaining wall scheme (cross-section)



Fig. 11. Use of a combination of RC struts and steel struts

INSTRUMENTATION & MONITORING

Since the station is located in a densely populated urban environment, surrounded by critical structures and utilities, an extensive instrumentation and monitoring scheme was implemented for the retaining walls, ground, groundwater and surrounding structures. Real time monitoring and a warning system

was established to alert key staff within the Contractor, Consultant and Authority organizations. Some of the instrumentation data, which validate the design, are presented in this section.

(a) Retaining Wall Deflections

Inclinometers were installed in the SBP wall piles and in soil behind the wall and typically comprised 2 to 4 inclinometers per design zone. The excavation has reached FEL and base slab has been cast at the time of writing this paper. It has been observed that where the excavation is fully in soil and rock is well below the FEL, the observed wall deflections (Figs. 12 and 13) are between 45-60% of the deflections predicted in excavation analysis (58/31mm vs. 106/72mm for west/east walls in zone G2). In contrast, where excavation is partially in soil and partially in rock (rock at shallow depths), the monitored wall deflection is very similar to the predicted deflections.

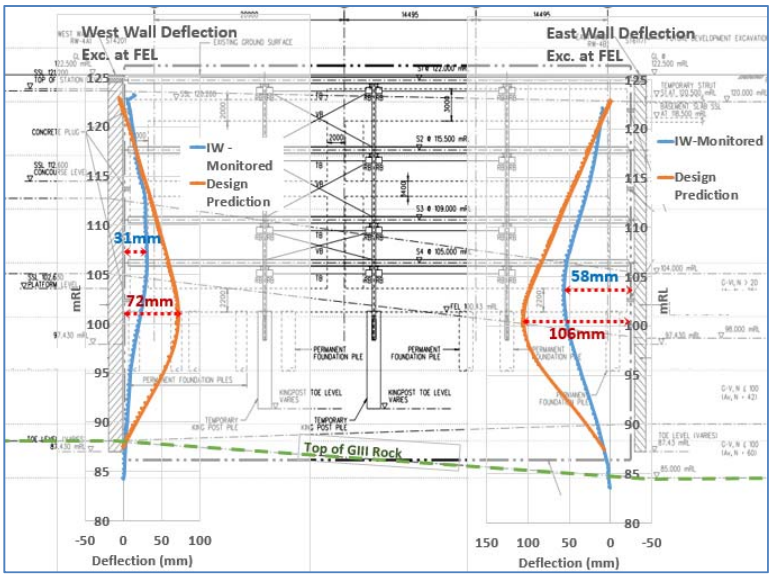


Fig. 12. Predicted vs. monitored wall deflections at a section with deep rock

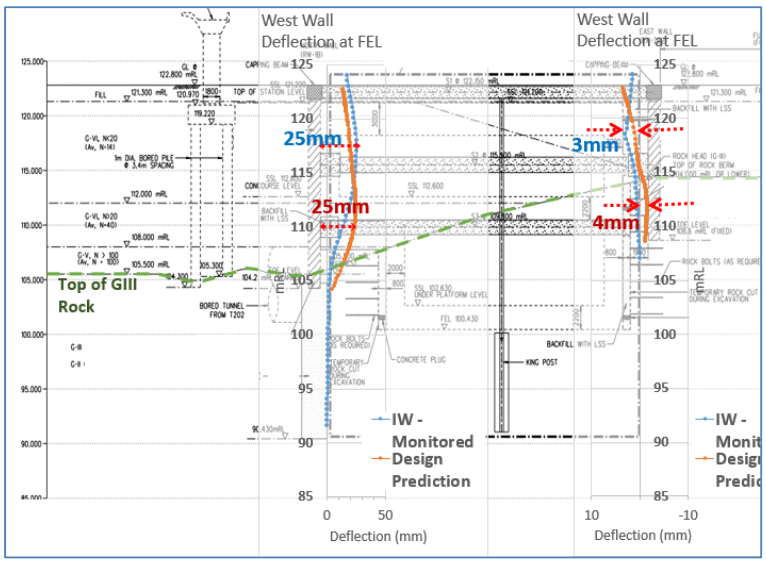


Fig. 13. Predicted vs. monitored wall deflections at a section with shallow rock

(b) Strut Forces

A comparison of observed strut forces is presented in Table 1. The key observations from the table are summarised below.

- In Zone F2, where rock is at shallow depth and RC struts are installed, the monitored strut forces are only 25 to 50% of the predicted strut forces.
- In zones G2 and G3, where rock is much deeper and retaining wall is subjected to full soil pressure, the monitored strut forces for S2, S3 and S4 level are between 40 and 60% of the predicted forces. Monitored forces at S1 level are between 80 to 110% of the predicted forces.

(c) Vibration Monitoring

Due to the presence of existing sensitive structures in close proximity to the station excavation, vibration monitoring was undertaken at all critical structures. A vibration limit (Peak Particle Velocity) of 10mm/s was adopted. The monitoring shows very small vibrations (<2mm/s) within 10m of the station excavation. This shows that conventional piling and excavation activities do not cause significant vibrations outside the excavation. The attenuation of vibration through soils is significant.

Table 1: Comparison of predicted and monitored strut forces

Zone F2 Strut Forces (3 Levels, RC Struts) *(Shallow Rock, 7 to 15m below Ground Level)*				**Zone G2 Strut Forces (4 Levels, Steel Struts, UB)** *(Deep Rock, 28 to 35m below Ground Level)*				**Zone G3 Strut Forces (4 Levels, Steel Struts, UB)** *(Deep Rock, 25 to 40m below Ground Level)*			
Strut Level	**Level**	**Predicted**	**Monitored**	**Strut Level**	**Level**	**Predicted**	**Monitored**	**Strut Level**	**Strut Level**	**Predicted**	**Monitored**
	[mRL]	[kN]	[kN]		[mRL]	[kN]	[kN]		[mRL]	[kN]	[kN]
S1	122.2	14723	7700	S1	122.0	1912	1650	S1	121.2	1340	1500
S2	115.5	36336	11500	S2	115.5	4940	2800	S2	115.5	5330	2850
S3	109.8	30284	9500	S3	110.0	6564	3300	S3	110.0	6718	2850
				S4	106.0	7944	3900	S4	106.0	9566	2400

(d) Groundwater Monitoring

Groundwater levels were monitored using piezometers and standpipes. Recharge wells were installed around settlement sensitive structures. It was observed that despite more than 10m embedment of retaining walls below the formation level, the groundwater table dropped by 5 to 12m just behind the retaining walls (see Fig. 14). However, near the sensitive structures away from the walls, recharge wells were effective in limiting the groundwater drawdown to within 2m below its original level.

It appears that the significantly smaller wall deflections and strut forces in some sections, as discussed in sections *(a)* and *(b)* above, are partially due to groundwater drawdown behind the wall. FE back-analysis of a couple of sections showed that a drop of 10m in groundwater level led to reduction of up to 30% in wall deflection and forces. However, the monitored wall deflections and strut forces on site are still significantly lower than the predictions in back analysis. It is considered to be a result of a combination of a groundwater drawdown and conservative soil parameters and soil model.

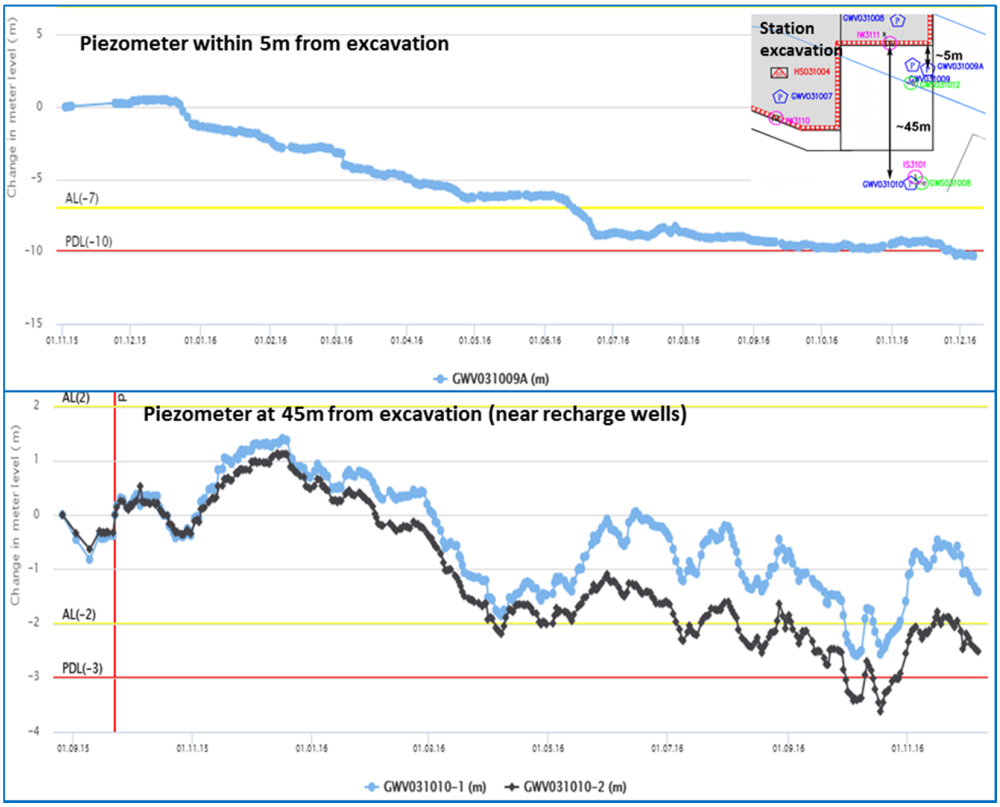


Fig. 14. Monitored groundwater drawdown

SUMMARY AND CONCLUSIONS

The key experiences from this case study can be summarised as follows.

- Systematic additional SI was useful in assessing design values of soil stiffness and achieving an optimized design of retention system. The monitored wall deflections and strut forces during construction have been found to be lower than the design prediction.
- Additional SI enabled greater confidence in rock levels and hence the required pile toe levels and pre-fabrication of pile reinforcement.
- Targeted field permeability testing resulted in significant reduction of fissure grouting in rock.
- Alternative low cost ground improvement technique using overlapping LSS piles were successfully used.
- It has been theoretically demonstrated that a short term flexural stiffness value of 0.5EI for a cracked section of secant pile walls is appropriate. Significant reduction in pile reinforcement was achieved by using this wall stiffness value.
- Systematic instrumentation and monitoring enabled safe construction and verification of design assumptions.

REFERENCES

CIRIA C580, 2003, Embedded retaining walls – guidance for economic design.

Civil Design Criteria – A1, for road and rail transit systems, E/GD/09/106/A1, 2010, Land Transport Authority Engineering Group, Singapore

A 16 M DEEP BASEMENT EXCAVATION IN KUALA LUMPUR KARST: MIXED RETENTION SOLUTION

Prasad PVSR, Mikias Yohannes, Serhat Baycan
Keller (M) Sdn. Bhd.

ABSTRACT

Kuala Lumpur Karst is a complex limestone formation that is characterized by presence of cavities, solution channels, pinnacles and floaters. Basement excavations in such geological formations are usually challenging, mainly owing to the unpredictable rock head depths and potential for groundwater inflow. Any excavation support system should have adequate robustness and water tightness. Traditionally, Secant Bored Pile walls (SBP) with struts are the preferred option for karst ground. This paper discusses a cost effective and innovative alternative solution for a particular site – using Deep Soil Mixing (DSM) and using Contiguous Bored Piles (CBP) together with Ground Anchors (GA). The site, located around one of the busiest areas of Kuala Lumpur, is a 5,700 m^2 commercial and residential development. A 16.0 m deep excavation was needed for four levels of basement and excavation support along the 275 m perimeter of the development. Within the site, the depth to rock head varied from 6 m to 19 m. The basis for each solution and conditions for its suitability are discussed in detail. Some design considerations and construction challenges are also presented. The performance of the two retention systems during excavation are presented, together with comparisons versus design predictions. Suggestions for future development are also given. Advantages of this approach compared to other traditional approaches are highlighted.

Keywords: Deep soil mixing, DSM, KL Limestone, karst, basement excavation, mixed solution

1. INTRODUCTION

The geology of Kuala Lumpur is among the most complicated and geotechnically challenging formations in South East Asia. The majority of the city falls into the Kuala Lumpur Limestone formation; which is a thick, highly-weathered and cavernous limestone. This formation is pure calcitic to dolomitic in composition, having infrequent schist and phyllite interbedding (Gobbett et al., 1973).

The KL limestone has a highly karstic topography dotted with cavities, ravines, interconnected subterranean channels, pinnacles, overhangs, floaters and slump zones (Tan, 2006). This results in erratic bedrock profiles even within short distances. It is not uncommon to see a precipitous rock head incidence within short distances in the same site. In most parts of the City, the bedrock is typically encountered ranging from very shallow depths to about 30.0 m. The exception to this is at the heart of the City, where Kenny Hill formation prevails above the KL limestone. In such cases the limestone bedrock can be encountered much deeper. The erratic rock head profile and the highly karstic nature of the KL limestone makes it a geotechnical challenge requiring careful consideration of suitable engineering solutions.

1.1 – Site Description

The site, located in downtown Kuala Lumpur, is abutted by a busy street on the North. Before development, the site previously served as a car park. To the west an access road separates the site from an empty lot; while on the east, the lot is bounded by light weight residential and commercial buildings. On the south side, the site is bordered by a road that separates it from a prominent Shopping Mall in the City. A layout plan and an artist's impression of the finished development is shown in Figure 1.

The site has an estimated area of 5,700 m^2 and a total perimeter length of about 275 m. The development is a mixed type consisting of a 56-storey commercial/SOHO tower with 4-levels of basement. The tower foundation was designed as a 3.0 m thick raft resting on the bedrock. Hence, construction of the raft

and 4 levels of basement necessitated excavation up to maximum of about 16.0 m deep. Due to the presence of limestone at depths shallower than the final excavation level across the larger part of the site, the excavation works have to be carried out mostly in rock.



Figure 1. Site layout plan (left), and artist impression of the intended development (right)

1.2 – Subsurface Investigation and Soil Parameters for Design

A total of 23 boreholes were available within the site. From the soil investigation data, the subsoil conditions are generally loose to medium dense, light grey silty Sand up to about approximately 7.0 m from the ground surface, save for a few localized pockets of decayed material, construction debris and soft slimes. Further below and overlying the limestone is a medium dense, silty Sand layer of grey appearance and having traces of gravel. Figure 2 shows the scatter plot of field SPT-N blow count values versus reduced levels for all the boreholes in the site. The idealized soil properties that was adopted for design is also shown in the same plot as a line, following a moderately conservative approach. The ground water table as indicated by the boreholes was approximately at 2.5 m below original ground level.

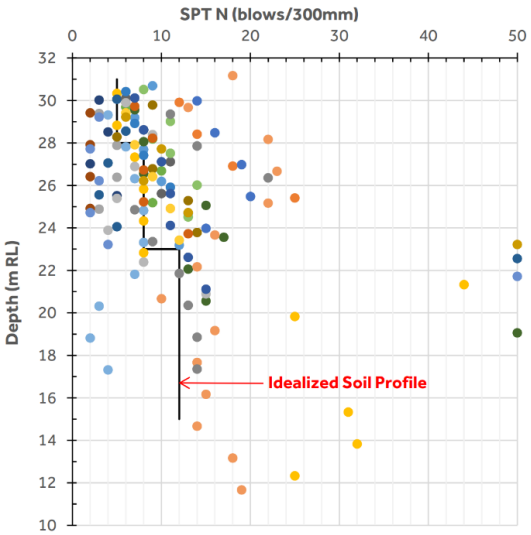


Figure 2. Scatter plot of field SPT-N versus reduced levels for all the boreholes in the site

From the borehole data that was available, the rock head incidence was seen to range from as shallow as 7.0 m up to as deep as 20.0 m below the ground surface. However, given the erratic nature of the

karst limestone profile, additional probing was necessary to be carried-out to determine the depth of the rock more accurately for detailed design purposes. Based on the borehole information, the limestone in the site varied from highly weathered limestone to sound limestone, exhibiting a wide range of rock quality designation (*RQD*). Based on unconfined compressive strength (*UCS*) tests the bedrock can be classified as medium strong to strong limestone, as the results ranged from about 20 MPa to 75 MPa. Figure 3 shows the scatter plot of *UCS* values versus depth, and *RQD* versus *UCS* strength of the rock samples that were tested.

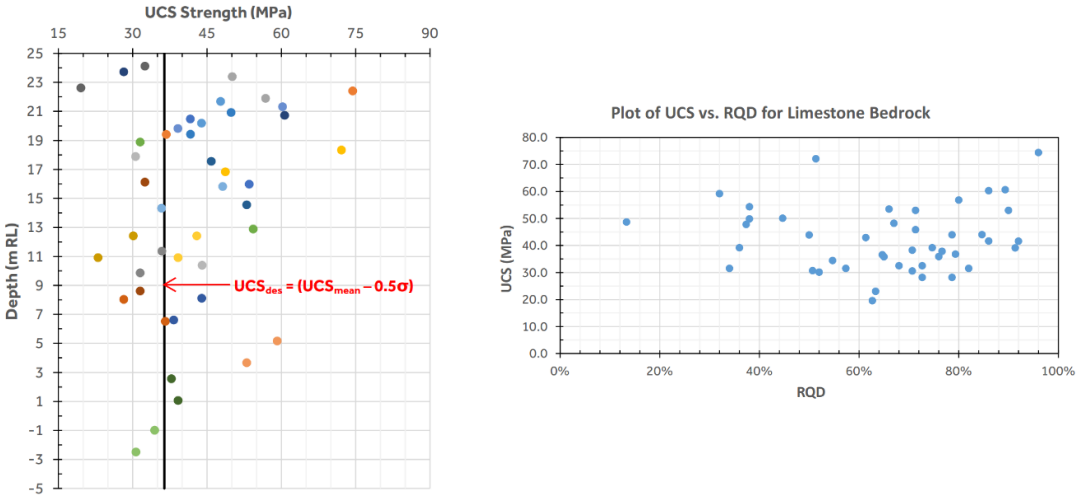


Figure 3. Scatter plot of rock samples' *UCS* value vs. reduced level (left), and plot of *RQD* vs. *UCS* of rock samples (right)

2. DESIGN AND ANALYSIS OF RETENTION SYSTEM

2.1 – Design Considerations

Keller carried-out rock probing along the site perimeter to check the depth of the rock and establish a rock head profile for design and construction purposes. A total of 65 numbers of probing points were carried out along the four walls of the site. On the West and South walls, probing points staggered in two rows were carried-out. While on the North and East walls points in single rows were considered.

The rock was found to be as shallow as 7.0 m and as deep as 18.0 m. On the North wall the rock profile showed some ravines or depressions were the rock was deeper. On the East wall the rock was found to be at an average depth of 9.0 m below the ground level. On the South wall the depth of the rock was found to be more erratic, ranging in depth from 8.0 m to 16.0 m within short wall lengths. In addition, based on the two rows of probing, it was concluded that the rock profile was slanting towards the excavation. In contrast, the two rows of probing on the West wall showed almost uniform rock profile, with an average of 8.0 m deep rock head. Figure 4 shows the rock probing results along the West and South walls.

2.2 – Conforming Design

The conforming design during tendering stage was a soldier pile system with timber lagging. The proposed soldier piles were UC steel profiles (UC 305×305×118 kg/m up to UC 305×305×283 kg/m) with 2.0 m socketing into the limestone rock and placed at 2.0 m centre-to-centre. The proposed wall would be restrained by a combination of removable ground anchors and corner strutting. The ground anchors proposed were also at 2.0 m centre-to-centre and of temporary, removable type. These were provided along the North, West and South walls; whereas, the corner strutting system was proposed along the East wall (buttressed against North and South walls). The reason to adopt strutting for this wall was due to inability to install ground anchors into the neighboring lot.

Some shortcomings in the conforming design permitted consideration of an alternative retention solution. Timber lagging and soldier pile system would not allow a dry excavation, as it is not watertight. This is especially crucial where the ground water table is high, such as the site in discussion. Moreover, the system would not be able to retain the soil properly since the laggings cannot form good contact or seal with the erratic rock head profile of karst formations. The strutting system proposed in the conforming design also included 38 king posts of UC profiles (UC 254×254×73 kg/m) to support the struts and cross members. This added more complications to the proposed system, as this would mean that excavation below the strutting would be delayed due to the high numbers of king posts.

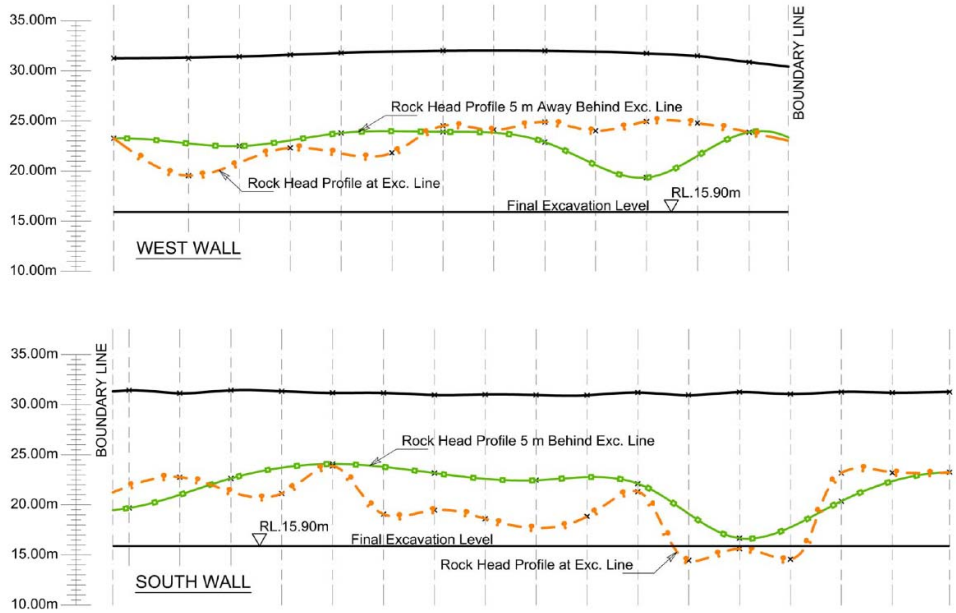


Figure 4. Probing point results of the rock head level at the West (top) and South (bottom) walls

2.3 – Selection of Retention Method

Due to the drawbacks in the conforming design, an alternative proposal was devised. A design using deep soil mixing (DSM) for shallow rock head areas and contiguous bored piles (CBP) was proposed. DSM block, as a gravity retention system, has been successfully used to support excavations in karst ground up to 10 m retained height previously. Where DSM would not be applicable (deeper rock head and/or space unavailability) it was proposed to use CBP and retrievable ground anchors. Cost comparisons were made to ensure that the proposal would be competitive.

Before the designs were finalized, physical rock probing was decided to be carried out, as described in Section 2.1. Due to space unavailability, DSM was ruled out for North and East walls (only 2.3 m was available from boundary line to excavation line). Hence, for these walls only CBP option was explored. Where space was available (West and South walls), the applicability of DSM was evaluated. Adequate rock probing was carried out to map out the rock profile at these walls. Since the rock profile was more consistent and shallower than 10 m, it was decided that DSM is an ideal application for the West wall. For South Wall, since the rock depths ranged from 8.0 m to 19.0 m, it was deemed that DSM would not be a suitable choice. Moreover, the rock profile showed that at certain sections the rock was dipping towards the excavation; hence necessitating a wider DSM block. For these reasons CBP option was preferred.

To address the water tightness issue of the conforming design, the proposed solutions provided suitable means to prevent water seepage into the excavation. DSM treatment effectively makes the ground impermeable as the cementation seals the voids in the soil matrix. The block treatment also cuts off potential water seepage across the rock–soil interface, as the individual columns would have variable

depths due to the karst formation. The gap between contiguous piles was proposed to be sealed using jet grout or jet mixed columns (JMC) having larger diameter than the opening. The jetting would ensure the formation of the columns against the CBPs, plugging any potential water seepage. The size of the JMC was selected such that the gap is adequately sealed after allowing for verticality deviations of the CBPs.

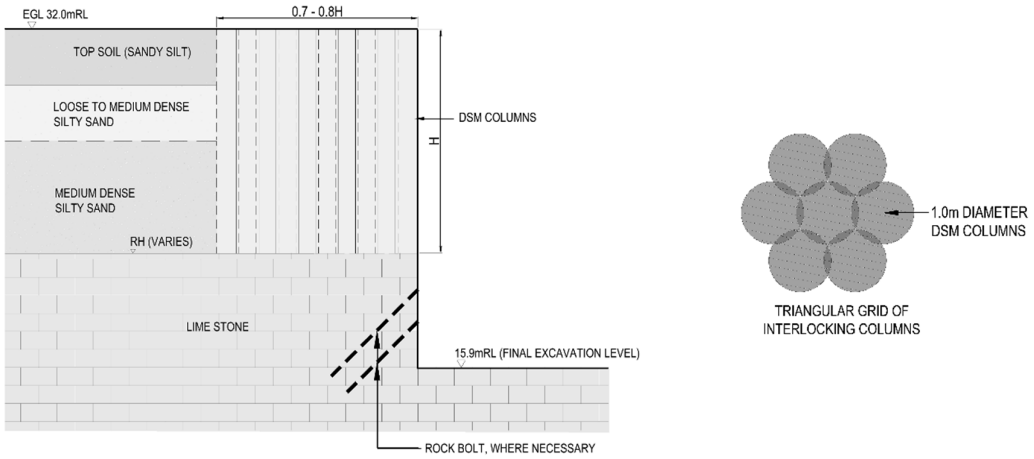


Figure 5. Typical DSM cross-section and details (West Wall)

To allow a faster and less congested excavation, it was also proposed to use only retrievable ground anchors as a means of retaining the CBP walls and avoiding the use of struts all together. As the adjacent lot was semi-vacant with few light-weight barracks, it was proposed to the Main Contractor to rent the land for the duration of the construction and install retrievable ground anchors into the lot. This was more favorable to the Client as it afforded a time saving by allowing faster and unobstructed excavation.

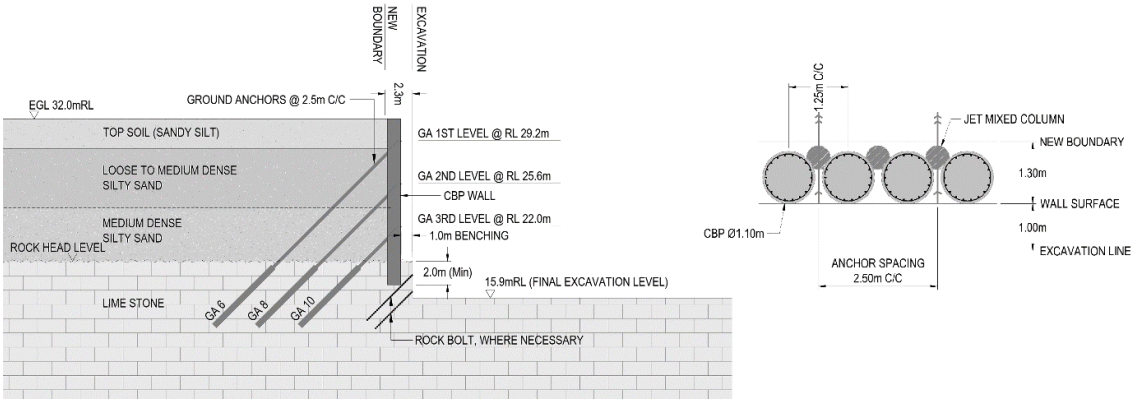


Figure 6. Typical CBP cross-section and details (North and South Walls)

2.4 – Design and Analysis of Alternative Proposal

For the alternative proposal, preliminary design were carried-out by hand calculations – with the help of in-house spreadsheets. For the detailed design stage, a number of plane strain finite element analyses were done using the geotechnical engineering program Plaxis 2D.

2.4.1 – Soil Parameters

Based on the soil investigation data, the soil layers were modelled by using the Hardening Soil constitutive model (*HSM*). Idealized soil profile as shown in Figure 2 was considered for design purpose. Since the soil on the site is predominantly sandy, all soils were modelled as drained. Drained

angles of shearing resistance as shown in Table 1 were adopted for each soil layer, whereas the effective cohesion was considered to be insignificant (taken as 0.5 kPa for modelling purposes).

Table 1. Summarized soil and rock properties

Soil Description (*HSM*)	γ_b [kN/m^3]	γ_s [kN/m^3]	c'_{ref} [kPa]	ϕ' [deg]	ψ' [deg]	E_{50}^{ref} [MPa]	E_{ur}/E [-]	m [-]	R_f [-]
Firm sandy SILT/ loose Silty SAND	16.0	18.3	0.5	27	0	5.5	3.0	0.75	0.9
Loose to medium dense Silty SAND	17.0	19.0	0.5	29	0	16.0	3.0	0.65	0.9
M/dense SAND with Silt/Gravel	17.3	19.3	0.5	32	2	24.0	3.0	0.65	0.9
Rock Description (*HB* Model)	γ_b [kN/m^3]	γ_s [kN/m^3]	σ_{ci} [MPa]	E' [MPa]	ψ_{max} [deg]	v' [-]	m_i [-]	GSI [-]	D [-]
Limestone	23.0	24.0	36	30,000	0	0.25	9	50	0.7

γ_b = bulk unit weight of material, γ_s = saturated unit weight of material, c'_{ref} = effective cohesion, ϕ' = effective angle of shearing resistance, ψ' = angle of dilation, E' = Young's modulus of material, v' = Poisson's ratio, E_{50}^{ref} = triaxial secant stiffness for soils, E_{ur}/E = moduli ratio of unloading–reloading, m = HSM model power for stress level dependency of stiffness, R_f = limiting failure ratio, σ_{ci} = uniaxial compressive strength of rock, E' = Young's modulus of material, ψ_{max} = dilatancy at zero stress level, m_i = Hoek-Brown material constant for the type of rock (intact rock), GSI = geological strength index for the rock, D = disturbance factor for the bedrock as a result of excavation.

The limestone bedrock was modelled using Hoek-Brown (*HB*) rock model by assuming an isotropic rock with no preferred jointing direction. The necessary input parameters were evaluated following Hoek et al. (2002), Marinos et al. (2007) and Marinos and Hoek (2000). Intact rock properties were evaluated first, and the laboratory or intact rock properties were reduced by incorporating the geological strength index (*GSI*) to reflect actual or in-situ rock characteristics. Additional relevant factors were also considered, such as the damage and stress relaxation effects due to rock excavation. Since the rock excavation was to be carried out by a third party, a no-blasting zone of 5.0 m from the walls was prescribed as a safeguard. Rock bolts were also prescribed if any unstable rock was noted on site during excavation. The idealized soil and rock input parameters adopted for detailed analyses are provided in Table 1.

The initial in-situ locked in stresses for the soils were considered based on K_o approach, where K_o was taken as (1- sin ϕ'). In addition to these, the ground water table was considered to be 2.0 m below the ground level. A surcharge load of 15 kPa was also considered on the retention side to account for the live load on existing roads. Moreover, over-excavation for up to 0.5 m below the final excavation level was considered. Seismic action was not considered in the design since Kuala Lumpur is not located in earthquake prone area.

2.4.2 – Design for DSM

The width of the DSM block was decided based on rock head depths from rock probing results. Attention was given to areas where the rock showed a slanting profile towards the excavation. For DSM wall, no rock benching was considered in order to allow the direct casting of permanent wall against the DSM wall, allowing cost saving of formwork erection and removal on the West wall.

The DSM block was designed for a target *UCS* of minimum 1.0 MPa. Such a value was specified based on internal stability and stiffness requirements. Using a relationship of *UCS* to Young's modulus of $(250 \times q_u)$, a design stiffness of 250 MPa was used (where q_u is the *UCS* target value of DSM samples, in MPa). For lack of a better constitutive model, DSM was modelled as a non-porous *MC* model having a cohesion value only. The DSM cohesion value is taken as $c_u = q_u/2$. An allowance for tensile stress up to 5% of the *UCS* strength was accounted for in the model. Detailed DSM properties that were adopted for design are as shown in Table 2.

Table 2. DSM properties adopted for detailed design

Soil Description (*MC* Model)	γ_b [kN/m^3]	*UCS* [MPa]	c_{ref} [kPa]	ϕ [deg]	v' [-]	*E* [MPa]	$\sigma_{t,max}$ [kPa]
DSM (non-porous)	21.0	1.0	500	0	0.30	250	50

γ_b = bulk unit weight of material, UCS = ***unconfined compressive strength of material,*** *c_{ref} = cohesion,* ***ϕ = angle of shearing resistance, E =*** *Young's modulus of material,* ***v' = Poisson's ratio,*** *$\sigma_{t,max}$ = maximum allowable* ***tensile stress.***

2.4.3 – Design for CBP

Design of the CBP wall was carried out by categorizing the wall stretches based on rock head profiles from the rock probing results. Based on the *UCS* strength values for the site, competent rock was specified to be as rock having *UCS* strength greater than or equal to 36.0 MPa (which is a representative value adopted on the moderately conservative side, refer Figure 3).

The CBPs were designed to be socketed minimum 2.0 m into competent rock. The side shear resistance of the rock was determined based on Horvath and Kenney (1979) approach. If no rock was encountered, the CBPs were continued for 5.0 m into the medium dense Silty Sand below the final excavation level. Where rock head was encountered shallower than final excavation depth, rock benching of 1.0 m was considered from CBP face. This allowed termination of piles encountering rock shallower than the final excavation depth. The benching was provided so as to provide the piles with enough rock to develop geotechnical capacity within the socket length and augment pile toe stability. It also acts as a buffer during rock hacking, so that the CBPs are not compromised.

Among the walls where CBP was proposed, the space at the East Wall was more restricted. This was due to the roof eave boards of the barracks at adjacent lot impinging into the site. Installation of bigger CBP diameter would result in potential damaging of these quarters by the piling rig's drilling tool. Thus, a smaller diameter of CBPs was selected for this wall (i.e. 0.8 m vs. 1.1 m for North and South Walls).

FEM modelling of CBPs was done in 2D plane strain condition considering 5-noded isotropic and end-bearing enabled plate elements. The input properties considered for the design are as shown in Table 3.

Table 3. Summarized CBP properties for FEM modelling

Type	Dia. [m]	*EA** [kN/m]	*EI** [kN.m^2/m]	*w* [kN/m/m]	*v'* [-]
CBP-T1	1.10	1.90×10^7	1.44×10^6	18.24	0.20
CBP-T2	0.80	1.32×10^7	5.29×10^5	12.70	0.20

Dia. = diameter of piles, EA = *axial* ***rigidity, EI*** *= flexural rigidity,* ***w = weight per meter width per meter run, v' = Poisson's ratio****.*

* An effective long term stiffness of 80% was considered

Based on the member forces envelop from Plaxis, the structural design of the CBPs was carried out. Axial loads on the CBPs were predominantly from the vertical component of ground anchor forces. The resulting axial forces ranged from 800 kN to 1,500 kN per pile, depending on ground anchor levels and retention height. The bending moments on the CBPs varied from 550 kN.m to 1,700 kN.m per pile. Based on these, the CBPs were designed to have reinforcement contents of 0.8% to 1.8%. The CBPs were designed for 40 MPa characteristic strength concrete.

2.4.4 – Ground Anchors

The CBP walls were designed to be supported by grouted ground anchors. The ground anchors were designed using retrievable, 15.2 mm dia. high tensile steel (Y1860C) strands. As the overburden soil is loose to medium dense sands, the fixed length of the anchors was designed to be socketed into the rock to get the necessary pull-out resistance. To shorten the length, the anchors were designed with a 45^o inclination. The anchors were chosen to be spaced at alternate gap between CBPs (i.e. 2.50 m at North

and South Walls, 1.90 m at East Wall). Cement grout of 30 MPa characteristic compressive strength was chosen for the ground anchors. Material properties of the different ground anchors that were used is given in Table 4.

Table 4. Summarized Ground Anchor properties for FEM modelling

Type	Free Length		Fixed Length				
	Strands' *EA* [kN]	Spacing* [m]	Dia. [m]	*EA* [kN/m]	*EI* [kN.m²/m]	*v'* [-]	f_s [kN/m]
GA6a	1.72×10^5	2.50	0.15	1.77×10^5	2.49×10^2	0.20	141.4
GA8a	2.30×10^5	2.50	0.18	2.54×10^5	5.15×10^2	0.20	169.6
GA10a	2.87×10^5	2.50					

Dia. = diameter of ground anchor, EA = axial rigidity, EI = flexural rigidity, f_s = limiting skin friction, v' = Poisson's ratio.

* Data shown only for 2.5m spacing ground anchors.

2.4.5 – Rock Fissure Grouting

To prevent seepage of water through exposed rock face, drilling and grouting was necessary. A row of curtain grouting was done in the rock at 3.75 m spacing around the perimeter of the excavation; secondary and tertiary points were added at intermediary locations as necessary when volume and pressure requirements were not met. The curtain wall was designed to be done from rock incidence up to 10.0 m below the excavation depth. Base grouting was specified at the excavation area to prevent seepage from the bottom of the pit. These points were designed to be carried out from final excavation up to a maximum depth of 5.0 m.

3. CONSTRUCTION OF RETENTION SYSTEM

3.1 – Construction and Excavation Process

The drilling and grouting works were carried out before the other products. This allowed some understanding on the nature of the bedrock in terms of depth and quality. The installation of the CBP was facilitated by the depth information obtained from the drilling work. The nature and quality of bedrock was also assessed based on the drilling information and grout intake. Figure 7 shows the spatial grout intake plot of all drilling and grouting works. In total, about 300 m³ of grouting was carried out for the project.

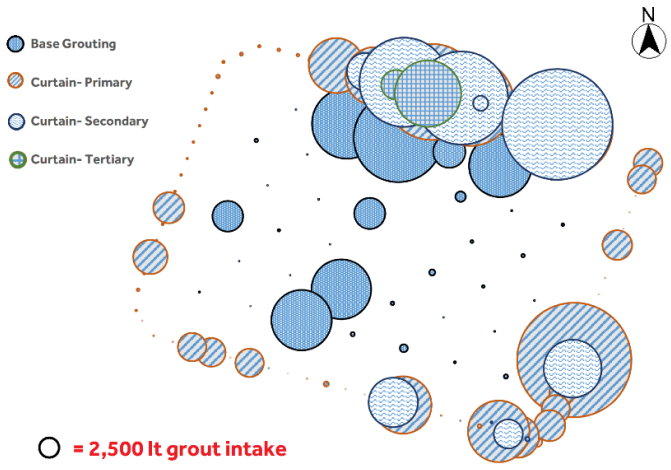


Figure 7. Spatial grout intake plot of all the drilling and grouting points carried-out

Based on this plot, it can be seen that on the North Wall a stretch of about 35.0 m was highly jointed and weathered bedrock. The grout intake was so much that secondary and tertiary points were added to

the curtain grouting (refer Figure 8a for exposed rock). This zone extended into the excavation area, as the neighbouring base grouting also recorded relatively higher intake (refer photo in Figure 8b). Similarly, on the South-East corner, a stretch of about 15.0 m showed highly weathered rock profile.

To act as a homogenous gravity wall, the DSM block was required to be mixed without the development of cold joints. The columns were mixed consistently and due attention was given to creating mechanical interlocking between each shift of DSM production. Samples at selected columns were cored and tested for *UCS* of the formed DSM. The minimum UCS value that was recorded was 1.60 MPa, which is above the target strength.

On site, point load tests for rock samples retrieved from each CBP rock coring were performed and point load strength indices evaluated ($I_{s(50)}$). The correlation between point load index strength and *UCS* strength is given by a general formula $UCS = k \times I_{s(50)}$, where k is a correlation factor, and for KL limestone the suggested values are 7 – 20 (eg. Liew et al., 2010). Based on the point load test on rock samples retrieved from each pile socketed in rock, the $I_{s(50)}$ vs. *UCS* correlation factor for this site was found to be approximately 13. When the inferred *UCS* values were lower than the design value, rock socket lengths were made longer. Extra socket lengths were decided based on correlated point load indices.

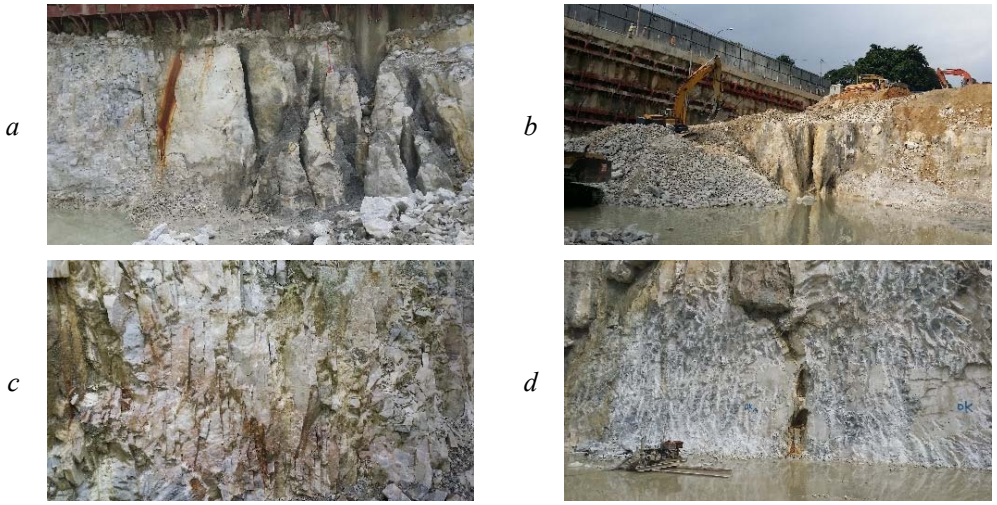


Figure 8. Exposed rock after excavation *(a)* massive to thinly bedded formation with wide burrows (North wall, where high grout intake was recorded), *(b)* pinnacled and fissured limestone exposed (middle of site), *(c)* fractured, thinly and vertically bedded formation (South wall), *(d)* solution channel in massive rock formation at DSM toe (West wall)



Figure 9. Faster excavation on DSM wall is afforded as no additional supports are needed

Installation of the ground anchors was done progressively. Since the DSM wall does not require ground anchors, the west part of the site was excavated at a faster pace. This meant the ground anchors' installation at the abutting walls (North and South) had to be well coordinated with the excavation progress (refer Figure 9). Installation of second layer ground anchors at the North wall initially caused

leakage through the anchor point. This was overcome by doing pre-grouting and post installation sealing plug. As the ground anchors were temporary and retrievable type, they were destressed and removed progressively. When a basement floor below a row of ground anchors was cast, those ground anchors were removed.

The excavation process was carried out reasonably fast, as the early completion of the DSM wall provided an area where excavation works can commence. Other than a few cases of leakage from ground anchor installation points, the seepage through the retaining walls or base of the excavation was insignificant. As such, dewatering of the water trapped inside the pit was done and the drawdown in the ground water table outside of the pit was not noteworthy.

3.2 – Challenges in Construction

One of the challenges in construction for this site was due to unforeseen ground conditions. Peaty soil with high organic content and wood pieces was encountered at a depth range of 3 m to 7 m in a localized area within the DSM treatment (refer Figure 10). Treating the area with DSM was not possible; hence, jet mixed columns were used to drill through the peaty soil, go up to the rock incidence and form mixed columns.

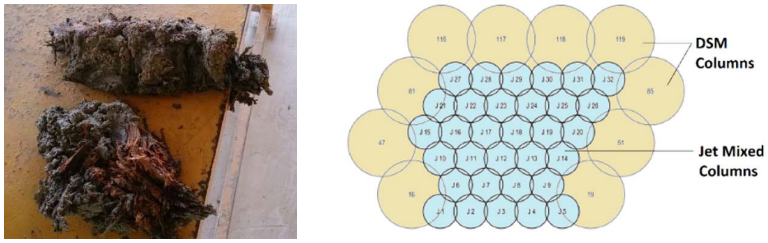


Figure 10. Peaty soil encountered at DSM treatment area (left), and rectification measure taken to replace affected DSM columns with JMC columns (right)

As excavation was undertaken by a third party, close supervision of the works was warranted. Among the issues encountered, one was relating to rock mining near DSM wall. It was prescribed in design specifications that rock blasting would not be conducted within 5.0 m of retention wall, and only mechanical hacking was expected for rock excavation close to the DSM and CBPs. The reality on site was different. In some cases, blasting was conducted as close as 1.0 m from the wall face due to delay in construction program. Compared to CBP walls, this caused concern particularly on the DSM wall, since it is unreinforced and cracking of the block can potentially lead to water seepage. Based on pertinent vibration codes (BS 7385-2), it was recommended to keep the vibrations peak particle velocity (PPV) at the DSM to less than 15 mm/s. Save for minor deformations at DSM toe, no significant damage was noted on the DSM wall. Vibration monitoring at the top of the DSM (approx. 15.0 m away from blasting point) showed the resultant PPV was 5.2 mm/s. Figure 11 shows the damage to the rock and DSM toe following the incident.



Figure 11. DSM toe and damage to rock below DSM following a close proximity blasting

On CBP walls, a source of concern was over-excavation of the proposed rock benching. This was as a result of hasty excavation works and highly jointed and weathered rock profiles. In one case, where the remaining benching was insignificant, additional level of ground anchors was quickly added to pin the CBPs and prevent potential pile toe instability (refer Figure 12).

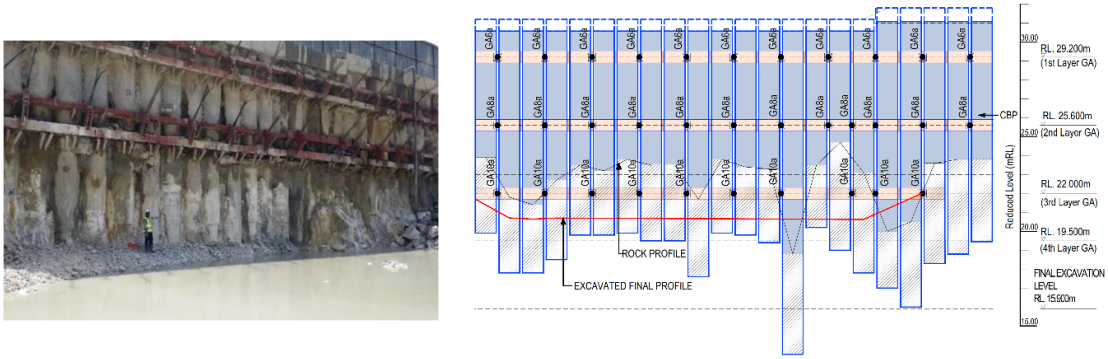


Figure 12. Over-excavation of rock benching (left), and remedial measures taken by adding a third row of ground anchors (right)

4. COMPARISON OF RETAINING WALL PERFORMANCE: EXPECTED VS. ACTUAL

The basement excavation and response of the retaining walls were monitored throughout the excavation and basement construction process. Wall lateral deformations along the four walls were monitored using eight inclinometers. About 19 numbers of ground and wall settlement markers were also installed to monitor the effect of excavation on surrounding areas, roads and buildings. Four standpipes were also installed around the walls to monitoring groundwater variation throughout the excavation period. Two of these had the dual purpose of ground water level monitoring and serving as recharge wells, if necessary. Layout plan of the different instruments is as shown in Figure 13.

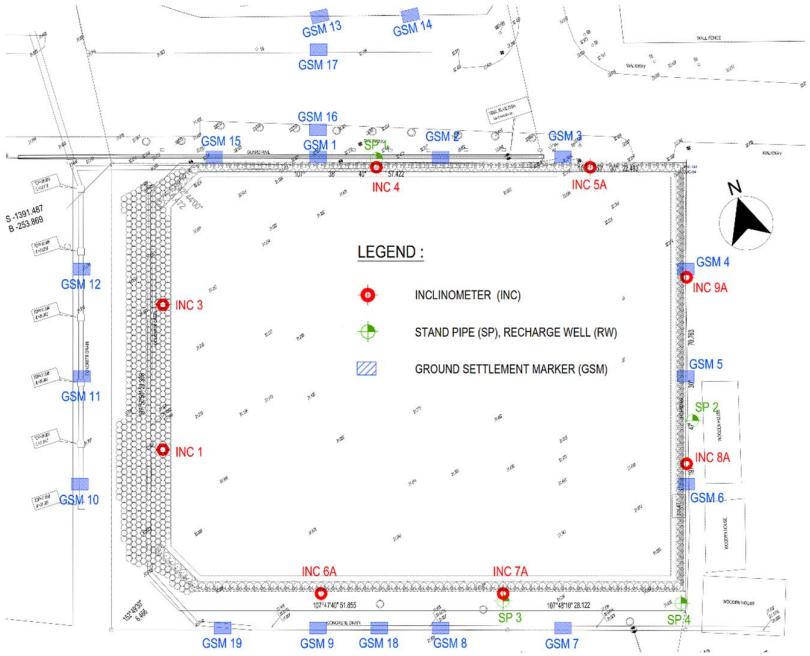


Figure 13. Instrumentation layout plan

Alert and alarm values, together with action plans were set up at the beginning of the excavation based on local construction practice. The maximum lateral movement of the wall was limited to 0.5% of the

excavation height. During the excavation works, monitoring of the installed instruments (inclinometers, ground settlement markers and standpipes) was carried out at a frequency of twice per week. This was gradually reduced to a weekly and fortnightly basis during basement construction and anchor destressing/removal.

From the monitoring data, it was noted that the DSM wall barely moved, showing a maximum lateral movement of about 1.0 mm up to the end of excavation period. The predicted maximum deformation from FEM modelling was about 8.0 mm. It is to be noted that in FEM modelling for simplicity the rock-soil/DSM interface is modelled as a straight plane (horizontal or otherwise). However, owing to the karstic profile of the rock, the actual rock–DSM interface is jagged. This allows more contact area and mechanical roughness, thereby providing higher basal resistance against sliding and resulting in a better performance of the block retaining wall.

In contrast, the CBP wall performance showed some variation. During each stage of excavation, the wall deformations were checked. The maximum lateral deformations ranged from a minimum of 3.0 mm to a maximum of about 20.0 mm. Generally, the actual performance of the CBP walls was better than the predicted deformation, as shown in Figure 14. Particularly at the South wall, the performance of the CBP wall was much better than the predicted due to better soil conditions than expected (Figure 14, bottom left). The dipping bedrock profile at this wall may have resulted in lower lateral pressures on the wall. The exerted surcharge load on this wall was also less than the design, since there was about 8.0 m clear distance to the road and the space was mostly vacant.

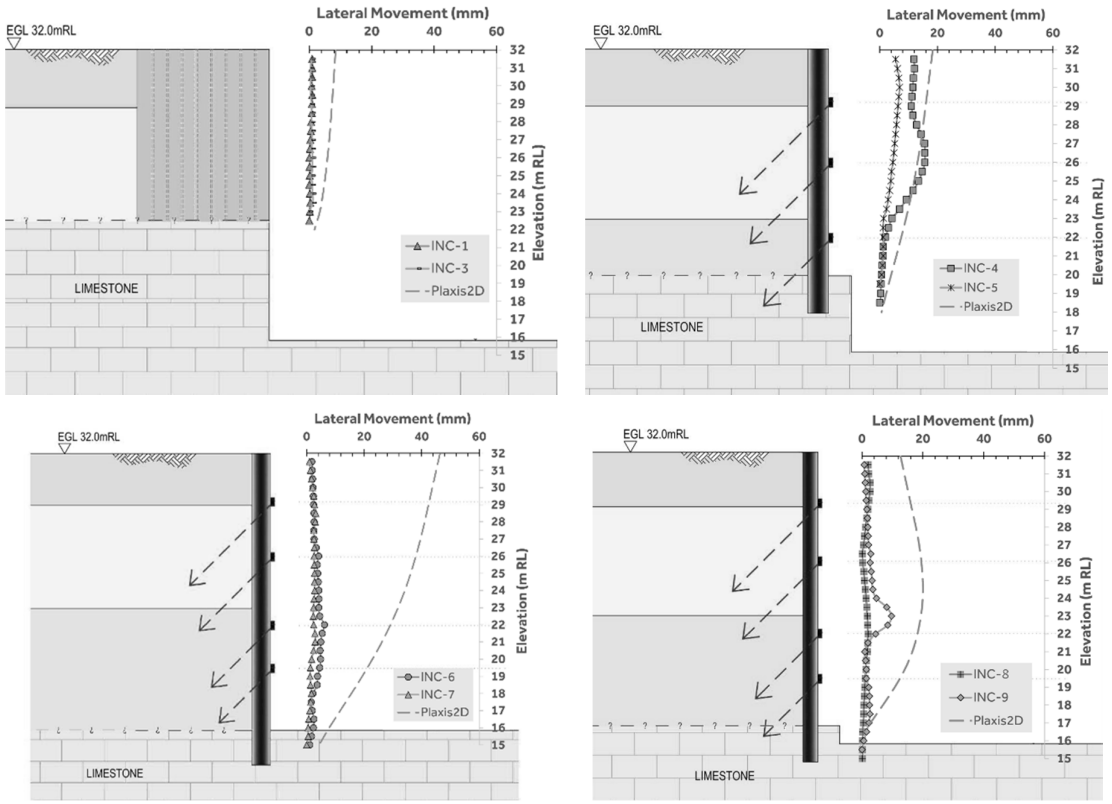
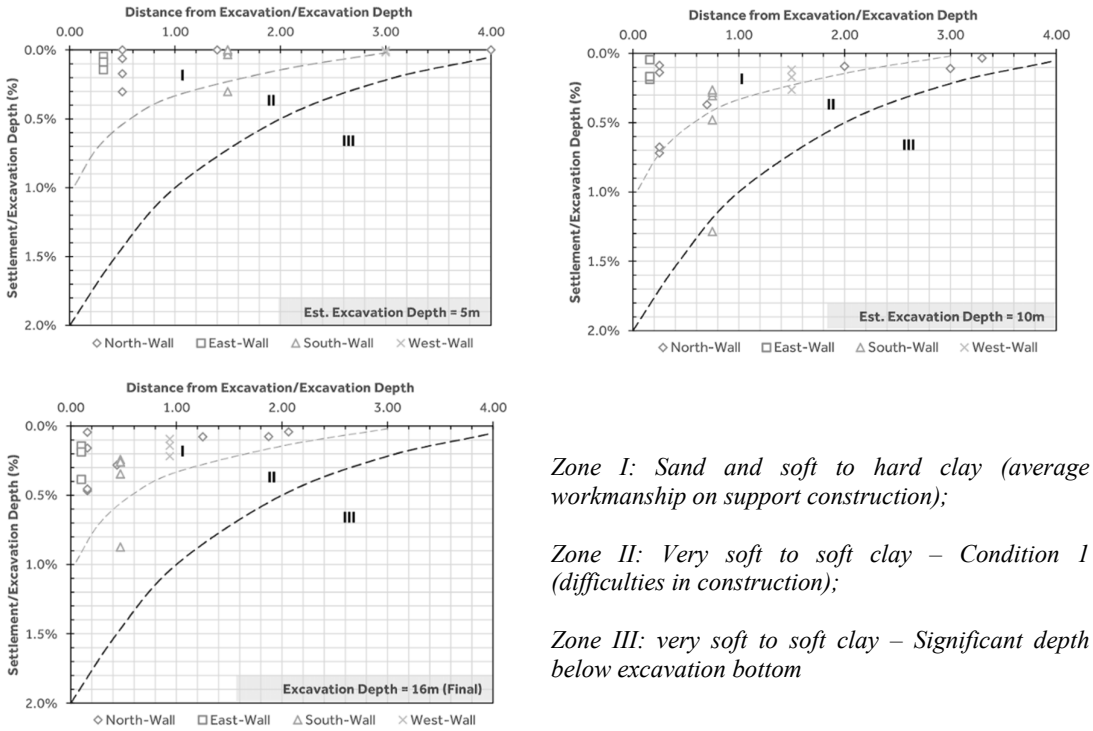


Figure 14. Comparison of predicted and actual wall deformations; West Wall (top left), North Wall (top right), South Wall (bottom left), and East Wall (bottom right)

The highest recorded lateral movement was at the North wall (INC-4), where highly-fractured limestone was encountered and the rock benching was over-excavated (Figure 14, top right). In another case at the East wall, where the rate of wall deformation was larger than predicted as a result of deeper rock head (INC-9 in Figure 14, bottom right), a corrective measure in the form of installing additional ground anchors at that level was carried out.

Plots of normalized ground settlement and distance of monitoring points from the excavation face for the different walls is shown in Figure 15. As shown in the monitoring results plotted in Figure 15, on one side of the site there was localized settlement of the ground. This was on a pedestrian walk way on the south west corner of the site. The reason behind the ground settlement was found out to be mainly due to loss of support to kerb wall. About 1.0 m high earth was removed behind the CBP walls upon which the kerb wall was leaning to make way for site offices and storages.

Further, the monitoring data recorded for this project will be used to refine designs for future basement excavation projects in similar ground conditions.



Zone I: Sand and soft to hard clay (average workmanship on support construction);

Zone II: Very soft to soft clay – Condition 1 (difficulties in construction);

Zone III: very soft to soft clay – Significant depth below excavation bottom

Figure 15. Normalized plots of ground settlement vs. excavation depth and distance from excavation face. Plots show actual, recorded settlements compared to Peck's (1969) plot for excavations

5. SUMMARY AND CONCLUSIONS

This project shows the effectiveness of mixed solutions for basement retention particularly in karst ground. The provided solution for excavation retention proved successful. Performance of the retention system was satisfactory and within the predicted movement envelop. Excavation was carried out efficiently; on account of no obstructions due to struts, no problems with ground water inflow, and faster excavation was possible.

Pre-execution site investigation works, such as rock probing, were vital to arrive at an optimized design. Precise mapping of the rock head profile was used to determine the wall types to be implemented. Using a mixed solution for the excavation retention enabled tailor-made solutions for each potential risk, while also allowing cost and time saving to the Client.

In this project, it was evident that the construction aspect of basement excavations is important. In karst ground, as the variables that affect the design are numerous, it was vital to follow the construction closely. The construction process of the retention system was examined closely to ensure the design is

being realized and the required quality is being achieved. Monitoring was carried out consistently and design was revised progressively when the need arose.

REFERENCES

Gobbett, D.J., Hutchison, C.S. and Burton, C.K., 1973. Geology of the Malay Peninsula.

Hoek, E., Carranza-Torres, C. and Corkum, B., 2002. Hoek-Brown failure criterion-2002 edition. *Proceedings of NARMS-Tac*, *1*, pp.267-273.

Horvath, R.G. and Kenney, T.C., 1979. Shaft resistance of rock-socketed drilled piers. *Deep Foundations*, pp.182-214.

Liew S.S., Khoo C.M., Tan S.T., and Loh Y.E., 2010, May. Review of Load Test Performance of Bored Pile Foundation in Weathered Meta-Sedimentary Formation and Kuala Lumpur Limestone. *The 17th Southeast Asian Geotechnical Conference Taipei, Taiwan*.

Marinos, P. and Hoek, E., 2000, November. GSI: a geologically friendly tool for rock mass strength estimation. In *ISRM International Symposium*. International Society for Rock Mechanics.

Marinos, P., Marinos, V. and Hoek, E., 2007. Geological Strength Index (GSI). A characterization tool for assessing engineering properties for rock masses. *Underground works under special conditions. Taylor and Francis, Lisbon*, pp.13-21.

Peck, R.B., 1969. Advantages and limitations of the observational method in applied soil mechanics. *Geotechnique*, *19*(2), pp.171-187.

Tan, B.K. 2006. Urban geology of Kuala Lumpur and Ipoh, Malaysia. *Engineering geology of tomorrow's cities. Geological Society, London, Eng Geol Spec Publ*, *22*.

Tan, Y.C. and Chow, C.M., 2006, August. Foundation design and construction practice in limestone area in Malaysia. In *HKIE-IEM Seminar on Geotechnical Works in Marble, Hong Kong*.

Topolnicki, M., 2004. In situ soil mixing. *Ground Improvement*, *2*, pp.331-428.

Yee, Y.W. and Chua, C.G., 2008. Case Studies: Deep Soil Mixing in Excavation. In *Seminar on Excavation and Retaining Wall*.

DETERMINATION OF BASAL HEAVE STABILITY FOR STRUTTED EXCAVATIONS SUPPORTED WITH JET GROUT BASE SLAB

Anthony T. C. Goh, Assoc. Prof., School of CEE, Nanyang Technological University, Singapore, +65-67905271, ctcgoh@ntu.edu.sg

ABSTRACT

For deep excavations in soft clay, it is common to use jet grouting piles (JGP) prior to excavation to minimize wall deflections and ground settlement, and to prevent basal heave instability. In this paper, finite element analyses were carried out to assess the basal heave factor of safety for excavations in soft clay supported by JGP. Comparison of the factor of safety from the finite element analyses with limit equilibrium methods was then performed. Subsequently, to account for the uncertainties in the soil and JGP properties, a simplified reliability analysis procedure is proposed to estimate the probability of basal heave failure for deep excavations supported by JGP.

Keywords: basal heave, clay, excavation, finite element, jet grout slab, factor of safety

INTRODUCTION

Jet grout piles (JGP) are often used to prevent basal heave instability and to minimize excessive wall and ground movements associated with deep excavations in soft clay deposits (Shirlaw 2003; Wen 2005; Ou 2006). The jet grouting process which is carried out prior to any excavation works produces a series of short overlapping grout columns resulting in a "continuous" base slab (commonly termed as jet grout pile or JGP) below the final excavation level that spans across the entire excavation (Gaba 1990; Hsieh et al. 2003; Ho and Hu 2006). Typically, the JGP thickness ranges from 2 m to 4 m.

The focus of this paper is on the assessment of basal heave instability for deep excavations in clay stabilized with JGP. Finite element analyses were first conducted to determine the basal heave factor of safety for deep excavations in clay with JGP. Comparisons were then carried out with factors of safety based on conventional limit equilibrium methods. Since the conventional factor of safety approach does not explicitly reflect the uncertainties of the soil and JGP properties, it is demonstrated in this paper that a simple reliability based approach (Hasofer and Lind 1974) can be used to assess the probability of basal heave failure.

LIMIT EQUILIBRIUM METHOD

For excavations is clay, the Terzaghi (1943), Bjerrum and Eide (1956) and Eide et al. (1972) methods which are based on bearing capacity theory, are commonly used to determine the basal heave factor of safety. Another commonly adopted method in Japan and Taiwan is the slip circle method which involves taking moments about the lowest strut level (JSA 1988; Hsieh et al. 2008; Luo et al. 2012). The slip circle method has also been applied for excavations with a JGP at the base by incorporating the undrained shear strength of the JGP. In the slip circle method, the basal heave factor of safety FS_{slip} is assessed by taking moments about the lowest strut level (Fig. 1)

$$FS_{slip} = \frac{M_r}{M_d} = \frac{R\int_0^{\theta+\pi/2} c_u d\omega + R\int_0^{\beta} c_{uJ} d\omega}{W(R/2) + q(R^2/2)} \quad [1]$$

where M_r = resisting moment; M_d = driving moment; R = radius of the failure slip circle; W = weight of the soil mass behind the wall and above the excavation level; q = surcharge pressure; H = excavation depth; D = wall penetration depth; B = excavation width; c_u = clay undrained shear strength; c_{uJ} = JGP undrained shear strength; θ and β = angles shown in Fig. 1.

In this paper, another limit equilibrium method called the modified Terzaghi method (Wong and Goh 2002; Goh et al. 2008) is also used to assess the basal heave factor of safety for excavations involving a JGP layer. In this method, it is assumed that failure occurs beneath the base of the wall and is partially resisted by the JGP-wall adhesion $f_s = \alpha_J c_{uJ}$ (Eide et al. 1972), as illustrated in Fig. 2, in which α_J is the JGP-wall adhesion factor. The factor of safety FS_{mT} can be expressed as:

$$FS_{mT} = \frac{5.7c_{ub}B_1 + c_{uh}H + c_{ud}D + f_sD}{(\gamma H + q)B_1} \quad [2]$$

where $B_1 = (B/\sqrt{2})$, H = excavation depth, and D = depth of wall penetration. The value of 5.7 in the first term of the numerator of Eq. [2] corresponds to the bearing capacity factor N_c for a rough footing. As illustrated in Fig 2, c_{uh} is the undrained shear strength of the clay from the ground surface to the final depth of excavation H, c_{ud} is the undrained shear strength of the clay from depth H to the tip of the wall, and c_{ub} is the undrained shear strength of the clay below the final excavation level.

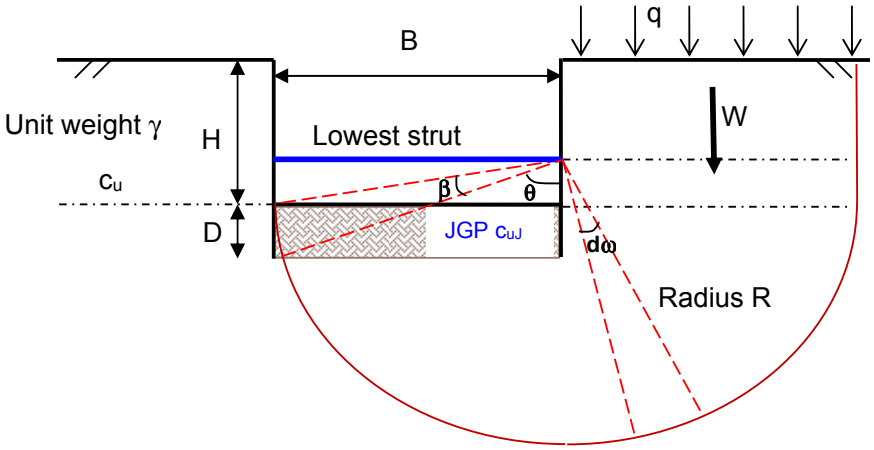


Fig. 1. Slip circle method for basal heave stability of jet grout pile

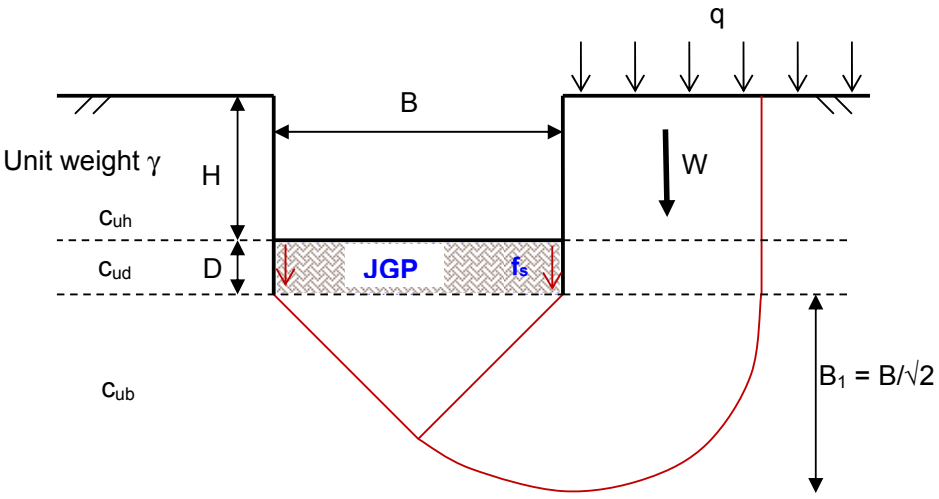


Fig. 2. Modified Terzaghi method for basal heave stability of jet grout pile

FINITE ELEMENT MODEL

Extensive plane strain finite element analyses were carried out to assess the basal heave factor of safety for excavations with JGP. The parametric study was performed using the finite element software Plaxis (Brinkgreve et al. 2011). A typical very refined mesh comprising 3,226 elements and 26,409 nodes is shown in Fig. 3.

Because of symmetry, only half the cross-section was considered. The soil was modeled by 15-noded triangular elements. The wall structural elements were assumed to be linear elastic and were modeled by 5-noded beam elements. The struts (not shown in Fig. 3) were modeled by linear elastic 3-noded bar elements. The interface elements that model the slippage between the soil and the wall consist of 10-noded joint elements. The shear response of the interface element is controlled by an elastic–perfectly plastic Coulomb shear strength criterion. The nodes along the side boundaries of the mesh were constrained from displacing horizontally while the nodes along the bottom boundary were constrained from moving horizontally and vertically. The right vertical boundary extends far from the excavation (~5B) to minimize the effects of the boundary restraints.

The Hardening Soil (HS) constitutive relationship was used to model the undrained behavior of the clay and the JGP. The HS model is an elastic-plastic soil model based on the classical plasticity theory (Schanz et al. 1999; Brinkgreve et al. 2011) for simulating the behavior of soils. The model involves frictional hardening characteristics to model plastic shear strain in deviatoric loading, and cap hardening to model plastic volumetric strain in primary compression. Failure is defined by the Mohr Coulomb failure criterion. This model has been used successfully for analyses of deep excavations by a number of researchers in Singapore (Teo and Wong 2012) and elsewhere (Finno et al. 2007; Bryson and Zapata-Medina 2012; Surarak et al. 2012). For this study, only cases with a homogeneous clay layer with constant undrained shear strength c_u were considered. The soil is assumed to be subjected to undrained shearing during excavation. The depth to the hard stratum is assumed to be large. The properties of the JGP (see Table 1) are based on common design values used in Singapore (Ho and Hu 2006). In addition, it is assumed that the wall has enough capacity not to fail under the action of deep-seated soil movements. A total of 55 different cases were analyzed. The range of geometrical properties of the excavation that were analyzed, and the assumed wall, JGP and soil properties are shown in Table 1.

The construction sequence simulation comprised the following steps: (1) the wall and JGP are installed ("wished into place") without any disturbance in the surrounding soil; (2) the soil is excavated uniformly in 2 m intervals, and struts are installed until the final depth H is reached. The stability of the excavation is then determined using the shear strength reduction technique. This technique has been used by various authors including Griffiths and Lane (1999), Hammah et al. (2007), Zhang and Goh (2012), and Do et al. (2013). The method is now available in many commercial finite element and finite difference programs. The procedure essentially involves repeated analyses by progressively reducing the shear strength properties until global failure occurs. This critical strength reduction value is taken to be the basal heave factor of safety FS_{FE}.

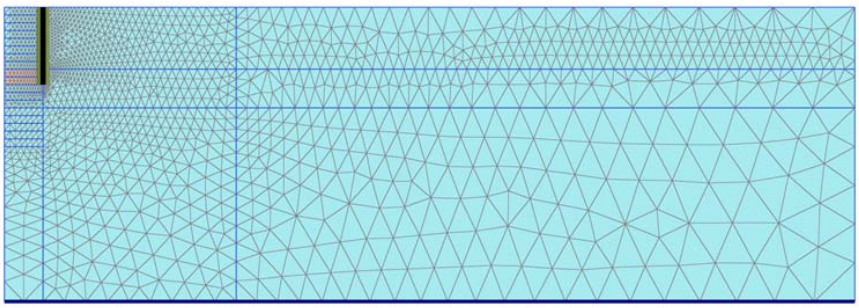


Fig. 3. Typical finite element mesh (struts not shown)

Table 1. Summary of JGP, soil and geometrical properties

Parameter	Range of values
Geometrical and wall properties	
Excavation width B (m)	10 – 60
Excavation depth H (m)	16 – 24
Depth of wall penetration D (m)	3 - 8
Thickness of JGP (m)	3 - 8
Wall stiffness EI (kNm^2/m)	4.032×10^6
Soil and JGP properties	
Soil unit weight γ (kN/m^3)	16
Soil undrained shear strength c_u (kPa)	30 - 80
Soil modulus ratio E_{50}^{ref}/c_u	300
Unloading and reloading stiffness E_{ur}^{ref}	$3\ E_{50}^{ref}$
Unloading and reloading Poisson's ratio υ_{ur}	0.2
Stress-dependent stiffness ratio m	0
Failure ratio R_f	0.9
JGP shear strength c_{uJ} (kPa)	300 - 500
JGP E_{50}^{ref} (MPa)	150
JGP-wall adhesion factor α_J	0.2 – 1.0

RESULTS

For brevity, only some general trends of the finite element analyses are highlighted. The influence of the width of the excavation B is shown in Fig. 4 for the cases with H = 16 m, D = 4 m, c_u = 50 kPa and f_s = 300 kPa. The basal heave factor of safety FS_{FE} decreases with the increase of the excavation width. Comparing the factor of safety with and without the JGP, the increase in FS_{FE} with the JGP is more significant for B ≤ 20 m. For example, for the case with B = 20 m, the installation of a 4 m thick JGP increased the basal heave factor of safety by 31% compared with a 16% increase for B = 30 m.

Fig. 5 shows the influence of the JGP-wall adhesion factor α_J on the factor of safety for the cases with B = 20 m, H = 16 m, D = 4 m, c_u = 50 kPa and c_{uJ} = 300 kPa. The factor of safety reduces significantly for $\alpha_J \leq 0.67$. For example, the installation of the JGP increased the FS_{FE} by 31% for α_J = 1, compared with an increase of 17% for α_J = 0.5. The results indicate that the interface friction between the jet grout slab and the wall is a key component of the resistance of the excavation system to basal heave failure.

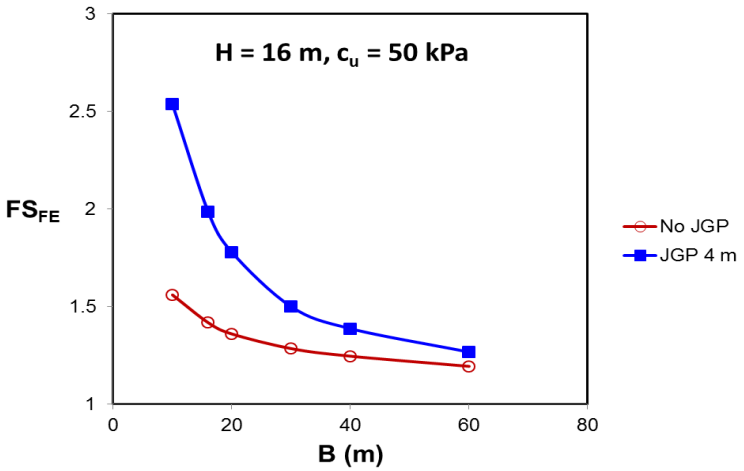


Fig. 4. Effects of excavation width B on FS_{FE}

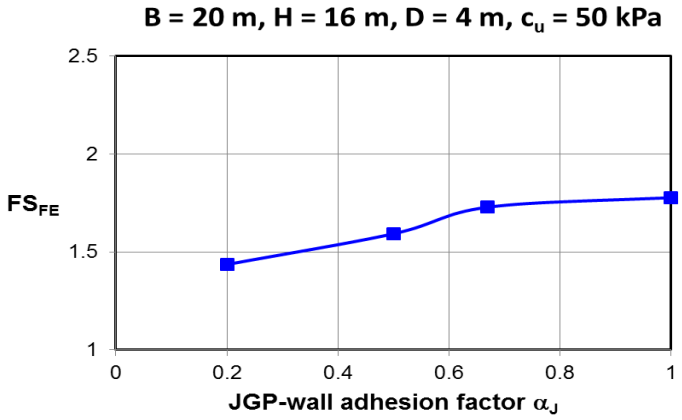


Fig. 5. Effects of JGP-wall interface adhesion factor on FS_{FE}

Fig. 6 shows the comparison of the factor of safety computed based on the slip circle method (FS_{slip}) and the modified Terzaghi method (FS_{mT}) with FS_{FE}. Generally, there is more scatter in the FS_{slip} predictions using the slip circle method compared with the predictions using FS_{mT}. The modified Terzaghi method generally predicts reasonable values of the basal heave factor of safety compared with FS_{FE}.

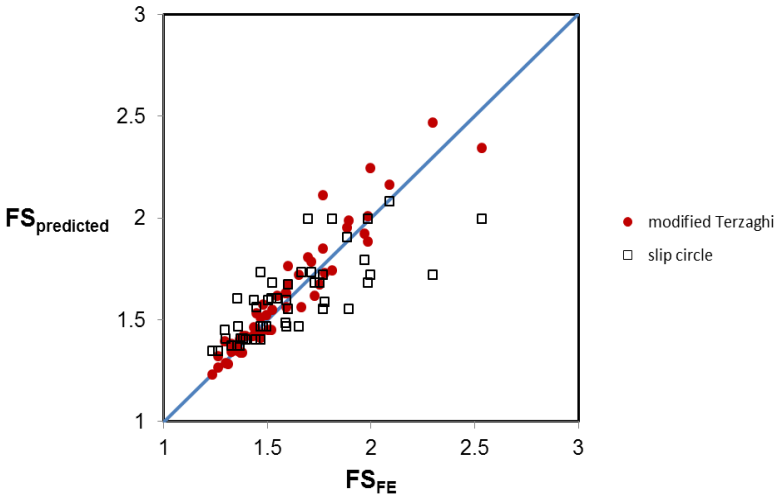


Fig. 6. Plot of predicted FS versus FS_{FE}

RELIABILITY ANALYSES

In order to quantify the inherent variability of the JGP and soil properties, a probabilistic approach using reliability analysis has been carried out. Clear expositions of the reliability approach are found in various publications (Ang and Tang 1984; Baecher and Christian 2003). In the reliability index approach (Hasofer and Lind 1974), the uncertainties in the design parameters (X_i) are represented by their mean value points (m_{Xi}) and standard deviations (σ_{Xi}), and safety is determined by measuring the shortest distance (measured in units of directional standard deviations) from the safe mean-value point to the most probable failure combination of the parameters on the limit state surface (Low 2005). Examples of the use of reliability to assess basal heave stability in conventional excavations without JGP can be found in Park et al. (2007), Goh et al. (2008), and Wu et al. (2010).

If the geometrical properties of the excavation (B, B_1, and H) and the depth of the wall penetration D are assumed to be deterministic, and the random variables (c_{ub}, c_{uh}, c_{uh}, f_s, γ and q) are normally distributed, then the limit state surface is linear (planar) and the reliability index β can be determined as (Goh et al. 2008):

$$\beta = \frac{5.7m_{cub}B_1 + m_{cuh}H + m_{cud}D + m_{fs}D - m_{\gamma}HB_1 + m_qB_1}{[(5.7B_1\sigma_{cub})^2 + (H\sigma_{cuh})^2 + (D\sigma_{cud})^2 + (D\sigma_{fs})^2 + (HB_1\sigma_{\gamma})^2 + (B_1\sigma_q)^2]^{0.5}} \quad [3]$$

in which the symbols m_{Xi} denotes the mean value and σ_{Xi} denotes the standard deviation for the random variable X_i. Based on Eq [3], analyses were carried out to assess the probability of failure P_f ($FS \leq 1$) for excavations in clays with FS_{mean} values ranging from 1.2 to 1.7, where FS_{mean} is the factor of safety computed using the mean values of the parameters. In all the analyses, $c_{uh} = c_{ud} = c_{ub} = c_u$, and the mean and the coefficient of variation COV of the surcharge adjacent to the excavation q and the unit weight of the clay γ are assumed to be unchanged ($mean_q$ = 10 kPa/m, COV_q = 0.2; $mean_\gamma$ = 16 kN/m^3, COV_γ = 0.15). Based on the database by Phoon and Kulhawy (1999) the inherent variability of the undrained shear strength of clay is 0.3. Hence, analyses were carried out assuming the coefficient of variation COV of the soil undrained shear strength (for simplicity, the term COV_{cu} is used) was 0.3, following which comparisons were carried out for COV_{cu} = 0.2.

The results of the analyses for COV_{cu} = 0.3 are shown in Fig. 7 and Table 2 for the cases with B = 20 m, H = 16 m, D = 4 m, and c_{uJ} = 300 kPa, while the results for COV_{cu} = 0.2 are shown in Fig. 8 and Table 3. The FS_{mean} is calculated based on Eq. [2]. The plots highlight that the same factor of safety can have significantly different levels of risk depending on the degree of uncertainty of COV_{cu} and COV_{fs}. The results indicate the significant influence of the COV_{fs} of the JGP-wall adhesion on the probability of failure P_f as the COV of f_s is increased from 0.1 to 0.6. As expected, for a given FS_{mean}, the probability of failure P_f increases as the COV_{fs} increases. For example, for FS_{mean} = 1.5 and COV_{cu} = 0.3, P_f increased 41% as the COV_{fs} increases from 0.1 to 0.4. For FS_{mean} = 1.5 and COV_{fs} = 0.6, the probability of basal heave failure is still fairly high (approximately 9%). The proposed reliability approach in Eq. [3] provides a systematic method for evaluating the influences of the uncertainties in the various parameters affecting FS_{mean} and to assist design engineers assess the acceptable level of risk.

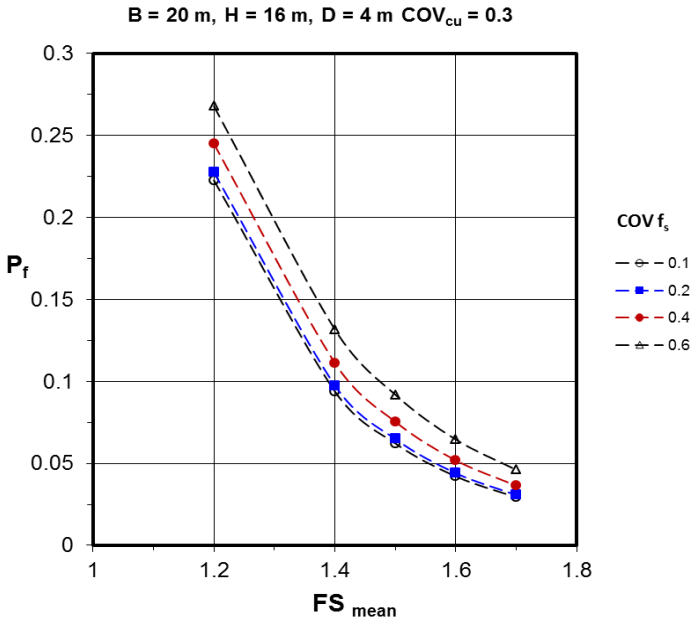


Fig. 7. Plot of P_f for COV_{cu} = 0.3 (B = 20 m, H = 16 m, D = 4 m, c_{uJ} = 300 kPa)

Table 2. Probability of failure for various COV_{fs} for COV_{cu} = 0.3

	P_f (FS ≤ 1)			
FS_{mean}	COV_{fs} = 0.1	COV_{fs} = 0.2	COV_{fs} = 0.4	COV_{fs} = 0.6
1.2	0.223	0.228	0.245	0.268
1.4	0.094	0.098	0.111	0.132
1.5	0.062	0.065	0.075	0.092
1.6	0.042	0.044	0.052	0.065
1.7	0.029	0.031	0.036	0.046

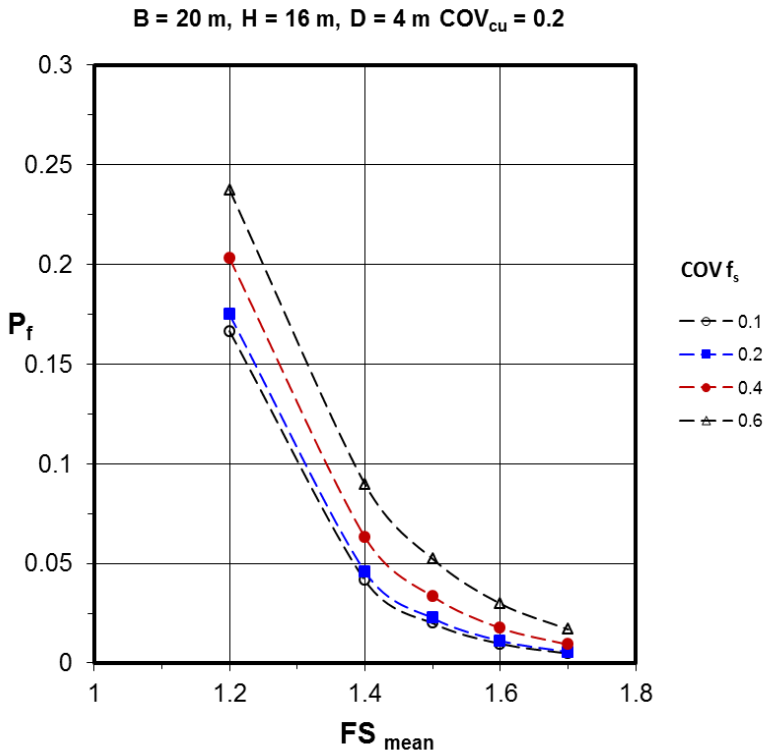


Fig. 8. Plot of P_f for COV_{cu} = 0.2 (B = 20 m, H = 16 m, D = 4 m, c_{uJ} = 300 kPa)

Table 3. Probability of failure for various COV_{fs} for COV_{cu} = 0.2

	P_f (FS ≤ 1)			
FS_{mean}	COV_{fs} = 0.1	COV_{fs} = 0.2	COV_{fs} = 0.4	COV_{fs} = 0.6
1.2	0.167	0.175	0.203	0.237
1.4	0.041	0.046	0.063	0.090
1.5	0.020	0.023	0.034	0.052
1.6	0.010	0.011	0.018	0.030
1.7	0.005	0.006	0.009	0.017

SUMMARY

Finite element analyses were carried out to assess the basal heave factor of safety for deep excavations in soft clay supported by JGP. A total of 55 different cases with different geometrical properties of the excavation, JGP and soil properties were considered. The basal heave factor of safety FS_{FE} was found to decrease with the increase of the excavation width. Comparing the factor of safety with and without the JGP, the increase in FS_{FE} with the JGP is more significant for $B \leq 20$ m. The finite element analyses also highlight that the interface friction between the jet grout slab and the wall is a key component of the resistance of the excavation system to basal heave failure.

Comparison of the FS_{FE} values with the predictions based on the slip circle method and the modified Terzaghi method was also performed. Generally, there is more scatter in the FS_{slip} predictions using the slip circle method compared with the predictions using FS_{mT}. The modified Terzaghi method generally predicts reasonable values of the basal heave factor of safety compared with FS_{FE}.

A series of reliability analyses were then carried out to assess the basal heave factor of safety for excavations supported by JGP. The results show that the same factor of safety can have vastly different levels of risk depending on the degree of uncertainty of the design parameters. The proposed reliability approach in Eq. [3] provides a systematic method for evaluating the influences of the uncertainties in the various parameters affecting FS_{mean} and can be used to assist design engineers assess the acceptable level of risk.

References

Ang, A.H.S. and Tang, W.H. 1984. Probability concepts in engineering planning and design. Vol. II - Decision, risk and reliability. John Wiley & Sons, New York.

Baecher, G.B. and Christian, J.T. 2003. Reliability and statistics in geotechnical engineering. John Wiley & Sons, New York.

Bjerrum, L. and Eide, O. 1956. Stability of strutted excavations in clay. Geotechnique. 6(1), 32-47.

Brinkgreve, L.B.J., Engin, E. and Swolfs, W.M. 2011. Plaxis user manual, PLAXIS bv, Netherlands.

Bryson, L. and Zapata-Medina, D. 2012. Method for estimating system stiffness for excavation support walls. J. Geotech. Geoenviron. Eng. ASCE 138 (9), 1104-1115.

Do, T., Ou, C.Y., and Lim, A. 2013. Evaluation of factors of safety against basal heave for deep excavations in soft clay using the finite-element method. J. Geotech. Geoenviron. Eng. ASCE 139 (12), 2125-2135.

Eide, O., Aas, G., and Josang, T. 1972. Special applications of cast-in-place walls for tunnels in soft clay in Oslo. Pub. 91, Norwegian Geotechnical Institute, Oslo, 63-72.

Finno, R.J., Blackburn, J.T., and Roboski, J. F. 2007. Three-dimensional effects for supported excavations in clay. J. Geotech. Geoenviron. Eng. ASCE 133 (1), 30-36.

Gaba, A.R. 1990. Jet grouting at Newton Station, Singapore. Proc. 10th Southeast Asian Geotech Conf., Taipei, Taiwan, SEAGC, 77-79.

Goh, A.T.C, Kulhawy, F.H., and Wong, K.S. 2008. Reliability assessment of basal-heave stability for braced excavations in clay. J. Geotech. Geoenviron. Eng. ASCE 134 (2), 145-153.

Griffiths, D.V. and Lane, P.A. 1999. Slope stability analysis by finite elements. Géotechnique 49 (3), 387-403.

Hammah, R.E., Yacoub, T., and Curran, J.H. 2007. Serviceability-based slope factor of safety using the shear strength reduction (SSR) method. The Second Half Century of Rock Mechanics 11th Congress of the International Society for Rock Mechanics, Taylor & Francis, 1137-1140.

Hasofer, A.M. and Lind, N.C. 1974. An exact and invariant first-order reliability format. J. Eng. Mech., ASCE 100 (1), 111-121.

Ho, C.E. and Hu, S. 2006. Numerical analysis of jet grout elements for braced excavation in soft clay. Proc. ASCE GeoCongress 2006: Geotechnical Engineering in the Information Technology Age, Atlanta, Georgia. 1-6.

Hsieh, H.S., Wang, C.C., and Ou, C.Y. 2003. Use of jet grouting to limit diaphragm wall displacement of a deep excavation. J. Geotech. Geoenviron. Eng. ASCE 129 (2), 146-157.

Hsieh, P.G., Ou, C.Y., and Liu H.T. 2008. Basal heave analyses of excavations with consideration of anisotropic undrained strength of clay. Can. Geotech. J. 45, 788-799.

JSA. 1988. Guidelines of design and construction of deep excavations. Japanese Society of Architecture, Tokyo, Japan.

Low, B.K. 2005. Reliability-based design applied to retaining walls. Geotechnique 55 (1), 63-75.

Luo, Z., Atamturktur, S, Cai, Y, and Juang, C.H. 2012. Reliability analysis of basal-heave in a braced excavation in a 2-D random field. Comp. Geot. 39, 27-37.

Ou, C.Y. 2006. Deep Excavation: Theory and Practice. Taylor & Francis Group, London.

Park, J.K., Blackburn, J.T., and Gardoni, P. 2007. Reliability assessment of excavation systems considering both stability and serviceability performance. Georisk 1 (3), 123-141.

Phoon, K.K. and Kulhawy, F.H. 1999. Characterization of geotechnical variability. Can. Geot. J. 36 (4), 612-624.

Schanz, T., Vermeer, P.A., and Bonnier, P.G., 1999. The hardeing soil model -formulation and verification. Proc., Beyond 2000 in Computational Geotechnics-10 years PLAXIS, Balkema, Rotterdam, 281-296.

Shirlaw, J.N. 2003. Jet grouting soft clays for tunneling and deep excavations – design and construction issues. Proc. 3rd Int. Conf., Grouting and Grout Treatment, ASCE 1, 257-268.

Surarak, C., Likitlersuang, S., Wanatowski, D., Balasubramaniam, A., Oh, E., and Guan, H. 2012. Stiffness and strength parameters for hardening soil model of soft and stiff Bangkok clays. Soils Found. 52 (4), 682–697

Terzaghi, K. 1943. Theoretical soil mechanics. John Wiley & Sons, New York.

Teo, P.L. and Wong, K.S. 2012. Application of the Hardening Soil model in deep excavation analysis. The IES Journal Part A: Civil & Struct. Eng. 5 (3), 152-165.

Wen, D. 2005. Use of jet grouting in deep excavations. In Ground improvement – case histories. Editors: B. Indraratna & J. Chu. Elsevier. 357-370.

Wong, K.S. and Goh, A.T.C. 2002. Basal heave stability for wide excavations. Proc. 3rd Int. Symp. Geotech. Aspects of Underground Construction in Soft Ground, Toulouse, 699-704.

Wu, S.H., Ou, C.Y., Ching, J., and Juang, C.H. (2010). Reliability-based design for basal heave in an excavation considering spatial variability. In: GeoFlorida 2010: Advances in Analysis, Modeling & Design, Geotechnical Special Publication No. 199, ASCE, West Palm Beach, Florida, 1914-1923.

Zhang, W.G. and Goh, A.T.C. 2012. Reliability assessment on ultimate and serviceability limit states and determination of critical factor of safety for underground rock caverns. Tunnel Underg. Space Technol. 32, 221–230.

PERFORMANCE OF FOOTINGS IN ROCK BASED ON SERVICEABILITY

CM Haberfield

1 INTRODUCTION

Around the world, there is a demand for larger structures, tall buildings and large bridges. While good footing design is important for all structures, it is even more important in the case of large structures. Recent experience with footing design for tall buildings (e.g. Burj Al Alam development and Nakheel Tower in Dubai, the Gate of Kuwait in Kuwait, the City Centre Project in Bahrain and Eureka Tower and Freshwater Place in Melbourne) has shown the benefits of investing in footing planning, design and construction (Haberfield, 2011, Poulos and Bunce, 2007).

The footing systems for most of these projects include the use of deep bored piles or barrettes (piles of rectangular cross-section). Many use piled rafts where the piles, while acting to support the load, are primarily used to reduce settlements. A clear understanding of the factors controlling the behaviour of the footing system is needed to enable a good engineering design to be achieved. This starts with a sound understanding of the ground characteristics and individual pile performance, including adequate collection of data and testing. The best footing solution can then be found using recent improvements in data collection and analytical techniques, complex and highly capable computer-based models and the availability of high speed computers.

This paper focuses on the axial performance of deep bored piles socketed into rock – both their individual performance and their performance as part of a larger footing system. Recent research and construction practice is discussed. In practically all cases, serviceability conditions control the behaviour of the footings. Methods of establishing the parameters for input into sophisticated computer programs are described. Application of the methods to case studies is included and it is shown that the behaviour of individual piles can be closely predicted. These developments lead to lower construction costs, better constructability and shortened construction time because of the better understanding of footing behaviour.

2 FACTORS AFFECTING PERFORMANCE OF FOOTINGS ON ROCK

For a typical pile-supported footing, it is necessary to consider both individual pile, pile group and raft performance. These require consideration of the behaviour of the ground immediately beneath the surface raft or footing, along the pile shaft, and at and beneath the pile toe (Figure 1). Immediately beneath the surface raft or footing, the important factors are strength for bearing capacity and stiffness for settlement and interaction effects. Along the pile shaft, of most interest are strength for bearing, excavatability and stability; stiffness for settlement and interaction effects; geology and permeability for pile stability and, most importantly, pile shaft resistance. At the pile toe all the above factors for the pile shaft are present and in addition the pile end bearing is of interest. Below the toe, stiffness for pile settlement is important to at least a depth of twice the building width.

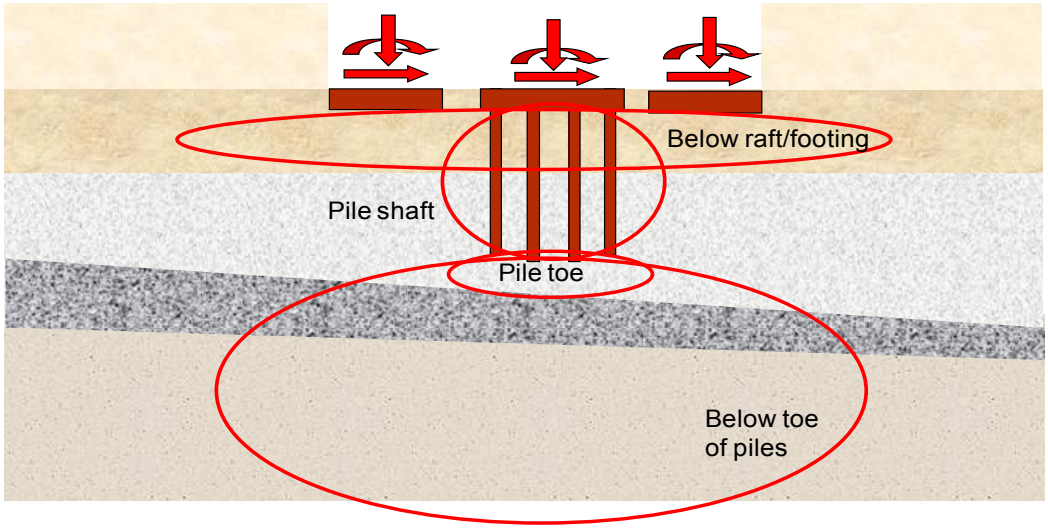


Figure1: Areas of interest for footing design

The principal factors affecting the performance of footings in rock (both individual piles and the entire footing system) are illustrated in Figure 2. For pile footings, construction issues include particularly the structural integrity of the pile shaft and the nature of the contact between the pile shaft and the pile concrete. The geotechnical design issues include the detailed interface properties, the joint geometry and boundary conditions and the rock properties (intact and mass). An understanding is needed of the strength, stiffness, permeability, geology and mineralogy of both the intact rock and the rock mass. This can lead to solving design issues of bearing capacity, serviceability, excavatability and stability of the piles that make up the footing system.

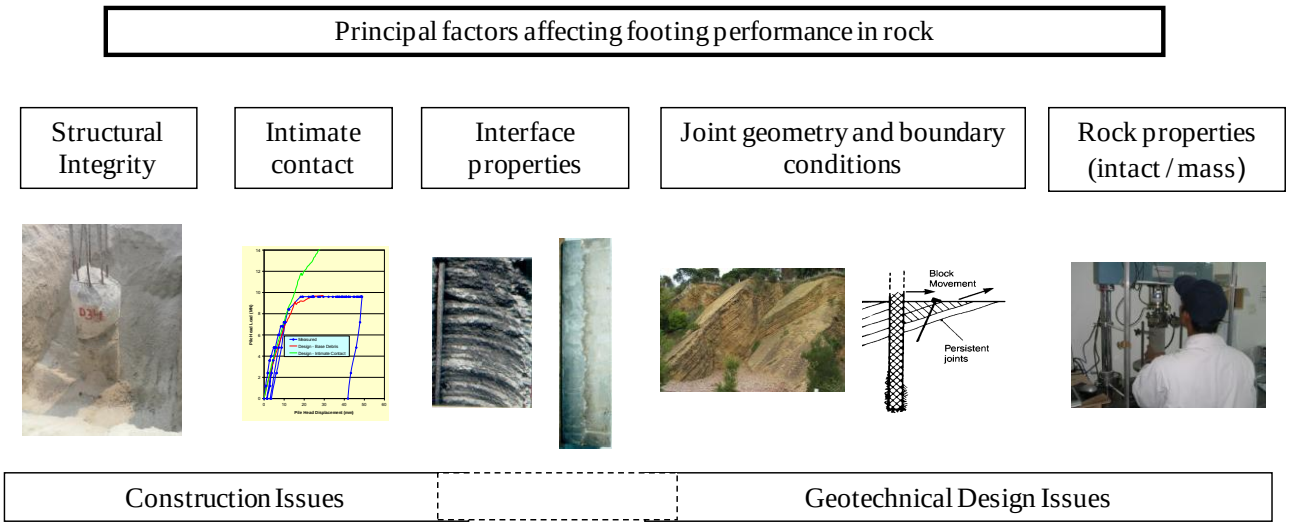


Figure 2: Factors affecting footing performance

Often, current design approaches group the geotechnical design issues together. This leads to misunderstanding of the true behaviour and conservatism and/or impractical and/or unsafe designs. However, before the performance of a footing system can be understood and effectively and economically designed, the performance of the individual components within the footing system need to be understood. As piles socketed into rock form a key component of these foundation systems, a detailed knowledge of the performance of piles socketed into rock is required.

3 AXIAL LOAD PERFORMANCE OF ROCK SOCKETED PILES

3.1 Background to rock socketed pile design and performance

Rock sockets can be constructed in rock materials ranging from very weak rock to high strength rock and from relatively intact rock to highly fractured rock. The nature and quality of the rock mass is one factor that has an impact on socket performance and needs to be accounted for in design.

Throughout the world, rock socketed piles have been, and are still by many engineers, designed by assessing estimates of allowable shaft and allowable base resistance, with little if any assessment of the displacement performance of the pile. Settlements are quoted based on experience rather than by calculation. The estimates of allowable shaft and base resistance are usually based on local ordinances, experience or empirical correlations with the uniaxial strength of the intact rock (e.g. see Figure 3).

There are several inconsistencies with this type of approach. These include:

i) specification of allowable shaft and base resistance values is not consistent with the limit state approach adopted in the current Australian Piling Code AS2159-2009.

ii) shaft and base resistance mobilise at different rates (see Figure 4). Typically, ultimate shaft resistance is mobilised at socket displacements of about 0.5 % to 1 % of socket diameter, whereas significant base resistance (even in clean sockets) is not mobilised until socket displacements of 10 % of socket diameter or higher. The rate of mobilisation of base resistance is further reduced if base debris is present. Simply summing factored ultimate base and shaft capacity values is not a valid approach due to the different mobilisation rates.

iii) Ultimate base resistance of piles in rock can be many (>5 and of the order of 10 to 20) times the uniaxial compressive strength (q_u) of the intact rock. For rocks with a q_u > 2 MPa, the concrete strength of the pile often governs the maximum design load of the pile. However, the displacements required to mobilise these loads can be significantly in excess of the serviceability requirements.

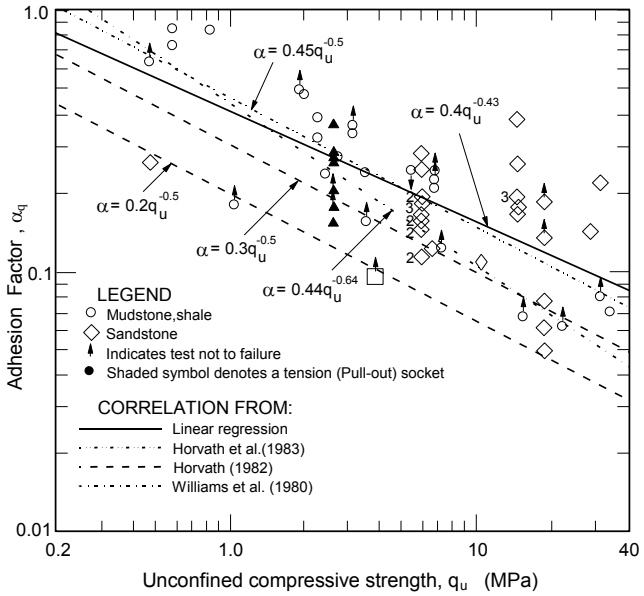


Figure 3: Empirical correlations between ultimate shaft resistance and rock uniaxial compressive strength (after Rowe and Armitage, 1984)

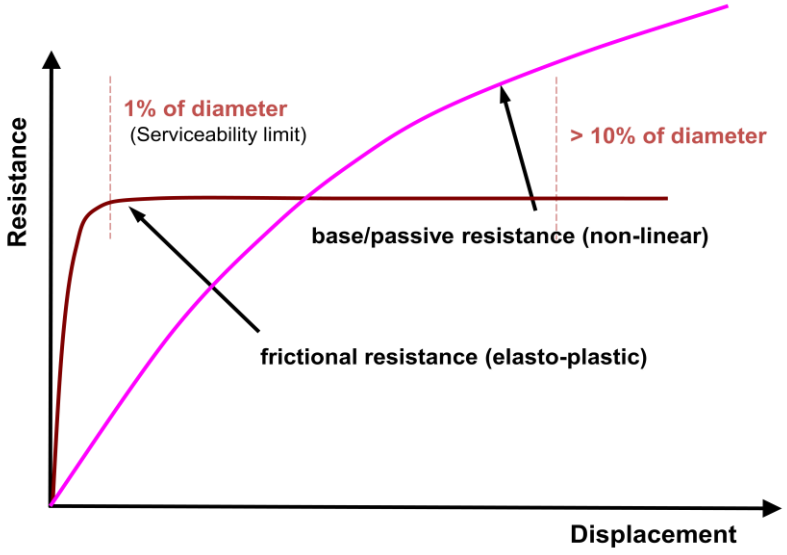


Figure 4: Rates of mobilisation of base and shaft resistance in rock socketed piles

A more rational approach is to design rocket socketed piles using techniques which account for the different mobilisation rates of shaft and base resistance. Such approaches need to be based on serviceability rather than working or ultimate load considerations as illustrated in the following example. The overall load-displacement response of a rock socketed pile is made up of contributions from the shaft and the base. If the base does not contribute to the response (due to the presence of base debris, for example), the load versus displacement response of the pile can be affected as shown in Figure 5 which shows the calculated load versus displacement response for 1 m diameter pile socketed into rock having a UCS of 3 MPa. There is a significant effect on response arising from the absence of base contribution but the effect decreases as the shaft length increases.

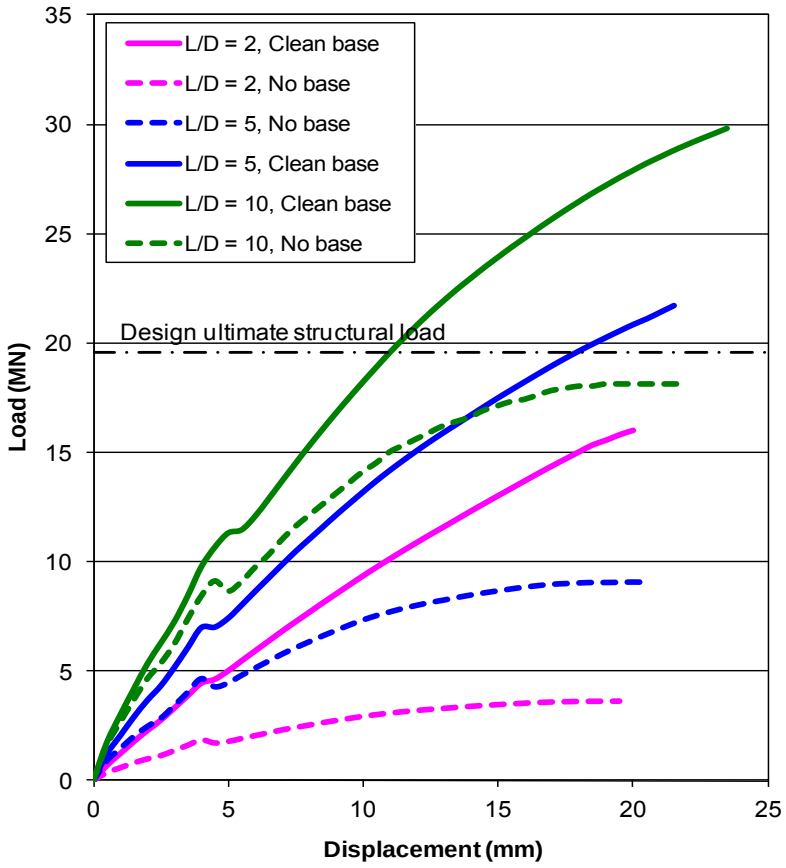


Figure 5: Pile load versus displacement performance depending on socket length, with and without base resisatnce

As illustrated by the above example, because of the different mobilisation rates of shaft and base resistance, the performance of most rock socketed piles at serviceability loads (SLS) is dependent predominantly on the shear resistance developed at the interface between the concrete shaft and the surrounding rock; i.e. shaft resistance. The base resistance also provides some resistance to the serviceability load, but in general its contribution is much less than shaft resistance (particularly for relatively long sockets in weak rock). For this reason it is common for rock socketed piles in relatively weak rock to be designed such that serviceability loads are carried predominantly by shaft resistance, and that the available base resistance is only relied on for ultimate loads (ULS).

For piles with short sockets (usually in more competent rock), base resistance is the primary component of socket resistance. As with long sockets, serviceability considerations also dictate the design of piles with short sockets.

Figure 3 could be interpreted to indicate that the uniaxial compressive strength (q_u) of the intact rock is the primary and only factor influencing the shaft resistance of piles in rock. This is not correct. While rock strength has an influence on shaft resistance, it is only one of many parameters that does so. Rock uniaxial compressive strength, provides a convenient and easily measured parameter for correlating shaft resistance values across a wide range of rock types (as shown in Figure 3).

The shaft resistance developed in a rock socket depends on many factors including shaft diameter, rock type, stiffness of the rock mass, strength of the intact rock and construction effects such as socket roughness, the thickness of smear zone or residual drilling fluid coating the socket walls and the pressure imposed onto the socket rock due to fluid concrete placement (e.g. Johnston, 1977; Williams and Pells, 1981: O'Neill and Hassan, 1994, Haberfield, 2000).

Shaft resistance is sensitive to a number of these parameters and as a result, socket performance can vary significantly from one site to another, even in the same rock type. This provides an explanation for the large scatter observed in published correlations between shaft resistance and rock strength (see Figure 3); for example Williams, Johnston and Donald (1980) or Rowe and Armitage (1984). The use of such empirical correlations requires the designer to choose a design shaft resistance from within a relatively wide scatter and as a result, a conservative assessment is usually made.

3.2 Shaft resistance considerations

3.2.1 Socket diameter and rock mass stiffness

The shaft resistance of the socket is a frictional response that depends on the normal stresses applied to the socket wall. It is not surprising then that interface roughness plays a critical role in the development of shaft resistance. The roughness of the pile-rock interface may vary from minimal to significant depending on the drilling method, the rock type, quality and jointing. Grooving of the rock socket to increase roughness may also be undertaken. As explained below, after pouring of the concrete pile an initial normal stress, σ_{no}, will be acting on the pile interface. On application of an axial load to the pile shaft, the shaft and rock mass will displace elastically until the shear stress at the interface becomes large enough to induce slip. Extensive laboratory experiments (Lam and Johnston, 1989; Kodikara and Johnston, 1994; Seidel and Haberfield, 2002a, Cheng, 1997) have shown that the stress at which slip occurs depends on the initial normal stress, the interface roughness, the residual friction angle of the rock and the degree of cementitious bond developed at the interface.

Once slip has initiated (usually at a relatively low shear stress unless the degree of cementation is high), geometrical constraints require that sliding will induce dilation on the socket interface, and an increase (Δr) in the socket radius. This dilation occurs against a surrounding rock mass that must deform to compensate for the enlargement of the socket diameter. An increased normal stress at the pile-rock interface results (Johnston, 1977).

The expansion of the socket can be approximated to the expansion of a cylindrical cavity in an infinite half space. Accordingly, the increase in normal stress, $\Delta\sigma_n$, for a socket can be related to the interface dilation Δr by

$$\Delta\sigma_n = \frac{E}{1+\nu}\frac{\Delta r}{r} \qquad (1)$$

where r is the original socket radius, E and ν are the rock mass Young's modulus and Poisson's ratio respectively. This expression can be rearranged to compute the normal stiffness, K, as

$$K = \frac{\Delta\sigma_n}{\Delta r} = \frac{E}{r(1+\nu)} \qquad (2)$$

Since the increase in socket radius due to dilation is relatively small compared to the initial socket radius, the normal stiffness, K, remains relatively constant. The shaft response is thus governed by a constant normal stiffness or CNS condition. The CNS condition is important to the work strengthening behaviour of socketed piles as progressive slip displacements of the shaft prior to peak resistance cause increasing normal stresses, and therefore increased interface shear strength.

Equation 1 predicts that the increase in normal stress on the pile-rock interface is dependent on the pile radius, the elastic deformation properties of the rock mass and the dilation of the interface (which depends on interface roughness). All of these parameters therefore have an impact on interface shear strength or socket shaft resistance.

The potential impact of socket diameter and rock mass stiffness (Young's modulus) on the shaft resistance versus displacement performance of a rock socketed pile in weak rock is illustrated by the following example. Consider a 0.9 m diameter rock socketed pile constructed in a weak shale which has a uniaxial compressive strength of approximately 3 MPa and a rock mass Young's modulus of 360 MPa. The socket is 1 m in length, has been roughened and the side wall cleaned of smear. An estimate of the shaft resistance versus displacement performance of the socket has been calculated using the analysis program ROCKET97 (Seidel and Haberfield, 2002b; Haberfield and Collingwood; 2006)). ROCKET97 has been tested against results from many static load tests on piles socketed into a range of rock types and found to provide an accurate estimate of measured socket performance (as set out later in this report). Other input parameters assumed for the ROCKET97 analysis include a residual friction angle of the shale of 24^o, an initial normal stress acting on the socket wall of 100 kPa and a mean roughness angle of 10^o. In each of the analyses described below only the relevant parameter (i.e. shaft diameter or rock mass Young's modulus) has been varied. All other parameters have been kept constant at the reference case values.

The potential calculated impact of varying only the shaft diameter (whilst keeping all other input parameters constant) is shown in Figure 6. It is clear from this figure that increasing the shaft diameter results in a decrease in the unit shaft resistance and in the initial stiffness of the socket displacement response. It is also evident that the decrease becomes less pronounced as the shaft becomes larger. The dependence on shaft diameter arises because of the constant normal stiffness condition - a larger shaft diameter means a lower normal stiffness and a smaller increase in normal stress with socket dilation, resulting in lower shaft resistance.

Figure 6 also indicates that two 600 mm sockets of a given length will carry the same load as one 2000 mm diameter socket of the same length (assuming of course that the structural capacity of the shafts is not exceeded). This outcome however depends on sockets of both diameters having a similar level of roughness. In practice, unless artificial roughening of the socket is carried out, the smaller diameter socket is likely to exhibit a lower level of roughness. Under these circumstances the increase in shaft resistance (from large diameter to small diameter) shown in Figure 6 is likely to be less pronounced.

The mass modulus of the rock is dependent on the rock strength and the discontinuities and other weakness in the rock mass. Rock mass modulus typically varies from a minimum of about 50 q_u for highly fractured rock to about 400 q_u for massive rock which is relatively free of discontinuities. For the assumed shale strength of 3 MPa, the mass modulus of the rock could potentially range from 150 MPa to 1200 MPa. Figure 7 shows the variation of shaft resistance for the example given above for rock mass moduli values varying between 75 MPa and 900 MPa. Figure 7 clearly shows that rock mass modulus has a significant impact on shaft resistance, with the higher modulus values resulting in significantly greater shaft resistance values.

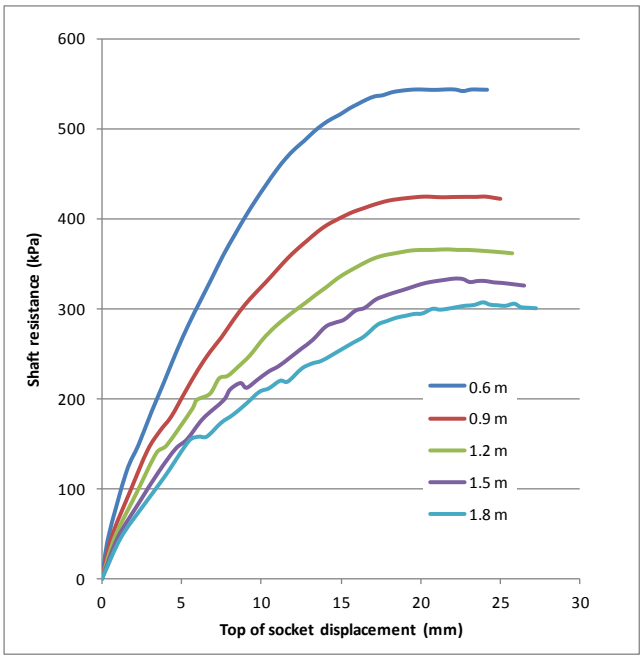


Figure 6: Calculated potential variation in shaft resistance with socket diameter

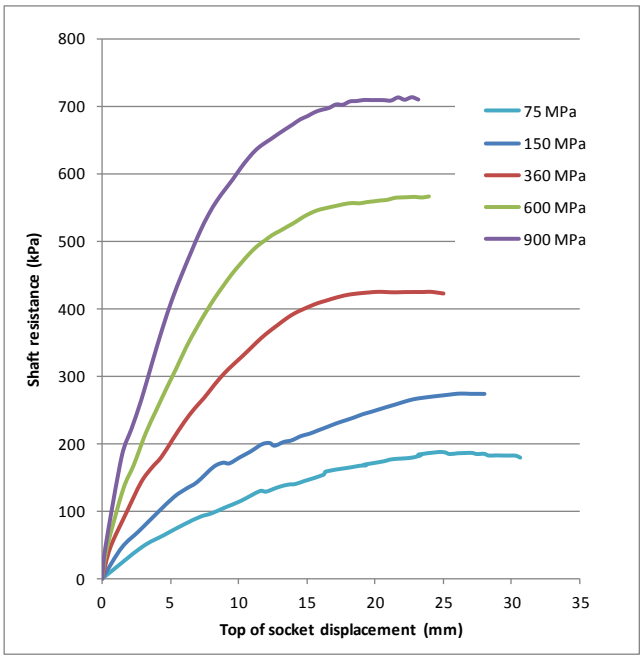


Figure 7: Calculated potential variation in shaft resistance with rock mass modulus

3.2.2 Pile length and initial normal stress

On completion of drilling, socket cleaning and placement of reinforcement, the concrete is placed into the socket usually either by free fall of by tremie. For a well constructed pile, the concrete pour produces an intimate contact with the base and walls of the socket and exerts a fluid pressure (or initial normal stress) on the side of the socket. The shaft resistance developed in the socket depends on the normal stress developed on the socket-rock interface which can be calculated from the sum of the initial normal stress due to concrete placements, σ_{no} and the additional normal stress ($\Delta\sigma_n = K\Delta r$) developed due to dilation (Δr) of the socket as follows:

$$\sigma_n = \sigma_{no} + K\Delta r \qquad (3)$$

Seidel and Haberfield (2002b) give recommendations for estimating the initial normal stress based on the work of Clear and Harrison (1985). For typical sockets, initial normal stress values could range from 25 kPa to 250 kPa. In general, the initial normal stress does not affect socket resistance significantly within the usual range of this parameter. However, if high initial normal stresses are generated by the use of expansive agents (e.g. Haberfield et al., 1994) socket resistance may be significantly increased.

Figure 8 shows the potential calculated variation of shaft resistance for the reference case pile set out above and for the expected range of initial normal stress from 25 kPa to 250 kPa. Only minor differences in peak shaft resistance are calculated across the range of normally expected initial normal stress values. However, the initial stiffness of the

response increases as the initial normal stress is increased. As a result, although a poor estimate of initial normal stress is likely to have only a minor influence on the predicted shaft capacity, it may have a major influence on the predicted displacements at working loads.

Figure 8 also shows that substantial improvements in pre-peak shaft performance can be obtained by artificially generating high initial normal stresses (e.g. 900 kPa shown in Figure 8) by (for example) use of expansive cements. Field investigations have been carried out by Haberfield et al. (1996) to see if this improved performance could be realised in practice. For relatively smooth sockets, significant increases in shaft resistance were achieved (three fold in some cases). However for very rough sockets, little if any increase in socket resistance was observed. In general initial stiffness increased with initial normal stress level. One potential disadvantage of using high initial normal stresses is the loss of ductility in the drilled shaft response. As shown in Figure 8 as the initial normal stress is increased to 900 kPa, the shaft response becomes much more brittle, with considerable loss of resistance after peak.

It should be noted that expansive agents are not commonly used in construction of rock socketed piles.

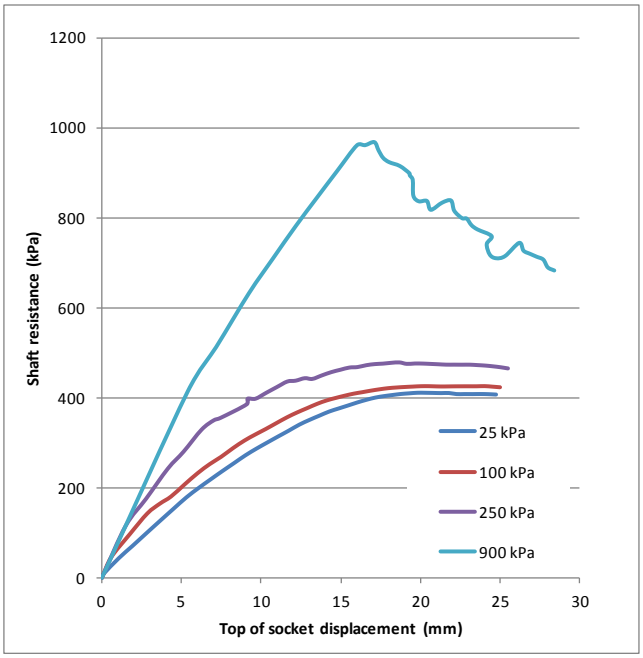


Figure 8: Calculated potential variation in shaft resistance with initial normal stress

3.2.3 Rock strength

To understand the significance of the rock strength, it is convenient to visualise the socket-pile interface as a rock joint made up of identical regular triangular asperities as shown in Figure 9(a). Such interfaces have been tested in direct shear by several investigators (e.g. Patton, 1966; Johnston and Lam, 1989; Seidel and Haberfield, 2002a) and two basic and apparently independent mechanisms have been identified : initial sliding along the surface of the asperities and then shearing through the intact asperities.

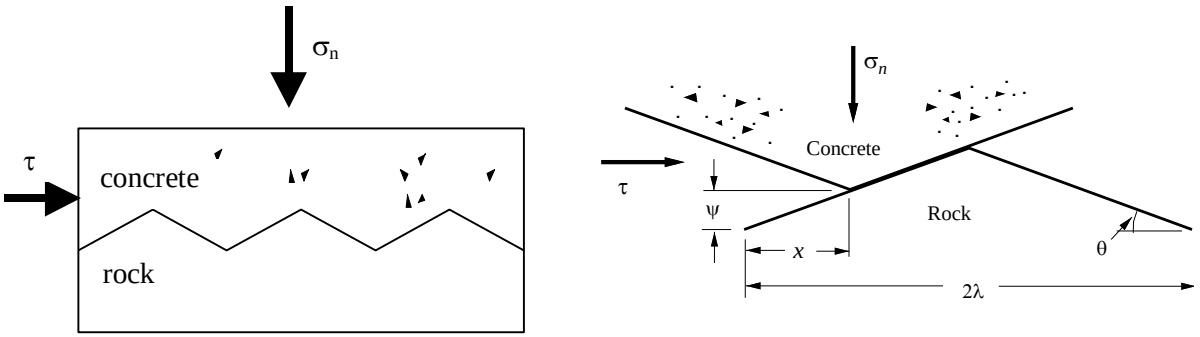
Initial sliding on uncemented interfaces is found to occur according to the following simple frictional relationship (Patton, 1966) :

$$\tau = \sigma \tan(\phi_b + \theta) \qquad (4)$$

where τ is the sliding shear stress, σ is the average normal stress applied to the joint, ϕ_b is the base or residual friction angle (ϕ_r) of the joint and θ is the asperity inclination.

After the initiation of interface slip, the contact area between the concrete and the rock is restricted to the leading asperity face, and progressively reduces as shear displacement progresses (Fig. 8b). Local normal stresses increase both as a consequence of the reduced contact area and as a result of the increasing normal stress due to dilation, ψ, and the CNS condition. A critical normal stress is reached at which the asperity can no longer sustain the loading and

individual asperity failure results. After asperity failure, post peak deformation continues by sliding along a failure surface through the rock asperity which is now at residual strength.



(a) Triangular asperity profile (b) Asperity during interface slip

Figure 9: Idealisation of socket roughness using regular triangular asperities

Although the approximation of a rock socket as a series of regular triangular asperities is simplistic, direct shear testing of more complex interfaces comprising random three dimensional roughness similar to that measured in rock sockets (e.g. see Figure 10) show that the two mechanism of sliding and asperity shearing still occur. However, the reasonableness of the simplification of three dimensional roughness as two dimensional asperities needed to be confirmed.

Pearce (2001) used CNS direct shear testing to investigate whether there were significant differences between the results obtained from testing interfaces comprised of two-dimensional ("prismatic") roughness as shown in Figure 9a) compared to interfaces that comprised three dimensional roughness as can be observed in Figure 10. No differences were found using a range of soft to hard rock interfaces. This provides confidence in the use of the two-dimensional asperity model in the theoretical approach to modelling roughness and shaft resistance.

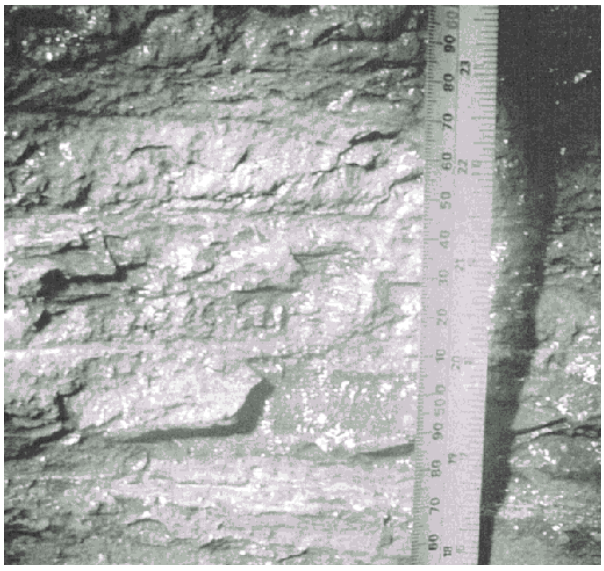


Figure 10: Photograph of a socket excavation in weak siltstone showing roughness of the socket

During shearing of a rough interface, deformations not only occur at each loaded asperity, but also for a finite area around each asperity. As a result of these elastic deformation fields, load sharing of the normal stress between asperities occurs. In general, the steepest asperities will attract the greatest load, and shallower asperities will be more lightly loaded, or may even carry no load as they come out of contact. At a finite displacement, the most highly stressed asperity will fail, and a proportion of its load will be gradually redistributed amongst other asperities. At any stage

during pile displacement there will be sliding, shearing and post peak sliding occurring simultaneously. All mechanisms contribute to both the shear strength and dilatancy of the interface.

From the above discussion it is clear that the shear strength of the intact rock (rather than the rock mass) controls failure of individual asperities within the interface. Either effective or total strength parameters can be used depending on the rate of loading. In general, loading rates are slow and effective strength parameters are appropriate. Where the strength of the rock exceeds the strength of the concrete, the strength parameters of the concrete should be substituted.

Due to the interdependence between strength and Young's modulus of intact rock it is not meaningful to vary the strength of the rock without varying the modulus of the rock. This makes it difficult to demonstrate the impact of rock strength alone on shaft resistance as has been undertaken above for other parameters.

The residual friction angle of the rock also has an impact on socket shaft resistance. The residual friction angle of the rock is a fundamental property of the rock and depends on the grain structure and mineralogy of the rock. For example, fine grained, mud rich rocks may have a residual friction angle of around 20^o, whilst the residual friction angle of (coarser grained) sandstone may be 35^o. The impact of residual friction angle (and therefore rock type) on shaft resistance for rock of the same reference strength and stiffness is indicated in Figure 11 – shaft resistance increases with increase in residual friction angle.

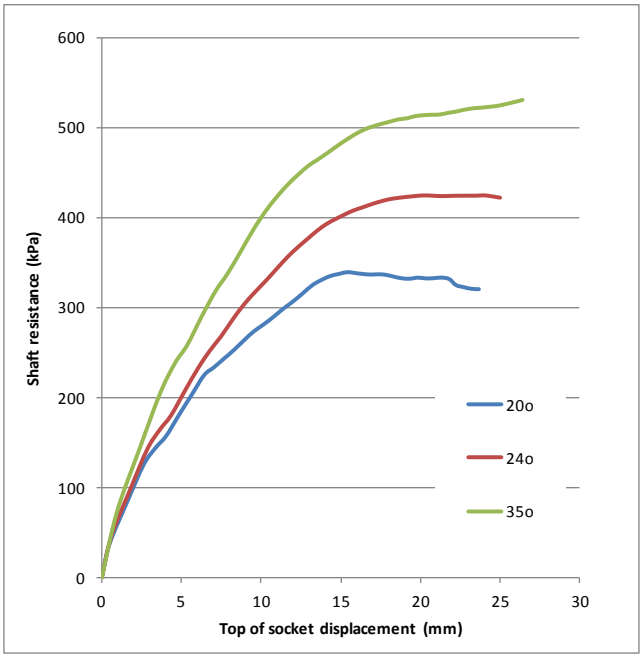


Figure 11: Calculated potential variation in shaft resistance with residual friction angle (or rock type)

3.2.4 Socket Roughness

The importance of socket roughness to the development of interface dilation, asperity failure, normal stress on the socket/rock interface and hence the development of socket shaft resistance is evident from the discussion above. The impact of socket roughness on shaft resistance, at least empirically, has been known for many years as is evidenced through the consideration of socket roughness in rock socket design techniques currently in use (see below).

For example, Pells et al (1980) provided an assessment of roughness based on observations of sockets drilled using various techniques in Sydney sandstone. This classification system utilises Roughness Classes R1 (relatively smooth) to R4 (sockets with grooves/undulations greater than 10 mm). The classification system provides a relatively crude assessment of socket roughness which has been widely used for design of sockets in Sydney sandstone. However the system is difficult to reasonably correlate to design shaft resistance values and does not appear to be applicable to other rock types.

Figure 12 shows the influence of socket roughness for the example pile set out above. For this example, socket roughness is defined by the effective roughness height (Collingwood, 2000) which is the average roughness height determined using a chord length (scale) of 50 mm (see below). An effective socket roughness of 3 mm indicates a relatively smooth socket and is on the lower limit of roughness measured in shale and siltstone materials with a UCS of about 3 MPa. A more typical effective roughness value for sockets in 3 MPa shale and siltstone which have not been subjected to mechanical roughening is about 6 mm, whereas maximum effective roughness for a mechanically roughened shaft in 3 MPa shale and siltstone is about 16 mm.

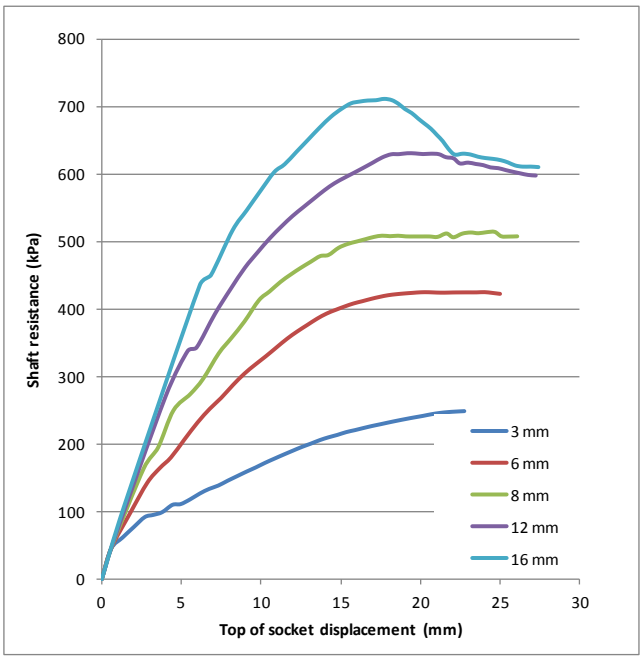


Figure 12: Calculated potential variation in shaft resistance with socket roughness (effective roughness height)

Figure 12 demonstrates how critical socket roughness is to shaft performance. Relatively smooth shafts will have a much lower capacity and lower stiffness than relatively rough shafts. Artificial roughening of sockets has a beneficial effect on shaft capacity. Although not shown in Figure 12, analysis and testing indicates that there is an upper limit to socket roughness beyond which very little increase in shaft capacity can be obtained by artificial roughening.

Socket roughness therefore has a profound influence on predicted socket performance, and as such it is essential that socket roughness be accurately characterised. The roughness of rock sockets varies with socket diameter, drilling technique, rock type and strength and rock discontinuities (bedding and jointing). Despite the central importance of this parameter, there is very little published data on socket roughness. Roughness in general is poorly understood, so it is not surprising that it is the estimation of this parameter that poses the greatest problem to designers.

Since the early 1980's, a number of techniques ranging from visual inspection to borehole callipers have been used to measure or characterise socket roughness. In general these techniques were either limited in their accuracy or have become unacceptable practice due to occupational health and safety issues. Collingwood et al. (1999) described a laser-based socket inspection device called SOCKETPRO that is capable of measuring socket roughness profiles (in dry sockets) to better than 1 mm accuracy. The device has been used to measure roughness profiles in a variety of rock types. SOCKETPRO is shown in Figure 13 and typical roughness profiles for fresh shale, basalt, moderately weathered sandstone and moderately weathered siltstone are shown in Figure 14. The profiles shown represent one vertical scan in each socket. Other scans in the same socket show similar roughness characteristics. In general, as the rock becomes harder and less fractured, the level of roughness decreases.



Figure 13: SOCKETPRO for field measurement of roughness

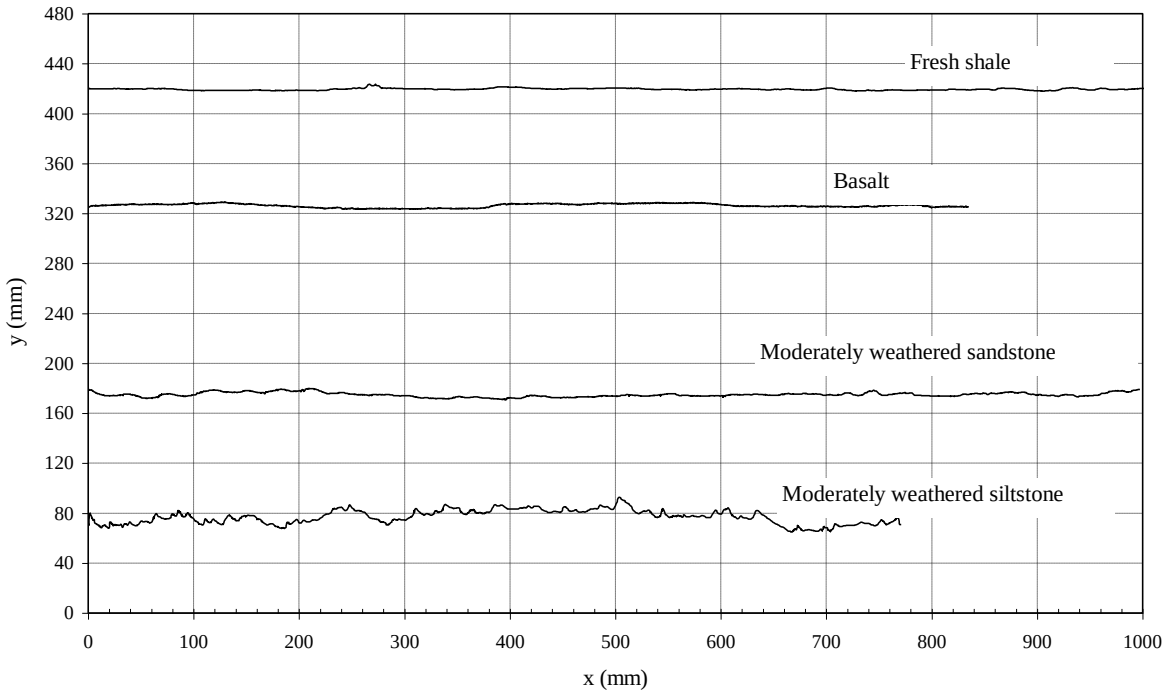


Figure 14: Typical measured roughness profiles of rock sockets in different rock types

The roughness profiles shown in Figure 14 can be analysed in a number of ways to produce roughness parameters that statistically describe the profile. The compass walking method, commonly used in the field of Fractal Geometry to determine fractal dimension, is one such method. A compass is opened to a set radius and then stepped across the profile. A chord is drawn from one intersection point to the next, thereby forming a profile consisting of chords all of the same length. The profiles that result from this process are illustrated in Figure 15. The inclination of each chord is determined and these inclinations are analysed to determine the mean chord angle and standard deviation of chord angle for that chord length. The distribution of chord angles appears to follow a Gaussian distribution (Reeves, 1985; Baycan, 1997). This process can be repeated for several different chord lengths (see Figure 15). Using trigonometry, the standard deviation of chord angle at each chord length can be converted into an effective roughness height. In general, as chord length increases, standard deviation of chord angle decreases and effective roughness height increases.

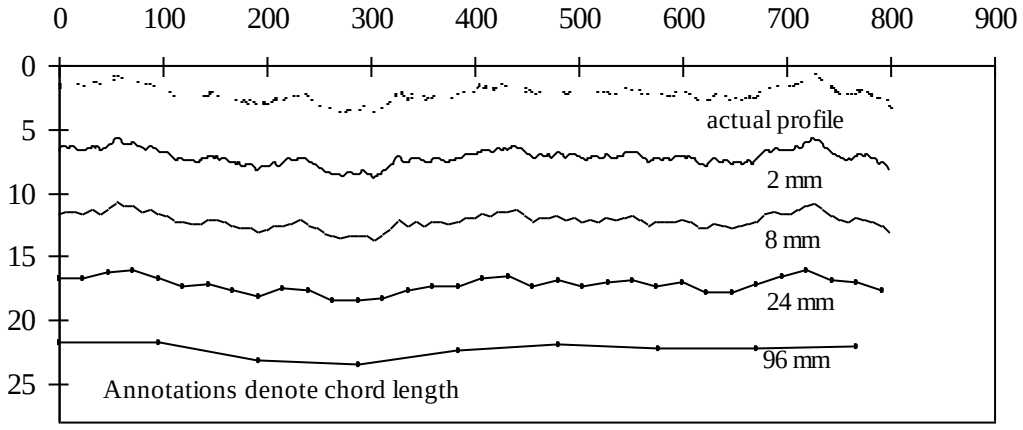


Figure 15: Approximation of roughness using the compass walking method

The advantage of using this approach is that it clearly identifies the scale effect of socket roughness. That is the roughness of the socket depends on the scale at which the discretisation is undertaken. Seidel and Haberfield (1995) provide further details on this concept. Of particular importance is the impact that roughness at various scales has on the development of shaft resistance in a rock socketed pile. Results of static load tests and laboratory direct shear tests (Seidel, 1993) indicate that while peak shaft resistance is dependent on the long wavelength (or large scale) roughness, it is the small wavelength roughness that influences deformation behaviour of the socket at working loads. That is, the greater the small scale roughness, the greater the rate of mobilisation of shaft resistance and the greater the stiffness of the load-displacement response of the socketed pile (Seidel 1995).

Seidel and Haberfield (1995) suggested that the scale (chord length) chosen for analysis should be about twice the displacement of interest. Thus, small wavelengths should be used for small displacement calculations and large wavelengths for large displacements. Figure 16 shows how this was applied to the calculation of the shaft resistance displacement relationship of a 22 m long, 900 mm diameter pile with a 9m long socket in weak calcareous siltstone (for a project in Bahrain). The relationship is calculated as the envelope to the individual curves calculated for one scale of roughness (chord length – e.g roughness height of 6.2 mm at 50 mm chord length) at a time. Figure 16 also shows the shaft resistance versus shaft displacement response measured from static load testing.

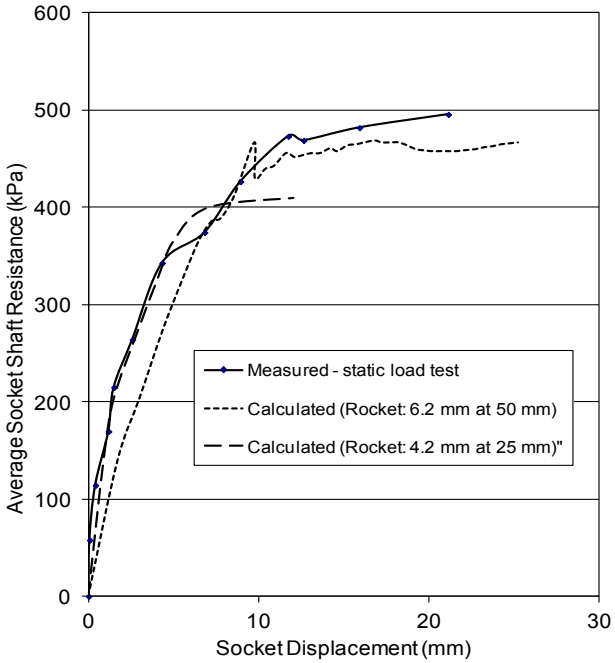


Figure 16 – Comparison of measured and calculated shaft resistance performance for roughness scales

For practical purposes it is found that roughness measured at a chord length of 50 mm provides a basis for undertaking socket design as it provides a reasonable estimate of ultimate shaft resistance and a conservative(but reasonable) estimate of shaft resistance versus displacement response of the rock socket.

Whilst artificial roughening of sockets will generally increase the ultimate shaft capacity of the rock sockets, it may not improve performance at working loads unless the small wavelength roughness is also increased (Haberfield et al. 1996). The intent of artificial roughening of sockets should not be to form grooves in the socket wall but to generally roughen the socket wall. The formation of steep sided grooves in the socket wall may actually be detrimental to socket performance as it enhances brittle rather than ductile load displacement performance and may achieve a lower socket resistance due to loss of the strengthening effects caused by dilation of the socket (which may not occur if groves are steep sided).

Whilst it is important that designers understand the impact of socket roughness on shaft resistance of rock sockets, it is unlikely that designers and piling contractors will routinely measure socket roughness until instruments such as SOCKETPRO become readily available. Even then, the measurement of socket roughness can be time consuming and expensive and may not be cost effective. SOCKETPRO is no longer operational and that there is no similar system in Australia available for the routine measurement of socket roughness.

Seidel and Haberfield (1995) recognised the issues of measuring socket roughness and published recommended upper and lower values of roughness parameters for rock socketed piles as a function of rock strength. This was later updated by Collingwood (2000) following an analysis of a large number of field pile tests in a wide range of rock types and strength. The Collingwood (2000) recommendation is shown in Figure 17. The effective roughness heights in Figure 17 correspond to a 50 mm chord length, which when used with ROCKET97 has been found to provide a reasonable estimate of ultimate shaft resistance and a conservative estimate of displacement.

Figure 17 indicates the maximum roughness occurs in rocks with a q_u of between 2 and 10 MPa, perhaps reflecting the weathering and jointing condition of these rocks. The higher degree of roughness in these materials is also observed in practice.

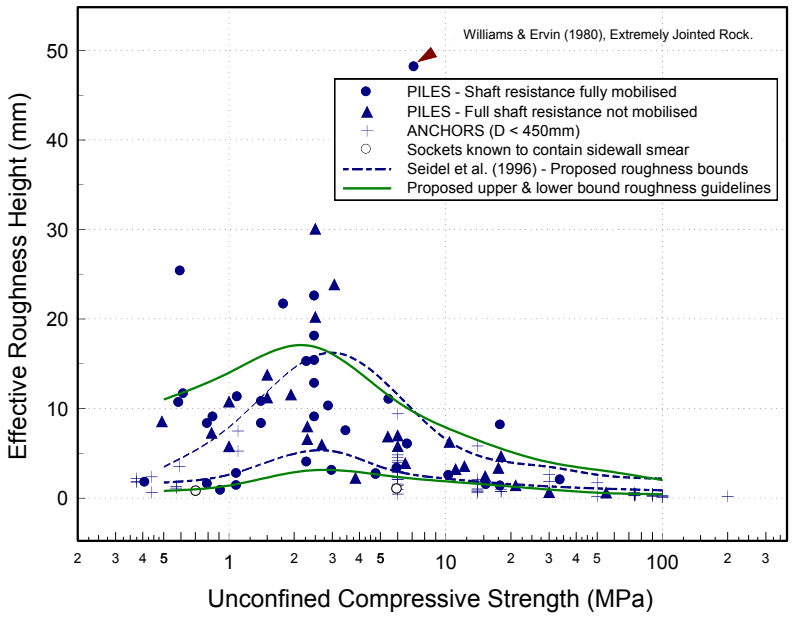


Figure 17: Variation of effective roughness height versus rock strength (After Collingwood 2000)

3.2.5 Integrity of concrete column

The above discussion was based on the assumption that the concrete forming the pile is in intimate contact with the side wall of the socket and the concrete column comprises concrete which meets the design structural strength and is free from defects or contamination. If the integrity of the concrete column is compromised then the design shaft resistance values and design pile performance may not be achieved. As set out later in this paper, the construction processes adopted for installation of the pile are a key factor in the pile achieving its design performance.

3.2.6 Bonding, smear and drilling fluid residue

In the design of rock socketed piles it is generally assumed that the socket side walls are constructed free from smear and/or drilling fluid residue. During excavation of rock sockets it is likely that some contamination of the socket wall will occur either through smearing of the rock while cutting or by coating of the socket walls with drilling fluid residue (e.g bentonite filter cake). Effective cleaning of the socket walls can remove most of this contamination and result in relatively clean sockets with shaft resistance values commensurate with those set out above.

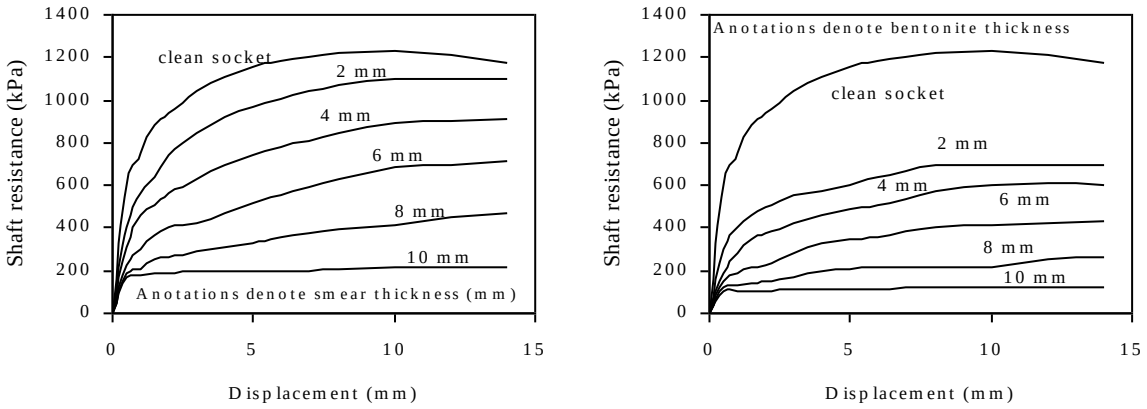
On the basis of the work of Holden (1984), Williams (1980) and Pells et al. (1980) for example, it is well known that the presence of smear and or drilling fluid residue on the socket walls can significantly reduce the shaft resistance of rock socketed piles.

Cheng (1997) investigated the effect of smear and drilling fluid residue on the performance of concrete-siltstone interfaces tested in direct shear in the laboratory. He found that polymer drilling fluids effectively precluded bonding, but otherwise did not significantly affect the performance of the interface. This was also found to be the case by O'Neill and his co-workers (e.g. Majano and O'Neill, 1993; O'Neill et al. 1995).

However, Cheng (1997) also found that interface shear strength and stiffness significantly reduced with increasing thickness of smear and bentonite filter cake. Cheng's assessment for the impact of rock smear and bentonite filter cake of a range of thicknesses for a 600 mm diameter, mechanically roughened socket in siltstone (q_u = 5 MPa and effective roughness height of 11 mm at 50mm chord length) are shown in Figure 18. Figure 18 clearly shows the importance of good construction practices and socket cleaning.

The examples set out in the previous sections of this paper have assumed that the socket wall is relatively clean. However it is likely that even with thorough cleaning, some smear or drilling fluid residue will remain. This may be enough to prevent a significant bond occurring between the concrete and the rock, or at best result in a variable bond.

The influence of bonding on socket performance has been investigated by Cheng (1997). Cheng carried out a large number of laboratory direct shear tests on bonded and unbonded concrete - siltstone interfaces. From these tests he concluded that the amount of bonding was extremely variable, even under ideal laboratory conditions and was very sensitive to the cleanliness of the rock surface. In general, bonded interfaces exhibited a stiffer response and higher shear strength at failure than unbonded interfaces. Ignoring bonding in the assessment of shaft resistance is therefore considered to be conservative.



(a) Rock smear (b) Bentonite filter cake

Figure18: Potential influence of socket wall contamination on socket performance

3.3.7 Summary

There are many factors which impact on the shaft resistance of piles socketed into rock. These include rock type, rock strength, rock mass modulus, socket diameter, depth of socket, socket roughness and socket cleanliness. It is important that the designer understand the impact of each of these parameters. However, it is perhaps more important that the designer understands that many of these parameters (and hence socket shaft resistance) are influenced by the socket

construction process and that if appropriate construction practices are not adopted for installation of the piles, then the design shaft resistance and pile performance may not be achieved.

3.3 Base resistance considerations

As rock socketed piles are often of relatively large diameter, the resistance provided by the base of the pile can be substantial. However as set out below, the calculation of a meaningful base resistance for a pile socketed into rock is not straight forward.

As with shaft resistance, empirical correlations between base resistance and rock strength are available in the published literature. For example Zhang and Einstein (1998) published the results of tests on piles having embedments into rock of more than three diameters. Their results are replotted in Figure 19, as the normalised mobilised base bearing pressure (q_b/q_u) against the normalised deflection (ratio of settlement to diameter). All results were for rock strength less than 10 MPa. The results show that large displacements are required to mobilise base resistance. However, all tests were terminated without a peak base resistance being reached. Figure 98 also indicates that a prudent estimate of base bearing pressure for a displacement of 10 % of diameter would be about 5 q_u unless the rock was highly fractured in which case a lower value would be advisable.

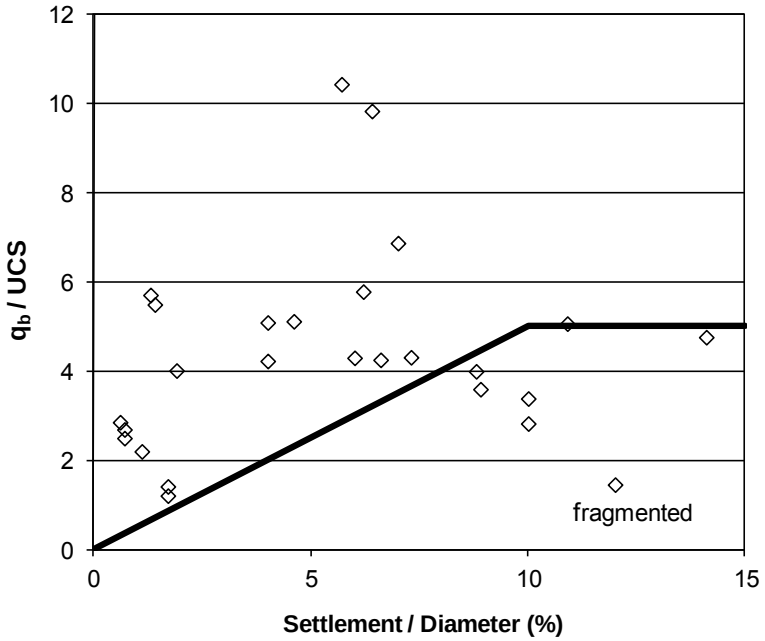


Figure 19: Load settlement relationship for piles socketed into rock

Similar conclusions can be drawn from the results of Williams (1980) for tests at three sites in siltstone around Melbourne (Figure 20). Ratios of embedment to footing diameter from zero (surface footing) to more than 20 were tested. Ultimate base resistance was achieved only in a few tests (indicated by the solid symbols in Figure 20) which had low embedment to diameter ratios (i.e. surface footings to embedment of two diameters below the ground surface). The low q_b/q_u values measured in some tests were due to insufficient load being applied to the piles to generate high base bearing pressures.

The results indicate:

- $q_b > 5\ q_u$ for surface footings
- $q_b > 10\ q_u$ for piles with embedment > 5 dia.
- ultimate bearing capacity was not reached for embedment > 2 dia.
- in extremely fractured rock, much lower bearing capacities were measured.

These results are considered to be typical of behaviour of piles socketed into rock.

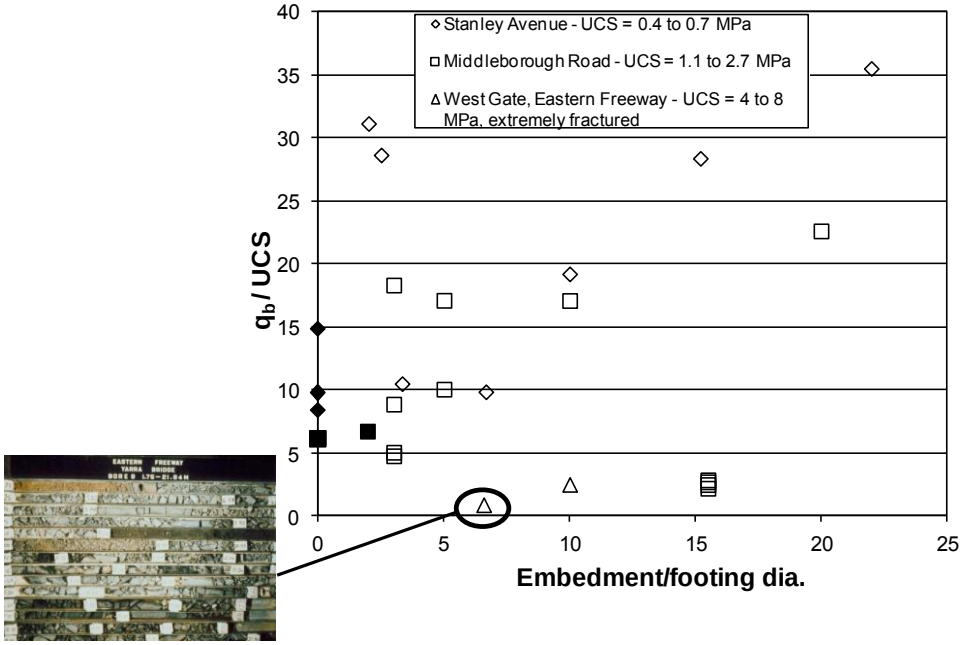
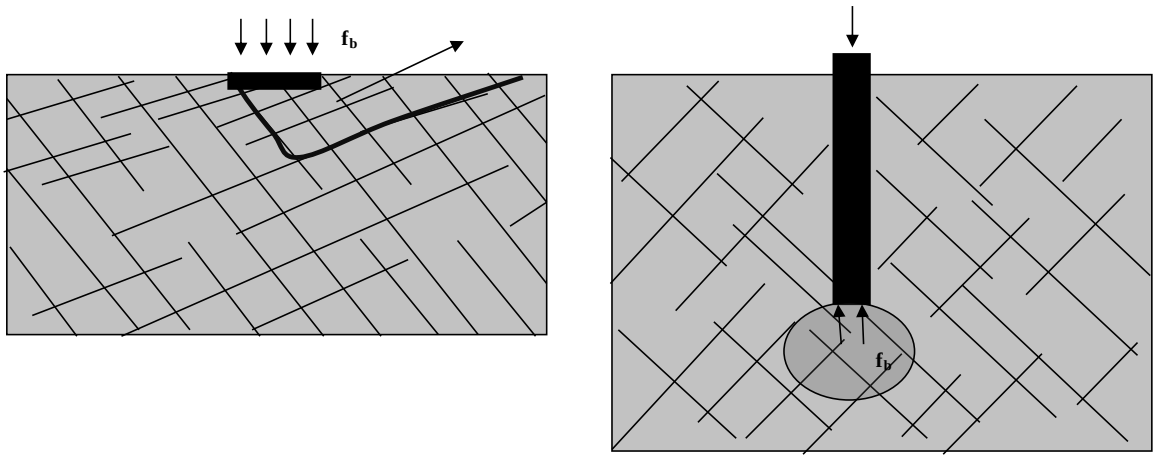


Figure 20: Load-settlement relationship for piles

The fact that very few field pile load tests in rock achieve peak base resistance is not surprising if the possible failure mechanisms in jointed rock are considered. For surface footings, (Figure 21a), joints can provide a preferred failure surface and clearly they limit bearing capacity. In contrast, for piles (Figure 21b), there is no theoretical limit to bearing capacity as a failure surface does not propagate to the ground surface. The jointed rock mass is assumed to be a dense, dilatant material. The stress bulb beneath the toe is confined by the stiffness of the surrounding rock, and dilation (as a result of shearing of the rock) increases this confining stress thereby increasing the resistance. This only occurs in relative dense dilatants rocks and is not applicable to high void ratio rocks (e.g. carbonate rocks). The load that can be supported by the pile is controlled in practical cases by settlement (serviceability) and not by bearing capacity.



(a) footing or short pile (b) pile

Figure 21: Possible failure surface for shallow footings and piles in jointed rock

The conclusion is that the ultimate end bearing capacity is reached at large displacement, if at all. In practice, this means that piles should be designed to satisfy displacement limitations, that is, serviceability will control. Piles should **not be** designed by applying a strength reduction factor to an estimated base bearing capacity without considering settlement.

What impact, if any, does joint orientation have on end bearing performance of piles in rock. There is little published information on the effects of joint orientation on the axial load versus displacement relationships of piles. Some insight

can be gained from theoretical analyses using programs such as UDEC. Figure 22 shows load-displacement relationships from UDEC for the base response of a pile in a jointed mass having the following properties:

- Uniaxial compressive strength q_u = 5 MPa
- joint spacing 0.5 m
- joint friction angle 30°
- joints at +45°/-45°, 60°/-30° and 0°/90°

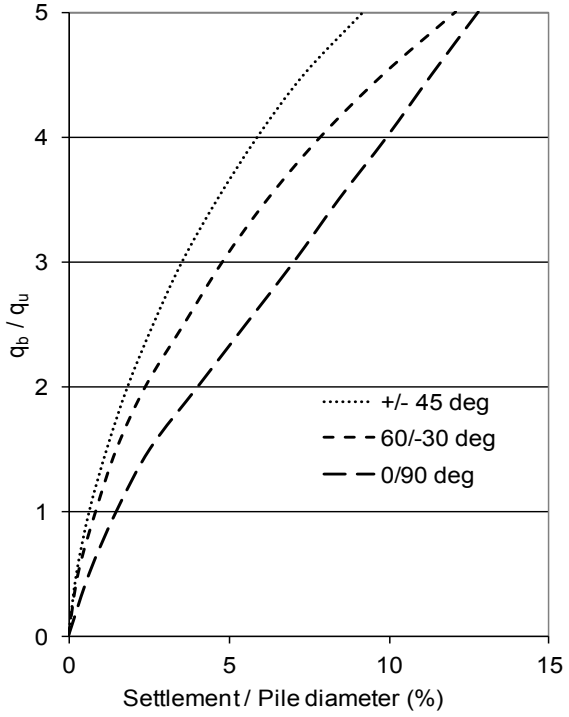


Figure 22: Theoretical response of base of pile on jointed rock

In Figure 22, q_b is the base bearing pressure. The results show that at the likely serviceability limits (settlement/pile diameter <1 %), there is a similar response for the joints at 45°/45° and 60°/30°, but the joints at 0°/90° give a less stiff response. Similar results were obtained using PLAXIS.

In practical terms there is little difference between the results for different joint orientations, especially in the light of the likely range in other variables. This indicates that modelling the jointed rock as a rock mass (continuum) is likely to be satisfactory.

When considering the ultimate capacity of piles on rock, this capacity may be limited by the maximum allowable stress in the concrete. Australian Standard AS3600 gives the maximum allowable compressive stress in concrete ranging between 0.27 f'_c and 0.45 f'_c, where f'_c is the characteristic strength of the concrete. If the maximum allowable concrete stress is taken as 0.5 f'c, then once the axial pile bearing stress (f_a) exceeds this value, the concrete strength limits the maximum pile base capacity.

For example, if f_a = 12 q_u, and f'_c = 50 MPa, then if the rock has q_u > 2 MPa (approximately), the pile base bearing capacity should not be a design issue, as concrete strength will control.

The above discussion has assumed that there is no debris at the base of the pile. This requires appropriate construction procedures to be implemented as set out later in this paper. The presence of base debris will not reduce the ultimate base resistance of the pile, but it will significantly increase the displacement required to mobilise the design base resistance. For this reason, it is imperative that rock socketed piles are constructed with clean bases, or alternatively, the piles should be designed such that serviceability load can be safely carried by (factored) shaft resistance only.

As set out later in this paper, even if accepted base cleaning methods are adopted and carried out competently, it is likely that some debris will remain at the base of the pile. If concrete is placed with a tremie, some of this base debris may be carried away on the top of the rising concrete column, whilst the remainder will tend to be pushed to the edge of the socket base, potentially forming an annulus of debris material around the outer edge of the pile. For this reason it is prudent to reduce the effective base area of the pile for serviceability calculations (unless a clean base can be ensured and confirmed). A reasonable and prudent assumption for design would be that 50 % of the base area is effective for serviceability calculations. The full base area may be used for ultimate limit state calculations, but the designer should be aware that the pile head settlement required to achieve this may be significant.

3.4 Available design methods

Although there are numerous methods for analysing the load displacement performance of rock socketed piles, only relatively few appear to be used commonly for design (at least in Australia). Pells (1999) groups the available design methods into 3 categories: elastic design (Rowe and Pells, 1980; Pells et al., 1980), design for side-slip (Rowe and Armitage, 1984; Carter and Kulhawy, 1987) and non-linear analysis (Williams et al., 1980; Seidel and Haberfield, 2002b).

3.4.1 Elastic design

A number of approaches have been devised in order to translate elastic solutions of pile load vs displacement perfomance into simple design tools. Pells and Turner (1979) presented a series of elastic solutions for shaft-only, base-only and combined shaft and base resistance piles determined from numerical integration of Mindlin's equations and finite element analyses. Two methods were proposed for accounting for the combined effect of shaft and base resistance. Both methods make use of simple estimates of limiting shaft adhesion and base resistance (i.e. 0.05 q_u and 0.5 q_u respectively for the Sydney Sandstone for which the method was specifically developed). Both values are predicated on a criterion of limiting settlement to 1% of diameter.

In the first method, for a given load requirement and pile diameter, the developed end-bearing at a displacement of 1% of shaft diameter is assumed to be fully available. Any deficit in capacity is assumed to be carried by the shaft, and the required shaft length is then determined from the shaft circumference and the allowable shaft adhesion. It is assumed that the shaft resistance is "plastic" (i.e. is constant after reaching initial peak), resulting in no transfer of load to the base, and therefore guaranteeing settlements of less than 1% of pile diameter. This method is not rigorous, as the strain fields from the assumed shaft and end-bearing components will not necessarily be compatible, and in practice the compatibility requirement will force some redistribution of resistance.

In the second method, the socket length is iteratively designed from charts provided for combined shaft and base resistance, thus taking into account elastic compatibility considerations. This second method results in longer pile sockets. This is essentially the same method as proposed by Horvath et al. (1983).

Pells (1999) adapted the second method to the limit state format and provided recommendations with regard to strength reduction factors. He also altered the determination of limiting shaft resistance from 0.05 q_u to include estimates from existing correlations with q_u (e.g. Figure 3).

The input parameters required to carry out an elastic analysis include the Young's modulus of the rock mass around and below the pile, the average peak shaft resistance and the ultimate base resistance of the pile.

3.4.2 Design for side-slip

Rowe and Armitage (1984), building on the work of Rowe and Pells (1980) presented design charts for piles including slip. The method is similar to, and requires the same input parameters as the elastic method described above.

The analytical solutions developed by Carter and Kulhawy (1987) can be used directly to estimate the load-displacement behaviour of the pile. Input parameters are similar to that required for elastic analysis.

3.4.3 Non-linear design

Williams et al. (1980) developed a non-linear design method by combining empirically measured pile load-displacement response curves with elastic solutions. By implementing a simple iterative procedure they were able to develop load-displacement predictions for both side-only and complete (side and base) piles. At the time, the resulting design method provided a significant improvement in design rational over existing methods, and was quickly accepted by local practitioners for the design of sockets in the Melbourne siltstone.

The rock joint model developed by Seidel and Haberfield (2002b) forms the basis of a pile design program called ROCKET97. The program allows the designer to divide the socket and overburden into a number of sub-layers that might represent different rock and soil types or different weathering conditions within the same rock type. For each sub-layer a number of fundamental input parameters are required. ROCKET97 then develops a τ-z (shear stress versus displacement) curve for each layer. These curves represent the behaviour of the concrete-rock interface for each sub-layer. To determine the overall pile response, the elastic shortening of the pile shaft and the vertical elastic deformations of the rock mass need to be considered. The elastic deformations of the rock mass are determined using the solution determined by Randolph and Wroth (1978). A reverse Coyle and Reese (1966) analysis (i.e. working from the top of the pile to the bottom rather than the bottom to the top) is then carried out to sum the contributions of each sub-layer and of the base. The base response is assumed to be elastic perfectly plastic, with the ultimate base resistance being input by the user. Base debris and enlarged (or smaller) bases can also be accounted for. The output is in the form of the pile head load – displacement response.

As with all theoretical techniques, the solutions obtained are dependent on the input parameters. ROCKET97 requires the following parameters to determine the τ-z curve for each sub-layer : socket diameter, initial normal stress acting on the socket wall due to wet head of concrete, peak intact rock strength parameters (cohesion, c' and friction angle, ϕ'), rock residual friction angle, ϕ_r, rock mass Young's modulus, E and Poisson's ratio, ν_m and socket roughness (mean asperity height, h_{av} and chord length, λ.

As almost all of these parameters can have a significant influence on shaft resistance (the exception being Poisson's ratio), it is imperative that the designer understands the influence that each has on the development of shaft resistance (as explained earlier in this paper). A detailed description of the models incorporated into ROCKET97 are described in Seidel (1995) and Seidel and Haberfield (2002a,b).

There are available a number of general pile analysis programs that are suitable for the design of rock sockets provided the input is appropriate. One in common use by piling contractors and geotechnical engineers is a software package called PIGLET (Randolph, 2004). The output obtained from PIGLET is a top of pile load displacement response. As PIGLET only allows the input of one stratigraphic unit along the pile length, an average socket shaft resistance and shear modulus needs to be assessed. Base resistance is input by specifying a base bearing pressure mobilised at a nominated displacement as a percentage of pile diameter. On the basis of the discussion above, for most moderately or less fractured rock masses, it would appear prudent to assume a base bearing pressure of 5 q_u at a displacement of 10 % of diameter. For more highly fractured rock masses a lower multiplier (than 5) on q_u should be adopted, or alternatively, a higher displacement ratio.

3.4.4 Stratigraphy

The rock stratigraphy present over the length of the socket and below the socket will dictate shaft and base resistance (respectively) and therefore pile performance. It is therefore important that a relatively accurate assessment of the rock stratigraphy over and below the likely socket depth be obtained from the ground investigation. This is particularly the case for sockets in interbedded weak sedimentary deposits (say q_u < 10 MPa).

Ideally such ground investigation should comprise cored boreholes using triple tube methods with unconfined compressive strength tests being conducted on the recovered core samples. Such testing should be undertaken on samples that are saturated or close to saturation. Insitu pressuremeter testing is also recommended (in weak rocks) to obtain a reasonable estimate of rock mass modulus. Point load testing is not recommended for weak rocks, but may be adequate for stronger rocks where the unconfined compressive strength of the rock is more than about half the design strength of the concrete.

From this information it is usually possible to identify a reasonable and prudent design stratigraphy over the depth of the socket. Each different stratigraphic layer can be assigned a different shaft resistance and modulus values for use in a displacement based design of the pile (see above). The presence of fractures and seams in the rock is accounted for in the assessment of shaft and base resistance and modulus and plays no further role in the assessment of design pile performance. Thick soft seams, if they are present can be treated as separate layers in the analysis.

Many rock socketed piles have a significant depth of overburden soil above the socket. Some designers ignore the contribution to shaft resistance from the overburden materials on the basis that its contribution as a proportion of the total capacity of the pile is not significant. However, if the overburden materials are relatively competent (stiff to hard clays, moderately dense or better sands etc) they can have a significant impact on the displacement performance of the pile particularly at service loads. For this reason, the contribution from competent overburden materials can be included in the pile design.

If the overburden materials over the pile length comprise rock over more compressible soil with the pile then socketing into the underlying rock (e.g. in some areas of Melbourne, piles penetrate through near surface Quaternary basalt then Tertiary sands and clays before socketing into Silurian siltstone) then the full shaft resistance which could potentially develop within the upper rock sequence should not be included in the design of the pile. This is because the presence of the underlying more compressible soil causes a significant portion of load shed in the upper rock sequence to be attracted back into the pile. As a result, for pile design, the shaft resistance attributed to the upper rock sequence should be limited to a maximum value equivalent to that of the ultimate shaft resistance in the underlying soil.

As with design of other pile types, negative skin friction (if relevant) needs to be considered in the serviceability performance of the pile and in the assessment of structural strength of the pile.

3.4.5 AS2159-2009 Considerations

Australian Standard AS2159-2009 "Piling-Design and installation" provides recommendation for design of piles. Section 4 of the Standard deals with the geotechnical design of piles. The design approach adopted in the Standard is to apply strength reduction factors to the design geotechnical strength of the pile calculated from estimates of ultimate shaft and base resistance. As set out above, this approach is not particularly suited to the design of piles socketed into rock due to:

i) the different mobilisation rates of shaft and base resistance and the high ultimate base resistance that can be achieved at very large pile displacements. This makes a meaningful estimate of ultimate base resistance to be used in design subjective and a potential source of disagreement; and

ii) the settlement of the pile (rather than ultimate capacity) is usually critical.

Nevertheless, the pile design still requires an estimate of an appropriate geotechnical strength reduction factor and the geotechnical strength of the pile should still satisfy code requirements.

4 CONSTRUCTION CONSIDERATIONS

The performance of a bored or rock socketed pile can be significantly influenced by the methodology used in its construction.

4.1 Pile Excavation Support

Bored pile construction may be carried out, depending upon the geotechnical conditions and the strata that must be penetrated, either by:

1. In stable, self supporting ground above the ground watertable by drilling shafts without support in the dry.
2. In wet or unstable ground overlying a stable stratum into which the piles are to be socketed by the installation of a permanent or temporary steel casing sealed into the top of the founding strata then drilling out the casing and drilling the pile socket into the founding strata in the dry.
3. In wet or unstable ground and in founding material where sockets may be unstable if drilled in the dry, piles may be constructed by installing either a permanent or a temporary casing to the top of the founding stratum and then drilling out the pile shaft inside the casing followed by drilling the rock socket with socket support provided by a drilling fluid. The socket should not be dewatered as this may induce socket instability.
4. In similar ground conditions to 3 above, a short temporary top casing could be installed followed by drilling the entire shaft and rock socket using temporary support provided by a drilling fluid to maintain shaft and rock socket stability. Drilling fluid support should be maintained through the drilling concreting process.

The load settlement performance of a bored pile will be significantly influenced by the processes used to construct the rock socket, to manage the drilling fluid (if any and the placement of reinforcement and concrete.

4.2 Socket excavation and cleaning

Socket excavation is achieved through use of appropriate drilling tools. Drilling tools should be of the correct diameter, and checked regularly for wear which may result in an undersized pile hole.

Where sockets are drilled in relatively weak rock (q_u < about 10MPa) the side walls of the socket should be roughened using mechanical means to stiffen the load deformation response of the socket and to help remove any smear on the socket walls. This is best achieved using one or more extended offset reaming teeth fitted to the outer diameter and at the base of the socket drilling or cleaning tool. Roughening of the socket walls and the removal of any smear is

accomplished by lifting and lowering the rotating roughening tool over the full depth of the socket. After roughening is carried out base cleaning will be required.

The purpose of mechanical roughening should **not** be to form grooves in the socket but to ensure a minimum level of overall socket surface roughness to meet design assumptions.

Roughening of sockets in rock with a unconfined compressive strength of greater than about 10 MPa to 20 MPa is problematic and may not be practical. In strong rock, water is often introduced into the socket during the drilling process to maintain efficient drilling, to cool the drill teeth and aid in spoil removal. The introduction of water also helps remove rock smear and clean the walls of the socket. In some hard rock types, washing of the socket may be advantageous.

Where casing is used, the casing diameter should be such that it provides clearance for excavation, cleaning and roughening tools.

After a pile socket has been drilled to the final design depth, the base of the socket must be cleaned of loose drilling debris to maximise the load settlement behaviour of the base of the rock socket if the pile design includes a component of base resistance. Base cleaning should still be undertaken even if the socket has been designed as a friction socket only with no contribution to the design load from the base. This is because socket cleaning promotes good construction practice and to reduce potential contamination of the concrete by debris. Figure 22 shows the results of ineffectual cleaning (and also poor concrete placement) in a pile socketed into weak siltstone.

Base cleaning is usually carried out using purpose-designed cleaning tools that conform to the base profile of the drilling tool used to excavate the socket. The cleaning tool must be designed to retain loose base debris and in sockets drilled under drilling fluid support the cleaning tool must incorporate a means of retaining base debris during withdrawal of the cleaning tool including suitable drilling fluid bypass tubes to minimise suction pressures being developed below the tool during its withdrawal.

Alternatively base cleaning may be carried out using airlifting, provided the location of the airlift inlet can be controlled and passed over the entire base of the socket. For deep large diameter sockets this may require the use of a purpose designed sweep airlift. In general, handling the airlift suction pipe from the surface and moving the top across the socket does not provide sufficient control of the base of the airlift and will not provide acceptable base cleaning.



Figure 22: Pile socketed into siltstone showing results of poor base cleaning

4.3 Drilling fluid management

Fluids that may be used to provide shaft support may include water, bentonite or polymer slurries. Drilling fluids provide support to the pile shaft and or socket by maintaining an excess fluid pressure inside the pile shaft above that of the surrounding ground water table. In relatively stable sockets the use of water alone may be sufficient. In weaker rocks and soft soils and sands, additional support may be required.

Additional support can be achieved using either bentonite or polymer slurry. Each of these slurries works in different ways to provide pile shaft and socket support. Correct care and maintenance of drilling fluid properties during drilling and concrete casting operations is critical for the construction of intact pile shafts and sockets, free from base debris.

An illustration of the impact of fluid management on base debris and pile performance is shown in Figure 23. This shows load test results for three test barrettes constructed at the site of the Nakheel Tower development (Haberfield and Paul, 2011) and tested using two levels of Osterberg Cells (O-Cells). The barrettes were 1.2 m by 2.6 m in plan area and were constructed to depths of 65 m (test barretes TB02 and TB03) and 95 m (TB01). The best available practice was adopted in their construction which was carried out using polymer-based fluid. The polymer was completely replaced following base cleaning, and a maximum sand content of less than 0.5 % was generally measured before concrete placement. The base of the piles was investigated using base coring and cross-hole sonic logging which penetrated through the base of the pile into the underlying ground. Despite adoption of best practice fluid management and base cleaning, the base coring and cross-hole sonic testing showed up to 0.1 m of debris generally across the full plan area of the base of the barrettes and up to 0.6 m of debris around the perimeter of the base of the barrettes.

As test barrettes, measurements of deflection were carried out at the pile toe (by tell-tales) and below the toe (in the rock using soil strain meters). When loaded, significant differences were found between the deflections measured at the pile toe, and those measured immediately below the toe, indicating that debris in the base had been compressed. During loading, water was expelled from open casings for the strain meters which had been extended to the surface. This observation gave independent evidence that the debris at the base was being compressed. It is noted that had these

casings not been present, it is quite likely that the base would have been observed to be incompressible, since there was no other way that water in the debris could be expelled in the short time the loading was applied.

Considerable care was taken in construction of these test barrettes. Nevertheless, debris accumulated at the base. One of the major contributing factors was considered to be ineffectual desanding . The length of the barrettes meant that the time to place the reinforcement cage was such that the delay between end of construction and concreting was up to 10 hours. Placement of the reinforcement cage through the upper uncased section of the barrette could also have exacerbated collapse of the walls, especially where the cages were slightly oversize.

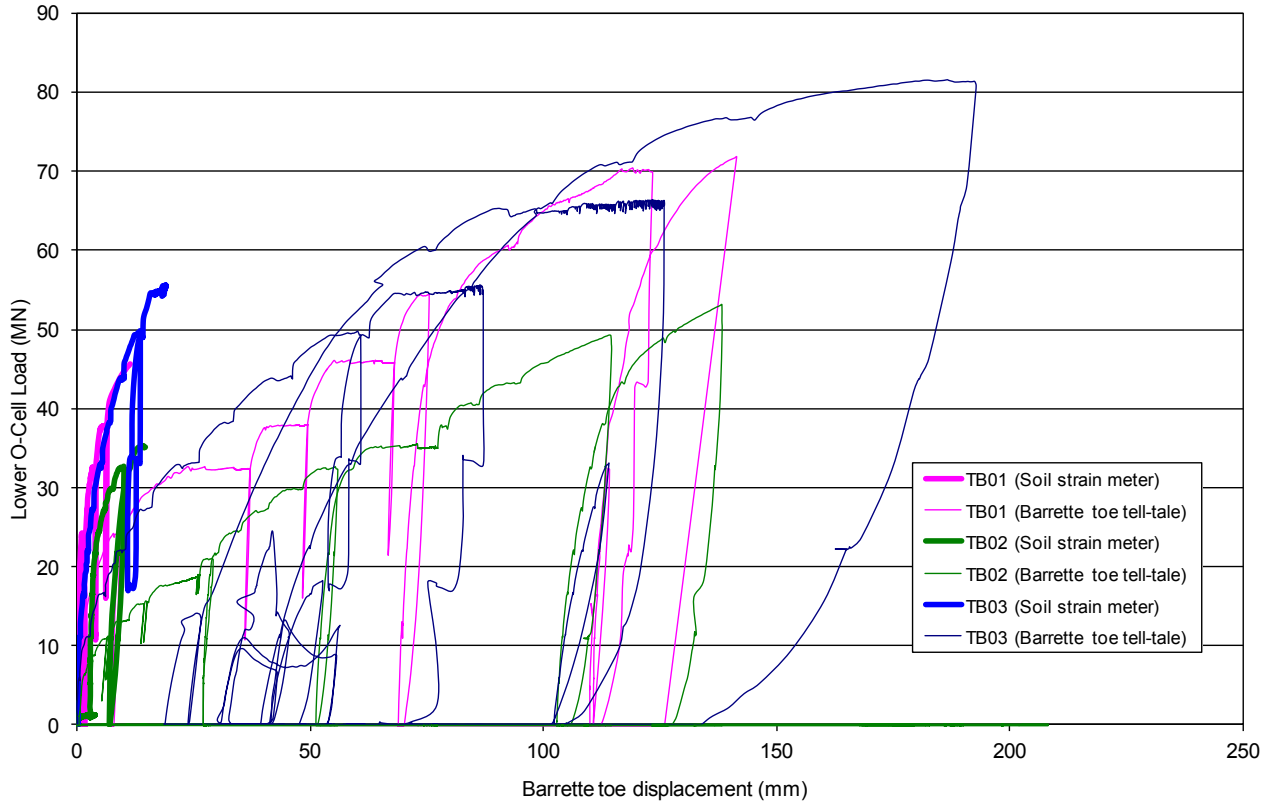


Figure 22: Effect of base debris on load-displacement response

4.3.1 Bentonite Based Drilling fluid

Bentonite drilling fluid provides support to the pile shaft and socket by providing a fluid with a specific gravity higher than that of water. Providing the bentonite slurry level in the pile shaft is maintained above the ground water level the bentonite fluid will tend to seep into the walls of the pile shaft. This forms a thin filter cake of the walls of the pile shaft and socket which increases shaft and socket stability. The bentonite fluid is thixotropic (it forms a gel if left undisturbed for sufficient time) and it can keep sand and clay particles in suspension.

To prevent an excessive build up of filter cake, which may affect socket shaft resistance, maintenance of the bentonite slurry properties during socket construction and concrete placement is critical. Fluid properties to be monitored include:

1. Fully hydrating the bentonite powder when mixed with water prior to introducing the fluid into the pile shaft excavation. This may be achieved by mixing dry bentonite powder with water typically at 5% by mass and storing the resultant fluid for 24 hours prior to use.
2. Maintaining bentonite slurry head in the pile shaft a minimum of 1.0 m above standing ground water level at all times during pile excavation. During drilling avoid rapid withdrawal of drill tools which may cause suction pressures to develop below the tool which may cause shaft or socket collapse and consider using a surge tank

to help maintain bentonite level in the shaft at a constant level, compensating for the volume of drill kelly bar inserted and removed from the pile shaft as the drilling tool is moved up and down the shaft.

3. Do not leave slurry in a completed pile socket more than 2 hours without agitation to prevent formation of excessive filter cake on the walls of the socket and pile shaft
4. After pile socket drilling is completed roughen the socket wall as noted above.
5. Clean the pile base as noted above.
6. Prior to the placement of pile reinforcement and concrete, de-sand and recycle the bentonite drilling fluid in pile shaft to achieve the properties presented in Table1
7. After de-sanding and recycling the bentonite in the pile to achieve the properties shown in Table 1 conduct a final base clean (if socket is designed for end bearing) using appropriate methods.
8. Place the reinforcement cage using suitable spacers to maintain cover to reinforcement.
9. Place concrete using tremie technique as soon as possible after reinforcement cage is placed.

Table 1: Bentonite fluid properties

Bentonite Slurry property	During Drilling	Prior to concreting
Bentonite concentration (bentonite mass/water mass %)	4 minimum	4
Specific Gravity	1.03 -1.2	1.03 to 1.08
pH	8-11	8-11
Viscosity (Marsh funnel seconds/0.945 L) field check	28-40	28-40
API sand content (%)	0 to 10	0 to 2 (up to 5 may be acceptable)
API fluid loss (ml/30 min)	10 max	10 max

Bentonite-polymer mixes may have different requirements that set out in Table 1.

4.3.2 Polymer based drilling fluids

The use of polymer drilling fluids or blends of polymer and bentonite fluid is increasing within the construction industry. Some advantages of polymer slurry include:

1. High yield – small quantities of polymer powder or liquid can make large quantities of drilling fluid.
2. Polymers are easier to mix and store than bentonite fluid.
3. Polymer slurries do not form a filter cake on the side walls of the pile shaft or socket and can provide superior performance in drilling soft rocks which may slake or swell on wetting.
4. Polymer slurries do not hold drilled spoil is suspension for any significant period of time so de-sanding and reconditioning of drilling fluid is not required.
5. Some polymer slurries are biodegradable, some may be reverted to water by adding bleach and in general polymer fluid is easier to dispose of than bentonite fluid.

There are several types of polymer drilling fluid additives available all of which have specific manufacturer's recommendations for use which should be adhered to. Because of their lower specific gravity, polymer slurries require a larger minimum head (preferably 2 m or more) above standing ground water level than do bentonite slurries.

As polymer is not effective in holding spoil in suspension for any significant period of time, it is important that prior to final base cleaning of the socket that sufficient time be given to allow any suspended solids to be deposited at the base of the socket to allow its removal in the base cleaning process.

4.4 Reinforcement placement

The placement of the reinforcement cage into the pile excavation has the potential to dislodge material from the side walls of the pile which may be deposited as debris at the base of the pile. Figure 24 shows the results of cross-hole sonic logging (a form of integrity test) in a test pile which used over-sized spacers resulting in accumulation of debris at the base of the pile. To minimise the potential for this to occur, reinforcement cages should be of the correct dimension, straight and fitted with circular spaces of correct size that freely rotate as the cage is lowered into the pile excavation.

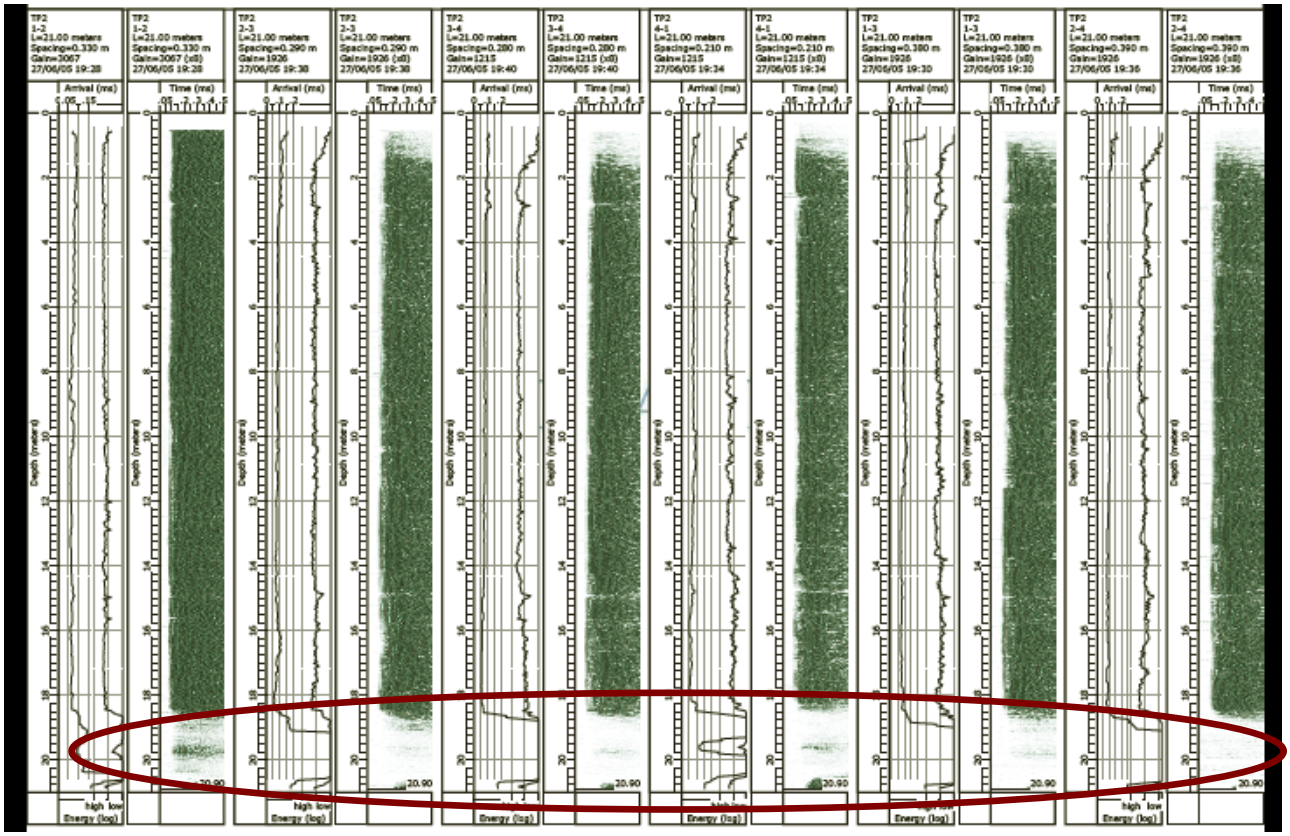


Figure 24: Results of cross-hole sonic logging test showing base debris issues due to use of oversized reinforcement cage spacers.

4.5 Concrete placement

Concrete properties and placement can have a major effect on the integrity and performance of bored cast in place socketed piles. Figure 25 shows a pile that has integrity issues due to poor concrete placement. This pile will never carry its design load – not because of geotechnical considerations, but due to insufficient structural strength of the concrete column.



Figure 25: Pile defect due to poor concrete placement procedures

For shafts and sockets constructed in dry stable strata and for which socket bases are free from base debris, concrete may be placed by free fall. This method involves the placement of concrete directly into the centre of the pile shaft from the surface. Concrete is allowed to free fall from the surface to the base of the pile. Provided the concrete is directed though a funnel or similar device so as not to strike, or fall though the pile reinforcement cage, segregation of the concrete may be avoided. If it is not possible to confirm that the base of the pile is free from debris then to mitigate the risk of contamination of the concrete with base debris, the concrete should be placed by tremie pipe as set out below.

For sockets which are stable, with slow water ingress it may be practical to dewater the socket and place concrete as above. However, if the socket has potential for instability or water inflows are relatively rapid, no attempt should be made to dewater the socket and concrete should be placed by tremie as set out below.

In wet sockets or for piles drilled under drilling fluid support, concrete must be placed via a tremie pipe. Placement of concrete where it drops through water or drilling fluid will cause segregation of the concrete and may not displace all of the drilling fluid. Pile sockets in weak or unstable ground should not be dewatered.

For correct tremie placement of concrete the following should be adhered to:

1. The tremie should comprise of metal pipes connected with waterproof joints.
2. The tremie should be assembled and lowered to the base of the pile socket after the drilling fluid in the socket has been appropriately conditioned and the reinforcement cage is placed
3. The base of the tremie should be sealed with a drop off plate or a flow separator (a charge of vermiculite, a greased sponge or rubber ball) should be placed on top of the drill fluid at the top of the tremie prior to concrete placement
4. Tremie mix concrete is then placed into a hopper at the top of the tremie pipe and concrete placement must be continued uninterrupted until flow though the tremie slows or stops. The tremie pipe is then raised taking care

to keep the bottom of the tremie pipe at least 2m to 3 m below the surface of the concrete and concrete flow recommences.

5. Measurement of the rise of the top of the concrete within the pile and noting the volume of concrete placed and tremie pipe location should be recorded during concrete placement
6. Tremie Concrete mix design and performance is critical for the construction of intact piles. A minimum cement content of 400 kg/m3 and a slump of 180 mm or more is recommended. Retarders and super plasticizers may be used. It is important to note that the first concrete placed into a pile is lifted to the top of the pile at the completion of concreting in a correctly managed tremie pour so retention of concrete slump and delay of initial set , to ensure that the first concrete is still fluid at the end of the pour is important.

Poor tremie practice can result in pile shafts with significant defects as shown by the cross-hole sonic logging results shown in Figure 26. This pile only achieved about 50 % of its design working load.

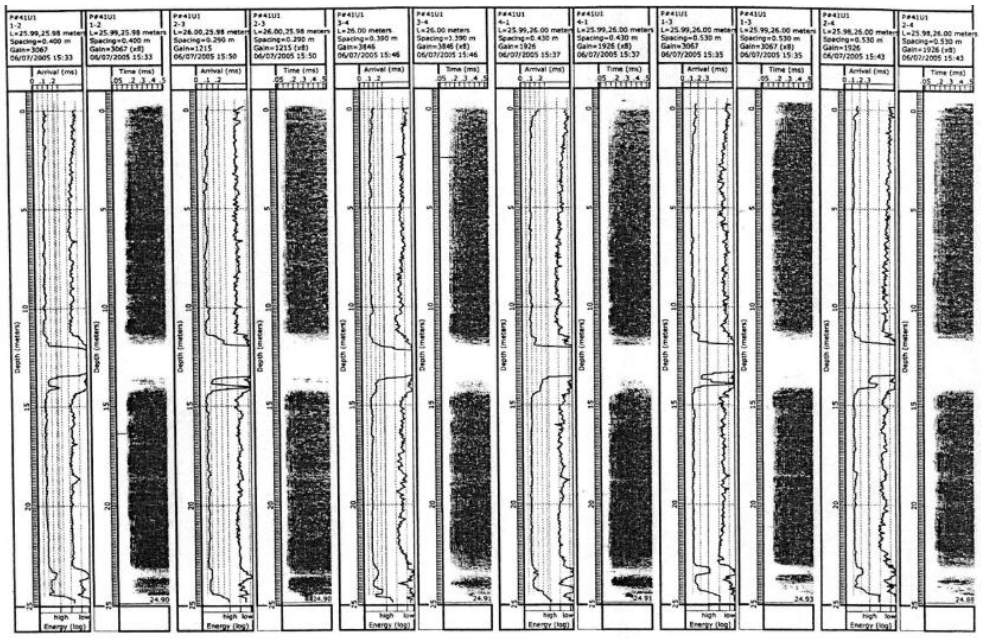


Figure 26: Cross-hole sonic logging results showing large potential defect in a pile shaft due to poor tremie procedures.

The processes of final socket cleaning and placement of reinforcement and concrete should be undertaken as a continuous process without any significant delays. If a significant delay is encountered between final clean and concrete placement then the reinforcement should be removed from the hole and the cleaning process repeated prior to replacement of the reinforcement and placement of the concrete. In some rock types, delay in concreting can result in softening of the rock and a reduction in pile load versus settlement performance, whilst in other rock types, a delay may not be detrimental. Some rocks may exhibit significant deterioration on exposures to air or water (e.g. slaking) which can make installation of bored piles impractical. Usually, such materials can be identified during the ground investigation by observing the recovered core or undertaking slake durability testing. As a general rule, it is prudent to keep delays during pile construction to a minimum.

Delays in pile installation may have an impact even in rocks that do not show any obvious signs of softening or slaking. For example, Figure 27 shows the measured socket shaft resistance versus socket displacement for two piles constructed in calcareous silststone with a UCS of 2 MPa. The piles were 0.75 m in diameter and had 9 m long sockets and were constructed under water. The pile concreted within 24 hours of drilling had significantly better performance than the pile concreted 18 days after drilling. The difference is attributed to softening of the weak rock in the shaft of the pile left open for 18 days.

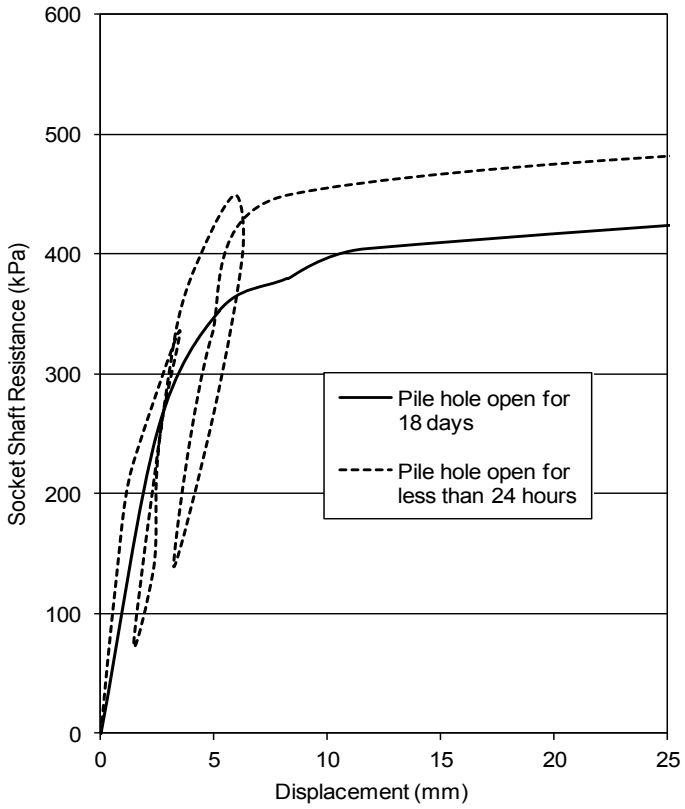


Figure 27: Effect of shaft softening on socket shaft resistance

4.6 Health and safety

There are many health and safety risks associated with the construction of piles. No piling should be undertaken until appropriate Health and Safety plans are provided and agreed to, and workers are properly inducted.

Bored piles are drilled using heavy tracked drilling equipment. The stability of the drilling rigs relies on an adequate working platform. A working platform certificate for the site should be obtained prior to any piling equipment mobilising to site. The working platform must be maintained during the works.

Care is required when working close to rotating machinery.

Workers are also in close proximity to the top of the pile shaft during drilling. The use of a short top temporary casing set about 1m above working platform level provides not only an access barrier but also serves to stabilise the ground around the top of the pile which helps with rig stability. Access should be controlled and suitable safety barriers erected to prevent workers accidently falling into the pile shaft.

Under no circumstances should personnel enter a pile hole. Surface inspections of pile hole excavations may only be carried out once appropriate protection barriers are in place. Personnel should not approach the pile hole while excavation is underway. Inspection of cuttings from the pile hole excavation should be made from the spoil dump.

Workers operating near the drilling rig should maintain eye contact with the operator and unauthorised personnel should be kept out of the area.

4.7 Engineering involvement

Engineering involvement prior to construction is recommended to confirm that the proposed piling method is consistent with the pile design assumptions. Method statements for installation of the piles should be submitted by the piling contractor for review by the designer. For design and construct projects, the piling method statement should be checked for consistency with the specification.

Engineering involvement during construction is recommended to confirm design assumptions and to confirm compliance with the specification. The scope of engineering involvement will depend on the project, the ground conditions, the design assumptions and the level of conservativeness assumed in the design of the piles.

In the past, some design assumptions (e.g. socket roughness, stratigraphy and cleanliness) have been confirmed by direct entry of engineers into the pile hole. For occupational, health and safety reasons, the entry of personnel into a pile hole is no longer considered acceptable. To the author's knowledge none of the major geotechnical consultants or piling contractors will permit manned entry into a pile hole. Major consultants and piling contractors have successfully designed and installed rock socketed piles for more than 20 years without requiring manned entry. Reference to manned entry of sockets should be removed from specifications and piling method statements.

The following design assumptions are considered impractical to confirm directly or without significant cost/delay to the project:

- Socket roughness
- Detailed stratigraphy (including joints and seams) in the socket
- Rock properties at the socket location

As a result, suitably conservative and prudent design assumptions should be made in respect to these design inputs (see recommendations below). Indirect confirmation of these design inputs can be obtained from appropriate testing of one or more piles.

Direct observation of sockets of shallow depth can be made using light and mirrors. Such observations should only be undertaken with appropriate fall protection and barricading in place. If the sockets require dewatering, then careful consideration should be given to the benefits obtained by direct observation compared to the risk of instability of the socket.

For deeper sockets, it may be practical to observe the socket using a down hole camera or similar. Unless specialised equipment is utilised (e.g. the SIDS device developed by VicRoads), cameras can only be effectively used if the socket is dewatered. This can significantly increase the potential for socket instability especially in weak rock below the water table. The confirmation and confidence that can be obtained by such inspections should be carefully considered in the context of risks to the pile, cost and delay to the project. Such risks can usually be offset at a lower cost by adopting suitably conservative design inputs and a relatively small increase in the length of the socket.

On some previous major projects in Australia, drilling a cored borehole at every pile location was adopted in lieu of manned entry and direct observation of the stratigraphy in the pile sockets. Drilling every pile location is expensive and time consuming and is unnecessary unless the geology is highly variable. As set out above, if the geology is relatively well defined and known, then there is little benefit in undertaking additional boreholes to locate fractures and weak seams in the rock. These have already been accounted for in the pile design assumptions and are unlikely to allow refinement of the pile design.

An example of a project where boreholes at pile locations were beneficial was the 270 m high Eureka tower in Melbourne. The subsurface stratigraphy at this site comprises upper basalt which covers about half the site underlain by alluvial deposits overlying weathered siltstone. About one half of the building is supported on piles which found within the upper basalt whilst the remaining half of the building (where there is no higher level basalt or it is relatively thin) is founded at much greater depth in weathered siltstone. As the thickness and quality of the upper basalt was variable, a borehole was drilled at many of the proposed pile locations to assess whether the quality and thickness of the basalt was a suitable founding material or whether piles needed to be extended to the siltstone.

A reasonable assessment of socket stratigraphy and rock properties at the socket location can be made by observation of the drilling rate and process, and of the drill cuttings and spoil by a suitably experienced geotechnical engineer. This process has been used successfully for many years by geotechnical consultants to confirm rock conditions in the socket. This process mitigates the risk of poorer than expected ground conditions (e.g. dykes) and allows pile lengths to be increased if necessary without delay to the project. The reverse is also true, where better than expected ground conditions can lead to a reduction in pile length (assuming reinforcement length and uplift requirements are met).

Engineering involvement during construction also allows independent confirmation that the pile installation conforms to the agreed method statement and promotes good construction practice. The engineer can observe the excavation,

cleaning and concreting processes and observe or undertake simple checks to confirm compliance. Such checks with respect to geotechnical issues commonly include:

- Observance of drilling method and rate, drill rig response and logging of socket excavation based on drill cuttings
- Inspection of roughening tool and cleaning bucket to confirm they are appropriate and in good working condition and that they are not extracted too quickly to cause pile excavation instability
- Observance of minimum level of drilling fluid in pile hole
- Observance of water level in pile hole (for essentially dry sockets with some water inflow) and potential for collapse of socket if dewatered or need for concrete placement by tremie
- Observance of volume of material recovered from excavation during cleaning – should be minimal at end of cleaning process
- Surface socket inspection if practical and safe to do so
- Observance of dipping of pile hole to confirm pile length and to "feel" for debris at base of pile
- Observance of test results for drilling fluids if appropriate, particularly prior to placement of concrete
- Observance of reinforcement and its placement ensuring that the reinforcement cage is straight and of correct diameter and appropriate spacers have been used
- Observance of tremie process, including use of tremie plug, initial placement of tremie at base of pile excavation, dipping to confirm height of concrete in pile hole, depth of tremie in concrete, concrete volume vs height curves
- Observance of good concrete at top of pile at end of concreting process
- Observance of any time delays

Satisfactory compliance with these aspects will usually result in a competent pile.

5. PILE TESTING CONSIDERATIONS

5.1 Load testing

The primary purpose of load testing of piles should not be to confirm design input parameters (e.g. soil and rock properties, roughness and cleanliness of socket) that have been assumed in the design but to confirm overall pile load vs displacement performance is consistent with the design and perhaps to confirm design pile shaft and base resistances are reasonable and achievable.

Confirmation of the load displacement performance of piles can be confirmed through pile load testing of trial piles or working piles. Typically testing of trial piles is taken to higher loads in an attempt to confirm design ultimate geotechnical capacity (noting that the actual ultimate pile capacity may not be practically achievable for piles socketed into rock). Load testing of working piles is usually to a nominated proof load to confirm satisfactory pile performance at serviceability load.

Pile load testing of bored piles can be carried out by static load testing, bi-directional load testing, statnamic load testing and high strain dynamic testing.

Static load testing is expensive and is (currently) rarely undertaken in Australia. It requires provision of reaction piles/anchors or kentledge to provide resistance to the applied test load. For bored piles, reaction is usually provided by reaction piles or anchors due to the high test loads required and the impracticality and occupational health and safety issues associated with using kentledge. Reaction piles and anchors can interact with the test pile and impact on the measured pile performance. For this reason, the test pile set-up needs to be carefully considered. In general, achieving the design ultimate geotechnical strength of a pile socketed into rock will not be practical as the design structural strength of the concrete will likely be exceeded prior to the pile achieving the design ultimate geotechnical capacity. Static load testing has a practical test load limit of about 30 MN.

Static load testing of piles socketed into rock is therefore generally limited to testing to design serviceability loading. Adequately installed piles tested to their serviceability load will not have fully mobilised either design ultimate shaft or base resistance and therefore confirmation of these parameters will not be possible using such testing.

Bi-directional load testing (e.g using Osterberg Cells) provides a more practical method (than static load testing) of achieving high test loads (e.g. the author has been involved in bi-directional testing that mobilised a pile capacity of approximately 250 MN). This test method utilises sacrificial jacks cast into the pile shaft and jacks one part of the pile against the other. The method is generally less expensive than a static load test and has been used with great success overseas to confirm pile performance up to design ultimate geotechnical capacity of piles with relatively long sockets. The method however is not practical for use in relatively short sockets which rely primarily on end-bearing resistance as the resistance provided by the pile shaft above the jack is not sufficient to achieve the required pile base bearing pressures. Bi-directional testing was successfully undertaken on test piles for the new Gateway Bridge in Brisbane.

It is usual to include strain gauges and other instrumentation into a trial pile tested by static load or bi-directional testing to better understand the performance of the pile. However as:

i) it is common for at least some of the instrumentation to malfunction during pile testing

ii) accurate interpretation of the strain gauge results to assess pile shaft and base resistance is difficult as it relies on an estimate of the concrete modulus which is not known accurately, and

iii) load tests on piles socketed into rock are unlikely to mobilise ultimate shaft or base resistance,

it may not be economical or cost effective to include all but basic instrumentation (e.g. to allow measurement of displacement and load) into the test pile.

Statnamic testing is not commonly used, but is a suitable testing method for bored pile socketed into rock. Statnamic testing utilises a much faster test rate than static or bi-directional testing and this needs to be accounted for in the analysis of the test results. Statnamic testing successfully mobilised a pile resistance of about 30 MN on two test piles for the 270 m high Eureka Tower in Melbourne. The test method is relatively expensive to undertake and requires specialist equipment.

High strain dynamic or PDA testing has been used extensively for load testing of continuous flight auger piles and less so for bored piles, socketed into rock. No instrumentation in the pile is required other than detachable strain gauges and accelerometers at the head of the pile. Testing is relatively inexpensive (compared to the other forms of load testing), but requires additional reinforcement in the top of the pile and for the pile head to built up above ground surface level. Test loads of up to about 30 MN can be practically achieved with a 20 tonne drop hammer.

The test results are interpreted using CAPWAP or similar signal matching software to provide a estimate of pile head load displacement performance under static loading, distribution of mobilised shaft and base resistance and mobilised pile capacity. One drawback from such testing and analysis is that the analysis of the test is not straight forward and is not understood by the majority of geotechnical engineers. For this reason, the analysis of the results is open to interpretation and potentially misrepresentation. In our experience, provided a capable analyst is used to interpret the test results, the results from PDA testing are consistent with those from static load testing.

This is illustrated by Figure 28 which provides a comparison of estimates of pile performance from dynamic testing/CAPWAP analysis and a field load. The CAPWAP analyses have been undertaken by 3 different analysts (from different testing companies) using the same dynamic test data. Analysts 1 and 3 appear to provide an estimate of static pile performance that is similar to that measured during static load testing. Analyst 2 provides a reasonable estimate for one pile test but over-estimates pile performance for the other test. The expertise and competency of such analysts appears to vary significantly. For this reason, the author recommends that analysis of the test results is carried out by an independent, competent, experienced and certified analyst. Such certification is provided by Foundation QA HSDPT (see http://www.hsdptregister.org/).

PDA testing also provides information on the integrity of the pile.

In summary, pile load testing can provide confirmation of the load displacement performance of piles socketed into rock and therefore provide a direct confirmation of pile performance and an indirect confirmation of pile design assumptions and construction method. Static load testing is not usually practical to undertake for piles socketed into rock. Bi-directional load testing can be practical for long sockets but due to its cost may only be considered for large heavy structures with high pile loads and long sockets (e.g. Gateway Bridge). High strain dynamic testing provides a

practical and less expensive method of confirming pile performance (load and integrity) for projects involving pile test loads up to about 30 MN, provided the analysis of the results is undertaken by an experienced and competent analyst.

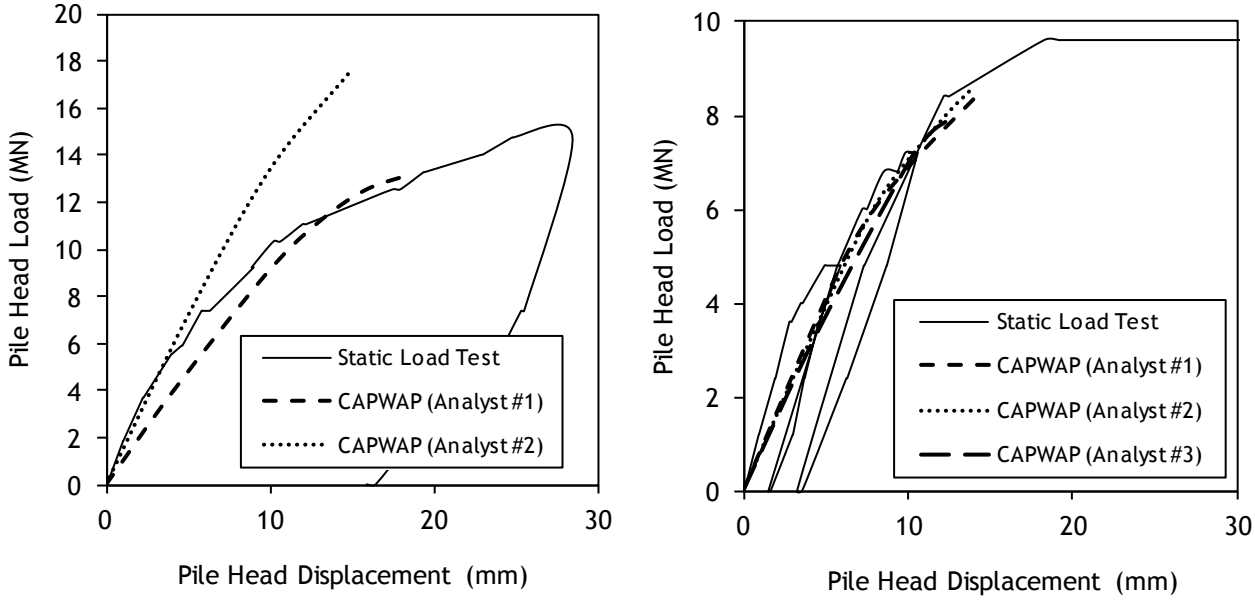


Figure 28: Comparison of pile load versus settlement performance from static load tests and dynamic testing/CAPWAP analyses of piles socketed into calcareous siltstone

5.2 Integrity testing

The adoption of good construction practices as set out earlier in this paper is an essential first step to achieving durable piles that are free from defects and that meet their design performance. If the pile installation method is poor or not suited to the ground conditions (e.g. dewatering pile excavations in weak fractured rock) then the potential for defects occurring in the pile shaft or at the pile base (base debris) is increased, thereby potentially impacting on pile performance and durability.

The integrity of a pile socketed into rock can be confirmed through pile integrity testing. No matter how good or conservative the design, if the structural integrity of the pile is inadequate, the pile will never perform as designed. Figure 25 shows an example of a pile which was excavated for inspection after integrity testing (PIT) showed up a fault.

Small strain pile integrity testing (PIT) or transient dynamic response (TDR) testing is a relatively cost effective way of confirming that the upper 10 pile diameters or so of the pile shaft is free from major defects. It is in common use in Australia and overseas, where it is typically applied to 100 % of working piles. The test does not require any special preparation of the pile but needs to be undertaken by a competent specialist tester/analyst. For piles in hard soil or stronger material longer than about 10 pile diameters, the PIT testing may not provide any information on the integrity of the lower portion of the pile (see below). An acceptable PIT test result does not guarantee that the pile is free from defects, it just means that no defect was detected. These tests provide no useable information on pile capacity.

Crosshole sonic testing is a more expensive method that provides a method of testing the integrity over the full length of the pile (but not the base of the pile). It has not been in common use in Australia, but is relatively common overseas. The test requires tubes of a specific diameter to be attached to the reinforcement cage and extend over the full length of the pile and therefore the piles for testing need to be selected prior to installation of the pile. For the test, a sonic transmitter and receiver are lowered down each pair of tubes in turn. The tests are undertaken by a competent specialist tester/analyst and provide detailed information on the integrity of the concrete between each pair of tubes. By repeating the test in alternate pairs of tubes, a very detailed measurement of the integrity of the pile between the tubes is obtained. The test is very sensitive and an anomaly in the signal may not necessarily represent a defect in the pile. Significant anomalies identified in the test may need to be investigated through further testing (e.g coring of the pile, excavation around the head of the pile if the anomaly is close to the surface, or high strain dynamic testing). The test is not able to identify defects outside of the reinforcement cage (e.g. lack of concrete cover) or below the base of the tubes (e.g. base debris).

Figure 29 compares the results of cross-hole sonic logging with PIT testing of a 26 m long pile. Initial interpretation of the PIT testing showed no obvious problems. However, static load testing showed unacceptable load-deflection behaviour. Subsequent to the static load testing, cross-hole sonic logging was undertaken. The results clearly show a problem with the pile material at depths between about 12 m and 14 m. The PIT testing was then reviewed and only showed a minor disturbance at that depth when maximum signal amplification had been carried out. Clearly at that depth the PIT is not sufficiently sensitive to detect anomalies.

High strain dynamic testing when competently used, also provides information on the integrity of the pile.

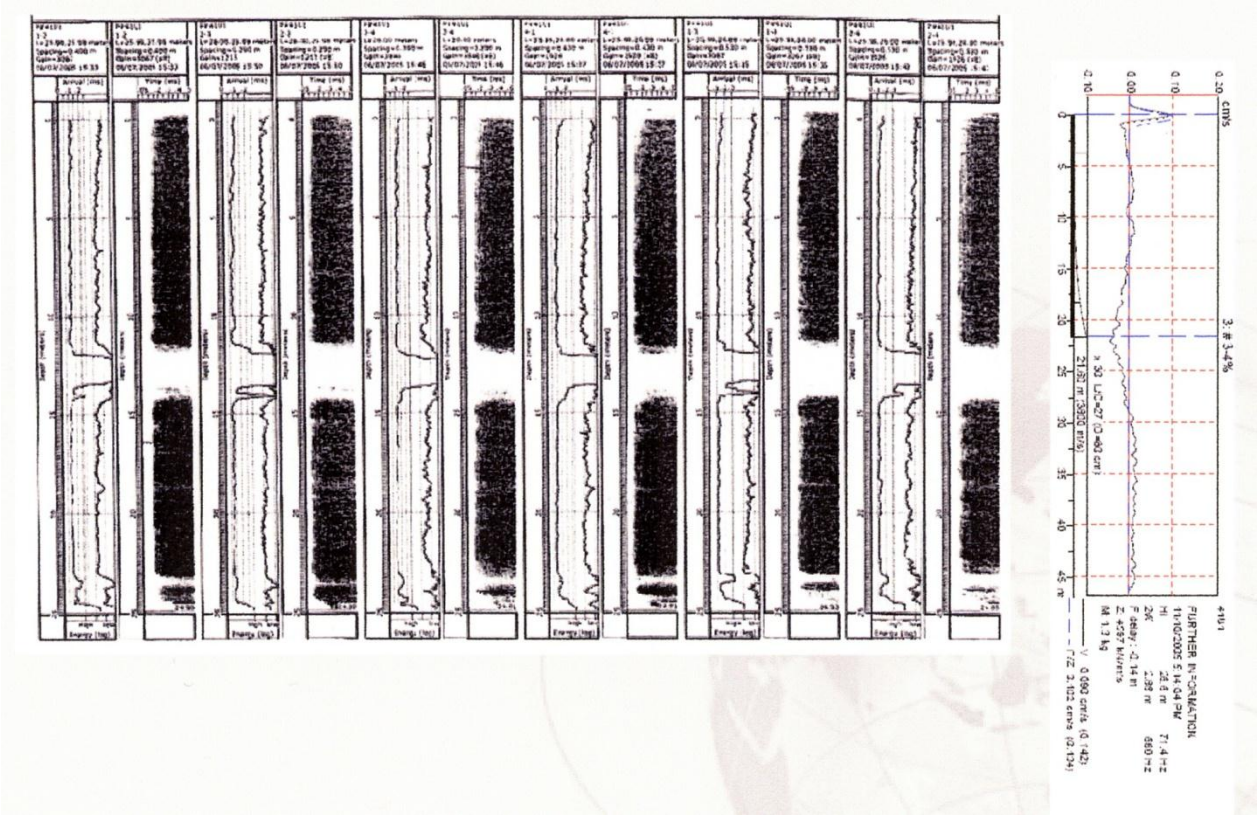


Figure 29: Comparison of cross-hole testing with PIT on 26 m Pile

6. RECOMMENDATIONS FOR ROCK SOCKETED PILE DESIGN, CONSTRUCTION AND VERIFICATION

As set out above, the load versus displacement performance of a pile socketed into rock is dependent on the properties of the rock, the pile dimensions and the construction method used to install the pile. As a result, pile design must consider the pile construction processes.

There are several proven methods available for the design of rock socketed piles. The choice of method should remain the decision of the designer. However, a design method which simply factors estimates of ultimate shaft and "ultimate" base resistance without considering the different rates of mobilisation of these resistances is overly simplistic. For well constructed piles installed by a competent and experienced piling contractor and following the construction and testing related recommendations set out below, then the geotechnical design of rock socketed piles can reasonably be based on the following:

i) A prudent and representative stratigraphy assessed from a reasonable interpretative geological model and supported by an adequate ground investigation.

ii) An adequate ground investigation which should comprise boreholes drilled into rock using triple tube methods unless impractical to do so. Unless impractical (due to unsuitable samples; e.g. close fracture spacing) unconfined compressive strength (UCS) testing should be carried out on representative core samples, with a minimum of one UCS test every 3 m within the rock material. In addition, point load strength index testing should be undertaken at a minimum of 0.5 m centres within the rock material. For rocks with uniaxial compressive strengths of less than about 5 MPa, insitu pressuremeter tests are recommended to be undertaken at a minimum of 5 m centres (but not necessarily in every borehole), with at least two tests in the one borehole. UCS tests should be undertaken on the rock core at each pressuremeter test location. UCS tests should be undertaken on samples that are saturated or close to saturation. In sedimentary rocks, point load and UCS tests should also have moisture content recorded.

iii) Prudent and reasonable estimates of rock mass Young's modulus and strength based on a prudent assessment of the results of the geotechnical investigation.

iv) Prudent and reasonable estimates of ultimate shaft resistance and rate of mobilisation of shaft resistance which consider the diameter of the socket, the rock type and fracturing, the mass modulus of the rock, the intact strength of the rock and a socket roughness and cleanliness that is consistent with the construction methods to be adopted. Information pertaining to estimates of ultimate shaft resistance can be obtained from:

a. Appropriate and proven analysis programs such as ROCKET97. It is generally not practical to measure roughness of sockets. Estimates of shaft resistance in roughened sockets should be based on lower quartile roughness values presented in Figure 17 (Collingwood, 2000). For sockets constructed without roughening lower bound values from Figure 17 should be adopted. The roughness classification system by Pells et al (1980) was developed for Sydney sandstone and its use for other rock types may not be appropriate.

b. Published correlations with UCS based on static load testing (e.g. Rowe and Armitage, 1984; Kulhawy and Phoon, 2000)

c. The results of constant normal stiffness direct shear testing on concrete rock interface samples

d. Design methods proposed by Rowe and Armitage (1984), Rowe and Pells (1980), Carter and Kulhawy (1987), Williams et al. (1980) and Seidel and Haberfield (2002b), or

e. The results of field pile load testing

Guidance for an estimate of the rate of mobilisation of ultimate shaft resistance can be obtained from:

a. Comments set out earlier in this paper;

b. The results of constant normal stiffness direct shear testing on concrete rock interface samples

c. Design methods proposed by Rowe and Armitage (1984), Rowe and Pells (1980), Carter and Kulhawy (1987), Williams et al. (1980) and Seidel and Haberfield (2002b), or

d. The results of field pile load testing.

Alternatively, it may be assumed that for highly fractured or less fractured rock masses, free of clay seams and shear zones, ultimate shaft resistance mobilises at a pile displacement of 1 % of pile diameter. For extremely fractured rock masses, or rock masses containing significant clay seams and shear zones, it may be assumed that a displacement of 5 % of pile diameter is required to mobilise the ultimate shaft resistance.

iv) Prudent and reasonable estimates of base resistance and mobilisation of base resistance with pile toe displacement that considers the pile construction method and the potential for base debris. The assumed ultimate base resistance should be no greater than 5 x q_u for relatively short rock sockets (a rock socket length less than five pile diameters) and up to10 x q_u for sockets with significantly deeper embedment. The ultimate shaft resistance should be assumed to be mobilised at a pile toe displacement of 10 % of pile diameter for highly fractured or less fractured rock masses, free of clay seams and shear zones and 20 % of pile diameter for extremely fractured rock masses, or rock masses containing significant clay seams and shear zones. If the piling contractor is unable to confirm through observation (or other approved methods) that a completely free base to the pile has been achieved then a reduced base area (50 % to 75 % of base area depending on the base cleaning methods adopted) should be assumed for estimates of base settlement performance. If there is concern regarding the cleanliness of the base, then the piles should be designed such that serviceability load can be carried by shaft resistance only with an appropriate strength reduction factor applied. In this way, base resistance is only relied on for ULS considerations.

v) For piles in relatively strong and massive rock (UCS greater than about 10 MPa and relatively wide spacing of joints) with relatively short sockets, the preferred approach is to use the elastic design methods set out above. An alternative approach is to sum factored ultimate base and shaft capacities values (as set out above) with strength reduction factors selected in accordance with AS2159-2009.

vi) Piles socketed into weak, soft and fractured rock (UCS less than about 10 MPa) usually require reasonably long sockets. For such applications, it is not valid to design pile sockets simply by summing factored ultimate base and shaft capacity values and/or use of elastic design methods. Instead, a non-linear design or analysis method (e.g. as set out earlier) should be used to calculate the design pile head load versus displacement performance. The analysis should incorporate estimates of shaft and base resistance and their mobilisation rates as set out under items iii) and iv) above with an appropriate factor of safety applied to settlement. It would seem prudent to apply a factor of safety of 2 to estimates of settlement (i.e. design settlement = 2 x calculated settlement) based on rock mass modulus values obtained from published correlations with q_u and fracture spacing or from using GSI (Hoek and Brown, 1997) or similar published methods. For settlement estimates based on rock mass modulus values obtained directly from field testing (e.g. pressuremeter) or from back-analysis of pile load tests, the safety factor could reasonably be reduced to 1.5.

vii) The socket should be of sufficient diameter and length to satisfy the project serviceability criteria for single piles (at serviceability load) and requirements of AS2159-2009 with respect to ultimate and serviceability limit state conditions and other relevant standards..

There are many proven procedures for the installation of rock socketed piles. The most appropriate procedures will depend on many factors, and will vary from site to site. An experienced and capable piling contractor is usually in the best position and has the expertise to deside on installation procedures. The author would advise against stipulating the construction methods to be adopted. However, the construction of rock socketed piles should:

i) only be undertaken after the piling platform has been designed and certified.

ii) preclude manned entry into sockets

iii) provide suitable protection to prevent personnel or equipment falling into pile holes

iv) only be undertaken after a method statement for the construction of the piles has been provided by the piling contractor and agreed to by the designer, engineer or authority if appropriate. The method statement should cover all aspects of the pile construction including health and safety, pile excavation, socket roughening, socket cleaning, drilling fluid management, reinforcement placement and concrete placement.

v) use industry accepted and proven practices unless direct confirmation of the results of a new practice is undertaken

vi) not require sockets to be dewatered for inspection or placement of concrete

vii) allow use of drilling fluids (where appropriate) provided the drilling fluids are properly managed, especially for sockets in rock that are susceptible to instability. The choice of drilling fluid (e.g. water, polymer, polymer-bentonite mixtures or bentonite) will depend on the ground conditions and the experience of the piling contractor.

viii) mandate roughening of all sockets with intact unconfined compressive rock strengths less than about 10 MPa

ix) mandate that suitable methods of shaft and base cleaning be undertaken even if base resistance is not relied on in the design of the pile. Current accepted practices include use of purpose-made cleaning and roughening tools that conform to the base profile of the socket excavation drilling tool, and/or using airlifting. Airlifting through tremie pipes and recirculating of reconditioned clean drilling fluid or bottom suction cleaning using a suitable down hole pump may be applicable in shallow sockets where base coverage of the pump or airlift inlet can be controlled (this is often impractical for deep holes). Vigorous airlifting in unstable sockets is not recommended as it can lead to socket collapse.

x) utilise reinforcement cages of the correct dimension, that are straight and fitted with circular spaces of correct size that freely rotate as the cage is lowered into the pile excavation

xi) use a tremie and good tremie practice for concrete placement in sockets containing any free water or drilling fluid, or for dry sockets where it is not possible to confirm that the base of the pile is free from debris

xii) be a continuous construction process without any significant delays between final socket cleaning and completion of concreting

An important part of the design process is the confirmation of design assumptions and that the piles are installed as set out in the agreed piling method statement. For this reason, a suitably qualified and experienced geotechnical engineer should be on site to observe the pile installation. The engineer should (as appropriate):

i) observe and record drilling method and rate, drill rig response and assess and describe socket materials based on drill cuttings

ii) confirm roughening and cleaning tools are suitable and in good working condition. Observe their use to confirm that they are not extracted too quickly to cause pile excavation instability

iii) observe and record the minimum level of drilling fluid in pile hole

iv) observe and record water level in pile hole (for essentially dry sockets with some water inflow) and assess the potential for collapse of socket if dewatered or need for concrete placement by tremie

v) observe and record qualitatively the volume of material recovered from excavation during cleaning – should be minimal at end of cleaning process

vi) observe the pile hole excavation from the surface if practical and safe to do so. Under no circumstances should any personnel enter the pile excavation or approach the pile excavation without appropriate barriers in place. Record results of observations.

vii) observe and record dipping of pile hole to confirm pile length and to "feel" for debris at base of pile

viii) review test results for drilling fluids if appropriate, particularly prior to placement of concrete. Formal records to be provided by drilling contractor.

ix) observe reinforcement and its placement confirming that the reinforcement cage is straight and of correct diameter and appropriate spacers have been used

x) observe and record tremie process, including use of tremie plug, initial placement of tremie at base of pile excavation, dipping to confirm height of concrete in pile hole, depth of tremie in concrete, concrete volume vs height curves

xi) observe and record the presence of uncontaminated concrete at top of pile at end of concreting process

xii) record any time delays

The on-site presence of a suitably qualified and experienced geotechnical engineer may be sufficient to provide confirmation that piles have been installed in accordance with the agreed method statements and are likely to meet design performance. However, if required, further confirmation of performance can be obtained through pile load and integrity testing. In the authors view:

i) all piles should be low strain integrity tested to requirements set out in AS 2159-2009. For piles with length to diameter ratios of greater than about 10 (in hard soil or stronger material), low strain integrity testing may not be able to detect defects within the lower part of the pile. For such applications, integrity should be confirmed using cross hole sonic testing or high strain dynamic testing (see below).

ii) for major structures with relatively heavily loaded rock socketed piles (with respect to structural strength) cross hole sonic tubes should be installed in up to 40 % of piles to be constructed and cross-hole testing be completed on a minimum of 50 % of the piles with tubes installed.

iii) in all projects that involve rock socketed piles (other than minor works) high strain integrity testing (and CAPWAP analysis) be performed on between 2 % and 5 % of working piles to verify serviceability load. Testing should comply with the recommendations set out in AS 2159-2009.

iv) for major structures with heavily loaded rock socketed piles consideration be given to undertaking a bi-directional load test on a working or trial pile to a minimum of serviceability load. Testing should comply with the recommendations set out in AS 2159-2009. Such tests should be carried out in lieu of static load tests which may be impractical to perform.

6. FOOTING SYSTEM PERORMANCE

The above discussion has focussed on the design, analysis, construction and verification of individual piles. A footing system can comprise a few to in excess of many hundreds of individual piles, groups of piles supporting pile caps or piles supporting shallow footings or rafts (e.g. piled raft). In such instances the interactions between piles and other foundation components can be significant and analyses which consider such interactions are required for the design of the footing system. This is particularly important for the design of a large heavy structure (e.g. a tall building) supported on a piled raft and founding in soft, weak or weathered rock. The interactions are usually not of significance if the piles found in medium to high strength rock as settlements and interactions are generally small.

As with the design of individual piles, in the design of pile groups, piled footings and piled rafts, serviceability and not strength is the critical factor. The problem, which is common to all footing systems, is to be able to estimate displacements at serviceability loads.

The areas of interest with respect to the assessment of footing displacement are shown in Figure 1. These areas of interest extend well beyond the rock adjacent to individual piles and can incorporate the ground to at least a depth of twice the footing width.

There are many proven, hand calculation methods and computer based analytical tools available to estimate the load versus displacement performance of individual piles, pile groups and global footing systems and which provide a quantitative assessment of foundation structure interaction which is required for design of the footing system and the load bearing elements of the structure. The more complex computer based tools (e.g. non-linear continuum (e.g. PLAXIS2D and 3D, FLAC2D and 3D) and discontinuum (e.g. UDEC, 3DEC) methods), in particular, are very powerful when used competently and the results are tempered with experience and judgement. However, although these tools are in general relatively easy to use, they are open to misuse especially if the analyst in inexperienced or does not have a good understanding of numerical methods, plasticity, soil and rock behaviour and constitutive modelling.

It is beyond the scope of this paper to provide a summary of the many analysis methods that are available and how they can be used in serviceability based design. A common misconception is that discontinuum methods (e.g UDEC) are required to model foundation structure interaction problems (e.g. footings and retention systems) in fractured rock. This is not the case. Reasonable results can usually be obtained from continuum models (e.g. PLAXIS and FLAC) provided reasonable and representative rock mass properties (which account for the structure in the rock) are assumed. In particular, the modelling of discontinuities is generally not required for piled footings subjected to axial load as the impact of the discontinuities can be incorporated into the rock mass properties. For some situations however where failure to a free surface can occur; e.g laterally loaded piles or retention piles, the orientation of discontinuities present in the rock mass may need to be considered. Many of the continuum methods that are commercially available allow a small number of discontinuities to be included in the analysis. For most applications the introduction of one to a few discontinuities into the model is sufficient to account for most credible and critical joint configurations.

One aspect that all the various analysis (both continuum and discontinuum) methods have in common is that to obtain meaningful results, appropriate input parameters (particularly for rock strength and deformation properties) need to be used. As in most applications the strength and deformation properties of the rock mass may not be known with sufficient confidence, it is good practice and prudent to undertake analyses assuming a range of credible properties for the rock mass. In some applications, probabilistic analysis may need to be undertaken to better quantify the potential for unfavourable settlement and rotation (e.g. under wind load) of the footing system.

The remainder of this paper provides some brief comments on the very important issue of obtaining relevant rock properties for analysis and design.

7. ROCK PROPERTY DETERMINATION

Assessment of rock properties for analysis and design should only be undertaken after the development of an adequate subsurface model of the site which is based on a reasonable understanding of the geology and geological history of the site. This may require an understanding of formation processes, how geological structures are developed and how subsequent factors affect the extent and depth of weathering. Without a reasonable understanding of the geological history of the site, any assessment of stratigraphy, rock structure and/or rock properties could be seriously in error.

One example of this was for the 1000 m plus Nakheel Tower in Dubai. Geotechnical investigations at the site by others indicated that the weak calcareous rock underlying the site was moderately to highly fractured. This had implications

for the assessment of mass modulus and strength and hence on the design of the footing system and estimate of displacements. The geological history of the area indicated the rock to be relatively young (Holocene age) and was unlikely to have experienced any activity which would have caused the rock to be fractured. The fractures observed in the core were attributed to the double tube coring methods used for the ground investigation. Subsequent ground investigation using triple tube methods showed the rock to be massive. Figure 30 compares the rock core obtained from double and triple tube coring for the Nakheel Tower project.

The geological model can provide a significant insight into the likely behaviour of the rock and of the rock properties. Confirmation of rock properties is usually obtained from the results of appropriate laboratory testing. However, the results of laboratory testing depend critically on the quality of the samples. This applies equally to tube samples in soil and core samples in rock. The sample quality can be significantly affected by the drilling method and the type of core barrel used in soft rocks, where stress relief and slaking may be important. Careful sealing, storage, transport and test preparation are also important if representative material properties are to be established by laboratory testing.

Rock samples should be tested as close to saturation as practical as like soil, their strength and stiffness properties depend on the degree of saturation. This should also apply (in general) to rocks that have been sampled above the water table. It is also important to maintain the insitu water content of rocks if testing or observation of samples is to be relied upon. Rock samples that have been allowed to dry out and are then resaturated for testing may not be representative.



Figure 30: Triple tube and double tube core barrel drilling

Even with the best sampling, sealing, storage and transporting practices, rock core samples will still undergo stress relief and disturbance. This is particularly evident in weak rocks sampled from depth. For the Nakheel Tower project, rock samples from up to 200 m depth were retrieved for laboratory testing. The recovered core samples (from below about 30 m depth) were often observed to delaminate within minutes of being brought to the surface. This was

attributed to the low permeability and low strength of the rock, the significant depth from which they were recovered and the sudden loss of confinement and water pressures as the core was sampled and brought to the surface. The samples were essentially blown apart by the internal pore water pressures (and possibly dissolved air). The delamination has an obvious and significant impact on the strength and deformation properties of the rock. Figure 31 compares the uniaxial compressive strength and modulus values measured in uniaxial compressive strength tests with those calculated from pressuremeter tests at the Nakheel Tower site. The modulus and strength parameters measured in the laboratory tests are significantly lower than calculated from the insitu pressuremeter tests. Subsequent bi-directional load tests on test barrettes installed at the site confirmed the higher modulus and strength values calculated from the pressuremeter testing (Haberfield and Paul, 2011).

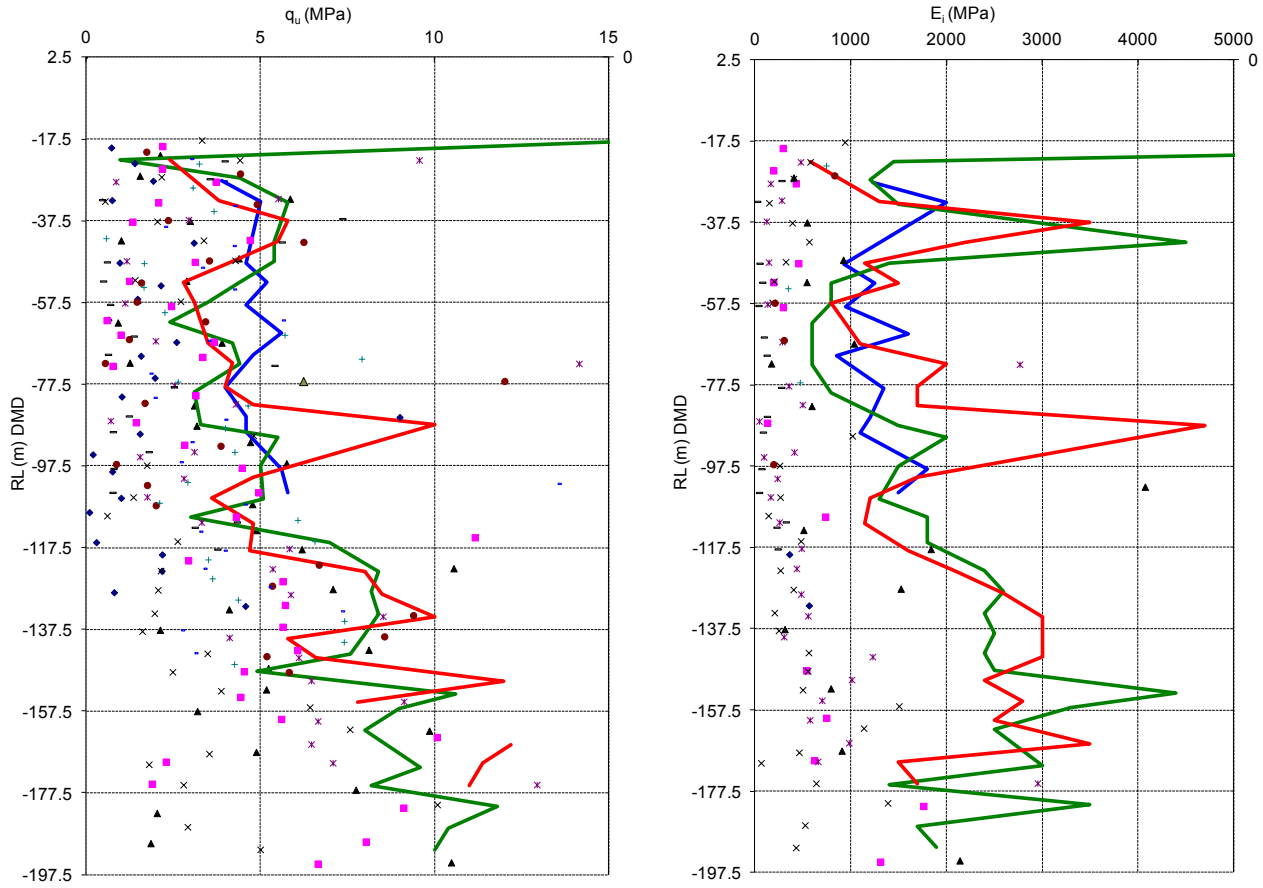


Figure 31: Comparison of strength (q_u) and deformation parameters (E_i) from laboratory tests (points) and insitu pressuremeter tests (lines).

Whilst carefully conducted insitu testing usually causes some disturbance and stress relief, the effects are much less than that can occur with rock samples obtained from coring. For this reason, in situ testing usually provides more representative estimates of properties for analysis and design. However, this does not mean that laboratory testing should not be carried out, even when extensive in situ testing has been undertaken As discussed below, laboratory tests can provide significant insight into the nature and constitutive behaviour of the rock which is difficult to obtain from insitu testing.

Unfortunately, the amount of laboratory and in situ testing undertaken for projects is less than ideal. For many projects, the assessment of rock strength and deformation properties is based on visual classification of weathering, with little or no testing of the rock. For some projects, standard penetration testing, point load testing and/or moisture content testing may be carried out to provide some confirmation of the strength as assessed from the visual classification of weathering. In the authors view, standard penetration testing even in soft rock is of little if any value (especially at deeper depths) and the practice should be discontinued in favour of higher quality tests.

The relative merits of carrying out more advanced insitu testing such as insitu pressuremeter testing, crosshole seismic testing and static load testing and more advanced laboratory testing such as triaxial testing (including unconfined

compressive strength testing) and direct shear testing are only realised by relatively few informed clients and hence are carried out on relatively rare occasions. The additional information obtained from such testing not only provides better estimates of rock strength and deformation properties but also provides a better basis for assessing practical footing construction procedures and construction risks.

Unfortunately, some ill-informed geotechnical professionals express the opinion that there is no benefit in carrying out more advanced testing to better establish the strength and stiffness parameters of the rock. Instead, they argue that a satisfactory footing design can be based on "experience" and a visual assessment of the rock. As a result, the design of the footing system is generally overly-conservative and can result in over-designed foundations, often at significant cost to the project, and in some cases the foundations may be impractical to build.

Ground investigations that include only basic and limited testing (e.g. SPT and point load strength testing) are often attractive to the client as they are inexpensive. However, for the relatively small additional cost to conduct a more thorough ground investigation with a reasonable component of insitu and laboratory testing, significant savings can be made in the construction of the foundations (Haberfield, 2012). Couple this with on-site presence during construction by experienced geotechnical professionals (to log sockets, confirm raft subgrade and carry out appropriate testing for example), a lower cost and lower risk foundation solution is generally achievable.

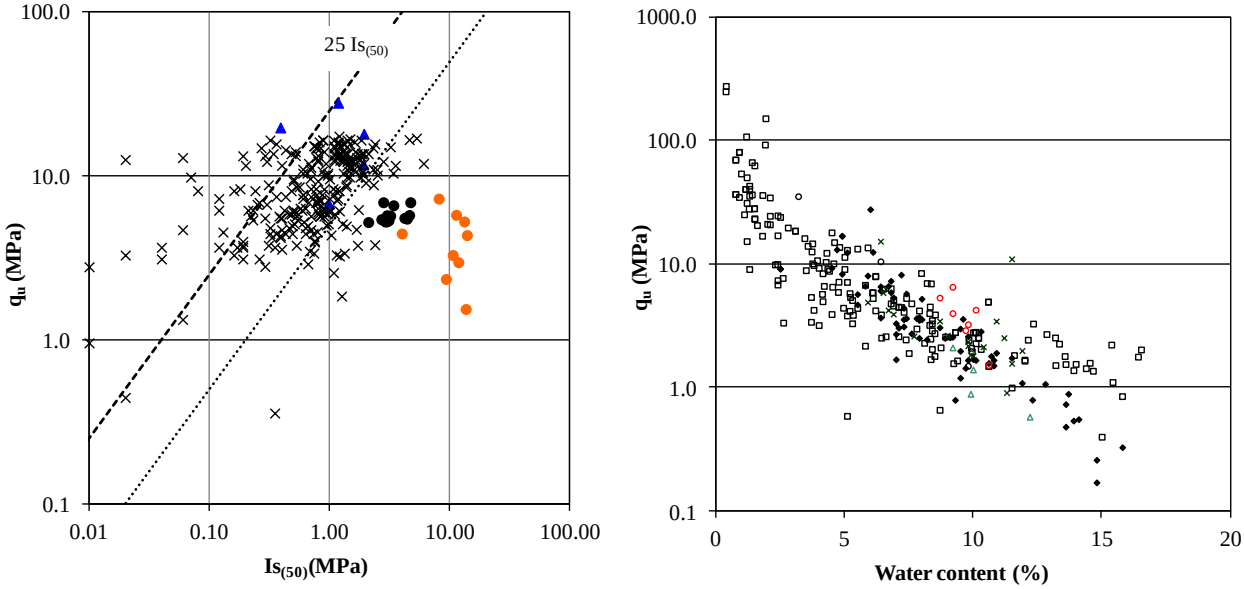
More extensive and appropriate ground investigations allow a better assessment of rock properties, which in turn allow a serviceability design based approach to be undertaken (rather than the working stress method). A serviceability based analysis/design approach allows an improved understanding of individual pile and footing system performance and construction techniques to be more fully utilised, and coupled with observations during footing construction, can reduce the risk and costs associated with installation of such footing systems.

The question arises therefore as to what laboratory and in situ tests are available and practical for testing of rock to allow a reasonable estimate of strength and deformation properties? What are the limitations of these tests and how are the test results best interpreted to obtain the rock properties required for analysis and design?

7.1 Laboratory testing for intact strength and modulus

The point load strength index ($Is_{(50)}$) has often been used as a quick and inexpensive means of estimating intact rock strength. Many factors influence the test result and its interpretation, including the difference between axial and diametral strength testing and nature of the failure mode. While attempts have been made to relate the results to unconfined compressive strength (q_u) values, such relationships appear to hold only for localised areas. Results for Melbourne siltstone covering a large number of sites are shown in Figure 32(a). There is a large scatter, and many of the results lie outside the relationships $q_u = 25\ Is_{(50)}$ and $q_u = 5\ Is_{(50)}$, suggesting such relationships are of little value in the general approach to estimating intact rock strength of this particular rock. However, $Is_{(50)}$ results can be useful for high strength rocks where the strength and deformation properties of the rock are usually not critical for footing analysis and design.

Empirical correlations with other sample properties have also been used and perhaps are of more practical use than point load strength index tests. Plots have been produced for Melbourne siltstone relating q_u to saturated moisture content (see Figure 32(b)) and have proved useful for a range of sites around Melbourne. Similar correlations between saturated moisture content and other rock properties (e.g. modulus and effective strength parameters) are also available (Chui, 1981). The fact that rock properties (especially for weak rocks) show reasonable correlation with saturated water content is not surprising as it is well known that the properties of soil are dependent on void ratio. Saturated water content is also a measure of the porosity or void ratio of the rock.



(a) (b)

Figure 32 Variation of uniaxial compressive strength (q_u) with point load strength index ($Is_{(50)}$) and saturated water content for Melbourne siltstone

Direct measurement of uniaxial compressive strength can be affected by the sample preparation (particularly saturation) and the testing rate adopted. All unconfined compressive strength tests (especially on weak rocks) should be carried out on samples that are as close to fully saturated as practical (usually obtained by soaking the samples in a bucket of water for 24 hours) and tested at a displacement rate that results in failure over at least 15 minutes. Experience has shown than even partial drying of samples can have a significant impact on strength and modulus measurements. The testing of saturated samples may preclude the use of strain gauges to measure intact modulus and a device which measures displacement over the middle third of the sample may be required. Modulus values calculated from end platen displacements can provide a significant underestimate of the actual intact rock modulus. If end platen measurements are used, the modulus should be estimated as a tangent modulus from the steepest gradient of the load vs displacement response.

Triaxial testing has been used to measure rock strength and may be better suited for soft rocks and rocks that slake when placed in water. Effective stress triaxial tests (consolidated drained and consolidated undrained with pore pressure measurements) can be used to obtain estimates of effective strength properties. However such tests should be single staged tests as the development of a failure plane in the first stage of the test can have a significant impact on the strength measured in later stages. In most applications which relate to the design of footing systems, the effective strength parameters of the rock are usually of minor importance and are therefore rarely tested for. As discussed above, it is the modulus of the rock that is of primary importance.

Various laboratory methods have been used to measure the intact rock modulus of rock in compression. The results show that, as for soils (e.g. Carter, 2005), the value measured is strain-dependent and strain-rate dependent. Figure 33 shows the results of Young's modulus measurements for a carbonate-cemented siltstone using resonant column and cyclic triaxial testing. The resonant column test results shown in Figure 33 may be an underestimates of the true small strain modulus due to equipment compliance issues with the test apparatus when testing material of relatively high stiffness. Such compliance issues are common with most laboratory based stiffness measurements of weak rock and need to be considered in the assessment of the test results.

The choice of a modulus for design therefore depends on the likely strain level for the loading condition. Values for analysis of earthquake, wind or static loading will each require an assessment of the relevant strain level and hence the appropriate modulus. Strain levels will also vary around the footing, with higher strains occurring near loads or excavations and reducing away from the areas. Non-linear finite element programs commonly used for analysis of foundation structure interaction problems (e.g PLAXIS and PLAXIS3D) include constitutive models that account for this variation in modulus with strain.

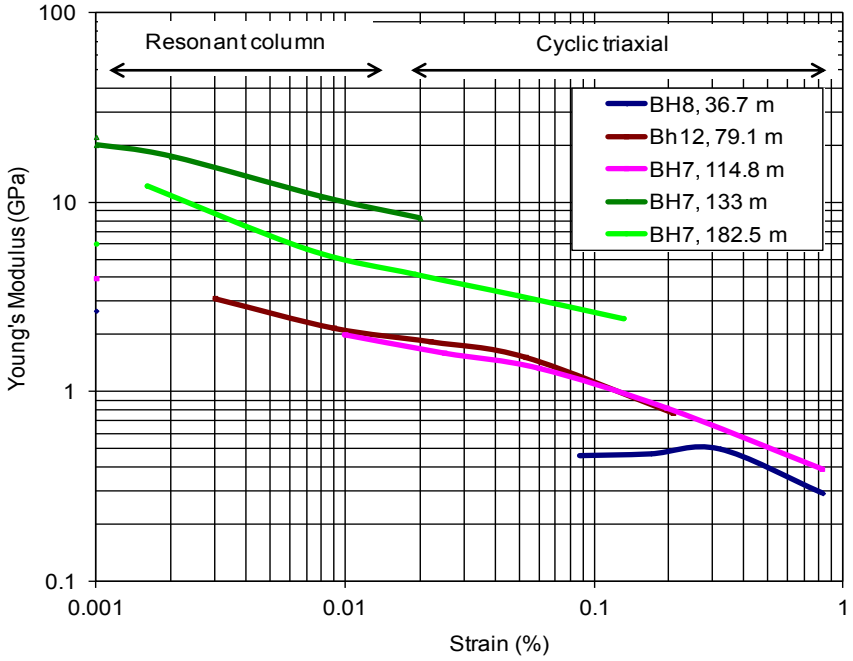


Figure 33: Young's modulus versus strain level for carbonate siltstone

The oedometer test is commonly used to estimate the one-dimensional compression characteristics of soil. Such tests may also be suitable for estimating the near one-dimensional compression of the ground directly underlying the base of the footing system for a tall building founded in very weak rock, for example. Such testing can also provide an indication of time dependent consolidation and creep settlements.

Attempts to measure the modulus of relatively stiff materials such as hard clay and very weak rock in laboratory oedometer tests require an appreciation of compliance effects and the application of high pressures. Oedometer testing is not suited to low strength or higher strength rocks. Figure 34 shows the results of a loading increment in an oedometer test on a carbonate-cemented siltstone for the Nakheel Tower project. The overall displacement measurement which includes platen compression is significantly larger than the sample displacement measured by direct methods. The creep observed in the platen measurements is also significant and not observed in the direct measurement. Oedometer testing of relatively stiff soil and weak rock therefore requires direct measurement of compression of the sample to obtain a reasonable estimate of constrained modulus.

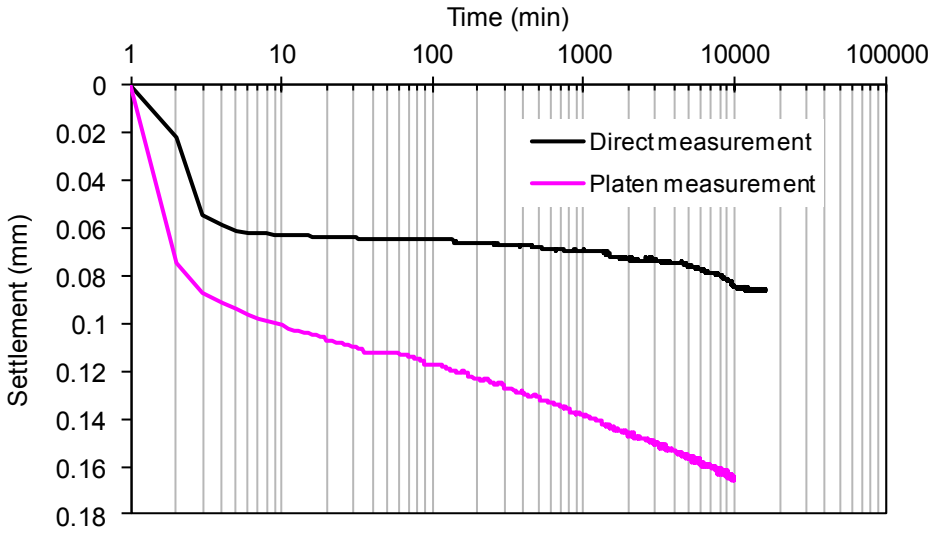


Figure 34: Effect of platen compression on measured response

7.2 Assessment of rock mass strength and modulus from intact values

In Section 6 it was noted that rock mass (continuum) models were able to provide a reasonable and practical approach to most foundation structure interaction problems (e.g. footings and retention systems) in fractured rock. In some applications however, e.g. retention systems or laterally loaded piles, it may be necessary to introduce (usually a small number of) discontinuities into the model to account for critical planes of weakness in the rock mass. Use of continuum methods to assess stability of slopes and excavation and temporary support of underground spaces in fractured rock may need special consideration and may be better suited to discontinuum or blocky rock models.

Some of the key inputs into the analysis of footing systems in rock masses is the selection of the rock mass strength, stiffness and dilation properties.

7.2.1 The Hoek-Brown criterion

One of the most flexible rock mass models is the Hoek-Brown Geological Strength Index (GSI) model. The Hoek-Brown failure criterion was developed in the 1970s to provide input for the design of underground excavations. In 1995, the specific classification system called the Geological Strength Index was introduced. Hoek and Marinos (2007) give a history of the development of the GSI to 2007.

The generalised Hoek-Brown criterion was introduced in 1994 (Hoek, 1994) and incorporated both the original criterion for excellent to fair quality rock masses and the modified criterion for poor to very poor quality rock masses. The criterion states:

$$\sigma_1' = \sigma_3' + UCS\left(m_b \frac{\sigma_3'}{UCS} + s \right)^a$$

$$m_b = f(m_i, GSI)$$

$$s = f(GSI)$$

$$a = f(GSI)$$

where m_b, s and a are generalised strength parameters of the rock mass

The Hoek-Brown GSI model is widely known and offers flexibility in its application to a wide range of rock mass quality. The two main inputs into the model are m_i and *GSI* - m_i is based on rock type whilst GSI is usually assessed visually from a set of charts which classify the rock mass according to rock structure (intact through blocky to disintegrated) and joint surface condition (from very good to very poor).

Szymakowski (2003) investigated the application of the Hoek-Brown criterion to the results of laboratory CNS direct shear tests on rock samples 270 mm thick, 400 mm wide and 280 mm high. He included a wide range of variables in these tests on rock having artificially-created joints. The rock had UCS values in the range of 1 to 5 MPa.. Five joint dips ranging from 0° to 90° to the shear plane were tested, and three different joint spacings were included. A summary of the results relating to the rock mass strength of the samples are shown in Figure 35. Figure 35 shows the measured peak shear stress versus normal stress on the failure plane, normalised with respect to the uniaxial compressive strength of the intact rock. Also shown are estimates of the rock mass strength using the GSI model and back-calculated estimated of fracture spacing "s". The recommended value of "s" from the GSI model for GSI = 62 is 0.0147 which is very close to the lower bound curve fit to the test data.

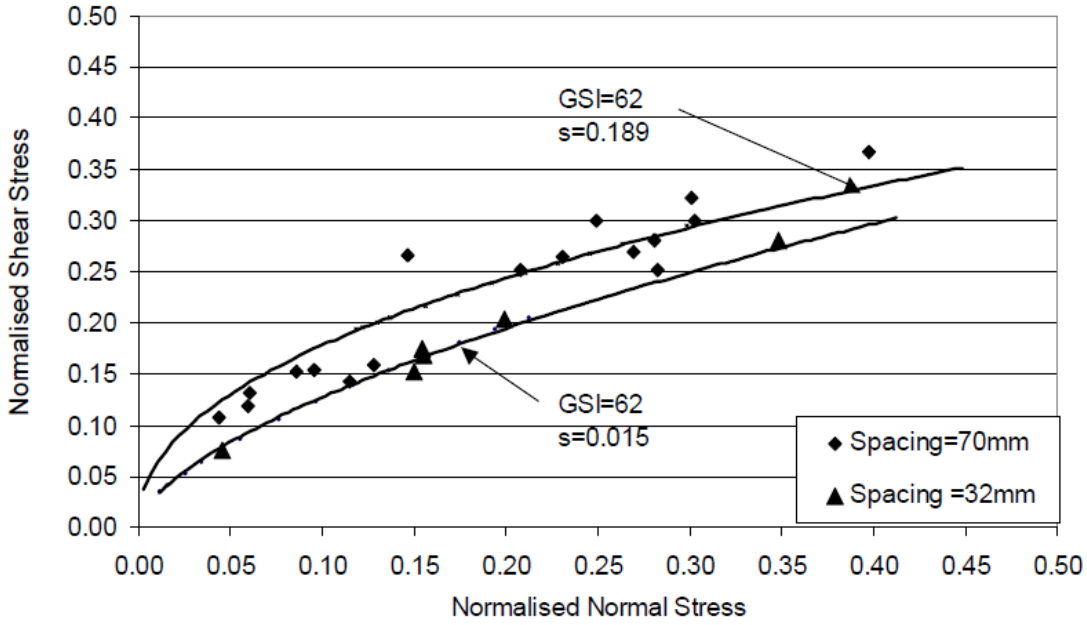


Figure 35 Normalised peak shear stress versus normal stress compared with Hoek-Brown (Szymakowski, 2003)

There was good agreement between the results and the predictions from the GSI, even though three different failure modes were identified, depending on the joint spacing and orientation of joints to the failure plane. However the results covered only one value of GSI and a small range of UCS values. Whether the GSI is a suitable model for prediction of rock mass strength (and therefore its value in predicting bearing capacity) is therefore not fully resolved.

7.2.2 Application of GSI to rock mass modulus prediction

Hoek and Diederichs (2006) have provided methods for empirical estimation of rock mass modulus. They established relationships between the rock mass modulus and GSI for a range of disturbance factors (D) between 0 and 1, based largely on analysis of published values from tests in China and Taiwan. Figure 36 shows the results expressed as the normalised modulus (E_m/E_i) against GSI. In the absence of direct measurement, the value of E_i can be established from UCS using proposed values of the modular ratio, MR (where $MR = E_i/UCS$).

According to Hoek and Diederichs, the reliability of measured values of E_i is often suspect because of specimen damage. This specimen damage has a greater impact on modulus than on strength and, hence, the intact rock strength, when available, can usually be considered more reliable.

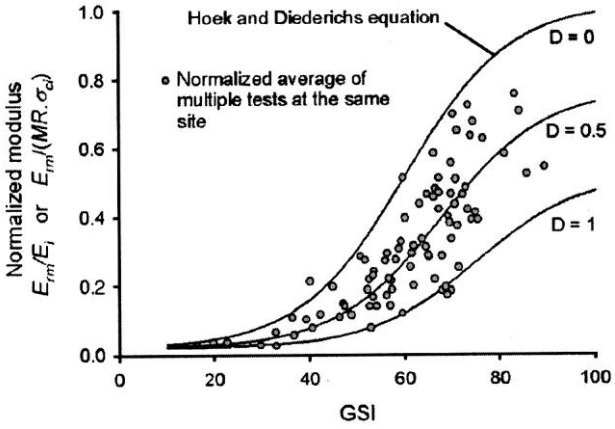


Figure 36 Normalised rock mass modulus versus GSI (Hoek and Diederichs, 2006)

7.3 Field measurement of rock mass modulus

Pressuremeter testing has been used to measure rock mass modulus and strength. However the interpretation of measurements is subject to a number of factors. These factors include the nature of the cavity expansion model adopted, the effects of radial cracking, disturbance and drainage. Modulus can be interpreted from the results of first loading or from any number of unload/reload loops. The first loading modulus is generally appropriate for analysis of piled foundations, whereas the unload/reload modulus is more appropriate for low strain applications such as in retaining wall design. Figure 37 shows a range of results of pressuremeter tests conducted in different rock types. A significant amount of information can be gained from the shape of the pressuremeter curves. For example, tests in fractured rock masses show a response with greater curvature than less fractured rock masses of the same intact rock strength and weathering. It is of benefit to compare pressuremeter curves from across a site to assess the relative strength and stiffness characteristics of the rock mass at different depths and locations.

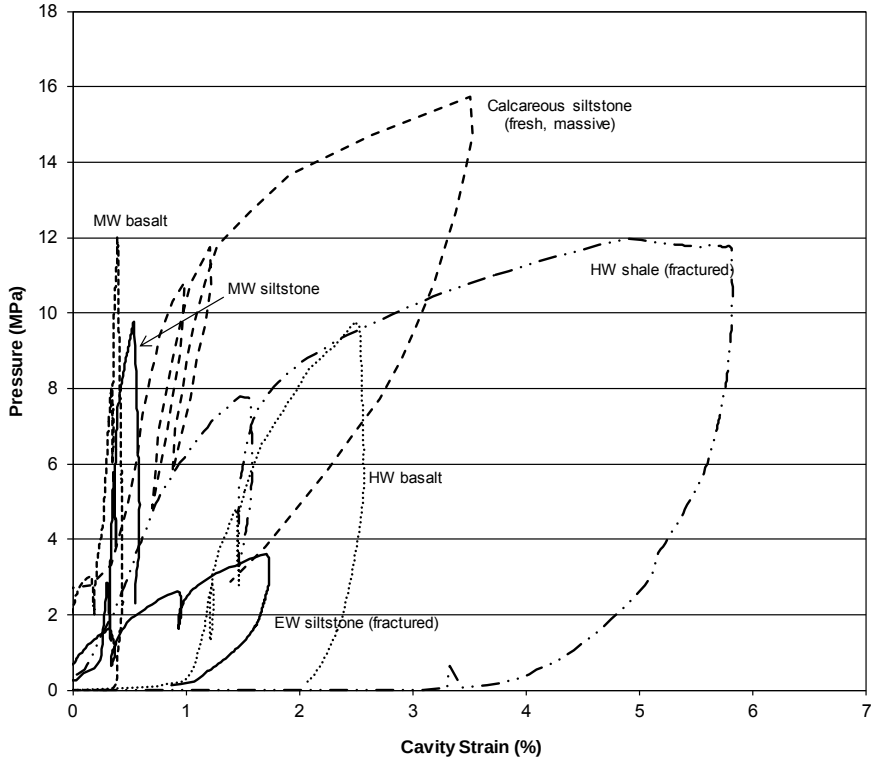


Figure 37 Typical pressuremeter results in different rock types

The interpretation of strength from pressuremeter test results is not straight forward and requires experience and some subjectivity, and if possible confirmation through other tests. It also requires the test to be carried to significant strain levels which are commensurate with yielding of the rock mass. This is rarely possible in rocks with uniaxial strengths greater than about 5 MPa even when using a high pressure pressuremeter (20 MPa capacity). Assuming relatively high strain levels are achieved in the test does not necessarily mean a reasonable estimate of strength can be made. An assumption that the test is undrained and application of pressuremeter analyses used for clay may result in significant over-estimates of strength. On the other hand the application of pressuremeter analyses for sand is also not applicable. Haberfield (1997) provides a curve fitting process which allows estimates of mass rock strength to be made, however these estimates are sensitive to a reasonable estimate of rock mass modulus. Significant over or under-estimates of strength can be made if the assumed modulus value is not reasonable. A reasonable estimate of insitu horizontal stress is not practical from most pressuremeter tests in rock – such values must usually be assumed and can have a significant impact on strength assessment.

Benson and Haberfield (2003) compared the estimates of rock mass modulus for Melbourne siltstone from three methods of measurement. Figure 38 shows the modulus values measured from plate load tests, from pressuremeter tests and inferred from pile load tests. In these tests, the geotechnical strength was usually not reached. Where values of the UCS were available, the results were generally contained within the limits, $E = 50\ q_c$ and $E = 400\ q_c$. This is consistent with the range proposed from GSI by Hoek and Diederichs, (2006).

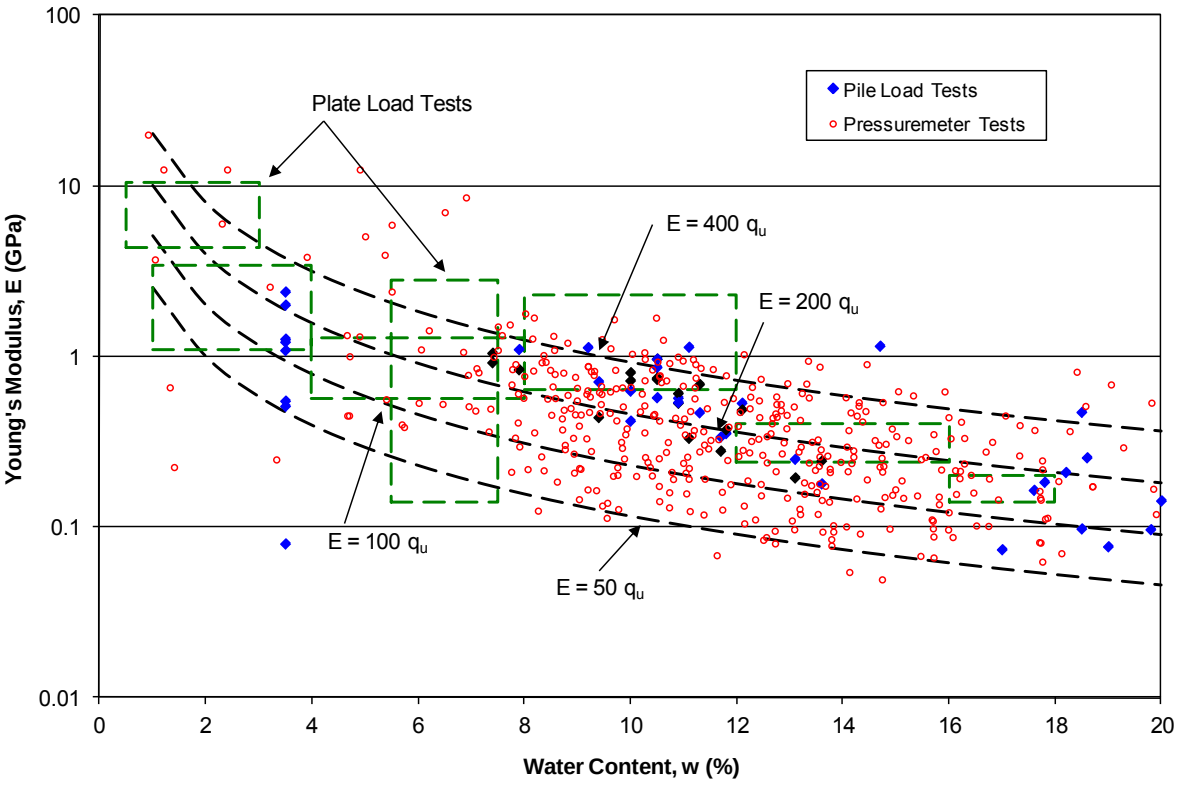


Figure 38 Young's modulus of Melbourne siltstone estimated from field tests (Benson and Haberfield, 2003)

An alternative method of estimating rock mass modulus was adopted at a site underlain by deeply weathered phyllite. The material proved impossible to sample for UCS or other testing, it slaked on exposure and pressuremeter testing was unsuccessful. Point load index tests on small pieces of core gave values of I_{s50} of less than 0.05 MPa. The design was for a bored pile footing system, albeit without much confidence in the design parameters for estimating settlement. On review of the footing system it was recommended that a precast pile be installed and PDA tested. From the interpretation of the PDA tests, a value of rock mass modulus was established. This showed that the building could be supported on shallow footings on the rock with acceptable settlements. Survey measurements undertaken during construction of the building indicated settlements within design estimates.

Cross-hole seismic and pressuremeter tests were used to measure rock mass modulus on a site underlain by carbonate-cemented siltstone. Figure 39a shows the results of these tests which were carried out to depths of up to 200 m. The small-strain cross-hole seismic tests gave estimates of modulus which ranged between about 3 to 7 times those measured in the pressuremeter tests at the same depths. This difference is consistent with the effects of strain level on modulus, see Figure 33. To obtain a modulus value for engineering design adopting the strain levels appropriate to field behaviour, the cross-hole values were reduced by a factor of five. Figure 39b shows the correspondence between the reduced cross-hole seismic values and the pressuremeter results. Subsequent pile load tests confirmed the design modulus values.

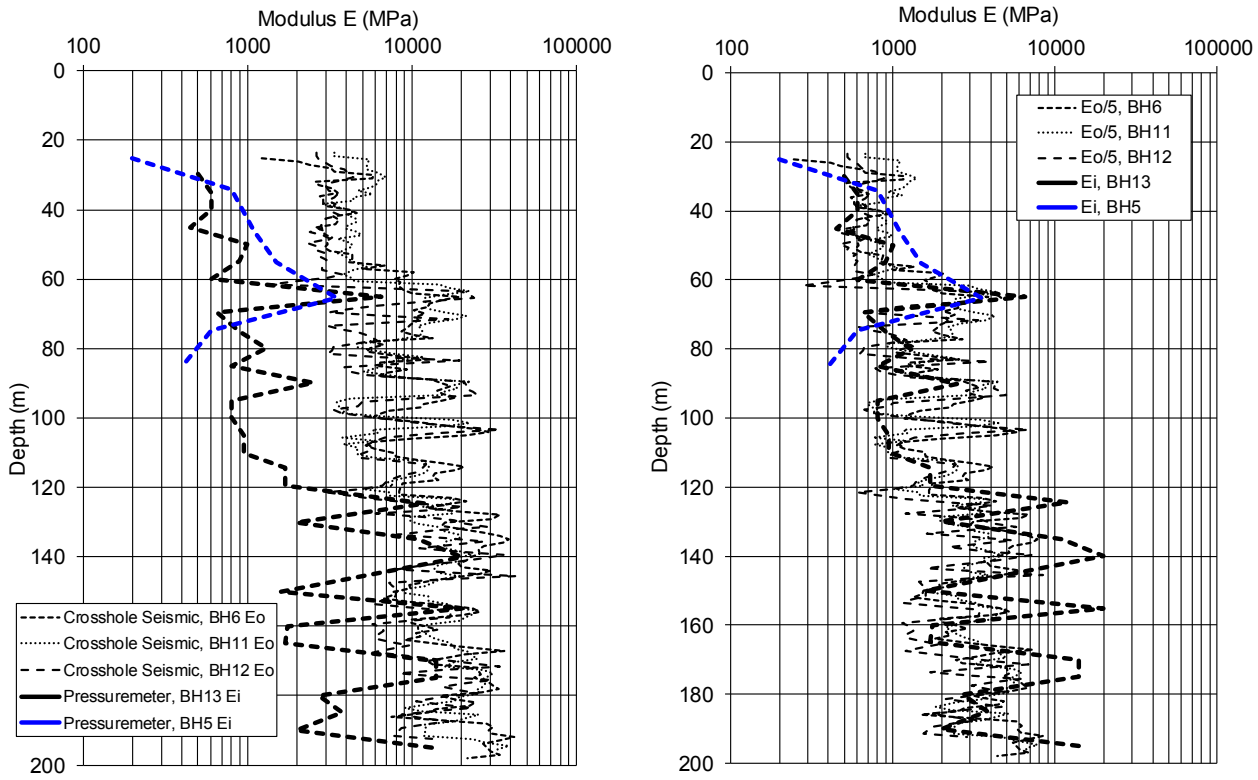


Figure 39aand b Comparison of pressuremeter and cross-hole seismic modulus

8 EXAMPLE APPLICATIONS

8.1 DESIGN FOR SERVICEABILITY

At Royal Domain Towers, Melbourne, the site conditions comprised a deeply-weathered rock profile of extremely to moderately weathered siltstone and sandstone, intersected by dykes. The dykes typically comprise material weathered to a stiff clay and pose a significant rick to pile performance. The foundation design was based on the use of socketed piles with serviceability loads ranging from 5 MN to 15 MN. The design serviceability condition was a pile head deflection of 1% of pile diameter. The 85 piles ranged in diameter from 0.75 m to 1.5 m.

A conventional investigation and design would suggest that piles with lengths of around 26.5 m would be required. A more sophisticated approach was recommended which included pressuremeter testing and laboratory UCS testing. The integrity of the design was protected by providing a geotechnical engineer on-site during pile construction to ensure the actual founding conditions complied with those assumed in the analysis and design.

For a typical 1.2 m diameter pile with a serviceability load of 15.3 MN, the conventional approach would lead to a pile length of around 26.5 m. The application of a more sophisticated testing approach and design for serviceability allowed the pile length to be reduced to 17 m, an overall saving of 9.5 m. There was also a greater confidence in the predicted

performance. Overall, the adopted pile design resulted in savings of 950 m in socket length, 950 m^3 in pile concrete and 1400 m^3 in spoil removal. In addition, the pile construction period was reduced by 42 days.

The integrated approach to investigation and design therefore provided significant cost and time savings to the project.

8.2 FLEXIBILITY IN DESIGN

The Northern Stand for the Melbourne Cricket Ground had site conditions comprising a profile of extremely to moderately weathered siltstone and sandstone extending from the surface. Based on geological interpretation of the site history a buried river channel was expected, and weathered dykes were present within the siltstone.

Three hundred piles were required for the building ranging in diameter from 0.6 m to 1.8 m with serviceability loads up to 30 MN. The ground investigation provided to tenderers was limited in scope and this, combined with a tight construction schedule, required an innovative approach to pile design.

The approach adopted was to drill each pile location with full-time engineering assessment of the rock conditions. A serviceability design was carried out using ROCKET97 to compute the required pile length for the design deflection under serviceability load. The approach provided significant time savings to the project which far outweighed the additional engineering input required.

8.3 GOING BEYOND EXPERIENCE

The planned Nakheel Tower in Dubai UAE will extend to in excess of 1 km in height making it the tallest building on earth. At about 2 Mt dead load it will also be one of the earth's heaviest buildings. The basement, around 105 m in diameter, is planned to extend to a depth of around 20 m (Haberfield et al, 2008). Construction commenced in early 2009, but was halted because of the Global Financial Crisis. As at end-2012, construction had not been resumed.

Subsurface conditions comprise soft calcareous rock extending to at least 300 m, the maximum depth explored. The highly saline groundwater table is at relatively shallow depth.

The initial investigation involved drilling boreholes to around 60 m depth with one extending to 120 m. Laboratory testing was carried out on nominally undisturbed samples. Because of stress relief the samples were considered partially disturbed and the results unreliable. The foundation analysis based on the results of this investigation indicated that piles would be required extending to at least 120 m depth. The estimated settlements were up to 500 mm with the potential for significant tilt of the building.

A detailed review of the results of the drilling, sampling and testing established that even though this work was quite detailed and of high standard, it was not adequate as a basis for sophisticated analysis. Also, it could not provide confidence in the predicted performance of the footing system. As a result, a further investigation was performed to the highest standard that could be achieved in the location. This included:

- drilling boreholes to depths of up to 300 m, with triple tube coring to ensure good sample recovery
- extensive laboratory testing for strength, stiffness and constitutive behaviour
- extensive insitu testing including pressuremeter and crosshole seismic tests
- testing of three full scale barrettes
- carrying out construction trials.

The results of the insitu testing allowed reliable constitutive models to be developed. These models were used in extensive 2D and 3D finite element and other analyses to arrive at the design of the foundations. These comprise barrettes up to 80 m in depth and carrying ULS loads of up to 90 MN. The results of the additional testing, interpretation and analysis meant the estimated total settlement was revised to around 80 mm with correspondingly lower tilt. Adopting a circular diaphragm wall for the basement solution allowed for the elimination of anchors for basement wall support. Figure 7 shows the foundation layout adopted.

Potential construction issues were identified and method statements were developed for the main aspects including integrity testing requirements for the barrettes. Without the level of sophistication in the investigation, analysis and design it is doubtful if the client could have had confidence that the geotechnical solutions for this world-ranked structure were achievable.

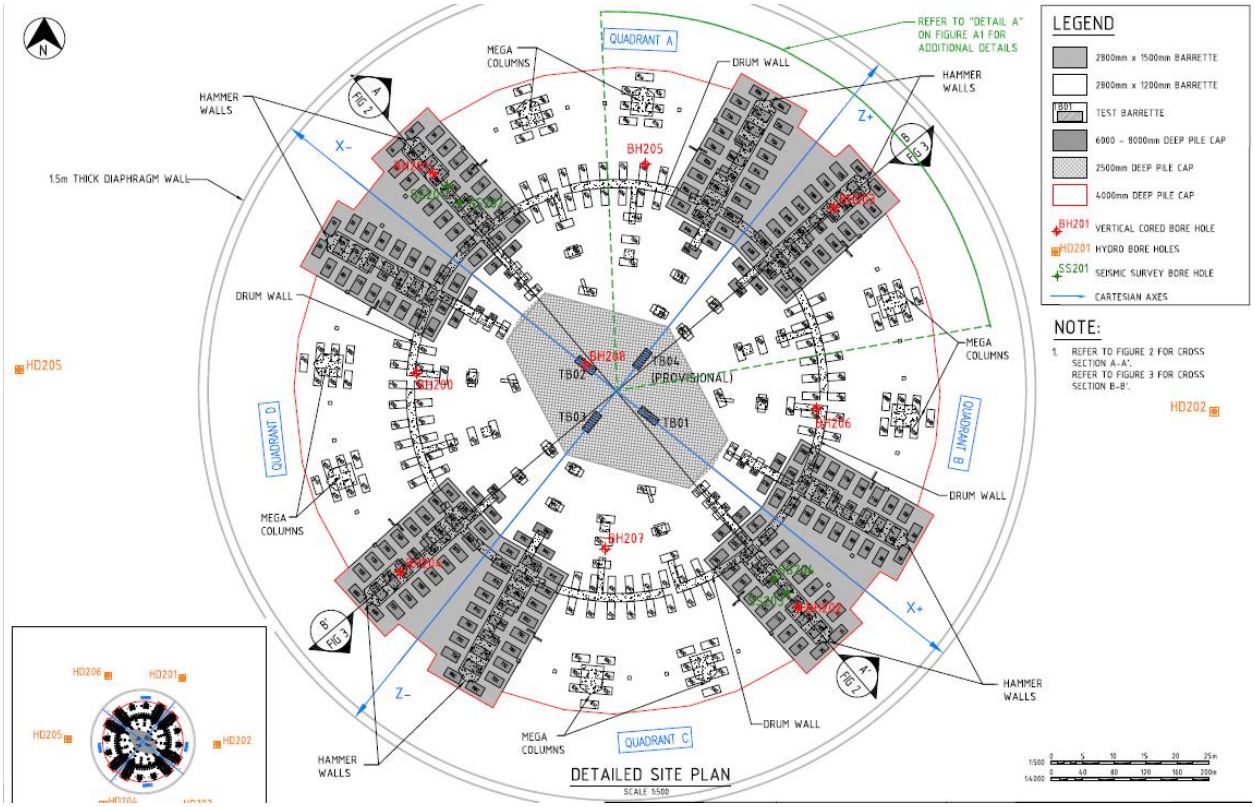


Figure 40 Nakheel Tower foundation plan

9 SUMMARY AND CONCLUSIONS

9.1 PREDICTION OF PILE RESPONSE

This paper has sought to illustrate the factors influencing the response of footings, and particularly piled footings, to load. Large and heavy structures are increasingly being supported on piles either as individual units or as significant components of piled rafts. An understanding of the pile response is critical in the assessment of these footing systems.

In practical terms, the design of individual piles will be controlled by deflection, that is, 'serviceability rules'. Where piled rafts are adopted, it is the deflection of the piles at serviceability loads which controls the load-sharing response between the piles and the raft.

Suitable methods are now available to adequately model pile, pile group and pile-raft load-deflection responses but these require quality and detailed ground investigation and quality pile construction and testing. Socket shear dominates pile performance. Socket shear is largely controlled by socket roughness and rock mass modulus and by pile construction. Estimates or measurements of rock mass and intact rock modulus are important input parameters into pile performance. Practical, direct measurement of rock mass modulus should be undertaken (e.g. by pressuremeter, cross-hole testing or load testing). In cases where this is not practical, rock mass modulus can be estimated from intact values and an assessment of GSI.

Careful control of construction is necessary for the performance of socketed piles to achieve the design assumptions. The contact between the concrete and the rock must be free from smear, drilling fluid residue, softened material and base debris. In practice this is managed by adoption of sound construction processes and application of site-specific QA procedures.

9.2 THE GEOTECHNICAL INVESTIGATION AND DESIGN PROCESS

Geotechnical investigation and design is often limited by the desire of clients to minimise the upfront costs for geotechnical work. However, benefits of good site investigation and design are potential savings in construction costs, potential for assessment of foundation alternatives and reduction of risk in groundworks. Table 2 illustrates typical

levels of investigation and design which could be categorised as basic, intermediate and comprehensive. Basic levels of investigation and design inevitably lead to increasing conservatism, and perhaps surprisingly, increasing risk and construction cost.

The challenge for geotechnical engineers is to be not satisfied with mediocrity as the tools are available to do much better.

Table 2 Geotechnical investigation and design process

Range of Investigation	**Basic**	**Intermediate**	**Comprehensive**
Ground Investigation	Geological maps, boreholes/pits geological history mapping		
Laboratory Testing	None	Moisture content UCS Point Load Strength Index	Triaxial (CUD, CD, cyclic) CNS direct shear Resonant column Local strain high pressure oedometer
Field Testing	Visual assessment, SPT		Pressuremeter RAX / joint orientation Surface/down hole geophysics Pile/plate load testing Hydrogeological testing
Analysis	None	Design charts Elastic analysis	Non linear finite element or similar Advanced constitutive models Discontinuum models
Design	Rules of thumb, Traditional values	Empirical methods	Serviceability - Based on results of analysis with “factors of safety” on settlement and capacity
Installation	None	Review of method statements and installation records Site presence	
Confirmation and verification	None	Footing/pile inspections PIT testing	Static load testing PDA & CAPWAP Cross-hole sonic Base coring

10 ACKNOWLEDGEMENTS

The information in this paper has been gained over many years in academia and consulting, through the research work of many people and involvement in many construction projects. Many of those that have contributed directly or indirectly are past colleagues and research students at Monash University – Ian Johnston, Ian Donald, Julian Seidel, Chris Powell, Serhat Baycan, Ben Collingwood, Jerry Szymakowski, Helen Pearce, Felix Cheng, and Bernie Francis. I would also like to acknowledge my colleagues in industry who have helped to implement the research into engineering practice and expanded my experience and knowledge through our interactions and the many projects we have worked on together. In particular I would like to acknowledge my colleagues at Golder Associates Pty Ltd - Jack Morgan, Gary Chapman, Max Ervin, Doug Goad, Jim Finlayson, Darren Paul, Neil Benson and David Gu.

The lecture of this paper was presented in 2007, and it has taken until now to document the lecture in this paper. Much of the impetus for completing the paper is owed to the Roads and Maritime Services of NSW as it was through their engagement that I was able to document my knowledge on the performance and design of rock socketed piles. I thank them for allowing the use of that documented information in this paper. I also gratefully acknowledge the assistance of the following organisations: the Department of Civil Engineering, Monash University and the Australian Research Council for support of the research into rock socketed piles; Golder Associates Pty Ltd for embracing the socketed pile

technology in their projects and providing support and allowing me the time to complete this work and Foundation Specialists Pty Ltd for the use of ROCKET.

11 REFERENCES

Baycan, S., 1997. *Improving the capacity of bored piles and ground anchors using expansive concretes*. PhD Dissertation, Department of Civil Engineering, Monash University, Australia.

Benson, N. and Haberfield, C.M., 2003. *Assessment of rock mass modulus*. 10th International Congress on Rock Mechanics, Johanessberg, Sth Africa.

Carter, J.P., 2006. *Who needs constitutive models.* EH Davis Memorial Lecture. Australian Geomechanics, Vol 41, No. 2, June, pp 1-27.

Carter, J.P. and Kulhawy, G.H., 1987. *Analysis and design of drilled shaft foundations socketed into rock*. Report 1493-4 for Electric Power Research Institute, Palo Alto, California.

Cheng, F.K.K., 1997. *A laboratory study of the influence of wall smear and residential drilling fluids on rock socketed pile performance*. PhD Dissertation, Department of Civil Engineering, Monash University, Australia.

Chiu, H.K., 1981. *Geotechnical properties and numerical analyses for socketed pile design in weak rock.* PhD Dissertation, Department of Civil Engineering, Monash University, Australia.

Clear, C.A. and Harrison, T. A., 1985. *Concrete pressure on formwork.* Construction Industry and Research Information Report 108, p32.

Collingwood, B., 2000. *The effect of construction practises on the performance of rock socketed piles.* PhD Dissertation, Department of Civil Engineering, Monash University, Australia.

Collingwood, B., Seidel, J.P. and Haberfield, C.M., 1999. *Laser based roughness measurement for design and verification of rock socket piles.* Proceedings 8th ANZ conference on Geomechanics, Hobart. 1: 375-382.

Coyle, H.M. and Reese, L.C., 1966. *Load transfer for axially loaded piles in clay.* Journal Soil Mechanics and Foundation Engineering Division., ASCE, 92(SM2):1-26.

Haberfield, C.M. 1997. Pressuremeter testing in weak rock and cemented sand. Geotechnical Engineering Journal, Proceedings ICE, July, Vol 125, pp. 168 - 178.

Haberfield, C.M., 2000. *Prediction of the initial normal stress in piles and anchors constructed using expansive cements.* International Journal for Numerical & Analytical Methods in Geomechanics, 24:305-325.

Haberfield, C.M. 2012. *Getting value from your site investigation*, Earthmover and Civil Contractor, March

Haberfield, C.M., Baycan, S. and Seidel, J.P., 1994. *Improving the capacity of piles in rock through the use of expansive cement additives.* 5th International Conference and Exhibition on Piling and Deep Foundations, Belgium, June: 1.2.1-1.2.7.

Haberfield, C.M., Baycan, S. and Seidel, J.P., 1996. *Field testing of bored piles in weak rock.* Proceedings 6th ANZ Conference on Geomechanics, Adelaide.

Haberfield, C.M. and Collingwood, B. 2006. *Rock socket pile design and construction: a better way?*. Proceedings of the Institution of Civil Engineers, Geotechnical Engineering 159, pp. 207-217.

Haberfield, C.M. and Paul, D.R. 2011. Footing Design of the Nakheel Tower, Dubai, UAE in Workshop on soil-structure interaction and retaining walls. Proceedings of the Technical Meeting TC207 ISSMGE, Dubrovnik, pp 35 to 52.

Haberfield C.M., Paul D.R. and Ervin M.C., 2008. Geotechnical design for the Nakheel Tall Tower, ISSMGE Bulletin, 2:4, 5-9

Haberfield, C.M. and Seidel, J.P.,2000. *The role of theoretical models in the analysis and design of rock socketed piles*, Developments in Theoretical Geomechanics, 465-488, Smith and Carter (eds), Balkema, Rotterdam

Hoek E., 1994. *Strength of rock and rock masses*, ISRM News Journal, 2(2) 4-16

Hoek, E., and Brown, E.T., 1997. *Practical estimates of rock mass strength.* International Journal Rock Mechanics and Mining Science and Geomechanics. Abstract, 34/8),1165-1186.

Hoek, E. and Diederichs, M.S., 2006. Empirical *estimation of rock mass modulus*, International Journal of Rock Mechanics and Mining Sciences, 43, 203-215, Elsevier

Hoek, E. and Marinos, P., 2007. *A brief history of the development of the Hoek-Brown failure criterion*, Soils and Rock, Vol 2

Holden, J.C., 1984. *Construction of bored piles in weathered rocks.* Research Report No. 34, Road Construction Authority of Victoria, Melbourne.

Horvath, R.G., Kenny, T.C. and Kozicki, P., 1983. *Methods for improving the performance of drilled piers in weak rock.* Canadian Geotechnical Journal., 20: 758-772.

Johnston, I.W., 1977. *Rock-socketing down under*. Contract Journal, 279: 53-53.

Johnston, I.W. and Lam, T.S.K. 1989. *Shear behaviour of regular triangular concrete/rock joints - Analysis.* Journal Geotechnical Engineering Division., ASCE, Vol. 115: 711-727.

Kodikara, J.K., and Johnston, I.W., 1994. *Shear behaviour of irregular triangular rock-concrete joints.* International Journal of Rock mechanics Min. Science and Geomechanics. Abstract., Volume 31(4):313-322

Kulhawy, F.H. and Phoon, K.K., 1993. *Drilled shaft side resistance in clay soil to rock*, Proceedings Conference on Design and Performance of Deep Foundations: Piles and Piers in Soils and Soft Rock, Geotechnical Special Publication No. 38, ASCE, 172-183

Lam, T.S.K. and Johnston, I.W 1989. Shear behaviour of regular triangular concrete/rock joints - Evaluation. Journal Geotechnical Engineering Division., ASCE, Vol. 115: 728-740.

Majano, R.E. and O'Neill, M.W., 1993. Effect of dosage and exposure time of slurries on perimeter load transfer in bored piles. Proceedings Second International Geotechnical Seminar on Deep Foundations on Bored and Auger Piles. Balkema, Rotterdam, Ghent, Belgium.

O'Neill, M.W. and Hassan, K.M., 1994. *Drilled Shafts: Effects of Construction on* Performance and Design Criteria. Proceedings International Conference Design and Construction of Deep Foundations, Orlando, Florida: 137-187.

O'Neill, M.W., Townsend, F.C., Hassan, K.M., Buller, A. and Chan, P.S., 1995. *Load Transfer for Drilled shafts in Intermediate Geomaterials-Draft Report*. FHWA-RD-95-172, US Department of Transportation, Federal Highway Administration, Virginia, USA.

Patton, F.D., 1966. *Multiple modes of shear failure in rock*. Proceedings 1st Congress International Society Rock mechanics. Lisbon, Vol. 1: 509-513.

Paul, D.R,, Haberfield, C.M. and Ervin, M.C. , 2010. *Laboratory and in-situ stiffness assessment in soft carbonate rock, Dubai, UAE*, Geologically Active – Williams et al (eds) Taylor and Francis Group, London

Pearce, H., 2001. *A micro-mechanical approach to the shear behaviour of rock joints*, PhD Dissertation, Civil Engineering Department, Monash University, Australia

Pells, P.J.N., 1999. *State of practice for the design of rock socketed piles*. 8th Australia-New Zealand Conference on Geomechanics. IEAust., Hobart, Tasmania, pp. 1-307 to 1-308.

Pells, P.J.N., Rowe, R.K. and Turner, R.M., 1980. *An experimental investigation into side shear for socketed piles in sandstone.* International Conference on Structural Foundations on Rock. Sydney, Balkema: 291-302.

Pells, P.J.N. and Turner, R.M., 1979. *Elastic solutions for the design and analysis of rock socketed piles.* Canadian Geotechnical Journal., 16: 481-487.

Poulos HG (2009) Tall buildings and deep foundations – Middle East challenges Proceedings of the 17th International Conference on Soil Mechanics and Geotechnical Engineering M. Hamza et al. (Eds.)

Randolph, M.F. and Wroth, C.P., 1978. *A simple approach to pile design and the evaluation of pile tests.* Behaviour of Deep Foundations, ASTM STP 670, R.Lundgren Ed.: 484-499.

Randolph, M.F. 2004. *PIGLET – Analysis and design of pile groups*. University of Western Australia. 2004

Reeves, M.J., 1985. *Rock surface roughness and frictional strength*. International Journal Rock Mechanics & Mining Sciences and Geomechanics. Abstract., Vol 22(6): 429-442.

Rowe, R.K. and Armitage, H.H., 1984. *The design of piles socketed into weak rock.* Report GEOT-11-84, University of Western Ontario, London, Canada.

Rowe, R.K. and Pells, P.J.N., 1980. *A theoretical study of pile-rock socket behaviour.* International Conference on Structural Foundations on Rock, Sydney, Balkema: 253-264.

Seidel, J.P., 1993. *The analysis and design of pile shafts in weak rock*. PhD Dissertation. Department of Civil Engineering. Monash University.

Seidel, J.P. and Haberfield, C.M., 1995. *The axial capacity of pile sockets in rocks and hard soils.* Ground Engineering, March : 33-38.

Seidel, J.P. and Haberfield, C.M., 1995. *Towards and understanding of joint roughness.* International Journal of Rock Mechanics and Rock Engineering, 28(2), pp. 69-92.

Seidel, J.P. and Haberfield, C.M., 2002(A). *A theoretical model for rock joints subjected to constant normal stiffness direct shear.* International Journal of Rock Mechanics and Mining Sciences, 39/ 5 pp 539-554.

Seidel, J.P., and Haberfield, C.M., 2002(B). *The axial capacity of pile shafts in rock – Prediction of field response.* Geotechnical Engineering Division ASCE.

Williams, A.F., 1980. *The design and performance of piles socketed into weak rock.* Ph.D. Thesis, Monash University, Melbourne, Australia.

Williams, A.F., Johnston, I.W. and Donald, I.B. 1980. *The design of socketed piles in weak rock.* International Conference on Structural Foundations on Rock. Sydney, Balkema: 327-347.

Williams, A.F. and Pells, P.J.N., 1981. *Side resistance rock sockets in sandstone, mudstone and shale.* Canadian Geotechnical Journal., 18: 502-513.

Zhang, L. and Einstein, H.H., 1998. *End bearing capacity of drilled shafts in rock.* Journal of Geotechnical and Geoenvironmental Engineering, ASCE, 124/7: 574-584.

DYNAMIC LOAD TESTING OF 2 METRE STEEL TUBULAR PILES DRIVEN INTO FOLIATED PHYLLITE BEDROCK

Bosco Poon, GHD Pty Ltd, Sydney, NSW, Australia, 61 29462 4849, bosco.poon@ghd.com
Geoff McKay, GHD Pty Ltd, Sydney, NSW, Australia, 61 29462 4847, geoff.mckay@ghd.com
Kim Chan, GHD Pty. Ltd., Sydney, NSW, Australia, 61 29462 4843, kim.chan@ghd.com
Luis Raúl Castañeda, Acciona and Ferrovial, Australia, 61 415 521 797, Lrcastaneda@afjv.com.au

ABSTRACT

Driven steel tubular piles of up to 2 m diameter have been used to support abutments and piers of a bridge over Nambucca River and floodplain. The bridge was designed by Arup-Aurecon Design Joint Venture (Lead Designers) with GHD leading the geotechnical design assessment in conjunction with Acciona Ferrovial Joint Venture (AFJV – Principal Contractor). Piles were to be driven through alluvium and founded on foliated Phyllite bedrock. The large diameter piles posed significant challenges on bearing capacity assessment and pile acceptance criteria, especially for anisotropic rock strength. Prior to pile driving, boreholes were drilled at each pile location, accompanied with a suite of rock index and UCS testing. AFJV and GHD oversaw geotechnical construction verification. All production piles were monitored with a Pile-Driving-Analyser to manage driving stresses and pile termination. Wave matching CAPWAP analyses were performed on 40% of the piles at the end-of-drive, or restrike, to satisfy specification requirements and limit over-driving. This paper presents discussions on the design and construction of the driven piles with findings from the extensive dynamic pile data obtained. Based on the shaft resistance distribution and toe resistance obtained from CAPWAP analysis, the mobilised pile shaft frictions f_s of the soil / rock materials, as well as the end bearing f_b of the founding Phyllite bedrock, are examined. The impact of the rock fabric foliation angle on the mobilised f_b, and the relationship between rock strength and the mobilised f_s are outlined.

Keywords: driven steel tubular pile, Phyllite, foliation, shaft friction, end bearing

INTRODUCTION

The Bridge over Nambucca River consists of a single bridge structure, comprising single substructures and separate superstructures. The 850 m long bridge facilitates the crossing of the Northbound and Southbound carriageways of the Pacific Highway Upgrade over Nambucca River, with central median barriers, separated by a horizontal clearance of 50 mm. The bridge is required to span over the Nambucca River, which is a navigational channel, and over the adjacent floodplains, including two local access roads and the existing Pacific Highway. The bridge superstructure consists of 21 simply supported spans, each comprises four 2.25 m deep precast post-tensioned U-Girders, with two girders across the width of each carriageway. The spans of girders vary from eleven spans of 39.5m and ten spans of 41.5 m. The floodplain section of the bridge was founded on up to 2m diameter steel tubular piles, designed to be driven through alluvial sediments and weak rock to nominal refusal on sound rock. Dynamic load testing using wave matching CAPWAP (CAse Pile Wave Analysis Program) analyses in conjunction with PDA (Pile Driving Analyser) were used to verify the pile integrity and mobilised capacity. This paper discusses geotechnical aspects associated with design and construction of driven piles. The methodology developed for construction to verify pile capacity and to meet acceptance criteria is outlined. Based on the shaft resistance distribution and toe resistance obtained from CAPWAP analysis, the mobilised pile shaft friction, f_s of the soil / rock materials, as well as the end bearing, f_b of the founding Phyllite bedrock, are examined. The impact of the rock fabric foliation angle on the mobilised f_b, and the relationship between rock strength and the mobilised f_s are outlined.

SUBSURFACE CONDITIONS

The geology of the bridge site is shown in Figure 1 and comprises alluvial sedimentary deposits from the Holocene and Pleistocene eras overlying Phyllite bedrock of varying degrees of weathering and strength. The Holocene deposits (Unit 2) are typically low strength silt and clay soils, which make up

of the upper 10 to 15 m of alluvial soils between Abutment A to Pier 9, then deepen to a maximum recorded thickness of 23 m at around Pier 11, before reducing in thickness northwards to 0 m just before Pier 20. The Pleistocene alluvial deposits (Unit 3) are generally reported to consist of medium dense to very dense gravels with various fines contents. For the southern viaduct up to the edge of the river bank, the relative thickness of the Pleistocene deposits is indicated quite consistently to be about 8 m. The Pleistocene thickness increases to about 14 m at around Pier 8, before reduces to typically 5-8 m thick between Piers 9 and 12, and further reduces to 2 m thickness between Piers 12 and 15 before pinching out.

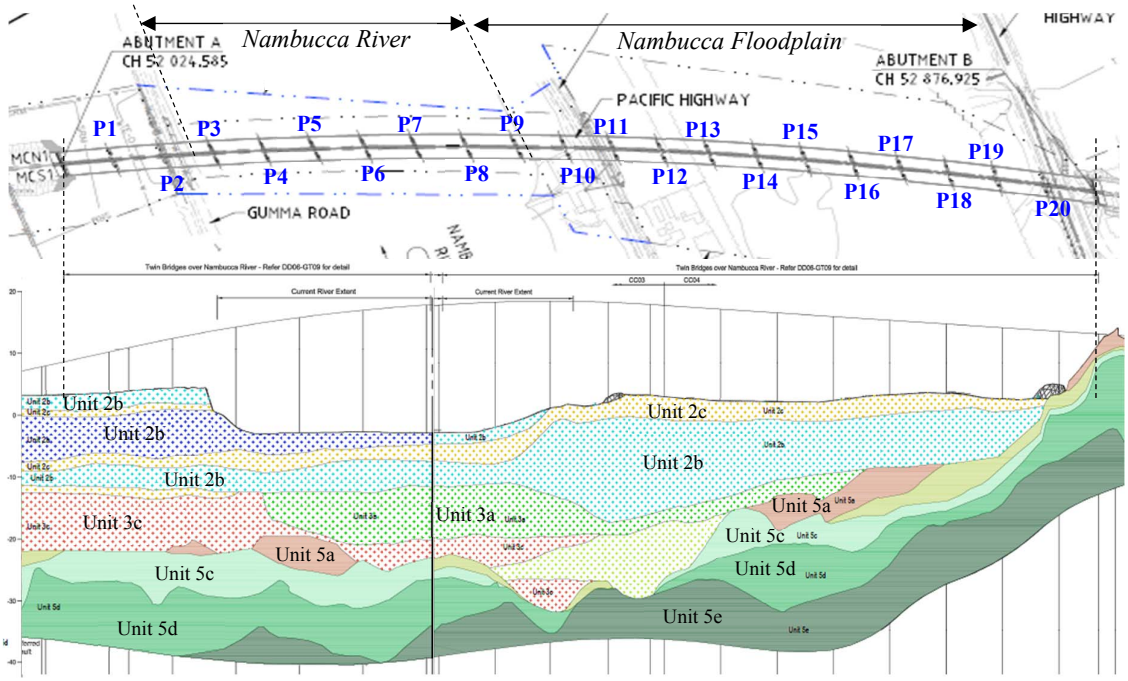


Fig. 1. Geological Longitudinal Section

Phyllites (Unit 5), ranging from residual soils to medium strength rock are typically encountered at depths of more than 25 m below ground level, with rock level rising towards Abutment B. The residual soil (Unit 5a) is only encountered north of Pier 13, where it attains a maximum thickness of 5m. The thickness of the extremely low strength Phyllite (Unit 5b) is variable. It is in the range of 2-4 m thick south of the River, less than 1 m to 1 m thick beneath the River, and 0-2 m thick north of the River. The thickness of the very low to low strength Phyllite (Unit 5c) typically ranges between 0.5-3.5 m, with localised thicker intersections at the southern abutment associated with the more intensely fractured and weathered zones, interpreted to be sub-vertically oriented fault zones of limited lateral extent. All boreholes drilled have encountered medium strength Phyllite (Unit 5d), with some extending into high strength Phyllite (unit 5e). The thickness of the Unit 5d ranges between 0.5-8 m. The Unit 5d/5e profile appears to be irregular, which could be related to the crenulation of the foliation within this area.

BRIDGE PILE FOUNDATION

Due to the variable nature of the geology and differing loading conditions for the bridge piers, a number of different founding arrangements have been adopted. Primarily driven steel piles have been used, with a steel driving shoe to improve driveability through the gravel layers and piles are founded on competent rock to obtain the required axial and lateral capacities

The southern spill through abutment comprises a 22.5 m wide reinforced concrete headstock, supported on five 1050 mm diameter steel driven tubular piles. The northern abutment is a 22.5 m wide reinforced concrete headstock, retaining structure with a spread footing. The piers consist of a reinforced concrete

headstock and two 1.8 m diameter columns. For the floodplain piers 1, 2 and 9 to 18, these columns are supported by two 2 m diameter steel driven tubular piles with 23 mm wall thickness. The river piers (piers 3-8) are similar in form with a headstock and two 1.8 m columns which are supported with a single pile cap. Piers 3, 4 and 8 are supported on four 1.2 m diameter steel driven piles. Piers 5, 6 and 7, which are the navigational piers subject to vessel impact loads, are supported on five 1.5 m diameter steel driven piles. All river piles have a wall thickness of 22 mm. Due to the shallower soil profile towards Abutment B, Piers 19 and 20 are supported on two 2 m diameter bored piles.

The upper section of the steel tubular driven piles has been designed as sacrificial for all locations. For the inland driven piles within the floodplain, a reinforced concrete infill extending to 10 m below pile head level is designed to act as the upper section of the pile, while the lower steel section of the piles (without concrete infill) relies on the steel. A corrosion allowance of 2 mm was assessed for the steel piles in the ground. The allowance was increased to 3 mm and 4 mm (location specific) to provide additional robustness at the request of the Principal. For the driven piles in the river, the concrete infill is extended from the pile head (at the underside of the pile cap at RL-0.8 m) to 10 m below riverbed.

The proposed driving shoes to be fitted at the toe of the steel tubular piles is 50 mm thick, which is the minimum thickness as required by the project Scope of Work and Technical Criteria (SWTC). While increasing the thickness of the driving shoe could increase the axial capacity of the pile, and potentially improve local buckling resistance at the toe, it could increase the risks of stress concentration and possible fatigue failure at the connection between the driving shoe and the general thinner steel tube wall section. In consideration of balancing axial capacity and drivability to achieve rock penetration, the minimum required driving shoe thickness of 50 mm as required by the SWTC has been adopted.

In compliance with SWTC requirement, a minimum of one borehole was drilled within 2 metres of the centre of each pier and abutment. For the flood plain piers with only 1 pile per pier, the drilled boreholes are essentially located at the pile locations.

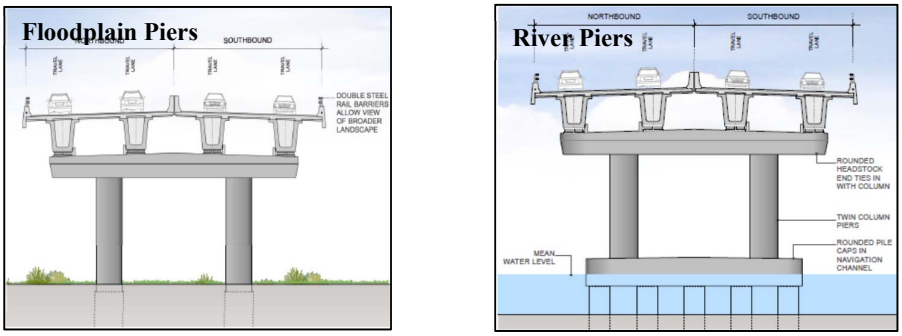


Fig. 2. Floodplain Piers and River Piers

PILE DRIVING REQUIREMENTS AND DRIVABILITY ASSESSMENT

Methodology for driven pile construction and verification

The maximum vertical design ultimate limit state (ULS) loads were 20.4 MN for the 2 m diameter piles in the floodplain and 11 MN for the 1.5 m and 1.2 m piles in the river. In accordance with the SWTC, all driven piles are to be extended to a sound rock bearing. In this context, the project specific Roads and Maritime Specification D&C B54 Driven Tubular Steel Piles requires that piles to be driven to nominal refusal in rock, and with the pile toe level installed to below a specified Minimum Penetration Level to satisfy lateral capacity. The refusal criteria that has been adopted is 13 mm set per 10 blows under the specified minimum net driving energy to mobilise 1.25 × ULS axial design load (P*). While piles are nominally to be driven to refusal in rock, extended driving to achieve refusal (after the required capacity has been reached) has a significant potential to result in damage to the steel tube. In these instances, dynamic testing may be utilised to validate the required capacity.

A minimum 14% of the total number of piles (8 out of total 56 piles) was nominated to be subject to Dynamic Pile Testing with wave matching to validate assumed capacity. D&C B54 requires that test piles are to be driven prior to remaining piles. The applicability of this clause in terms of logistics has been considered during the design, and it has been agreed in the context of access that test piles were to be installed (and dynamically tested) ahead of the production piles in the vicinity. The test regime for the test piles was undertaken in accordance with the project specific D&C B54, and was to include: (i) Restrike test after a minimum period of 20 hours, (ii) Dynamic Testing with CAPWAP signal matching analysis to confirm the required pile resistance, and (iii) Validation of geotechnical pile resistance for individual piles at 1.25 times the applicable pile design axial load as demonstrated by dynamic testing of that individual pile. Figure 3 outlies the adopted methodology for driven pile construction and verification, which has been developed on the basis of SWTC requirements, as well as from a constructability standpoint.

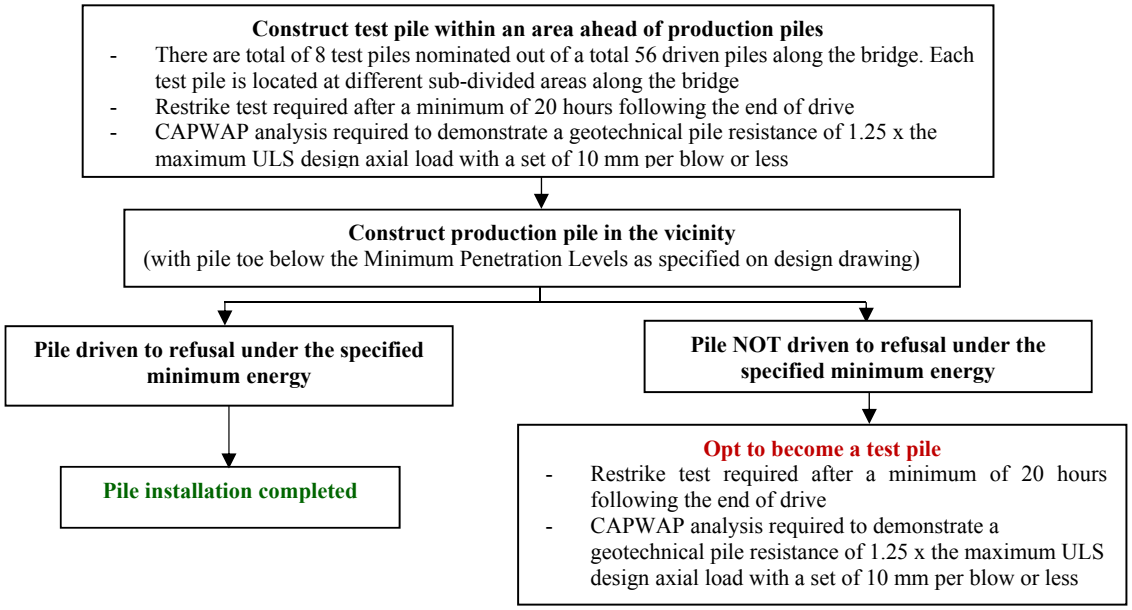


Fig. 3. Methodology for driven pile construction and verification

As an additional construction control, Pile Driving Monitoring with PDA was to be undertaken on all piles during driving to validate penetration to rock, monitor the actual transferred net driving energy and the driving stresses in the piles, estimate the mobilised capacity of the piles, assess pile integrity (e.g. pile condition and pile damage), eccentricity during driving and assist in determining the final penetration resistance in driving and restriking.

Considerations in drivability assessment

Driveability analysis based on wave equation approach (using software program GRLWEAP 2005) has been undertaken to assess the expected driving energy requirements and the associated compressive stresses generated in the pile during driving. Within the GRLWEAP analysis, the static resistances are modified to consider potential loss of shaft resistance due to full loss of setup. The adopted setup factors for clayey materials including residual clay, Holocene and Pleistocene alluvium are 1.5. For the deeper clayey gravel layers, it has been noted from past projects that the fines content in the gravels is typically sufficient to develop a degree of setup, hence a setup factor of 1.2 was adopted. For Phyllite bedrock, a setup factor of 1.2 was considered for Unit 5b (extremely low strength), and 1 for Unit 5c or better.

To achieve the ultimate capacity that satisfy 1.25 × ULS indicates that the minimum required net driving energy is about 370 kJ for the 2 m diameter piles to be driven to nominal refusal. The hammer used for this operation was a 28t Junttan HHK 28S hydraulic boasted hammer. It applied up to 450 kJ of energy with a 1.5 m drop. Sensitivity analyses conducted during design have shown that excess internal friction

or pile plugging would result in driving conditions exceeding the assumed 370 kJ net driving energy. However, these conditions were considered less likely for large diameter piles. For design purposes, the base analysis case has considered external skin friction only. Full internal skin friction (i.e. same values as to the external) was limited to application at the driving shoe only. Skin friction was not applied along the inner wall of the pile shaft and soil plugging was not considered in the base case analysis. In addition to the minimum net driving energies, assessments were also conducted to determine the maximum driving energies corresponding to the induced maximum driving stresses of 0.9 f_{sy}, where f_{sy} is design yield stress of steel (= 350 MPa).

PILE DRIVING PERFORMANCE

In addition to the 8 nominated test piles, 14 out of the remaining 48 production piles have also become test piles during construction, since a practical refusal with less than or equal to 1.3 mm set per blow was not achieved under the specified minimum net driving energy in the expected founding medium strength rock, while the PDA monitoring has indicated the required capacity. It was decided in these instances to opt for the alternative verification method by restrike with CAPWAP analysis in order to avoid risk of pile damage due to prolonged hard driving, as well as the need for additional splices with increasing rock penetration.

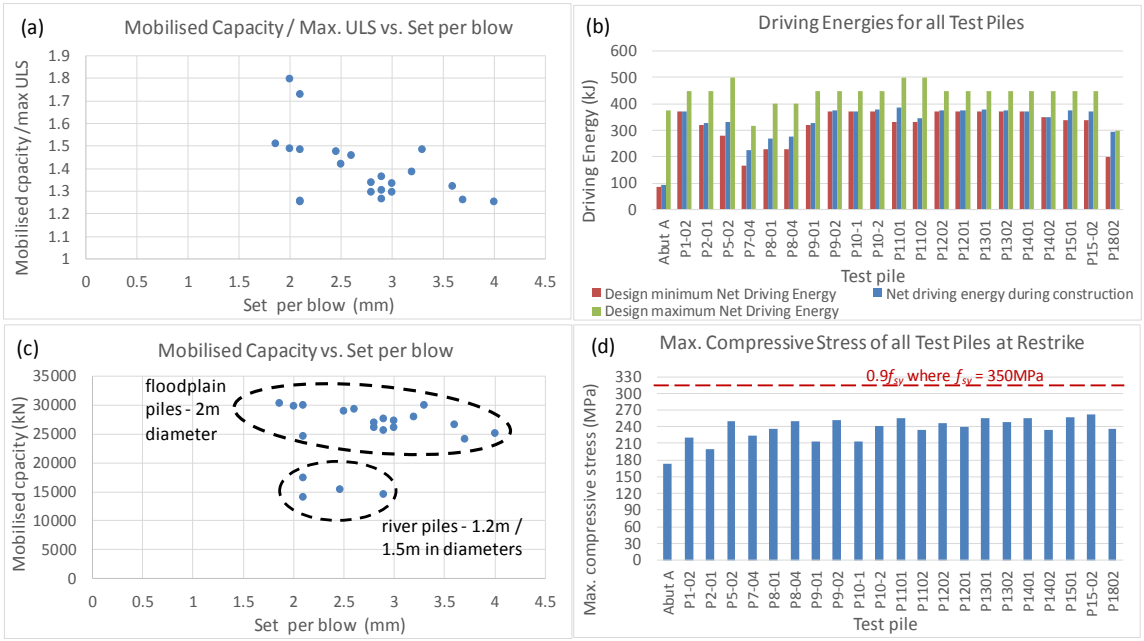


Fig. 4. (a) Mobilised capacity / design ULS vs. set per blow; (b) Driving energy for all test piles; (c) Mobilised capacity vs. set per blow; (d) Maximum compression stress for all test piles

Figure 4a shows that all test piles were driven to 2-4 mm set per blow, with a mobilised axial capacity typically about 1.25 – 1.5 times the maximum design ULS axial load. Rule-of-thumb guidance indicates that a test blow that produces a permanent set of 2.5 mm or less may not measure the full ultimate capacity, but only a mobilised resistance. However, such a test would still have value as a proof test since the mobilised capacity exceeds the required load. Figure 4b shows that the net driving energy at restrike were within the envelope of the design minimum and maximum net driving energies, typically about 1 – 1.2 times the design minimum values and about 0.6 – 0.8 times the design maximum values (adopted to limit driving stresses). Figure 4d indicates that the maximum compressive stresses of the piles at restrike were all below 0.9 f_{sy}, where f_{sy} is design yield stress of steel (350 MPa). The restrike capacities for the floodplain piles and the river piles averaged 26 MN and 15 MN, respectively (Fig. 4c). Shaft resistance accounted for an average of 30 – 40% of total pile capacity. CAPWAP analysis indicated an overall strength gain along pile shaft between the end of drive and restrike, with a set up factor of 1.2 – 1.4. However, there is also a corresponding relaxation at the pile toe resistance, with a

relation factor of about 0.8 – 0.9. The changes in the shaft and toe resistances tend to compensate, and the overall pile capacity may be regarded unchanged.

CAPWAP analysis indicated that skin damping factors were typically 0.6 – 1.4 s/m, which are generally higher than the adopted values of different soil types as suggested in the literature (Fig. 5a). The toe damping factors in the medium strength Phyllite were about 0.2 – 0.3 s/m (Fig. 5b), which are slightly lower than typical value of 0.5 s/m for all materials as suggested in the literature. Consistent with the literature suggested value, skin quakes were about 2.5 mm (Fig. 5c). Toe quakes were typical 3 – 5 mm, which are higher than the adopted 1 mm for competent rock (Fig. 5d).

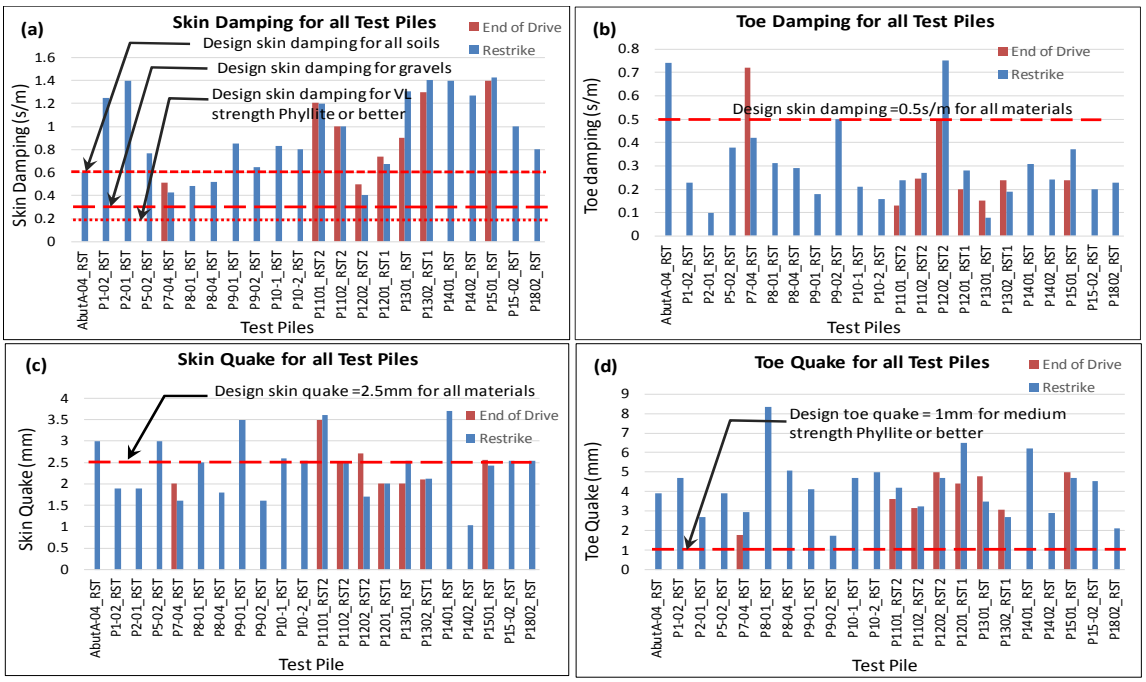


Fig. 5. (a) Skin damping; (b) Toe damping; (c)Toe quake; (d) Skin quake for all test piles

BACK-ANALYSED SHAFT FRICTION AND END BEARING FROM CAPWAP ANALYSIS

CAPWAP analysis is capable of determining shaft resistance distribution and toe resistance. It provides a valuable tool to correlate the shaft friction and end bearing with material types and properties. This section focuses on these correlations in details, beginning by examining the end bearing as it contributes to 60 – 70% of pile capacity, then progresses upwards to shaft frictions in a bottom-up review approach.

End bearing capacity in medium strength Phyllite

The Phyllite bedrock is typically a low-grade metasedimentary rock characterised by a foliated, fine grained rock with a lustrous micaceous sheen when fresh. The Phyllite typically exhibits a deep gradational weathering profile. The very low to low strength Phyllite (Unit 5c) is commonly mottled brown-orange/grey, with an indistinct low angle (5° to 25° degrees) foliation fabric, which becomes more distinct with depth. The medium strength (Unit 5d) and high strength (Unit 5e) is commonly grey-dark grey with a distinct foliation fabric usually at 5° to 25° which is often wavy/undulating or crenulated. Figure 6a shows a plot of unconfined compressive strength (UCS) versus point load strength $Is_{(50)}$ that were obtained specifically from the founding medium to high strength rock at the bridge site.

When fitting the scattered data with a curvilinear trend line, it can be seen that the slope is steeper for the low to medium strength rock than for the high strength rock. Also, the curvilinear line gives a better fit for the data than a linear line, since the R-squared value is closer to 1. When plotting $UCS/Is_{(50)}$ versus $Is_{(50)}$ as shown in Fig. 6b, it can be seen more clearly that the UCS / $Is_{(50)}$ ratio is indeed higher for the

low to medium strength rock (about 16 – 17) than for the high strength rock (about 12 – 13), hence supporting the use of the curvilinear line for fitting the data as shown in Fig. 6a.

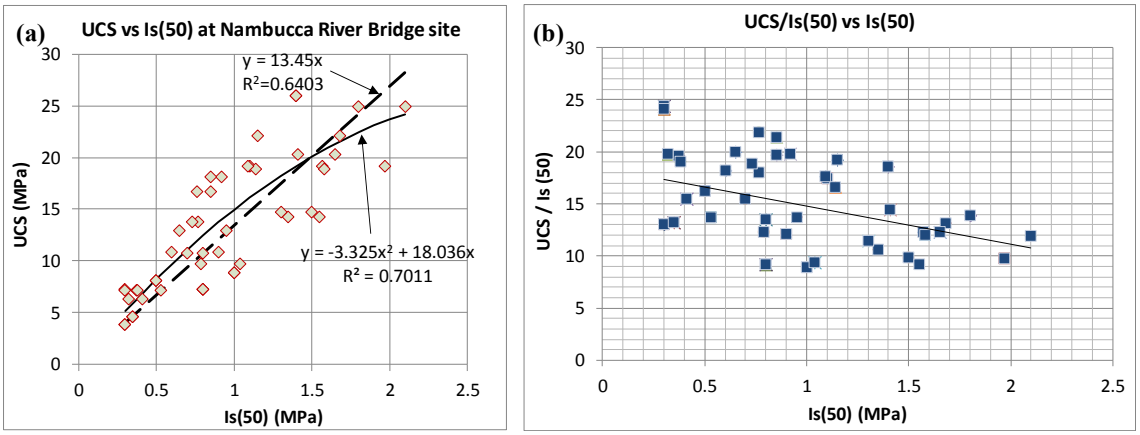


Fig. 6. (a) UCS vs. $Is_{(50)}$ of medium to high strength Phyllite; (b) UCS/$Is_{(50)}$ vs. $Is_{(50)}$

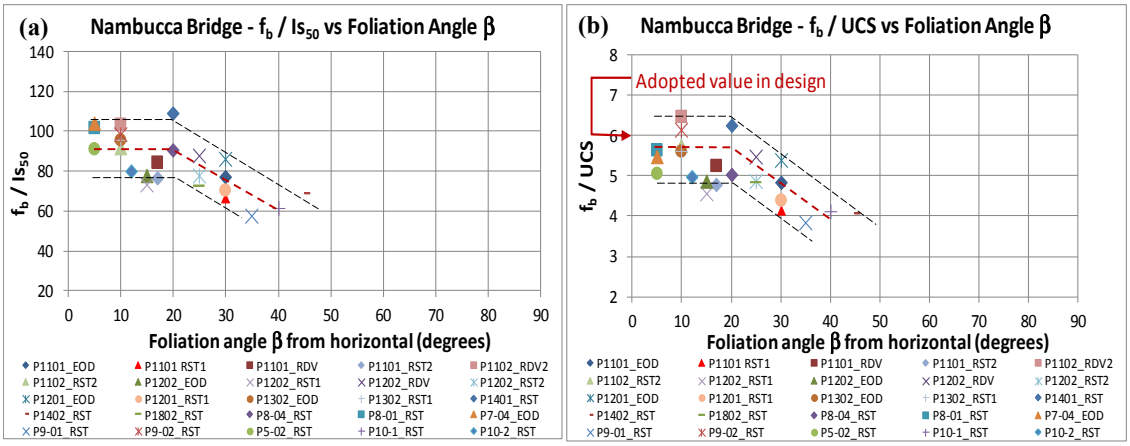


Fig. 7. (a) f_b / $Is_{(50)}$ of medium to high strength Phyllite vs. foliation angle β (from horizontal); (b) f_b / UCS of medium to high strength Phyllite vs. foliation angle β (from horizontal)

Inspection of rock cores indicate that the pile toes of all test piles pull up in unweathered rocks with defect spacing of 300 mm or greater. Figure 7a shows the CAPWAP results for end bearing pressures f_b at the end of drive and restrike, normalised by the $Is_{(50)}$ value at the pile toe level and plotted against the foliation angle β (measured from horizontal) of the Phyllite rock also at the pile toe level. Note that the f_b was assessed based on dividing the toe resistance (from CAPWAP) by the area of the driving shoe annulus without considering soil plugging. The $Is_{(50)}$ and the foliation angle β at the toe level were examined from the boreholes drilled at the pile centres for the floodplain piles, and within 2 m from pile centres for the river piles. Figure 7b shows a plot of f_b / UCS vs. β, which was inferred from Fig. 7a by considering the UCS/$Is_{(50)}$ relationship outlined in Fig. 6. Both Figs. 7a and 7b indicate a reduction of end bearing beyond a β of about 20˚. This may be due to the fact that the internal angle of friction for the schistosity plane is typically about 20˚. Loading on a shallow plane with β < 20˚ may experience an intact rock capacity. Loading on a steeper plane with β > 20˚ may experience a lower capacity due to the impact of rock foliation. Fig. 7b indicates that for β < 20˚, f_b /UCS is about 5.5, which is consistent with the adopted design value and published records for intact rocks. This also supports the notion that the driven tubular piles are unplugged. For β > 20˚, f_b /UCS reduces to about 4 at β = 40˚. Research works by Hoek and Brown (1980) has suggested a U-shaped rock anisotropy, such that the f_b /UCS ratio may continue to reduce to a lowest at β = 60˚, then rises up slightly as β increases from 60˚ to 90˚. The

current bridge site, however, does not have test data with β beyond 45˚ to demonstrate this trend anticipated.

Shaft friction in Phyllite

The steel tubes driven with open ends are helpful in achieving the penetration of rock to reach virtual refusal on a hard unweathered stratum. The penetration lengths into rock for all test piles are typically 2-5 m. Figure 8 shows the CAPWAP results for shaft friction, f_s in rock at the end of drive and restrike, plotted against the averaged $Is_{(50)}$ value in the rock socket materials. Note that f_s was assessed based on dividing the unit resistance registered in CAPWAP by the outer perimeter of the pile only. No shaft resistance from the internal pile wall has been considered in the back-analysis. For low to medium strength rock with $Is_{(50)}$ = 0.2-0.3 MPa, the back-analysed f_s is up to about 280 kPa. The f_s does not increase, but actually reduces to as low as 160 kPa for medium to high strength rock with $Is_{(50)}$ = 1 MPa. Figure 8 also plots the corresponding driving set, ranging from 2 mm to 5 mm set per blow under similar net transfer energy of 375 kJ, but in the different rock strengths. There does not seem to show a distinct pattern between the mobilised f_s and strain (or the driving set). Thus, the lower mobilised f_s in the high strength Phyllite cannot be related satisfactorily to strain alone. Another plausible explanation is that the medium to high strength Phyllite tend to crush more and suffer a drop in the confining stress surrounding the steel tubular pile, possibly leading to a lower than expected shaft resistance. The rock crushing mechanism is reflected in the UCS testing in high strength rock shown in Fig. 9a. Conversely, the low strength Phyllite tends to exhibit expansive strain as it bulges during failure. This is exemplified by the UCS test result for low strength rock shown in Fig. 9b. Therefore, the failure mechanism of low strength rock provides the confinement required to mobilise the pile shaft friction of the steel driven pile.

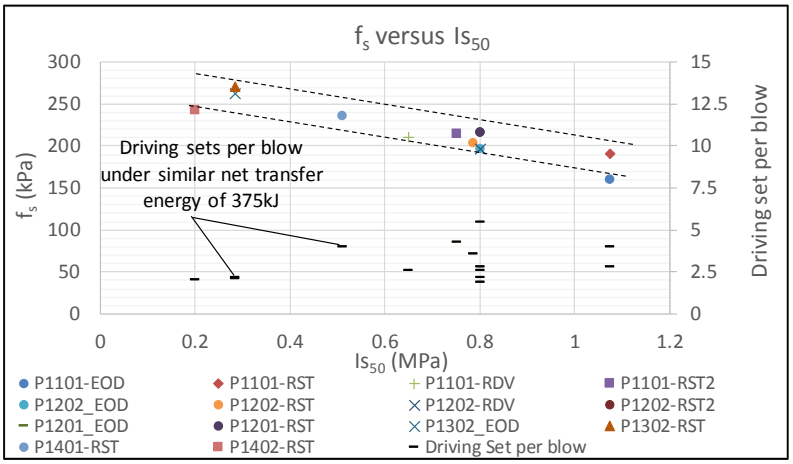


Fig. 8. f_s vs. $Is_{(50)}$ of Phyllite rock

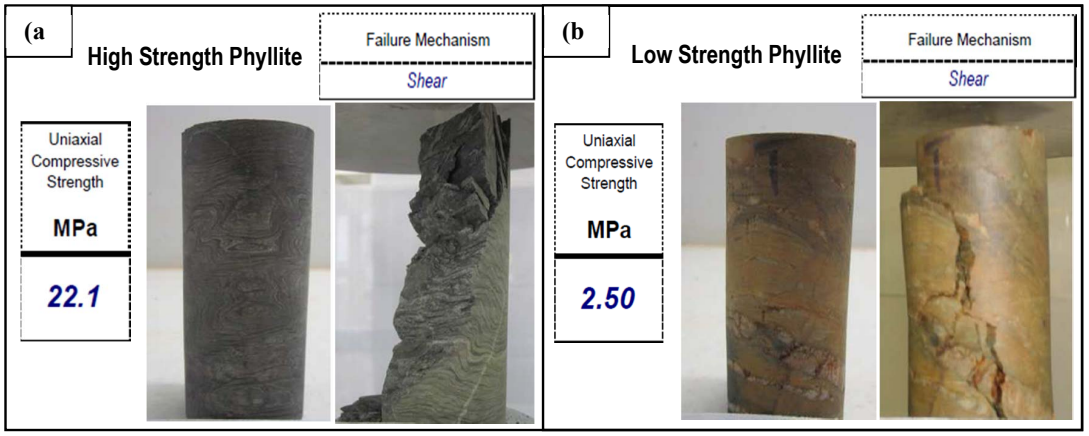


Fig. 9. Typical UCS test results for (a) high strength Phyllite; and (b) low strength Phyllite

Shaft friction in gravels

The Phyllite rock is generally overlain by gravels. The thickness of the gravel layer is typically 5-8m, but could increase to about 10 m at around Pier 9. The loose gravels are largely mixed with sands/silty sand and are considered as Holocene. Conversely, the medium to very dense gravels are considered as Pleistocene, and they comprise typically fine to coarse grained gravels, sandy gravels and silty gravels. The relative density of the gravel encountered can be conveniently inferred from the SPT blow count (N) and the effective overburden pressure using the chart shown in Fig. 10. However, it is acknowledged that this chart was originally developed by Coffman (1960) for sands rather than for gravels.

Figure 11 shows a plot of effective overburden pressure verse f_s in gravels at restrike. Note that the f_s was assessed based on dividing the unit resistance registered in CAPWAP by the outer perimeter of the pile only. No shaft resistance from the internal pile wall has been considered in the back-analysis. For granular material, the shaft friction will increase with effective vertical stress σ_v' until a critical depth and beyond which the shaft friction is relatively constant. With the σ_v' experienced in the gravels at depths 24-32 m below ground, the f_s back-analysed may be considered as the limiting shaft friction developed along pile shaft. It can be seen that the back-analysed f_s values are segregated in well-defined ranges. More interestingly, the back-analysed f_s for dense and medium dense gravels, are comparable with the limiting f_s values as suggested by American Petroleum Institute (API) (2011) for very dense and dense sands, respectively. For the loose sand/gravel mixtures, API (2011) recommends to use CPT-based methods for assessing f_s. The cone resistance in the loose materials is typically about 2 – 4 MPa. Figure 11 shows the assessed f_s using different CPT-based methods. All of the methods compared reasonably well with the back-analysed f_s values. Note that for the Simplified ICP and Offshore UWA methods, the assessed f_s values are related to the soil depth in relation to the embedded pile length. For the present bridge site, the loose sand/gravel mixtures are typically encountered at depth 20 – 28 m, and the pile toes are typically 6 – 8 m below these materials.

Shaft friction in clays

The mobilised shaft friction in alluvial clays is relatively low compared with that of gravels and rock. CAPWAP results indicate that the mobilised f_s at restrike for soft to firm alluvial clays (undrained shear strength, S_u = 20-30 kPa) is generally less than 10 kPa. For stiff/very stiff clays with S_u = 50-75 kPa, the mobilised f_s (at restrike) is generally less than 20 kPa. These mobilised f_s values are in the order of 2.5-5 times less than the design values calculated using the α-method outlined in API (2011). The reason for the lower mobilised f_s in the alluvial clays is twofold: (1) full mobilisation of shaft friction in end bearing pile is less likely to have achieved, and (2) setup continue to occurs days after restrike, hence the mobilised f_s at restrike is not the ultimate shaft friction.

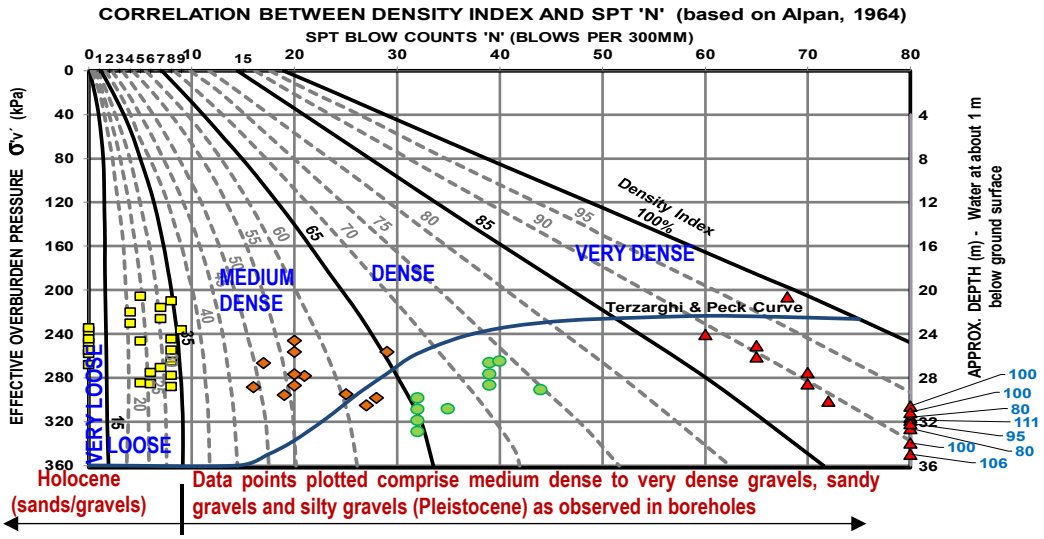


Fig. 10. Vertical effective stress vs. SPT blow count for gravel materials

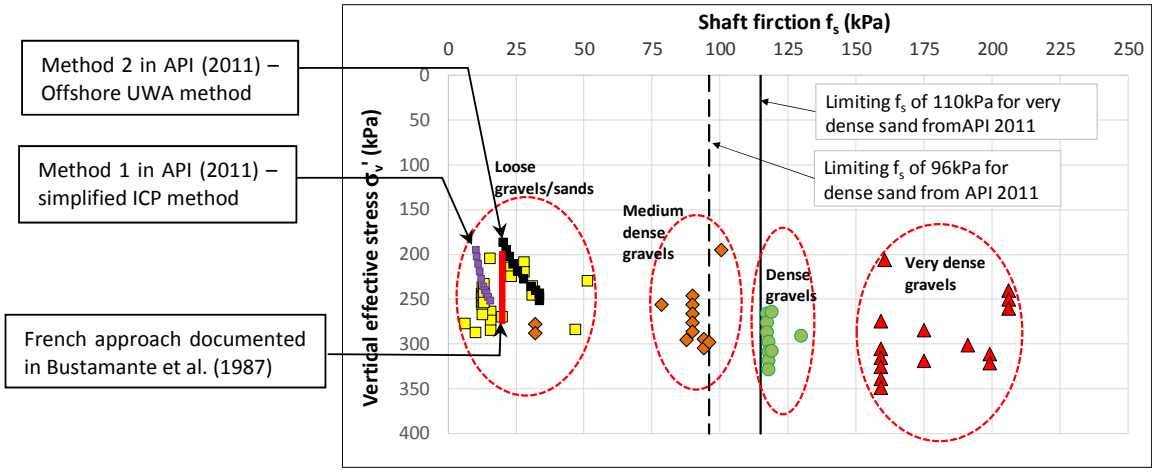


Fig. 11. Vertical effective stress vs. pile shaft friction f_s for gravel materials

CONCLUDING REMARKS

Driven steel tubular piles of up to 2 m diameter have been used to support abutments and piers of a bridge over Nambucca River and floodplain. The piles were designed to be driven through alluvium and founded on foliated Phyllite bedrock. Prior to construction, boreholes were drilled at each centre of the 2 m diameter piles. Wave matching CAPWAP analyses were performed on 40% of the piles at the end-of-drive, or restrike, to satisfy specification requirements and limit over-driving. In addition, PDA was undertaken on all piles during driving to validate penetration to rock, monitor the actual transferred net driving energy and the driving stresses in the piles. CAPWAP analysis indicated that the toe resistance accounted for 60-70% of pile capacity. The pile toes of all test piles pull up in unweathered medium to high strength Phyllite with defect spacing of 300 mm or greater. The f_b/UCS ratio for the founding rock is about 5.5 for rock foliation angle β (from horizontal) of less than 20˚. For $\beta > 20$˚, f_b/UCS reduces to about 4 at $\beta = 40$˚. This may be due to the fact that the internal angle of friction for the schistosity plane is typically about 20˚. For the pile shaft friction, CAPWAP indicated a lower mobilised f_s in the medium to high strength Phyllite than in the low to medium strength Phyllite. This may be related to the rock crushing mechanism such that the low strength rock provides better contact with the steel wall and the confinement required to mobilise the pile shaft friction than that of the medium to high strength rock. The pile shaft friction in the gravel materials has been examined and compared with calculated f_s for sands given by API (2011) method which is the current industry standard. For alluvial clays, it is observed that the mobilised f_s is well below that indicated by conventional API recommendations.

ACKNOWLEDGEMENTS

The authors acknowledge the contributions of the all parties involved in the design and design approvals including NSW Roads and Maritime Services (project Principal), Acciona and Ferrovial Joint Venture (Principal D&C Contractor), and Arup Aurecon Design Joint Venture (Lead Designer). Any opinions, findings, conclusions, and recommendations in this paper are those of the authors and do not necessarily reflect the views of Roads and Maritime Services.

REFERENCES

American Petroleum Institute Recommended Practice 2GEO, 2011. Specific requirements for offshore structures. Part 4 – Geotechnical and foundation design consideration. First edition.

Bustamante, M., Frank, R. & Gianeselli, L., 1987. Le dimensionnement ds fondations profonde. Bull. Liaison LabsP. Et CH149, May-June, 13-22.

Coffman, B.S., 1960. Estimating the Relative Density of Sands Civ. Eng'g (ASCE), Vol. 30, No.10.

Hoek, E, and Brown, E.T., 1980. Underground excavation in rocks. London: The Institution of Mining and Metallurgy.

DESIGN AND CONSTRUCTION OF PILE-SUPPORTED MECHANICALLY-STABILIZED-EARTH SLOPE STABILIZATION

Nasr Sheta, Ph.D., P.E., Langan Engineering and Environmental Services, Parsippany, NJ, USA
Phone: 201-220-7720, Email: Nsheta@Langan.com

ABSTRACT

After Hurricane Sandy, the stability of an earth slope in the Atlantic Highlands, New Jersey in the United States was deteriorating due to slumping soils and erosion from flooding. A slope stability evaluation indicated the slope did not satisfy the requirements of the local building code. A triple-tier, pile-supported and mechanically stabilized earth wall was designed and constructed to stabilize the slope. The construction was planned from a 3-m-wide roadway and, because of rough terrain and limited work space at the site, a cast-in-place drilled-pile construction was deemed impractical due to slow pile production. An alternative procedure was utilized by pre-drilling holes, and installing precast tip-and-shaft-grouted (PCTSG) piles, which extended to competent soils to improve slope stability. A grade beam, connecting the PCTSG piles along with soldier beams and concrete lagging were used to form the lowest tier of the slope stabilization, while the middle and higher tiers were built as mechanically stabilized earth. The stability of the proposed stabilization was analyzed using 2-D non-linear finite elements. After construction, monitoring of the wall continued for about 8 months to check its performance, and indicated lateral and vertical wall movements were less than 25 mm and 6 mm, respectively, indicating effective slope stabilization.

Keywords: Slope, stabilization, pile, finite element, geogrid-reinforced

INTRODUCTION

Stabilizing earth slopes using piles to connect near-surface unstable soils to underlying stable ground masses has been investigated by many researchers, who presented various approaches to evaluate the contribution of the pile system towards improving the stability of the slope. Some of these approaches consider the piles as structural elements receiving forces from the upper sliding ground mass and transmitting these forces to the underlying stable one. The force from the top sliding mass is applied at between one third and one half of the pile embedment into the top sliding mass, Anagnostopoulos et al. (1990), Fukuoka (1977) and Matsui et al. (1988). The point of application of the sliding force was explored based on successful case histories while addressing the safety factors for both geotechnical and structural design, Vessely A. et al. (2007). The development of numerical analysis techniques utilizing the method of finite elements (FE) also enabled better analysis and design of slopes stabilized using piles. A FE-based approach was successfully utilized to design slope stabilization with target safety factor based on the shear and bending demands and the spacing of the piles, Pradel D. et al. (2010).

After Hurricane Sandy in October 2012, the stability of many properties constructed atop earth slopes located along the coast of the Atlantic Ocean has become a concern due to storm-induced erosion. This paper presents the analysis, design and construction of a hybrid slope stabilization system utilized at one of these storm-impacted properties, which is located in the Atlantic Highlands, New Jersey in the United States. The subject property consisted of a two-story residential dwelling and a parking structure, and was built on top of an about 8-m-high earth slope having crest at about elevation 10 m (el 10) and toe at about el 2.

The property is located in an area known as “the Highlands”, which has a history of actively slumping soil blocks, Minard J. P. (1974). A timber retaining wall with a height of about 1.5 m was previously built at slope crest. This timber retaining wall was severely deflecting, and surface grades behind the wall were slumping, indicating an ongoing slope movement, see Fig. 1. During Hurricane Sandy, the earth slope experienced significant toe erosion due to wave action and storm surge, and portions of the slope toe were washed out due to flooding. The stability of the entire slope was questionable, which

necessitated performing stability evaluations to provide recommendations for possible corrective measures.



Fig. 1. Deflecting Timber-Sheeting Wall at the Top of the Existing Earth Slope

SUBSURFACE INVESTIGATION AND SOIL PROFILE

Six borings were performed as a part of a subsurface investigation associated with past construction at the subject site. The borings extended about 8 to 15 m below the top of the slope, and were performed using a tripod hand-operated rig, because of limited accessibility. Standard penetration tests were conducted in all borings, and soil samples were obtained and classified in accordance with the Unified Soil Classification System (USCS). The subsurface conditions consisted of an about 1.5-m-thick surficial loose fill, mainly composed of sand intermixed with various amounts of silt, clay and gravel. The fill is underlain by successive layers of sand, clay and clayey sand / sandy clay overlying denser glacial till material consisted of sand, clay and gravel. Soil parameters were evaluated based on a series of laboratory and field tests, including Atterberg Limits, sieve analysis, unit weight determination, unconfined compression and Standard Penetration. A design soil profile was established as indicated in Fig. 2.

STABILITY ANALYSIS OF EXISTING SLOPE AND RETAINING WALL

A stability analysis was performed for the existing slope and timber retaining wall, considering the conditions existed after Hurricane Sandy. The analysis utilized 2-D finite elements and the soil profile and parameters shown on Fig. 2. A surcharge of 5 kN/m^2 was applied at the top of the slope behind the timber retaining wall. The soil mass was modeled using 15-node triangular plane-strain elements, and the retaining wall was modeled as elastic beam (plate) elements. Since the purpose of the analysis was to evaluate the safety factor against slope failure, the soil was modeled as an elastic-perfect-plastic material obeying Mohr-Coulomb failure criterion. The analysis utilized the strength reduction method (SRM) to evaluate the safety factor against slope failure. The FE mesh used to analyze the slope is given in Fig. 3.

The results of the stability analysis indicated that the existing slope had a safety factor of less than 1.2, and that the timber retaining wall at the top of the slope experienced significant deformation and distress, which agreed well with field observations. Since the International Building Code – New Jersey Edition requires a minimum safety factor of 1.5 against slope failure, slope stabilization was necessary for the existing slope and the adjacent residential and parking structures.

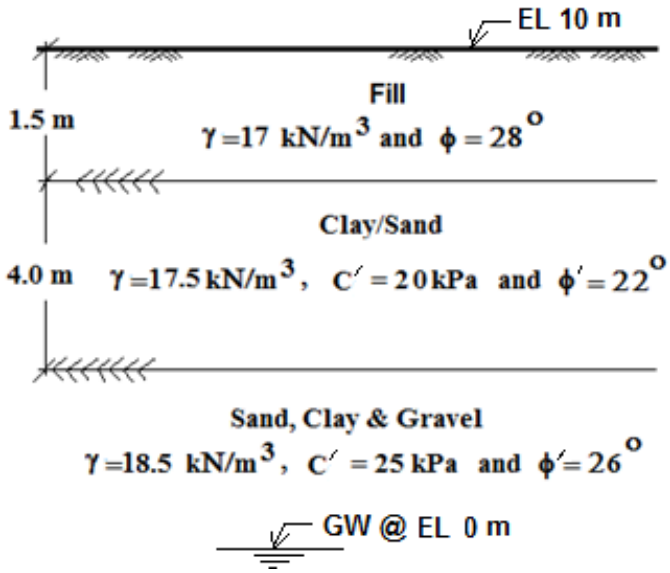


Fig. 2. Design Soil Profile and Parameters

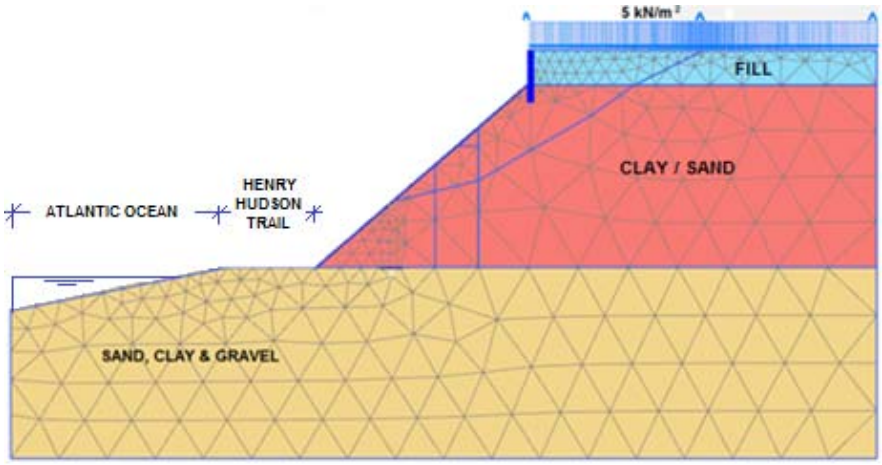


Fig. 3. Finite Element Mesh used for Slope Stability Analysis for Existing Slope

LIMITATIONS OF DIFFERENT SLOPE-STABILIZATION ALTERNATIVES

The challenges at the site were not only to stabilize the slope, and to provide lateral support for the soil mass below the existing residential structure, but also to achieve this goal at a cost that is affordable to an owner of a single-family house, which typically prices at about $1,000,000 at the area where the property is located. Different alternatives were explored including steel sheet piles, driven piles and concrete retaining walls. Because the safety against slope failure was not in compliance with the requirements of the local building code, it was necessary to adopt a stabilization system that penetrates surficial soils to deeper competent strata, thus providing additional sliding resistance, and improving the slope stability. Driving timber or steel sheet / pipe piles results in vibrations that can impact the adjacent structures within 3 m from the slope crest and, consequently, pile driving was excluded. Concrete retaining walls were also discussed; however, unless built at the toe of the slope, a concrete retaining wall can decrease the slope stability. Also, building a concrete retaining wall capable of supporting 9 m of soil would require significant cost, and the initial cost obtained from local contractors to build conventional retaining-wall slope stabilization was on the order of $750,000.

In addition, accessibility limitations dictated a specific type and size of equipment required to install such slope stabilization if it is to be constructed at reasonable cost. Therefore, it was vital to develop a slope stabilization design that accounts for site limitations, and can be constructed at reasonable cost.

PILE-SUPPORTED TRIPLE-TIER REINFORCED-EARTH SLOPE STABILIZATION

After evaluating different options, it was decided to build a reinforced-earth, triple-tier retaining wall to stabilize the slope. It was also decided to design the lower tier of the wall as a pile-supported soldier-beams (H-Piles) and concrete lagging, and extend the supporting piles deep to ensure safety against deep-seated failure. Fig. 4 shows a section and perspective views of the proposed slope stabilization.

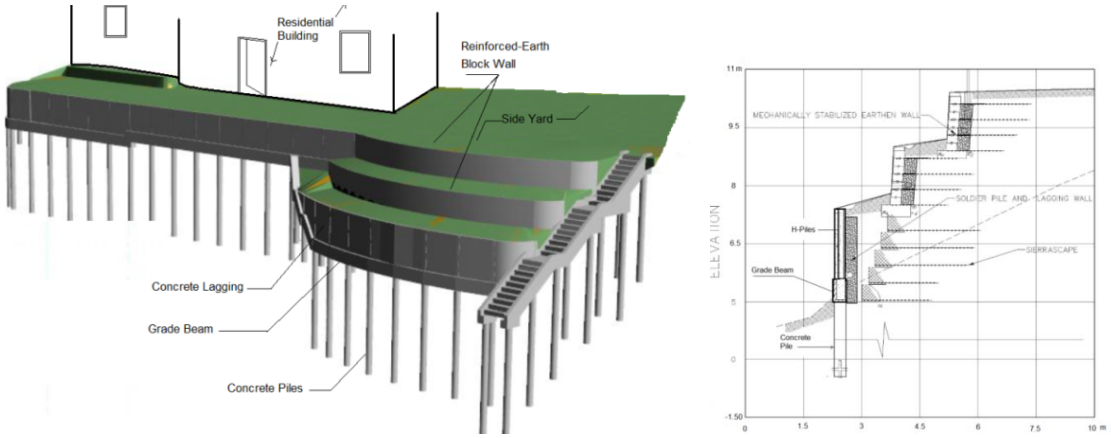


Fig. 4. Section and Perspective Views of the Proposed Triple-Tier Wall Slope Stabilization

The piles supporting the lowest tier were designed to be 0.30-m-diameter cast-in-place concrete piles, because of limitations on the size of the pile drilling equipment. The center-to-center pile spacing was typically 1.5 m. The piles were also designed to support a 0.4-m-wide by 0.6-m-deep cast-in-place concrete grade beam that supports the soldier beams and concrete lagging wall. The drilled piles were planned to be installed at about 1/3 of the slope height above the toe, using a drilling rig working from the 3-m-wide Henry Hudson Trail adjacent to the slope toe. The piles were designed to extend to deeper competent soils, so they can transmit forces from the upper ground mass subject to sliding to the lower more-stable competent soils and, hence, improve the slope stability. The concrete grade beam was designed to resist torsion, resulting from bending moments and shear forces acting on the soldier beams supporting the concrete lagging subject to lateral soil pressures. The second and the third tiers of the retaining wall were designed as reinforced earth having decorative segmental-block facing to provide an attractive façade for the proposed slope stabilization.

STABILITY ANALYSIS OF THE PROPOSED SLOPE STABILIZATION

A stability analysis, similar to that conducted for the existing slope, was performed for the proposed slope stabilization and earth retention including the pile-supported soldier beam and concrete lagging as well as the geogrid-reinforced tiered wall. The stability analysis was based on the soil profile and parameters shown on Fig. 2. The FE method was, again, used to perform the analysis utilizing the mesh in Fig. 5. The results of the stability analysis indicated that the proposed slope stabilization will increase the safety factor against slope failure from less than 1.2 (obtained for conditions existed before slope stabilization) to about 1.8, which exceeds the requirements of the local building code of a minimum safety factor of 1.5 against slope failure. The slip surface associated with the obtained factor of safety is shown on Fig. 6.

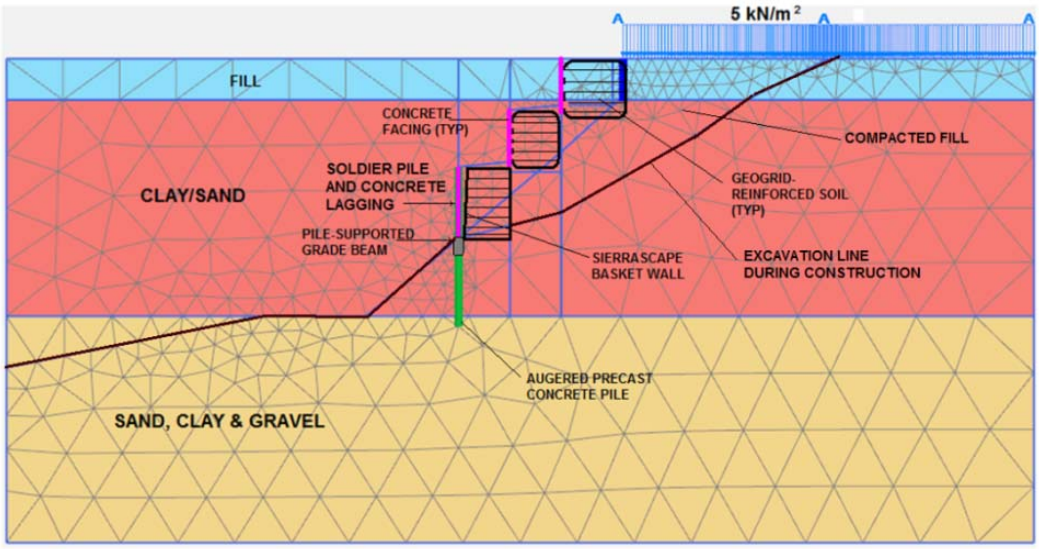


Fig. 5. Finite Element Mesh used for Proposed Slope Stabilization Analysis

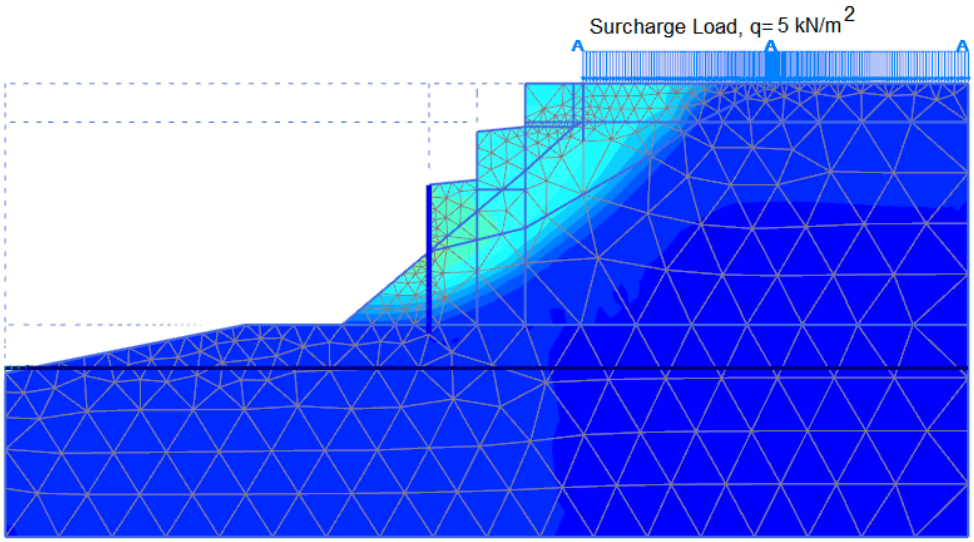


Fig. 6. Displacement Results from Stability Analysis of the Proposed Slope Stabilization

CONSTRUCTION OF PRECAST TIP- AND SHAFT-GROUTED CONCRETE PILES

The installation of the lowest-tier wall concrete piles was started by constructing the piles as augered-cast-in-place (ACIP) elements. Because of the rough terrain of the slope as well as the limited maneuver at the site, the pile production was limited to 3 piles per day, resulting in significantly high cost for piling. Therefore, it was decided to install precast concrete piles in pre-augered holes, rather than ACIP piles. A main advantage of using precast piles was to manufacture the piles at a remote site, then, transfer them to the project site, after concrete reached reasonable strength that allowed for pile handling. This resulted in more-efficient utilization of construction materials, and in manufacturing the rebar and piles in a much larger space than the limited one available at the project site, which significantly reduced the piling cost.

The main concern of installing precast piles in pre-augered holes was ensuring the integrity of the interface between the precast pile shaft and the pre-augered hole (i.e. ensuring no voids exist along soil-pile interfaces, which may impair the lateral performance of piles). Different approaches were discussed to ensure effective filling of the pre-augered holes after installing the precast piles, hence, providing lateral stability to the precast piles and soldier-beam and lagging wall supported on the concrete grade beam. However, it was foreseen that traditional backfilling and compaction of the pre-augered holes after inserting the precast piles would not yield satisfactory result, and an alternative approach was developed.

During manufacturing the precast concrete piles, and during the installation of the rebar cage, an about 25 mm-diameter PVC grouting tube, aligned along the pile centerline, was tied to the rebar cage. The top of the PVC grouting tube was about 0.6 m outside the top of the pile, and the tip of the tube was about 50 mm below the tip. About 0.15 m above the tip of the pile, 4 grout exits uniformly distributed along the pile circumference, and extending about 25 mm outside the pile, were provided as shown in Fig. 7. The cage with the grouting tube was, then, placed in a formwork and the pile concrete was poured. After the hole was drilled, the pile was inserted into the hole, and held with a sling to make the pile tip about 0.25 m above the bottom of the hole. The grouting tube was, then, connected to a pump injecting grout through the tube down to the exits at the bottom of the pile, pushing groundwater and loose soil out of the hole. The grouting process continued until fresh grout was observed at the top of the hole, and the grouting pressure reached a minimum of 250 kN/m^2. The pile was, then, pushed down to the bottom of the hole, and was left for a minimum of 3 days before cutting the grouting tube and constructing the grade beam.



a) Grout Tube at Pile Top **(b) Grout Exits at Pile Tip** **(c) Grouting Process**

Fig. 7. Precast Tip- and Shaft-Grouted Concrete (PCSTGC) Pile Construction

CONSTRUCTION OF LOWEST-TIER WALL TO ACCOUNT FOR FUTURE SETTLEMT

Existing grades were raised by about 2.5 m at the area around the slope toe to build the lower-tier of the wall, which would result in long-term settlement. The soil mass behind the soldier-beam wall was designed and constructed as a self-standing geogrid-reinforced earth independent of the soldier-beam and concrete lagging, by utilizing Sierrascape-basket system as shown on Fig. 8. After installing the

Sierrascape-basket system, the space between the concrete lagging and the Sierrascape baskets was left without backfilling for about 4 weeks. The purpose of this installation sequence of the Sierrascape baskets and geogrid-reinforced earth behind the concrete lagging was to initially minimize lateral soil pressures acting on the soldier-beam wall and the PCTSGC piles. As soils underneath the area around the slope toe consolidate and compress due to increased overburden stresses, the Sierrascape and geogrid-reinforced earth wall will tend to move / rotate and impose more lateral pressures on the concrete lagging and on the PCTSGC piles. Installing the Sierrascape baskets and leaving the space behind the concrete lagging without backfilling for 4 weeks helped mitigating lateral pressures on the concrete lagging, during the compression / consolidation of soils underlying the area around the slope toe. Also, the interaction between the PCTSGC piles, the soldier-beam and concrete lagging wall, as well as the Sierrascape wall helped improving the behavior of the entire slope stabilization, and minimized wall deformations.

MONITORING OF PILE-SUPPORTED REINFORCED-EARTH SLOPE

The construction of the proposed stabilization was started around end of December 2013, and completed early April 2014, i.e. construction period of about 4 months. Upon finalizing the construction, 16 elevation control points were installed on the soldier beams at the locations indicated on Fig. 9. Both vertical and lateral movements of these elevation control points were monitored for about 8 months. Monitoring data indicated total lateral movement of the lowest tier of the wall was within 25 mm (i.e. perpendicular to the wall face), and total vertical downward movement (i.e. settlement) was less than 5 mm, which indicated effectiveness of the slope stabilization utilized.



(a) Top View of the Wall **(b) Side View of the Wall**

Fig. 8. Sierrascape and Geogrid-Reinforced-Earth behind Soldier-Beam and Concrete Lagging



Fig. 9. Locations of Post-Construction Monitoring Points

CONCLUSIONS

A cost-effective pile-supported mechanically-stabilized-earth slope stabilization was successfully designed and installed. The concrete piles supporting the lowest tier of the wall were utilized to increase the stability of the earth slope as they were extended deep enough to cut the potential slip surface, thus increasing the force to resist sliding. The concrete piles were also utilized to laterally support the concrete lagging and the mechanically stabilized soil behind the lagging. An innovative pile installation procedure was developed by constructing the piles as pre-augered PCTSGC elements, to overcome very rough terrain and limited work space at the project site, as well as to control the cost of proposed stabilization. Such innovative design resulted in reducing construction cost from about $750,000 (for conventional concrete-retaining-wall stabilization) to slightly above $200,000. Post-construction monitoring indicated the vertical movement of the utilized stabilization was insignificant, and the lateral movement was less than 25 mm, which indicated efficient slope stabilization design and performance.

REFERENCES

Cala M. and Flisiak J. (2003) Slope stability analysis with numerical and limit equilibrium methods, Computer Methods in Mechanics; CMM.

Dawson, E., Roth, W. and Drescher, A. (1999) Slope stability analysis by strength reduction, G´eotechnique, vol. 49, no. 6, pp. 835–840.

Duncan, J. (1996) State of the art: limit equilibrium and finite element analysis of slopes, Journal of Geotechnical Engineering, vol. 122, no. 7, pp. 577–596.

Griffiths D.V. & Lane P.A. (1999) Slope stability analysis by finite elements, Geotechnique, Vol. 49 (3): pp. 387-403.

Minard J. P. (1974) Slump Blocks in the Atlantic Highlands of New Jersey, Geological Survey Professional Paper 898.

Pradel, D., Garner J. and Kwok, A. (2010) Design of Drilled Shafts to Enhance Slope Stability, Proc. of the 2010 Earth Retention Conf., Bellevue, Washington, US.

Richards, K. and Reddy, K. (2005) Slope Failure of Embankment Dam under Extreme Flooding Conditions: Comparison of Limit Equilibrium and Continuum Models, Proc. of the Geo-Frontiers 2005 Conf., ASCE, Austin, Texas, US.

Sarma, S., (1979) Stability analysis of embankments and slopes, Journal of the Geotechnical Engineering Division, vol. 105, no. 12, pp. 1511–1524.

Vessely, A., Yamasaki K. and Storm, R. (2007) Landslide Stabilization Using Piles, Proc. of 1st North American Landslide Conf., CO, US.

APPLICATION OF INNOVATIVE UNDERREAMED GROUND ANCHORAGE WITH CAPSULE

Zhong Liu, Central Research Institute of Building and Construction of MCC Group, Beijing, China, 0086-18601969086, zzliu8@163.com
Gang Guo, Central Research Institute of Building and Construction of MCC Group, Beijing, China, 0086-18611211727, charlie4322@163.com

ABSTRACT

In response to an increasing demand of anchored structures for underground space and transportation infrastructure in China, an innovative underreamed ground anchorage system was created. The novel anchorage system has provided more efficient functions with higher capacity at lower cost, because of the enlarged cylindrical body (known as ECB) sealed in capsule at bottom of anchorage. This paper presents the detailed structure of innovative anchorage system and its special features. To investigate the bearing mechanism of new anchorage, we evaluate its performance and failure mode based on the experimental results, and also indicate its strain-hardening load-displacement relationship. Unlike the shaft anchorages, it is identified no overall failure to be found in soil surrounding the underreamed anchorage. More importantly, the anchorage capacity is governed by the base resistance, which takes more than 80% of total pullout capacity resulting from the contribution of ECB. Finally a case history of anti-floating project introduces the new combined construction approach and procedure, which has provided the contribution to the quality control and cost efficiency.

Keywords: innovation, anchorage system, ECB, bearing behaviour, failure mode, application

INTRODUCTION AND BACKGROUND

The construction boom over two decades in China has resulted in an increasing demand for underground space and slope stability. The infrastructures market requires the more efficient anchorage systems for retaining structures, resisting uplift forces and slope protection. The major concern focuses on gaining higher capacity and lower cost resulted from perfecting anchorage systems. There are three main anchorage systems designed to achieve the above objectives: ① single bore multiple anchorage system (Barley 1997), ② regroutable anchorage system (Smoltczyk 1991), ③ underreamed anchorage systems (Xanthakos 1991). Generally, the concept ③ comparing with the other two, can be more competitive due to its distinct advantages. To improve the performance and durability of ground anchorages under the complex geological conditions and diversified engineering requirements, a number of different underreamed anchorage technologies had been used, which included cone - shape anchorage described by Liao, Wu and Shu (1997) in Taiwan, Soilex anchorage developed in Sweden (Massarsch et al. 1997), Soletanche anchorage proposed in France, blasting anchorage used in Czechoslovakia (Hobst and Zajic 1986), jet-grouting anchorage innovated in Europe (Anon 1988), as well as deep mixing anchorage created in Japan (Cheng et al. 2000).

The underreamed anchorage systems have the remarkable advantages compared to the shaft anchorage system. However, there are also some weaknesses inherent in the underreamed systems. For instance, the mechanical underreamed anchorage is unsuitable in sand or waterbearing ground, because the enlarged hole is easy to collapse, and it is hard to ensure the quality of anchorages. On the other hand, relying on the blasting in deep hole, the geometrical space and dimension of enlarged hole is uncontrollable, meanwhile, the continuous blasting operations may easily cause the serious ground deformation and the negative effects to the completed anchorages.

The jet grouting anchorage system was initially proposed in Europe in 1980's, which, then, has been widely used in China. Chinese code “Technical specification for underreamed anchorage by jet grouting” (JGJ/T282-2012) requires that the strength of fixed anchor by jet grouting shall be more than 20 MPa. But, in the practice the strength of cement soil is usually less than 10 MPa, and it is easy to

lead to the insufficient strength of ECB. In order to avoid the tension cracks produced in permanent ground anchorages, the compression underreamed anchorages are reasonably recommended in design, however it can hardly meet the requirement of Chinese code "Technical code for engineering of ground anchorages and shotcrete support" (GB 50086 - 2015) with 30 MPa grout strength. The other drawback relates to quality control, e.g. how to ensure the reaming dimension and volume of enlarged body has been still unsolved by current jet grouting technique, which is affected by various construction parameters.

In order to solve the aforementioned problems of the traditional underreamed anchorages, a patented ground anchorage system with capsule was successfully developed in China in 2008. The evolution and the concept of new underreamed anchorage system is illustrated in Figure 1. Liu at el. (2014) found the obvious differences between two anchorage systems, especially the load-displacement curve of underreamed anchorage demonstrates the monotonic rising along with increasing displacement, and the behavior of Q-S curve displays a hardening characteristic in Figure 2. Figure 3 depicts the innovative ground anchorages with capsule excavated on site.

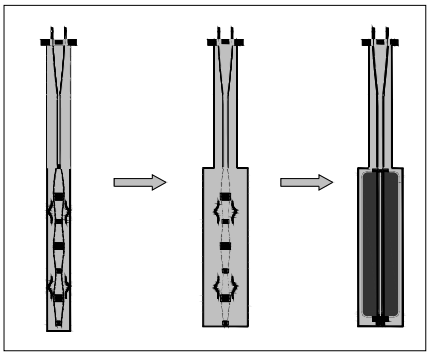


Fig. 1 Evolution of anchorage systems

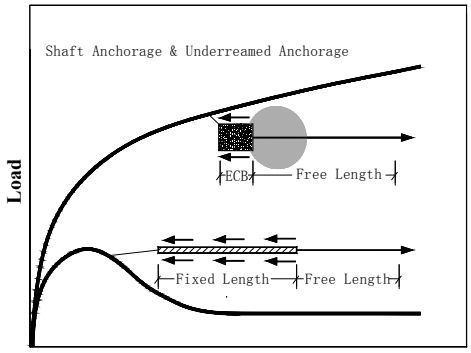


Fig. 2 Load – Displacement curves





Fig. 3 Photos of underreamed anchorages with capsule on site

STRUCTURE OF INNOVATIVE ANCHORAGE SYSTEM

Unlike the existing underreamed anchorage systems, the proposed anchorage system consists of the patented structure of ECB device, which comprises two sealing steel cover plates propped by hollow steel tubes, a sleeved grouting pipe, an air exhaust valve, and a thin foldable capsule. The tendons either strands or bars can pass through the hollow steel tubes and can be fixed on the end bearing plate with anchor block and gripping wedges or nuts (Figure 4). The capsule is made of special materials including high density polyethylene (HDPE), polyvinylchloride (PVC), and poly-p-phenylene terephthalamide (PPTA). The capsule around the central steel structure can be folded in diameter of 130 mm, which can be inserted into the borehole with diameter of 160 mm. In the construction phase, the ECB device with tendons can be installed by means of borehole drilling, under-reaming by jet grouting or mechanical reamer, and inflated by grout injecting. By utilizing such ECB device, the cement grout-filled cylindrical body with pre-designed grout volume can be achieved below ground.

In the practice, the nominal diameters of ECBs range from 0.4 m to 1.0 m, and their lengths vary from 1.0 m to 3.0 m depending on the soil properties and the tension load designed.

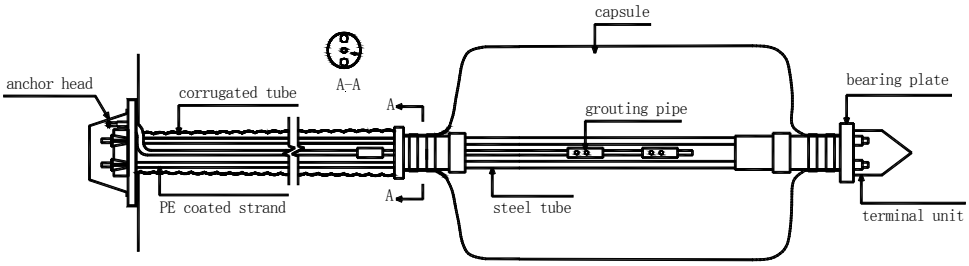


Fig. 4 General configuration of new anchorage system with capsule

The innovative anchorage system has been implemented in many deep excavation, anti-floating and slope protection projects since 2011, and it is suitable for various soil formations covering clay, silt, loess, sand, gravel and weathered rock. The advantages of the new technology contain higher capacity, better safety, more reliable quality and cost efficiency. The key structure features of this new system (Liu et al. 2012) are listed as follows:

- Sleeved grouting pipe, air exhaust valve, hollow steel tubes and capsule to be key components;
- Compression and anti-corrosion structure to be used for the anchorage system;
- Capsule to be able to be folded and expanded to the size and volume required;
- Properties of capsule to be able to meet requirements of strength, deformation and permeability;
- Capsule of ECB device to be able to maintain the injection pressure after grouting;
- ECB devices to be manufactured in factory and assembled easily with tendons on site.

Relying on above key structure and assembling technique, the ECB device with tendons can be easily inserted into the borehole within the diameter of 150 mm~180 mm, and the capsule can be inflated by the cement grouting with water/cement ratio ranging from 04 to 0.45, and injection pressure varies from 1 MPa to 3 MPa in the practice. According to completed projects and various ground conditions, the actual geometrical shape and dimension of ECB devices can be adjusted based on the required tension load of anchorages. Besides, the compressive strength of ECB shall be over 40 MPa and capsule shall be enclosed in surrounding dense cement soil.

In past 6 years, due to the technical, environmental and economical advantages, this innovative anchorage system has been promoted in 17 provinces in China, and more than 150 deep excavation, anti-floating and slope protection projects were accomplished. By employing the new anchorage technology, the 10%~20% total cost has been reduced for the projects of anchored structures, and the amount of steel strand and cement has been cut down by 20%. In sum, this anchorage system is playing an increasingly important role in Chinese sustainable development.

MODEL TESTS FOR UNDERREAMED ANCHORAGE

Differ from the shaft anchorage, there is an expanded section on underreamed anchorage, so its bearing capacity derives from the skin resistance of small section and enlarged section, and the base resistance of ECB as well. To make the bearing behavior of underreamed anchorage clear, the characteristics of these three parts should be studied separately. Meanwhile, the investigation of the failure mode of underreamed anchorage is also vital for applying the new anchorage system. Hence the model tests of bearing characteristics and failure mode were carried out.

In the model experiments, the research object was the model of underreamed anchorage with the geometric similarity ratio of 1:10, and the reaction of the soil around anchorage during uplifting process was researched in the symmetrical form. In the investigation of the anchorage bearing

behavior, the dimension of test anchorages included the length T from the top of ECB to the soil surface, the diameter D and the length L of ECB, and the entire model anchorage was T + L long. The model tests were operated in the assembled sand box, in which the model foundation was prepared through stratified sand raining with medium quartz sand. The properties of the simulated foundation are shown in Table 1.

Table 1 Physical - mechanical parameters of simulated foundation

Density /g·cm^{-3}	Coefficient of uniformity	Friction angle / °	Cohesion /kN·m^{-2}	Poisson's ratio/υ	Specific gravity
1.49	1.9	40.0	0.0	0.26	2.67

The ECB models of anchorages were made of steel cylinders with different dimension and connected with screw bar in 8 mm diameter. In order to distinguish the end bearing capacity from total tension load, a circular pressure sensor was set on the upper surface of ECB as in Figure 5. During the tests, the total load (Q), the corresponding displacement (s) of the anchorage top and the corresponding end bearing capacity (q) of each loading step were all measured and recorded.

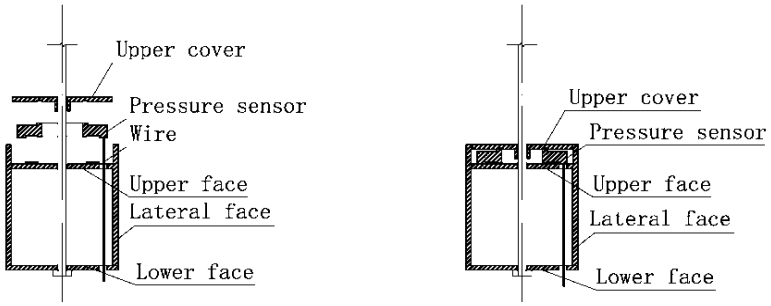


Fig. 5 Model of ECB with load pressure sensor

As to symmetrical model tests, the law of deformation field was studied, and the sand box and model anchorage were both cut into half scale according to the symmetry principle of mechanics, seen in Figure 6 (a). The deformation field of soil around anchorage was captured and described. Figure 6 (c) shows the frontal side of sand box with thick glass, and model anchorage, surveying sensors, digital camera and studio strobes were adopted as well. When the anchorage was pulled vertically, the tension load, the displacement and the deformation picture of each test step were all recorded. After testing, the deformation value of soil around anchorage could be accurately calculated.

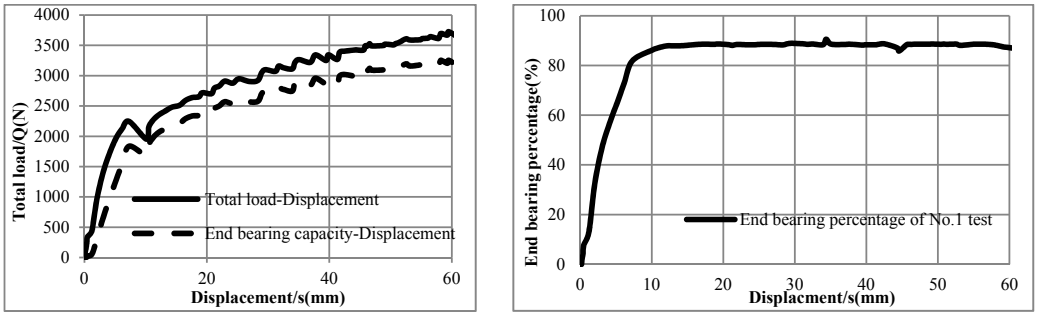


(a) Test system sketch **(b) Photo of model test system** **(c) Photo of symmetry test**

Fig. 6 Sketch and photos of model test system for underreamed anchorage

Figure 7 demonstrates the total tension load versus displacement curve and the end bearing capacity versus displacement curve, in which the ECB with 100 mm diameter and 150 mm length in embedment depth of 950 mm in sand. The pair of curves shows clearly that the Q-s curve and q-s curve keep increasing. The two curves get almost the same increasing pace and the both trends are also

similar. For studying the relationship between the total tension load and the end bearing capacity, Figure 7 (b) provides a meaningful curve of the q/Q versus displacement.



(a) Q-s curve and q-s curve **(b) q/Q-s curve**

Fig. 7 Test curves of model test No.1 with the embedment depth of 950 mm

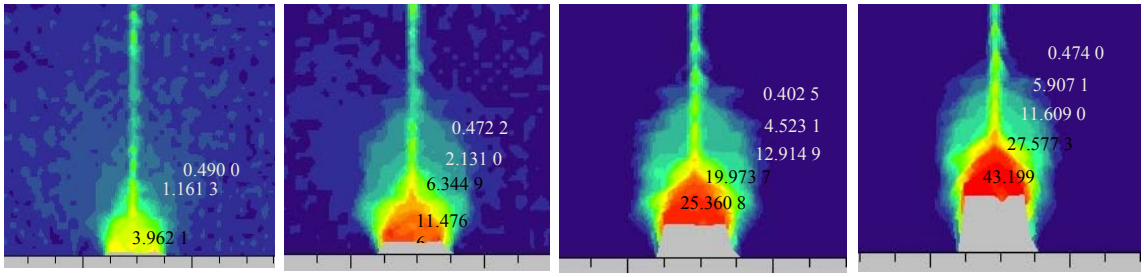
q/Q-s curve states the developing law of the percentage of the end bearing capacity in the total tension load with the increasing vertical displacement. The curve has a rapid increase before the displacement of 10 mm, and then it changes to be a flat straight line. The development trend illustrates the end bearing capacity ratio goes up rapidly from zero, and the percentage nearly keeps still after the displacement is over 10 mm, it means that the percentage of end bearing capacity in the total tension load tends a constant value. In order to research the regularity of the percentage variation, Table 2 lists the test results in different embedment depths. The alteration of the percentage can be found in the fifth column. It indicates that the anchorage buried in deeper foundation has the higher end bearing capacity percentage. For example, the percentage of the embedded depth in 950 mm is 88.34%, while the value is 84.56% of the embedded depth in 450 mm. And at least 80% anchorage capacity is taken by the base resistance of ECB if the ratio of T/D is over 4.5.

Table 2 Test results summary of underreamed anchorages

No.	Expanded length L (mm)	Expanded diameter D (mm)	Embedment depth T (mm)	End bearing percentage q/Q (%)	Ultimate capacity Q (N)	Corresponding displacement s (mm)
1	150	100	950	88.34	3725.96	60.00
2	150	100	850	85.99	2888.06	60.00
3	150	100	750	85.22	2370.28	60.00
4	150	100	650	85.18	2056.04	60.00
5	150	100	550	84.69	1408.72	60.00
6	150	100	450	84.56	998.62	41.48
7	150	100	350	56.25	729.12	25.36

In investigating the soil deformation field in tests, the model ECB with diameter of 60 mm and length of 100 mm was buried in the depth of 850 mm. The partial amplified details of displacement calculated in photos are shown in Figure 8. These enlarged pictures captured by digital camera reveal that the deformation zone looks like a balloon and grows bigger with the increasing extension of anchorage. During the loading process, the deformation zone is buried throughout below the soil surface. From Figure 8, the regular pattern of the displacement distribution can be found through analyzing the representative displacement values of sand particles in the colored area. Figure 8 (a) to Figure 8 (c) demonstrate that the zone of moved particles gets larger with the pulling out of anchorage. Comparing Figure 8 (c) and Figure 8 (d), one can see that there is little change in the zone of moved particles after the anchorage displacement reaches 27.8mm, and the dark compacted zone moves up with ECB. The phenomenon illustrates the deformation zone not to expand any more, when the anchorage pulling out reaches certain condition, however the deformation zone on the top of ECB is further compacted.

The unique failure feature is to emerge the local shear failure in soil surrounding anchorage, on the other hand, the compacted area moves up and the yielding zone gets denser, it leads to the improvement of soil shear strength and the increase of bearing capacity. Therefore, the pictures in Figure 8 can well explain the reason why the Q-s curves of underreamed anchorage in Figure 2 and Figure 7 (a) can keep going up and demonstrate the strain-hardening load-displacement relationship.



(a) Displacement of 5.8mm (b) Displacement of 13.8mm (c) Displacement of 27.8mm (d) Displacement of 44.8mm

Fig. 8 Soil displacement contours around undereamed anchorage in model test

NEW COMBINED CONSTRUCTION APPROACH

There are two new combined approaches to be proposed for construction, ① jet-grouting plus capsule expanding, ② mechanical under-reaming plus capsule expanding. While here only the approach ① is presented, which consists of the processes of drilling, jetting, ECB device to be inserted and grouting in- and outside capsule. With the help of the patented liquid-controllable drilling tool, the process of drilling - jetting - grouting can be carried out in one phase (Liu et al. 2008). It simplifies the construction procedure and improves site productivity. By the combined approach, the installation quality can be controlled by the simple way, in which the target volume of cement grout will be accurately injected into the capsule. In this way, this combined approach can solve the most problems of the traditional underreamed anchorage systems in construction.

Utilizing the innovative ECB devices, the enlarged boreholes can be maintained in various soils, and the controllability and reliability of the new anchorage system can be enhanced, because the designed dimension and compressive strength of the enlarged body can be enforced based on low water cement ratio, high grouting pressure and target grout volume during the capsule injection process. Moreover the combined approach is easily to execute, to provide higher confining pressure around ECB and to improve the surrounding soil of ECB. Normally, the compressive strength in 7 days of the cement grout in capsule shall be higher than 40 MPa, which completely meets the technical regulations for the application of compression anchorages.

In stiff clay, dense sand or weathered rock layers, jet grouting can easily bore a large hole in stiff ground, and then the inflatable capsule can quickly expand into an enlarged body in sequence without any problem. The new approach of jet-grouting plus capsule expanding can extend not only more applicable formations, but also improve the construction quality and productivity. On the other hand, the durability of new anchorages system will be significantly upgraded by using the double corrosion protection for permanent anchorages.

BACKGROUND OF A CASE HISTORY

The case history is a 30000 m^2 mixed-use development located in Kaifeng city in China, which comprises 14, 22, 27, 32-storey tower blocks and the large 3-level basements as well. Due to the -0.5m groundwater level, the scenario of tension piles with the diameter of 600 mm in the length of 17 m was proposed to resist the hydrostatic uplift. However, after comparing an alternative design of the

innovative underreamed anchorages with capsule, the client decided in favor of the optimizing scenario because this new anchorage system could provide the obvious benefits as below:

- More than 30% total cost of anchored structure for resisting uplift force to be cut down;
- Construction period to be reduced from 100 days to 45 days by using 20 tower rigs;
- No soil spoils to be transported outside and to provide the friendly environment.

The site ground condition is shown in Figure 9, being typical Kaifeng sequence of fill, silt, silty clay and fine sand. The deposits were primarily brought down by Yellow River, and the geotechnical conditions vary both in vertical and horizontal direction, soil parameters are presented in Table 3.

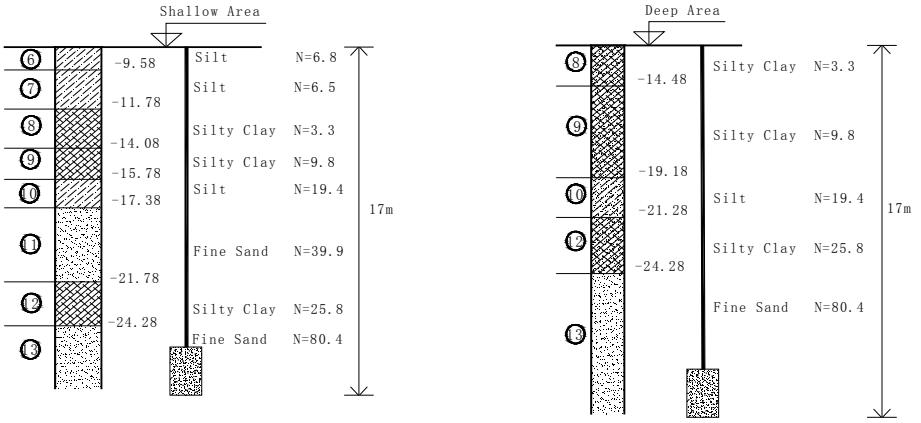


Fig. 9 Typical ground conditions and position of ECB

Table. 3 Soil parameters adopted in design

Stratum	SPT Value	γ kN/m^3	C_u kPa	φ' °	Stratum	SPT Value	γ kN/m^3	C_u kPa	φ' °
⑥Silt	6.80	19.40	6.50	16.40	⑩Silt	19.40	19.60	7.00	23.00
⑦Silt	6.50	19.40	7.00	17.50	⑪Fine sand	39.90	20.00	0.00	36.00
⑧Silty clay	3.30	18.20	11.00	9.50	⑫Silty clay	25.80	19.40	20.00	26.20
⑨Silty clay	9.80	19.00	15.50	9.50	⑬Fine sand	80.40	20.00	0.00	41.00

In this project, the scenario of innovative underreamed anchorages provided the optimum solution, both from program perspective and cost efficiency. According to the anti-floating design, the length of total 4450 anchorages varied from 11 m to 17 m based on soil conditions. The alternative design required the ultimate capacity of permanent anchorages as 1200kN with a safety factor of 2. In the anchorage design, the fixed length was 3 m, the same as the length of ECB, the free length varied from 8 m to 14 m and the diameter of ECB was 600 mm. Besides, the combined construction approach ① for the new underreamed anchorages included fabricating, installing, grouting and stressing procedures, the construction procedure included the following stages:

- ECB devices and strands fabrication: to connect each ECB device with four Φ17.8 mm strands solidly on site, and all strands to be covered with HDPE sheath;
- Anchorages installation: to drill and to enlarge the boreholes by jet grouting and to put the ECB devices with strands into the holes in proper position;
- Grouting: to inject the target grout with water/cement ratio 0.40～0.45 into the capsule at first, and then to screw the grouting pipe off the capsule and to re-inject the borehole with the same cement grout thereafter;
- Anchorages stressing: to stress the strands of anchorage up to the tension load of 600 kN, and then the load of 400 kN was locked off for each anchorage.

In Figure 10, there are more than ten tower rigs to be used during the installing the underreamed anchorages with capsule on the construction site.



Fig. 10 Photo of construction site in Kaifeng city project

RESULTS OF PROVING TESTS AND ACCEPTANCE TESTS

The aim of proving tests was to ensure the suitability of the new anchorage system for the project, and the combined construction approach ① was applied in this project and preliminary trials. The proving test anchorages were installed from the ground surface, and the length of two underreamed anchorages was 27 m, including 24 m free length and 3 m fixed length with the diameter of 600 mm. In the installation, the ECB devices were placed into fine sand layer ⑬ with the density established from SPT value around 80.

The two test anchorages with capsule were tested to the failure in preliminary trials. The test results indicated the ultimate capacity of 1200 kN attainable using the underreamed anchorage system, the displacements versus the ultimate tension load were separately 228.5 mm and 174.2 mm. The failure of test anchorages resulted from the part of strands broken during the tests. It means, the test anchorages could supply higher capacity if more strands or larger cross section of strands were used in the anchorages.

The priority of the acceptance tests is to establish the safety factor by overloading in a short period, usually to the 1.5×working load as the requirement of Chinese code "Technical specification for underreamed anchorage by jet grouting" (JGJ/T282-2012). Considering the importance of this project, the 1.8×working load was chosen as the acceptance test load. The test results has testified the excellent quality of innovative underreamed anchorages, which are demonstrated in Table 4 based on the data submitted by the independent test company. Except No.2 anchorage, the displacements of the 43 test anchorages are less than 90 mm, these results of accepted tests indicate all the underreamed anchorages to be on the safe side.

Table 4. Acceptance test results of 44 anchorages on site (test load = 1080kN)

No.	Displacement (mm)	No.	Displacement (mm)	No.	Displacement (mm)	No.	Displacement (mm)
1	80.71	12	89.91	23	55.47	34	80.82
2	129.42	13	53.92	24	57.22	35	76.59
3	63.56	14	79.58	25	76.21	36	88.56
4	56.50	15	63.02	26	64.85	37	61.17
5	71.67	16	64.03	27	78.61	38	70.11
6	67.51	17	71.90	28	64.25	39	61.67
7	58.76	18	81.65	29	66.67	40	61.90
8	68.53	19	58.12	30	73.55	41	59.67
9	62.62	20	57.06	31	73.73	42	77.36
10	76.94	21	64.57	32	85.65	43	55.18
11	77.89	22	77.61	33	74.05	44	63.91

CONCLUSIONS

The following conclusions are obtained through revealing the innovative anchorage system, the lab-experiment finding and the achievement in the practice.

1. The most important characteristics of underreamed anchorages demonstrate the strain-hardening load-displacement behavior, which results from its unique failure mode and better bearing mechanism. It is also identified that the local shear failure is found in soil surrounding the expanded body and the anchorage capacity is governed by the base resistance, which takes more than 80% of total anchorage capacity in the most model tests.

2. The innovative ECB device, including the inflatable capsule, sleeved grouting pipe, air exhaust valve, hollow steel tubes and compression-type structure, was created for the advanced anchorage system, and this patented structure is bringing many benefits in various kinds of the technical and economical aspects.

3. Based on the case description, the combined construction approach of jet-grouting plus capsule expanding has been verified as the efficient technology for installing the innovative underreamed anchorages with capsule, which has contributed to the quality control, time saving and execution convenience in the projects.

REFERENCES

Barley, A.D., 1997. The single bore multiple anchor system. Ground Anchorages and Anchored Structures, Proceedings of the International Conference Organized by the Institution of Civil Engineers and held in London, UK, pp. 65-75.

Smoltczyk, U., 1991. Grundbau – Taschenbuch. Berlin: Ernst & Sohn, Vierte Auflage Teil 2, 815 p.

Xanthakos, P.P., 1991. Ground anchors and anchored structures. Canada: John Wiley & Sons, 686 p.

Liao, H. J., Wu, K.W. and Shu, S.C., 1997. Uplift behaviour of a cone-shape anchor in sand. Ground Anchorages and Anchored Structures, Proceedings of the International Conference Organized by the Institution of Civil Engineers and held in London, UK, pp. 401-410.

Massarsch, K. R., Oikawa, K., Ichihashi, Y., et al., 1997. Design and practical application of soilex anchors. Ground Anchorages and Anchored Structures, Proceedings of the International Conference Organized by the Institution of Civil Engineers and held in London, UK, pp. 20-21.

Hobst, L. and Zajic, J., 1986. Anchoring in rock and soil. Translated by Wang, S. J., Beijing: Central Research Institute of Building and Construction, Ministry of Metallurgical Industry, 312 p. (in Chinese)

Anon, 1988. Jet grouted anchors put to the test. Ground Engineering, pp. 16-17.

Cheng, L. K., Fan, J. L., Han J., et al., 2000. Ground anchorage. Beijing: China Architecture and Building Press, pp. 35-45. (in Chinese)

Chinese Code, 2012. Technical specification for underreamed anchorage by jet grouting (JGJ/T282-2012). Beijing：Chinese Building and Construction Press. (in Chinese)

Chinese Code, 2015. Technical code for engineering of ground anchorages and shotcrete support (GB 50086-2015). Beijing：China Planning Press. (in Chinese)

Liu, Z., Guo, G., Zhang, Y., et al., 2014. Construction technology and application of underreamed anchorage with capsule. Chinese Journal of Geotechnical Engineering, Vol. 36(2): pp. 205-211. (in Chinese)

Liu, Z., Guo, G., Zhang, Y., et al., 2012. Mechanical behavior and new construction technology of underreamed ground anchorage in anti-floating project. Proceedings of 11th Science and Technology Seminar on Underground Engineering cross the Strait Tunnel, Taiwan, C15: pp. 167-174. (in Chinese)

Liu, Z., Yang, S., Zhao, Y. F., et al. 2008. Construction method of underreamed anchorage with the drill tool of combination of drilling, jetting and grouting. Patent: CN101260669. (in Chinese)

EFFECTS OF INSTALLATION PARAMETERS OF DRILLED DISPLACEMENT PILES ON IN SITU STRESS CONDITIONS IN STIFF CLAYS

Martin D. Larisch, Brian Perry Civil, Auckland, New Zealand, +64274055406, martinla@fcc.co.nz

Martin D. Larisch, Geotechnical Engineering Centre, School of Civil Engineering, The University of Queensland, Brisbane, QLD, Australia, +61419799701, m.larisch@uq.edu.au

David J. Williams, , Geotechnical Engineering Centre, School of Civil Engineering, The University of Queensland, Brisbane, QLD, Australia, d.williams@uq.edu.au

Alexander Scheuermann, Geotechnical Engineering Centre, School of Civil Engineering, The University of Queensland, Brisbane, QLD, Australia, a.scheuermann@uq.edu.au

ABSTRACT

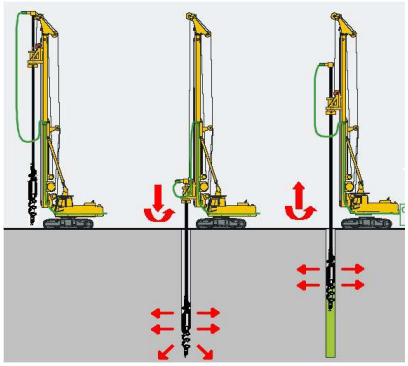
Drilled displacement piles (DDP) have been used around the world for decades as foundation elements for structures and embankments. Typically the pile toes are designed to penetrate into stiff or dense soil formations to achieve sufficient base resistance. Recent research at The University of Queensland in Brisbane, Australia has discovered that the *in situ* stress conditions in stiff to hard clays is directly related to pile installation rates, which in turn are a function of the piling rig capacity and ground conditions. With adequate and constant pile penetration rates *in situ* stress conditions in the stiff to hard clay are increased by about 40%, resulting in significantly higher pile capacities. If pile penetration rates are too slow the *in situ* stress conditions are reduced considerably by remoulding and shearing of the clay, potentially causing reduced pile capacities. The paper presents the results of full-scale test piles at a stiff to hard clay site installed using different full-scale piling equipment.

KEYWORDS

Drilled displacement piles, pile installation effects, CFA piles, CPT, pile load capacity, pile design

INTRODUCTION

Drilled displacement piling (DDP) is a piling technique in which a hollow stem, fitted with a purpose built displacement tool at the bottom, is drilled into the ground. Dissimilar to non-displacement piles, like Continuous Flight Auger (CFA) piles or conventional rotary bored piles drilled with kelly bars, the soil is not excavated during the DDP penetration process, but is displaced laterally and to a lesser extent vertically. The cavity created by the drilling tool is filled with highly workable concrete during the extraction process. The DDP technique is very economical providing high production rates and creating only marginal drill spoil, which has led to its increased global usage during the last decade. The typical DDP installation process is described in Figure 1.



1. Set up auger at pile position and install cap to close concrete outlet at auger tip.
2. Install auger by rotating clockwise and applying vertical pull down force.

   Drill auger to design depth; the displacement body of the auger pushes the soil cut by the auger tip into the surrounding ground.
3. Pump concrete through hollow auger stem and extract auger while rotating clockwise, always maintaining positive concrete pressure with the auger embedded in fresh concrete.

   Install reinforcement into fresh concrete, if required.

Fig. 1. Typical installation process of DDP (after Bauer company brochure)

DDP are typically installed using standard Continuous Flight Auger (CFA) piling equipment. Consequently, applicable piling rig monitoring systems should be utilized for quality assurance. The depth of DDPs is similar to the applications and limitations of the CFA method, typically ranging from 15 m to 25 m (49 to 82 ft.) depth for standard rigs and up to 40 m (131ft.) for large piling equipment. As the drill resistance of the DDP tool is governed by the full displacement effect of the tool, diameters usually range between 270 mm and 450 mm (10 to 17.7 in.). Larger diameters are not recommended as the steel connection between the drill tool and the stem would fail for high torque machines or less powerful rigs would reach early refusal. In both scenarios constant minimum penetration rates could not be achieved which directly influences the DDP performance as highlighted in the following chapters.

DRILLED DISPLACEMENT AUGERS

As described by Larisch et al (2012) 'Drilled displacement piles were invented in the 1960's in Europe. The Atlas Pile was a pioneer of a bored, full-displacement pile, followed by the Omega pile as the flagship of the next generation of DDPs (Figure 2). With the development of hydraulic piling rigs and the increasing torque and thrust capacities of these machines, DDPs became more economical and over the past few decades several different auger shapes have been developed. The augers shown in Figure 2 are all referred to as DDP augers, but generally fall in two different groups: (a) short augers (Atlas / Fundex) and (b) long auger systems (Omega, de Waal, others).

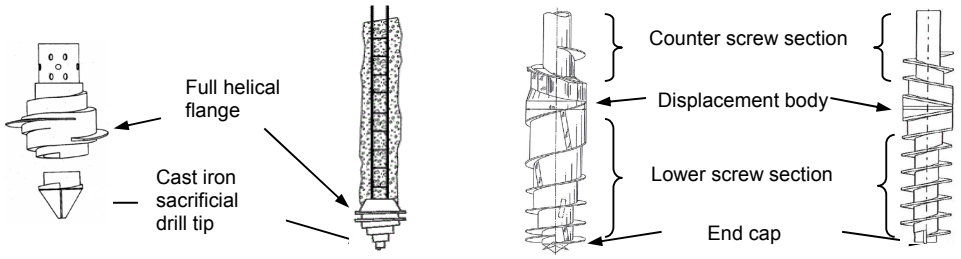


Fig. 2. Selection of different DDP augers, the short augers systems Atlas and Fundex (left) and long auger systems Omega and de Waal (right) show different performances

The Atlas and Fundex systems rely on a short, single, full-helical flange to cut the soil and pull in the displacement body, with little or no soil transport. The compact displacement bodies displace the soil. Usually, high torque capacities are required for these pile types, since a large amount of soil displacement occurs and the cast iron, auger-shaped drill head of the Fundex system is sacrificial. In contrast, the Atlas drill head is extracted and only the drill tip is left in the ground. The installation of reinforcement is carried out prior to concrete placement for both systems via the hollow casing or auger stem, unlike that described in Figure 1. Both piling systems are niche products in Northern Europe.

Omega and de Waal displacement augers are examples of long DDP systems. They are designed with longer flighted sections and the lower auger sections are used for cutting and transporting the soil to the displacement body of the auger. The counter screw sections, located above the displacement body, re-displace soil that has collapsed into the cavity behind the auger during the extraction process. The auger geometry of Omega and de Waal augers seems comparable. However, the Omega auger is a progressive displacement auger as the stem diameter of the lower auger section progressively increases towards the displacement body. During drilling, the soil is displaced progressively along the lower auger section. The de Waal auger can be defined as a rapid displacement auger, since the displacement body has a larger diameter than the auger stem. Soil displacement occurs rapidly at the displacement body and only marginal displacement is expected below and above it. Installation torque and pile capacities should be lower for rapid displacement augers compared to progressive augers (Slatter 2000).

The general working principles of screw auger tools has been described by various authors and the most accepted theories about auger mechanics of screw auger piles can be found in the relevant literature (Viggiani 1993, Fleming 1995, Slatter 2000).'

It is important to understand the influence of the auger geometry and the installation parameters (e.g. penetration rate, torque, auger rotation) on the stresses and displacements generated in the formation during DDP installation. These have a direct influence on the load-settlement behaviour of the piles.

Auger Model after Vigianni (1993)

In a paper discussing the use of CFA piles in Italy, Viggiani (1993) carried out a detailed analysis of the soil transport and displacement characteristics of this auger type. He developed an auger model and by equating the volume of the auger stem introduced with the volume of material removed during the installation process, Viggiani derived the following equation for the minimum velocity at which a CFA tool could be installed without loosening the surrounding soil:

$$V_{a(min)} \geq nl\,(1 - (d_o^2/d^2)) \qquad [1]$$

Where $V_{a,\,(min)}$ = minimum penetration rate (m/min), n = rate of rotation of the drill tool (rev/min), l = auger pitch (m), d = outer auger diameter (m) and d_0 = auger stem diameter (m)

From equation (1), it is evident that the ratio of stem diameter to flight diameter (d_o/d) influences the allowable penetration rate. Even though Vigianni's formula was originally developed for CFA piles, the method was found to be suitable for drilled displacement piles in fine-grained soils (Larisch 2014).

For this research project and in this paper, DDP augers are referred to as rapid displacement augers.

SCOPE OF RESEARCH

Over the past two decades research around the globe has been carried out to understand the behaviour of DDPs in granular soil formations and the influence of installation parameters on pile load capacities (Slatter 2000, Schmitt and Katzenbach 2003).

The influence of the installation parameters (penetration rate, rotational torque and revolutions of the drill tool) on stress development and stress changes during the installation of DDPs in fine-grained soil has not been investigated in detail. This paper explores this topic in detail and presents field measurements that were recorded at a field test site in Lawnton, Queensland (Australia) on two different test piles installed with different installation parameters using similar DDP augers.

THE FIELD TEST SITE AT LAWNTON, QLD, AUSTRALIA

The Lawnton test site comprised stiff to hard clays down to about 7 m (23 ft.) below ground level, underlain by gravel and decomposed rock formations as shown in Figure 3.

Two initial cone penetration tests (CPT) were carried out together with two boreholes, to ensure that each test pile location was covered by sufficient ground investigation data. Undisturbed samples from each borehole were used to carry out laboratory tests (tri-axial test, odometer tests) for the determination of geotechnical parameters for the test site.

Two 4 m (13 ft.) long drilled displacement test piles were installed into the stiff to hard clay formation as shown in the soil profile of the test site displayed in Figure 3. The parameters of the stiff to hard clay were used to model a typical bearing layer for a piled foundation using DDPs.

Usually, DDPs need to be installed to penetration depths of 2 to 4 m (6.5 to 13 ft.) into suitable bearing layers, which often consist of stiff to hard clay, to achieve sufficient base and shaft resistances. Hence, a pile depth of 4 m (13 ft.) was selected. The additional 3 m of hard clay below the proposed pile toe levels ensured that the test piles were not influenced by the gravel layer.

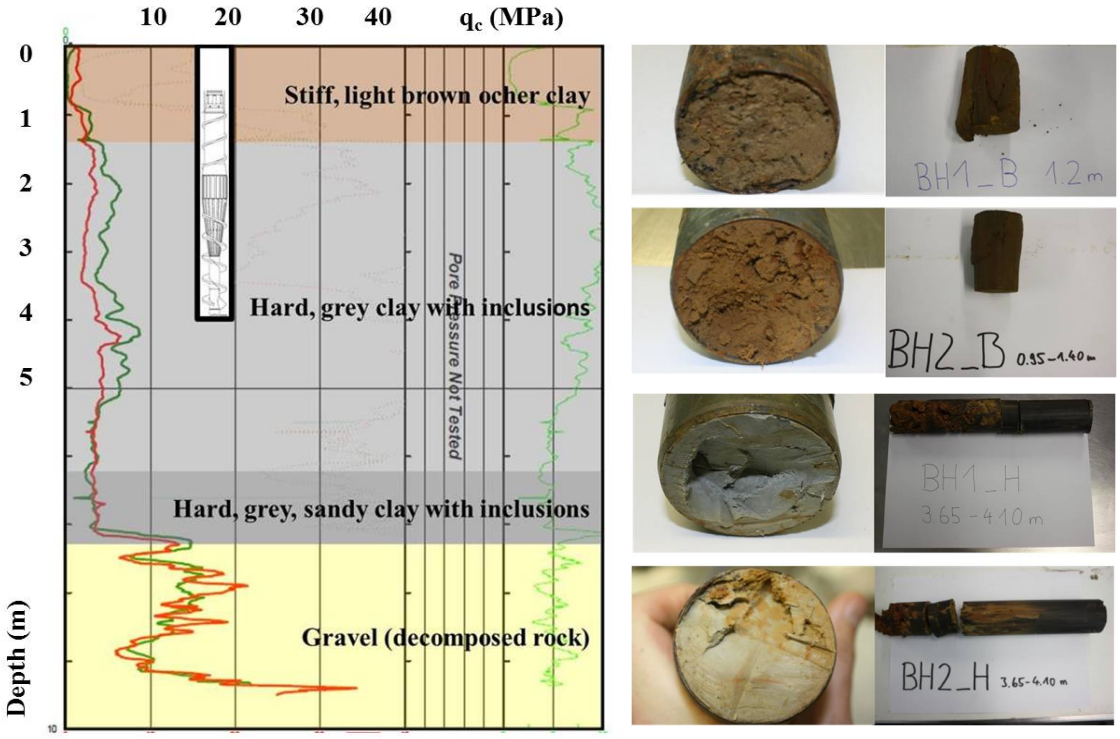


Fig. 3. Soil profile at field test site at Lawnton (Australia), CPT profile (left) and core samples of stiff, light brown ocher clay (top right) and hard, grey clay (bottom right)

CONSTRUCTION OF TEST PILES

Two test piles (D and E) were installed using identical DDP augers of 450 mm (17.7 in.) in diameter. The test auger is defined as a rapid displacement auger (Larisch et al., 2012). Both test piles were installed in similar ground conditions using the same tool geometry (Table 1).

Table 1. Auger details for DDP test piles

Auger details	**Rapid Displacement Auger**	
Outer diameter (flights and displacement body)	450 mm	17.7 in.
Inner stem diameter (inner tube at the bottom)	250 mm	9.8 in.
Height		
Lower Section	1,500 mm	59.0 in.
Displacement Body	500 mm	19.7 in
Counter Screw Section	1,000 mm	39.4 in.
Total	**3,000 mm**	**118.1 in**
Upper Flight Pitches	250 mm	9.8 in.
Bottom Flight Pitch	100 mm	3.9 in.



For the installation of the test piles, two different piling rigs were utilised, as specified in Table 2.

Table 2. Comparison of the two piling rigs used for the tests

Piling Rig details	Piling Rig A	Piling Rig B
Operational weight (ton)	120	85
Year of manufacture	2008	1985
Rotational torque (kNm)	280	120
Vertical thrust (kN)	300	150
Automatic drill assistant	YES	NO

The installation rate for the rapid displacement auger was calculated according to Vigianni's formula (equation (1)), from which the minimum constant penetration rate was determined to be:

$V_{a,\,(min)} \geq 1.8$ m/min

Test pile D was installed with the less powerful piling rig B, whereas test pile E was installed with piling rig A. The penetration rates of the different test piles are displayed in Figure 4.

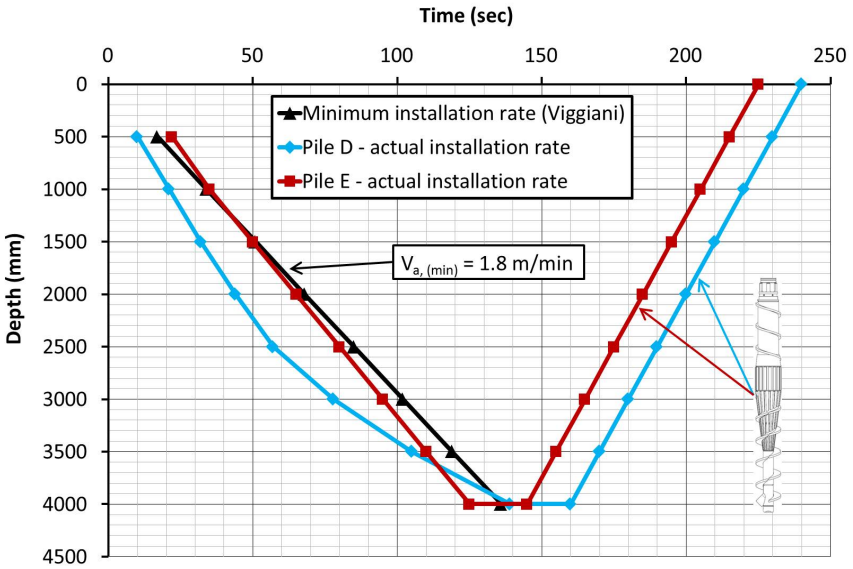


Fig. 4. Summary of installation rates for test piles D and E compared with the minimum rate

The installation records of test pile D indicated that the smaller piling rig could not maintain the penetration constant at the required rate of 1.8 m/min (due to increased resistance of the drill tool in the stiff to hard clay).

Test pile E was installed with the more powerful piling rig, supported by an automatic drill assistant and a penetration rate of about 2.0 m/min was achieved for the full depth of 4 m (13 ft.), which fulfilled the minimum requirement of Vigianni's formula.

Pile installation records

The pile installation records for both tests piles are shown in Figure 5. The rig monitoring system Jean Lutz was used to record the penetration rate, torque, tool rotation, extraction rate as well as concrete pressure and volume. The latter parameters are not included in the records shown as this paper is concerned with the installation factors only.

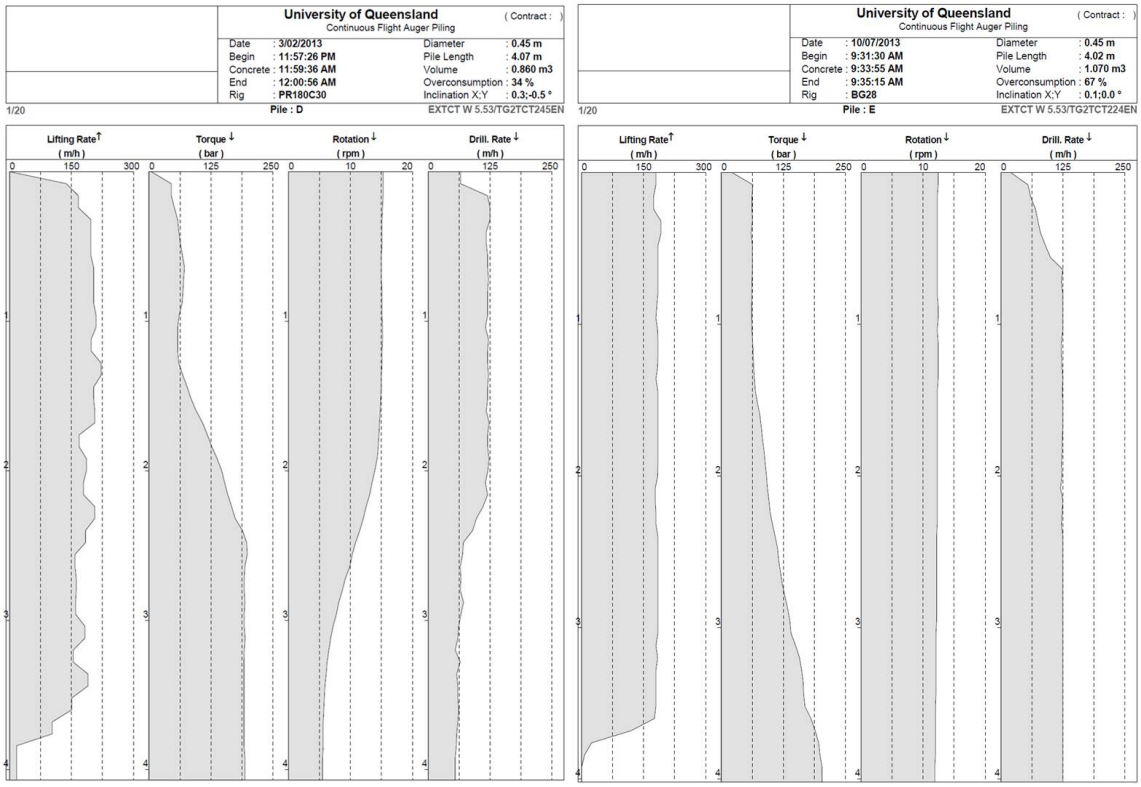


Fig. 5. Pile monitoring record for test piles D (left) and test pile E (right)

For test pile D, the maximum torque capacity of the piling rig was reached at about 2.5 m (8.2 ft.) depth. Below this depth the rotation of the drill tool as well as the penetration rate slowed down. Unfortunately, the vertical pull-down force could not be displayed, but it is obvious that the tool penetration over the last 1.5 m (4.9 ft.) socket penetration is almost constant despite the rotations slowing down linearly. The extraction rate was constant at 3 m/min; however, due to the manual control of the tool extraction a slight variance can be observed.

The installation record for test pile E presents a completely different scenario. The torque increased linearly down to the ultimate 4 m (13 ft.) drill depth. The rotation of the drill tool as well as the tool penetration rate were controlled by the rig computer (not manually by the rig operator) and were able to be maintained constant, despite the increased drill resistance as seen for test pile D. The extraction rate of the DDP auger for test pile E was also carried out by the automatic drill assistance and shows a constant value of 3 m/min.

Cone penetration testing (CPT) to determine installation effects

Cone penetration testing (CPT) is a fast and reliable method of conducting *in situ* soil exploration for the support of embankments, retaining walls and pavement subgrades, or for bridge foundations and the determination of pile load capacities.

Initial CPTs were carried out at the locations of the two test piles to measure 'undisturbed' ground conditions. Seven days after the installation of the test piles two additional CPTs were carried out at each test pile location in order to determine the total effective changes in the clay formation as a result of the installation of the two test piles. It was assumed that one week after pile installation the pore water pressure caused by the drilling process was fully dissipated.

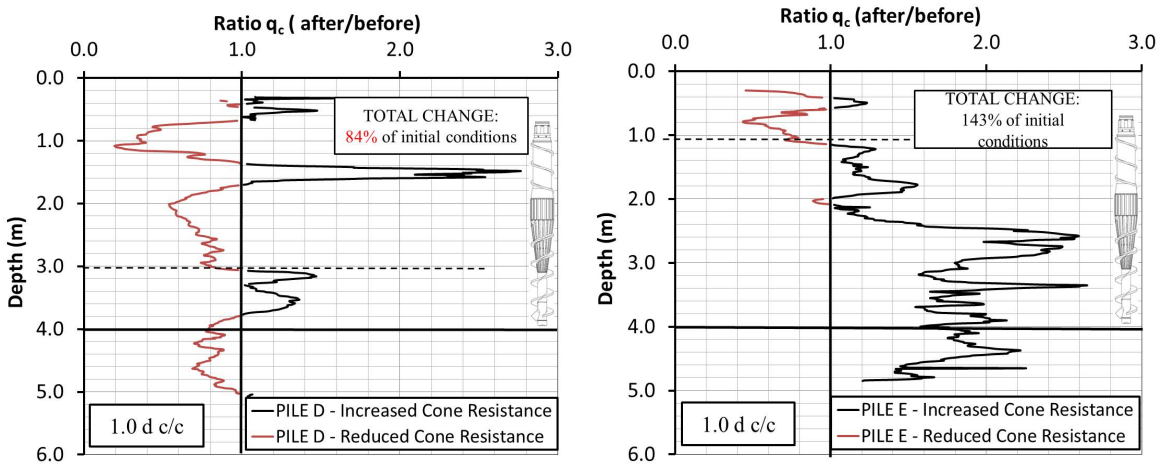


Fig. 6. Ratio of cone resistance qc after and before installation for pile D (left) and pile E (right)

The two additional CPTs at each test pile location were carried out 225 mm (8.86 in.) from the edge of the pile shaft (which is equivalent to one pile diameter from the pile axis) and the average of both measurements was taken to evaluate the soil profile after pile installation. In order to determine the influence of the pile installation process on the effective stresses in the clay at both test pile locations, a plot displaying the ratio of q_c (after / before) was developed as shown in Figure 6. A ratio of < 1 indicates weakening of the soil formation as result of pile installation, and a ratio of > 1 indicates an increase in soil strength due to pile installation.

ANALYSIS OF RESULTS

The use of inadequately powered piling rigs or the choice of inadequate installation rates of DDPs could lead to more than 15% stress reductions in stiff to hard clay formations. Whereas the stress reduction at the upper part of the pile shaft could be related to soil heave (Larisch et al. 2015), the stress reduction below the pile toe and along the lower part of the pile shaft (except the bottom 25%) are an indication of clay remoulding. There the clay is sheared and heavily disturbed as a result of the decreasing tool penetration rate. The spike shown for pile D in Figure 6 at about 1.75 m (5.7 in.) depth is a localized phenomenon likely related to a boulder.

The installation of the DDP tool using a sufficient penetration rate according to Vigianni's formula increased the stresses in the Lawnton clay by about 43% during the installation of test pile E. There is a notable increase below the pile toe and along the lower section of the pile shaft. The small improvement in the q_c ratio along the upper part of the shaft could be related to soil heave.

CONSEQUENCES FOR PILE DESIGN

Bustamante and Gianeselli (1998) introduced a design method for DDPs that is based on *in situ* test results. The authors have used the CPT data from this research to estimate the pile capacities of the DDPs in Lawnton clay for: (a) undisturbed ground, (b) test pile D (inadequate installation parameters), and (c) test pile E installed with adequate penetration rates according to Vigianni's formula.

The results are displayed in Figure 7 and the method by Fleming (1992) was used to predict the load-settlement behaviour of the respective test piles. It was predicted that test pile E could achieve about 950 kN (96.87 tf.) ultimate geotechnical capacity, which is greater than 30% of the pile load estimated for the undisturbed ground conditions (720 kN or 73.42 tf.)). It was predicted that test pile D, installed with insufficient installation rates could achieve only 680 kN (69.34 tf.), which is 5% less than the target design pile capacity.

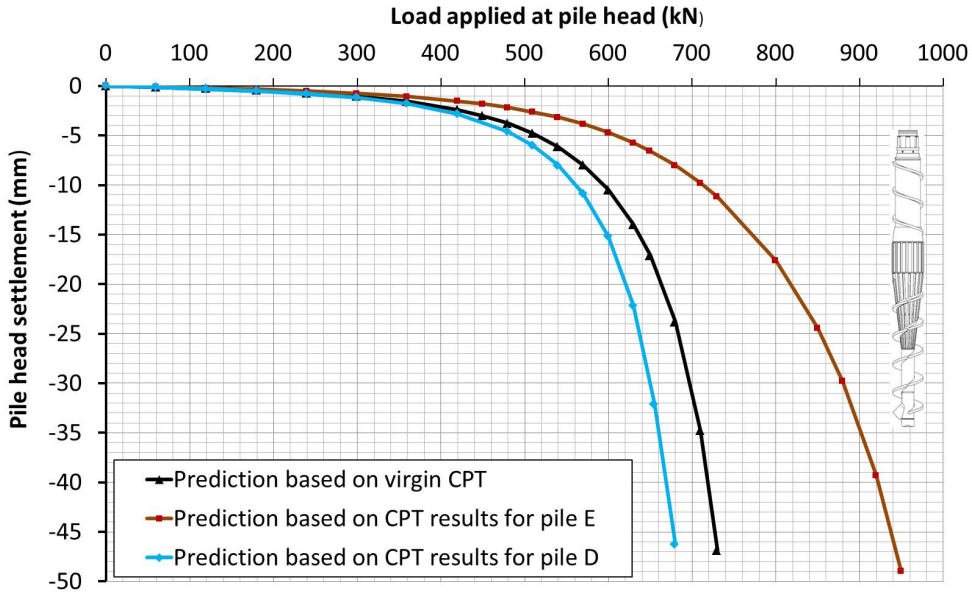


Fig. 7. Predicted load-settlement behaviour of test piles D and E

The predicted difference of about 30% increased ultimate load capacity in similar ground conditions and identical drill tools is purely a result of the optimized installation rates of DDPs into stiff /hard clays.

Well accepted piling codes and standards (e.g. AS2159-2008, BS EN 12699:2001) do not allow for adjustments based on installation effects. Some authors (Van Impe 1988, Bustamante and Gianeselli 1998) developed general design methods for CFA and DDP mainly relying on *in situ* soil test results (i.e. CPT, SPT, PMT), but none of the authors incorporates adjustment factors taking different installation effects into account for the design.

SUMMARY AND CONCLUSIONS

The research has shown that the stresses in the stiff to hard clay formation at Lawnton can be changed significantly by the installation of drilled displacement piles (DDPs). Vigianni's formula (even though it was developed for CFA piles) provides a good indication of the minimum penetration rates for DDPs installed into stiff to hard clay formations.

Compliance with minimum installation rates for DDPs in stiff to hard clay increased the effective *in situ* stresses in the soil formation by 43%. Decreasing tool penetration reduced the effective stresses by 16%. Consequently, the installation parameters of DDPs in the stiff to hard Lawnton clay had a significant influence on the predicted pile capacities of the DDPs.

The authors strongly recommend the specification of installation rates for piling projects and the introduction of installation factors to allow for changing installation rates during construction.

The use of underpowered piling rigs which are not able to maintain the minimum penetration rate need to be allowed for. On the other hand, pile capacities could be increased or penetration depths into bearing layers reduced if adequately-powered piling rigs are used for DDP installation.

The authors strongly recommend carrying out pre-construction pile load tests to verify the site specific ground conditions for the estimated installation parameters.

ACKNOWLEDGEMENTS

The authors thank the ARC Linkage scheme and industry sponsors Piling Contractors, Golder Associates and Insitu Geotech Services for their valuable support of the research.

REFERENCES

AS 2159-2008. Piling – Design and Installation , Standards Australia

Bauer, FDP: Full-displacement pile system - Process and equipment. Company brochure, Bauer Maschinen GmbH, Schrobenhausen, Germany

Bottiau, M., Meyus, I.A., Van Impe, P.O. and Russo, G. 1998. Load testing at Feluy test site: Introducing the Omega B* pile. Proceedings of the 3rd International Geotechnical Seminar on Deep Foundations on Bored and Auger Piles, Ghent, Belgium, 19–21 October 1998, pp. 187–199

Bustamante, M. and Gianeselli, L. 1998. Installation parameters and capacity of screwed piles. Proceedings of the 3rd Int. Geotechnical Seminar on Deep Foundations on Bored and Auger Piles, Ghent, Belgium, 19–21 October 1998, pp. 95–108

EN 12699:2000. Execution of special geotechnical work – Displacement piles, European Committee for Standardization, Brussels

Fleming, W.G.K. 1992. A new method for single pile settlement prediction and analysis, Geotechnique, No. 3, pp. 411–425

Fleming, W.G.K. 1995. The understanding of continuous flight auger piling, its monitoring and control. Proceedings of the Institution of Civil Engineers Geotechnical Engineering, pp. 157–165

Larisch, M.D., Williams, D.J. and Scheuermann, A. 2015. Influence of pile installation techniques on heave volumes in clays. 12th Australia New Zealand Conference on Geomechanics, February 2015, Wellington, New Zealand, pp. 143-150

Larisch, M.D. 2014. Behaviour of stiff, fine-grained soil during the installation of screw auger displacement piles. PhD thesis, The University of Queensland, Brisbane

Larisch, M.D., Williams, D.J. and Slatter, J.W. 2012. Load capacity of auger displacement piles. Proceedings of the Int. Conference on Ground Improvement and Ground Control (ICGI 2012), Wollongong, Australia, pp. 739–745

Schmitt, A. and Katzenbach, R. 2003. Particle based modeling of CFA and soil displacement piles. Proceedings of the 4th Int. Geotechnical Seminar on Deep Foundations on Bored & Auger Piles, Ghent, Belgium, 2–4 June 2003, pp. 217–224

Slatter, J.W. 2000. The fundamental behaviour of displacement screw piling augers. PhD thesis, Monash University, Melbourne

van Impe, W.F. 1988. Consideration on the auger pile design. Proceedings Deep Foundations on Augered and Bored Piles I. Balkema, Rotterdam: 193 - 218.

Viggiani, C. 1993. Further experiences with auger piles in Naples area. Proceedings of the 2nd Int. Geotechnical Seminar on Deep Foundations on Bored & Auger Piles, Ghent, Belgium, 1–4 June 1993, pp. 445–455

ROCK SOCKET CAPACITY CERTIFICATION USING THE POINT LOAD INDEX TEST

Burt G. Look, Foundation Specialists Pty Ltd, Brisbane, Queensland, Australia, (+61) 7 3831 4600, blook@foundationspecialists.com.au
David W. Lacey, Foundation Specialists Pty Ltd, Brisbane, Queensland, Australia, dlacey@foundationspecialists.com.au

ABSTRACT

Certification of foundation capacity during the construction phase is often assessed by strength or weathering state descriptors based on visual observations. This case study used the Point Load Index (PLI) test as a quantitative tool in the construction certification of a pile's design capacity. Construction phase tests were completed on irregular sized rock samples whilst comparable design phase testing was completed on intact rock core samples. Statistical comparisons were made to assess the repeatability between the PLI tests, with best-fit Probability Distribution Functions (PDFs) determined for both datasets. Pronounced differences were observed based on the PDF adopted to characterize the PLI dataset, the consequence of which would be a significant change to the pile's design capacity. The adoption of the lower quartile value is shown to satisfy both design conservatism and construction simplicity requirements. The commonly held belief that rock samples produced during socket excavation may be biased towards the higher strength portion of the rock mass, is shown to be invalid for this site. As the central bridge piers were certified using Plate Load Tests (PLTs), the resultant load-settlement relationships were compared with the PLI strength assessments made for similar materials recovered from the adjacent abutment piles.

Keywords: Cast in Place (Bored) Piles, Point Load Index, Rock Socket, Construction Inspection, Certification

INTRODUCTION

The upgrade of the Foxwell Road Overpass across the Pacific Motorway in South East Queensland required the duplication of an existing four span bridge structure. The foundations of the new bridge included the installation of 1.2m diameter cast in place (bored) piles at the bridge abutments and 900mm diameter cast in place (bored) piles below a retaining wall to be constructed adjacent to the existing abutment.

The site geology was dominated by the Palaeozoic Neranleigh–Fernvale Beds, predominantly comprised of argillite, sandstone and greywacke. Limited soil materials existed at the site, with Extremely Weathered (EW) rock typically encountered within metres of the existing ground surface. The exception to the existence of shallow rock were locations where existing filling of the site had occurred – i.e. approach embankments to existing bridge structure.

Capacity of pile sockets is typically assessed onsite by descriptive rock strength or weathering assessment. Such descriptors encompass a wide range of values and lack precision. Due to the subjectivity of such assessment techniques – a factor of 3 is often observed in terms of strength assessment based on one's interpretation of rock strength descriptors alone – uncertainty on site often occurs regardless of whether a lower bound, average or other characteristic design parameter applies.

At the Foxwell Road Overpass site, certification of the abutment bored piles at this site required – as specified by the designer in project documentation – a quantitative rock strength assessment based on the results of the Point Load Index (PLI) test (with results standardized to a 50mm diameter rock sample, $I_{s(50)}$). The project specification required PLI tests to be completed onsite during the excavation of the piles, upon representative samples of the competent sandstone / argillite. PLI testing was to be undertaken at regular 500mm depth intervals for the full length of the pile rock socket, with the mean value of the compiled dataset specified to be not less than the value shown for the shaft

resistance on the project's geotechnical schedule, which is summarized in Table 1. Each abutment had design strength parameters assigned, based on the designer's interpretation of ground conditions and strength variation across the site (i.e. inferred from closest boreholes).

Table 1. Design Pile Schedule for abutment piles with anticipated 3m rock socket

Location	Design (mean) Point Load Index – $I_{s(50)}$ (MPa)		Ultimate Limit State Axial Compression Load (kN)
	Shaft	Base	
Abutment A	0.7	1.1	2927
Abutment B	0.6	0.8	3556

The designer specified requirement for rock strength assessment by the completion of PLI testing to be completed during the construction phase assumed:

- The distribution of the PLI parameter dataset – obtained from the intact rock cores during the Site Investigation (SI) – would be equivalent to that from the (irregular) samples available for testing during rock socket excavation. Assuming that the distribution of PLI results was equivalent, then the characteristic PLI parameter from the SI would be equivalent to that required to be exhibited by the samples during rock socket excavation;
- The testing of irregular lump samples tested during construction results would be equivalent to that obtained from testing of the intact rock core samples tested during the SI (i.e. $I_{s(50)}$ data from PLI testing irregular samples is directly comparable to $I_{s(50)}$ data from testing of intact rock cores); and
- Both the SI and pile excavation process yield similar material samples to undergo testing (e.g. tested samples from SI are not isolated to larger / stronger sections of recovered rock core whilst samples from rock socket excavation are not biased to the stronger portion of rock mass that resists crushing during excavation).

Although all resultant rock strength index parameters were normalized – in this case to $I_{S(50)}$ values as per the applicable Australian Standard, *AS4133.4.1* (2007) – uncertainty remained as to the relationship between tests completed during the design phase and piling works. The local relevant regulatory authority's construction standard – *MRTS63 Cast-in-place piles* (2016) – specifically identifies that rock strength assessment based on rock samples returned by the pile excavation process is "not adequate" for the certification of the pile's rock socket. The rationale behind this specified limitation is that PLI testing of recovered rock samples could potentially over-estimate the *insitu* rock strength of the rock mass present within the rock socket; as the pile excavation process could crush the comparatively weaker rock materials and thus any produced PLI dataset would be biased towards the higher strength rock portion.

As detailed within this paper, the designer's assumptions have been tested by statistical comparison the PLI datasets complied from both assessment phases of the project. The repeatability of the PLI test programs were assessed, along with presentation of the limitations of the PLI test method being used for such Quality Assurance (QA) purposes. The limitations of the PLI test method proposed are initially presented with general statistical implications of such data. Site specific data is then presented, and the reliability of this method of rock socket assessment is discussed.

POINT LOAD INDEX TEST

Point Load Index (PLI) testing involves rock samples – either irregular lump hand specimens or cylindrical rock core – being broken by the application of a concentrated load using a pair of conical platens. Broch & Franklin (1972) and Bieniawski (1975) first detailed the test, with the test methodology now standardized (e.g. *AS4133.5.1*, 1993). Although the PLI result is an index of material strength, it remains popular because of the relative speed and low cost of the test as compared to carrying out a Uniaxial Confined Strength (UCS) tests.

The relationship between PLI and UCS test results is known to be at least both rock type and strength range specific (if not also site-specific). The relationship is also recognized to vary based on the samples: (i) moisture condition; (ii) size; and (iii) shape, along with (iv) the PLI test orientation (axial or diametral), due to rock anisotropy and defect orientation. Although the PLI:UCS multiplier of 23.7 (i.e. UCS ≈ 24 x PLI) as presented by Broch and Franklin (1972) is often adopted in the absence of site-specific data, the application of this generic multiplier to all results can be misleading and unreliable as this multiplier was defined for hard rocks only (UCS ≥ 25 MPa). Subsequent studies (e.g. Bieniawski, 1974) warned that the PLI test should be used very cautiously upon weaker rocks, and strength determination via the UCS alone is recommended.

At the Foxwell Road Overpass site, from the data available from the site investigation, a PLI: UCS ratio of between 5.9 and 6.2 (refer Figure 1) was determined to apply based on the adoption of the full (site wide) PLI: UCS test pairs (n = 14) or isolated to the test pairs recovered from boreholes completed in the vicinity of the overpass pile locations (n = 6) respectively. Negligible rock anisotropy was observed to exist at this site, however it was noted that all rock strength testing was completed upon Moderately Weathered (MW) or Slightly Weathered (SW) rock materials. Using this relationship and the schedule values (refer Table 1) the bridge pile's design (mean) rock strength parameter was inferred to be UCS ≥ 3.7 MPa and UCS ≥ 5.0 MPa for pile shaft and base respectively.

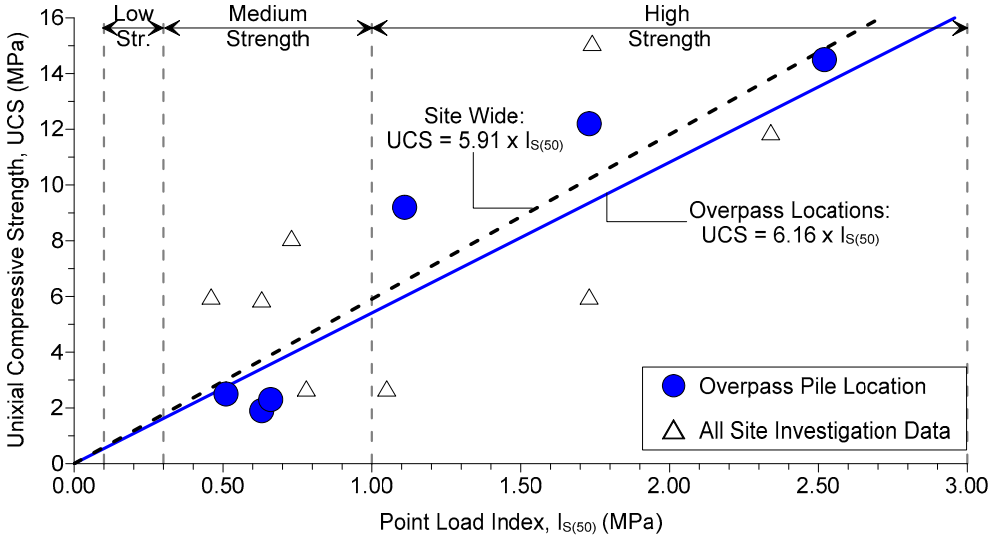


Fig. 1. PLI: UCS relationship for the Foxwell Road Overpass Site (Site Investigation data only)

AS1726 (1993) adopts the PLI $I_{S(50)}$ parameter as a rock strength classification measure, as summarized in Table 2 and annotated on Figure 1. Due to the range of $I_{S(50)}$ associated with each descriptive term, the quantitate assessment of an $I_{S(50)}$ parameter based on a strength descriptor alone can produce have a wide range of results. Note that not all 7 descriptors included in *AS1726* are shown in Table 2, as the minimum rock strength required by the Foxwell Road site's rock socket design was 'medium strength' (i.e. PLI = 0.3 – 1.0 MPa).

Table 2. Strength of Rock Material (except from *AS1726*, 1993)

Symbol	Term	$I_{S(50)}$ (MPa)	Field Guide
L	Low	0.1 to 0.3	Easily scored with a knife; indentations 1mm to 3mm show in the specimen with firm blows of the pick point.
M	Medium	0.3 to 1	A piece of core 150mm long by 50mm diameter can be broken by hand with difficulty.
H	High	1 to 3	A piece of core 150mm long by 50mm diameter cannot be broken by hand but can be broken with a single firm blow.
VH	Very High	3 to 10	Hand specimen breaks with pick after more than one blow

STRENGTH VARIATION – SITE INVESTIGATION / DESIGN PHASE

The Probability Distribution Function (PDF) is the relative likelihood a random variable will assume a particular value. The area under a PDF is unity. Although the normal distribution is the simplest distribution to understand, but is not always directly relevant to soils and rocks materials. The normal PDF, although commonly adopted for material modelling, suffers from allowing impossible (negative) values to exist within the fitted function. This error is exacerbated within datasets that contain a higher Coefficient of Variation (COV). Thus the appropriateness of alternative distribution models needs to be assessed and goodness-of-fit tests are commonly used for this purpose to discern differences between a hypothesized and the observed distribution.

Look and Wijeyakulasuriya (2009) and Look (2015) discuss the characterization of the strength properties, through goodness-of-fit tests, and demonstrated the normal distribution model is not appropriate for the lowest 10th fractile when fitted to rock strength test datasets. For strength datasets with low COVs then the normal PDF may apply, however Schnieder and Schnieder (2011) posited that once the reported CoV exceeds 30% (0.3) a Log-Normal distribution should be assumed. Look and Wijeyakulasuriya (2009) similarly concluded a Log-Normal distribution would be preferential over a normal distribution for PLI test datasets, as they typically demonstrated COVs of 40% to above 100%. Thus, for any specified mean PLI - $I_{s(50)}$ parameter the rock strength should be expected to not vary beyond a value equivalent to twice the mean $I_{s(50)}$ parameter (i.e. COV $\leq$ 100%).

For the PLI dataset (n =30) compiled from testing of the rock core recovered during the site investigation of the Foxwell Road Overpass site the Log-Normal function was found to be the 2nd highest ranked PDF (with only the Inverse Gaussian PDF ranked higher). The significant difference in interpretation of a characteristic $I_{S(50)}$ parameter based on the adoption of either a Log-Normal or Normal PDF is demonstrated in Table 3 and Figure 2. The following implications for the site become evident within this comparison:

- If a normal PDF is adopted negative values would result for the lower 3% fractile;
- The median is equivalent to the mean for the normal PDF, however such a value should not be considered a characteristic design parameter due to the high strength samples producing a left skew in the PDF and the high CoV associated with the PLI dataset;
- A right skewed Log-Normal function is well fitted to the dataset (i.e. median < mean), supporting the recommendations of previous researchers for datasets displaying COVs in excess of 30%;
- The designer's nominated shaft friction requirement of 0.6 to 0.7 MPa reflects the lower quartile values – also coinciding with the approximate point of equality between the Log-Normal and normal PDFs – for the Foxwell Road Overpass site.

Table 3. Comparative PLI values ($I_{S(50)}$, MPa) based on PDF adopted for site investigation dataset

Percentile	Normal PDF	Log-Normal PDF
1%	-0.23	0.34
10%	0.35	0.50
25% (Lower Quartile)	0.68	0.66
50% (Median)	1.06	0.91
75% (Upper Quartile)	1.43	1.30
90%	1.77	1.81
99%	2.35	3.31
Standard Deviation	0.55	0.62
Coefficient of Variation (CoV)	52%	58%
PLI Dataset – Average (n = 30)	1.06 MPa	

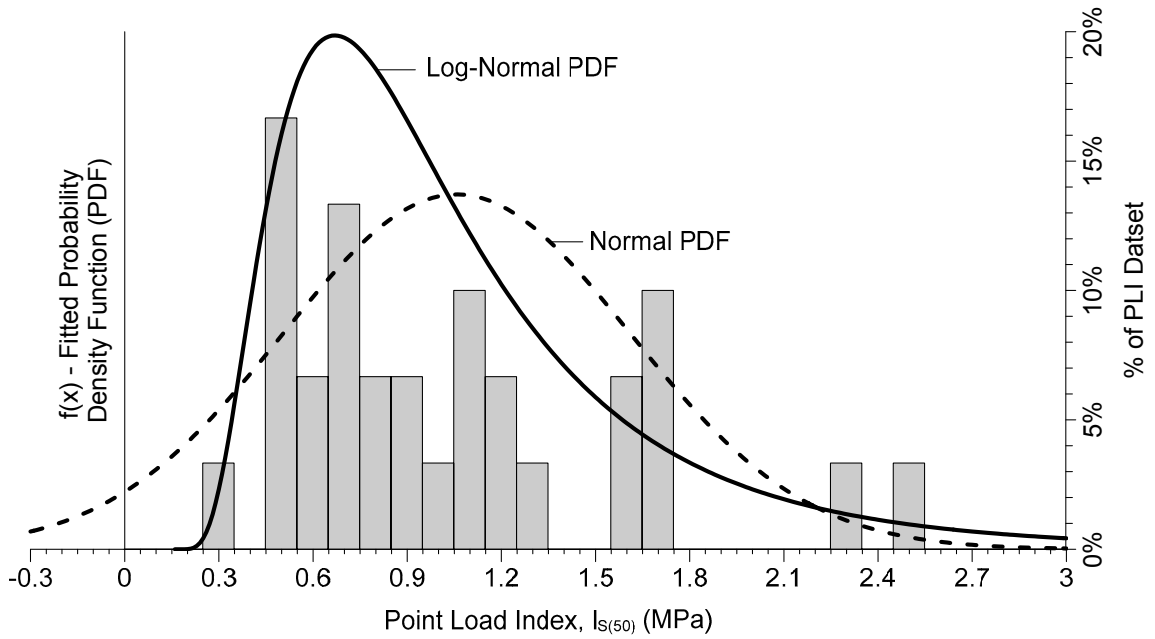


Fig. 2. Comparative PDFs for PLI dataset at the Foxwell Road Overpass (site investigation data)

STRENGTH VARIATION – CONSTRUCTION PHASE

As identified previously, the PLI testing of irregular rock samples recovered during rock socket excavation are not typically utilized for quantitative material characterization due to the expectation that the recovered materials would only be representative of the stronger component of the rock mass. In order to evaluate if the construction phase PLI dataset exhibited such a bias, the results of the 119 tests completed upon rock fragments returned to the surface during the pile socket construction were assessed and compared to the PLI test results of the site investigation.

Table 4 summarizes the $I_{S(50)}$ statistics compiled for the pile shaft of each overpass abutment (comprised of 5 piles each). The required rock socket strength was achieved at all locations and both the lower quartile and median $I_{S(50)}$ parameter for each abutment are comparable. As presented in Table 4, Abutment B displayed significantly higher variability within the PLI dataset in comparison to Abutment A. Without the identification and prior removal of outliers – the threshold of which is defined results more than 1.5 times the interquartile range below / above the lower / upper quartile value respectively – an (incorrect) higher mean $I_{S(50)}$ parameter would have been determined.

Table 4. Pile design schedule requirements compared with results of onsite PLI testing of full rock socket

Location	Design (mean) $I_{s(50)}$	Construction Phase Point Load Index Testing – $I_{s(50)}$ (MPa)				
	Pile Shaft		Lower Quartile	Median	Mean	CoV
Abutment A	0.7 MPa	Full Dataset (n = 51)	0.6	0.7	0.8	52%
		Outliers Removed (n =48)				38%
Abutment B	0.6 MPa	Full Dataset (n = 68)	0.6	0.7	1.1	111%
		Outliers Removed (n =58)			0.7	33%

Figure 3 presents the box-and-whisker plot of the full PLI data associated with each abutment, which displays the distribution of the dataset and comparative frequency of outliers within each abutment's dataset. The outlier points present within Figure 3 influence the fitted PDF and thus creates the unrealistic negative values when the normal PDF is adopted.

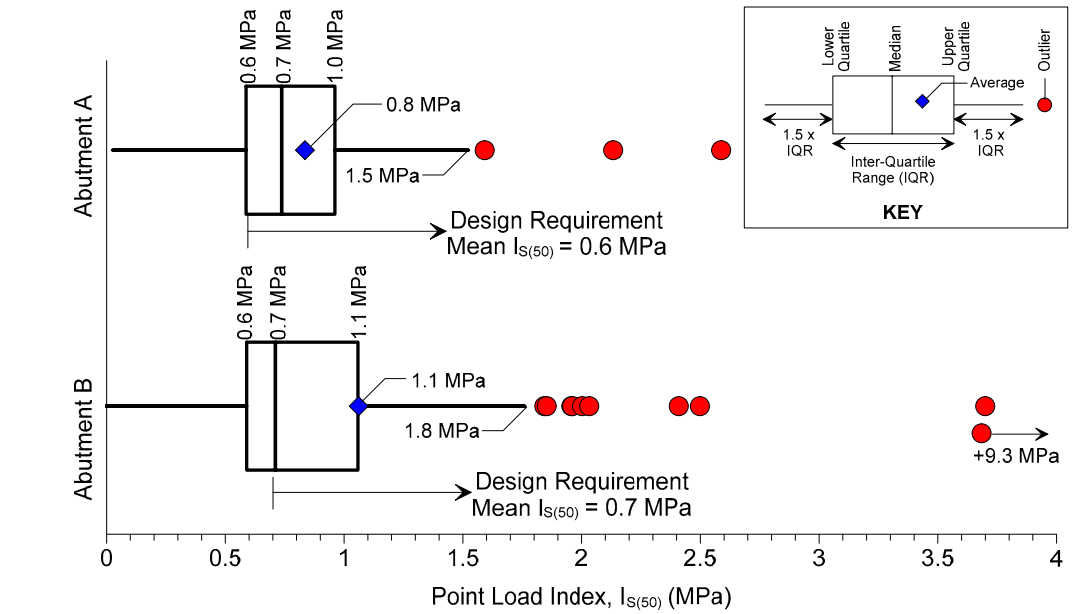


Fig. 3. Point Load Index (PLI) dataset compiled at each abutment during construction phase

Such PLI analysis was further extended to each of the individual piles present at each abutment (5 piles per abutment), as presented in Figure 4. Two of the piles present at Abutment B indicate significantly higher strength rock materials were present within the rock socket, with Pile B1 reporting a median $I_{S(50)}$ parameter 140% higher than the equivalent parameter observed in the weakest pile of Abutment B (Pile B5). A similar, comparatively higher $I_{S(50)}$ strength parameter was observed in a single pile of Abutment A (Pile A1). Overall, the median parameter associated with Abutment A piles was slightly higher than that observed at Abutment B.

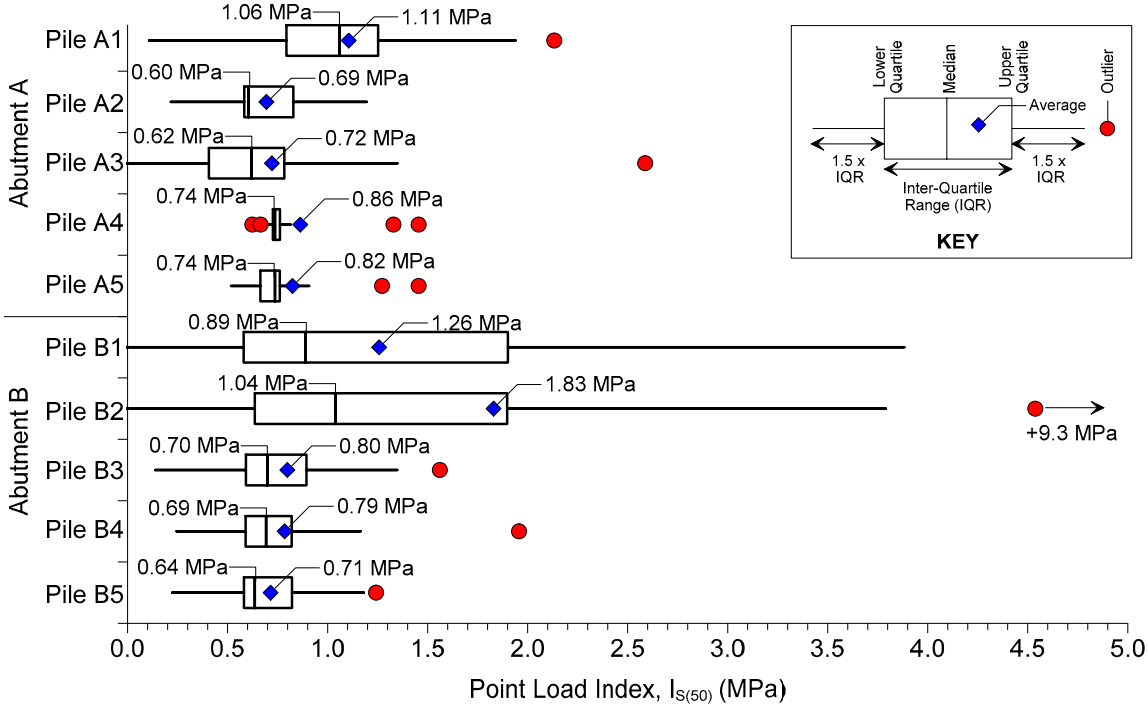


Fig. 4. Distribution of Point Load Index Tests at each individual pile location.

COMPARISON BETWEEN SITE INVESTIGATION AND CONSTRUCTION PHASE DATA

As per the analysis completed on the site investigation data, both a normal and Log-Normal PDFs were fitted to the construction phase PLI dataset (n = 119). A summary of the fractiles associated with the fitted PDFs are presented in Table 5, and compared to the corresponding PDFs determined for the SI datasets.

Table 5. Comparative PLI values ($I_{S(50)}$, MPa) based on PDF – Site Investigation and Construction Phase rock socket datasets

PDF Type	Log-Normal PDF			Normal PDF		
Project Phase	Borehole / Site Investigation	Rock Socket / Construction		Borehole / Site Investigation	Rock Socket / Construction	
Dataset	All	All	Largest Samples	All	All	Largest Samples
1%	0.34	0.34	0.32	-0.23	-1.21	-0.04
10%	0.50	0.45	0.43	0.35	-0.24	0.31
25% (Lower Quartile)	0.66	0.56	0.52	0.68	0.33	0.52
50% (Median)	0.91	0.76	0.67	1.06	0.96	0.74
75% (Upper Quartile)	1.30	1.09	0.87	1.43	1.60	0.96
90%	1.81	1.60	1.14	1.77	2.16	1.16
99%	3.31	3.22	1.85	2.35	3.14	1.51
Standard Deviation	0.62	0.60	0.32	0.55	0.94	0.33
Coefficient of Variation (CoV)	58%	64%	43%	52%	103%	45%
PLI Dataset – Average (MPa)	1.06 (n = 30)	0.96 (n = 119)	0.74 (n = 25)	1.06 (n = 30)	0.96 (n = 119)	0.74 (n = 25)

Using the normal PDF fitted to the full construction dataset, the COV of 103% is significantly higher than the 52% and 45% calculated for the site investigation and irregular shaped construction phase PLI datasets respectively. However, the dataset size associated with the full construction PLI dataset is four times larger than the other datasets. Negative $I_{S(50)}$ values – an impossible result – occurred for the initial 15% of the normal PDF fitted to the full construction dataset.

The Log-Normal PDF was again identified as the more appropriate PDF (in comparison to the normal PDF) for the compiled PLI datasets as evidenced by the consistent CoVs returned and the absence of negative $I_{S(50)}$ parameters. When the Log-Normal PDF was used, the results were approximately comparable (within ~15% of each other) for the full dataset compiled during both the site investigation and construction phase sof the project. Such a result demonstrates that, once the appropriate PDF was utilized to describe the PLI dataset (i.e. Log-Normal), then no bias was present within the strength index values displayed by the rock fragments recovered during the excavation of the pile rock socket.

No evidence that only stronger rock fragments were surviving the pile excavation technique was observed within the PLI dataset, with the range of $I_{S(50)}$ values reported by the tested irregular lump samples mirroring the full range observed in the initial borehole rock core and very similar CoVs being determined for both datasets. In fact, for all fractiles the Log-Normal PDF fitted to the rock socket / construction phase dataset calculated a lower $I_{S(50)}$ parameter than the comparable borehole / site investigation dataset value.

The effect of the larger irregular sample size was also examined, with the 25 largest sized irregular lump particles isolated and analyzed independently. As summarized in Table 5, little size effect was demonstrated. The larger particles showed similar COV and lower characteristic $I_{S(50)}$ values to either of the full PLI datasets, and an absence of the higher strength proportion of rock materials (i.e. higher $I_{S(50)}$ fractiles associated with the larger sized particles dataset were consistently lower than the comparable fractile of the full dataset). This suggests that the larger particles that survived the rock socket excavation process were not necessarily those of highest strength.

ROCK MASS MODULUS FROM PLATE LOAD TESTS (PLTs)

At the location of each of the Foxwell Road Overpass piers, a number of static Plate Load Tests (PLTs) were completed upon the same material unit as encountered at the base of the abutment piles. The coincidence of such tests allowed the comparison of the *insitu* rock mass modulus (E_m) with the results of the PLI index tests. The designer stated an E_m parameter of 150 MPa was required to be demonstrated by onsite PLTs. This value, when compared to the minimum UCS of 5 MPa – previously identified for use as the pile toe design strength parameter – represents a direct UCS:E_m multiplier of 30. Such a multiplier was significantly lower than that expected to be exhibited by the founding material based on the available site investigation data.

Previous research (e.g. Hobbs, 1974) suggests that in sandstone materials the Modulus Ratio that related the UCS and the intact rock modulus, E_i, would be 275 to 300. Based on the borehole records of the recovered rock core an RQD of 40 – 70% was typically observed the materials encountered at the base of the piles, which would necessitate an E_i / E_m reduction factor (K_E) of between approximately 0.20 (Bieniawski, 1984) and 0.30 (Carter and Kulhawy, 1988). Accordingly the UCS: E_m ratio was expected to be between 55 and 90 for the medium strength sandstone utilized to support shallow pier foundations at the Foxwell Road Overpass site.

Four (4) PLTs were undertaken at the two (2) central bridge piers, with *insitu* composite modulus (E_m) parameters of 250, 330, 325 and 440 MPa being reported from analysis of the reloading cycle (E_{V2}) of the PLT (average E_m = 336 MPa). Adopting the minimum design UCS (5 MPa), this returned a UCS: E_m multiplier of 67.2 (with a range of 50 to 88 based on all E_m observations). Such a value falls well within the range of the UCS: E_m modulus ratio that was expected to be exhibited by the site materials. Similarly, the equivalent UCS produced by multiplying the lower quartile of the PLI dataset that represents the tests completed at the pile toe ($I_{S(50)}$ = 0.8 MPa) with the overpass site-specific PLI: UCS ratio (6.2) would yield a slightly higher UCS: E_m modulus ratio range (59 to 91, average of 70).

As illustrated previously by Lacey and Look (2015), the input UCS parameter required to reproduce the onsite observed *insitu* rock mass modulus varies based on the design procedure utilized. Applying two (2) previously published non-linear relationships between UCS and E_m – along with the Log-Normal relationship fitted to the pile toe PLI dataset (having been determined as per the methodology presented for the pile shaft) – the percentile of the PLI dataset that would be required to be input to replicate the average E_m observed onsite has been determined.

Table 6 summarizes the average observed E_m parameter back-calculated by the adoption of a very conservative log-normal PLI parameter (<5th percentile of fitted dataset). Incorporation of the lower quartile PLI value ($I_{S(50)}$ = 4.8 MPa) within such design methods would have predicted an E_m parameter that exceeded 75% of the values observed within the PLTs completed onsite. Use of the median PLI value reproduced the upper bound (maximum) observed E_m in one of two non-linear UCS: E_m equations considered (Prakoso, 2002).

This shows direct comparisons between these 2 distinct certification tests did not provide a reliable predictive approach. Using the Log-Normal PDF, a 5% PLI fractile appears to represent an upper bound parameter suitable for prediction of the serviceability (modulus) parameter. In comparison a lower quartile value is recommended to be adopted for the direct use as the characteristic strength (PLI) parameter.

Table 6. 'Characteristic' UCS and PLI Values (MPa) required to replicate observed E_m values

Reference		Rowe & Armitage (1987)	Prakoso (2002)
Defined Relationship		$E_m = 215 \times (UCS)^{0.5}$	$Log_{10}(E_m / UCS) = 2.73 - [0.49 \times Log_{10}(UCS / p^{a})]$
Lower Bound	E_m = 250 MPa	UCS = 1.35 MPa $I_{S(50)}$ = 0.22 MPa < 5% Percentile	UCS = 2.02 MPa $I_{S(50)}$ = 0.33 MPa < 5% Percentile
Average	E_m = 336 MPa	UCS = 2.44 MPa $I_{S(50)}$ = 0.40 MPa < 5% Percentile	UCS = 3.60 MPa $I_{S(50)}$ = 0.58 MPa < 5% Percentile
Upper Bound	E_m = 440 MPa	UCS = 4.19 MPa $I_{S(50)}$ = 0.68 MPa 13th Percentile	UCS = 6.10 MPa $I_{S(50)}$ = 0.99 MPa 50th Percentile (median)

CONCLUSIONS

Typically a descriptive strength (or weathering) approach is taken in field assessment of rock socket strength. At the site considered herein a quantitative approach based on the PLI testing of bored pile rock sockets was instead implemented. The application of the Log-Normal PDF to characterize the both the site investigation and construction phase PLI datasets demonstrated that the construction phase dataset reflected the full strength range exhibited by the site investigation testing, and did not result in a biased dataset that over-estimated the characteristic *insitu* rock strength. Accordingly, the results observed by this study suggests there is potential for use of PLI results from tests completed upon rock fragments recovered during rock socket excavations, and dispels the common belief that samples produced during socket excavation only represent the strongest portion of the rock mass. Other studies would be required to confirm the PLIs applicability for use as an onsite validation technique over a wider range of materials.

As outliers affect the derived characteristic values, the PLI dataset mean was not coincident with the median value when a normal distribution was applied. The mean and median are not considered appropriate values for rock socket assessment, and should not be used for characterization of the rock mass. Instead, the lower quartile value is recommended as it provides a simple site assessment approach to assess the rock socket strength value during construction, and was demonstrated to be the approximate point of equality between the fitted Log-Normal and normal PDFs of both the site investigation and construction phase PLI datasets.

The completion of PLTs in the same material as the PLI testing of the pile toes also allowed the assessment of the relationship between rock strength tests and *insitu* rock mass modulus (E_m) parameters. The results of this suggested that typical non-linear strength – stiffness relationships require a very conservative (5th percentile maximum) rock strength parameter and appropriate PDF in order to replicate the composite rock mass modulus parameter observed through onsite testing.

REFERENCES

Australian Standards (1993). *AS1726 – Geotechnical site investigations*. SAI Global

Australian Standards (2007). *AS4133.4.1 – Method of testing for engineering purposes - Rock strength tests - Determination of point load strength index*. SAI Global

Bieniawski, Z.T. (1974). "Estimating the strength of rock materials", *Jour. South African Institute of Mining and Metallurgy*, Vol. 74, No. 8, pp. 312-320.

Bieniawski, Z.T. (1984). *Rock Mass Design in Mining and Tunnelling*, Balkema, Rotterdam, The Netherlands

Broch, E. and Franklin, J.A. (1972). "The Point Load Strength Test", *Int. Jour. Rock Mech. & Min. Sci*., Vol. 9, No. 6, pp. 669-697.

Carter, J.P. and Kulhawy, F.H. (1988). *Analysis and design of drilled shaft foundations socketed into rock*, Report EL-5918, Palo Alto: Electric Power Research Institute, 190p.

Hobbs, N.B. (1974). "Factors affecting the prediction of settlement of structures on rock with particular reference to the Chalk and Trias", in *Proc. of Conf. on Settlement of Structures*, Cambridge, pp. 579-654

Lacey, D. and Look, B (2015). "Characteristic design modulus for rock socket pile design", in *Proc. 12th Australia New Zealand Conference in Geomechanics*, Wellington, New Zealand, P051

Look, B. (2015). "Appropriate distribution functions in determining characteristic values", in *Proc. 12th Australia New Zealand Conference in Geomechanics*, Wellington, New Zealand, P014

Look, B. and Lacey, D. (2013). "Characteristic values in rock socket design", in *Proc. of 17th Int. Conf. on Soil Mechanics and Geotechnical Eng. (18th ICSMGE)*, Paris, France, 2 -6 September, p. 2795 – 2798.

Look, B.G. and Wijeyakulasuriya, V. (2009). "The statistical modelling for reliability assessment of rock strength", in *Proc. of 17th Int. Conf. on Soil Mechanics and Foundation Eng.*, Alexandria, Vol. 1, pp 60 – 63.

Prakoso, W.A. (2002). *Reliability-Based Design of Foundations on Rock for Transmission Line & Similar Structures*, Doctoral (M. Sc.) dissertation, Cornell University.

Queensland Transport and Main Roads (2016). *MRTS63 Cast-in-place piles,* Main Roads Technical Specifications.

Rowe, R. K. and Armitage, H. H. (1987). "A design method for drilled piers in soft rock", *Canadian Geotechnical Journal*, 24 (1), pp.126–142

Schneider H.R. and Schneider M.A. (2013). "Dealing with uncertainties in EC7 with emphasis on determination of characteristic soil properties" in *Modern Geotechnical Design Codes of Practice*, P. Arnold, G.A. Fenton, M.A. Hicks, T.Schweckendiek and B. Simpson (eds.), IOS Press, Amsterdam, pp. 87–101

Table of Contents

Challenges in the Design and Construction of Deep Foundations for Transportation Infrastructure Projects (Abstract Only)
Dan Brown, P.E., Ph.D., D.GE 1

Construction Methods and Quality Outcomes for Bored Cast-In-Situ Piles - A Review of Current Practice
Ben Collingwood and Jim Slatter 2

Design of a Raft Assisted Piled Foundation for a High Rise Prefabricated Hotel Structure in Perth, WA
Lucie Spencer and Craig Butterworth 20

Performance of Large-Diameter Bored Pile Socketed in Sandstone and Siltstone in Thailand
Zaw Zaw Aye, Thayanan Boonyarak, Nutthapon Thasnanipan and Sereyroath Chea . .35

Pile Foundation Solutions in the Deep Quaternary Sediments of Botany Bay
Paul A. O'Brien, Thomas G. Cuniowski, Gary A. Chapman. 45

The Application of Rapid Load Testing in Singapore
Soon-Hoe Chew, Peter Middendorp, Joost Bakker and Gilbert Chuah 56

Ground Improvement by Dynamic Replacement within Intertidal Mangrove Mud Environment, Ichthys LNG, Darwin
D. Mitchell, P. Vincent and J. Racinais. 66

Monitoring of an Embankment Project Using Rigid Inclusions and Vacuum Consolidation during and after Construction
Stephen Buttling and Rui Zhong 81

Design, Construction, and Long-Term Monitoring of a Pile-Supported LNG Tank in Savannah, Georgia
Guoming Lin, Ph.D., G.E., D.GE, Cheng Lin, Ph.D., P.E. 91

Quality Control and Testing of Jet Grouting and Its Interpretation in Relation to the Christchurch Town Hall Restoration Project
Paul Marsden, David Chadwick, Mathias Delapille and Chris Hughes 104

Design, Construction and Design Validation through High Strength Testing (PDA) of CFA and DD Foundations
Stefano Pirrello 116

Centrifuge Modelling of Displacement Piles and Installation Effects
L. King, A. Bouazza, J. Gniel, C. Gaudin and C. O'Loughlin 126

Analysis of Soil and Structural Thermal Response of a Field Scale Geothermal Energy Pile
Mohammed Faizal and Abdelmalek Bouazza 134

Lateral Response of Pole on Engineered Driven Timber Pile Footing at Ararat Windfarm Terminal Station (Abstract Only)
Frank Albrecht and Brian McCarthy 143

Designing Piles for Seismic Events
H. G. Poulos 144

Artificial Ground Freezing – A Typical Application for the Underpass of an Existing Metro Station in Rome
Bruno Vingiani and Alessandro Bertero 172

Resonance Pile Driving with Zero Ground Vibration
Mathew Janes, M.E.Sc., P.Eng and Mark Johnson 183

Level Crossing Removal Project – Package 1
David Chong, Chris Crowe, Andrew Middleton and Mick Stadter 193

Value Engineering through Systematic Site Investigation and Design Optimization – A Case Study
Dr. Manish Tiwari, Frances Badelow, Dr. Lu Yitan 203

A 16M Deep Basement Excavation in Kuala Lumpur Karst: Mixed Retention Solution
Prasad P. V. S. R., Mikias Yohannes and Serhat Baycan 215

Determination of Basal Heave Stability for Strutted Excavations Supported with Jet Grout Base Slab
Anthony T. C. Goh 229

Performance of Footings in Rock Based on Serviceability
C. M. Haberfield 239

Dynamic Load Testing of 2 Metre Steel Tubular Piles Driven into Foliated Phyllite Bedrock
Bosco Poon, Geoff McKay, Kim Chan and Luis Raúl Castañeda 292

Design and Construction of Pile-Supported Mechanically-Stabilized-Earth Slope Stabilization
Nasr Sheta, Ph.D., P.E. 302

Application of Innovative Underreamed Ground Anchorages with Capsule
Zhong Liu and Gang Guo 310

Effects of Installation Parameters of Drilled Displacement Piles on In Situ Stress Conditions in Stiff Clays
Martin D. Larisch, David J. Williams and Alexander Scheuermann 320

Rock Socket Capacity Certification Using the Point Load Index Test
Burt G. Look and David W. Lacey 329

The Nonlinear Constitutive Behaviour of Coode Island Silt
Kaveh Ranjbar Pouya, Ali Tolooiyan and Rae Mackay 339

Brickworks Marketplace Ground Improvement, Adelaide
Andrew Middleton and Mark Wyatt 349

Case Study: Load Transfer Analysis on an Instrumented Augercast Pile Using EDC Strain Gauges and Geokon Rebar Strainmeters
Swamy Avasarala, Santosh Mummaneni, Vamshi Vemula and Dr. Sastry Putcha .356

CFA Pile Design Parameters in Sand
Stuart Coutts 367

Deep-Sea Quay Wall for Offshore Wind Energy Terminal on Maasvlakte 2 Rotterdam – NL
Patrick van der Schaaf, Bsc Eng. 377

Dynamic Pile Testing at the Five Mates Bridge
Jonathan G. Cannon 384

Failure Modes for Embankments over Ground Improved with DCM Column Walls beneath the Slope
Manasi Wijerathna and D. S. Liyanapathirana 391

Improvement of Soil Properties by Basalt Fibre Reinforcement
Ramanathan Ayothiraman and Anurag Singh 403

Innovative Design for Retaining Structures Using Combined Products
Dr. Alexander Zöhrer and Clifford Taylor 413

Newest Developments in Quality Control and Soil Mixing for Actual and Future Demands
Franz-Werner Gerressen 425

Observing Friction Fatigue Using High Strain Dynamic Pile Testing
Ronald Damen and Dion Denes 434

ShaftCam: A Practical and Cost Effective Solution to Drilled/bored Pile Hole Inspection
Swamy Avasarala, Santosh Mummaneni and Dr. Sastry Putcha 446

Small-Strain Behaviour of Artificially Cemented Sand in Deep Mixing Application
Alireza Mohammadinia, Mahdi M. Disfani, Arul Arulrajah and Stephen Darmawan ..452

Wrigley Field – The 1060 Project
Darren S. Diehm P.E. 462

A System with Local Strain for Studying Shear Modulus Degradation of Cement Treated Clay with Fibers
Huawen Xiao, Siang Huat Goh, Min Sunn Ye, Kai Yao, Fook Hou Lee and Wei Wang 472

Microstructure of Bio-Cemented Coarse Sand
Aamir Mahawish, Abdelmalek Bouazza and Will P. Gates 482

Pile Foundation Response to Ground Vibration from Rock Blasting
Laddu B. Jayasinghe, Anthony T.C. Goh, Zhiye Zhao, Hongyuan Zhou and Yilin Gui .492

Risk-Based Approach in Drilled Shaft Design for Infrastructure Projects
Ramanujachari Kannan, P.E. D.GE., F.ASCE 499

THE NONLINEAR CONSTITUTIVE BEHAVIOUR OF COODE ISLAND SILT

Kaveh Ranjbar Pouya, Geotechnical and Hydrogeological Engineering Research Group (GHERG), Federation University Australia, Victoria, Australia, +61459332381, k.ranjbarpouya@federation.edu.au

Ali Tolooiyan, Geotechnical and Hydrogeological Engineering Research Group (GHERG), Federation University Australia, Victoria, Australia, +61437244557, ali.tolooiyan@federation.edu.au

Rae Mackay, Geotechnical and Hydrogeological Engineering Research Group (GHERG), Federation University Australia, Victoria, Australia, +61407912230, rae.mackay@federation.edu.au

ABSTRACT

A major part of Melbourne's central business district is underlain by a very soft silty clay deposit known as Coode Island Silt (CIS). Due to the low strength of CIS, most construction in the region is based on pile foundation systems. Traditionally, the design of pile foundations is mostly based on empirical and analytical methods. However, numerical methods such as Finite Element Methods (FEM) can be utilised for more accurate estimation of the bearing capacity and deformation of pile foundation systems, especially in complex loading scenarios. Unfortunately, no systematic effort is made yet to calibrate a realistic nonlinear constitutive model to describe the geomechanical behaviour of CIS in a numerically based solution. Among the nonlinear constitutive models, the Hardening Soil (HS) model is an advanced hyperbolic model which accounts for the nonlinearity of stress-strain relationship as well as the stress dependency of the soil stiffness. In this study, the HS model is calibrated based on laboratory tests performed on CIS. Also, to validate the accuracy of the calibration, the well-known cavity expansion theory is employed to model the CPT cone tip resistance (q_c) in CIS, and results are compared against the measured CPT q_c profile at the field.

Keywords: Coode island silt, hardening soil model, cone penetration test, cavity expansion method

INTRODUCTION

A large percentage of world's coastal areas are covered with soft marine clay deposits. Having very low shear strength and high compressibility, the alluvial deposits are known as one of the most problematic soil layers for the design and construction of infrastructure facilities. A major part of Melbourne's central business district is underlain by a very soft silty clay deposit known as Coode Island Silt (CIS). Basically, there are two main solutions for construction in such weak soil conditions. One is the use of pile foundations transferring the applied load to deeper and stronger soil layers, and the second one is to employ ground improvement techniques such as using deep soil mixing columns to improve the bearing capacity of the soil. In both cases, a practical geotechnical design should incorporate both stability analysis and deformation analysis to achieve a cost-effective and reliable solution. Most of the classic solutions for stability analyses such as limit equilibrium analysis disregard the stress-strain relationship of the soil for the sake of the simplicity (Chen, 2007; Sokoloviskii, 1965). In a similar simple approach, most of the past studies of deformation analysis have been established on the basis of linear elasticity. However, it is well recognised that the soil stress-strain behaviour is highly nonlinear even at very small strains (Burland, 1989). Hence, for a precise deformation analysis of the foundation of important geotechnical structures, the application of advanced nonlinear constitutive models is extremely beneficial. Precise deformation analysis is essential as geotechnical designers have to predict the displacement of geotechnical structure and the adjacent soil as well as the induced displacement and forces to adjacent structures. This issue is more highlighted recently in the analysis, and design of highly important infrastructures as geotechnical engineers are facing new challenges in the analysis and design of infrastructures in congested areas. Rapid population growth, especially in the major cities all around the world necessitates the design and construction of more integrated infrastructure facilities. Consequently, geotechnical engineers should employ more advanced design approaches to address the new challenges in geotechnical engineering practice. Complicated geometries, different loading scenarios and the application of

nonlinear deformation models which is believed to be essential for a precise deformation analysis, necessitate the application of numerical methods to satisfy most of the design requirements.

As nonlinearity is one of the most important features of geomaterials, many researchers have worked on the development and validation of advanced nonlinear constitutive models. With the advances in computer hardware technology, the application of these advanced and computationally expensive nonlinear constitutive models has become more popular among the researchers and designers. Although obtaining the good quality input parameters requires extensive laboratory experiments, application of the advanced and complicated stress-strain models usually requires more input parameters. Prior to the application of the constitutive model, the input parameters have to be calibrated and verified based on a systematic procedure. The basic idea of the calibration is to minimise the difference between observations from field/laboratory experiments and the predictions from numerical analysis. Although calibration of a geotechnical constitutive model seems simple at first glance, it is often a time consuming and difficult iterative procedure, when the number of input parameters is considerably large. Unfortunately, no systematic effort is yet made to calibrate a constitutive model to describe the nonlinear geomechanical behaviour of CIS in a FEM based solution. In this study, the nonlinear elastoplastic Hardening Soil (HS) model in the finite element framework is calibrated for CIS. Also, to validate the accuracy of the calibration, the well-known spherical cavity expansion theory is employed to model the CPT cone tip resistance (q_c) being compared against the measured CPT q_c profile at the field reported by Aurecon (2013). The calibrated parameters in this study can be used by other engineers in commercial finite element packages to achieve a realistic prediction of deformation of either shallow footings or deep pile foundations. This will result in a more reliable and cost-effective design which will be of interest to geotechnical engineers and designers as well as their clients. This paper describes details of laboratory tests, numerical analyses, calibration method, and validation processes adopted for calibration of HS model for the CIS.

COODE ISLAND SILT

As explained by Ervin (1992), there are four major geological units in the Yarra delta known as: Port Melbourne Sand (PMS), Coode Island Silt (CIS), Fishermen's Bend Silt (FBS) and Moray Street Gravel (MSG). Among these units, CIS has always been receiving extensive attention amongst geotechnical engineers in Melbourne area due to the challenges associated with its low shear strength and high compressibility. CIS is a soft silty clay containing marine shelly material and is widespread in the upper 10 to 20 m of the alluvial deposit of the major part of Melbourne's central business district as well as Port Melbourne and South Melbourne. Although it is known as silt, CIS contains a considerable amount of clay. The XRD test on CIS samples was conducted in the Mineralogy and Geological Laboratory of Federation University Australia using a Panalytical XPert Powder Diffractometer. The XRD test results obtained for CIS shows the presence of Kaolinite, Illite, and Montmorillonite up to 14 %, 13 % and 1.5 %, respectively.

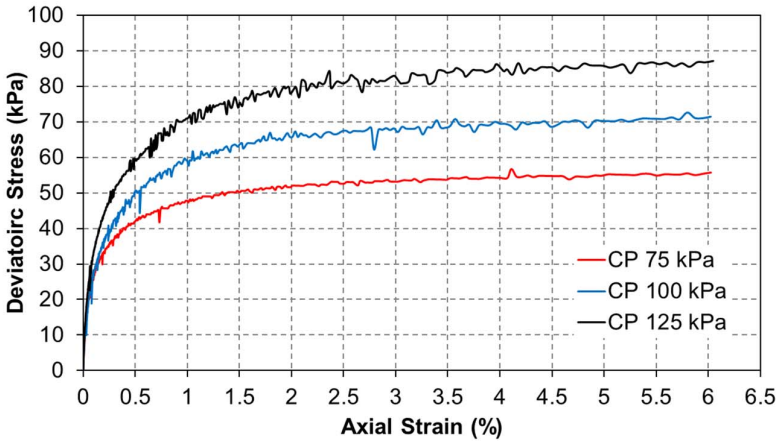
LABORATORY TESTS FOR EVALUATION OF STRENGTH AND STIFFNESS PARAMETERS

The CIS samples were reconstituted by mixing air dried material with water to achieve soil-water mixture with 50% moisture content, representing the average in-situ moisture content at the field. The soil slurry was poured into clear cylindrical PVC moulds of 50 mm diameter and 130 mm height. The mixture was placed into the moulds in three equal height layers, and a slight manual vibration was applied to remove air bubbles. The moulds were covered at top and bottom with filter papers and capped with porous stones. A pressure of 70 kPa was applied in a loading frame to reproduce the field pre-consolidation pressure, which has been reported previously to lie between 40 and 70 (Abdelmalek et al., 2004). After consolidation, the sample was extruded in the same direction as filling with the aid of a hydraulic sample extruder to avoid grain disorientation. All the CIS samples were 50 mm in diameter and minimum of 110 mm in height after extruding.

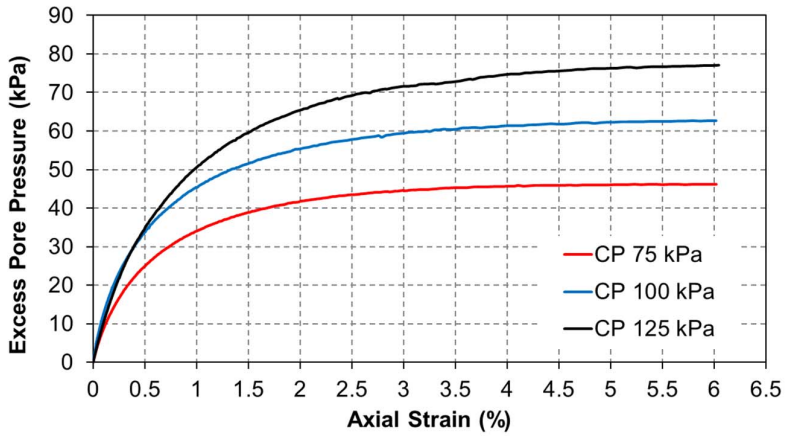
The extruded sample was then prepared for triaxial testing. Both ends of the samples are capped with triaxial porous stones to provide drainage and maximise the chance of perfect contact with loading pedestal. As the CIS sample is of very low permeability, the triaxial consolidation step takes unreasonably long. To speed up the consolidation progress, a filter strip cage using Whatman No.54 filter paper was wrapped around the sample based on the ASTM (2011). Finally, the sample was enclosed with rubber membrane and sealed by O-rings against the pedestal and the top loading cap. To place the rubber membrane around the sample, a split-mould membrane stretcher was used to minimise the risk of sample disturbance and also possible misalignment of the filter paper strips.

Consolidated Undrained (CU) triaxial test was performed on the remoulded CIS samples in three different effective confining pressures of 75 kPa, 100 kPa and 125 kPa. Considering the value of pre-consolidation pressure of 70 kPa applied in the loading frame, all the triaxial samples are in the state of normally consolidated. All the samples were subjected to the back water pressure of 200 kPa for the aim of saturation prior to consolidation stage, and a B-value of 0.95 was achieved. Using the filter paper cage, the required time for consolidation was found to be less than 2 hours for all the samples depending on the applied effective cell pressure. As the consolidation is used to bring the samples to the required effective stress state, the consolidation step has to be continued till the sample's volume change is not significant and minimum of 95 % of the excess pore pressure has been dissipated BS1377 (1990). All triaxial tests were strain-controlled, and the rate of strain for each test was calculated based on the volume change during consolidation phase according to the BS1377 (1990).

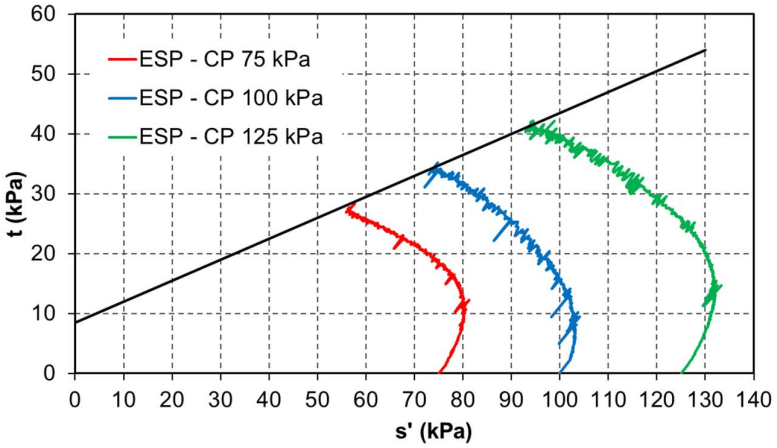
The results of the triaxial tests performed on the CIS samples are presented in Fig. 1. Figure 1(a) shows the relationship between the deviatoric stress and the axial strain in different effective confining pressures. With the increase of axial strain, the deviatoric stress increases until it reaches a peak value at an axial strain of about 4% - 5% for all three samples. The peak deviatoric stresses are 56 kPa, 70 kPa, and 88 kPa for effective confining pressures of 75 kPa, 100 kPa and 125 kPa, respectively. Figure 1(b) shows the development of excess pore pressure with the axial strain in different cell pressures, and Fig. 1(c) shows the effective stress paths in the t-s' plane are illustrated. Parameter t is half of the difference between maximum and minimum principal stresses, while s' is half of the sum of maximum and minimum principal stresses. The triaxial test results showed in this figure indicate that the internal friction angle of CIS is about 21˚ (slope of the failure envelope), and the cohesion is about 10 kPa (obtained from the y-intercept of the failure envelope).



(a)



(b)



(c)

Fig. 1. Consolidated undrained triaxial test on CIS; (a) Deviatoric stress versus axial strain (b) excess pore pressure versus axial strain (c) stress path, s versus t'

HARDENING SOIL MODEL

The most remarkable feature of Hardening Soil (HS) model comparing to elastic-perfectly plastic models is the capability to represent the nonlinear hyperbolic stress-strain relationship of the soil which results in a more realistic prediction of soil deformations. The original HS model was first formulated by Schanz et al. (1999) based on the hyperbolic stress-strain relationship introduced by Duncan and Chang (1970). A full description of the HS model and its formulation is not within the framework of this study and can be found in Brinkgreve et al. (2012), and Schanz et al. (1999). Herein, we only focus on some of the most important features of the HS model and the practical use of input parameters. The hyperbolic stress-strain relationship is in the form of Equation 1.

$$-\epsilon_1 = \frac{1}{E_i}\frac{q}{1-{}^{q}/_{q_a}} \qquad [1]$$

where, ϵ_1 is the axial strain, q is the deviatoric stress, E_i is the initial stiffness, and q_a is the asymptotic value of the shear strength. q_a is related to the ultimate deviatoric stress q_f by Equation 2.

$$q_a = \frac{q_f}{R_f} \quad [2]$$

where, R_f is the failure ratio implying that failure occurs when $R_f = 1$. The default failure ratio in Plaxis is given as 0.9. The ultimate deviatoric stress is defined as shown in Equation 3.

$$q_f = (c.\cot\varphi - \sigma_3')\frac{2\sin\varphi}{1-\sin\varphi} \quad [3]$$

The initial stiffness parameter is related to E_{50} by the use of Equation 4.

$$E_i = \frac{2E_{50}}{2-R_f} \quad [4]$$

where, E_{50} is the stress dependent secant stiffness modulus for primary loading corresponding to 50% of the ultimate deviatoric stress. The E_{50} parameter is preferred to the initial modulus E_i as it is more difficult to determine the initial tangent modulus experimentally (Schanz et al., 1999). The E_{50} parameter can be determined from Equation 5.

$$E_{50} = E_{50}^{ref}\left(\frac{c\cos\varphi - \sigma_3'\sin\varphi}{c\cos\varphi + p^{ref}\sin\varphi}\right)^m \quad [5]$$

E_{50}^{ref} is the drained reference secant stiffness modulus corresponding to the reference confining pressure p^{ref} (Brinkgreve et al., 2012; Schanz et al., 1999). The level of stress dependency is governed by the power *m* in the equation. As a practical approach, the reference secant stiffness modulus for drained conditions can be approximated from the one obtained from consolidated undrained triaxial test through Equations 6 and 7 (CUR195, 2000).

$$E_{50}' = E_{50}^{u}.\frac{1+\upsilon'}{1+\upsilon_u} \quad [6]$$

$$E_{50}' \approx 0.7\,.E_{50}^{u} \quad [7]$$

where, $\upsilon'$and υ_u are drained and undrained Poisson's ratios, respectively. In the HS model, strains are modelled accurately by incorporating three different input stiffness parameters. The second stress dependent stiffness modulus corresponds to the unloading and reloading stress paths and is determined by Equation 8.

$$E_{ur} = E_{ur}^{ref}\left(\frac{c\cos\varphi - \sigma_3'\sin\varphi}{c\cos\varphi + p^{ref}\sin\varphi}\right)^m \quad [8]$$

Similar to the secant stiffness modulus for primary loading, the unloading-reloading stiffness is a stress dependent parameter, and the parameter *m* controls the level of this dependency. E_{ur}^{ref} is the reference unloading reloading stiffness modulus which corresponds to the reference pressure. The reference unloading reloading stiffness can be determined from both oedometer and triaxial tests. Plaxis gives the default value of E_{ur}^{ref} equal to $3E_{50}^{ref}$. However, a practical estimation for clays suggests $E_{ur}^{ref} = (2to6)\,E_{50}^{ref}$(Obrzud and Truty, 2013). Another stiffness modulus which deals with the isotropic compression and oedometric loading is the tangent stiffness modulus for the primary isotropic compression loading which can be determined by Equation 9.

$$E_{oed} = E_{oed}^{ref}\left(\frac{c\cos\varphi - \sigma_1'\sin\varphi}{c\cos\varphi + p^{ref}\sin\varphi}\right)^m \quad [9]$$

E_{oed}^{ref} is the reference tangent stiffness modulus for the primary isotropic compression and can be determined from oedometer test or estimated from the E_{50}^{ref}.

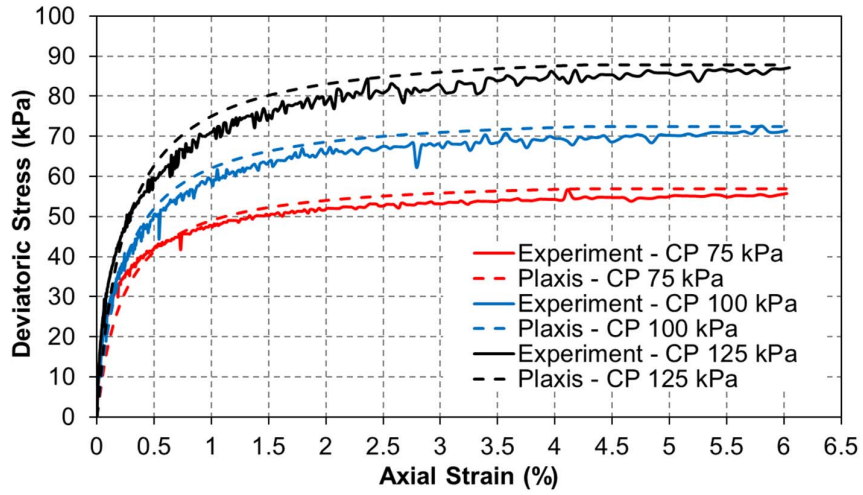
FINITE ELEMENT MODELLING AND CALIBRATION OF HARDENING SOIL MODEL

For the purpose of the calibration procedure, a triaxial compression test is modelled using Plaxis 2D (Version 2016.01). The triaxial test is modelled in an axisymmetric analysis with sample dimensions of 100 mm in length and 50 mm in diameter. The leftmost boundary is the axis of symmetry. Vertical displacements are restricted at the bottom of the model while the horizontal displacements are free. The 15 node triangular elements are used in the numerical model. The calculation consists of two phases, in the consolidation phase; the confining cell pressure is applied all around the sample and will be followed by the next phase which is the axial compression of the sample to failure.

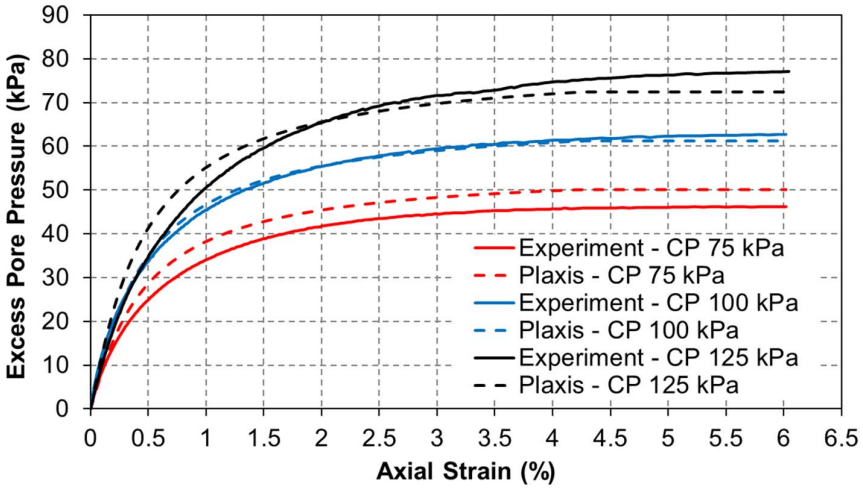
The reference secant stiffness modulus for CIS was measured to be about 18 MPa from the consolidated undrained triaxial test. As mentioned in the Equation 7, the drained reference secant stiffness can be approximated from the one obtained from consolidated undrained triaxial test. Although a reduction factor about 0.7 has been suggested based on the elasticity theory, the factor of 0.35 was found to be suitable for the presented calibration practice. This is due to the fact that, like most soft soils, CIS undergoes a considerable amount of plastic strain when the deviatoric stress increases to the level of 50% of the ultimate strength at failure. The reference pressure is 100 kPa as the default setting in Plaxis and the same value is assumed in this study as it is the effective confining pressure for one of the performed triaxial tests. E_{ur}^{ref} and E_{oed}^{ref} are respectively measured as 39.9 MPa and 3.5 MPa from an unloading reloading triaxial and oedometer test performed on CIS samples. As suggested in Plaxis manual, the power *m* can be assumed as unity for soft soils. In this calibration practice, the power *m* was varied in the numerical analysis of triaxial and oedometer tests until a reasonable match between the numerical and the experimental results were obtained for the all three effective confining pressures. The power *m* of 0.95 was found to be most suitable for the calibration CIS. The acceptable agreement has to be satisfied for both stress-strain and excess pore pressure-strain curves. However, a perfect match on excess pore pressure curves is hard to attain as the pore pressure in the triaxial test is measured by a sensor at the bottom rather middle of the sample and a slight difference between the model and the experiment is expected at the start of the test till the pore pressure equalisation take place throughout the whole sample. As shown in Fig. 2, a good agreement exists between the predictions by the HS model and the triaxial test results for stress-strain and pore pressure-strain curves for all the three confining pressures. As shown, the nonlinear stress-strain behavior of the CIS and the stiffness reduction during primary loading can be well captured by the use of HS model and such an exact prediction of stress-strain behavior results in a more precise deformation analysis of geotechnical structures in CIS. The HS model input parameters for CIS are summarised in Table1 1.

Table 1. Hardening Soil Model Parameters for CIS

Parameter	Description	Value
φ	Internal Friction Angle (Degree)	21
c	Cohesion (kPa)	10
R_f	Failure Ratio	0.87
ψ	Dilation Angle (Degree)	0
E_{50}^{ref}	Reference Secant Stiffness in Drained Triaxial Test (MPa)	6.3
E_{oed}^{ref}	Reference Tangent Stiffness For Oedometer Primary Loading (MPa)	3.5
E_{ur}^{ref}	Reference Unloading/Reloading Stiffness (MPa)	39.9
m	Exponential Power	0.95
v_{ur}	Unloading/Reloading Poisson's Ratio (Default Setting: 0.2)	0.2
p^{ref}	Reference Pressure (Default Setting: 100 kPa)	100



(a)



(b)

Fig. 2. Laboratory and numerical simulation of consolidated undrained triaxial; (a) deviatoric stress versus axial strain (b) excess pore pressure versus axial strain

CAVITY EXPANSION METHOD AND VALIDATION OF CALIBRATED PARAMETERS

In order to validate the suggested parameters, they have been used to model the CPT q_c profile in a CIS and the results of modelling were compared against the CPT results at the field. The cavity expansion theory deals with the expansion (or contraction) of a cavity in a medium with given properties. The expansion (or contraction) results in the change of both stress and strain fields throughout the medium. Cavity expansion method has been extensively employed by other researchers to study significant fundamental engineering problems such as the bearing capacity of deep foundations, cone penetration, dilatometer and pressuremeter testing, underground excavation and tunnelling. The geometry of cavity (spherical or cylindrical) and the mechanical properties of the surrounding medium are the two important features in any cavity expansion solution which control the extent of complexity of the governing equations.

In this part of study, authors focused on the analysis of spherical cavity expansion theory to model the CPT cone tip resistance (CPT q_c) profile in a layer of CIS. The developed CPT q_c profile was then

compared against the profile gained from field test to validate the capability of the calibrated HS model in modelling the elastoplasticity of CIS. The analogy between cavity expansion and cone penetration test was first studied by Bishop et al. (1945) concluding that the pressure required to produce a hole in an elastoplastic medium is related to the pressure which is required to expand a cavity of the same volume in the same medium. As the cavity expands inside the soil, the pressure inside the cavity increases and eventually reaches a constant value which is called limit pressure. As described by Yu and Mitchell (1998), there are two steps required to apply the cavity expansion theory to predict the cone tip resistance. The first step is to develop the theoretical solutions to find the so-called limit pressure induced by the cavity expansion. The second step is to relate the obtained limit pressure to the cone tip resistance. A considerable amount of work has been done on the development of cavity expansion solutions in both clay and sand from very simple stress-strain models such as linear elastic to more realistic nonlinear stress-strain models. A full description of the cavity expansion theory development in geomechanics can be found in Yu (2000). Several researchers have suggested different equations to correlate the limit pressure with the CPT q_c value. Among them, the correlations developed by Ledanyi and Johnston (1974), Vesic (1972), and Silva (2005) are very popular for cohesive soils. Also, the correlations developed by Baligh (1976), Yu and Houlsby (1991), Randolph et al. (1994), and Yasufuku and Hyde (1995) have been proven to be successful for cohesionless soils.

In the current study, spherical cavity expansion analysis is performed in Plaxis finite element code using the model developed by Tolooiyan and Gavin (2011). In this model, an axisymmetric analysis is performed with the left-hand boundary of the model as the axis of symmetry, the vertical and horizontal displacements are restrained at the bottom of the model, and the horizontal displacements are restrained at the rightmost boundary. The mesh is 10 m wide and 21 m deep. A 1 m thick dummy layer is used at the top of the 20 m deep soil deposit. Different stress levels corresponding to different depths are modelled by varying the unit weight of the dummy material. The spherical cavity expansion is then carried out by applying small steps increasing the volumetric strain of the cavity. For a full description of the cavity expansion methodology in Plaxis, please refer to Tolooiyan and Gavin (2011), and Tolooiyan (2011).

The limit pressure values were determined from the radial stresses developed inside the cavity due to the applied volumetric strain, at different depths from 10 m to 22m. Finally, the limit pressure at each depth was then converted to the q_c value using the correlation proposed by Silva (2005) as shown in Equation 10.

$$q_c = \sqrt{3}\, c' + p_{lim} + \sqrt{3}(p_{lim} - u)\tan\delta \qquad [10]$$

where, c' is effective cohesion, p_{lim} is the limit pressure, δ is the soil-cone interface friction angle, and u is the induced excess pore water pressure. The interface friction angle is assumed to be equal to the friction angle of the soil as suggested by Yu (2000). Using Equation 10, the CPT q_c value for each depth is calculated. The developed CPT q_c profile and the magnitude of excess pore water pressure from numerical analysis in Plaxis are compared against the ones from the field test (see Figure 3). This comparison presents an excellent agreement between the numerical analysis and the field test results.

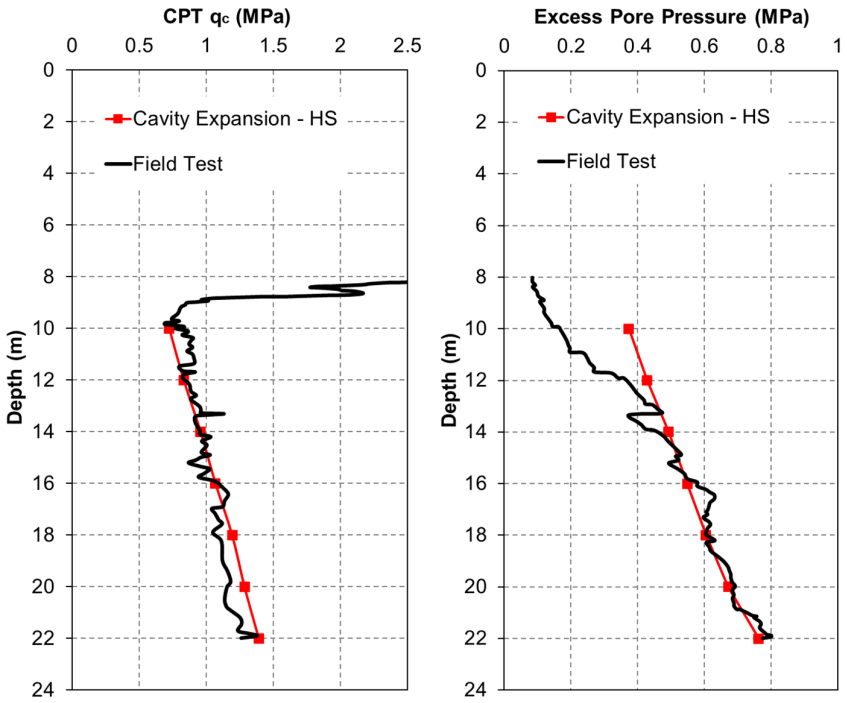


Fig. 3. Comparison between the results of numerical analysis and field investigation; (a) CPT q_c profile, and (b) excess pore pressure

SUMMARY AND CONCLUSION

In this study, the calibration of HS model for CIS has been explained. Series of consolidated undrained triaxial tests were performed to determine the strength and stiffness parameters for the HS model. The analysis of spherical cavity expansion was numerically performed in the Plaxis finite element package to calculate the cavity limit pressure which was then correlated to the CPT q_c value. The obtained CPT q_c profile was finally compared against the CPT results at the field. An acceptable agreement between the numerical analysis and the field investigation results was gained which validates the capability of the HS model in modelling the elastoplasticity of CIS and the accuracy of the suggested parameters.

A realistic constitutive soil model should be able to take into account the most fundamental features of the soil behaviour such as nonlinearity and the stress level dependency. Comparing the stress-strain and stress path curves from the triaxial test and the numerical modelling reveals that the HS model is effectively capable of representing such fundamental behaviour of CIS. This capability is crucial for modelling geotechnical structures in problematic CIS. Considering the complexity of the HS model formulation, a higher computational cost and effort should be expected in the analysis of geotechnical structures with the HS model comparing to modelling using linear elastic-plastic models. However, the importance of a precise deformation analysis is so highlighted recently in the design of highly important infrastructures that justifies the computational cost associated with the application of the advanced models.

Authors believe that the suggested HS model's parameters for CIS can be incorporated in FEM packages by geotechnical engineers for realistic deformation analysis of geotechnical infrastructures in Coode island area which finally results in more reliable and cost-effective design.

REFERENCES

Abdelmalek, B., Kwan, P.S., and Chapman, G., 2004. Strength Properties of Cement Treated Coode Island Silt by the Soil Mixing Method, Geotrans 2004. ASCE, pp. 1421-1428.

ASTM, 2011. Standard Test Method for Consolidated Undrained Triaxial Compression Test for Cohesive Soils, D4767. ASTM International.

Aurecon, 2013. Port Capacity project-civil works, 7T231883-RPT-200-GEO- Geotechnical Report, Aurecon Australia Pty Ltd.

Baligh, M.M., 1976. Cavity expansion in sands with curved envelopes. Journal of the Geotechnical Engineering Division ASCE 102.

Bishop, R.F., Hill, R., and Mott, N.F., 1945. The theory of indentation and hardness tests. Proceedings of the Physical Society 57, 147-159.

Brinkgreve, R.B.J., Engin, E., and Swolfs, W.M., 2012. PLAXIS 2D The Netherlands: PLAXIS B.V.

BS1377, 1990. Soils For Civil Engineering Purposes, Part 8. Shear Strength Tests (Effective Stress).

Burland, J.B., 1989. Small is beautiful: the stiffness of soils at small strain. Canadian Ceotechnical Journal 26, 499-516.

Chen, W.F., 2007. Limit analysis and soil plasticity. J. Ross Publishing.

CUR195, 2000. Backgrounds on numerical modelling of geotechnical constructions, Part 3. CUR Centre for Civil Engineering Research and Codes, Gouda, The Netherlands.

Duncan, J.M., and Chang, C.Y., 1970. Nonlinear analysis of stress and strain in soils. Soil Mechanics and Foundation Division Journal ASCE 96, 1629-1653.

Ervin, M.C., 1992. Engineering properties of Quaternary age sediments of the Yarra Delta, Engineering Geology of Melbourne, Victoria, Australia, p. 407.

Ledanyi, B., and Johnston, H.H., 1974. Beahviour of circular footings and plate anchors embedded in permafrost. Canadian Geotechnical Journal 11, 531-553.

Obrzud, R., and Truty, A., 2013. The hardening soil model - a practical guidebook, Technical Report Z Soil.

Randolph, M.F., Dolwin, J., and Beck, R., 1994. Design of driven piles in sand. Geotechnique 44, 427–448.

Schanz, T., Vermeer, P.A., and Bonnier, P.G., 1999. The hardening soil model: formulation and verification, Proceedings of the beyond 2000 in computational geotechnics: 10 years of PLAXIS international, Rotterdam (The Netherlands), pp. 281-296.

Silva, M.F., 2005. Numerical and physical models of rate effects in soil penetration. University of Cambridge.

Sokoloviskii, V.V., 1965. Statics of granular media, First Edition ed, New York.

Tolooiyan, A., 2011. FE approaches to evaluate the end bearing capacity of foundations on sand using in-situ test results, PhD thesis. University College Dublin, Ireland.

Tolooiyan, A., and Gavin, K., 2011. Modelling the cone penetration test in sand using Cavity Expansion and Arbitrary Lagrangian Finite Element Methods. Computers and Geotechnics 38, 482-490.

Vesic, A.S., 1972. Expansion of cavities in infinite soil mass. Journal of the Soil Mechanics and Foundation Division ASCE 98, 265-290.

Yasufuku, N., and Hyde, A.F.L., 1995. Pile end bearing capacity in crushable sands. Géotechnique 45, 663-676.

Yu, H.S., 2000. Cavity expansion methods in geomechanics. Kluwer Academic Publishers, The Netherlands.

Yu, H.S., and Houlsby, G.T., 1991. Finite cavity expansion in dilatant soils: loading analysis. Géotechnique 41, 173–183.

Yu, H.S., and Mitchell, J.K., 1998. Analysis of cone resistance. a review of methods. Journal of Geotechnical and Geoenvironmental Engineering ASCE 124, 140-149.

BRICKWORKS MARKETPLACE GROUND IMPROVEMENT, ADELAIDE

Andrew Middleton, Principal, Douglas Partners, Brisbane, Queensland, Australia, 0421 583 241, Andrew.Middleton@douglaspartners.com.au
Mark Wyatt, National Retail Manager, Badge Constructions, Queensland, Australia, 0458 303 783, Mark.Wyatt@badge.net.au

ABSTRACT

The Brickworks Marketplace Project is a significant shopping centre development in inner north west Adelaide constructed by Badge Constructions in 2014 and 2015. The site was a former brickworks with a deep pit containing various extents of uncontrolled fill which was to remain on site, and with a remaining void up to 6 m in depth. The existing uncontrolled fill was improved using the High Energy Impact Compaction system, and the pit backfilled using a quarry crusher byproduct selected by trial and a recycled crushed concrete and bricks and compacted in deep lifts. This approach resulted in significant savings in compaction time, cost and building foundations. The settlements of various parts of the completed works have been monitored since February 2015 and this monitoring has demonstrated small settlements which meet the user's constraints.

INTRODUCTION

The Torrensville Brickwork Markets project involved the transformation of a former brickworks and clay pit site into a regional 17,000m2 shopping centre, opening in June 2015.

The site was a former brickworks with adjoining clay borrow pit. The clay pit had been partially backfilled over many years with 'uncontrolled' fill comprising 'clean' soil, bricks and kiln dust typically of the following thicknesses:

- of the order of up to 7 m to 10 m but locally up to 15 m in the western part of the site
- 2 m to 5 m in the south-eastern part of the site; and
- less than 0.5 m in the north-eastern part of the site

Anecdotal reports suggested compaction of some of the fill may have been undertaken, although this not able to be confirmed nor records obtained.

Initially it was proposed to take up the existing uncontrolled fill, sort and recompact or remove to landfill, followed by backfilling in conventional means over 500,000 cubic metres of imported filling to a thickness of up to approximately 6m to backfill the former pit. This work represented a significant cost and was not economically viable.

During early negotiations, the contractor proposed an alternative to retain and ground improve the existing filling on site, and to backfill the pit with fill placed and compacted in deep lifts, thereby significantly improving the economics, environmental and community impacts of the proposed works. The developer agreed to the proposal with the following performance criteria:

- a settlement of ≤10 mm after 10 passes by the Impact Compactor (on existing subgrade areas);
- a bearing capacity of 250 kPa for high level footings;
- a maximum long term differential settlement of 40 mm (measured over 16 m), ie. 1 in 400; and
- a minimum modulus of 40MPa.

A specialist subcontractor providing High Energy Impact Compaction (HEIC) was selected to provide the required ground improvement, and proposed the use of a compactor using a 3-sided 14t drum

module with a drop height of 230mm giving a rating of 3,220 Tonne-mm (175kJ Kinetic Energy). This equipment on site during construction is shown in Figure 1.



Figure 1 –Impact Compactor

TREATMENT OF EXISTING UNCONTROLLED FILLING

The existing filling was ground improved using the 3-sided HEIC compactor, with between 20 passes and 50 passes applied to meet the requirement for ≤10mm induced settlement for 10 passes.

Differential GPS unit was used to take height and position readings after each 10 passes of the compactor and compared to the requirement. Examples of settlement data presentation are given below in Figures 2 and 3. Typically settlements of the subgrade of the order of 100mm up to 200mm were induced by the compactor.

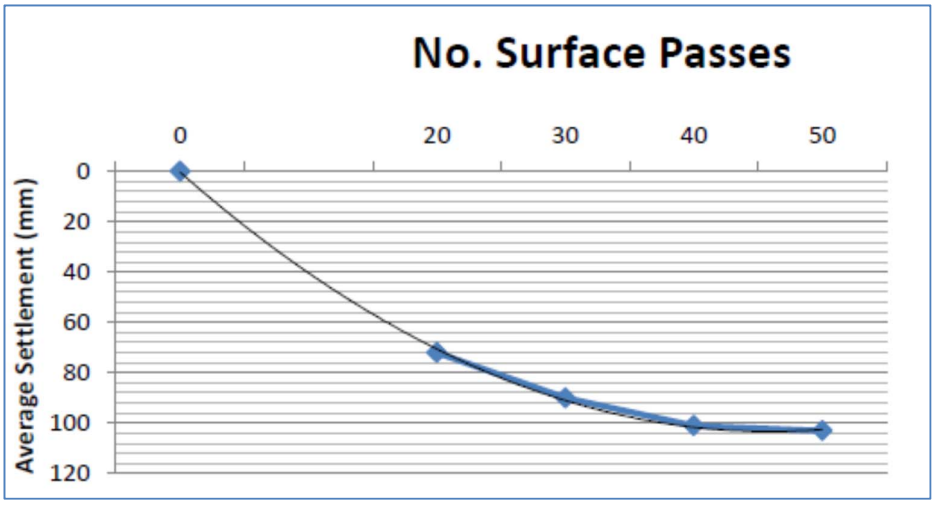


Figure 2 – Example of Induced Settlement Graph

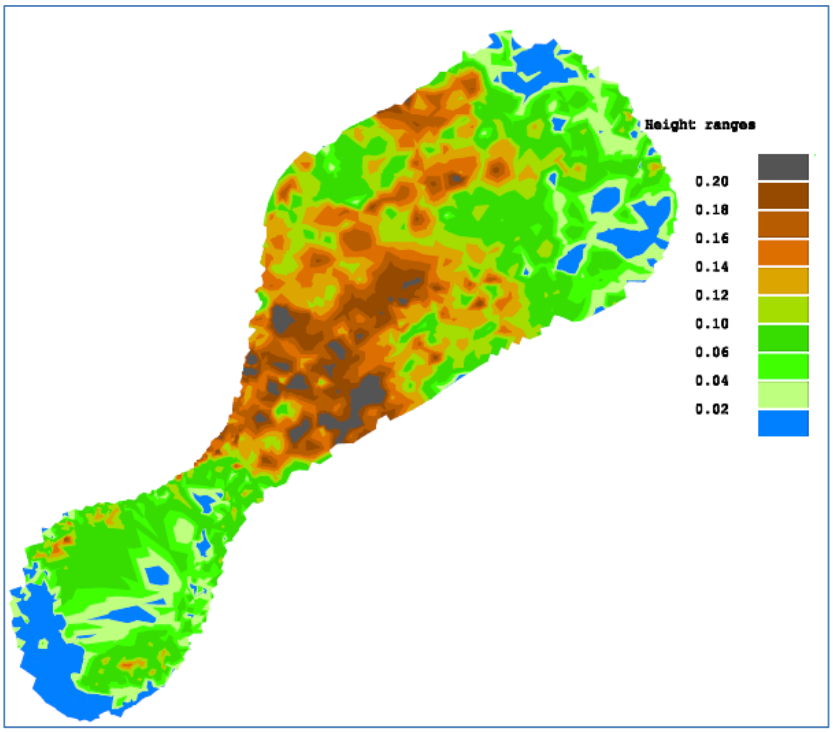


Figure 3 – Example of Total Compaction Induced Settlement Plot (height range in m)

The compactor was also fitted with an accelerometer in the drum module to measure deceleration of the drum when impacting the ground. Readings were taken during the first pass, and then again on the final pass, and plotted in conjunction with the differential GPS readings of position. These readings provide a useful indication of change in relative ground stiffness due to the compaction process, and areas of sites that may not be significantly improving which may require other intervention measures. The HEIC contractor produces these readings as Compaction Impact Response (CIR) plots. An example of a CIR plot is given in Figure 4 below.

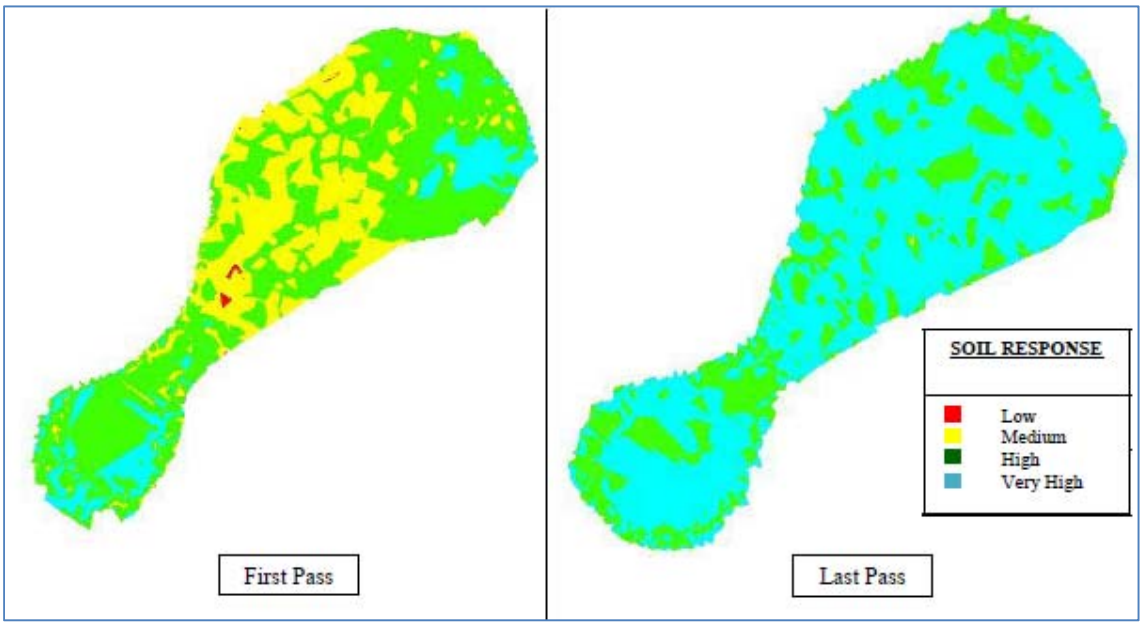


Figure 4 – Example of Compaction Impact Response Plot

Throughout the treatment of the existing filling, several areas that were unlikely to respond well, or did not respond well to the impact compaction were identified, and modified treatment approaches taken. These areas included areas of kiln waste and a pit loosely backfilled with bricks.

The area of kiln waste was in excess of 5m in depth, and presented as a firm clayey silt in nature. This material was considered unlikely to respond well to impact compaction. Based on assessed settlements, the material was excavated to 3m depth, a bridging layer installed and then filled over with controlled fill. The excavated material was able to be incorporated into filling in the carpark area by careful blending with waste bricks.

A pit approximately 5m in depth backfilled with loose bricks was identified by induced compaction settlements in excess of 0.4m, well in excess of any other induced settlements experienced during the works, and by failure to achieve an acceptable Compaction Impact Response. This area was ultimately treated by excavation and replacement with imported fill. The bricks were able to be recycled by incorporation into the fill by blending with kiln waste as described above.

DEEP LIFT FILL MATERIAL SELECTION AND TRIALS

The project specification nominated a sand material with not more than 5% fines (<0.075mm) content resulting in relatively high permeability, and being single size somewhat difficult to compact without significant water. Traditionally, clean sands would be most effectively compacted (in areas with good drainage) using water with heavy vibratory equipment; however in this case the former brock pit presented poor drainage conditions, and water is a relatively limited resource in Adelaide.

The specification alternatively allowed for a waste derived fill with maximum linear shrinkage of 7% and maximum “plastic shrinkage” of 10%. A number of fill sources were identified, primarily comprising quarry industry byproducts or recycled construction materials, offering cost and environmental benefits for the client and contractor. Natural sources of sand were some distance from the site, involving considerable cost, trucking resources, carbon impact, use of a non-renewable resource and increased road user and community impacts of additional truck movements on Adelaide roads and streets.

The alternative materials considered included a sand sized “crusher dust” byproduct, a “20mm quarry rubble” (silty gravelly sand crushing byproduct with CBR >45% and linear shrinkage < 3%), and a range of recycled construction materials including crushed concrete (PM20-2) and crushed brick.

Compaction trials were undertaken initially using the sand sized crusher dust, initially preferred because of cost and supply quantities, with layers of approximately 0.7m thicknesses were adopted. The sand sized crusher dust was found to have a silt fines content of approximately 15% to 20%. The works found that the moisture contents needed to be well dry of optimum, as the materials were unacceptably ‘spongy’ under passage of compaction equipment with near to optimum materials, and compaction was inhibited, as is commonly experienced with sands with significant silt content. The early trial results with a placement moisture between 5% and 6% (compared to an optimum moisture content of 9%), showed achieved dry density ratios (Standard compaction) of 85% to 92% for the lower level of the layer being compacted, and as low as 90% in the upper part of the layer being compacted. This material was subsequently rejected and alternative materials sourced and used.

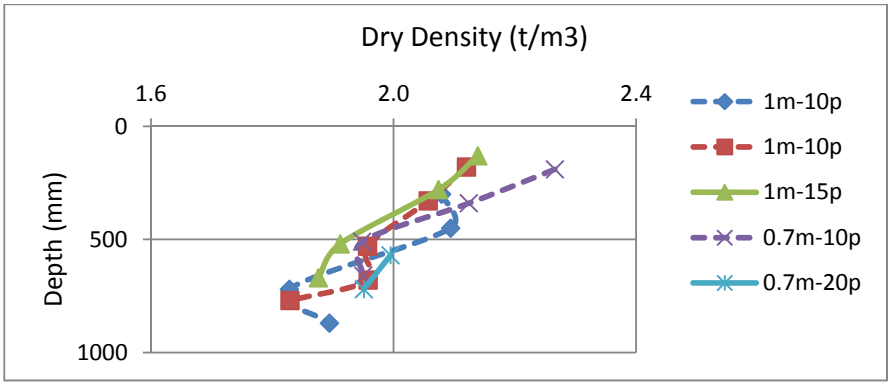


Figure 5 – Typical Density Results of Initial Compaction Trial Pad

Two materials, a 20mm quarry rubble and a PM20-2 crushed concrete and brick were subsequently trialed and selected as the preferred imported fills. The particle size distribution of the recycled product is shown below in Figure 6. The maximum dry density of the quarry rubble and crushed concrete and brick was of the order of 2.25 t/m3 and 1.85 t/m3 respectively, and the optimum moisture contents of the order of 7% and 14.5% respectively.

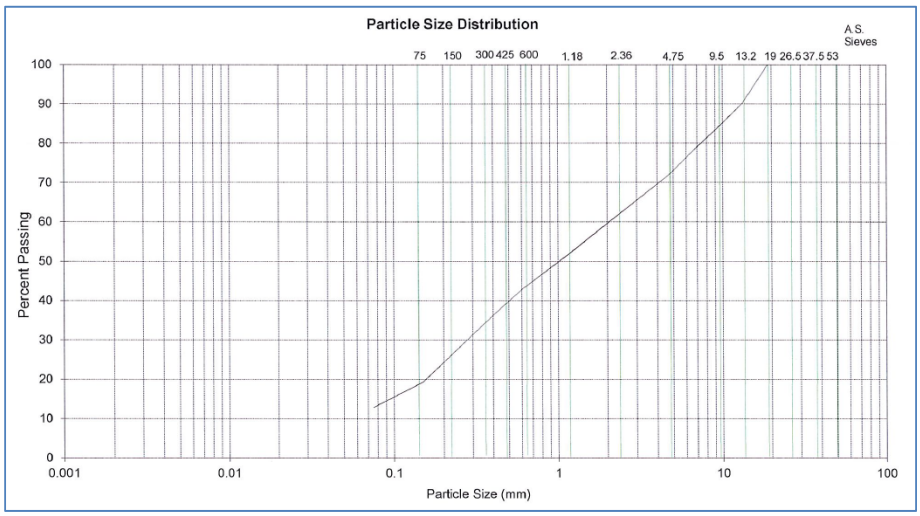


Figure 6 – Typical Particle Size Distribution for Recycled Product

DEEP LIFT COMPACTION

The majority of the backfilling of the pit was carried out between early May and mid August 2014, with in excess of 500,000m^3 of fill imported and compacted in this time. The rate of fill imported was constrained because of capacity constraints on local road network, and consequently the two Impact Compactors were utilized significantly less than half of the time.

Where the depth of fill transitioned at the northern edges the excavation was benched to provide a fill depth transition to meet the settlement criteria.

An exclusion zone for the impact compactors was initially employed around the heritage listed kiln and chimney stack, with a vibration limit of 3mm/sec adopted for the structures. Vibration monitors with automated alerts and warning alarms was installed for the compaction work. During the works the 2mm/sec amber warning was exceeded when the impact compactor approached to a distance of 22m of the structures. Conventional compaction equipment was subsequently used within 25m of the structures and no further exceedances were experienced.

Typically 20 passes of the compactors were employed, with settlement monitoring after 10 passes to assess when effective compaction had been achieved. Upon completing the compaction of each layer, compaction control testing was carried out by use of nuclear density meter testing, and Dynamic Cone Penetrometer testing with approximate correlations established during the compaction trial and early fill layers. Dry density ratios of close to 100% (Standard compaction) were typically able to be achieved after 20 passes. An example of typical results of the density testing is illustrated in Figure 7.

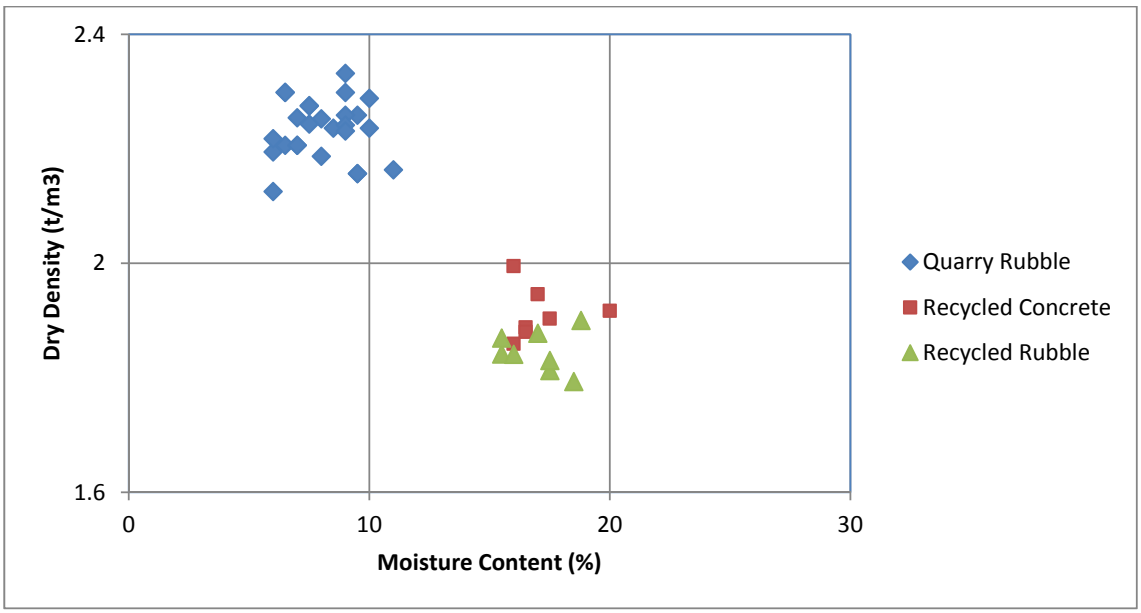


Figure 7 -Typical Density Test Results for Deep Lift Fill

Upon completion of the fill placement, twenty four plate load tests were undertaken in the proposed building areas to confirm bearing capacity, elastic modulus and insitu CBR. The typical results of this testing are summarised in Table 1.

Table 1. Summary of Typical Plate Load Test Results

Material	Bearing Capacity* (kPa)	Elastic Modulus (MPa)	Insitu CBR (%)
Shallow fill over natural clays	85 – 200	20 – 45	7 – 30
'Wet' filling#	50 – 170	10 – 40	3 – 23
Compacted filling	300 - >400	45 – 80	35 – 80

Note: * at 1.25mm plate deflection # subsequently removed and reworked

SETTLEMENT MONITORING

Surface settlement monitoring points were established at various locations around the completed project, typically installed on building columns or carpark kerbs. Readings have been taken since February 2015. Some typical results of this monitoring are shown graphical in Figure 8. Other areas of site have typically measured settlements not exceeding 15 mm. It is noted that some of the settlement observed on columns prior to Day 200 can be attributed to elastic 'take up' of footings during construction of the building superstructure, in particular the roof.

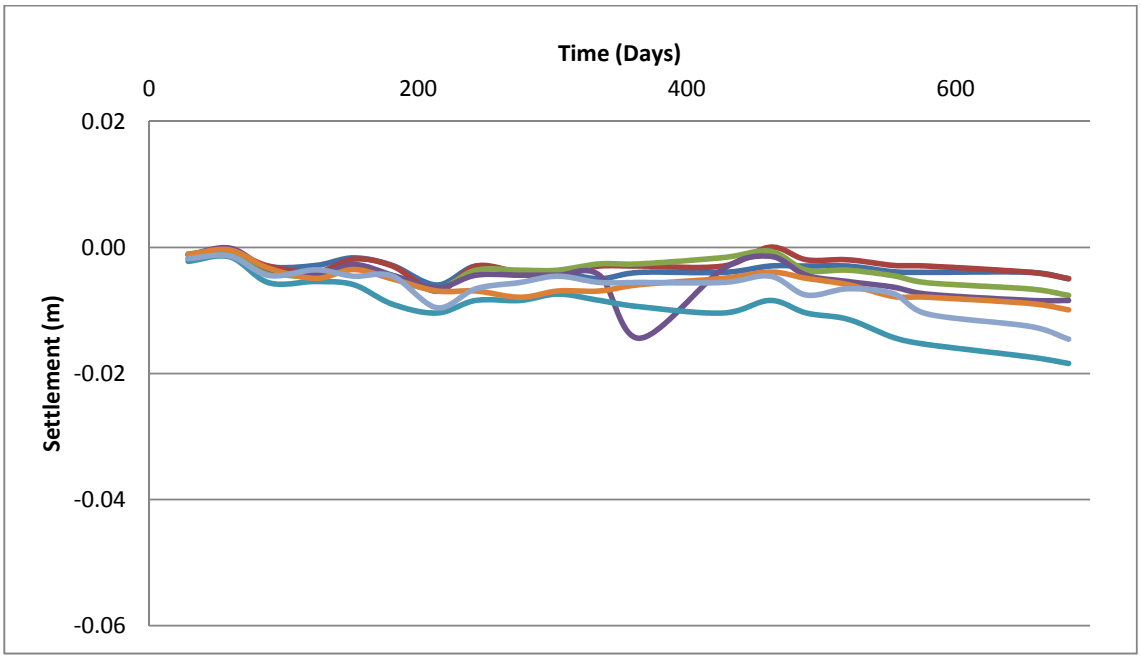


Figure 8 – Typical Settlement Monitoring Results

SUMMARY AND CONCLUSIONS

Impact compaction was carried out on existing uncontrolled fill at this site using a 14t 3-sided compactor achieved induced settlements of 100mm to 200mm typically, but locally more than 0.4m where a pit of loose bricks was present.

Deep lift placement and compaction was adopted for the 6m depth of backfill. A silty sand 'crusher dust' was trialed, but found to require dry placement for effective compaction and was subsequently rejected. Recycled or byproduct materials that were found to acceptably compact included a silty gravelly sand 20mm quarry rubble and recycled PM20-2 crushed concrete and bricks. Layer thicknesses of 0.7m and up to 1.0m were found to typically achieve a dry density ratio of close to 100% (Standard compaction) with 20 passes of an impact compactor.

The results of plate load testing indicated bearing pressures of at least 300kPa and soil modulus values of at least 45MPa for the material compacted by deep lift methods, meeting client requirements. Significantly lower values were measured in areas of natural soils or 'wet' fill. The results of settlement monitoring since February 2015 indicates total settlements of the building and carpark generally not exceeding 15mm, well within the client's performance requirements.

ACKNOWLEDGMENTS

Acknowledgement is made to Badge Constructions Pty Ltd who have provided kind permission for publication of this paper, and is also made to Landpac Technologies Pty Ltd who have permitted reproduction of the Compaction Induced Settlements and Compaction Impact Response information from the project.

CASE STUDY: LOAD TRANSFER ANALYSIS ON AN INSTRUMENTED AUGERCAST PILE USING EDC STRAIN GAUGES AND GEOKON REBAR STRAINMETERS

Swamy Avasarala[1], Santosh Mummaneni[2], Vamshi Vemula[3], Dr. Sastry Putcha[4]

[1] President, Aver Technologies, Inc., Virginia USA, +1-703-580-8907, swamy@avertechnologies.com
[2] Project Manager, Aver Technologies, Inc., Virginia USA, +1-703-580-8907, santosh@avertechnologies.com
[3] Project Engineer, Radise International, Florida, USA, +1-561-841-0103, vamshi.vemula@radise.net
[4] Chief Engineer, Smart Structures, Florida, USA, +1-561 841-0103, sputcha@smartstructures.com

ABSTRACT

This paper presents the results from a case study on the comparison of two strain acquisition instrumentation technologies, Geokon rebar strainmeters and Embedded Data Collectors (EDC) for the DC Water Main Pump Station project, in Washington D.C. These two instrumentation systems were installed by AVER in a single 18-inch (0.45 m) diameter augercast pile (with one-1.25 inch (3.175 cm) dywidag bar) at critical locations to determine the load transfer mechanism and establish a comparison between strain/load measured with these two systems along the pile. A quick static load test was performed on the test pile as per ASTM D1143 standard.

Prior to the installation of the pile, a 24-inch (0.6 m) diameter outer casing was installed to the proposed cutoff elevation of -22.5 feet (-6.85 m) to discount the frictional resitance within the upper overburden zone. The pile was then drilled through the outer casing to the tip elevation of -65.02 feet (-19.8 m) with inner casing within the overburden zone. Strainmeters along with EDC were installed on dywidag bar at various locations and then wet set into the concrete following auger retrieval. The loads measured with EDC and Geokon sensors were within 15% percent of each other.

Keywords: rebar strain meters, EDC strain gauges, augercast pile, loads, load tests

PROJECT BACKGROUND

Project Background & Requirements:

Like any other foundation piles, augercast piles are extensively used in the public and private sector structures in the United States for many years. It is a common practice to perform static compression (ASTM D1143), tension (ASTM D3689), and lateral load tests (ASTM D3966) depending on the project requirements. In recent years, embedded strain sensors, manufactured by Smart Structures, USA has gained prominence for its use to collect both static and dynamic measurements for driven piles. In addition, AVER has successfully used EDC for collecting long term static measurements for an abutment drilled shafts for I-95 Hotlanes project in Virginia, USA.

Geokon sisterbar strain gages are widely used in the foundation industry to monitor the load transfer mechanism within pile foundations throughout the world. As the Geokon strainmeters are vibrating wire and are welded to a sister bar, there is often a debate within the engineering community with regards to what modulus to use when converting measured strains to loads. EDC sensors, unlike Geokon strain gages are embedded directly into the concrete and therefore do not have the same concern.

For the first time, the EDC strain gages were used in augercast pile foundation at the DC Clean Rivers Project in Washington DC, USA. The project consisted of new Combined Sewer Outflows (C.S.O's), surge tanks, and connecting channels supported by over 150 augercast piles. Each pile was 18 inches (0.45 m) in diameter with one 1.25 inches (31.75 mm) dywidag bar and lengths ranging between 70 to 80 feet (21.3 to 24.3 meters). The axial compression loads ranged from 440 to 480 kips (1957 to 2135 KN). The project specifications required axial compression and tension load tests for the proposed piles. This paper presents only the results from axial compression load test and load transfer measured along the pile with Geokon and EDC strain sensors.

Augercast Test Pile Information:

Pile Length= 77.6 feet (23.67 m) long
Pile Reinforcement =1.25-inch (3.17 cm) diameter dywidag bar, Grade 150 ksi (1034 MPa)
Achieved Grout Strength (fc') = 4720 psi (32.54 N/mm^2)
Elastic Modulus of Concrete (E_c=5700*√(fc'))= 3916 ksi (27000 MPa)
Required Test Load = 240 Tons (2135 kN)
Ground Elevation at the time of test= +10.58 feet (3.22 m)
Proposed test pile cutoff Elevation = -22.5 feet (-6.85 m)
Plan Tip Elevation = -65.02 feet (-19.8 m)

Soil Profile Information:

The soil profile at this project site location was summarized in the Table 1 below.

Table 1: Soil Profile Information

Elevation (feet)	Elevation (meter)	Soil Classification (USCS)	SPT "N" Value
10.43 to -0.5	3.7 to -0.15	SM	7
-0.5 to -12.5	-0.15 to -3.81	CL	9
-12.5 to -18	-3.81 to -5.48	MH	8
-18 to -25	-5.48 to -7.62	CL	5
-25 to -29	-7.62 to -8.84	MH	5
-29 to -41	-8.84 to -12.49	SP-SM	33
-41 to -45	-12.49 to -13.72	SM	66
-45 to -56	-13.72 to -17.07	SC	60
-56 to -60	-17.07 to -18.29	ML	68
-60 to -67.5	-18.29 to -20.54	SC	50/3"

INSTRUMENTATION AND TEST PROCEDURE:

Background Information of Geokon and EDC sensors:

The test pile was instrumented with Geokon rebar strainmeters model 4911A at 7 locations and with 2 sets of EDC sister-strain gauges (each set has two strain gauges connected with a 12-feet (3.66 m) wire) at critical load transfer locations.

Geokon Rebar Strainmeters Model 4911 has a vibrating wire strain gauge and a thermistor attached to a No. 4 sister bar to record strains and temperature readings at the installed sensor location.

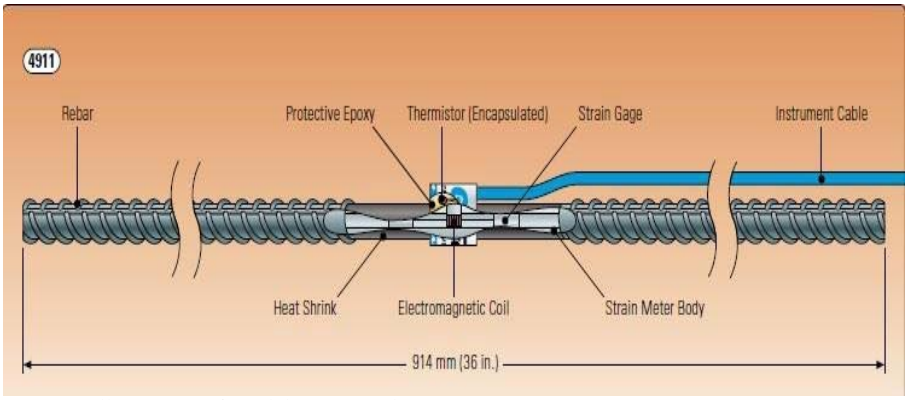


Figure 1: Illustration of Model 4911 A rebar strainmeter

Embedded Data Collectors are heat and corrosion resistant half bridge strain sensors with temperature and signal processing unit that can be utilized to measure strains under static and dynamic load conditions.



Figure 2: EDC-Wireless monitoring system in action during baseline readings at DC water project.

Instrumentation Plan and Installation

For the feasibility of performing static load test and construction sequence considerations, the project contractor chose to install the proposed foundation from the existing ground elevation instead of from the proposed cutoff elevation. To properly simulate the actual pile behavior under the static loads, prior to the installation of the pile, a 24-inch (0.61 m) diameter outer casing was first installed to the proposed cutoff elevation of -22.5 feet (-6.85 m) to prevent frictional resitance within the upper overburden zone. The pile was then drilled through the outer casing to the pile tip elevation of -65.02 feet (-19.8 m) by setting an inner casing within the overburden zone.

Since there was no frictional resistance within the cased overburden zone (between elevation +10.58 feet (+3.22 m) to the cutoff elevation of -22.5 feet (-6.85 m)), Geokon rebar strainmeters G1 and G2 were installed at elevation +7.3 feet (+2.22 m) and pile cutoff elevation of -22.5 feet (-6.85 m), respectively, to measure strain readings that would represent the applied loads. The remaining six Geokon rebar strainmeters were installed between the pile cutoff and pile tip elevation at the locations indicated in Table 2.

Table 2: Geokon Rebar Strainmeter locations

Geokon Sensor Number	Rebar Strainmeter Depth (From Ground EL.) feet (meter)	Approx. EL. at Strainmeter Location feet (meter)
G1	3.25 (0.99)	7.33 (2.23)
G2	31.25 (9.52)	-20.67 (-6.30)
G3	38.25 (11.65)	-27.67 (-8.43)
G4	45.25 (13.79)	-34.67 (-10.56)
G5	52.25 (15.92)	-41.67 (-12.70)
G6	59.25 (18.05)	-48.67 (-14.83)
G7	66.25 (20.12)	-55.67 (-16.96)

In addition, two sets of EDC strain gauges were also installed on to the dywidag bar to measure strain readings at critical load transfer locations as indicated in Table 3. Each EDC strain gauge set has two strain gauges connected with 12 feet (3.6 m) wire in between the gauges.

Table 3: EDC strain gauge locations

EDC Sensor Number	EDC strain gauge Depth from Ground Elevation feet (meter)	Approximate Elevation at EDC strain gauge location feet (meter)
S1	65.78 (20.05)	-55.2 (-16.82)
S2	52.78 (16.08)	-42.2 (-12.86)
S3	49.08 (14.95)	-38.5 (-11.7)
S4	35.08 (10.69)	-24.5 (-7.47)

The Geokon strainmeter sisterbars along with EDC sensors with cables were fastened to dywidag bar with zip ties. The EDC sensors were installed by suspending each sensor (with clear space) with metal straps

protruding from wire cage that was wrapped around the dywidag bar to provide sturdiness and prevent the sensor from collapsing onto the bar during placement into the concrete.



Figure 3: Geokon rebar strainmeters and EDC strain gauges attached to dywidag bar.

In addition, to save the instrumentation below the pile cutoff elevation for long term monitoring during service loads, excess wiring was planned for each sensor and was pushed inside a 2-inch (5 cm) diameter and 10 feet (3 m) long PVC pipe. The PVC pipe was strapped to the dywidag bar with zip ties just above the proposed cutoff Elevation of -22.5 feet (-6.85 m). The PVC pipe was sealed at both ends to prevent grout flow through the pipe so that the wires from strainmeters (G2 through G7 and S1 to S4) can be spliced and used for long term monitoring purposes at a later date.



Figure 4: Sealed PVC tube attached to dywidag bar (with extra EDC & Geokon cables inserted for long term monitoring)

***Augercast Test Pile Installation*:**

Prior to the installation of the augercast pile, a 24-inch (0.6 m) outer casing was installed to the proposed cutoff elevation of -22.5 feet (-6.85 m) to discount the frictional resitance within the upper overburden zone. The pile was then drilled through the outer casing to the tip elevation of -65.02 feet (-19.8 m) with the inner casing within the overburden zone.

The pile hole inside the inner casing was grouted with concrete as the auger was retrieved. The dywidag bar with instruments and centralizer bars was then lowered into the wet concrete. Subsequently, a one inch (2.54 cm) telltale steel tube was also wet set into the concrete. Upon installation of dywidag bar into the grout, baseline readings were taken from both Geokon strainmeters and EDC strain gauges to confirm that all the sensors were functioning. A 0.5 inch (1.25 cm) telltale rod was used to measure the pile tip displacement.

Quick Static Axial Compression Load Test Procedure:

Axial compression static load test setup was carried out by general contractor, in accordance with project submittals and ASTM D1143 standard. A total of four, 18-inch (0.45 m) reaction augercast piles were installed as part of the load test setup. The following is a general description of the test procedure and results obtained.

- The test pile was instrumented with Geokon strainmeters (G1 through G7), EDC strain gauges (S1 through S4), two dial gauges (Pile Top), two piano wires and one telltale rod for measurement of strain and pile displacement during the load applications.
- During the loading cycle, the test load was applied through a 500-ton load cell in increments of approximately 10% of the maximum test load of 480 kips (2135 kN).
- Each load application during the loading cycle was held for 5-minute period and corresponding strain measurements, dial gauge readings, tell-tale readings, piano wire readings and survey levels of all 4 reaction piles (R1, R2, R3 and R4) were recorded.



Figure 6: Geokon and EDC monitoring unit read out units during static load test

- During the 7th load increment, at an applied load of 150 tons (1334 kN), the supporting beams (R2 and R3) slightly swayed out of alignment and therefore the load test was aborted and the load was released.
- Two additional cross beams were welded to the transfer beams to provide additional support.
- The static load test was restarted and loads were again applied initially in increments of 20% until 300 kips (1335 kN) and followed by 10% standard increments to the maximum test load of 480 kips (2135 kN).
- The maximum test load of 480 kips (2135 kN) was retained for one hour and all the measurements were taken.
- During the unloading cycle, loads were reduced in decrements of approximately 25% of the maximum test load of 480 kips (2135 kN).
- Each load application during the unloading cycle was held for 5-min period and corresponding measurements were recorded.

***Axial Compression Static Load Test Data Analysis & Results**:*

The following is a summary of our test results from axial compression load test on the augercast test pile:

- The raw Geokon field recorded readings were converted from micro seconds to micro strains and corresponding loads (Ɛ*A*E) at each strainmeter location were obtained by multiplying the strain with pile cross sectional area and the elastic modulus of concrete.
- Baseline Geokon and EDC Readings were recorded prior to the test to determine relative strain increase due to loading during the test.
- The elastic modulus of concrete was determined based on the empirical relationship of 57000 times the square root of the compressive strength (ACI 318-08, 2008) (4720 psi or 32.54 MPa).
- The loads measured at G1, G2 and S4 (at the cutoff elevation of -22.5 feet (-6.85 m)) locations should be similar as soil friction within the overburden (casing zone) was zero.
- The loads measured by EDC strain gauges and Geokon rebar strainmeters at corresponding sensor locations were observed, in general, to be within 15%, with EDC load measurements slightly on the higher side.

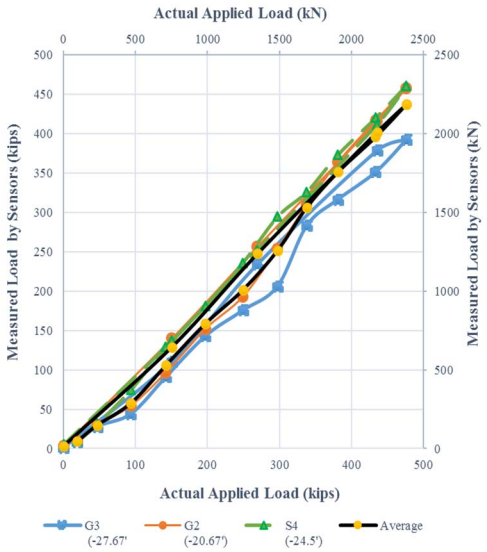


Figure 7a: Geokon Loads vs. EDC loads at cut off EL.

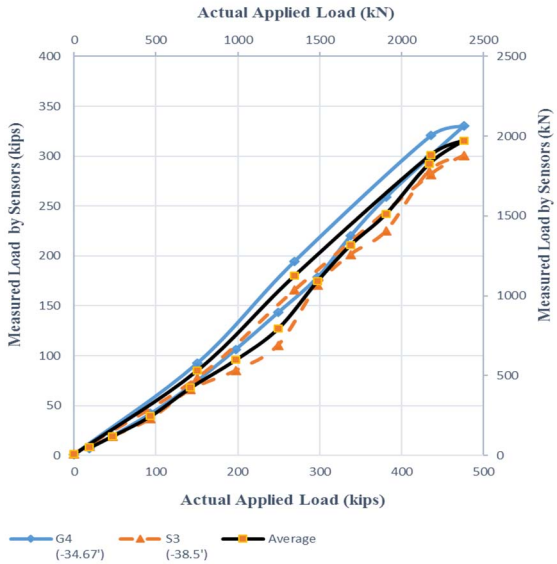


Figure 7b: Geokon loads @-34.67' vs. EDC loads@ -38.5'

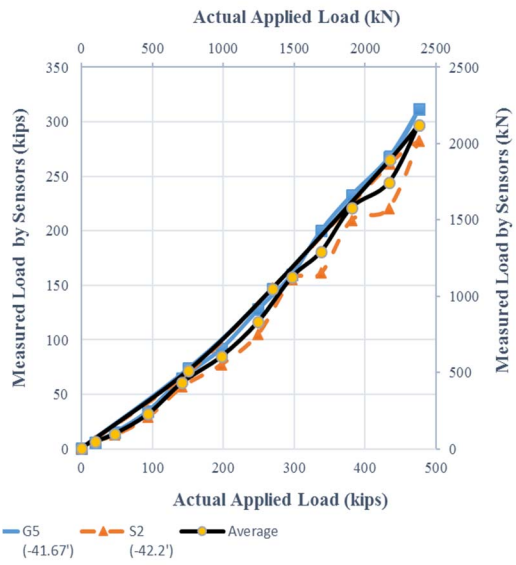


Figure 7c: Geokon loads @-41.67' vs. EDC loads@ -42.2'

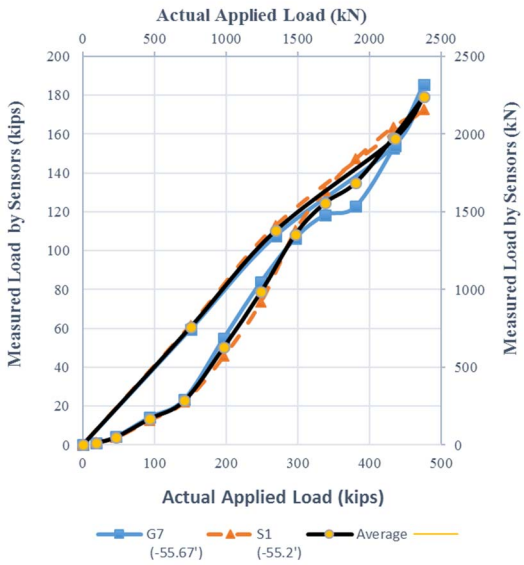


Figure 7d: Geokon loads @-55.67' vs. EDC loads @ -55.2'

- The average unit skin friction was computed between two consecutive levels of strainmeters by subtracting the load transfer computed from corresponding strain gages and a summary was presented in Table 4.

Table 4: Unit Skin Friction (ksf) calculated from loads measured by Geokon and EDC sensors

Actual Applied Load (480 kips/2135 kN)	**Unit Skin Friction from Geokon and EDC Sensors**			
	Geokon		**EDC**	
	Midpoint Between Sensor Elevations feet (meter)	**Unit Friction ksf (kPa)**	**Midpoint Between Sensor Elevations feet (meter)**	**Unit Friction ksf (kPa)**
	Overburden	~0.0 (0.0)	Overburden	~0.0 (0.0)
	-24.17 (-7.37)	1.99 (95.2)	--	--
	-31.17 (-9.48)	1.88 (90.01)	-31.5 (-9.60)	2.42 (115.87)
	-38.17 (-11.63)	1.05 (48.35)	-40.2 (-12.25)	1.66 (79.48)
	-45.17(-13.76)	1.79 (85.7)	-48.7 (-14.84)	1.79 (85.7)
	-52.17 (-15.90)	2.02 (96.72)	--	--

- Geokon sensors predicted slightly lower skin friction values than EDC sensors at several sensor locations as identified in Table 4.

- At 480 kips (2135 kN) load increment, the unit skin friction measured from Geokon and EDC sensors were 2.02 ksf (96.7 kPa) and 1.79 ksf (85.7 kPa), respectively. The load measured at S1 and G7 sensor locations include the combination of end bearing and skin friction between these sensor locations and pile tip.
- Therefore, the skin friction from these sensor locations was projected to the pile tip elevation by assuming the same unit friction.
- The net load transfer/end bearing to the pile bottom based on Geokon strainmeter readings was 90 kips (400 kN) (185.5 kips in load at G7 – (3.14 * 1.5 feet *2.02 ksf *10 feet) =90 kips).
- The end bearing calculated based on unit skin friction of 1.79 ksf from EDC strain gauges was 88 kips (391 kN) (172.2 kips – (3.14*1.5 feet*1.79 ksf *10) = 88 kips).
- Therefore, the end bearing values predicted based on unit skin friction from EDC/Geokon strainmeters matched well.
- The load displacement for pile top (dial gauge) and bottom (telltale reading) along with Davisson failure line were plotted below in Figure 7.

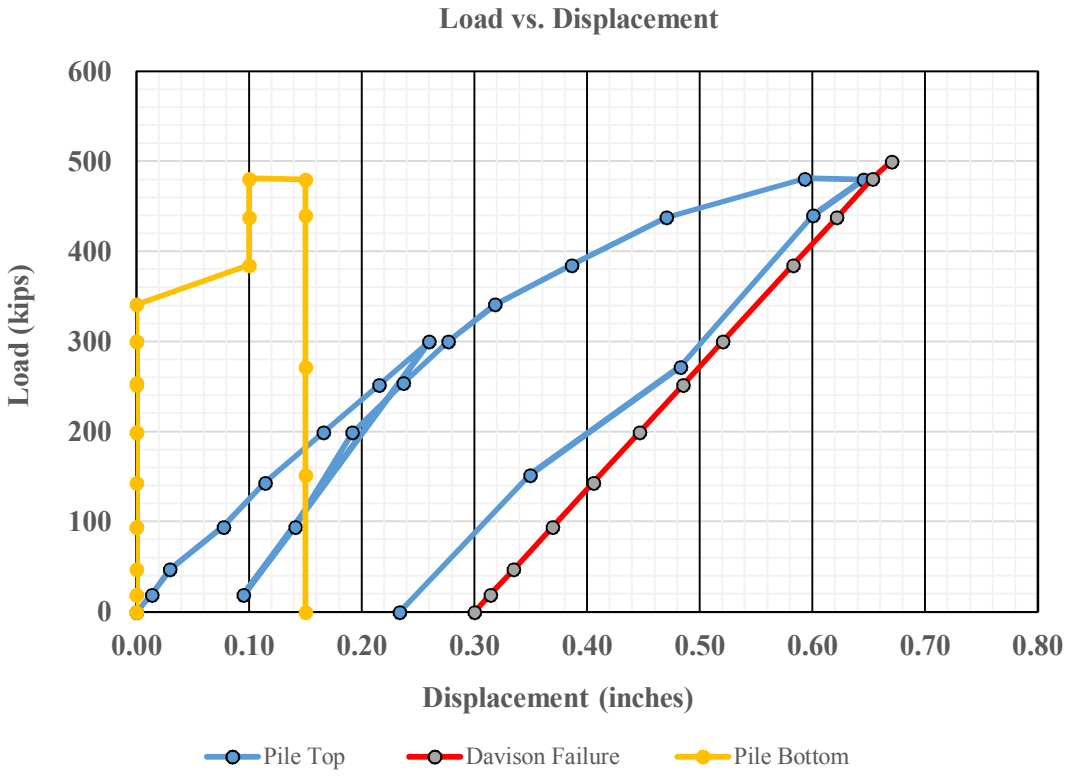


Figure 7: Load Displacement graph along with Davison Failure line for the load test.

- For the applied maximum load of 480 kips (2135 kN), the total movement of the pile was 0.645 inches (16.3 mm), with net permanent pile displacement of 0.23 inches (5.8 mm).
- The telltale reading for the pile bottom showed approximately 0.15 inches (3.81 mm) at the end of the test which was comparable to final pile set of 0.23 inches (5.8 mm).
- Davisson (1972) failure displacement for a maximum load of 480 kips (2135 kN) was 0.65 inches (16.51 mm) which was slightly higher than 0.645 inches (16.38 mm) measured at this load. The fact that the load was transferred to the bottom segment of the augercast pile clearly

demonstrates that the skin friction on the upper segments of the pile was completely mobilized during the test.

CONCLUSIONS

Based on axial compression load test results and strain measurements from Geokon and EDC gauges, the following were our conclusions:

- The loads calculated from strains measured with EDC and Geokon sensors at each location and the estimated concrete elastic modulus from empirical formula of $E_c = 57000 \sqrt{(fc')}$ (ACI 318-08, 2008) yielded consistent results.
- As expected, load measurements from Geokon rebar strainmeters (G1 and G2) and EDC strain gauge (S4) measurements at cut off elevation of EL. -22.5 feet (-6.85 m) matched well with applied jack load (within casing no loss of load was anticipated from skin friction)
- Loads measured by Geokon and EDC gauges at approximately similar sensor elevations matched well in general, with variations between 5 to 15 percent. The measured load difference between EDC and Geokon sensors reduced to 5 percent as the load increments increased to 480 kips (2135 kN) (highest load application).
- The estimated end bearing capacity by projecting the unit friction computed from EDC (S1) and Geokon (G7) sensors matched well and were within 5 percent (90 kips (400kN) from Geokon vs. 88 kips (391kN) from EDC gauges).
- It was found that EDC sensors had an advantage over traditional vibrating wire rebar strain meters for their ability to measure both static and dynamic strains and their ease of use in wireless data collection.
- The difference in transferred loads measured using both the systems (Geokon and EDC sensors) can possibly be attributed to slight variation in their corresponding locations and concrete modulus from empirical formula used for converting the strains measured from EDC sensors embedded in concrete as well as Geokon strainmeters welded to rebar.
- The use of EDC sensors supplments the static load test as these sensors can also be embedded in production piles and their capacity can be ascertained utilizing dynamic testing methods and further determine the applicability of static load test results across the project site at a small cost.
- Overall, static strain measurements using EDC strain gauges were in-line with traditionally used Geokon strainmeters and therefore, can be a viable alternative for future projects.

REFERENCES

Davisson, M.T. (1972) “High capacity piles” Proceedings, Lecture Series, Innovations in Foundation Construction, ASCE, Illinois Section, 52 pp.

American Concrete Institute (A.C.I) Committee (2008), Structural Building Code: American Concrete Institute (A.C.I 318-08), Code Section 8.5.1 Modulus of Elasticity, PP107.

Geokon. (2013). Rebar strainmeter: for measuring strains in foundation, slurry walls, etc. Retrieved from http://www.geokon.com/content/datasheets/4911-4911A_Rebar_Strainmeter.pdf

Smart Structures (2010). Embedded Data Collectors (EDC) to perform both dynamic load testing and determine load transfer in foundation, slurry walls, etc. Retrieved from http://smart-structures.com/technology/EDC-embedded-data-collector/index.html

CFA PILE DESIGN PARAMETERS IN SAND

Stuart Coutts
Belpile

ABSTRACT: This paper presents an overview of the author's experience related to the assessment of the base capacity of straight shafted and enlarged-base bored piles in sand. A design approach based on CPT q_c is described which has been calibrated using a database of load tests. The importance of correct installation techniques with instrumentation are illustrated and a discussion is presented on the current use of high strain dynamic testing to validate compliance with design. An example of a recent project with high quality instrumented load test data illustrates the close match to the proposed best practice approach and also highlights the importance for consideration of the effects of stress relief for deep foundations installed in deep excavations.

1 INTRODUCTION

Continuous Flight Auger (CFA) piles are the bored foundation pile of choice for sand deposits across Australia. The evolution of the determination of the base resistance of CFA piles has been shaped by available investigative techniques, calculation methods, and calibration of designs with laboratory and field testing. The Cone Penetration Test (CPT) has been widely used in Western Australia (WA) where the test has been commercially available via multiple contractors for more than 25 years. On the East coast, the adoption of CPT testing has been slower with a transition from traditional Standard Penetration Testing (SPT) still occurring. Dynamic pile load tests are often used to derive parameters.

The influence of pile installation on performance is commonly misunderstood and is an important element on any discussion of pile capacity for CFA pile types. The interface between the base of the constructed pile and the in-situ soil has an influence on capacity such that a poorly constructed pile base will have limited (if any) contribution to pile performance within the normal working range, generally within a 10 mm movement. The research presented in this paper pertains to CFA piles (no drilling fluids) and enlarged base piles constructed using CFA techniques under drilling fluids such that clean pile/base interface is targeted. Developments in modern piling equipment and instrumentation allow the pressure and volume of delivered concrete/grout to piles to be accurately monitored at various stages of installation such that repeatable 'best practice' can be achieved. The changes in soil conditions that occur due to the disturbance of the install technique are also important.

Although the results of this research are likely applicable to bored piles, the interface between the pile and in-situ soil (shaft and base) need to be considered for various installation techniques. The effects of stress relaxation (due to removal of soil above pile base and adjacent shaft), time to concreting, and the zone of disturbed soil around the pile shaft are paramount.

2 INSTALLATION CONSIDERATIONS

The pile mix (concrete/grout) and interface with the in-situ soil are also an important consideration. For example, coarse grained, poorly graded, dry, clean sand will be partially permeated by most pile mixes; such that the influenced soil will be enhanced and in instances the overall effective pile dimensions increased. Permeation of the disturbed zone of a pile or anchor shaft along with scale effects (Lehane 2009) can have significant effect on shaft capacity and shaft frictions significantly exceeding expected are not uncommon based on 'theoretical' dimensions. Advancements in mix technology and mix techniques also have a large influence on the pile/soil interface. The ability of the piling rig and augers to excavate a plumb and gauge hole can also have a large influence on the zone of soil disturbed adjacent the constructed pile with a resulting influence on capacity.

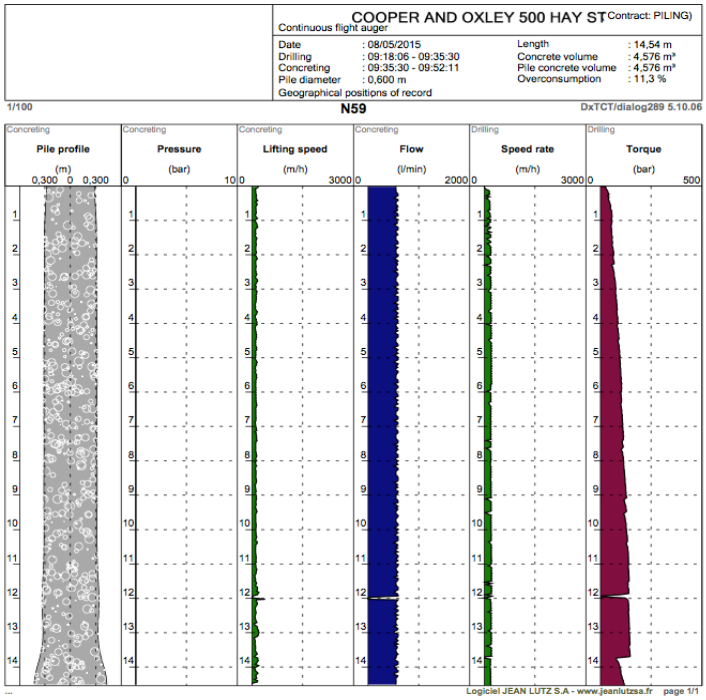


Figure 1. Example of remote access (live) instrumentation

The author believes best practice for a well constructed CFA pile base is to over-drill the pile base once pressurised delivery of concrete/grout has commenced. The objective is to minimise disturbance (stress relief) of the in-situ soil near the pile tip utilising the pressurised pile mix. Pre-instrumentation, it was not uncommon for some rig operators to consistently deliver higher base resistances on a test piles than other operators.

3 BASE CAPACITY DETERMINATION

The Standard Penetration Test (SPT) and corresponding design methods rely on a derivation of a bearing capacity factor from an assessed soil friction angle. This bearing capacity factor is multiplied by the effective overburden stress at the pile base to determine ultimate end bearing stress; this approach is described by Berezantsev *et al*. (1961) and others. The calculated capacity is an ultimate capacity consistent with a large strain bearing capacity failure and hence a large pile base movement. There is considerable scope for error with this calculation method in that a small error in the assessment of friction angle can result in a magnified error in derived bearing capacity (N_q). Inherent problems also occur with derivation of parameters based on SPT as reported by de Mello (1971).

Inconsistent with general International practice, the derivation and proof of capacity in Australia is often solely via modified high strain dynamic tests that were originally intended for evaluation of preformed driven piles. In numerous sand soil profiles compliance with AS2159 (1978, 1995, and, 2009) has often not been met in that the applied blow is insufficient to fully mobilize pile capacity because the magnitude of the blow would induce cracking and permanent pile damage. Commercial pressures have seen an increase in the application of dynamic tests such that deflection response and base capacity are being predicted with little or no calibration to static tests. The Australian Standard, AS2159, is clear on the limitations of dynamic testing and is consistent with international practice including that detailed in the federation of Piling Specialists Handbook on Pile Load Testing February 2006 (UK).

High strain dynamic tests can readily be performed on CFA piles in sand and they offer clear benefits in terms of time and cost savings, when correctly utilised. However, it is considered by the author, that predominant current Australia practice of using dynamic tests as the principle proving test for CFA piles is highly flawed and inconsistent with best international practice.

The University of Western Australia (UWA) has progressively established one of the world's largest geomechanics research centres with associated testing facilities such as drum and beam centrifuges and state-of-the-art laboratories. A significant research effort into understanding the behaviour on bored piles in Perth sands began with the UWA thesis of Coutts (2000), who describes research into the uplift capacity of a new enlarged-base bored pile. The shaft is constructed using conventional CFA techniques but it has the added enhancement of an enlarged base, which is created using a belling tool and drilling fluid. The methods available at that time to determine axial capacity of this pile type yielded a large variance in predicted capacity. The resulting research examined the failure mechanism in sand and derived capacity predictions related to the CPT.

Continued development of commercial applications of enlarged base and conventional CFA piles associated with R & D at UWA has resulted in some notable publications e.g. Lehane (2009), Le Viet & Lehane (2016). Initial research utilized multiple centrifuge tests (more than 100 No.) calibrated with full-scale load tests to derive design methods. Over the past 15 years, a large number of full-scale load tests have been carried out on conventional and enlarged base piles with several tests utilizing multiple strain gauges to assist in assessment of the relative contribution of the shaft and base to stiffness and capacity.



Figure 2. Prototype pile exhumed from ground

Since the mid 1980's an ongoing database of soil conditions and tests has been used to develop correlations between CPT tests and appropriate design parameters. More recent research has concentrated on the prediction of shaft and base parameter selection based on CPT data. Predictions of capacity are now typically within 10% of actual results from load tests. Deflection responses are also being accurately predicted.

There are large differences between calculation methods employed by various consultants and piling contractors, with difference of up to 300% not being uncommon. In the majority of instances designed solutions are not calibrated with static load tests. High strain dynamic tests are often solely used to validate designs. In many instances low partial factors of resistance (ϕ_g) values are combined with overestimates of base capacity and this practice leaves clients with the impression that designs are conservative. A review by the author of pile displacements induced in dynamic tests

indicates that these are often insufficient to mobilise an appreciable proportion of the end bearing. As a consequence, the extrapolation to displacements at which base capacity is defined is highly uncertain.

The accurate derivation of end bearing parameters is less critical when the base capacity represents a small proportion of capacity. However, recent failures in WA have highlighted the significant over-prediction of base capacity in sand as 'Industry norm'. This paper will present appropriate design parameters that are based on the R & D conducted by the author's piling company using experiences gained in over 1200 commercial piled projects, many of which incorporated load testing (static and dynamic). Parameters for shaft resistance are not discussed although it is noteworthy that the variance between the results of this research and Industry norm tend to be less pronounced when deducing shaft capacity.

A number of high strain dynamic tests have been carried out by the author in parallel with static tests; across a range of sand sites and with a range of CFA pile types including enlarged base. The objective has been to calibrate dynamic testing to increase use as a proving tool. The objective was the commercial windfall that comes with a more economical method of determining pile performance. Despite a significant body of work over more than 20 years working with industry experts such as CMR Testing, Professor Mark Randolph and Professor Barry Lehane, the ability to use a high strain dynamic test on CFA piles as a stand-alone proofing method has proved problematic.

Following a visit to the UK in the late 90's the author met with testing and design personnel from piling and testing organisations across the Industry. Similar conclusions had been arrived at based on significantly larger bodies of work.

Fleming and England (2001) carried out more than 2000 static load tests with significant effort to calibrate pile capacity to dynamic testing. The outcome was the recommendation that dynamic methods are unsuitable for assessing the base capacity for bored/CFA pile types, and that the static pile base characteristics are best modelled using static test methods. Fleming found that this is primarily due to rate effects. The faster the loading rate (as in a dynamic test), the higher the over-prediction of base stiffness and (by extrapolation) the higher the inferred base capacity. It is noted here that base capacity in compression is defined at a base movement of 10% of the pile base diameter. At this movement, the base stress is largely controlled by the stiffness of the sand and is not controlled by a large scale bearing capacity (shear failure) mechanism.

The author appreciates the benefits that dynamic testing offers and believes that the test provides a relatively quick and inexpensive method of carrying out pile capacity verifications. However, the use of a dynamic test as a stand-alone method to determine base capacity for CFA piles is incorrect and reckless. This is a message that has been delivered to the Australian Piling Community at National conferences on numerous occasions.

4 FAILURE MECHANISM

Figure 3 illustrates the failure mechanism around a model pile with an enlarged base in dense sand. The testing was carried out utilising the UWA centrifuge facility. The objective of using a centrifuge is that small scale tests can be carried out under a higher gravitational force. This ensures that tests are performed at typical in-situ stress levels, hence avoiding well known scale effects associated with 1g model tests. The flow-around type of sand movement at large pile base displacements is clearly evident; this mechanism is not consistent with the traditional N_q type formulations mentioned previously.

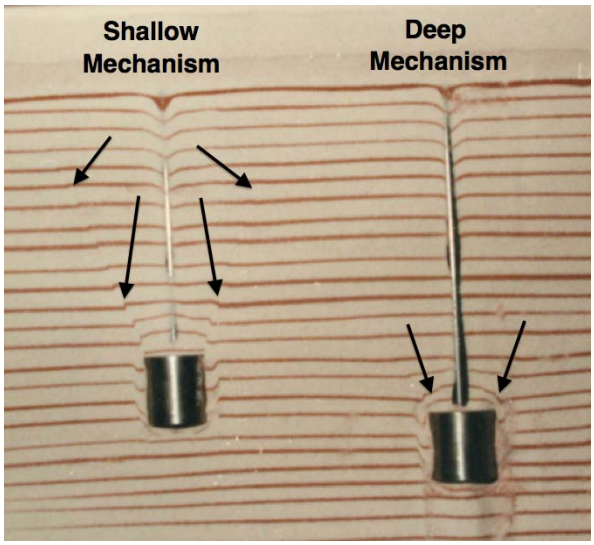


Figure 3. Photo of failure mechanism around enlarged-base pile

The photo was the result of trial and error to identify the failure mechanism and involved a complex process of sample preparation, testing, post test preparation and removal of a section/slice of the tested matrix to expose the disturbed sample. Consistent with prior research a 'critical' embedment was identified whereby the failure mechanism changes from failure that connects to the surface to a local 'cavity expansion' type failure. Coutts (2000) proposed a material flow mechanism around the enlarged base as the base is displaced.

The model testing was used to derive a rational design basis for the assessment of the uplift performance of enlarged base piles. Figure 4 shows a computer generated stress profile around an enlarged-base pile tested in compression. Studies such as this are used to assess optimum enlarged base configurations for compression and tension applications.

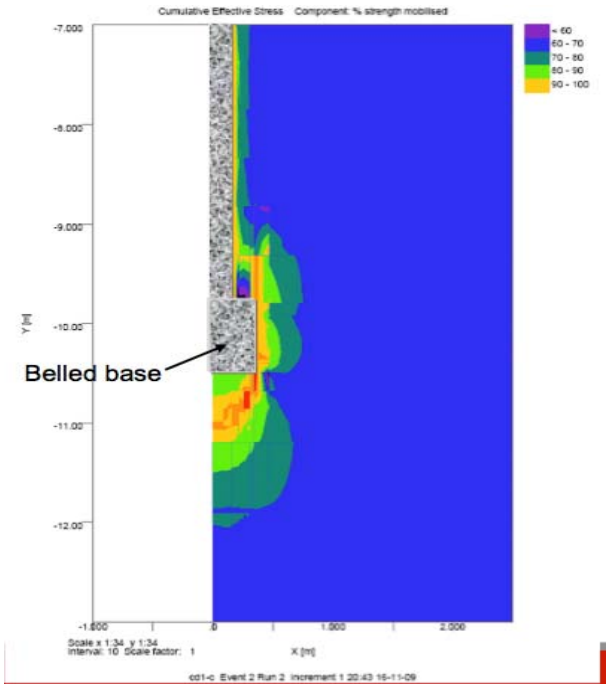


Figure 4. Mean effective stresses around enlarged base pile

Deflection is often ignored in pile design with focus on capacity. Working loads that give acceptable settlements are often derived by applying a suitable factor to capacity. Interestingly, many designers/contractors assume that this factor is ϕ_g, which is the required AS2159 factor on the ultimate limit state. AS2159 explicitly requires an independent assessment of pile settlement under working loads. An intrinsic risk with application of a global factor to derive an acceptable working load is that an over-estimate of end bearing will result in a higher proportion of available capacity on the pile base leading to significantly larger than predicted movements. The author has commonly observed, for example, that over-prediction of base capacity by a factor of 2 can result in pile deflections at working load that are up to 10 times those obtained using a reasonable estimate of base capacity and stiffness. Pile testing should reflect the information desired and as such load settlement at working load levels is essential for design.

Along with SPT correlations, the remaining soils investigation tools common to the Australian SI environment for sands comprise seismic methods, pressuremeter and CPT. Seismic methods utilise a bulk sample to generate a small strain stiffness modulus. This technique is useful but is generally only of direct use in design when assessing the effects of interaction of piles in pile groups on the overall group settlement. Pressuremeters are useful research tool but are expensive, while SPT N values are prone to error due to drilling disturbance and due their operator dependence. The CPT is therefore the most reliable test where correlations can be obtained for bored/CFA piles in sand.

5 CPT METHOD

The CPT provides a continuous sounding over the pile depth and to a suitable depth below pile tip encompassing the influence zone of the pile base. Most published design methods for CFA piles in coarse grained soil assume a proportional relationship between q_c and the end bearing (q_b) i.e.

$$q_{b0.1} = \alpha_b \; q_{c,avg} \qquad (1)$$

where $q_{b0.1}$ is the ultimate end bearing resistance defined at a pile base displacement of 10% of the pile diameter and $q_{c,acg}$ is an appropriately averaged q_c value in the vicinity of the pile tip. Work by Lehane (2009) resulted in the revised 'best fit' expression deduced as:

$$q_{b0.1} = (2.4 \pm 0.7)\; q_c^{0.5}\; \sigma'_v{}^{0.25}\; p_a^{0.25} \qquad (2)$$

where p_a is reference stress taken equal to atmospheric pressure (=0.1 MPa) with the same units as those employed for q_c and σ'_v. The design method is supported by a database of pile tests in Perth sand and by the numerical analysis of wished in place piles in normally consolidated sand. The effects of over consolidated aged deposits, which may be expected to be appreciably stiffer will result in higher values than equation 2 calculates. Figure 5 shows the correlation between theorectical and actual predictions based on the Lehane method combined with Belpile database of tests.

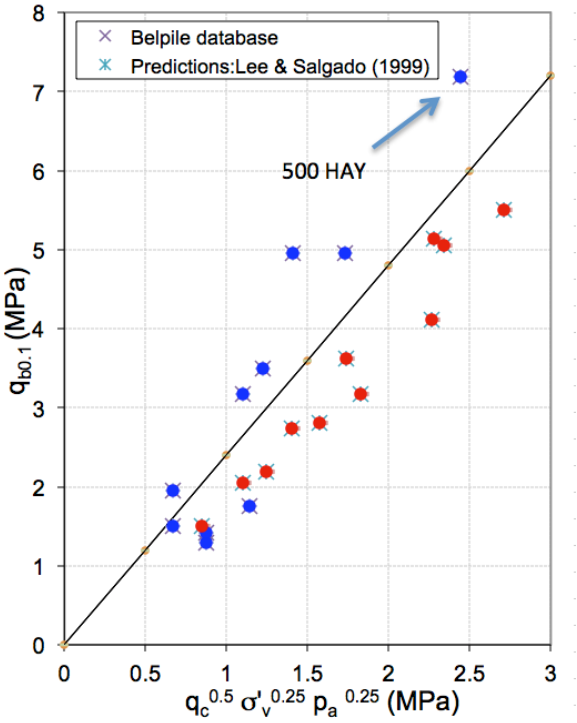


Figure 5: Relationship between $q_{b0.1}$, σ'_v and q_c

6 CASE HISTORY: PILES IN EXCAVATION

It is instructive to consider a typical case history performed by the author's piling company, Belpile Pty Ltd. Numerous 'Top-Down' construction projects have been delivered by Belpile and one of the often ignored characteristics with this type of construction is its sensitivity to the settlements of individual piles. The structural rigidity that arises naturally with conventional 'Bottom-Up' construction tends to reduce effects of differential stiffness of piles. For 'Top-Down' construction, there is a higher proportion of dead load on the piles for a given level of structural rigidity and hence greater sensitivity to differential pile settlements.

A recent project at 500 Hay Street, Subiaco in Perth was performed by Belpile and involved a revision of the pile design method to allow for the stress relief associated with excavation for a three level basement after the test pile was completed and the contract piles were constructed.

An initial prediction of the change in pile load settlement behaviour post excavation was undertaken using finite element (Plaxis) analysis. Due to a large established database of full scale load tests correlated with CPT q_c values, the preferred approach was to assess the CPT profiles pre/post excavation and assess the accuracy of current empirical correlations. The basis for prediction of the change in CPT value employed was the following relationship proposed by Jamiolkowski et al (1985) for normally and overconsolidated silica sands:

$$D_r = \frac{1}{2.93} ln\left(\frac{q_c}{205p'^{0.5}}\right) \qquad (3)$$

Where q_c and p' are expressed in kPa and p' is the mean effective stress derived using an estimate in-situ K_0 value. The sand at Hay St. could be assumed to be initially normally consolidated and therefore the K_0 profile after excavation can be deduced from equation (4) after Mayne & Kulhawy (1982):

$$K_0 = (1-\sin\phi')\ OCR^{\sin\phi'} \qquad (4)$$

where the sand friction angle, ϕ', was taken equal to 35° and the overconsolidation ratio (OCR) was calculated as the ratio of the pre-excavation vertical effective stress (σ'_{v0}) divided by the post-excavation, σ'_v. p' for input to equation (3) is then determined as:

$$p' = (1 + 2K_0)\ \sigma'_v/3 \qquad (5)$$

It is noted that the relative density before and after excavation can be assumed to be the same due to the high incompressibility of sand

To assess the applicability of this approach, CPTs were undertaken from the pre-existing ground levels and compared to those undertaken at both basement 1 (5m deep) and basement 3 level (11m deep). Test locations were selected to ensure an adequate distance was maintained from edge of excavation. Testing was undertaken 3-4 weeks minimum post excavation to ensure time dependent effects were minimised.

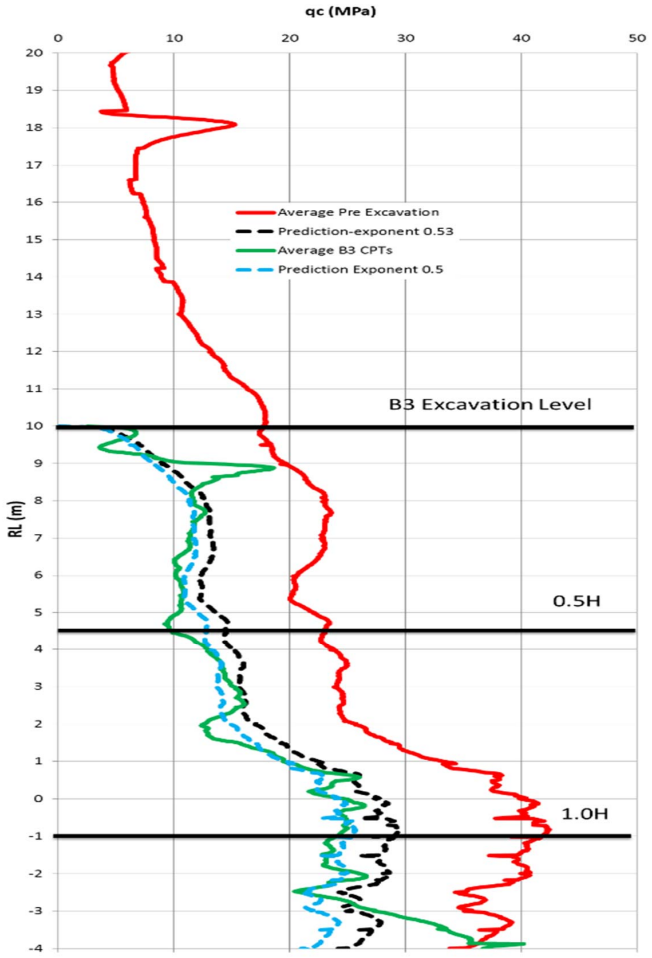


Figure 6. CPT reduction due to excavation

Figure 6 compares the pre/post excavation q_c profiles for the 2 excavation depths while Figure 7 compares the post excavation qc values with those predicted using the prediction approach outlined above. The following observations are made:

- The results of the basement 1 testing (5m) suggest a slightly higher exponent of 0.53 in equation (3) provides a better match to the post excavation q_c value, while the B3 testing suggests the original formulation provides a more accurate prediction.
- Predictions appear to be more reliable over a depth equivalent to the height of excavation (1H).
- On this particular site, variable cementation below RL1-2 results in poorer predictions at greater depths.

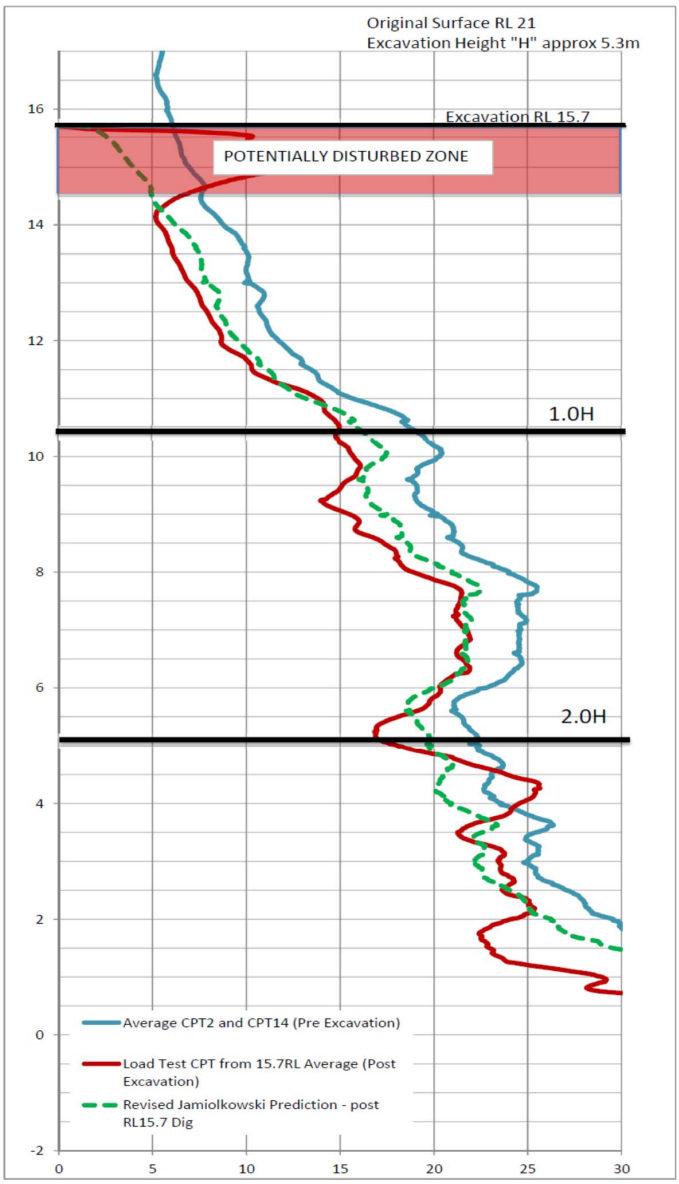


Figure 7. Measured and predicted post excavation CPT q_c values

Following such a significant change in overburden, there was a doubt as to whether Belpile's establish shaft and base correlations would provide valid prediction of pile performance. To assess this an instrumented full scale static load test was undertaken from the basement 1 level. Back calculation of pile strain gauge data indicated a slight increase in the α_b factor (equation 1) could be justified when used in conjunction with the reduced q_c profile. Importantly, if the original q_c was employed, with no account taken of stress relief, the base stiffness and capacity would have been over-estimated leading to larger pile

7 CONCLUSIONS

(i) Proving the base capacity for CFA piles in sand in Australia using Dynamic Testing leads to over-optimistic assessments of base stiffness and capacity, due to the need to extrapolate records to a pile settlement of 10% of the pile diameter.
(ii) CPT testing provides the best stand-alone SI tool for evaluating CFA pile capacity in sand with the method of Lehane (2009) providing a good approximation of the base resistance of a well-constructed CFA pile.
(iii) Consistent with International practice and the intent of AS2159 (Australian Piling Code), static load tests need to be carried out to validate design parameters for CFA pile design with focus on deflections being paramount.

8 REFERENCES

Berezantzev V.C., Khristoforov V. and Golubkov V. (1961). Load bearing capacity and deformation of piled foundations. Porc. 5th Int. Cof. On Soil Mech. and Found. Engineering, Paris, 2, 11-15.

Coutts S. G. (2000) The uplift capacity of an enlarged base pile in sand. MSc thesis, University of Western Australia.

De Mello, V. F. B., 1971, The Standard Penetration Test. *Proc 4th Panamerican Conference on Soil Mechanics and Foundation Engineering*, 1: San Juan, pp. 1–86.

Fleming K., Weltman A., Randolph, M. and Elson K. (2009). *Piling engineering*, Taylor and Francis, CRC press, London.

Jamiolkowski, M., Ladd, C. C., Germaine, J. and Lancelotta, R. (1985). New developments in field and laboratory testing of soils. *Proc. 11th Int. Conf. on Soil Mech. Found. Engng*, San Francisco, 1, 57–153

Lehane B.M. (2009). Relationships between axial capacity and CPT q_c for bored piles in sand. Keynote Lecture, *Proc. 5th International Symposium on deep foundations on bored and auger piles*, Ghent, 1, 61-76, Taylor Francis Group, UK.

Mayne, P.W., and Kulhawy. F.H. (1982). K_0-OCR relationship in soil. ASCE Journal of the Geotechnical Engineering Division, 108: 85 1-872.

Viet Doan, L. and Lehane, B.M. (2016). The influence of pile diameter on the relationship between the unit shaft friction of bored piles in sand and the CPT end resistance. *Proc. 69th Canadian Geotechnical, Geo-Vancouver*, October 2016

DEEP-SEA QUAY WALL FOR OFFSHORE WIND ENERGY TERMINAL ON MAASVLAKTE 2 ROTTERDAM – NL

Author: Patrick van der Schaaf Bsc Eng.
Manager Business Development Woltman Piling & Drilling Rigs, Dieseko Group
Sliedrecht, The Netherlands
Phone +31 184 430900
Email p.vd.schaaf@woltmanrigs.com

ABSTRACT

During 2016, foundation piling works were completed to allow for the construction of a production and storage/handling terminal in Rotterdam. It is there that steel foundations will be produced for offshore wind farms and the oil and gas industry. Several Dutch contracting companies were involved in constructing: foundations for an assembly hall, a barge quay and a deep-sea quay wall. For the hall foundations, cast in situ concrete vibro piles were created. Open ended steel casing piles were also installed due to very high cone resistances which made it impossible to perform cast in situ piles in certain areas. The quay wall was constructed with open ended steel casing piles in combination with sheet piles. A deep-sea quay wall was also constructed to provide enough storage area for the offshore mono piles. This project was unique and challenging due to the use of different foundation technologies in challenging circumstances and soil conditions. This paper will give an insight into the Dutch use of varying foundation piling techniques for deep-sea quay wall constructions. It can be concluded that even experienced local contractors can be surprised by variations in soil conditions. It will also show how the contractors adapted to the difficult circumstances.

PROJECT OUTLINE

The project consisted of a barge quay near the assembly hall with a length of 500 metres, width of 42 metres and a height of 35 metres, and a
deep-sea quay wall 480 metres in length. This paper concentrates on the foundation works for the construction of the deep-sea quay wall. The construction of the deep-sea quay wall consisted of a combination of open ended steel casing piles with a diameter of Ø 1420 mm and a wall thickness varying between 21 and 23 mm. The lengths of the steel casing piles varied between 32 and 37 metres. Between the steel casing piles triple PU 28 sheet piles were installed with lengths varying between 26 and 29 metres. In the Netherlands, a combination of open ended steel piles and sheet piles is known as a “combi wall”. For the deep-sea quay wall a steel combi wall was shored with steel H- section profiles that were driven in a raked position whilst being injected with grout, so called MV-piles. The MV piles for this project consisted of steel HEB 600 sections with lengths from 52 up to 59 metres and were installed with angles varying between 42.5 and 47.5 degrees. For a detailed overview regarding the project specifications reference is made to table 1 which is presented below.

Table 1. Project specifications for the deep sea quay SIF terminal

Description	Number [pcs]	Dimensions [mm]	Lengths [m1]	Steel quality
Open ended steel casing pile	145	Ø 1420 x 21/23	32 – 37	X70
Steel triple sheet pile	145	3 x PU 28	26 – 29	S355GP
MV piles	113	HEB 600	52 – 59	S355J2N

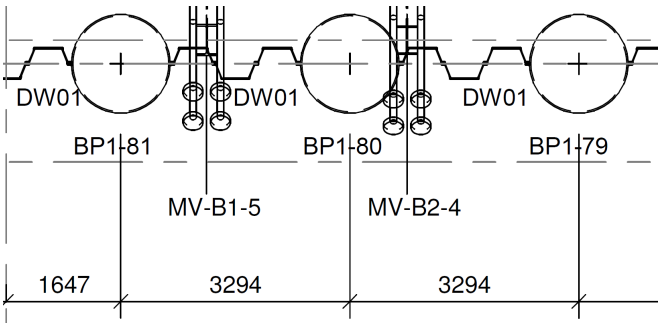


Fig 1. Configuration combi wall

PROJECT APPROACH

The new SIF terminal will be located on a new harbour area in Rotterdam – Maasvlakte II, which consists of reclaimed land. In 2008 land reclaimation works over an area of 20 km2 near Rotterdam started to create a new harbour area located in the North Sea near the already existing harbour area of Maasvlakte I. From this 20 km2 of new land, Maasvlakte II uses almost 10 km2 for sea protection structures and infrastructure such as roads, railways, harbours and harbour quays. The remaining 10 km2 is available for commercial use such as the chemical industry, distribution and container terminals. The new harbour area of Maasvlakte II was designed with a depth of 20 metres specifically for large container ships. This makes it more accessible than the surrounding harbours in Belgium and Germany which have limited depths.

It was its depth of 20 metres that created the challenges in constructing this new wind energy terminal with its deep-sea quay wall. Ordinarily, to construct combi walls it is common to first drive open ended steel casing piles. After the steel casing piles have been installed, sheet piles are driven between the steel casing piles where the clutches of the open ended piles and sheet piles interlock each other. The common working method for deep-sea quay combi walls in the Netherlands is to first drive the open ended steel casing piles with a vibratory hammer until refusal. The remaining part of the open ended steel casing piles can then be driven by a diesel or hydraulic impact hammer. For this project, the open ended steel casing piles Ø 1420 mm were driven with a PVE 110 M vibro hammer which has a maximum centrifugal force of 2198 kN and a maximum frequency of 1350 rpm. The piles were driven to a depth of approximately 24 metres with a vibratory hammer. The remaining part of the piles were driven with a Delmag D-160 diesel hammer.



Fig 2. Installing of open ended steel casings in progress

A smaller PVE 2350 VM vibratory hammer was used to drive the triple connected PU28 sheet piles to the required depth, between the open ended steel casings. Previous project experience at the Maasvlakte I area nearby indentified that waterjetting could support the drive-ability of sheet piles. However, due to the high pore water pressures in the new reclaimed soil layers at the Maasvlakte II project, waterjetting did not provide satisfactory results. For this reason it was decided to perform pre-drilling to a depth of 15 metres in order to support the drive-ability of the PU28 sheet piles. Together with pre-drilling of the sheet pile locations bentonite was poured into the boreholes to reduce the soil friction on the sheet piles and to the support the drive-ability.

DRIVE-ABILITY PREDICTION

Before the start of the piling operations the piling contractor requested that the Dieseko Group performed a drive-ability assessment of the open ended steel casing piles Ø 1420 x 23 mm with a length of 37 metres. For this assessment the ICE-vibro geodrive prediction program was used. With this computer program drive-ability predictions can be made based on the (sheet)pile specifications, pile lengths and soil profile. Based on a representative cone penetration test graph, known as CPT graph, the drive-ability program predicted that with a PVE 110 M vibrohammer the open ended steel casing could be driven to a maximum depth of approximately 24 metres below working level.

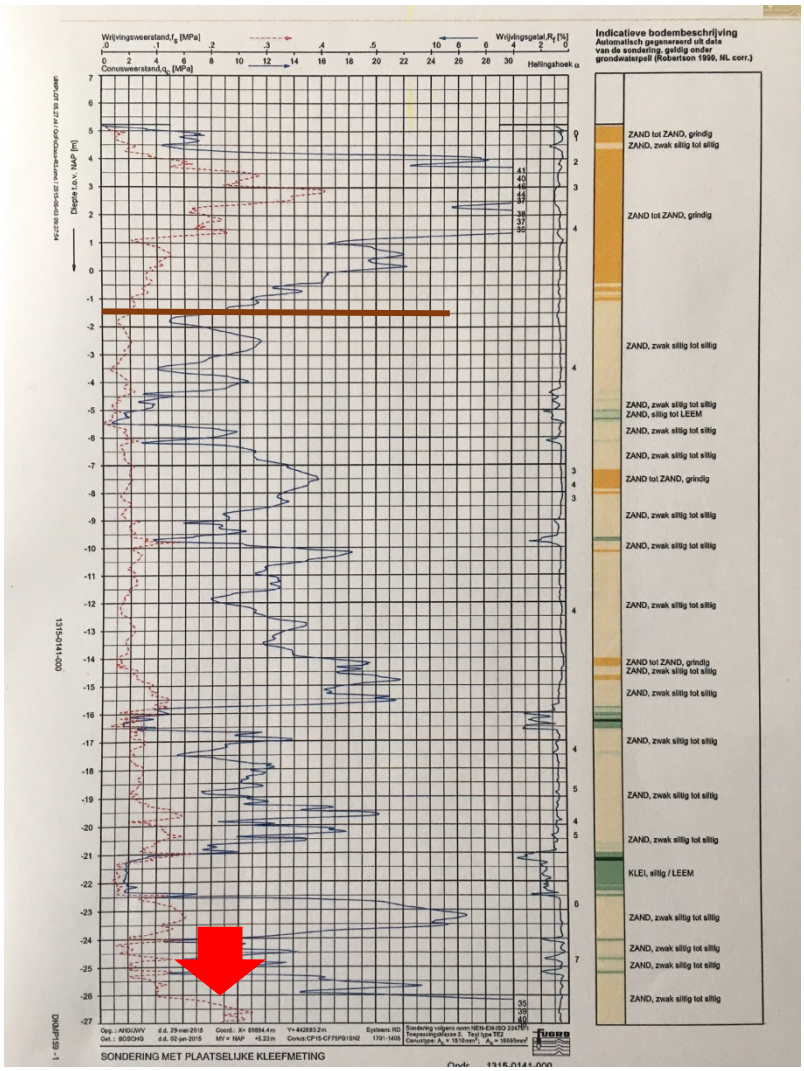


Fig 3. CPT graph

The CPT graphs shows the presence of dense sand layers from NAP +5,0 to NAP 0.0 metres. NAP is the abreviation for Normaal Amsterdam Peil (translated: Normal Amsterdam Level) which is the reference level for height survey levels in the Netherlands. The piling operations for the SIF terminal were performed from a working level of NAP -1.5 metres. Based on the drive-ability prediction that the open ended steel casing piles could be driven to a level of NAP -1.5 minus 24 metres = NAP -25.5 m. This level is marked with the red arrow in the graph. The following figure shows the results of the drive-ability prediction.

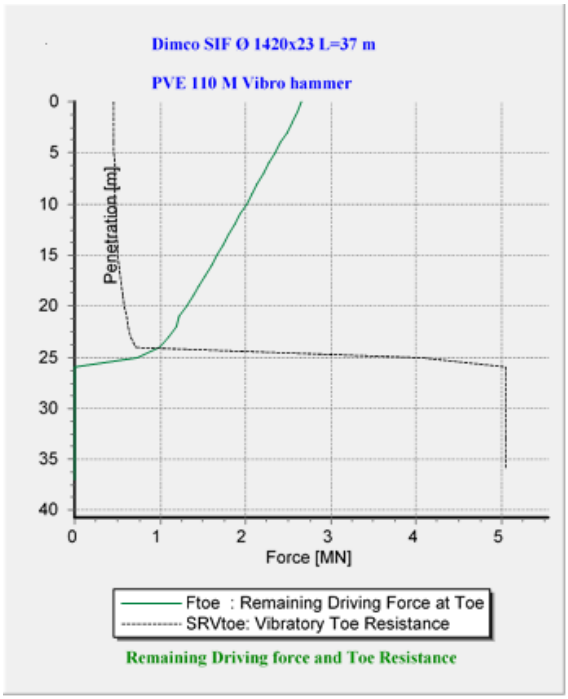


Fig 4. Results drive-ability prediction open ended steel piles Ø 1420 mm

The dotted line in figure 4 indicates the soil resistance at the toe of the casing pile whilst being driven. The second line indicates the remaining driving force at the toe of the pile. The level where both lines cross can be considered as the maximum level for the vibratory hammer to reach with sufficient penetration speed. Below the cross point of the lines at a level of -24 metres, equal to NAP – 25.5 m the penetration speed will drop to a level where this can be considered as refusal. In other words from this point, the vibratory hammer can be switched with a diesel- or impact hammer to continue pile driving to the required pile toe depths, in this case to a level between NAP -34.0 and -39.0 metres.

PILING OPERATIONS DEEP-SEA QUAY WALL

The piling contractor followed a specific work method for installing the open ended steel casing piles and the sheet piles. Working with the drive-ability prediction the piling contractor decided to drive the open ended steel casing piles with a Woltman 160 PR piling rig fitted with a leader guided PVE 110M vibratory hammer up to a depth of 24 metres below working level. With this set-up the first row of open ended steel casing piles was pre-driven into the soil. Another piling rig, a Woltman 1000 PDS equipped with a leader guided diesel hammer Delmag D-160, drove the open ended steel casing piles to the required pile tip level. As a quality check, blow counts of the Delmag D-160 diesel hammer were registered during the driving operations. In general, at pile toe finish level, the blow count over the final 25 cm ranged between 34 and 40 blows. This in relation to CPT values increasing 50 MPa of cone resistance over more than 10 metres depth.

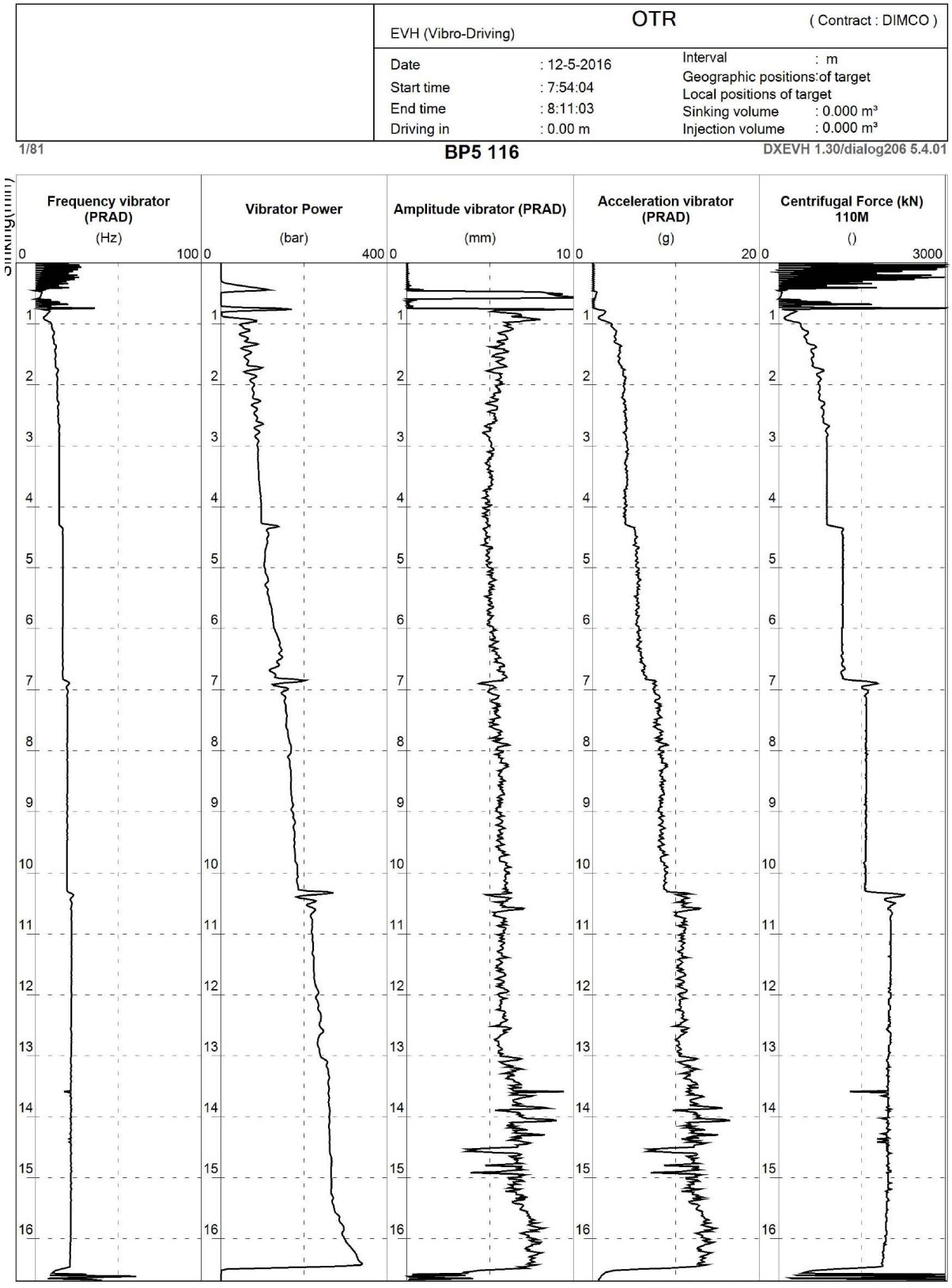


Fig 5. Example of monitoring information during driving open ended steel casing piles

MONITORING

Due to high quality standards on the project, the vibrations from the driving of the open ended steel casing piles with the PVE 110 M vibratory hammer were monitored by electronic registration equipment. The vibrations for driving the sheet piles were also monitored. Figure 5 shows information about the registered driving time, frequency of the vibratory hammer, amplitude, acceleration and centrifugal force for the open ended steel casing piles. Each casing pile and sheet pile was monitored during the operation of piling works. A comparison between the drive-ability prediction and the monitoring results of the open ended steel casing piles is presented in table 2.

Table 2. Comparison drive-ability prediction with monitoring results

Drive-ability prediction	Monitoring results
SRV toe = 500 – 1000 [kN]*	600 - 2000 [kN]
Max. frequency 1350 rpm**	20- 25 Hz = 1200 – 1500 rpm
Max. amplitude 11,5 mm***	6 – 7 mm

Remarks to table 2

* The maximum value of SRV toe is based on the level where refusal is expected

** Max. frequency according the specification sheet of a PVE 110 M vibratory hammer

*** Max. amplitude is the mathematical amplitude of the vertical deflection. Suppliers of vibratory hammers refer to the double value of the amplitude which is 22,9 mm for a PVE 110 M

SUMMARY AND CONCLUSIONS

Despite the piling contractor having prior experience working in the harbour area of Rotterdam the drive-ability of the open ended steel casing piles was predicted before the start of the piling operations. The drive-ability prediction showed that a PVE 110 M vibratory hammer could be expected to drive the open ended steel piles to a depth of approximately 24 metres. After reaching that particular depth they were advised to drive the casing piles to the required depth by a diesel- or impact hammer. During pile driving with a vibratory hammer the performance was monitored by an electronic measuring system. With this system it was possible to read the driving time, frequency, driving force and amplitude. When the drive-ability prediction was compared with the monitoring results it showed that the prediction was quite reliable. The open ended steel casing piles were driven with a vibratory hammer to a depth of approximately 24 metres below working level. The type of vibratory hammer suggested - a PVE 110 M, was sucessful in driving the piles to the predicted level. To ensure an efficient piling operations the piling contractor switched to piling rigs and drove the remaining part of the open ended steel casing piles with a Delmag D-160 diesel hammer. The blow counts at the pile toe levels varied between 34 and 40 blows per 25 cm indicating that the diesel hammer had sufficient energy for this purpose and therefore was suitable for the job. For driving the PU28 sheet piles no drive-ability prediction was performed prior to the piling works. Based on local experience the piling contractor decided to use a PVE 2350 VM vibratory hammer for driving the sheet piles, combined with pre-drilling in combination with bentonite filling. Although waterjetting is a common solution in that particular harbour area it turned out that for this project this method was unsuccesful due to the recent land reclamation works causing high pore water pressures. Nevertheless the piling contractor was able to adapt to the challenging circumstances and executed the piling works in a succesful and efficient way. However, for future projects, it may be advantageous to also predict the drive-ability of the sheet piles. Monitoring results can also give valuable information about the piling works.

REFERENCES

Paul van den Berg, personal communication, September 19, 2016, Company: DIMCO, City: Dordrecht NL, E-mail: van.den.Berg.Paul@deme-group.com, phone +31 (0)78 632 10 20

Martijn van der Biessen, personal communication, September 19, 2016, Company: DIMCO, City: Dordrecht NL, E-mail: van.der.biessen.martijn@DEME-group.com, phone +31 (0)78 632 10 20

Jan Kees Klippel, personal communication, July 15, 2016, Company Hakkers, City: Werkendam NL, E-mail: jkk@hakkers.com, phone +31(0)183 - 50 11 22

Mark Meeuwsen, personal communication, January 11, 2017, Company: MUC, City: Terheijden NL, E-mail: M.Meeuwsen@bv-muc.com, phone +31(0)76 5933450

Reference list

Vibro technology and how a vibratory hammer works 2014, Company: Dieseko Group, City: Sliedrecht NL, E-mail: info@diesekogroup.com, phone +31 (0) 184 410 333

DYNAMIC PILE TESTING FOR THE FIVE MATES BRIDGE

Jonathan G Cannon, Independent Geoscience Pty Ltd, Melbourne, Victoria, Australia,
indgeo@optusnet.com.au

ABSTRACT

This paper will describe dynamic pile testing conducted during installation of driven octagonal precast prestressed concrete piles used as the foundation for this bridge. The piles were long and hence spliced. A number of the piles showed damage near the splices and the damage location was near the ground surface so that the damage could be verified using visual inspection. The piles and splice configuration are still in use today without modification. Further WEAP driveability analysis has been conducted which demonstrates the effect of the splice on pile stresses and a likely failure mode. A slight modification is proposed to the splice that should prevent the damage on future projects.

Key words: Prestressed concrete piles, dynamic pile testing, damage, stresses

INTRODUCTION

The bridge site is located on the Olympic Way, Route 41, about 20km north of the regional centre of Albury, NSW. For a long distance north of the site the Olympic Way "shadows" the main Melbourne to Sydney rail line and is located on the Western side and in close proximity. At the bridge site there was previously a sharp dog-leg in the road and a right angle level crossing with the road changing to the Eastern side of the rail line, eventually joining up with the Hume Highway, which in turn now becomes a ring-road through the eastern outskirts of Albury. The dog-leg and rail crossing had warning signs and bells, speed restrictions and rumble strips to warn approaching motorists to reduce speed. Site distance was exceptionally good.

Approximately 2years before construction a group of five "high spirited" young men from the local area were driving south on the Olympic Way adjacent to a south-bound train. It is understood they interacted with the train crew for a period of time. Unfortunately the car and train collided at the level crossing and all of the young men were killed. There were outpourings of grief in the local community and a decision was made to replace the level crossing with a road-over-rail bridge.

The bridge was highly skewed with two piers and two high level abutments with fill embankments on both approaches.

GROUND CONDITIONS

The site is open grazing country with approximately level ground at the site with surrounding low hills. The geology was unremarkable with consistent stiff clays for a considerable depth.

The design required driven precast prestressed pile foundations with the piles to be driven to a considerable depth.

Hard driving with high tension stresses were evident from the start of driving and a variety of different pre-bore lengths were adopted in an attempt to minimise driving and potential for damage. At the abutments the pile locations were predrilled for at least the full embankment depth.

PILES

The piles were 550mm octagonal prestressed concrete with the pier piles being single piece and the longer abutment piles being two-piece with a "standard" epoxy glued box splice. Pier piles and the initial length of the abutment piles were 24m. The add-on piece used at the abutments was 12m. Pile concrete was grade 50MPa.

The pile prestress was provided by 15.2mm wire tendons tensioned before the casting of concrete and then released after curing and cut at the ends of the piles. Consequently there is a short length at the ends of pile where the prestress is not fully transferred and the concrete is not effectively "protected" by the prestress. Some text book estimates show prestress is not fully transferred until 50diameters (760mm) but others suggest this could be much greater – even 70% greater (1292mm).

The piles had a higher than normal prestress of 12.9MPa and also had a greater than normal content of longitudinal reinforcing, which extended full length.

SPLICE DETAIL

The "standard" pile splice is a glued epoxy box splice that was very strong and apparently designed for full strength in compression, tension and bending, however there was still a contractual requirement for the splice to be located at least 5m below ground at the end of driving. The splice comprised an external galvanised steel sleeve or box that was 10mm wall thickness and two metres in length, being a metre on each section. There were also six 38mm dowel bars and the pile section within the joint had a doubling of the longitudinal reinforcing. The dowels and extra reinforcing stopped at the same location as the steel sleeve, being 1m from the end of the pile section. The dowels were cast into the top pile sections and epoxy glued into the bottom pile section. The steel sleeve was glued to both top and bottom pile sections. The box was glued to the bottom pile section before the top pile section was placed.

It is understood the tension was to be carried along the pile length by prestress and the longitudinal reinforcing. At the joint the tension has to be transferred through the dowels and the external box. If the transfer of prestress is the longer of the estimates above, then there is a small zone beyond the splice of 200-300mm that is not fully "protected" from tension by the prestress and therefore vulnerable to damage.

PILE DRIVING AND TESTING

Driving commenced with the single length pier piles. The author was present during the initial testing and very high tension was evident from the very start of driving. The pile driving contractor was made aware of the potential for damage but he had the conflicting requirements of having to strike the pile with sufficient energy to achieve penetration in the stiff clay while not striking the pile too hard in order to prevent damage. In the end the practicality of achieving penetration won out over avoiding the risk of damage to the piles. Dynamic pile testing was conducted for the full length of driving each pile. Very high tensions exceeding the prestress were evident. However no damage, other than micro cracking was evident. An example of test results early and late in the driving of one of the pier piles is shown in Figures 1 and 2. These show the dynamic test measurements presented as the impact wave travelling down the pile (WD) and the reflection coming back up the pile from the toe (WU) versus time. TS is the time scale and TB is the time at the beginning of the graph. At the start of driving the "rise" of the (negative) reflection from the toe, being the time from zero to maximum of the wave is the same as the "rise" in the applied wave. By the end of driving the "rise" of the reflection is considerably longer, about double, suggesting considerable micro cracking. Experience at other projects suggested that when very long single piece sections of these prestressed piles are driven the slow "rise" can be evident from the beginning of driving owing to micro cracking caused during transport and by handling stresses. With regard for the prestress to hold any micro cracking tightly closed this was not considered to be "damage" to the pile, but it is indicative of the very high tensions evident during driving.

Driving of the first length of the abutment piles was similar.

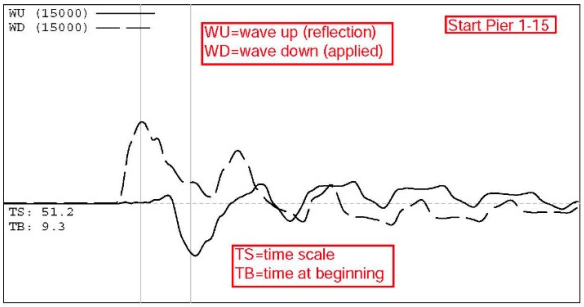


Figure 1 Dynamic test data at start of driving a pier pile

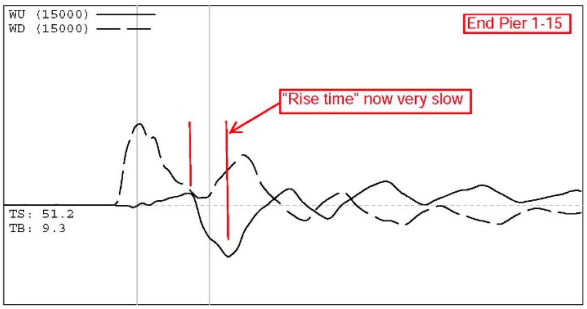


Figure 2 Dynamic test data at end of driving a pier pile

Testing of the Abutment piles after splicing also showed high tension stresses but, in addition, a BTA (an assessment of pile "damage" see reference 1) developed soon after re-driving recommenced after the addition of the second pile length and this became worse with driving, suggesting that it was not simply the splice but almost certainly a real damage to the pile. See Figure 3. The BTA was located not at the end of the concrete sections in the middle of the box splice but at the bottom of the box splice.

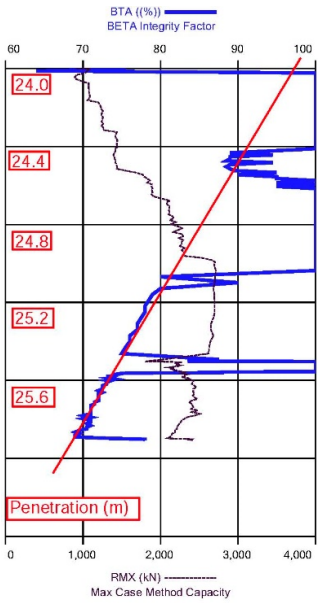


Figure 3 Beta reducing during re-driving

When the BTA reduced to where the pile was considered "damaged," driving was stopped. As the additional penetration achieved with the splice was not very great, being about 1m, the pile was excavated and inspected. Damage was visually confirmed. See figure 4.



Figure 4 Pile 68 Beta = 68 showing open cracking, spalling about 100mm below box splice

Testing was conducted on following abutment piles and each showed a similar BTA at a similar location indicating the piles were damaged. All piles were damaged about 100mm below the splice. See figure 5.



Figure 5 Multiple piles showing open cracking, spalling about 100mm below box splice

There was clearly a problem with the driving of the spliced piles in the ground conditions evident at the site. In order to progress the work without turning the project into a research exercise the abutment

piles were replaced one for one with steel tubes of similar size and at the initial locations and design penetrations.

The author has seen similar behaviour in similar spliced prestressed piles on several other projects. It is also understood that there have been discussions with groups of the client, designers and construction contractors in regard to the problems of damage to prestressed piles with splices but the author was not invited to the discussions and is not aware of the results. However, use of driven prestressed piles now appears to be uncommon, with most projects having bored cast-in-place piles specified, even though they are more expensive. Alternatives using driven piles are typically not accepted.

SUBSEQUENT CONSIDERATIONS

The PDA Case method (reference 2) considers the piles as a uniform section. CAPWAP (reference 3) was also conducted with the piles considered as a uniform section. However the box splice for these octagonal piles was quite massive with considerable additional steel cast into and glued into the pile section. Steel has a modular ratio of about five times that of concrete and the box and extra reinforcing together with dowel bars add very considerably to the impedance (EA/c) of the pile, with a relative increase of about 42%.

Subsequent GRLWEAP analysis (see reference 4) suggests that once the increased impedance at the box splice is taken into account the stresses below the splice are higher, but only about the level of the prestress, so the problem of breakage is most probably at least partially related to tension being too high within the development length of the prestress. See Figure 6. There is also some effect of the upward travelling tension wave being reflected back down by the increase in impedance of the massive splice. At half wave length there is the back of the upward travelling tension wave plus the front of the tension wave being partially reflected and travelling down. The author considered the effect of the reflections would be significant but analysis suggests this is not the case and that the effect is minor.

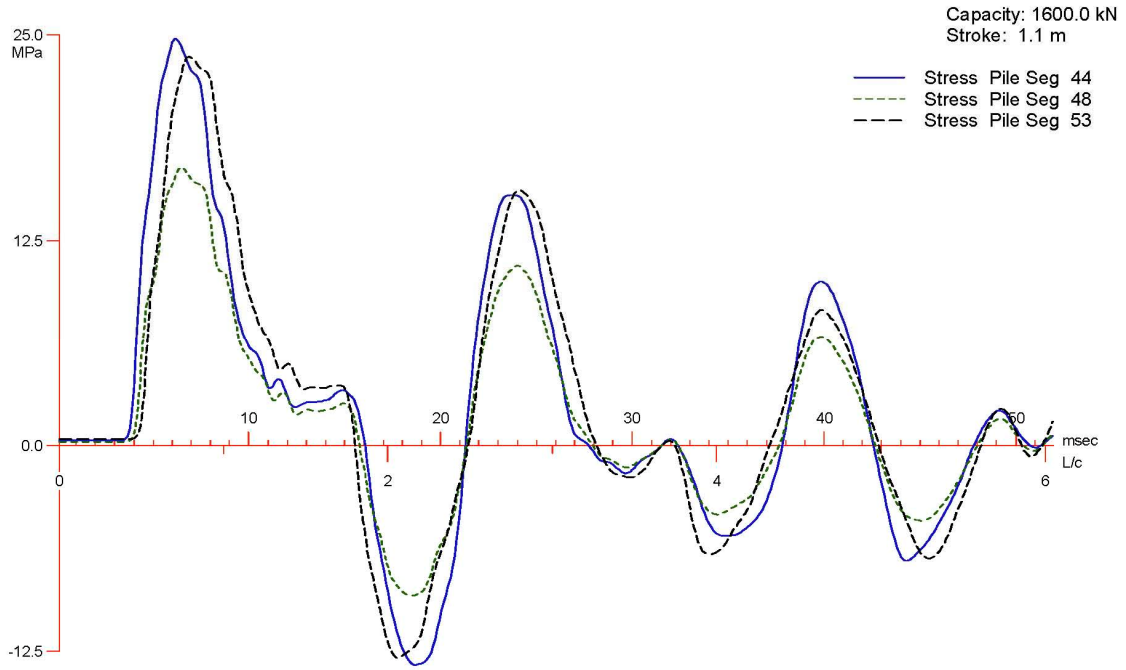


Figure 6 Stress at the top (segment 44), middle (segment 48) and immediately below (segment 53) the box splice

Damage is occurring in the bottom section of these spliced piles about 100mm below the splice so the solution to the problem is to lower tension stress at the top of the bottom section. This can be done by decoupling the lower section by not gluing it into the splice. The splice then transfers compression only. The top of the bottom section becomes a free end to an upward travelling tension wave and by

definition the tension stress has to be zero. See Figure 7. This also has the additional advantage that the top section is also “protected” from the upward tension.

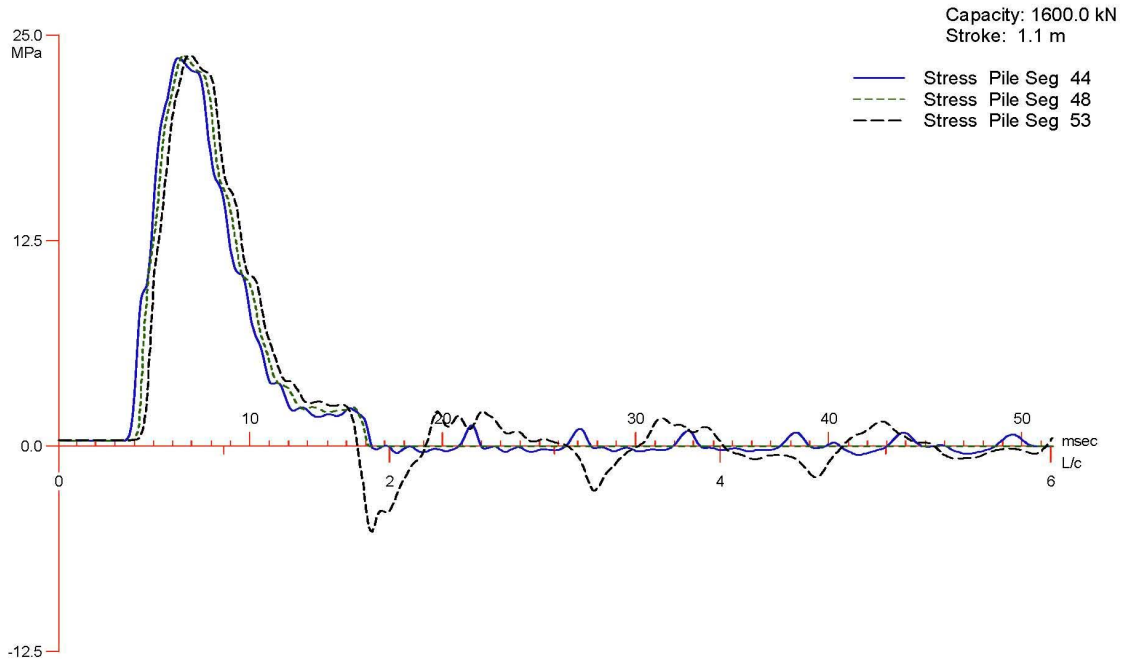


Figure 7 Stresses at the top (segment 44), middle (segment 48) and bottom (segment 53) of the box splice not glued

The box and additional splice dowels will ensure the top section remains in line with the bottom section but the splice will not transfer moment or tension. The splice would thus need to be located at sufficient penetration that moment is not an issue. Tension loading is generally very small or nil and in many cases is not real but only nominal. Small design tension requirements can be changed by re-aligning piles and/or adding mass to the structure.

However, having an unglued splice can result in "odd" driving behaviour. The initial blow is transferred in compression for the full length but when the upward tension wave is stopped at the splice, the bottom section will move slightly downward away from the top section. The subsequent blow will have a very high displacement with very little energy needed for driving because the top section only needs to "catch up" to the bottom section, which has "pulled away" from the top section. The pile will appear to have a small set, big set, small set, big set etc. It may be necessary to place another cushion layer within the splice to stop concrete to concrete impact during the "catch up" blows. The driving should always be finished on a blow with big set to ensure the top section of pile is in contact with the bottom section.

CONCLUSIONS

Long prestressed piles with a splice can be driven without damage. You only need to avoid gluing the bottom section into the splice. However the piles cannot support tension.

If there is a requirement to maintain a tension capability of the pile then further testing would be required to investigate the effect of a longer glued box splice. Alternatively use of an end-plate together with wedges on the prestress wires at the splice end of the pile would significantly reduce, or remove entirely, the development length of the prestress in the concrete.

REFERENCES

1. Rausche, F., Goble, G.G. January 1979. Determination of Pile Damage by Top Measurements. ASTM Special Publication 670: Philadelphia, PA; 500-506
2. Likins, G.E. March 1981. Case Method. Second Seminar on the Dynamics of Pile Driving, Boulder CO, Pile Dynamics Inc
3. Pile Dynamics Inc., 2006, CAPWAP for Windows Manual
4. Hussein, M., Rausche, F., Likins, G.E., 1988. Wave Equation Analysis of Pile Driving: Methodology and Performance. 6th National Conference on Microcomputers in Civil Engineering

FAILURE MODES FOR EMBANKMENTS OVER GROUND IMPROVED WITH DCM COLUMN WALLS BENEATH THE SLOPE

Manasi Wijerathna*, PhD Candidate, D.Wijerathna@westernsydney.edu.au
D.S. Liyanapathirana*, Associate Professor of Geotechnical Engineering,
s.liyanapathirana@westernsydney.edu.au
*School of Computing, Engineering and Mathematics, Western Sydney University, Penrith, NSW, Australia

ABSTRACT

Deep cement mixing is a popular soft ground improving technology that improves the bearing capacity and settlement characteristics of natural soil. When Deep Cement Mixed (DCM) columns are installed attached to each other in a wall configuration, the walls are capable of resisting bending moments and shear forces in the direction transverse to the columns. Therefore, installing DCM walls beneath the embankment slope perpendicular to the alignment of the embankment is a proper solution to prevent excessive lateral deformations of the embankment. Previous research studies have shown that failure patterns of DCM column walls are different to failure patterns of individual DCM column rows, under lateral loads. This study investigates the failure patterns of embankments where DCM column walls are located beneath the slopes, with respect to DCM wall strength, DCM column wall width and the spacing between DCM walls. 2D and 3D numerical models developed using the ABAQUS/standard finite element programme, were used in this investigation. Results show that the DCM wall strength and width of the DCM wall have a significant influence on the failure mode and the critical failure surface of the embankment. 3D simulation results demonstrate that the failure due to soil extrusion between columns was less pronounced in embankments improved with DCM walls, due to the interaction between the DCM walls and the surrounding natural soil.

Keywords: deep cement mixing, column-supported embankments, finite element modelling, failure modes

INTRODUCTION

Embankments constructed over soft ground are highly susceptible to global slope failure and excessive displacements due to combined effects of vertical and lateral loads beneath the embankment slope (Zheng et al., 2009, Han and Gabr, 2002). The overall stability of the embankment can be significantly improved by improving the soil beneath the slope of the embankment using Deep Cement Mixed (DCM) column rows or overlapped DCM column walls (Jamsawang et al., 2015, Larsson and Broms, 2000, Topolniki, 2004, Broms, 1999). According to the literature, the improved ground experience different failure modes other than shear failure, such as separation of columns, overturning, shear failure along the columns or dowel action (Broms, 1999). Some of the failure modes reported by Broms (1999) are shown in Fig. 1. The ultimate failure mode depends on the geometry and the strength of the improved ground (Jamsawang et al., 2015, Kitazume and Maruyama, 2006, Kitazume and Maruyama, 2007).

Kitazume and Maruyama (2006) studied the performance of DCM column improved ground under embankment loading, using centrifuge model tests. They observed that the failure pattern of the embankment shifted from slip circle failure to collapse failure of columns, after improving beneath the embankment slope with DCM column rows. Jamsawang et al. (2015) reported that the failure mode of a DCM wall improved embankment changes with the penetration depth of the DCM walls.

The DCM wall spacing, improvement area along the slope and elastic modulus of the DCM wall also affect the factor of safety of the embankment (Jamsawang et al., 2015). Zheng et al. (2009) investigated the performance of an embankment improved with a geosynthetic layer and DCM walls implemented parallel to the centreline of the embankment, with respect to modulus of DCM wall and spacing between DCM walls. According to their study, the efficiency of DCM wall increased with increasing elastic modulus of DCM wall and became steady at large values of elastic modulus.

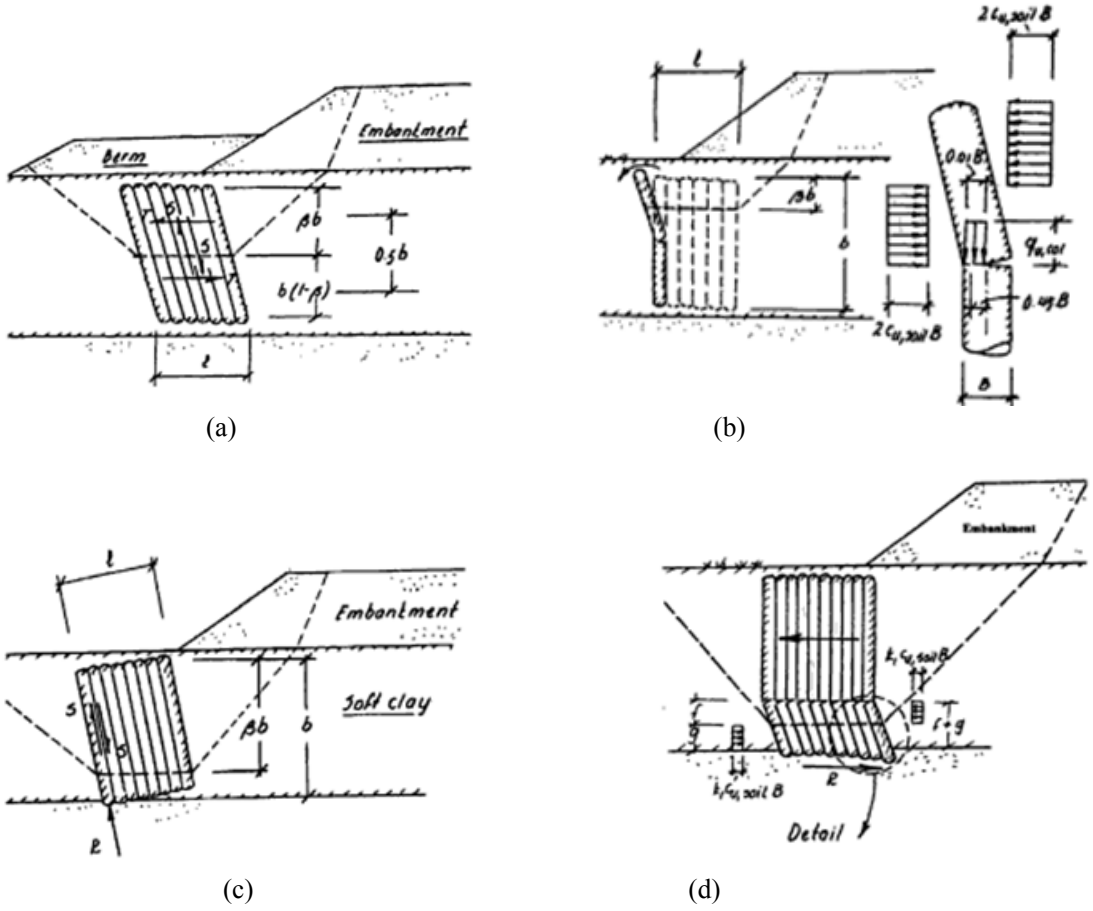


Fig. 1: Different failure modes of DCM column wall supported embankments (Broms, 1999) (a) Shear failure of column wall, (b) Failure by separation and dowel action at top of the column wall, (c) Overturning failure of column wall, (d) Failure by separation and dowel action at the bottom of the column wall

It is important to understand the evolution of failure patterns for embankments over column improved ground with respect to DCM column configuration and mechanical properties of columns, since the failure envelope of DCM improved embankments is characterised by many failure modes (Kitazume and Maruyama, 2006, Kitazume et al., 2000). However, no study has been carried out to investigate the failure modes of embankments improved with only DCM column walls underneath sloping sides. This study investigates the failure modes of a general embankment improved with DCM column walls beneath the slope of the embankment, in the direction perpendicular to the centreline of the embankment, with respect to elastic modulus of the DCM wall, width of the DCM wall and wall spacing. The response of maximum lateral deformation, settlement and soil intrusion, with respect to aforementioned influential parameters were studied using numerical models based on the finite element method.

DESCRIPTION OF THE TEST EMBANKMENT

A general embankment located on a soft clay deposit was selected for the study. Fig. 2 shows the cross section of the test embankment and the arrangement of DCM walls beneath the slope of the embankment. The foundation soil deposit consisted of three soil layers: a 10 m thick soft clay layer, a 5 m thick silty sand layer and a 5 m thick stiff to hard clay layer. The ground water table was at the ground surface. The height of the embankment was 5.5 m. The width of the embankment was 30 m at the crest level and 52 m at the base level. The gradient of the embankment slope is 2:1. The soft clay layer beneath the slope of the embankment was improved with 11 m wide and 10 m deep attached DCM column walls. Each DCM wall consists of eighteen 0.8 m diameter DCM columns with 0.2 m overlap. The column walls were spaced at 1 m centre to centre distance.

The embankment was constructed in 5 stages. In the first four steps, fill layers of 1 m thickness were completed. Each 1 m layer was applied over a period of 10 days. The fifth fill layer is 1.5 m high and it was completed over 15 days.

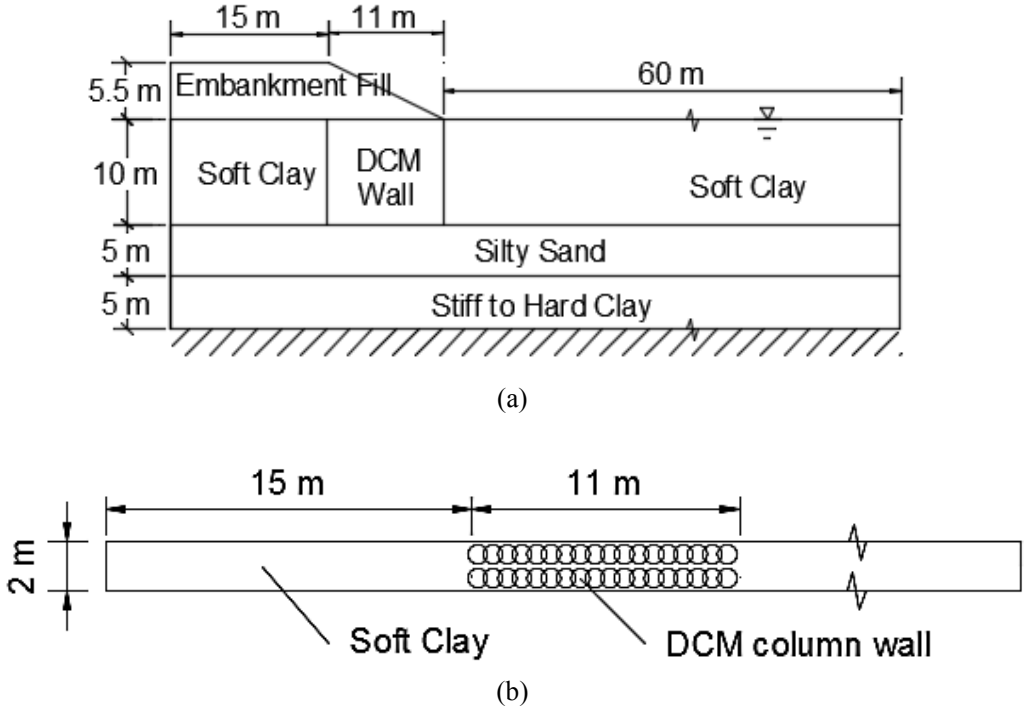


Fig. 2: Geometry of the embankment and layout of the DCM column walls (a) Section view (b) Plan view

NUMERICAL MODEL

The investigation was carried out using the numerical models of the embankment developed in ABAQUS/Standard finite element program. Only half of the embankment geometry was modelled due to the symmetry of the problem and simulated as a two-dimensional plane strain problem. The DCM walls were idealised into 2-D plane strain walls assuming equivalent mechanical properties, while keeping the DCM wall width identical to the actual geometry (Adams, 2011, Yapage et al., 2014, Navin, 2005). In this method the equivalent elastic modulus (E_{eq}), equivalent cohesion (c_{eq}) and

equivalent friction angle (φ'_{eq}) of the improved area of the foundation were calculated using Equations 1, 2 and 3, respectively.

$$E_{eq} = \frac{E_c A_c + E_s A_s}{A_c + A_s} \quad [1]$$

$$c_{eq} = \frac{C_c A_c + C_s A_s}{A_c + A_s} \quad [2]$$

$$\varphi'_{eq} = \tan^{-1}\left(\frac{nA_c \tan\varphi'_c + A_s \tan\varphi'_s}{nA_c + A_s}\right) \quad [3]$$

where E_c and E_s are elastic modulus of DCM walls and soil, respectively; A_c and A_s are area of DCM walls and soil, respectively; c_c and c_s are cohesion of DCM walls and soil, respectively; φ'_c and φ'_s are effective friction angle of DCM walls and soil, respectively; and n is stress concentration ratio (ratio of stress over DCM wall to stress over surrounding soil). The 3D numerical model of the embankment yielded an average stress concentration ratio of 3.5. Therefore, $n = 3.5$ was adopted in calculating φ'_{eq} .

Finite element mesh and element type

DCM column walls, soft clay, silty sand and stiff to hard clay were modelled using eight-node quadratic elements with reduced integration and pore pressure degrees of freedom at the corner nodes (CPE8RP). The embankment fill was modelled using eight-node quadratic elements with reduced integration and without pore pressure degrees of freedom (CAX8R). Elastic perfectly plastic material behaviour was assumed for DCM walls. Three soil layers and embankment fill were modelled using Mohr Coulomb constitutive model.

Mesh convergence was evaluated using models with element size of 1 m, 0.5 m and 0.25 m. The model with 0.5 m elements predicted the deformations with a difference of less than 0.001 m compared to the mesh with 0.25 m elements. Therefore the mesh with 0.5 m elements was adopted since it saves a considerable analysis time compared to the mesh with 0.25 m elements.

Boundary conditions

The stiff to hard clay layer was assumed to rest on the bedrock and vertical and horizontal translations of the bottom boundary were restricted. The bottom boundary and the two vertical boundaries were considered as impermeable. The pore water pressure was set to zero at the ground surface level where water table exists. A symmetrical boundary condition was assigned along the vertical face across the embankment centreline. The vertical boundary at the sloping side of the embankment was set at 60 m away from the embankment toe to minimize the boundary effects. Zero horizontal displacements were assigned to the vertical boundary at the sloping side of the embankment.

Material parameters

The material properties for soft clay layer, silty sand layer, stiff to hard clay layer and embankment fill are shown in Table 1. The soil profile used in this study is similar to the soil profile at the Ballina bypass project given by Yapage et al. (2014). Void ratios for the soil layers are based on the values published by Yapage et al. (2014), derived using field measured water contents of each layer and a specific gravity of 2.7. Although the derived values are high for the soft clay, silty sand and stiff to hard clay, they were not altered as they are based on the field measurements. Also in this case, since

the Mohr Coulomb model is used to simulate the soft clay, silty sand and stiff to hard clay, void ratios adopted in the model does not have any impact on the numerical results because void ratio is not an input model parameter for the constitutive model.

According to the literature, unconfined compressive strength of DCM soil (q_u) range from 0.2 MPa to 2.7 MPa (Jamsawang et al., 2015, Bruce and Bruce, 2003, Kasama et al., 2012). Cohesion (c') and elastic modulus of DCM soil (E) were assumed to be proportionate to q_u. Elastic modulus of DCM soil can vary from 75–300 q_u in dry mixed DCM soil (Navin, 2005, Bruce et al., 2013). Therefore, $E = 100q_u$ was assumed in this study. The cohesion of the DCM soil can range from 0.4-0.5 times q_u(Andromalos et al., 2000, Broms, 1999, Bruce and Bruce, 2003, Topolniki, 2004). The relationship between c' and q_u, adopted for this study was $c' = 0.4q_u$. Permeability, unit weight, void ratio and Poisson's ratio of DCM soil were assumed to be equal to those of the soft clay. Yapage et al. (2013), investigated the friction angle and cohesion of cement mixed soils considering triaxial data for a number of cement mixed clays. By drawing Mohr circles, they have given a range of cohesion and friction angle values for cement mixed soils. Utilising their results, a friction angle of 28^0 was assigned to the DCM column walls.

Table 1: Material properties used for soft clay, silty sand and stiff to hard clay

Parameter	Soft clay	Silty sand	Stiff to hard clay	Embankment fill
γ_{sat} (kN/m^3)	18	18	16.5	19
Permeability (m/s)	1×10^{-8}	8.3×10^{-7}	5×10^{-10}	-
Void ratio, e	2.2	2.2	2.0	-
ν	0.3	0.3	0.3	0.3
c' (kPa)	1	1	1	1
E (MPa)	5	15	17	20
φ'	25	30	25	30

RESULTS AND DISCUSSION

Performance of the DCM wall improved embankment is discussed in this section, using lateral displacement and settlement response of ground with respect to the elastic modulus of DCM wall, width of the DCM wall and wall spacing.

Effect of elastic modulus of DCM wall

The horizontal displacement beneath the toe of the embankment, at the end of construction is plotted in Fig. 3 for the case without DCM walls and the cases with DCM walls with elastic modulus ranging from 12.5 MPa – 125 MPa. The lateral displacements are relatively large when the ground is not improved with DCM walls. The maximum lateral deformation beneath the toe of the embankment reduced by 27% (from 55 mm to 40 mm) when the ground is improved with DCM column walls with an elastic modulus of 12.5 MPa and a cohesion of 50 kPa. The lateral displacements reduced further with increasing elastic modulus of DCM wall. However, the reduction in lateral deformations decreased with increasing elastic modulus as illustrated in Fig. 4. The reduction in lateral deformation

is negligible when the elastic modulus exceeds 75 MPa. It indicates that the failure mode of the embankment at elastic modulus less than 75 MPa is different from failure mode of the embankment when the elastic modulus is greater than 75 MPa.

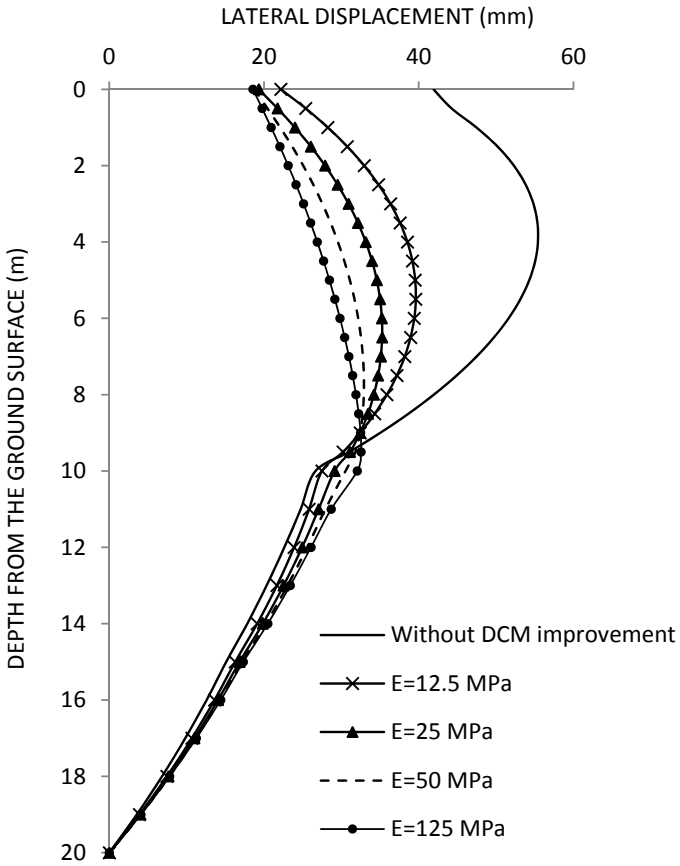


Fig. 3: Lateral displacements beneath the toe of the embankment for different elastic modulus values of DCM wall

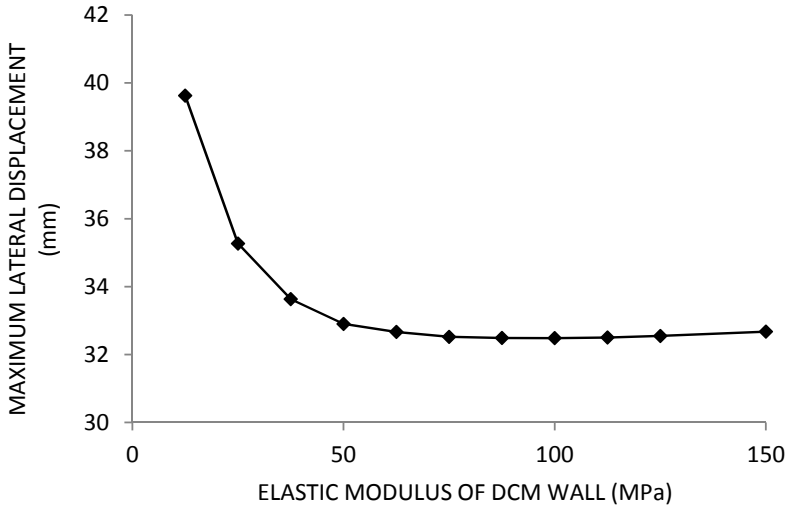


Fig. 4: Variation of Maximum lateral displacement beneath the toe of the embankment with increasing elastic modulus of DCM wall

This phenomenon can be explained using Figs 5(a) – 5(c), where evolution of lateral displacement at different construction stages is plotted for different values of elastic modulus. As shown in Fig. 5a, in the ground without DCM wall, the lateral displacement at a depth of 4m shows the most rapid deformation in response to increasing embankment load. The large deformations in the soft clay layer indicates that the ground fails in slip surface shear failure, with the failure surface passing at a 4m depth beneath the toe of the embankment. Similar to the unimproved ground, the point of maximum lateral deformation corresponding to weakest failure surface observed for the ground improved with a DCM wall with elastic modulus of 12.5 MPa (Fig. 5(b)) is located at around 7.5 m depth. Even though the DCM wall did not yield under the applied embankment load, the DCM wall clearly showed bending deformations. The depth to the maximum lateral deformation increases with increasing elastic modulus (Fig. 3) indicating an increase in depth to the critical failure surface. Eventually, the point of maximum lateral deformation reaches the bottom of the DCM wall when elastic modulus of the wall is close to 75 MPa. Beyond this point, the elastic modulus of the DCM wall is sufficiently high so the DCM wall does not bend under embankment loading. As a result, as shown in Fig. 5(c), the DCM wall showed tilting movement without significant bending deformations. Therefore, the reduction in lateral displacements as a result of increased resistance to bending moments becomes negligible at large elastic modulus values of DCM wall.

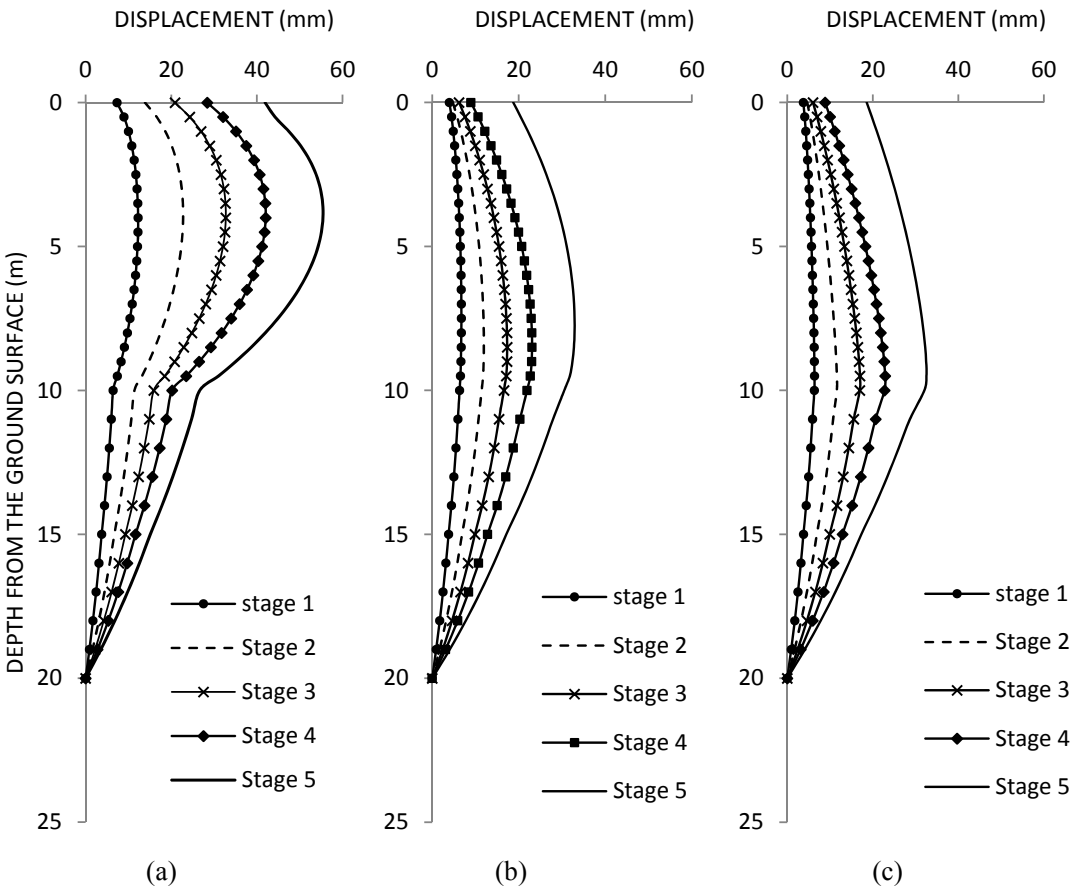


Fig. 5: Evolution of lateral displacements in the ground with construction stages (a) without DCM wall improvement, (b) when elastic modulus of DCM wall is equal to 12.5 MPa, (c) when elastic modulus of DCM wall is equal to 125 MPa

Fig. 6 shows the variation of vertical settlement along the base of the embankment at different elastic modulus values of DCM wall in comparison with vertical settlement in the unimproved ground. As shown in Fig. 6, the maximum vertical settlement was observed at the centreline of the embankment for all the cases. Maximum settlement was increased by 9 mm when the ground is improved with DCM walls. Maximum settlement did not change significantly with increasing elastic modulus of DCM walls. However, the settlement beneath the slope of the embankment reduced significantly after implementing DCM column walls and the settlements reduced further with increasing elastic modulus of DCM walls. The settlements show a sudden drop across the DCM wall – soft clay interface at large elastic modulus values of DCM wall. In the actual ground, this might cause slip along the vertical edge of DCM wall – soft clay interface.

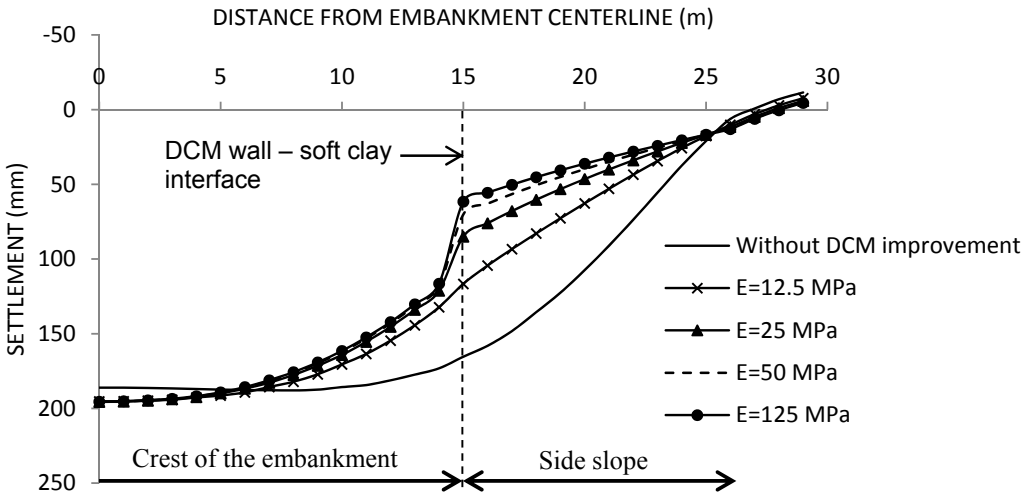


Fig. 6: Vertical settlement along the base of the embankment with changing elastic modulus of DCM wall

Effect of wall width

The maximum lateral deformations beneath the toe of the embankment at the end of construction, for different widths of the DCM wall are shown in Fig. 7. The cohesion and elastic modulus of DCM walls were equal to 200 kPa and 50 MPa respectively, for all the cases discussed in this section. The location of the wall was fixed at the toe of the embankment. The specified wall width was obtained by moving the vertical edge of the wall, which is close to the embankment centreline.

As shown in Fig. 7, lateral deformations reduced with increasing DCM wall width. However, the reduction in lateral deformations corresponding to a given increment in the DCM wall width reduced when increasing the width of the wall. The rate of reduction of maximum lateral deformation with DCM wall width is steady beyond the DCM wall widths greater than the length of the slope of the embankment (11 m).

With increasing DCM wall width, the depth to the point of maximum lateral deformation was increased (Fig. 8). A similar response in lateral deformations was observed when increasing the elastic modulus of DCM walls. However, the deformation pattern of the DCM wall did not change even when the width of the DCM wall is large as 16 m. The DCM wall showed bending deformations for all the widths considered (Fig. 8).

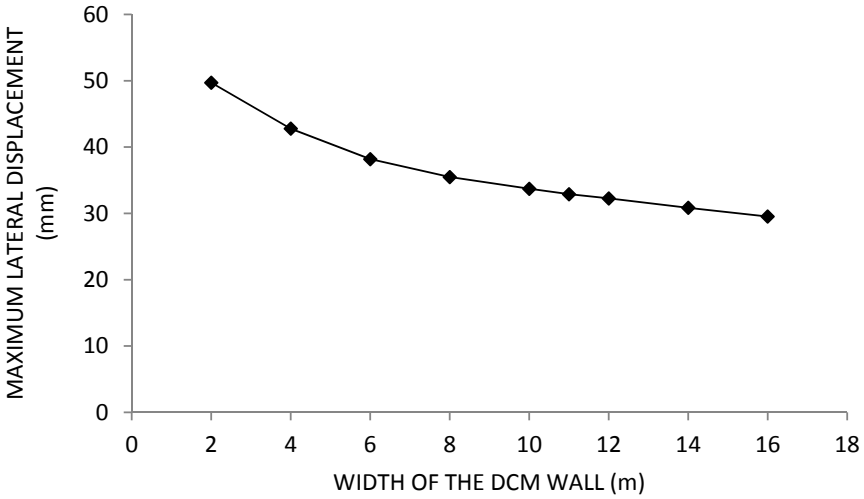


Fig. 7: Variation of Maximum lateral displacement beneath the toe of the embankment with increasing width of DCM wall

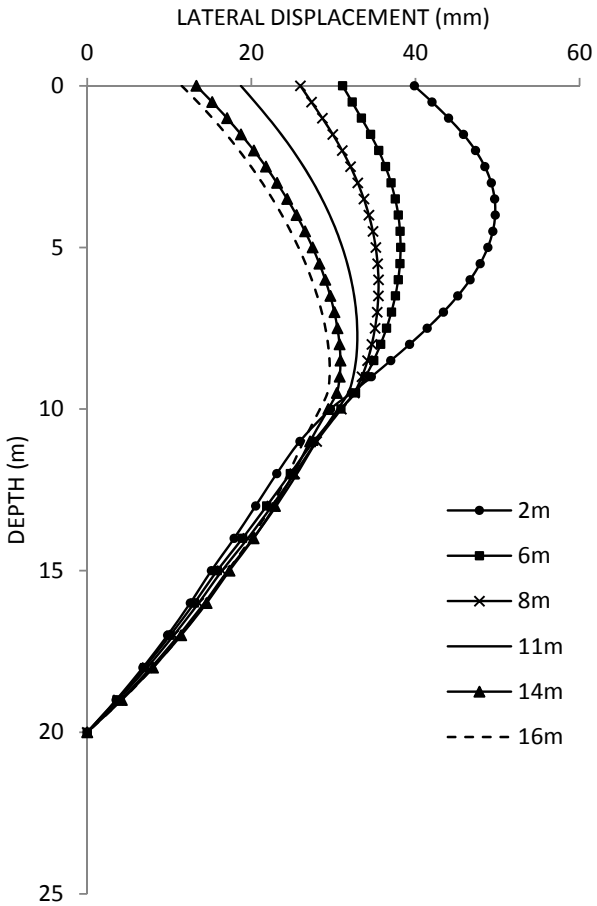


Fig. 8: Lateral displacements beneath the toe of the embankment for different widths of DCM wall

Effect of spacing between DCM walls

In a 2D plane-strain model the effect of spacing between the DCM walls when the strength properties are fixed, is expected to be similar to the effect of elastic modulus when the spacing is fixed, since both approaches finally affect the equivalent properties of the wall. This section intends to investigate the soil movements in between the DCM column walls when the equivalent properties are fixed. Therefore, four cases with different combinations of DCM wall cohesion and spacing, which yields the same equivalent properties and hence same lateral deformations in the 2D model, were selected. The details of selected cases and corresponding ground displacements are summarised in Table 2.

Effect of spacing between DCM walls on the ground deformations was studied using 3D finite element numerical models. The maximum lateral deformations beneath the toe of the embankment were obtained at the end of construction. As shown in Table 2, the results obtained from 2D numerical models agree well with the 3D numerical model results. Therefore, it can be concluded that, the 2D idealisation of the DCM column wall improved ground, used in this study predicts the ground displacements with a reasonable accuracy up to DCM wall spacing of 2.6 m.

In the 3D numerical models, the maximum lateral displacement of the DCM wall was larger than that of the surrounding natural soil for all four analysis cases. These results indicate that the embankment load has effectively transferred onto the DCM wall even when the spacing is as high as 2.6 m. The soil extrusion in between DCM walls was not observed in the ground. This may be due to the proper interaction between DCM walls and natural soil in DCM wall improved embankments.

Table 2: Details of analysis cases and maximum lateral deformations obtained for each analysis case

Analysis case	Cohesion of DCM wall (kPa)	Elastic modulus of DCM wall (kPa)	Spacing between DCM walls (m)	Maximum lateral deformation beneath the toe of the embankment (2D) (mm)	Maximum lateral deformation beneath the toe of the embankment (3D) (mm)	
					On DCM wall	On natural soil
1	150	37500	1.2	34.2	34.1	33.8
2	200	50000	1.7	34.2	34.3	33.8
3	250	62500	2.1	34.2	34.5	33.8
4	300	75000	2.6	34.2	35.0	34.0

CONCLUSIONS

Failure modes of embankment side slopes improved with DCM walls were investigated in this study using 2D and 3D numerical models.

The failure mode of the embankment shifted from bending failure to tilting failure with increasing elastic modulus of DCM wall. At lower elastic modulus values, where bending failure occurs, the maximum lateral deformations beneath the toe of the embankment reduced and the depth to the point of maximum lateral deformation increased with increasing elastic modulus.

The lateral deformations in DCM wall reduced with increasing width of the DCM wall. Lateral deformations reduced significantly with increasing DCM wall width, when the width of the wall is less than length of the slope of the embankment. The depth to maximum deformation increased with wall width. However, deformation pattern shows bending deformation for all the widths considered.

The effect of wall spacing was evaluated using 3D numerical models with four different combinations of DCM wall cohesion and wall spacing designed to yield same lateral deformation. 3D model results showed a good agreement with 2D model results in terms of lateral deformations. According to 3D model results, the maximum lateral deformation was observed on DCM column walls in all four cases. This means embankment loads are effectively transferred to the DCM walls, although the spacing between DCM column walls are large in the options with large cohesive strength. The failure due to soil extrusion was not observed in the analysed cases. This may be a result of the good interaction between DCM wall and surrounding natural soil assumed in this study.

REFERENCES

Adams, T. E. 2011. *Stability of levees and floodwalls supported by deep-mixed shear walls: Five case studies in the New Orleans area.* Ph.D. dissertation, Virginia Tech Blacksburg, VA.

Andromalos, K. B., Hegazy, Y. A. & Jasperse, B. H. 2000. Stabilization of soft soils by soil mixing. Proceedings of the Soft Ground Technology Conference, United Engineering. Geotechnical Special Publication, Foundation and ASCE Geo-Institute, Noordwijkerout, Netherlands, May 28 – June 2, 194-205.

Broms, B. 1999. Keynote lecture: Design of lime, lime/cement and cement columns. International Conference on Dry Mix Methods: Dry Mix Methods for Deep Soil Stabilization, Stockholm, Sweden. Balkema, Rotterdam, 13-15 Oct, 125-153.

Bruce, D. A. & Bruce, M. E. C. 2003. The practitioner's guide to deep mixing. In Grouting and Ground Treatment. Geotechnical Special Publication No. 120, Third International Conference, New Orleans, La.: American Society of Civil Engineers, Reston, Va., 10–12 February 2003, 474-488.

Bruce, M. E. C., Berg, R. R., Collin, J. G., Filz, G. M., Terashi, M. & Yang, D. S. 2013. Federal Highway Administration design manual: deep mixing for embankment and foundation support, FHWA-HRT-13-046. . US Department of Transportation, Federal Highway Administration, McLean, VA.

Han, J. & Gabr, M. 2002. Numerical analysis of geosynthetic-reinforced and pile-supported earth platforms over soft soil. *Journal of geotechnical and geoenvironmental engineering,* 128 (1)**,** 44-53.

Jamsawang, P., Voottipruex, P., Boathong, P., Mairaing, W. & Horpibulsuk, S. 2015. Three-dimensional numerical investigation on lateral movement and factor of safety of slopes stabilized with deep cement mixing column rows. *Engineering Geology,* 188**,** 159-167.

Kasama, K., Whittle, A. J. & Zen, K. 2012. Effect of spatial variability on the bearing capacity of cement-treated ground. *Soils and Foundations,* 52 (4)**,** 600-619.

Kitazume, M. & Maruyama, K. 2006. External stability of group column type deep mixing improved ground under embankment loading. *Soils and foundations,* 46 (3)**,** 323-340.

Kitazume, M. & Maruyama, K. 2007. Centrifuge model tests on failure pattern of group column type deep mixing improved ground. Proceedings of the Seventeenth International Offshore and Polar

Engineering Conference. International Society of Offshore and Polar Engineers(ISOPE), Cupertino, California, USA,, 1293-1300.

Kitazume, M., Okano, K. & Miyajima, S. 2000. Centrifuge Model Tests on Failure Envelope of Column Type Deep Mixing Method Improved Ground. *Soils & Foundations,* 40 (4)**,** 43-55.

Larsson, S. & Broms, B. B. 2000. Shear box model tests with lime/cement columns-some observations of failure mechanisms. ISRM International Symposium, Melbourne, Australia. International Society for Rock Mechanics.

Navin, M. P. 2005. *Stability of embankments founded on soft soil improved with deep-mixing-method columns.* Ph.D. dissertation, Virginia Polytechnic Institute and State University,Blacksburg, VA.

Topolniki, M. 2004. In situ soil mixing. *In:* MOSELEY, M. P. & KIRSCH, K. (eds.) *Ground improvement.* 2 nd Edition ed.: Spon Press, Taylor & Francis Group, New York, NY, USA.

Yapage, N., Liyanapathirana, D., Kelly, R., Poulos, H. & Leo, C. 2014. Numerical modeling of an embankment over soft ground improved with deep cement mixed columns: Case history. *Journal of Geotechnical and Geoenvironmental Engineering,* 140 (11)**,** 04014062 1-10.

Yapage, N., Liyanapathirana, D., Poulos, H., Kelly, R. & Leo, C. 2013. Numerical modeling of geotextile-reinforced embankments over deep cement mixed columns incorporating strain-softening behavior of columns. *International Journal of Geomechanics,* 15 (2)**,** 04014047 1-18.

Zheng, J., Chen, B., Lu, Y., Abusharar, S. & Yin, J. 2009. The performance of an embankment on soft ground reinforced with geosynthetics and pile walls. *Geosynthetics International,* 16 (3)**,** 171-181.

IMPROVEMENT OF SOIL PROPERTIES BY BASALT FIBRE REINFORCEMENT

Ramanathan Ayothiraman, *Associate Professor, Dept. of Civil Engg., IIT Delhi, New Delhi-110016, India, araman@civil.iitd.ac.in*
Anurag Singh, *B.Tech Student, Dept. of Civil Engg., IIT Delhi, New Delhi-110016, India, anuragsingh1727@gmail.com*

ABSTRACT
An experimental program was undertaken to investigate the effects of randomly distributed basalt fibre on the index and engineering properties of Dhanori clay and to compare its performance with the properties of soil reinforced with polypropylene fibre. In the present investigation, 7 groups of soil samples were prepared at four different percentages of basalt fibre and polypropylene fibre content and tests were done for measuring their consistency limits, compaction characteristics, unconfined compression strength and consolidation properties. The test results indicate that the inclusion of basalt fibre in Dhanori clay resulted in significant improvement in properties. The improved properties are not comparable with polypropylene fibres, nevertheless, the improvement by basalt fibres is able to meet the typical design target values and the cost is very much less than synthetic fibres. More importantly, basalt fibres are environment friendly.
Keywords: Basalt fibre, Polypropylene fibre, Dhanori clay

INTRODUCTION

Construction of buildings in low lands with engineered filling, flexible and rigid pavements for highways/airfields, and embankments for highways/railways are also part of major infrastructural development in addition to construction of tall buildings, bridges/fly overs, major dams and underground structures. The later projects require different improvement techniques than that is adopted in the former projects. Ground improvement techniques such as use of reinforcement inclusions within soil found as an effective and reliable technique. Especially such modification by fibre reinforcement, is primarily possible in engineered filling, pavements subgrade and embankments, where surface mixing is easier; and may not be feasible when stabilization/modification is required for deeper depths. In comparison with conventional reinforcement using geosynthetics (strips, geotextile, geogrid, etc.), there are some advantages in using randomly distributed fibre as reinforcement. In past few decades, the discrete fibres are simply added and mixed randomly with soil, in much the same way as cement, lime, or other additives.

There are several studies (Ziegler et al. 1998; Puppala et al. 2000; Bei-xing et al. 2004; Cai et al. 2006; Tang et al. 2007, 2012, 2016; Abdi et al. 2008; Viswanadham et al. 2009; Le et al. 2015) that investigated the behaviour of polypropylene fibre-reinforced soil and reported that an increase in fibre content caused an increase in strength and shrinkage potential but brought on the reduction of swelling potential. The length of fibres had an insignificant effect on soil characteristics, whereas fibre contents proved more influential and effective. A study on rubber fibre conducted by Hambirao and Rakaraddi (2014) mentions that tensile cracking of clays can be improved with the inclusion of short rubber fibres, optimum fibre content was about 15 % of weight of soil. Several experimental studies (Babu et al. 2008; Chaple and Dhatrak 2013; Vibhakar and Nahta 2014; Soundara and Senthilkumar 2015; Goyal et al. 2015; Jayasree et al. 2014, 2015) were conducted on coir fibre-reinforced soil and concluded that it helped in reducing the swell potential and 1% fibre by weight of the soil almost doubled the CBR value. Martins et al. (2015) found that 4% of sisal fibre by weight of the soil reduced the visibility of cracks. Pillai and Ayothiraman (2012), Ayothiraman et al. (2014) and Sahu et al. (2016) have demonstrated that human hair fibres can be used to improve the properties of both fine grained and coarse grained soils.

Although there are several studies on use of different type of fibres (synthetic fibres/natural fibres), studies on use of basalt fibre in reinforcing the soil (Dorigato and Pegoretti 2011; Pandian et al. 2014) are very limited. This paper presents the results of experimental investigation carried out in the laboratory on index, strength and compressibility characteristics of basalt fibre-reinforced soil.

MATERIALS

Soil

Dhanori soil (Fig. 1) has been used in this study and the various index and engineering properties of the soil are summarized in Table 1.

Table 1. Properties of Dhanori clay

Engineering Properties	Value
Specific Gravity	2.65
Liquid Limit	37.1
Plastic Limit	22.5
Plasticity Index	14.6
Maximum dry density	1.72
Optimum moisture content	17.0



Fig 1. Dhanori clay.

Fibres

The lightweight, strength and deformation properties of fibres make them effective materials in various foundation-engineering problems. The inclusion of randomly distributed fibre significantly increased the peak compression strength and other index and engineering properties (Cai et al. 2006). In many case, fibre can be cost effective. Polypropylene and basalt fibres used in the present study are shown in Fig. 2. The physical and chemical properties of basalt and polypropylene fibres are given Table 2.

FIBRE-REINFORCED SOIL

It is reported in literature that the optimum percentage of fibre content typically lies in the range of 0.5-1% by weight of soil. Therefore, in the present study, three different percentages of fibre content, i.e. 0.5%, 1.0% and 1.5% by weight of soil are considered for both polypropylene and basalt fibres. Tests were done on both unreinforced soil and reinforced soil for comparing the performance of fibre reinforcement. Fibers were randomly mixed with soil by hand and proper care and time were spent for preparing a homogenous mixture at each stage of mixing. It was observed that with increases in fibre %, it was difficult to mix fibre and fibres and soil were segregating from each other, and fibre lumps were formed. The index and engineering properties such as consistency limits, compaction characteristics, UCS and compressibility of the clayey soil reinforced with fibres were determined through lab testing. Specimens for strength tests were made by the static compaction method. The specimens were prepared at their respective maximum dry density and optimum moisture content, obtained from standard proctor compaction test. UCS tests were performed on specimens at the strain rate of 0.38 mm/min (0.5%) until specimens failed or a strain of 10% was reached. Consolidation tests were done on specimens as per standard procedures.

Table 2. Physical and chemical properties of basalt and polypropylene fibre

Physical and Chemical Properties	Value	
	Basalt	Polypropylene
Fiber type	Single	Single
Average Diameter	13 micron	34 micron
Average Length	12 mm	12 mm
Tensile Strength	4.5GPa	35GPa
Elastic modulus	105GPa	38GPa
Environment Friendly	Yes	No



(a) (b)

Fig 2. (a) Basalt and (b) Polypropylene Fibres.

DISCUSSION OF RESULTS

Consistency Limits

Fig. 3 shows that there is a marginal increase in LL, PL, and PI of the soil which may be attributed to the fact that fibre absorbs water itself. The surface roughness that prevails on the fibre tend to absorb some moisture which is very marginal. However, this marginal change is insignificant from the view point of practice.

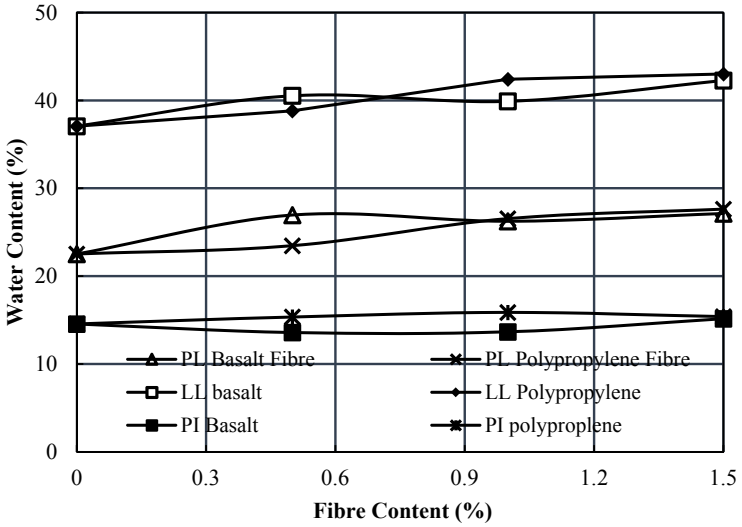


Fig 3. Variation of consistency limits with fibre content.

Compaction Characteristics

Standard Proctor tests were performed in the current study. Multiple trials were conducted in order to get more reliable results for comparison. The results of compaction tests are summarized in Table 3. It is seen from the table that the Maximum Dry Density (MDD) decreased with an inclusion of fibres owing to the light weight nature of fibres, but the Optimum Moisture Content (OMC) increased slightly.

Table 3. OMC and MDD of Fiber-Reinforced Soils

Fibre Content (%)	OMC (%)		MDD (g/cc)	
	Polypropylene Fibre	Basalt Fibre	Polypropylene Fibre	Basalt Fibre
0.0	17.0	17.0	1.72	1.72
0.5	18.4	19.3	1.67	1.66
1.0	19.3	20.0	1.64	1.68
1.5	20.3	20.0	1.60	1.68

Influence of fibre content on MDD and OMC of Dhanori-fibre mixture is shown in Fig. 4 and Fig 5 respectively. It is seen from Figs 5 and 6 that the increase in OMC in soil reinforced with both fibres are practically same. This indicates that fibre type may not significantly affect the OMC, and the slight increase in OMC is primarily due to moisture absorption of fibres. It is also seen from these figures that MDD for Basalt reinforced soil shows a lower rate of decrease than polypropylene fibre-mixed soil with increasing fibre content. However, higher fibre content (beyond 1.5%) of Basalt fibre shows a reduction in MDD similar to polypropylene fibres.

Unconfined Compressive Strength (UCS)

The unconfined compressive strength of both unreinforced and reinforced soils obtained from the stress-strain curves of uniaxial compression tests is summarized in Table 4. The undrained shear strength of clay is half of the UCS value and are also presented in Table 4. It is seen from Table 4 that the UCS value of reinforced soils is higher than unreinforced soil. The increase in strength of basalt fibre-reinforced soil with percent fibre is relatively smaller than the increase in strength of polypropylene fibre-reinforced soil (Fig. 6).

Table 4. UCS and Shear Strength for Fiber-Reinforced Soils

Fibre Content (%)	Unconfined Compressive Strength (kPa)		Undrained Shear Strength (kPa)	
	Polypropylene Fibre	Basalt Fibre	Polypropylene Fibre	Basalt Fibre
0.0	178.2	178.2	89.1	89.1
0.5	179.0	181.9	89.5	90.9
1.0	234.9	186.0	117.5	93.0
1.5	222.4	208.1	111.2	104.1

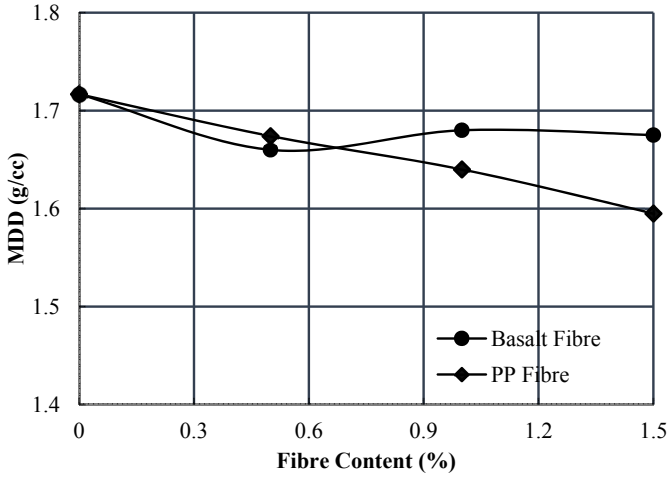


Fig 4. Influence of fibre content on MDD of Dhanori-fibre mixture.

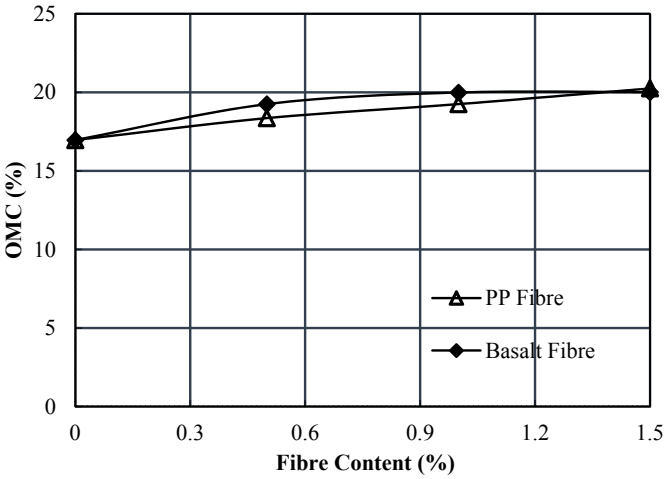


Fig 5. Influence of fibre content on OMC of Dhanori-fibre mixture.

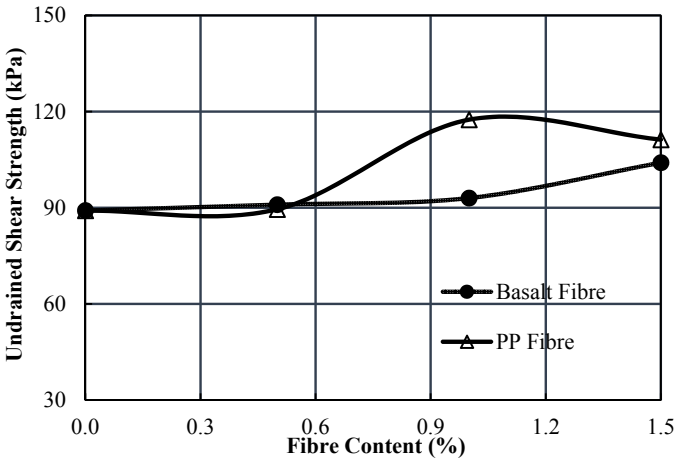


Fig. 6. Effect of fibre reinforcement on shear strength of soil

The typical failure of specimens as observed after the UCS testing is shown in Fig. 7. It is seen from the figure that the unreinforced specimen exhibits brittle failure (Fig. 7a), whereas the specimens reinforced with fibres exhibit brittle-ductile behavior at low fibre content, and behavior changes to completely ductile with an increase of fibre content. At large fibre content, the strength also reduces, as the whole matrix become highly compressible at same load.

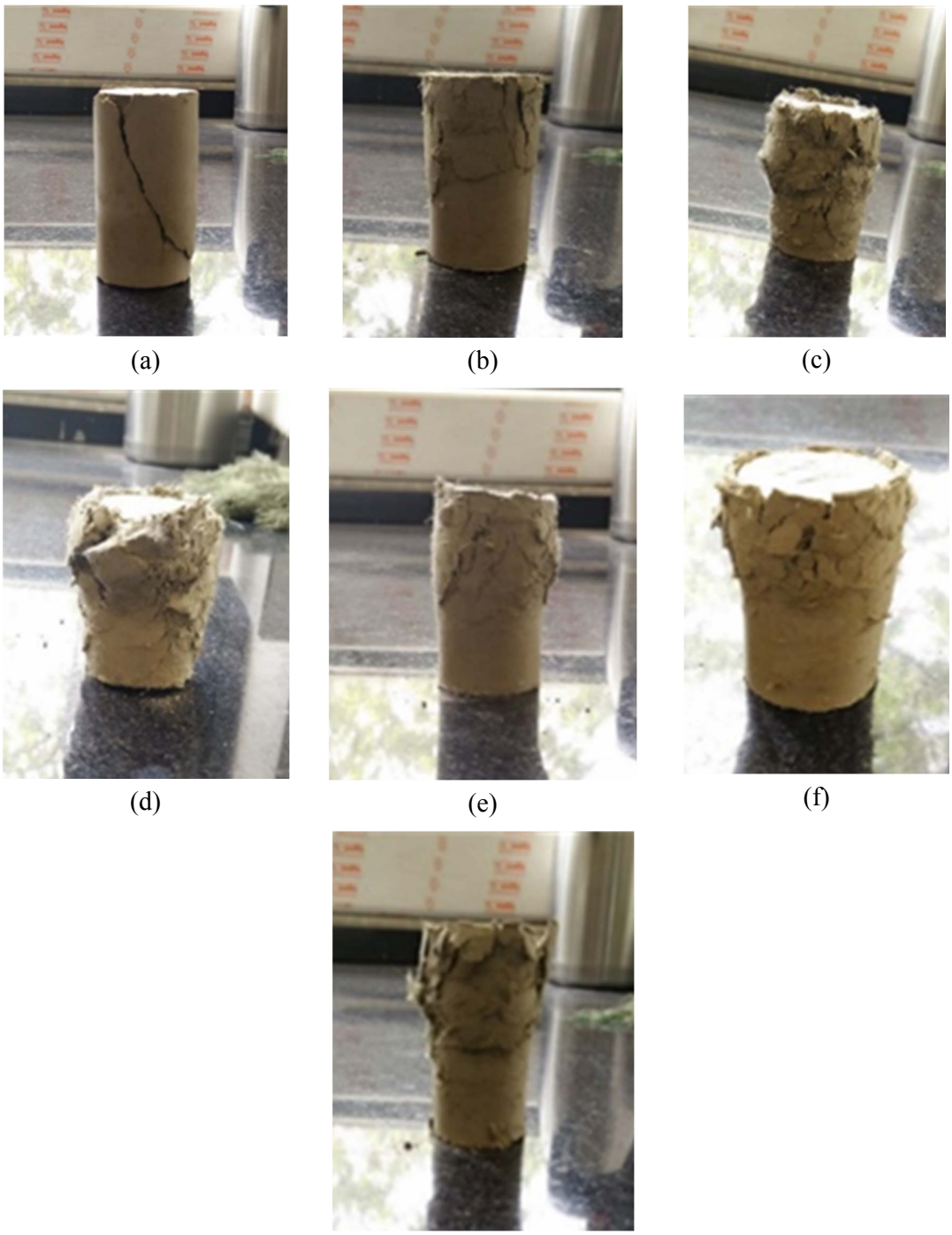


Fig 7. Typical failure of specimens as observed in UCS tests (a) Unreinforced; (b) 0.5 % Polypropylene; (c) 1% Polypropylene; (d) 1.5% Polypropylene; (e) 0.5% Basalt; (f) 1% Basalt; (g) 1.5% Basalt.

Compressibility of Clay

One-dimensional consolidation tests were conducted on both unreinforced and reinforced soils prepared at their respective maximum dry density and optimum moisture content. It was ensured that the specimens were saturated before the start of loading for consolidating them as per standard procedures. The variation of void ratio with pressure (*e*-log *P* curve) is shown in Fig. 8. The compression index of soil was estimated from the *e*-log *P* curve, and its variation with fibre content is also shown in Fig. 9.

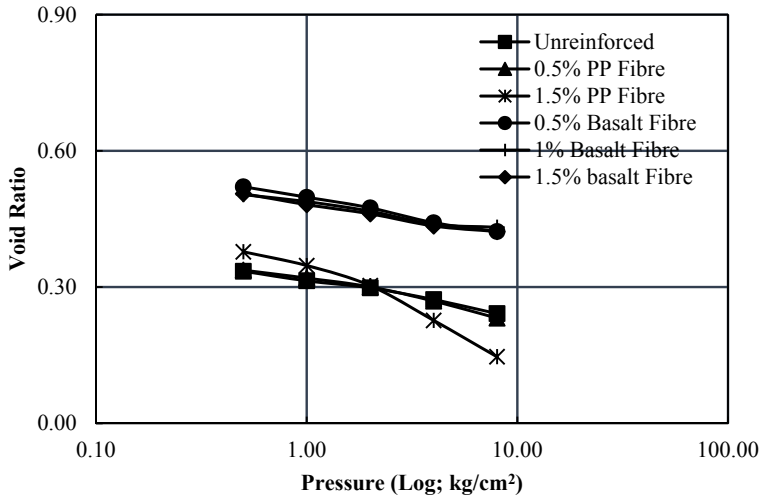


Fig 8.Variation of void ratio with pressure (log scale) for different fibre content.

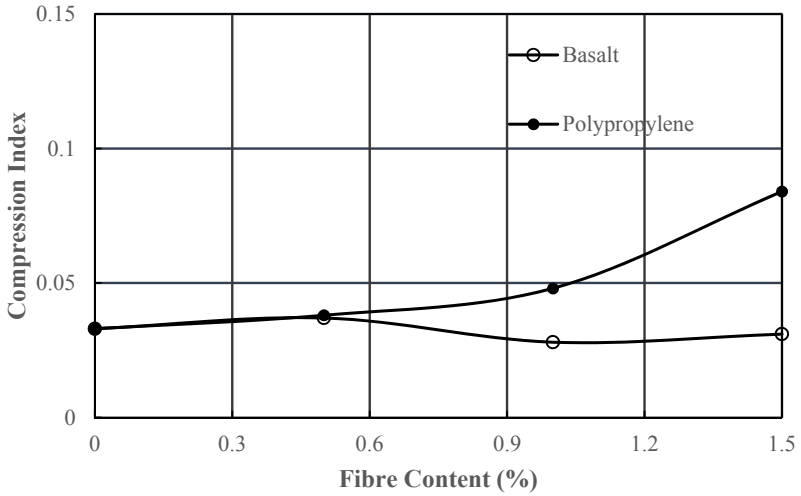


Fig 9. Influence of fibre content on compression index of Dhanori clay.

It is observed from Figs. 8 and 9 that the addition of basalt fibres does not affect the compressibility significantly within the percent fibres tested. This may be owing to the fact that basalt fibre consists of natural minerals having specific gravity similar to soil, therefore the compressibility of soil reinforced with basalt fibre is not affected. However, soil reinforced with polypropylene fibres beyond 1 % exhibits relative high compressibility and thus reached a low void ratio at high vertical/consolidation pressure. But at low vertical pressures, even 1.5% reinforced soil exhibits nearly same compression index to that of natural soil. This means, that for applications involving low vertical stresses, both types of fibres can be used to improve the strength properties of clay soils, without bothering about issues of compressibility.

From the results of consolidation tests, other engineering properties, such as coefficient of volume compressibility, coefficient of consolidation and permeability of unreinforced and reinforced soils are computed and are summarized in Table 6. It is seen from the table that the permeability of soil increases with an increase of fibre content, as the presence of fibres allow the water to flow along the interface of fibres and soil. This observation is consistent for both basalt and polypropylene fibres, and both types of fibres show similar order of increase of permeability values, irrespective of their respective diameter/size. Due to increase of permeability of soil with fibre content, the coefficient of consolidation also increases with the fibre content. This indicates that the time required for 90% consolidation in the field for clayey layers may reduce significantly, thus consolidation settlement could be achieved in a relatively shorter time.

Table 6. Summary of Consolidation test

Fibre Content (%)	C_v ($\times 10^{-6}$ m^2 /sec)		m_v		k ($\times 10^{-6}$ m/sec)	
	Basalt Fibre	Polypropylene Fibre	Basalt Fibre	Polypropylene Fibre	Basalt Fibre	Polypropylene Fibre
0	1.54	1.54	0.07	0.07	0.03	0.03
0.5	2.02	1.38	0.07	0.09	0.14	0.11
1	1.91	3.37	0.08	0.03	0.15	0.10
1.5	2.55	2.35	0.09	0.11	0.23	0.24

SUMMARY AND CONCLUSIONS

An experimental study was carried out to evaluate the engineering behavior of clay soil reinforced with basalt fibre and an effort was made to assess its performance over polypropylene fibre-reinforced soil. Dhanori clay is tested with and without reinforcement, for assessing it's both index and engineering properties in the laboratory. Fiber content was varied from 0 to 1.5%. From the analysis and interpretation of results of laboratory investigation, the following conclusions are arrived at:

1. The consistency limits: LL, PL, and PI of the fibre-reinforced clay is practically not affected by the fibre inclusion.

2. The compaction behavior is affected by fibre inclusion, and the maximum dry density is found to reduce slightly with an increase of fibre content, and marginal increase in OMC is noted.

3. It is noticed that the stress-strain behaviour has changed from brittle to ductile with inclusion of basalt fibre. This observation is the same for polypropylene fibre as well. The UCS value of fibre-reinforced soil increases with reinforcement of both fibres, which indicates that an increase in shear strength of soil. The percentage increase in shear strength of soil is about 17% for basalt fibre and about 25% for polypropylene fibre. It is also found that at large fibre content (> 1 %), the strength also reduces, as the whole matrix become highly compressible at same load.

4. It is noticed that the inclusion of basalt fibres does not affect the compressibility characteristics of soil significantly, which is due to fact that basalt fibre consists of natural minerals having specific gravity similar to soil. However, this conclusion largely depends on applied vertical pressure levels and application types. For applications involving low vertical stresses, both types of fibres can be used to improve the strength properties of clay soils, without bothering about issues of compressibility.

5. The permeability of soil increases with an increase of fibre content. This may be due to flow of water along the interface of fibres and soil, and fibres help in enhancing the flow path for the water. This observation is consistent for both basalt and polypropylene fibres.

6. The coefficient of consolidation of soil also increases with the fibre content which may help in accelerating the rate of consolidation in the field.

It is to be noted that the above conclusions are drawn from the laboratory investigation, which may need to be verified with the field observation, as and when the data is made available.

REFERENCES

Abdi, M.R., Parsapajouh, A. and Arjomand, M. A. (2008) "Effects of Random Fiber Inclusion on Consolidation, Hydraulic Conductivity, Swelling, Shrinkage Limit and Desiccation Cracking of Clays", International Journal of Civil Engineering. 6(4): 284-292.

Ayothiraman, R., Bhuyan, P. and Jain, R. (2014), 'Comparative studies on performance of human hair and coir fibres against synthetic fibres in soil reinforcement.' 2nd Annual International Conference on Architecture and Civil Engineering (ACE 2014): 222-227.

Babu, G. L. S., Vasudevan, A. K. and Sayida, M. K. (2008) "Use of Coir Fibers for Improving the Engineering Properties of Expansive Soils", Journal of Natural Fibers, 5(1): 61-75.

Bei-xing, L., Ming-xiang, C., Fang, C. and Lu-Ping L. (2004) "The Mechanical Properties of Polypropylene Fiber Reinforced Concrete", Journal of Wuhan University of Technology-Material Science Education, 19(3):68–71.

Cai, Y., Shi, B., Ng, C. W. W. and Tang, C. (2006) "Effect of Polypropylene Fiber and Lime Admixture on Engineering Properties of Clayey Soil", Engineering Geology, 83(3-4):230-240.

Chaple, P.M. and Dhatrak, A.I. (2013) "Performance of Coir fibre Reinforced Clayey Soil", The International Journal of Engineering and Science (IJES) 2(4): 54-64

Goyal, P., Trivedi, A. S. and Sharma, M. (2015), "Improvement in Properties of Black Cotton Soil with an Addition of Natural Fibre (Coir) Derived From Coconut Covering", International Journal of Engineering Research and Applications, 5 (3):36-37.

Hambirao, G. S. and Rakaraddi, P. G. (2014), "Soil Stabilization Using Waste Shredded Rubber Tyre Chips", IOSR Journal of Mechanical and Civil Engineering (IOSR-JMCE), 11 (1): 20-27.

Jayasree, P. K. Balan, K., Peter, L. and Nisha, K. K. (2014) "Volume Change Behavior of Expansive Soil Stabilized with Coir Waste", Journal of Materials in Civil Engineering, 27(6): 04014195(8)

Jayasree, P. K. Balan, K., Peter, L. and Nisha, K. K. (2015) "Shrinkage Characteristics of Expansive Soil Treated with Coir Waste", Indian Geotechnical Journal, 45(3):360–367.

Le, C., Zhi-Bin, L. and Shu-Zhong, Z. (2015), "Influence of Polypropylene Fiber-Reinforcement on Consolidation and Compression Characteristics of Kaolin", Rock and Soil Mechanics, 36(S1): 372-376

Martins, A.P.S., Silva, F.A. Toledo Filho, R.D. (2015) "Mechanical Behavior of Self-Compacting Soil-Cement-Sisal Fiber Composites", Key Engineering Materials, 634: 421–432.

Pillai, R.R., and Ayothiraman, R. (2012), 'An innovative technique of improving the soil using human hair fibres', Third International Conference on Construction In Developing Countries (ICCIDC-III) "Advancing Civil, Architectural and Construction Engineering & Management" July 4-6, 2012, Bangkok, Thailand

Puppala, A. J., and Musenda, C. (2000) “Effect of Fiber Reinforcement on Strength and Volume Change in Expansive Soils”, Transportation Research Record 1736, Transportation Research Board, Washington, D.C.

Sahu, R., Ayothiraman, R. and Ramana, G. V. (2016), “Shear behavior of sand reinforced with human hair fibres”. 19th Southeast Asian Geotechnical Conference & 2nd AGSSEA Conference (19SEAGC & 2AGSSEA), pp. 395-397, Kuala Lumpur Malaysia.

Soundara, B, Senthil kumar, K. P. (2015) “Effect of Fibers on Properties of Clay”, International Journal of Engineering and Applied Sciences (IJEAS), 2(5): 123-128.

Tang, C. S., Shi, B., Cui, Y. J., Liu, C., and Gao, L. (2012) “Desiccation Cracking Behavior of Polypropylene Fiber-Reinforced Clay Soil.” Canadian Geotechnical Journal 49(9):1088–1101.

Tang, C., Shi, B. Gao, W., Chen, F. and Cai, Y. (2007) “Strength and Mechanical Behavior of Short Polypropylene Fiber Reinforced and Cement Stabilized Clayey Soil”, Geotextiles and Geomembranes 25:194–202.

Tang, C., Wang, D., Cui, Y., Shi, B., and Li, J. (2016) “Tensile Strength of Fiber-Reinforced Soil”, Journal of Materials in Civil Engineering, 28(7): 04016031

Vibhakar, N. N. and Nahta, S. (2014) “Study of the Effect of Coir Fibre Reinforcement on the Strength Parameters and CBR Value of Clayey Soil”, International Journal of Engineering Research & Technology (IJERT), 3(4): 471-479.

Viswanadham, B.V.S., Phanikumar, B.R. and Mukherjee, R. V. (2009), “Swelling Behaviour of a Geofibre-Reinforced Expansive Soil”, Geotextiles and Geomembranes, 27(1): 73–76.

Ziegler, S., Leshchinsky, D., Ling, H. I., Perry, E. B., (1998) “Effect of Short Polymeric Fibers on Crack Development in Clays”, Soils and Foundations, 38(1): 247–253.

INNOVATIVE DESIGN FOR RETAINING STRUCTURES USING COMBINED PRODUCTS

Dr Alexander Zöhrer, Keller Grundbau GesmbH, Austria, +43 3137 3767 1274,
a.zoehrer@kellergrundbau.at
Clifford Taylor, Keller Ground Engineering, Sydney, Australia, +61 408 801 089
c.taylor@kellerge.com.au

ABSTRACT

The execution of deep basement excavations under narrow conditions is one of the most challenging tasks in geotechnics. The vicinity of neighbouring buildings, roads, and underground structures such as sewers or power lines, quite often prohibits the application of standard solutions. In addition, legal considerations in the use of adjacent properties is becoming increasingly difficult. This paper will present some innovative approaches to overcome the above-mentioned challenges based on several case studies from central Europe. For every project the design approach as well as the techniques used for execution will be explained, detailing both the advantages and the limitations of the applications. One case study shows a deep basement excavation (approx. 17m) in the centre of Prague, Czech Republic. This project featured many challenging boundary conditions (narrow construction area, high ground water table, jet grouting column embedment into bedrock, constraints regarding use of ground anchors due to property rights, etc). The realisation of the complex design is described and illustrated in detail. Other case studies will show the combined application of bored piles with jet grouting and also explain the design of vertical prestressed anchors for retaining walls.

Keywords: innovative, deep excavation, boundary conditions

INTRODUCTION

The development of urban areas has always presented challenges, from access for equipment and materials to the rectification of existing foundations in unknown condition. Compounding these is the increasingly stringent requirements to retain, maintain and reduce impact on culturally and historically significant structures. As available space is becoming more limited, optimisation of real estate has resulted in buildings getting higher and their basements deeper below ground. Two or more basement levels are quite common, with typical excavation depths ranging from 5 to more than 10m. Additionally, we are faced with neighbouring buildings that are equally high, deep and massive. These buildings directly adjacent the retaining structure require underpinning to limit settlement, and in cases where they are within just a few meters, this building mass generates additional earth pressure for the retaining wall to support, resulting in complex loading cases.

This paper highlights several common challenges and explores the measures implemented to overcome them. The challenges and examples of either design based solutions or practical applications will focus on the following topics – the limitations of conventional geotechnical construction methods, overcoming challenging geology and the requirement for watertight basement constructions.

LIMITATIONS OF CONVENTIONAL METHODS

There is a wide range of techniques available that can solve some of the challenges outlined above. Each of them has its advantages but also limitations. The determination of the technique or combination thereof best suited to the application is often dependant on numerous parameters. Soil and ground water conditions and the dimension and arrangement of the basement excavation are key considerations. Of increasing importance is the legal considerations when wanting to utilise adjacent property subsoils for

soil nails and or ground anchors required to complement a retaining system. A common solution is to install embedded walls in combination with one or more layers of ground anchors or internal struts. The walls are typically executed as secant pile walls or diaphragm-walls, the latter more suited to large projects offering sufficient space for the equipment required in construction of these elements. The application of soldier or contiguous pile walls is typically limited to excavations above the ground water table and jet grouting walls can be used under and in front of existing buildings. With sheet pile walls applicable for limited soil and depth conditions.

However, there are extensive reasons to consider alternative solutions. The vicinity of underground structures, power lines, sewers, etc. limit the application of ground anchors due to clearance or impact issues. Some European cities have prohibited the use of public ground during construction which also limits the use of ground anchors and nails as these are typically installed outside the building footprint into adjacent land. An additional consideration is the drilling procedure required to install anchors below the ground water table, it is technically very challenging and increases the risk profile of the project. Struts as substitutes for ground anchors heavily influence the construction sequence, and basement excavations with larger dimensions or non-rectangular/uniform layouts result in strutting systems being prohibitively difficult and expensive. To install stiff elements like piles, d-walls or sheet pile walls, large and heavy equipment is required to operate in limited or restricted space. Small and adaptive rigs are available to install jet grouting columns, but such retaining systems usually require additional layers of anchors or struts to compensate for their lack of reinforcement elements.

Innovative solution: Vertical anchors in combination with jet grouting columns

To overcome some of the above mentioned limitations, jet grouting techniques can be supplemented with vertical prestressed anchors. Jet grouting columns are applicable in a wide range of soils and can be executed under limited space and headroom conditions. The shape and arrangement of the jet grouting wall can be adjusted to suit the design and site requirements resulting in a highly versatile solution. One limitation being the requirement for multiple layers of ground anchors to resist the applied forces.

Design principle: Jet grouting walls without anchors (structural elements) are classified as gravity walls, the self-weight of the wall plays the most significant role in the support of the retained material. If anchors are incorporated in the retaining system, jet grout walls are then classified as composite retaining structures (Powrie, 2004). Design checks for jet grouting walls are identical to all other retaining structures with the exception for the internal stability of the wall. The failure mechanism is assessed by calculating and evaluating the line of thrust, which is defined as the locus of points through which the resulting forces pass in a retaining wall. To keep the structure stable, the position of the line must stay within certain limits. Depending on the design approach, these limits are defined by the core of the cross section for a conservative approach up to a limit dependant on the yield stress of the material. Put simply, the bending capacity of a jet grout wall increases if the vertical stress inside the wall increases. This general behaviour is optimised with the combination of vertical prestressed anchors. The anchor head of the vertical anchor is placed at the top of the wall and when stressed the resultant force is acting as an external vertical force applied through the wall, this additional vertical force increases the internal vertical stress of the wall. The bond length of the anchor is situated either close to the bottom of the wall (System A, Fig. 1) or below the wall (System B, Fig. 1). System B is only possible if the soil below the wall is very stiff as this system also increases the stress of the material between the bottom of the wall and above the bond zone.

By utilising this solution both the required number of anchor layers as well as the required thickness of the jet grouting wall can be reduced. The vertical anchors can be installed after completion of the jet grouting columns and before the excavation starts, reducing the influence on the excavation sequence and providing scheduling advantages.

Figures 1 and 2 below show the cross section and analysis showing the resultant line of thrust for a site executed in Bratislava, Slovakia. In addition to the above mentioned advantages, this design enabled the advantage of providing a water tight structure and also avoided the need for anchors installed below the ground water table. This is a key consideration when confronted with soils of high permeability as any drilling below the ground water level is very difficult and risky.

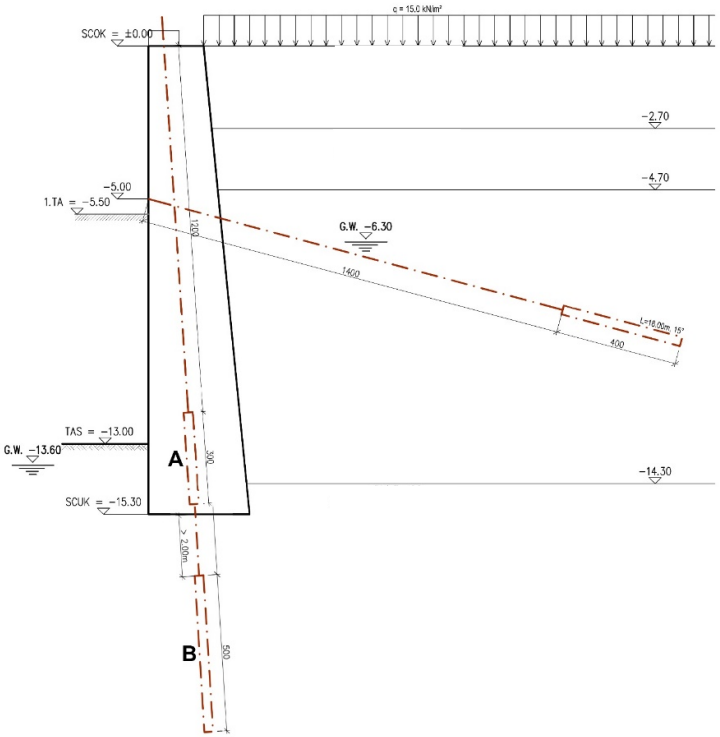


Figure 1: Cross section showing bond length of vertical anchor inside of jet grouting column (A) and below (B)

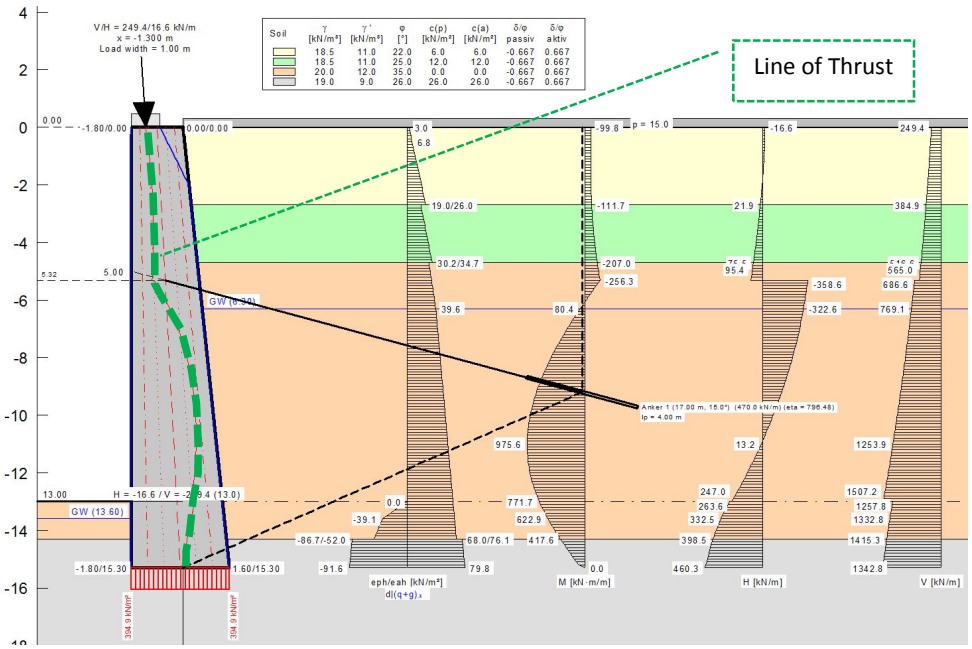


Figure 2: Model analysis of above shown cross section for case A (anchor within column)

A critical component of the system is the anchor head and its configuration. As the forces applied to the wall are comparably large in order provide a significant internal stress increase, the bearing of the anchor head must be capable of distributing the anchor force as homogeneously to the top of the wall as possible. Concrete blocks or beams are typically the most efficient solution. Evidenced below in Figure 3 is a bearing failure at the top of the column resulting from an insufficient bearing surface.



Figure 3: left: Poorly detailed anchor head; right: basement excavation with concrete anchor bearing caps/blocks

Innovative solution: Buttress walls

Another approach utilised in reducing the required number of anchors or ultimately avoid the requirement for anchors at all, is to consider a substantially thick wall. Such walls consist of multiple rows of columns which form a contiguous body. The design principle of buttress walls as opposed to a contiguous body is to omit columns from the second or subsequent row and rely on soil enclosed between the remaining columns to contribute sufficient mass to the stabilising unit. This results in a reduction to construction costs. To quantify the advantages of buttress walls Racansky (2008) investigated this design approach based on 3-dim Finite Element analysis (Figure 4).

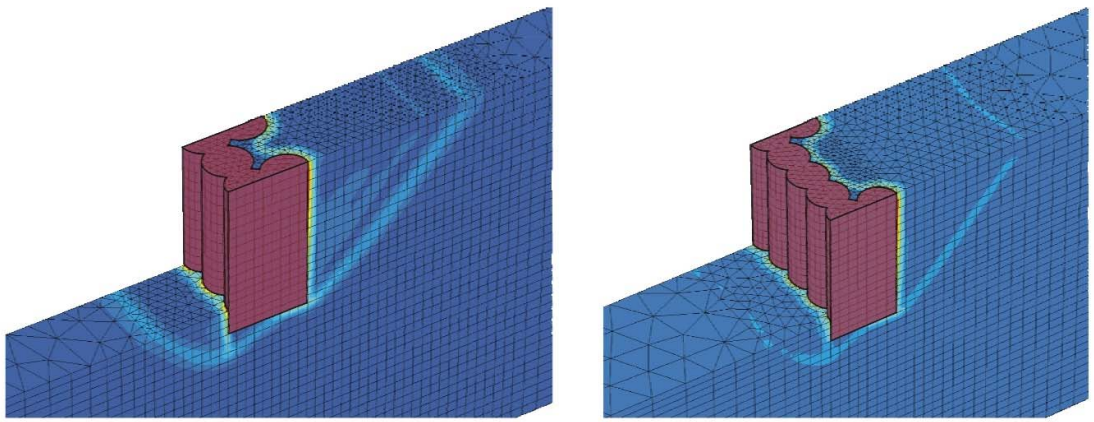


Figure 4: 3-dim Finite Element analysis to derive factor of safety

Analysis was undertaken for the extreme case of a continuous wall consisting of two rows of columns (S0). Several alternative but equivalent cases are shown in Figure 5) (S1-Sinf). As a result, by omitting every second column of the second row, the wall still performed close to the fully contiguous wall. A significant finding considering the treated volume has been substantially reduced. To simplify the design, diagrams with equivalent thicknesses based on the same factor of safety were developed, with the spacing of the buttresses dependant on the prevalent soil conditions. Buttress jet grouting walls have been particularly successful in Bratislava, Slovakia, as they perfectly complement the typical soil profile.

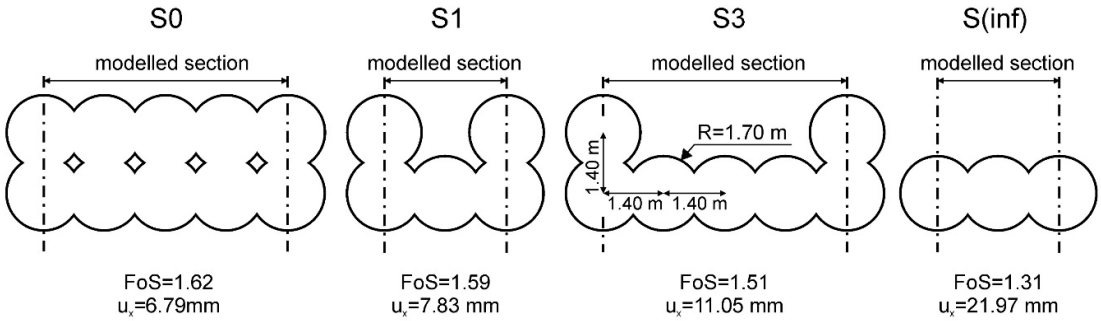


Figure 5: Analysed systems of jet grouting columns as Buttress Walls

CHALLENGING GEOLOGY

Some of the historical cities in Central Europe such as Vienna and Graz in Austria, or Prague, Czech Republic, have a particular soil profile providing significant challenges. Below an approximate 1 to 3m thick layer of fill or debris, there is a water bearing layer of quaternary sands and gravels up to 10m in thickness with tertiary stiff to solid silts forming the underlying layer. It is this lower layer of fines that makes the application of several techniques very difficult. The ability to penetrate with driven sheet piles into the stiff layer is very limited, and jet grouting, which is a common solution to treat the gravel layer, is limited by the achievable diameters within this lower layer. Piles, and in larger projects also d-walls are applicable, however, cheaper and more versatile solutions are often required by the client.

Innovative solution: Layered solutions using combined products

Example of use: Close to the city centre of Prague a new building with several levels of basement had to be constructed. The excavation level reached several meters into the stiff silt formation. Due to very confined available space, applications requiring the use of large rigs and equipment were not possible – diaphragm-walls and bored piles. Therefore the designer had to utilise techniques that could be executed with comparably compact equipment.

Figure 6 below shows an overview of the multiple different elements used in the retaining system. Jet grouting walls were used to underpin the adjacent building and form a water tight sealing wall. The bottom of the jet grouting columns were designed to be within the transition zone to the stiff layer of fines. As the columns have no embedment, no horizontal stresses could be applied to the base of the columns. Therefore at least two layers of ground anchors or struts needed to be placed. Below the columns shotcrete and soil nails were designed to retain the silty layer. As the vertical stress at the base of the columns cannot be supported by the thin shotcrete layer, this would have resulted in a ground failure. To combat this failure mechanism additional micropiles were used to transfer the vertical loads of the columns deeper into the underlying strata bypassing the soilnail wall.

To understand the behaviour of such a complex retaining system, Finite Element analysis was used to create a very detailed model of all the structural elements and their reactions during each construction sequence (Figure 7). One of the significant advantages of the design was the ability to adjust it to all local variations, including the soil profile, loads and foundation levels of the adjacent buildings, and excavation levels.

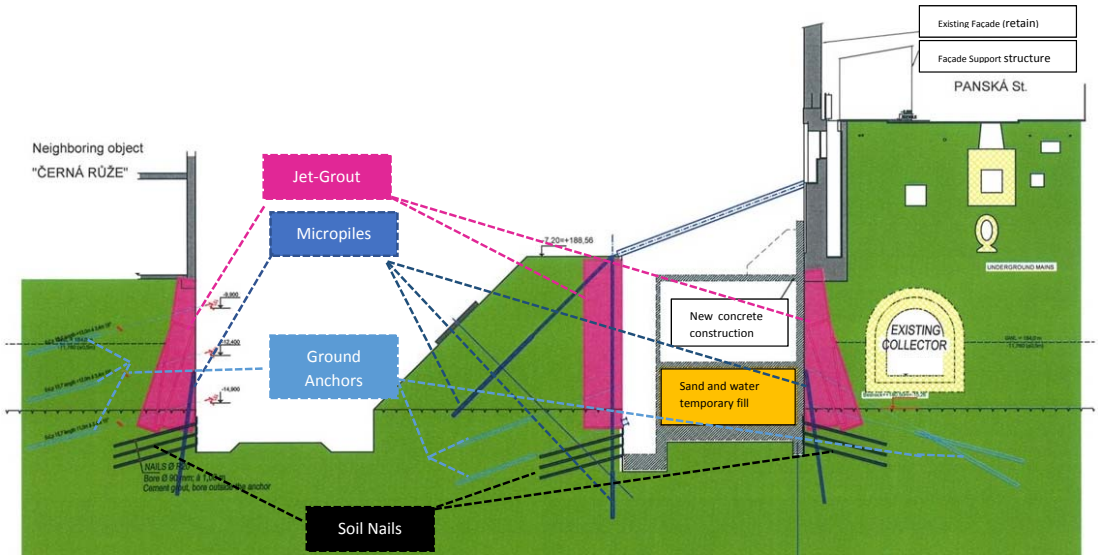


Figure 6: Cross section of site Na Příkopě, Prague

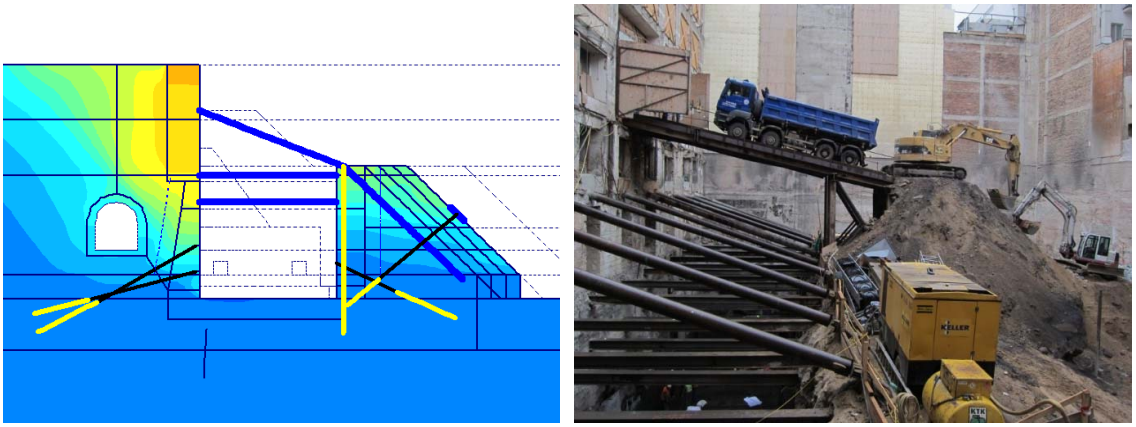


Figure 7: Comparison of Finite Element analysis (left) and execution (right)

WATER TIGHT RETAINING SYSTEMS

In many instances basement excavations extend below the ground water table. This results in the retaining structure having to resist not only the earth and water pressure but the additional requirement of forming water tight structure. One of the most commonly used systems is the hard-soft secant pile wall. From a design perspective this type of retaining construction is actually a split system, with the unreinforced primary piles prevent the water inflow between the secondary load bearing piles. These primary soft piles also distribute the earth and water pressure forces acting on them towards the stiffer reinforced secondary piles. However, much of the load distribution has already occurred behind the wall by means of arching effects within the soil.

Innovative solution: Contiguous pile wall with jet grouting sealing

When considering a secant pile wall, the designer is limited in choice of the pile spacing as it is a geometrical resultant of the pile diameter. Reinforcement within the secondary piles determined by the loading conditions. If you consider a contiguous pile wall in place, this limitation is removed, therefore the spacing of piles can be selected in order to optimise the design. Generally this results in a more cost effective solution but creates its own issues with water ingress within the untreated/replaced soil between each pile. In this example the space remaining between the piles is filled with jet grouting columns that can be perfectly adjusted to suit the resultant spacing of the piles, again the flexibility of the getting solution is suited to rectification works on piles that have been installed outside of verticality requirements causing water inflow issues. Equivalent to the primary (soft) piles of a secant pile wall, the columns transfer the earth and water pressure to the secondary (hard) piles. During basement excavation, any protrusion of the jet grout column within the basement excavation can be easily trimmed. As these elements are not subjected to significant loads, the design can be further optimised by using semi (half) columns instead of full columns (Figure 8).

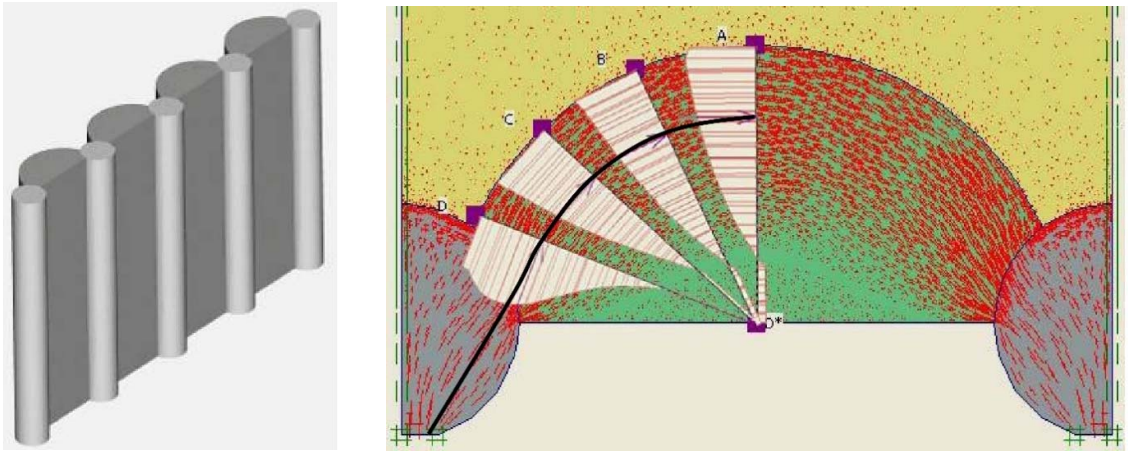


Figure 8: left: Jet grouting semi (half) columns between reinforced piles; right: normal stresses showing arching distribution

Design checks required for the columns are as follows: confirmation of the compressive strength of the jet grouting (soilmix) material and check of the shear stress at the interface to the pile. Stadlbauer (2010) analysed the stress distribution of various layouts, ranging from pile spacing similar to a secant pile walls up to larger spacing's of 3.0m. in which up to three jet grouting columns were modelled in between the secondary piles. Note: the secondary (hard) piles are installed as primaries when considering a jet-grout contiguous wall.

Figure 9 shows a design with two semi columns. As evidenced by the stress distribution and failure mechanism it can be determined that the critical component is the connection between the columns. The resultant arching mechanism passes very close to the edge of the columns, leading to local concentration of stresses. The phi/c-reduction of the Finite Element analysis (right picture in Figure 9) shows the shear stresses at failure. Moreover, Stadlbauer (2010) investigated the influence of geometrical imperfections of the initial column as well as pile position in combination with unfavourable inclinations.

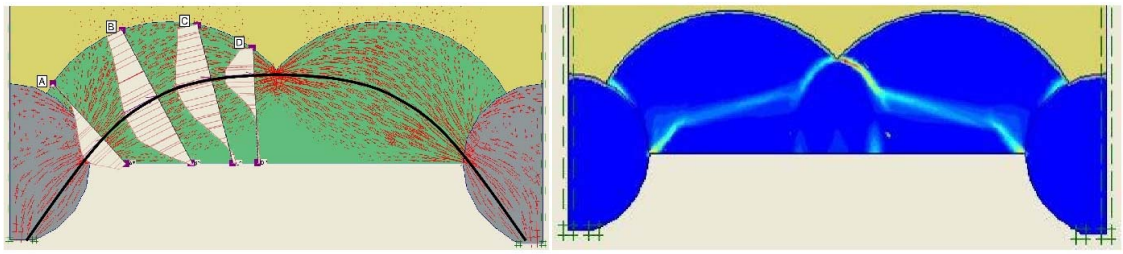


Figure 9: Application of two half columns; left: stress distribution; right: failure mechanism;

As an additional improvement full or semi columns can be substituted by thin jet grouting elements known as lamellas (Figure 10, left). With the installation of such thin elements the execution quality and quality management on site is extremely critical. Small deviations, especially for the direction of the lamellas, could result in the reduction of the contact area with the pile. Therefore, such systems are usually applied below the final excavation level.



Figure 10: left: application of jet grouting lamellas instead of half columns; right: trimmed jet grouting columns between piles

Innovative solution: Cutter soil mixing in combination with propping and ground anchors

Example of use: Seven story residential development with 2 level basement carpark in Northbridge, Perth, Western Australia. A number of construction techniques were incorporated to overcome a collection of the above mentioned challenges. The client was receptive to an innovative approach in providing an economical solution that also had to limit the impact on an existing historically significant building, located within the proposed basement footprint. As the carpark extended beneath the heritage building an underpinning solution had to be developed.

The soil profile consisted of a sandy fill with some construction rubble to approximately 2.0m over a fine to medium grained sand generally medium dense to dense with some silt and thin layers of stiff to very stiff clay between 7m and 9m extending between 12 and 15m depth. These sandy layers were overlying a 10m thick layer of stiff to hard sandy to silty clay containing 1m thick sand layers. A key consideration was the groundwater table located at 1 to 2.5m below ground level. The high water table in sandy material meant a dewatering solution would not be viable, therefore a watertight retaining wall embedded in the underlying clays was required.

The initial design options consisted of conventional driven sheet piles or a hard-soft secant pile wall. To avoid damage to the heritage building caused by vibratory construction methods sheet piling was discarded early in the design process. An alternative to the secant pile wall (Leach, 2014) in the form

of a Cutter Soil Mix Wall (CSM) was proposed. The CSM method provided a number of advantages over conventional piling. Higher production rates, comparably smaller equipment, reduced spoil disposal and a key consideration in the quality and surety of a watertight wall.

As a relatively new technology to Australia, there was no available historical data of CSM used in an underpinning application. Furthermore, without proven strength and stiffness properties of the soilmix material available in time to suit an expedited construction sequence, a conservative approach was taken with the inclusion of steel Universal Beam (UB) sections within the wall to provide lateral and vertical loading capacity. To supplement this capacity temporary ground anchors were required across the majority of the site with the exception of one boundary where the owners of the adjacent building did not provide consent to install any element beneath the footprint of their building. Figure 11 below outlines the multiple boundary conditions and techniques utilised.

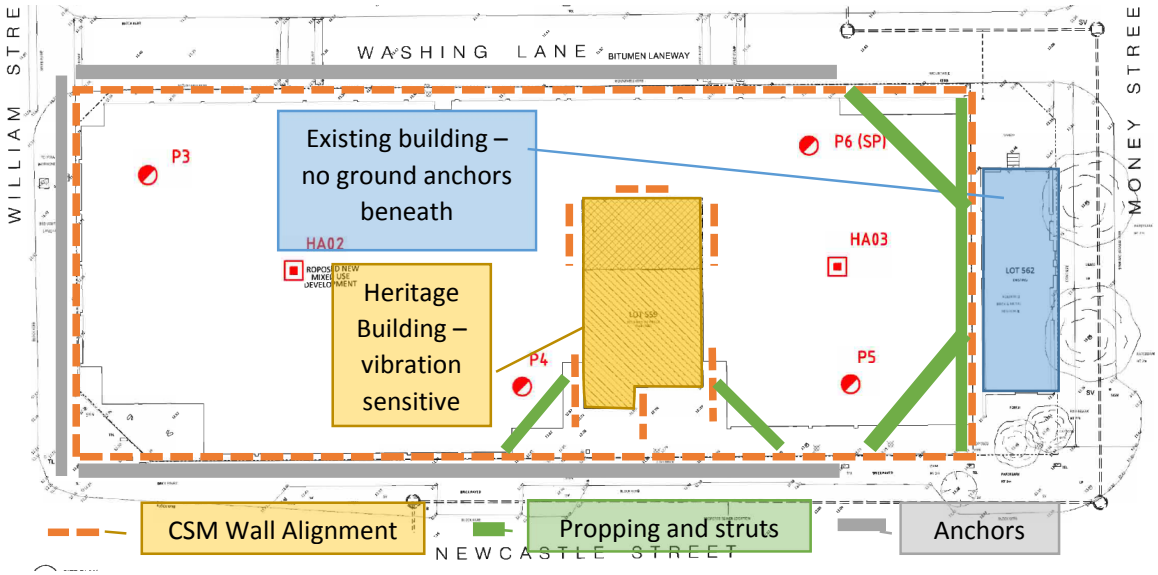


Figure 11: Multiple boundary conditions resulting in multiple techniques



Figure 12: left: CSM installation adjacent sensitive structure; right: part excavated basement with propping and struts

To further the optimisation of the construction programme and provide additional commercial savings the temporary ground anchor design included detailed modelling with the WALLAP software package. Again the soilmix material was conservatively assumed to provide no structural capacity other than that

of groundwater cutoff. The anchors were modelled to complement the lateral restraint of the UB sections and versatile multi-use wales provided flexibility in positioning and installation. Below in Figure 13 can be seen extracts form the model for staged construction sequences and associated bending and shear force loading.

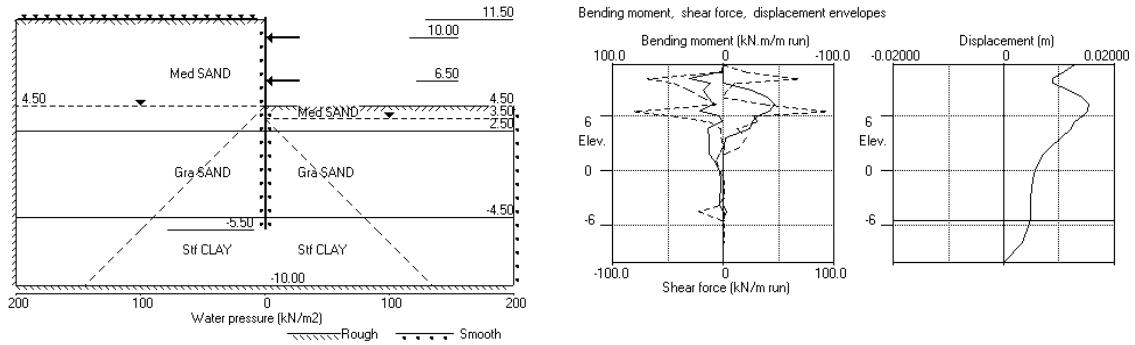


Figure 13: left: staged model; right: predicted bending, shear and displacement values

By adopting a multi-strand post grouted anchor construction, bonded within the sand strata, significantly higher load capacities could be applied to each anchor. This resulted in the reduction of the initially assumed number of anchors required by a full 33%. A propriety system was developed to ensure post grouting manchette tubes protruding from the wall below the water table did not cause inflow of water or running sands into the basement excavation before final sealing and lock-off could be achieved. Shown below in Figure 14 is an example of the anchor model in combination of the CSM and UB wall.

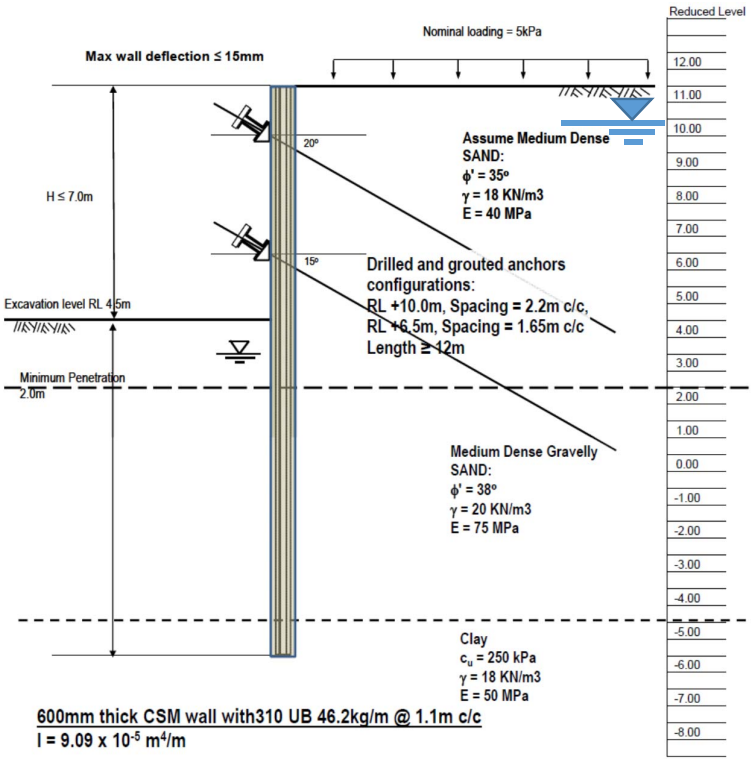


Figure 14: Multi-strand post grouted temporary ground anchor model in conjunction with CSM wall reinforced with UB sections

The combination of these multiple techniques not only significantly reduced the construction programme but resulted in no structural damage to the heritage building during the entire construction sequence (Figure 15).



Figure 15: Excavated basement with underpinned heritage building

CONCLUSIONS

As new building sizes increase, and the available or usable space in cities decreases, the design of urban projects is becoming more and more complex. Quite often conventional solutions do not complement all boundary conditions or are simply too expensive. During the development of a solution, designers should be conscious that special geotechnical conditions within the project exist and it is important to have an understanding of available techniques and products, including their advantages, limitations, performances and cost. However, in-depth knowledge of all techniques is not universally available to many designers or consultants. Fortunately specialist geotechnical contractors can provide alternative or optimised solutions based on their experiences and knowledge, thus can add considerable value to the project as a whole.

REFERENCES

Chris G. Leach, 2014. Use of CSM to support a heritage building, DFI 1943; publication #100 (IC-2014).

Powrie, W., 2004. Soil Mechanics - Concepts & Applications. 2nd ed. Spon Press.

Racansky, V., 2008. Design of jet grouting structures, Ph.D. Thesis, Brno University of Technology, Czech Republic.

Stadlbauer, J., 2010. Numerical investigation and optimisation of an intermittent bored pile wall with jet grouted bracings and development of an analytical model for design. Diploma Thesis, FH Joanneum Graz, Austria.

NEWEST DEVELOPMENTS IN QUALITY CONTROL AND SOIL MIXING FOR ACTUAL AND FUTURE DEMANDS

Franz-Werner Gerressen, BAUER Maschinen GmbH, Schrobenhausen, Germany, Franz-Werner.Gerressen@bauer.de

ABSTRACT

New developments are required day by day. On the one hand site to improve the actual situation, on the other hand site to create the future and to ensure that future demands can be fulfilled. This requires for instance the development of technical support systems, which enable a more constant and quality ensured installation of special foundation products like piles. As part of the quality control, real time installation control of the production process, data transfer and reporting systems become more and more important ensuring the five dimensions of a jobsite. That means not only the three well known dimensions (width, height, depth) are cover, but also the dimension of time and money. Beside small, but important, details, also the demand of extending the use of methodologies in terms of getting deeper or allow their use in various soil conditions require the development of new tools and equipment. Therefore, the paper will describe some of these new approaches and activities required for these new developments. It will describe also the main equipment which will be needed to execute these works under the various conditions

Keywords: Electronic, Assistant Systems, Soil Mixing

INTRODUCTION

New developments are required day by day. Either to improve the actual situation, or to create the future and to ensure that future demands can be fulfilled. Therefore, there is an increasing demand for the development of e.g. “Little Helpers”. “Little helpers” are for example technical support systems, which enable a more constant and quality ensured installation of special foundation products like piles, for example an assistance system like the later explained “drilling” assistant. As part of the quality control, real time installation control of the production process, data transfer and reporting systems become more and more important ensuring the five dimensions of a jobsite. In a second part the focus will be given to new approaches for soil mixing application. Adjustments of tools or equipment to extend the range of possible usage as well in terms of soil conditions as in treatment depth.

“LITTLE HELPER”

General

The B-Tronic System enables you to efficiently operate, maintain, and administer individual machines as well as entire fleets. It helps you to securely monitor and precisely evaluate your projects and work processes. The system is an integrated system for controlling all operations and visualizing actual operating parameters in real-time on a large interactive touch-screen monitor.

In addition to these basic operational data, general machine operating parameters (e.g. engine data) are also acquired and monitored. The display of current machine operating states and error messages is a valuable aid for targeted and effective fault finding by service personnel on site, but also by specialists based at the offices, as data can be transferred real time via internet connection. This does not only allow the control of equipment and installation process including relevant reporting, it also allows comparing

“virtual reality” and “reality”, hence planned and actual execution, which enables the project manager to control not only the schedule, but also the use of budget.

A special focus was given in the past to the development of so called assistance systems. These systems relieve the operator by automating or repetitive operations with the B-Tronic system. They help to prevent faulty operation of the machine and therefore protect both man and machine. Automatic, fast control processes increase the drilling performance and reduce wear of both, equipment and tools. Assistance systems thereby ensure a consistently high production quality. Actually more than 20 different assistant systems are available for various applications.

Assistance Systems - Controlling the installation process, e.g. by using a “Drilling” and “Concreting“ Assistant

Most rigs can be equipped with electronic software for use with the so called "Drilling Assistant", which modulates the optimal rate of penetration and crowd force during the drilling process for an optimal speed of rotation of the drilling tool, especially working in single pass methods like Continuous Flight Auger (CFA), Full Displacement Piles (FDP) and Cased CFA. The desired initial parameters can be input by the rig operator with the help of simple onscreen menus.
By using a programmable "extraction assistant", the speed of extraction and volume of concrete can be adjusted. This involves measuring the volume of concrete continuously throughout the concreting process and automatically regulating the speed of extraction based on the concrete flow rate.
The "Assistants" are integrated into the general electronic monitoring and control system B-Tronic. They ensure the piles are installed to a high and consistent quality standard. All important data is displayed on the operators monitor (Figure 1).

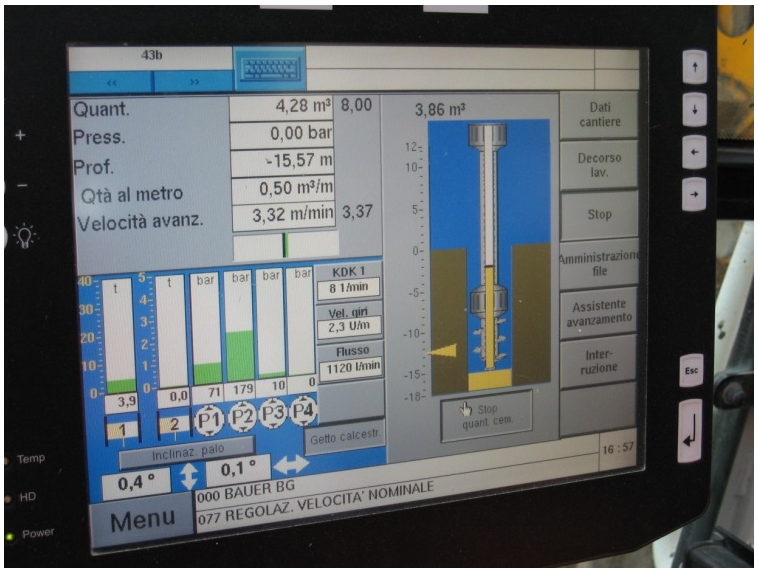


Fig. 1: Exemplary B-Tronic display during the concreting process in automatic extraction mode

iCFA

The iCFA system is a development to fulfil the growing demands in quality assurance for the installation of CFA piles. For instance, the monitoring of a higher concrete pressure than earth pressure is required. As usually the concrete pressure is measured at the top of the drill string, the real pressures in the ground are much higher than required and can cause unnecessary concrete overconsumption and in a worst case scenario blockages of the concrete line. The iCFA system is now equipped with a pressure sensor at the

bottom of the drill string which allows a more accurate pressure measurement and therefore provides potential cost savings in concrete overconsumption. In addition, the iCFA drilling rod measures as well the inclination of the pile at the bottom of the drilling string.

As measurement at the bottom is quite complicate, a special drill string was developed. A specific feature is that the data transmission is not done by cable, but by inductive data transmission through the auger joints, which were somehow eponym for the "i" in the name. Figure 2 shows the general configuration and highlighted details of such a drill string.

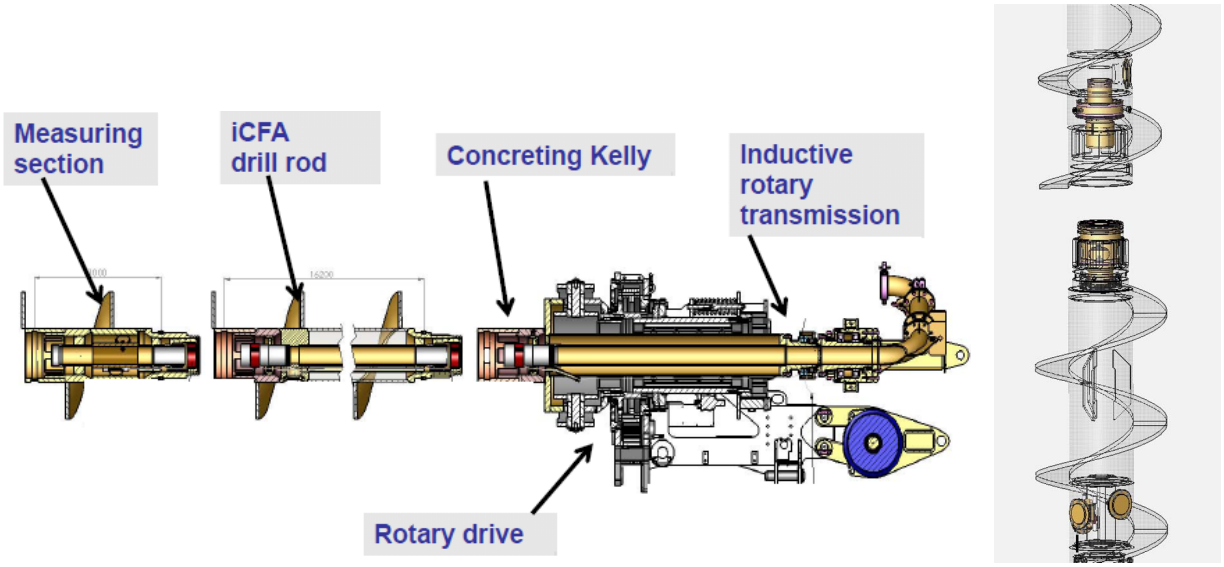


Fig. 2: Configuration of the iCFA, relevant parts of I-System are highlighted in the drill string (right detail)

These are only a few examples how to deal with more and more complex demands. Real time installation control, data transfer and reporting systems become more and more important and will serve also future demand ensuring the five dimensions of a jobsite.

NEW SOLUTIONS IN SOIL MIXING TECHNOLOGIES

Single Column Mix – Double Head (SCM-DH)

The Single Column Mix – Double Head (SCM-DH) method of deep mixing has been in operation now for a couple of years. Since it is not new to install single mix columns, the benefit of this new tool needs to be explained. As the name says, the system works with a double rotary head. This ensures that two counter-rotating mixing tool components achieve exceptionally intensive levels of mixing between soil and slurry. Therefore, the newly developed SCM-DH Single Column Mixing Tool for Double Rotary Drives represents a significant improvement of the single column mixing tool, as it enables to move the borderline of suitable soils for soil mixing applications. A major advantage that can be gained from the soil mixing method is the possibility to provide a number of solutions to a site that is being developed using the system for support to the new loadings, services to the site, temporary retaining walls, sewers or inspection pits that may be in or below the soil mixed mattress. Designing ahead of the works, additional soil mixed columns can be installed to facilitate the requirements for various proposals. Due to the fact that the counter-rotating mixing tools act like a compulsory mixer, the grade of achievable homogeneity allows intensive levels of mixing between soil and slurry and the construction of soil mix columns not only in granular soils but also in cohesive soils where soil mixing usually gets to its limits.

Working procedure

The general sequence of installing a SCM-DH column as shown in figure 3 starts with the preparation of the pre-excavation. Aim of the pre-excavation is to accommodate overflow, which might be created during the soil mixing process. After positioning the SCM-DH machine, the mixing tool is drilled into the ground at a continuous rate by the rotary drive of the drill rig. During the penetration the soil will be cut by the outer mixing tool. At the same time a fluid (e.g. cement slurry) is pumped by a slurry pump through to a flexible hose to a flush head on top of the rotary drive and the inner mixing tool. The fluid nozzles are located at the lower mixing blade layer of the inner mixing tool. The injection rate depends on the soil conditions and the required mechanical properties of the mixed column. Due to the counter rotating parts of the mixing tool, high shear forces can be applied to the soil.

After reaching the final mixing depth, the mixing tool is pulled out of the ground while it continuously rotates and mix the soil with the fluid. If necessary, reinforcement (e.g. steel beams) could be installed into the fresh mixed column.

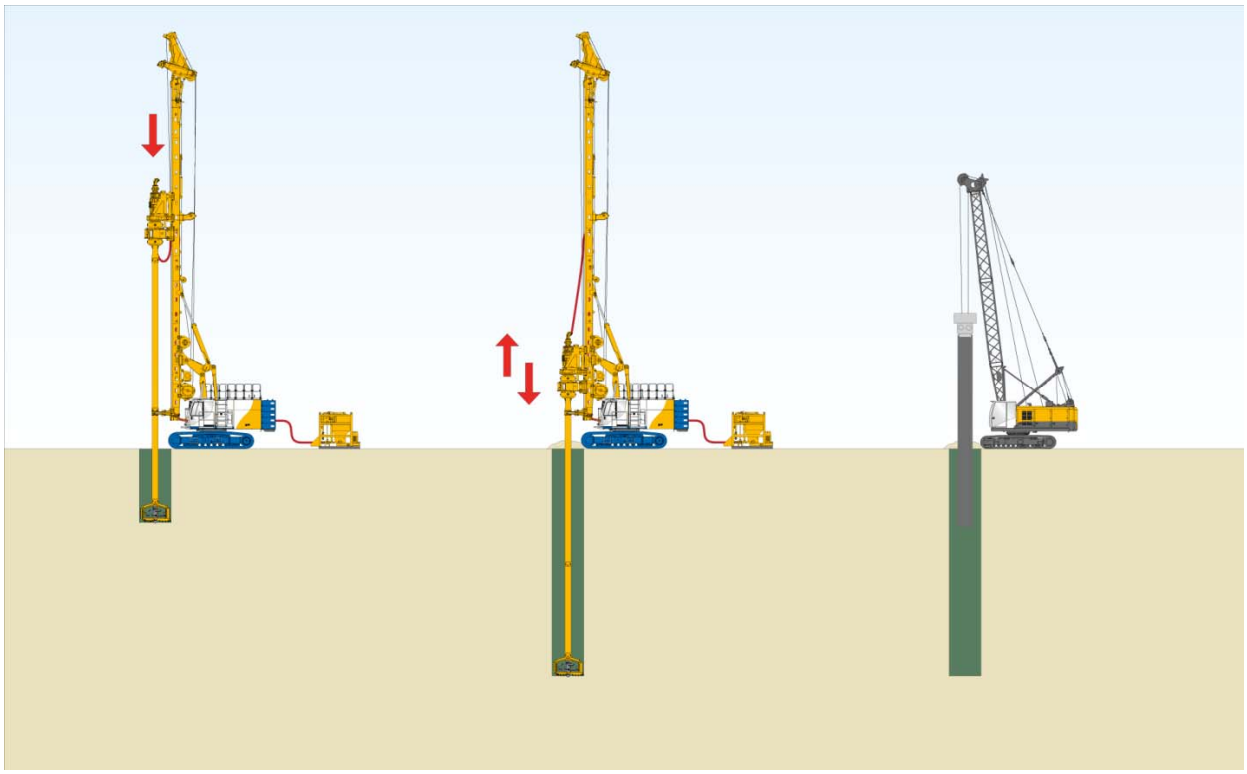


Fig. 3: Working principle SCM-DH

Equipment

Due to the robust design it is currently possible to create column diameters up to 2.4 m as shown in figure 4. Large diameter mixing offers a high potential for soil improvements at high performance, but also the right auxiliary equipment needs to be considered.

A sufficient set up of slurry supply capacity, mixers and pumps, is required to ensure that the mixing can take place at the best performance. Due to the achievable diameter and depending on the installation speed for the various applications, the required pumping capacity can be in a range of 500 – 1,500 l/min which would require mixing plant capacities of up to 90 m³/h.

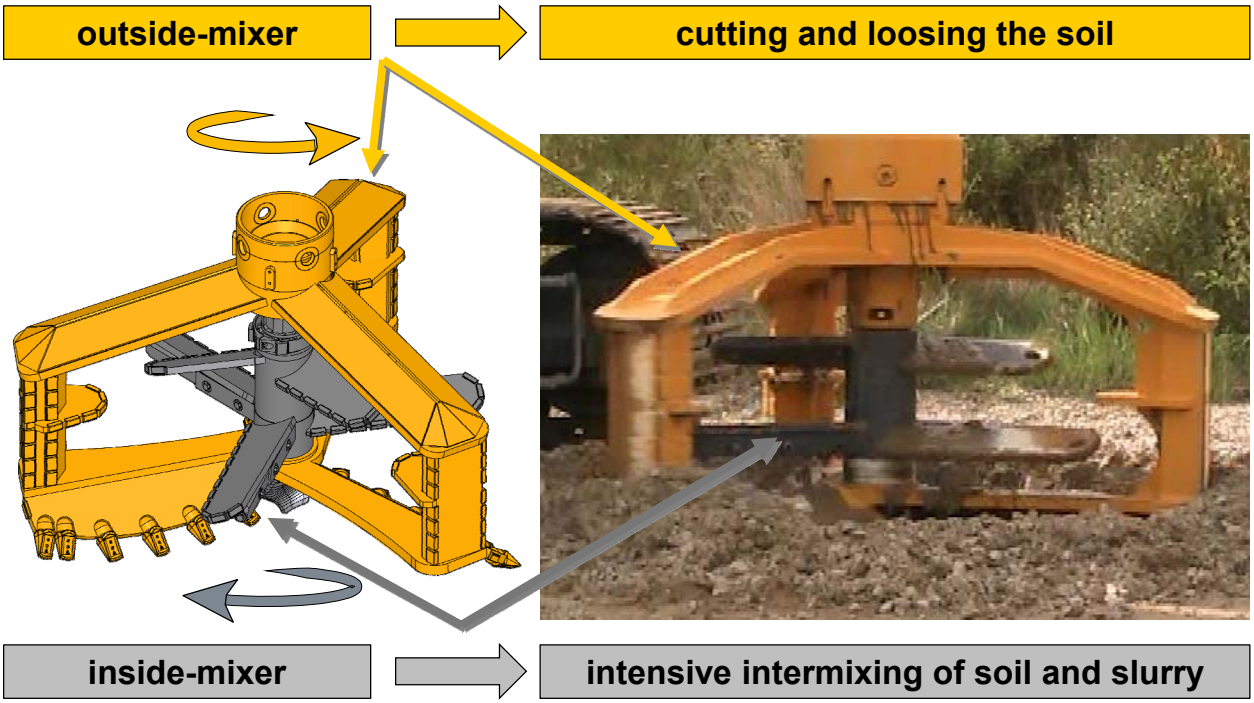


Fig. 4: SCM-DH Mixing tool

Having established the success of the SCM-DH system, several opportunities can be considered for its use. Following applications have been carried out successfully to date:

- Deep Drainage Corridor
- Bearing Capacity Ground Improvement
- Uniform Settlement Control to Variable Ground Conditions
- Retaining and Cut-Off Walls
- Vibration Reduction Barrier
- Mass Mixing to Depths greater than 4.0m
- Building Foundations
- Slope Stabilization

Exemplary reference for SCM-DH

For a new highway in Rumania there was a need to stabilize the slopes when the highway cuts into it. The soil conditions, as far as known, were described as a firm to stiff clay followed by a stiff to very hard Marl (see figure 5). The soil investigation was carried out using the Dynamic Penetration - Super Heavy (DPSH) test procedure, a test comparable to the SPT penetration Test.
For final mixing depth which was expected to be up to 16 m, an increase in soil resistance could be expected compared to the known Marl. The increase of resistance and the expected increase in installation time, also based on fits experiences made during test column installation, lead in a change of the installation procedure. Therefore, the 2-phase installation was introduced. That means, the penetration and liquefaction of the soil on the down stroke was done by injecting water; the final mixing was carried out on the upstroke by adding cement.

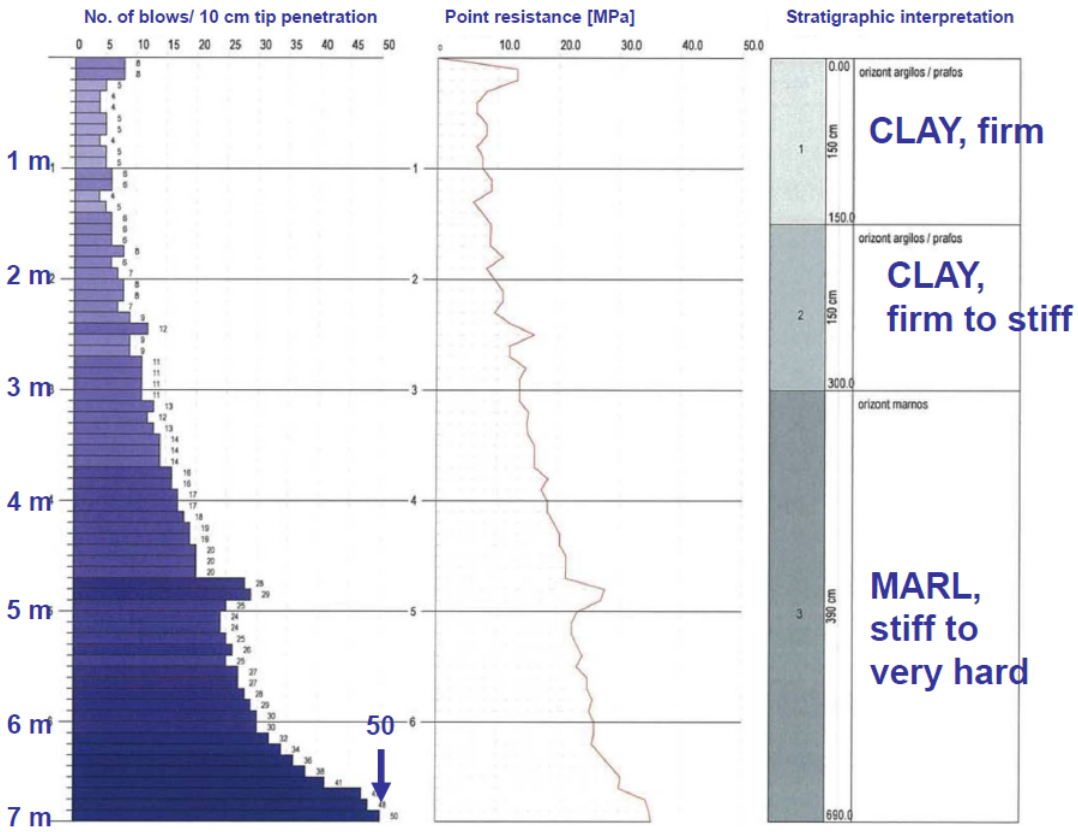


Fig. 5: Soil information for the upper part, tested by Dynamic Penetration - Super Heavy (DPSH)

Figure 6 shows an exemplary column head. Besides wet sampling also coring was done for quality control (see figure 7). Even the core shows the existence of some clay lumps, the overall mixing quality, especially for these soil conditions, can be seen as sufficient.



Fig.6. Top of the column head

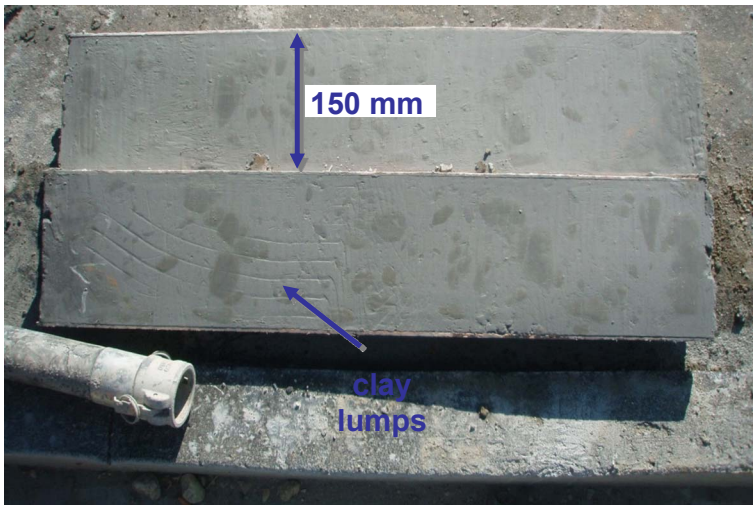


Fig. 7. Core with some clay lumps inside

Cutter Soil Mixing (CSM) – new levels in depth achievement

General

One of the main differences, in comparison with other soil mixing methods, is the mixing wheels which rotate about the horizontal axis. The design of the mixing tool was based on experience with designing trench cutters. The use of cutting/mixing wheels allows for effective penetration of hard soil layers. The design of the mixing head with the so-called reamer plates, provides a very good intermixing of soil and injected slurry.

Depending on the required properties of the soil mix elements and local conditions, different amounts of cement (if necessary bentonite) have to be injected by the CSM mixing head into the soil.

A typical construction sequence is as follows:
a) Construction of an open guide trench for retaining excess slurry.
b) Mixing of the soil mass during penetration to the final depth as appropriate slurry is simultaneously introduced. Depending on the prevailing conditions, either bentonite slurry is added to the mixing process as cement slurry is introduced into the soil during penetration. The volume of slurry injected is determined by the rate of cutter penetration.
c).During upstroke, additional slurry is injected to provide the final design soil cement proportions for construction of the wall panel.
d) A continuous panel is formed by the construction of individual panels in an alternating sequence of overlapping primary and secondary panels. Secondary panels can be constructed immediately after completion of primary panels, i.e. “wet-into-wet”. The cutter technology does, however, also enable cutting into panels that have already gained strength, i.e. “hard-into-hard”.
e) To utilize the wall as a structural retaining wall, steel beams (UB/IPB sections) are inserted into the freshly mixed wall panels.

The CSM method can be adapted to local conditions in different ways. In mixing applications with production times less than approx. 2 hours per element, a one phase mixing procedure may be used. In the one phase procedure, the final slurry product consists of cement and water or a cement, bentonite and water mixture, which is injected on both the down stroke and the upstroke of the machine. Advantages of this procedure include the additional mixing of the cement/soil on the down stroke and the simplicity of only having one slurry mix.

When mixing time per element can be expected to be longer than the initial setting time of the injected cement slurry, a two phase system should implemented. During the two phase method, non-hardening slurry is used for liquefaction on the down stroke until the final mixing depth is reached. During the upstroke, then cement slurry will be injected and mixed into the element. This method prevents the mixing tool from being ‘trapped’ in the panel if the panel construction time exceeds the initial setting time for the cement slurry. This so called two phase method becomes more and more important, as depth requirements are increasing.

As the Bauer cutter mixer (BCM) mixing unit is either mounted on a guided Kelly bar or on a wire rope-suspended cutter frame, for both types new depth records were achieved in 2015/1016. Project demands required new developments to enable possible mixing depth of 53 m (Figure 8) for the Kelly guides system and 80 m for the rope suspended system (Figure 9).

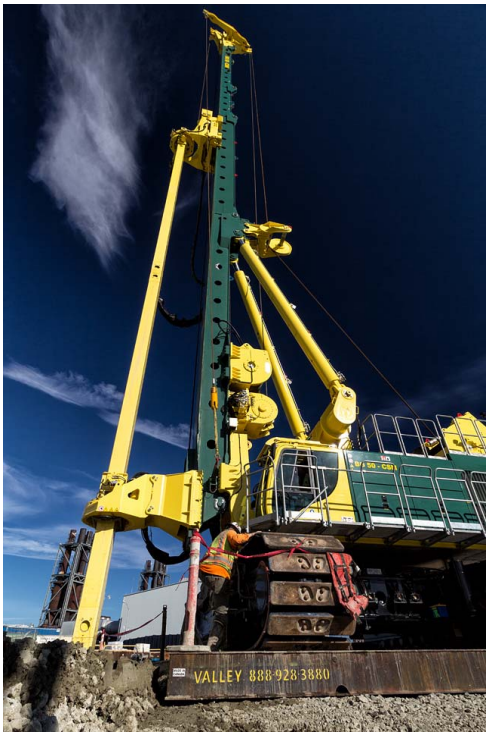


Fig. 8: BG 50 with BCM 10 for 53 m,


Fig. 9: MC 64 with BCM 10 for 80 m

Reference for shaft type retaining wall with cut-off wall function for nuclear power plant decommissioning

In Eureka, California a shutdown nuclear power plant (Humboldt Bay Power Plant) will be decommissioned completely. Therefore, a shaft with retaining and cut-off wall function had to be installed around the subsurface located reactor. Due to the local soil conditions the world deepest Kelly guided CSM panels had to be installed to key into a sufficient watertight clay layer and seal the shaft against groundwater, see figure 10

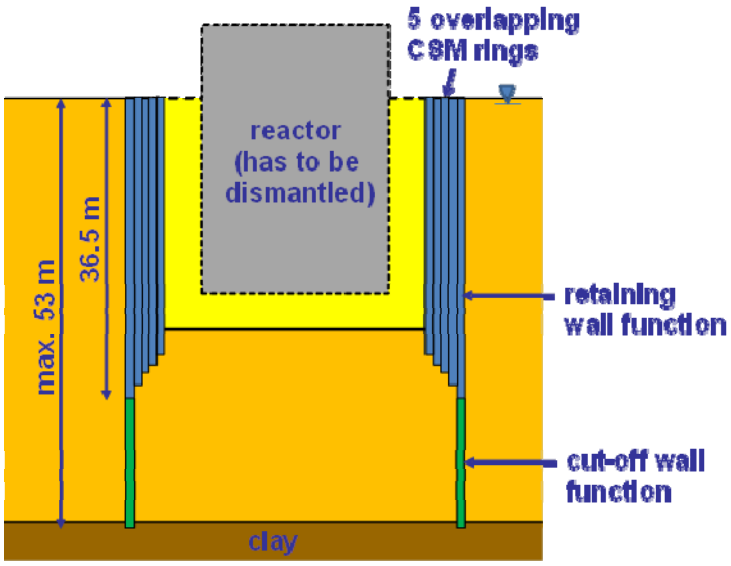


Fig. 10: General layout for the CSM installation

To prepare a sufficient support for the excavation pit and the surrounding soil the shaft, consisting of 5 overlapping CSM rings with a mixing width of 1000 mm each, were installed. Due to the mixing depth the installation time per panel exceeded the initial time of the cement slurry. Hence, the 2-Phase method was used. The 2-Phase method also had the advantage that the backflow material, which was created during the mixing process, could be recycled and the bentonite slurry reused. Thereby, the material which had to be disposed could be reduced – a major advantage in contaminated soils.
The mixing depth of the most outside ring was extended up to 53 m to key into a clay layer. In the depth between 36.5 m and final mixing depth, the injected amount of cement slurry could be reduced during the mixing tool extraction due to the required lower wall strength.
To reach the new record mixing depth for Kelly guided CSM panels a BG 50 with 10.5 m and 4 m long mast extensions was used. Additionally a steering device was mounted between the CSM mixing head and the Kelly to minimize the deviations y-axis. Also a BG 40 with a CSM mixing head were on side and helped to install the panel with mixing depth up to 36.5 m.(see figure 11)



Fig. 11: BG 50 and BG 40 during CSM installation, the old reactor building between both machines

CONCLUSION

Real time installation control, data transfer and reporting systems become more and more important and will serve also future demand ensuring the five dimensions of a jobsite. The “Little Helpers” will relieve the operator and will help to ensure constant quality: In addition they will provide cost saving potentials as well for wear and tear as for materials like concrete.

Pushing the boundaries for the use of applications either in limited suitable soils or for greater depth will require an ongoing development in equipment and tools. It can be seen that are already some steps done, but this will be a never ending process.

REFERENCES

F.-W. Gerressen, M. Schöpf, E. Stötzer, May 2009, CSM-Cutter Soil Mixing - Worldwide experiences of a young soil mixing method, Deep Mixing 2009, Okinawa

OBSERVING FRICTION FATIGUE USING HIGH STRAIN DYNAMIC PILE TESTING

Ronald Damen, Brian Perry Civil, Auckland, New Zealand, ronaldd@fcc.co.nz, +64 9 526 3515

Dion Denes, Foundation Specialists Group, Melbourne, VIC, Australia,
ddenes@foundationspecialists.com.au, +61 3 9417 4333

ABSTRACT

Friction fatigue is the loss of soil-pile friction around the shaft area of the pile. It has been observed during impact driving of piles, and has been modelled to a limited degree using physical scale models. This paper proposes the use of high strain dynamic pile testing to assess and quantify friction fatigue in impact driven piles. The method is applied to two case studies: one on a project off the north-west coast of Australia and one on a South Pacific Island. On both sites calcareous sand layers are present. Pile Driving Analyzer (PDA) monitoring has been conducted during impact driving of steel piles, which allowed for assessment of shaft resistance development both with depth and with progressive driving, by use of wave equation signal matching. Lessons are drawn from the case studies to improve future observations.

Keywords: friction fatigue, dynamic pile testing, calcareous sand

INTRODUCTION

Friction fatigue is the loss of soil-pile friction around the shaft area of the pile, under cyclic loading or during pile driving. The phenomenon has been frequently observed in some non-silica sands, such as pumice sands and calcareous sands and has been the subject of academic study.

The occurrence of friction fatigue impacts the driving behaviour of piles and the shaft friction component of the ultimate geotechnical strength ($R_{d,ug}$). If potential friction fatigue is not recognised in the design phase of a project, required pile toe levels can be significantly underestimated. This could lead to extra cost and delays, or, if no adequate pile verification is conducted, to geotechnical failure or underperformance of piles. This is especially true in remote locations, such as Pacific islands, where calcareous material is often present.

A better understanding of the phenomenon would aid both pile design and driveability assessment.

This paper proposes the use of high strain dynamic pile testing to assess and quantify the effect of friction fatigue from impact driving. Two case studies are presented in which high strain dynamic testing has been conducted on driven piles in calcareous sands to illustrate the method.

BACKGROUND

Friction fatigue

The geotechnical strength of piles is composed of the resistance to static loading by the base of the pile and the shear resistance between the shaft of the pile and the adjacent soil. The latter is often referred to as the shaft resistance or shaft friction.

During impact pile driving, a decrease in shaft resistance is often observed. Although this phenomenon is also observed during vibratory pile installation, this paper deals predominantly with impact driving. This decrease in material strength from the tip of the pile influences the shaft resistance and may be either temporary or permanent. Temporary reduction in shaft resistance is common in cohesive soils and is thought to be caused by excess pore water pressure, which has insufficient time to dissipate. This phenomenon, commonly referred to as set up, is observed to a significantly lesser extent in non-cohesive materials such as clean sands (Rausche et al., 2004).

Friction fatigue is the loss of shaft resistance due to volume reduction as a result from pile driving. During impact pile driving, rearrangement and repacking of sand grains occurs, which leads to volume reduction (White and Bolton 2002, White and Lehane 2004, White 2005). In crushable soils, such as calcareous or pumice sands, further repacking can occur due to diffusion of the fine broken particles, which settle away from the pile-soil interface into the more open matrix of unbroken particles further afield (White and Bolton, 2002). This leads to a reduction in normal stress at the pile-soil interface, which reduces the friction at this interface.

It has been observed in a number of soil types, amongst which calcareous sands (Angemeer et al., 1973) and has been subject of academic study (e.g. Murff, 1985; Poulos, 1989; Randolph 1994; White and Bolton, 2002; Denes, 2016). White and Bolton (2002) conducted calibration chamber tests, in which a pile was jacked into sand. Due to continual shearing at the pile-soil interface, a zone around the pile underwent volume reduction, which reduced normal stress acting on the pile. Gavin and O'Kelly (2007) found that the side friction of monotonically installed piles was significantly greater than of piles that underwent cyclic installation. However, it was found that a small number of load cycles was sufficient to reduce the shaft friction on a monotonically installed pile to the same level as a cyclic installed pile.

Friction fatigue has been related to the 'h/D' effect, where 'h' is distance from pile toe and 'D' is pile diameter. (Figure 1). This effect is associated with the decrease of horizontal effective stress (radial stress) at a given depth, as the pile toe penetrates deeper and the soil is sheared by an increasing pile length passing the point. A reduction in horizontal stress relates to a decrease in shaft resistance and therefore, the higher the h/D ratio, the larger the decrease in shaft resistance (down to a residual value).

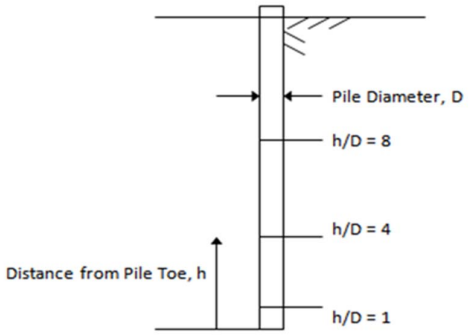


Fig. 1. 'h/D' ratio

Experiments conducted by White and Lehane (2004), using both monotonic and cyclic installation, suggest that the h/D ratio may be indicative of the amount of cyclic loading (number of blows) a pile underwent during impact hammer installation (Denes, 2016).

Calcareous sand

Calcareous sand is composed of calcium carbonate, and is formed from shells and skeletal remains from marine organisms such as coral, molluscs and calcareous algae (Poulos, 1989). Calcareous sand exhibits a porous hollow structure (see Figure 2), with a rough surface.

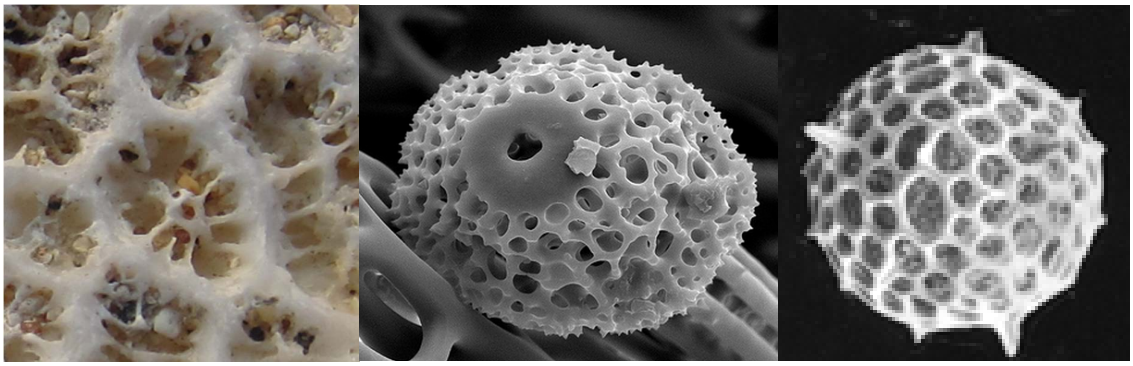


Fig. 2. Close ups of calcareous particles showing high inter particle porosity

The high void ratio makes calcareous sands highly crushable. In addition to this, calcareous sands may also be cemented, which increases the brittle response to pressure. The effective friction angle is usually higher than for most silica sands (Poulos, 1989) and can exceed 50 degrees (Murff, 1987). Poulos (1989) showed that normal stress reduces as shear displacement increases for calcarenite core samples under a series of monotonic loading. Shear resistance reduction in calcareous material was observed at a number of tests (Angeneer et al., 1973; Murff, 1987).

High strain dynamic pile testing

High strain dynamic pile testing uses strain gauges and accelerometers that are in most cases attached to a pile. The gauges are used to capture the stress wave traveling down the pile as a result from driving hammer impact, and its reflected stress wave traveling up the pile. There are multiple proprietary systems on the market. In the case studies discussed below, the Pile Driving Analyzer (PDA) from Pile Dynamics has been used.

In high strain dynamic testing a stress wave is applied to the pile by a large impact hammer. As this stress wave (Wave Down) travels down the pile, the pile moves and displaces the surrounding soil. The mobilised soil resistance is partially reflected back up the pile as compression waves. These reflected waves are cumulative added together to generate an upward travelling wave ('Wave Up' or WU) response. Hence, the WU response provides an indication of the total dynamic soil resistance around the pile and changes in soil resistance during pile driving. The upward travelling stress wave also provides an indication of the resistance below the toe of the pile, but this will not be investigated in this paper.

It is important to note that the WU response is a dynamic response, which incorporates both the static and dynamic frictional resistance. As such, the WU response should be used as a guide only to indicate the potential resistance.

A more detailed understanding of the pile-soil resistance profile can be obtained by a back-analysis process called signal matching. The signal matching process models the pile as an elastic body of masses and springs, and models the pile-soil interface as a series of elasto-plastic static resistance springs and linear dashpots. This allows for separation of the dynamic resistance from the static resistance. The model is adjusted until it yields a stress wave signal that matches the actual measured signal. The signal matching can be carried out using proprietary software such as AllWave-DLT or CAPWAP. The latter has been used in the case studies.

Signal matching does not yield unique solutions. It is possible to obtain the same match quality for different solutions and significant differences may be found in the proportion of shaft resistance to end bearing. In order to increase the likelihood of establishing a credible signal match, the process should be conducted by an experienced engineer, who has access to geotechnical information, hammer and pile details and set measurements. When conducted properly, the signal matching may provide a high level of information on the soil-pile interface over the length of the pile.

PROPOSED APPROACH

In order to assess the occurrence of friction fatigue under impact driving, we propose the following approach:

1. Perform full drive monitoring of pile driving using dynamic testing;
2. Review Wave Up response at regular blow count intervals;
3. Perform signal matching analyses at regular blow count intervals;
4. Compare shaft resistance for selected depths, at regular blow count intervals.

Full Drive Monitoring

Friction fatigue is considered to develop during driving, and has been related to the driven length of the pile (h/D) or the number of driving cycles or blows (Denes, 2016). In order to capture the development of friction fatigue during driving, full drive monitoring has to be conducted. Gauges are attached to the pile prior to impact driving and data is collected for each blow. Driving sets are recorded for the full length of impact driving.

Review Wave Up response

As discussed above, the WU response provides an indication of the dynamic soil resistance around the pile. As dynamic testing monitoring in undertaken for the full length of the pile, the WU response at various increasing pile penetrations can be compared. This response provides a quick and easy visual assessment to observe the development of the shaft resistance acting on the pile, even though the WU response is a dynamic response, which incorporates both static and dynamic frictional resistance.

Signal Matching Analysis

Signal matching is required to remove the dynamic effects and allow the static shaft resistance to be determined, based on the measured WU response. Signal matching requires some engineering effort, so it is essential to carry out signal matching on a selection of blows. For example, signal matching could be carried out at every 5m penetration. From the comparison of WU responses, however, it may be found that a certain zone is of more particular interest, which can subsequently direct the signal matching effort.

Comparison of Shaft Resistance

Shaft resistance profiles resulting from signal matching can be compared to assess and quantify friction fatigue. The shaft resistance profiles can be plotted for easy and intuitive comparison. Degradation of shaft resistance can be quantified by calculating the shaft resistance in a certain point at given intervals as a proportion of peak shaft resistance. This can then be compared to potential causes, such as h/D or number of blows. Examples of the shaft resistance comparison are illustrated by the case studies below.

CASE STUDIES

We have applied the approach to two case studies, in which dynamic pile testing has been conducted on driven piles in calcareous (coralline) sands. Case study 1 discusses a site on an island off the north-west coast of Australia. Case study 2 discusses a site on an island in the South Pacific Ocean.

Case study 1

This case study discusses a project on an island off the north-west coast of Australia. The case study is also discussed in more detail by Denes (2015; 2016). The project comprised 508mm steel circular hollow section (CHS) piles, with a 12.7mm wall thickness, and no thickening on the top or toe of the piles. Piles were driven using a 1.3t hydraulic drop hammer, with a maximum drop height of 1.3m.

Due to the remote location, no site specific geotechnical investigation was carried out. Our understanding of the geological conditions has been based on an extensive desktop study, local observations and geotechnical reports in similar environments. Nearby geological information was reviewed which detailed that the piling area occurred in the lower terrace of the island. This lowest terrace is composed of bedded marine calcarenite, thick reefs and phosphatic and talus deposits (from erosion of the surrounding limestone - micritic calcarenites - cliffs). This lowest terrace level was created at the last glacial period, approximately 124,000 years ago, where the water level was approximately 60-70 (up to 120) meters below current sea level. The generalised geotechnical profile is expected to consist of an upper layer of 15m calcareous sandy sediments, carbonate sands, coral, phosphate sediments and talus, overlying porous limestone layers, varying degrees of cemented sand layers, sand layers composed of coral, coralline limestone, shells, carbonate sands and silts (Denes, 2015).

PDA monitoring and analysis of the data have been carried out on a test pile, which was driven 39m below sea bed level. PDA monitoring commenced from 6m penetration.

The WU responses for various penetrations of the test pile are shown in Figure 3. The response has been modified to only show the length of penetration of the pile (i.e. the pile toe response has been removed for clarity).

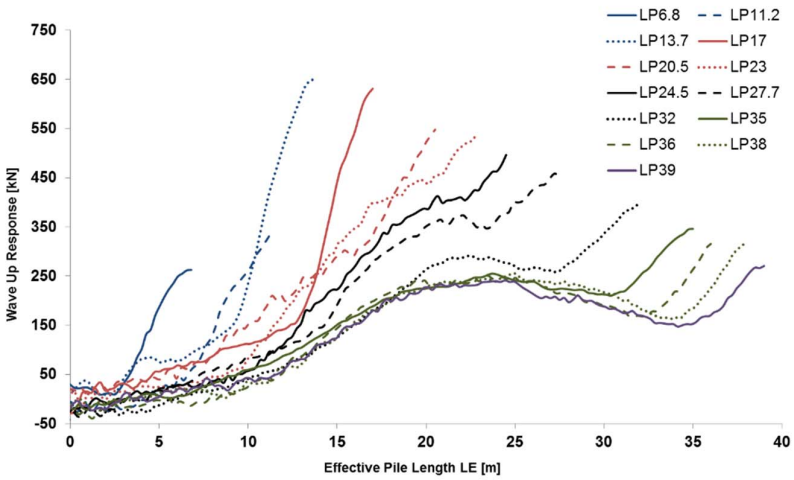


Fig. 3. Wave Up response vs effective pile length – case study 1

As discussed in the Background, the WU response is indicative of the shaft resistance of the pile. Figure 3 shows that the WU response reduces with increasing penetration. This suggests that the shaft resistance reduces due to driving. It is noted that the decrease in WU response trends towards a residual value. It is also noted that the sudden increase in WU response at 13.7m penetration corresponds to harder driving: between 13 and 15m penetration, the blow count increases from approximately 150 to 300 blows/m, and then drops back to 150 blows/m again. This harder driving may indicate a layer with more resistance, which would provide an explanation for the sudden increase in WU.

Following the review of the WU response, signal matching was conducted to further analyse the development of shaft resistance during driving (or with increased penetration). Modelling a reduction in shaft resistance provided improved match quality.

Alternative models were reviewed which included the addition of impedance (or pile area) due to potential internal plugging mechanisms. Although the solutions presented are not unique, the models adapted were consistent and the model was credible in regards to the geotechnical profile derived from the desktop study and local observations. The adjacent pile to the test pile discussed in this case study was assessed by both a static tension test and high strain dynamic testing at end of drive. Signal matching was carried out using the same end of drive soil model as for the test pile. The estimated resistance in uplift from signal matching was 222kN, which was based on 60% external shaft friction and a load reversal factor of 0.8. This was confirmed by the static load test, which demonstrated 'failure' (near-continuous displacement at constant load) at 225kN. The test pile discussed in the case study was modelled with a similar shaft resistance model to the adjacent pile and driving records demonstrated similar driving behaviour (Denes, 2015).

Figure 4 shows the shaft resistance profiles resulting from signal matching plotted against depth, for representative blows of increasing pile penetration.

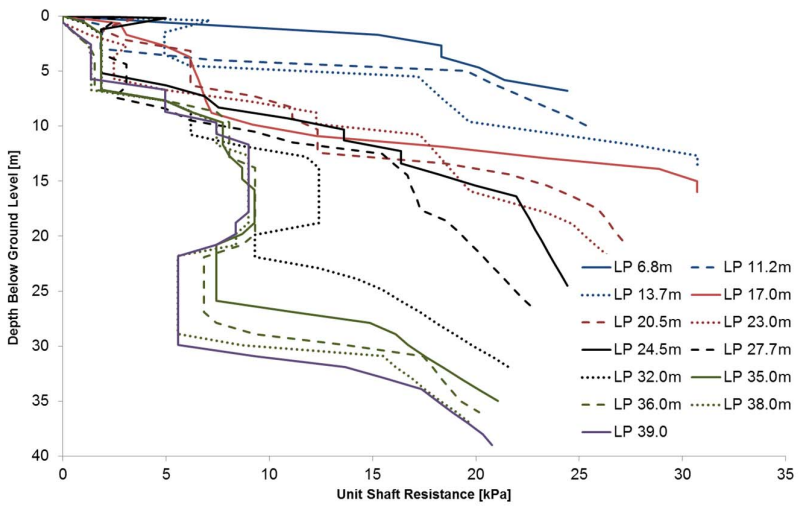


Fig. 4. Unit shaft resistance vs depth below ground level – case study 1

The results of the signal matching are representative of the PDA data. The trends in estimated shaft resistance follow a similar pattern as the WU response: a decrease of shaft resistance with increased penetration, down to a residual strength in the upper 25m of the pile.

Case study 2

This case study discusses a project on an island in the South Pacific Ocean. The project comprised of 610mm CHS piles, with a 16mm wall thickness. A 0.5m long section with a wall thickness of 40mm has been welded at the toe of the pile, resulting in an external driving shoe. Piles were pitched and vibrated to refusal, and subsequently impact driven, using custom built 6t and 10t crane suspended drop hammers.

A total of 11 machine boreholes with Standard Penetration Tests (SPT) have been conducted. The generalised soil profile consists of coralline sands and silts, with shell fragments, overlying basalt gravels and MW-SW basaltic rock. Some cobbles and boulders were found during drilling of the machine boreholes. Top of rock is varied, at approximately 50-75m below ground level.

One test pile with an approximate length of 70m was monitored for the last 16m of impact driving (i.e. after initial vibratory installation to 45m penetration). The initial objective of this test was to monitor driving stresses and hammer efficiency.

The WU response for various penetrations of the test pile is shown in Figure 5, modified to only show the length of penetration of the pile.

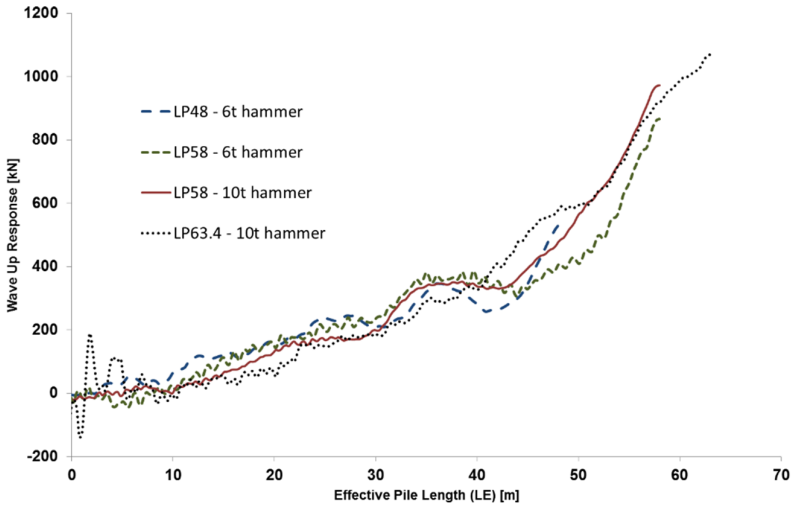


Fig. 5. Wave Up response vs effective pile length – case study 2

Figure 5 does not indicate a clear reduction in shaft resistance with increasing penetration, which could be related to the imparted energy into the system, resulting in varying dynamic forces. For case study 1, the imparted energy for the full length of driving was fairly consistent, mainly due to the use of a hydraulic hammer. For case study 2, at different levels of penetration, the weight of the hammer varied (6t hammer to 10t hammer) as well as the drop height (increased from 1 to 4m). Adding to this is the variable hammer efficiency transfer, due to the hammer / guide set-up (see Figure 6). As the WU response is measuring the dynamic response, a higher dynamic force from an increase in energy results in a higher WU response. Hence, a decrease in shaft resistance due to friction fatigue may be less evident if energy transferred into the pile varies greatly between blows. In order to remove the dynamic component from the response, and eliminate the influence of varying energy, signal matching is required.

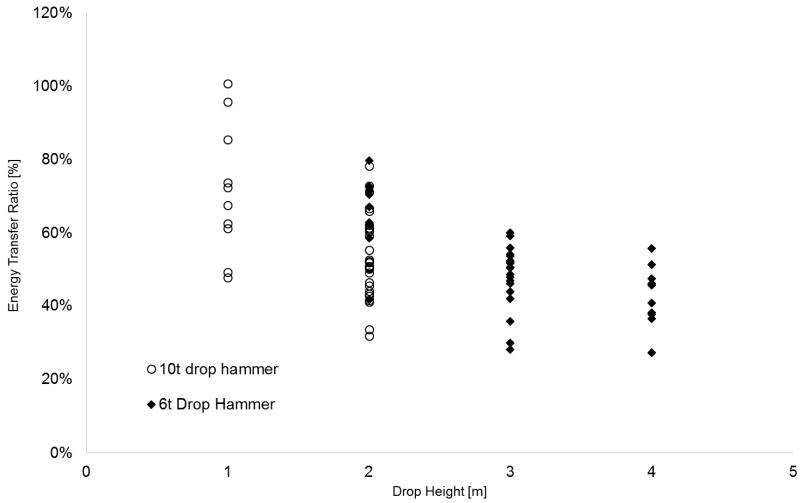


Fig. 6. Energy transfer ratio vs drop height – case study 2

Figure 7 shows the shaft resistance profiles resulting from signal matching plotted against depth, for representative blows of increasing pile penetration. Some degradation of shaft resistance now appears to be present, most notably at greater depth, which could indicate that the upper layers have already been reduced to a residual resistance. However, no test data is available for the early stage of driving, since the pile was installed using a vibratory hammer for the first 45m and it is possible that the vibratory installation has caused shaft resistance degradation prior to the start of the measurements.

An approach to assess the influence of vibratory driving for future projects could involve high strain dynamic testing of the piles using an impact hammer prior to and after vibratory installation. Alternatively, the Vibratory Driving Analyser (VDA) (de Neef et al., 2013) might be used instead of PDA.

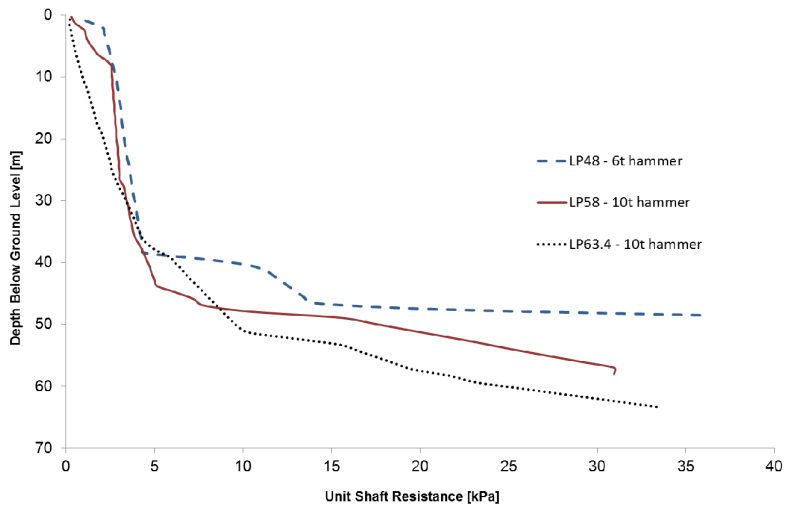


Fig. 7. Unit shaft resistance vs depth below ground level – case study 2

Combined Results

In order to further qualify the loss in peak shaft resistance, the percentage of peak shaft resistance has been plotted for both case studies. Peak shaft resistance has been defined as the shaft resistance encountered on the first pass of pile (no higher shaft resistance values were encountered after the passing of the pile toe). The percentage of peak shaft resistance is obtained by dividing the unit shaft resistance at a certain depth horizon, by the peak shaft resistance. All shaft resistance values result from the signal matching process.

For Figure 8, the peak shaft resistance has been plotted against the number of hammer blows given after the pile toe has reached the depth horizon. For example, the bottom right data point shows the percentage of peak shaft resistance 7000 blows after the pile toe had reached 5m depth.

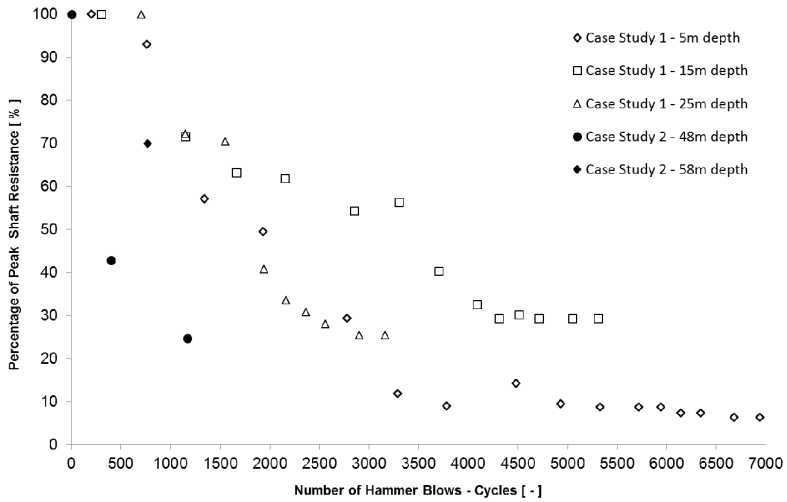


Fig. 8. Percentage of peak shaft resistance vs number of hammer blows – both case studies

In Figure 9, the percentage of peak shaft resistance has been plotted against the h/D ratio, with h being the distance between the depth horizon and the pile toe, and D the pile diameter.

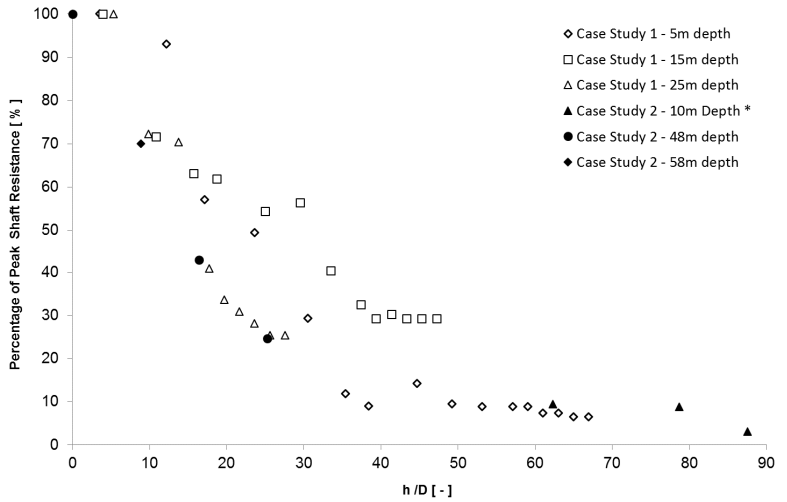


Fig. 9. Percentage of peak shaft resistance vs h/D ratio – both case studies

For case study 1, depth locations of 5m, 15 and 25m below seabed have been selected. For case study 2, depth locations of 10m, 48m and 58m have been selected.

For case study 2, the peak shaft resistance at 10m has been inferred to be 30kPa.

Comparing the number of blows to the relative decrease in shaft resistance only seems to provide meaningful correlation for case study 1, where there is a consistent hammer energy applied for the full length of the pile. There was no pile length vibrated into position for this pile.

However, the results from both case studies appear to correlate well with the h/D ratio, regardless of the type of installation.

Based on visual assessments, Denes (2016) has argued that the data from case study 1 suggests a slightly stronger correlation with number of blows, compared to h/D ratio. However, the h/D ratio may provide a more practical design approach, since it eliminates the need for a driveability analysis in early stage of the design, as well as eliminates the effects from vibratory driving, varying drop heights, hammer weight and hammer efficiencies, providing the pile is fully mobilised during driving. The method proposed in this paper will allow for further quantitative analysis of the correlation between both number of blows and h/D ratio with shaft resistance reduction due to friction fatigue.

It is emphasized that the data shown in Figures 8 and 9 are derived from 2 case studies only and should not be regarded as a basis for design. The quality and quantity of the data obtained from the case studies was limited due a number of factors, including remote locations, limited available time for testing and focus on production. However, the authors believe that the case studies illustrate the potential of dynamic testing in the further study of friction fatigue and provide some valuable lessons for future (research) projects.

SUMMARY AND CONCLUSIONS

Dynamic pile testing has been proposed as a method for assessing and quantifying friction fatigue. The method can be applied to full sized production piles in a construction environment. Data obtained from dynamic pile testing may be combined with numerical modelling and laboratory scale tests to further enhance the understanding of friction fatigue. The method could be applied to materials other than calcareous sands, e.g. pumice sands and any type on contracting sand/soil.

The two case studies discussed indicate that the method can provide meaningful data that can contribute to a better understanding of the phenomenon. The case studies also highlight some potential issues that could influence the results.

Case study 1 provided more consistent results than case study 2, which is expected to have been both the result of more consistent hammer energies, as well as the (untested) vibratory installation of a significant section of the pile in case study 2. Data quality of future projects will be enhanced by using a hammer with consistent energy input (such as hydraulic hammers operating at consistent drop height). If vibratory installation is a significant part of the driving process, it is recommended that dynamic testing is conducted prior to and after the vibratory installation or an alternative method (e.g. using VDA) should be developed to quantify the impact of vibratory installation on friction fatigue.

The method proposed in this paper will allow for further quantitative analysis of the correlation between both number of blows and h/D ratio with shaft resistance reduction due to friction fatigue.

REFERENCES

Angemeer, J. Carlson, E. and Klick, J.H., 1973. Techniques and results in offshore pile load testing in calcareous soils. Proceedings, 5th Annual Offshore Technology Conference, Houston, Texas, pp. 677-692.

De Neef, L., Middendorp, P. and Bakker, J., 2013. Installation of monopiles by vibrohammers for the Riffgat Project. Proceedings of the Institute for Soil Mechanics and Foundation Engineering, Technische Universität Braunschweig, Germany, 14 pages.

Denes, D., 2015. Observing friction fatigue on calcareous material: a progressive breakdown of shaft resistance for piles driven into calcareous material as observed during dynamic pile testing. Masters Subject, University of New South Wales.

Denes, D., 2016. Observing friction fatigue on calcareous material. Proceedings, 5th International Conference of Geotechnical and Geophysical Site Characterisation.

Gavin, K.G. and O'Kelly, B.C., 2007. Effect of Friction Fatigue on Pile Capacity in Dense Sand. Journal of Geotechnical and Geoenvironmental Engineering, ASCE, January 2007, pp. 63-71.

Goble, G.G. and Rausche, F., 1979. Pile driveability predictions by CAPWAP®. Proceedings, International Conference on Numerical Methods in Offshore Piling, ICE, London, pp. 29-36.

Murff, J.D., 1987. Pile capacity in calcareous sands: state of the art. Journal of Geotechnical Engineering, Vol. 113, No. 5 – May, pp. 490-507.

Poulos, H.G., 1989. The mechanics of calcareous sediments. John Jaeger Memorial Address. Australian Geomechanics, pp. 8-40.

Rausche, F., Robinson, B., Likins, G.E., 2004. On the prediction of long term pile capacity from end-of-driving information. Current practices and future trends in deep foundations, Geotechnical Special Publication No. 125, DiMaggio, J. A., and Hussein, M. H., Editors, American Society of Civil Engineers: Reston, VA. pp. 77-95.

White, D.J. and Bolton, M.D., 2002. Observing friction on a jacked pile. Centrifuge and constitutive modelling: two extremes. S.M. Springman, Editor, A.A. Balkema Publishers, pp. 347-354.

White, D.J. and Lehane, B.M., 2004. Friction fatigue on displacement piles in sand. Geotechnique 54, No.10, pp. 645-658.

White, D.J. (2005) A general framework for shaft resistance on displacement piles in Sand. Frontiers in offshore Geotechnics: ISFOG 2005 – Gourvenec and Cassidy. Taylor and Francis Group, London.

SHAFTCAM: A PRACTICAL AND COST EFFECTIVE SOLUTION TO DRILLED/BORED PILE HOLE INSPECTION

Swamy, Avasarala[1], Santosh Mummaneni[2], Dr. Sastry Putcha[3]

1 President, Aver Technologies, Inc., Virginia USA, +1-703-580-8907, swamy@avertechnologies.com

2 Project Manager Aver Technologies, Inc., Virginia USA, +1-703-580-8907, santosh@avertechnologies.com

3 Director, Aver Instruments, Inc., Virginia, USA, +1-561-841-0103, drputcha@averinst.com

ABSTRACT

Inspection of bored pile hole bottom prior to placement of concrete is one of the most crucial element of foundation design and construction, especially for end bearing piles. Pile hole bottoms that are not cleaned well for sediments could potentially result in settlement. Although many projects have specifications in-place for drilled pile hole inspection, they are rarely implemented as the current available tools are either unsafe or cumbersome and costly, thus making it very unattractive for owners and contractors. Further, sometimes the post-construction nondestructive quality control testing such as PIT or sonic logging on piles resulted in unanswered questions related to soft bottom. This generates costly disputes with additional testing including concrete coring and possible repairs. Currently, there are several bored pile bottom inspection devices in USA, namely, SID, DID, and SQUID which can either provide video and photo documentation or measure sediments.

"*ShaftCam*", a patented advanced Digital Borescope, was invented to address the issues related to pile hole bottom inspection with its ability to measure sediments as well as photo and video documentation. Shaftcam device consists of 8-inch diameter bell with a camera, led lights, air hose connection and penetrometer with digital measurement that are connected to a control power box and laptop through a cable. The bell is fitted with a round clear open fiberglass skirt to form an open chamber. A simple motorized winch frame allows the user to lower the ShaftCam equipment gently to the bottom of the shaft at the desired location. Once the bell with camera is lowered to the bottom of the hole, air is pumped into

the clear chamber to displace the water/slurry/polymer and get a clear view of the hole bottom to record the conditions and measure the sediment thickness and resistance. The skirt can also be enclosed and lowered to the desired location to allow for inspection of shaft walls.

ShaftCam weighs less than 15 lbs. (6.8 kgs) in water and allows for inspection of the hole by one person in less than 30 minutes. Use of ShaftCam has saved significant time and money and thus allowed owners and contractors to readily accept and implement the quality control measures in many projects in USA over past few years.

Current Pile Hole Bottom Inspection Regulations

Pile hole bottom cleanliness requirements vary widely from State to State throughout USA. The regulations vary from measuring the sediments with a weighted tape to camera inspection. The Federal Highway Administration (FHWA) specifications mandates the thickness of sediments at pile hole bottom to not exceed an average thickness of 0.5 inches (12.5 mm) and the maximum thickness of 1.5 inches (38.1 mm) for piles that rely on end bearing. Some DOT's mandate for 50% of the pile bottom area to not have more than 0.5 inches (12.5 mm) and the remaining 50% to not exceed 1.5 inches (38.1 mm) of sediments prior to placement of reinforcing steel cage and concrete.

Inspection Devices

There are not many devices currently available in the market for inspecting the bored pile hole bottoms. Majority of the pile holes are inspected with either physically going down the hole in a man basket for dry holes and with a weighted tape in case of wet holes.

In addition to weighted tape method, equipment such as SID-1, SID-II, Mini-SID, DID and SQUID were sporadically used to inspect the pile bottoms. However, due to their size, cost of ownership, and higher operating costs, SID's and SQUID devices are not widely implemented in majority of the projects, even though the specifications call for inspections.



Figure 1a: Shaft Inspection Device (SID)



Figure 1b: Mini-SID

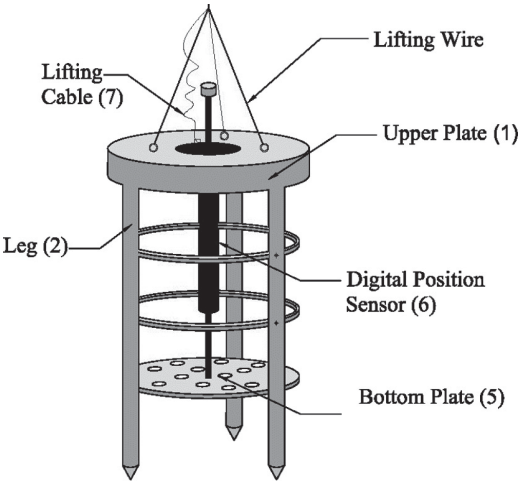


Figure 1c: Ding Inspection Device (DID)



Figure 1d: Shaft Quantitative Inspection Device

The SID/mini SID allows for visual inspection of pile bottoms using a camera and uses nitrogen to displace the slurry/water. They also require a crane to lower the equipment. SQUID on the other hand is primarily a device to measure the thickness of the sediments and soil strength to some degree. However, the SQUID requires use of the drilling equipment for use and does not facilitate visual inspection. The DID equipment is much smaller in size but operates with a similar working principle with the ability to measure sediment thickness and limited ability to measure the strength of soil. However, it does not have the capability to present a visual evidence of bored pile bottom. It is with this background, "*ShaftCam"* – a

patented advanced digital borescope was developed to make the pile hole inspection easy, quick and cost effective.

ShaftCam and Inspection Procedure:

ShaftCam consists of 8-inch diameter bell with a pan and tilt camera, led lights, air hose connection and penetrometer with digital measurement that are connected to a control box and laptop through a cable.



Figure 2: Shaftcam components with motorized lowering equipment

The bell is fitted with a round clear open fiberglass skirt along with a spring loaded penetrometer to form an open chamber. An air-hose is connected to the bell on one end and a small 6 gallons, 150 psi (1 MPa) portable air compressor air pump on the other end. A motorized lowering frame allows the user to lower the ShaftCam equipment gently to the bottom of the pile at the desired location.

Once the bell with camera is lowered to the bottom of the hole, air is pumped into the clear chamber to displace the water/slurry/polymer and get a clear view of the hole bottom to record the conditions and measure the sediment thickness and resistance.



Figure 3: Pan and tilt camera inside Shaftcam.

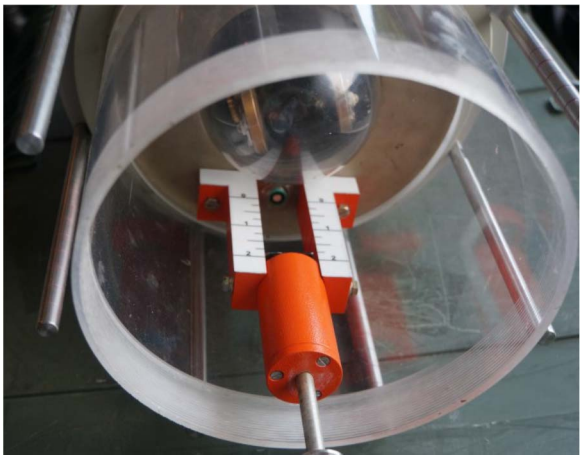


Figure 4: Calibrated Spring loaded penetrometer inside Shaftcam

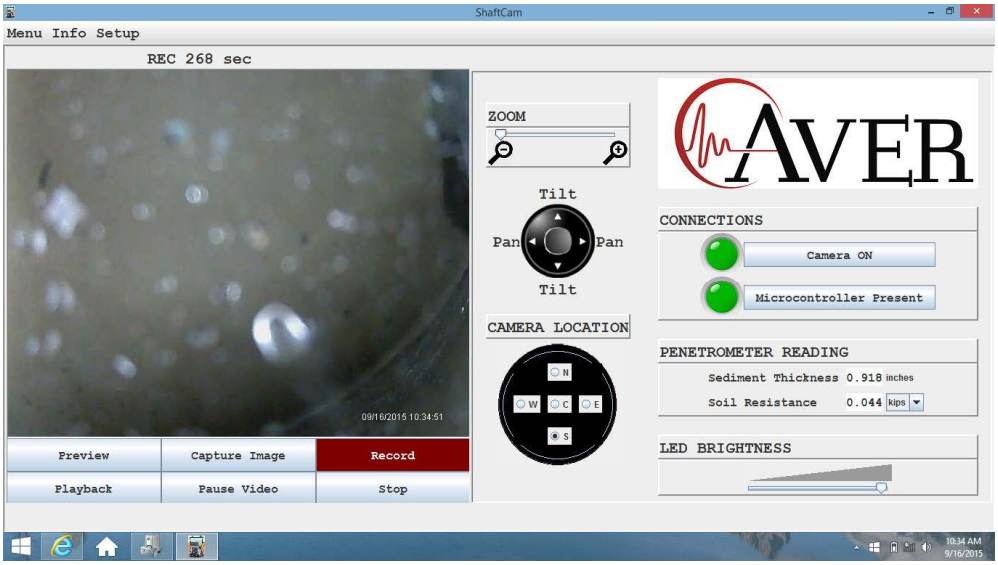


Figure 5: Shaftcam software operation during shaft bottom inspection

The pan and tilt camera has the zoom in capability and can be operated from the ShaftCam software to get close-up view and inspect the pile hole bottom. The LED lights with the ability to control the intensity allows for clear viewing of pile bottom. The calibrated spring loaded penetrometer (2 inch (51mm) long) with ultrasound sensor is used to distinguish

between the sediments/soft material and natural bearing strata and measure its thickness and resistance. The ShaftCam software outputs the sediment thickness and soil resistance (measured to the limit of 2 ksf) and is displayed on the screen with time and date stamped.

ShaftCam is easy to use (one-man operation) and is relatively light weight (<25 lbs (11.34 kg) above water and <15 lbs (6.8 kg) under water). ShaftCam also uses of air instead of nitrogen or other gas, and takes less than 30 minutes for setup and inspection of 5 areas within the pile. The skirt of ShaftCam can also be enclosed and lowered to the desired location to allow for inspection of pile walls.

ShaftCam Inspection Results:

ShaftCam was successfully used in many projects by contractors throughout USA. The following are some screenshots taken during inspection under different soil conditions.

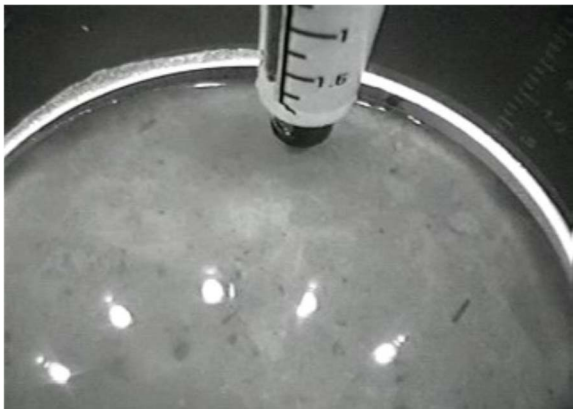


Figure 6a: Rock Bottom in a shaft.



Figure 6b: Disintegrated rock.



Figure 6c: Side walls in a shaft.

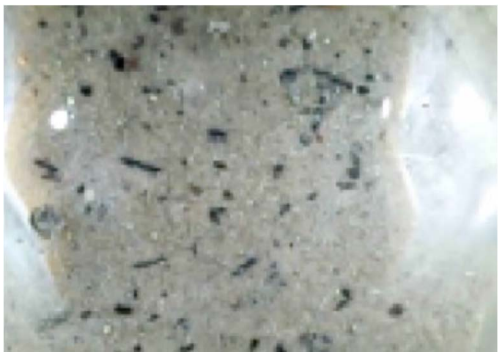


Figure 6d: Sand bottom

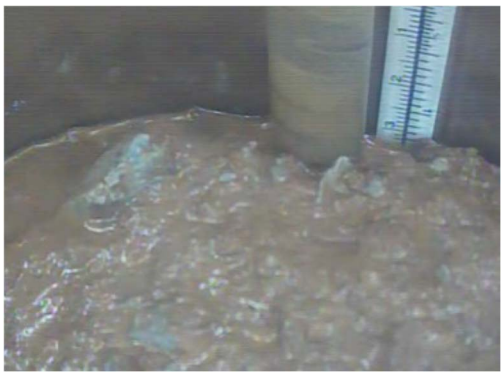


Figure 6e: Clay bottom



Figure 6f: Digital Penetrometer with silty sand sediments

Conclusion

ShaftCam has proven to be a cost-effective way to perform bored pile bottom inspection. This portable technology has made it easier for the contractors/consultants to work in tough environments and yet finish the inspection in relatively short time. Due to its relative ease of use, it has become much easier for the owners and contractors readily accept and implement the quality control measures in many projects in USA over past several months. Availability of these kind of tools allows the designer to have confidence in implementation of his/her design and possibly facilitate reduction in factor of safety that is otherwise not possible.

SMALL-STRAIN BEHAVIOUR OF ARTIFICIALLY CEMENTED SAND IN DEEP MIXING APPLICATION

Alireza Mohammadinia, Post-doctoral research fellow, University of Melbourne, Melbourne, Victoria, Australia, +61383441393, alireza.mohammadinia@unimelb.edu.au

Mahdi M. Disfani, Senior Lecturer, University of Melbourne, Melbourne, Victoria, Australia, +61383445972, mahdi.miri@unimelb.edu.au

Arul Arulrajah, Professor, Swinburne University of Technology, Hawthorn, Melbourne, Victoria, Australia, +61392145741, aarulrajah@swin.edu.au

Stephen Darmawan, Director, Geotesta Pty Ltd, Melbourne, Victoria, Australia, +61395628808, sd@geotesta.com.au

ABSTRACT

Deep mixing using cementitious compounds is an in-situ method of ground improvement for improving the strength, compressibility of loose sand. Artificial light cementation can increase the stiffness of loose sands significantly and reduce the settlement of loose deposits. The increase in contact area between the particles with a thin layer of cementitious agent depends on the confinement and void ratio of the soil mass. Hence, the stiffening effect of cementation not only depends on the type and amount of cementing agent and inter-particular force chain of loose deposit but also depends on the stress level at the time of cementation. In addition, the cementation effect in loose deposits can be deteriorated at relatively low strain levels. Decementation softening can cause detrimental and irreversible impacts on the soil deposit. This study investigates the effect of initial confinement and subsequently the initial void ratio at the time of cementation on small strain behaviour and decementation softening of cemented loose sand under k_o loading. The effect of inter-particular contact of sand particles based on the specific surface area and also soil density was also investigated by means of shear wave propagation. This study present insightful information on effect of primary consolidation stress levels, density of soil and cementation level on softening and collapse of loose deposits improved using deep soil mixing technique. Better understanding of soil-cement interaction by optimization of binder content for deep mixing activation can lead to increasing the level of confidence in using this technique in ground improvement applications.

Keywords: Deep mixing; ground improvement; shear modulus; cemented sand; soil structure

INTRODUCTION

The Progressive growth of societies and population has led to fast development of cities and surrounding infrastructures. The young sediments on the periphery of major cities especially in the coastal areas was traditionally avoided for construction due to weak quality of soil. The economic development of these areas in conjunction with concentration of population challenged the geotechnical engineers for construction at these sediments and weak deposits (Oliveira, et al., 2011).

A variety of methods have been used to treat weak deposits and reduce the settlements at ground surface such as preloading, partial or complete replacement, stone columns and timber or concrete piles. Selecting appropriate geotechnical parameters has been vastly emphasized by researchers and empirical correlations is widely used for obtaining reliable values for design (Poulos, 1989). Although piled supported system are efficiently used for heavy structures, ground improvement with deep soil mixing (DSM) is a applied for supporting five to nine story buildings (Han, et al., 2002). DSM, also known as wet soil mixing, is a ground improvement technique that improves the soils characteristics by mechanically mixing soil with cementitious binder slurry. DSM is a faster and relatively cheaper method of construction of piles by eliminating the high cost and time restriction for preparation of pile installation. Deep mixing methods was developed in Japan in 1960s and was developed worldwide to be an economical method of ground stabilization for light structures. However, the relatively high cement content used for DSM applications (up to 400 kg/m^3), leaves a high carbon footprint.(Bruce, et al., 2013).

DSM is mostly applied for soils with a maximum relative moisture contents of 60 percent (Burke, et al., 2001). Sandy soils will reach a much higher strength with less binder content compared to clayey soils (Burke, et al., 2001). Unconfined compressive strength (UCS) is one of the most important parameters used in the design and quality control of soil-cement columns (Han, et al., 2002). Boehm (2004) reported 28 days UCS strength of up to 7 MPa for sandy soils, up to 3 MPa for silty layers and up to 2 MPa for clayey and organic soils. Depending on the application, DSM can increase the relative strength to in situ soil two times in a mass stabilization while it can increase the bearing capacity up to 15 times (Boehm, 2004).

Soils vary widely in their ability to be mixed based on type, strength, water content, plasticity, stratigraphy and texture and generally wet mixing is considered an economical option for creating soilcrete up to 30 m depth (Bruce, et al., 2013). Organic content, moisture content of soil, cement type and content, curing condition, time and pH of the soil environment are identified as key factor in strength development of the soil mix (Ye, et al., 1994). DSM can be applied to almost any type of soil even organic soils; however, some soils may need pre-treatment or/and consume significant amount of binder up to 40 percent of the treated volume (Bruce, et al., 2013, Burke, et al., 2001). The significant amount of binder (generally Portland cement) in the process of deep mixing project can be a setback for economic justification of project. In addition, the carbone footprint of using Portland cement has a significant penalty on environment (Scrivener and Kirkpatrick, 2008). Replacing traditional Portland cement with alternative binders, such as alkali activated fly ash (FA), can significantly reduce the CO_2 emission significantly (Provis and van Deventer, 2014). This paper investigates the application of low-calcium alkali activated materials for stabilization of weak deposit by employing deep soil mixing.

The interaction between the soilcrete column and weak surrounding soil and behaviour of lightly cemented mass of soil in the vicinity of stabilized soil can have an important impact on the settlement behaviour of the stabilized area (Bruce, et al., 2013, Han, et al., 2002). Although light cementation is often sufficient to increase the stiffness of soils on small strain levels and decrease the liquefaction susceptibility, it can be easily destroyed during the construction due to installation/mixing loadings of piles in the deposit. Artificial cementation by leaked binders can repair the loose contact between the main structure and surrounding soil mass. This study aims to develop a non-destructive method of measuring the inter-particular bond by coupling electromagnetic waves. In addition, recognizing the existing cementation in the soil mass could result in a more economical design.

EXPERIMENTAL STUDY

A typical uniformly graded angular quartz sand was used for experimental program. The relatively uniform angular quartz sand (D_{50} = 0.24 mm, e_{min}= 0.602, e_{max}=0.832, uniformity coefficient C_u=1.63) was used for investigation of behaviour of cemented soil. The particle size distribution and shape of the sand is shown in Fig. 1 and Fig. 2 respectively.

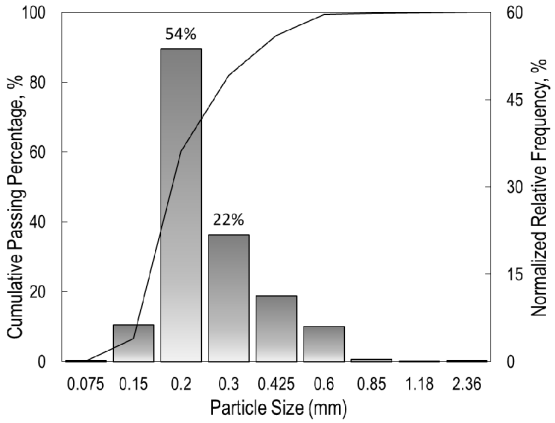


Fig. 1. Particle size distribution of the sands

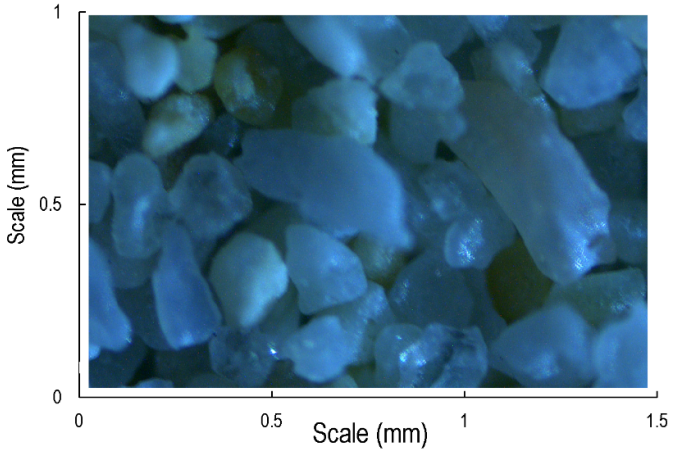


Fig. 2. Shape of sand particles

As suggested by Han, et al. (2002) UCS is conventionally used for design and quality control of soil-cement columns. A minimum UCS value of 700 kPa was suggested by Taki and Yang (1991) for a support cut-off wall constructed with DSM method. Small strain behaviour and strength development of cement treated sand has been previously reported by Consoli and Foppa (2014). Ribeiro, et al. (2016) studied the effect of water content on strength development of cement treated sand. They found that regardless of the cement dosage, the highest UCS strength is observed in the proximity of optimum moisture content obtained from compaction curve. At optimum moisture content, water is concentrated at the grains contact forming rigid hydrated gel at contacts; however if the moisture content is not enough the hydration process will not progress properly leaving weak contact between the aggregates. Alternatively, the excessive water content will increase the void ratio and hence will elongate the length of the gel bonding the grains. In addition the excess water which is not fully utilized in the hydration process will leave a porous gel and reduces the final strength (Ribeiro, et al., 2016). The variability of the moisture content of the weak deposit is a limiting factor in determination of the accurate mix design (Rebata-Landa and Santamarina, 2006). Researchers have attempted to reduce the final water content of the mix by methods such as dry mixing and reducing the water content of cement grout (Bruce, et al., 2013, Burke, et al., 2001, Taki and Yang, 1991).

Table 1. Chemical composition of Portland cement and FA

Chemical	Fly ash (wt.%)
AL_2O_3	25.56
SiO_2	51.11
CaO	4.3
Fe_2O_3	12.48
K_2O	0.7
MgO	1.45
Na_2O	0.77
SO_3	0.24
LoI[a]	0.57

[a]Loss on ignition

In this study, class F FA (specific gravity G_s=2.4) was used as the precursor to replace Portland cement for stabilization of the fine sand (Table 1). Due to low calcium content of the class F FA, grade D sodium silicate solution (Na_2SiO_3) was used as the alkali solution to accelerate the hydration process of the FA. Sodium silicate was previously used as an alkali activator for low calcium FA (Provis, et al., 2005). The specific gravity of sodium silicate solution used in this study was 1.53 where the ratio of SiO_2/Na_2O, also known as modulus ratio (M_s), was equal to 2.0. The cylindrical UCS specimens with 38 mm diameter and 76 mm height was prepared using wet tamping method and were sealed in plastic and were cured for 7 days prior to testing. The sensitivity of the fly ash stabilized sand to moisture content as well as the sensitivity to alkali activator is presented in Fig. 3. The UCS test were performed according to ASTM D1633 (2007) with a loading rate of 1 strain per minute.

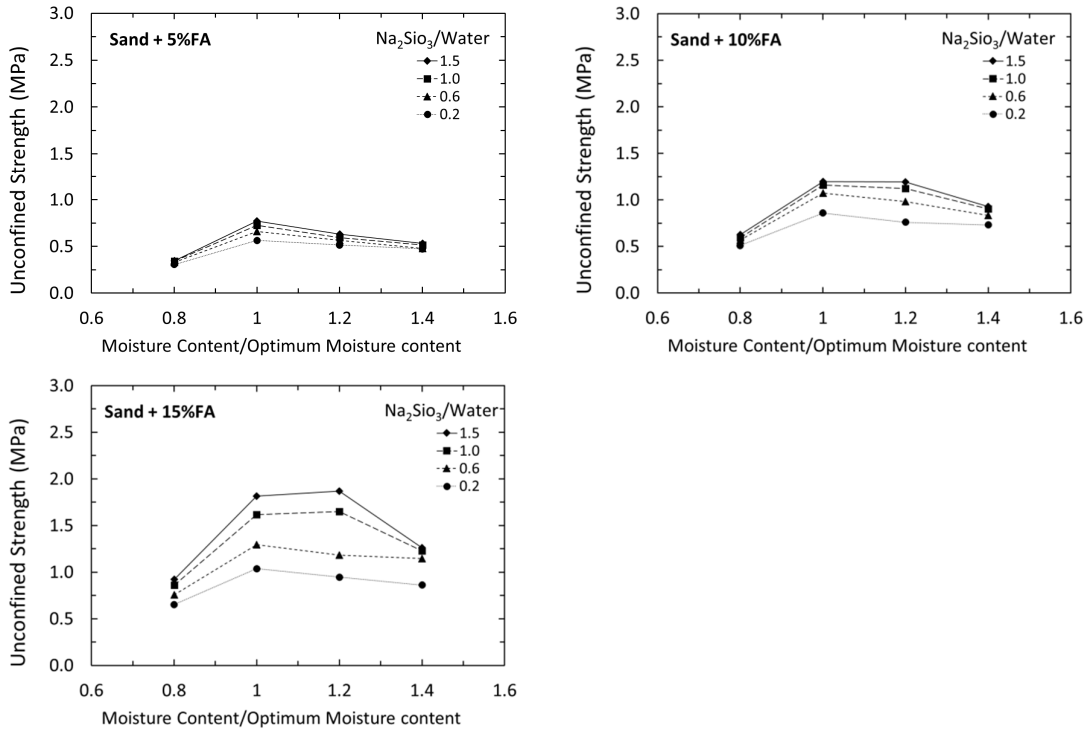


Fig. 3. Strength development of 7-day cured alkali activated FA-sand

Increasing the precursor content from 5% by weight to 15%, which is equivalent to additive content of approximately100kg/m^3 and 300kg/m^3 respectively, is increasing the UCS value. At low FA contents the scarcity of the precursor limits the hydration process and even the excessive amount of Na_2SiO_3 solution and high pH value is not improving the strength of the blend. It can be noted that best strength

in the blends was observed when samples were mixed at optimum moisture ratio. Evidently, the UCS strength development is clearly witnessed when the precursor content is increased to 10% (approximately 200kg/m^3). In addition, poor strength development can be observed for low ratios of sodium silicate, i.e. Na_2SiO_3/water = 0.2 and 0.6. A similar observation of under-development of hydration process for low activator content can be developed for the additive content of 15% FA. However, it should be noted that the maximum UCS value was observed at a higher moisture contents than optimum.

LIGHTLY CEMENTED SOIL

In designing the deep mix columns the diameter and spacing of the columns are not merely dependent on the strength of the stabilized soil. The effective diameter of stabilized columns also depends on couple of other parameters such as relative density of the deposit, permeability of the soil, the pressure of the injected grout and the expected loading condition (Bruce, et al., 2013, Taki, 2002). In cases that deep mixing is not used for water proofing and the stabilized columns are not required to overlap, the interaction between the soilcrete column and the surrounding soil should be evaluated. The soft clay layers was reported to completely lose the strength at the interface of pile and stabilized material due to excessive build-up of water pressure during construction/installation in short term (Shen, et al., 2008). This behaviour is less significant but similar in silty/sandy soil. However the "influenced zone" around the stabilized soil which is 1-2 m from the stabilized column, depending on the type of the soil, is lightly stabilized and regains strength after dissipation of the excess pore pressure induced by shear stresses during installation. The soil showed improved characteristics in long term up to 30% increase compared to initial strength of the soil (Shen, et al., 2008). These loose lightly cemented soils often exhibit collapse, and progressive failure behaviour.

It is often observed that the difference between the stabilized column and surrounding soil is relatively high and the failure is dominated by softening of the surrounding soil. Debonding of the particle and softening of the soil structure was observed under triaxial loading conditions (Dalla Rosa, et al., 2008). However the sampling loads can cause softening of the specimens (Yun and Santamarina, 2005) and development of debonding cannot be studied separately. In this study the deterioration of stiffness at small strain under k_o loading for lightly stabilized loose and dense sand was evaluated by a non-destructive test approach. The precipitation of the cementing agent around particles creates a composite system. The load bearing of the composite system depends on stiffness of soil skeleton (E_{Esk}) and binder (E_{bin}). The initial loose/dense state of the soil can significantly influence the stiffness of the soil matrix (E_{Esk}). Regardless of the ratio of E_{Esk}/E_{bin}, the binder is reducing the stress concentration between the aggregates; however, this may lead to brittle failure of the cemented soil (Yun and Santamarina, 2005).

Measurement of shear wave velocity traveling through a soil mass can often provide valuable information about the packing, relative density and cementation characteristics of soil mass. Observation of changes in shear velocity can further enlighten the process of softening and changes in stiffness of the soil mass. A simple oedometer cell was chosen to test effect of light cementation on sand under k_o loading (Fig. 4). Two bender element was hosted on the top and bottom platen of the oedometer cell to transfer a sinusoidal shear wave through the cemented/uncemented sand. The bender elements were shielded electrically and were grounded to prevent electrical cross talk (Lee and Santamarina, 2005). A signal generator (RIGOL DG1022) was used to generate a 2kH sine wave. The transmitted and received signal are digitized with a sampling frequency of 400 kHz.

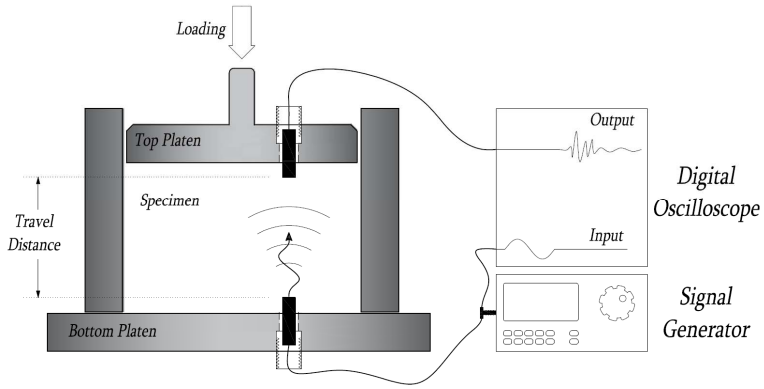


Fig. 4. Transformation of wave through top and bottom cap of Oedometer cell

Unbound sand specimens were prepared in loose state by funnelling method.Dry sand was tamped in four equal layers to create the dense state. The cemented sand and alkali activated FA stabilized sand was prepared at the optimum moisture content. The sand and the binder/activator was thoroughly mixed and was placed inside the cell and was tamped with different energies to produce loose/dense states. It was noted similar to study by Yun and Santamarina (2005) that the stabilized samples showed higher void ratios which is due to capillary forces induced by presence of water in stabilized sample. The effect of capillary is more prominent in loose samples where specimen are produced without tamping (Rao, et al., 1995). Capillary stabilization is most pronounced in the loose specimens, which are placed without tamping (Rao et al. 1995). Once the cell is filled, the upper plate is placed on top of the specimen and the initial void ratio is determined.

The variation in shear wave travel time during loading and unloading in lightly FA stabilized specimens is presented in Fig. 5. The increase in mean stress during the k_o loading reduces the travel time and the shear velocity increases. The variation of velocity versus stress and volume change trends during loading and unloading are presented for a deeper interpretation of debonding and stiffness changes in lightly stabilized sand.

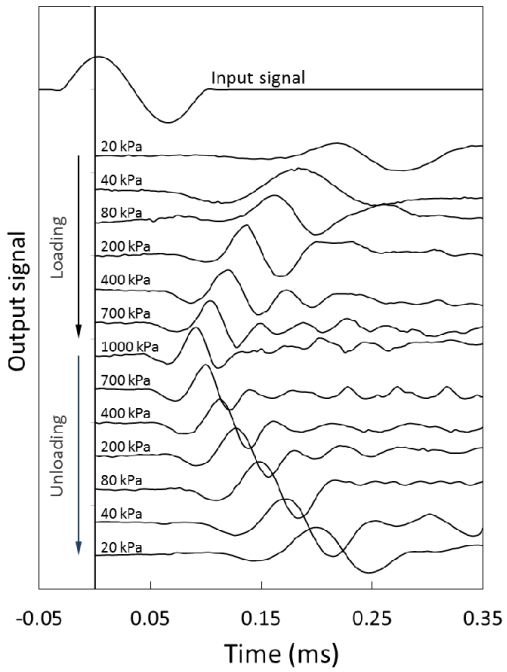


Fig. 5. Received shear wave for loading and unloading of loose sand stabilized with 2% FA (initial void ratio, e0 = 1.15)

Volume change

The change in void ratio is a direct indication of decementation and collapse of binder structure (Cuccovillo and Coop, 1999, Rao, et al., 1995). The volume change behaviour of unbound sand at loose and dense state are presented in Fig. 6.a as a reference. The FA stabilized sand was cured under a mild pressure of 22.2 kPa and a higher pressure of 100 kPa. The shear wave and deformation of cemented sand was measured in steps before the curing sitting pressure. The sample was then left under confinement for 1 day to be cured and then the cycle of loading unloading was completed. In the early stages of loading the binder carries the load and the stabilized soil have a relatively elastic behaviour (Fig. 6.b. and Fig. 6.c.). Although the volumetric behaviour of the dense specimens are mostly controlled by the inter-particular contact of the aggregates and no significant change in the void ratio can be observed during loading and unloading (Fig. 6.b. and Fig. 6.c.), loose specimens experience softening of the structure at yield vertical stress σ'_y during higher stress levels of loading and hence a major reduction in void ratio can be observed for 2% FA stabilized sands. In addition, it should be noted that increasing the sitting curing pressure delays the softening of the stabilized sand significantly.

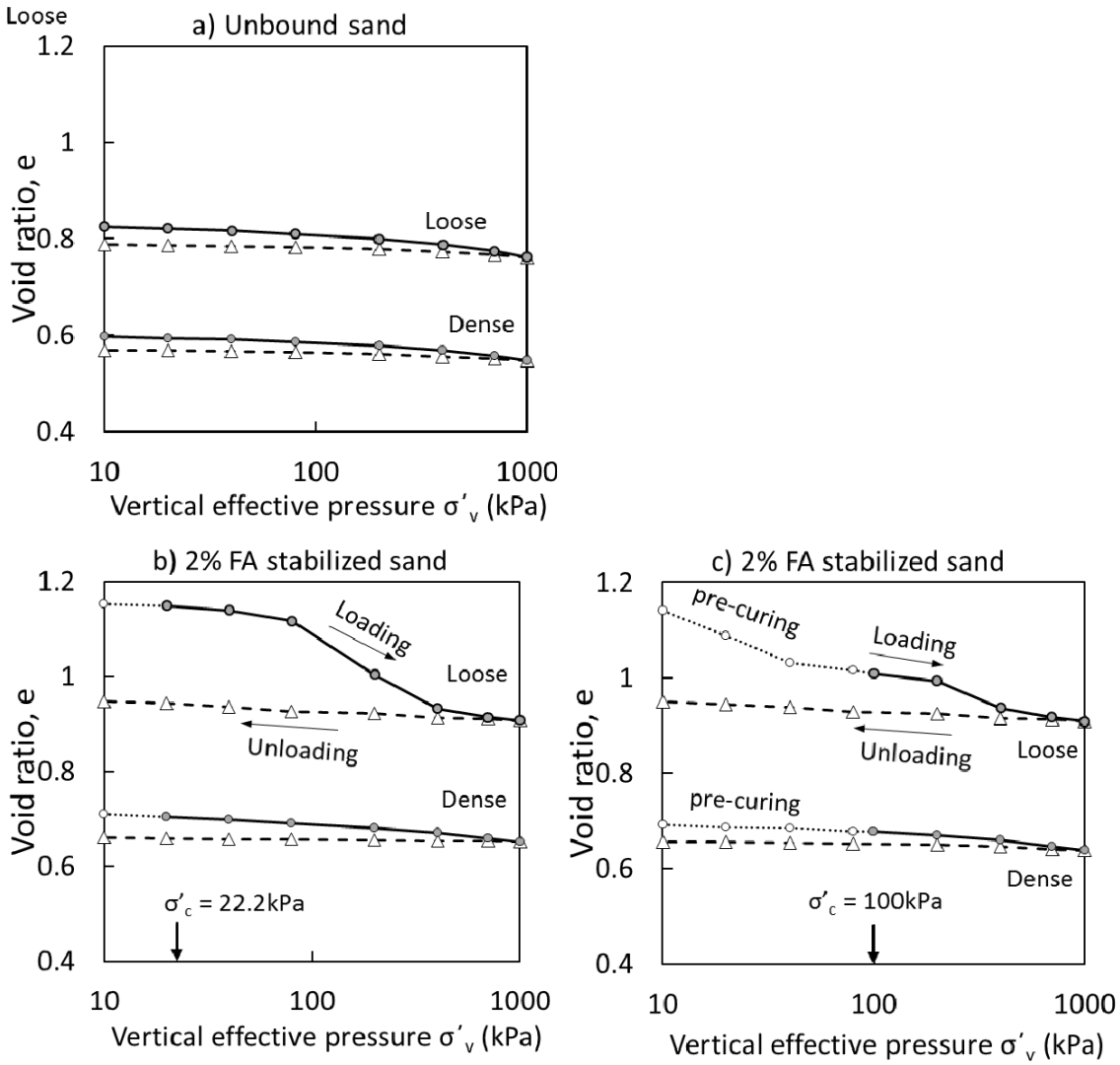


Fig. 6. Variation of void ratio with vertical effective stress in Oedometer cell: σ'_c = curing pressure

Variation of shear velocity under k_o ***loading***

As the mean stress (vertical stress) increases, the shear wave velocity of unbound sand increases almost constantly (Fig. 7.a.). The unloading plot is parallel to loading plot and slightly on the top of the loading plot as the horizontal stresses are locked in the sand (Yun and Santamarina, 2005). The 2% FA stabilized loose samples cured under mild confinement show a sudden decrease in shear velocity (stiffness) in the same vertical stress proximity that the decementation was observed in volume change plot (see Fig. 6.b. and Fig. 6.c.). The shear velocity of the decemnted specimen never falls lower that of unbound sand and shows a similar increase with stress. The shear velocity on unloading curve is decreasing relatively constant and crosses the loading curve. The dense specimen cured under mild sitting curing pressure are showing a relatively similar behaviour to that of unbound sand at a higher shear velocity /stiffness.

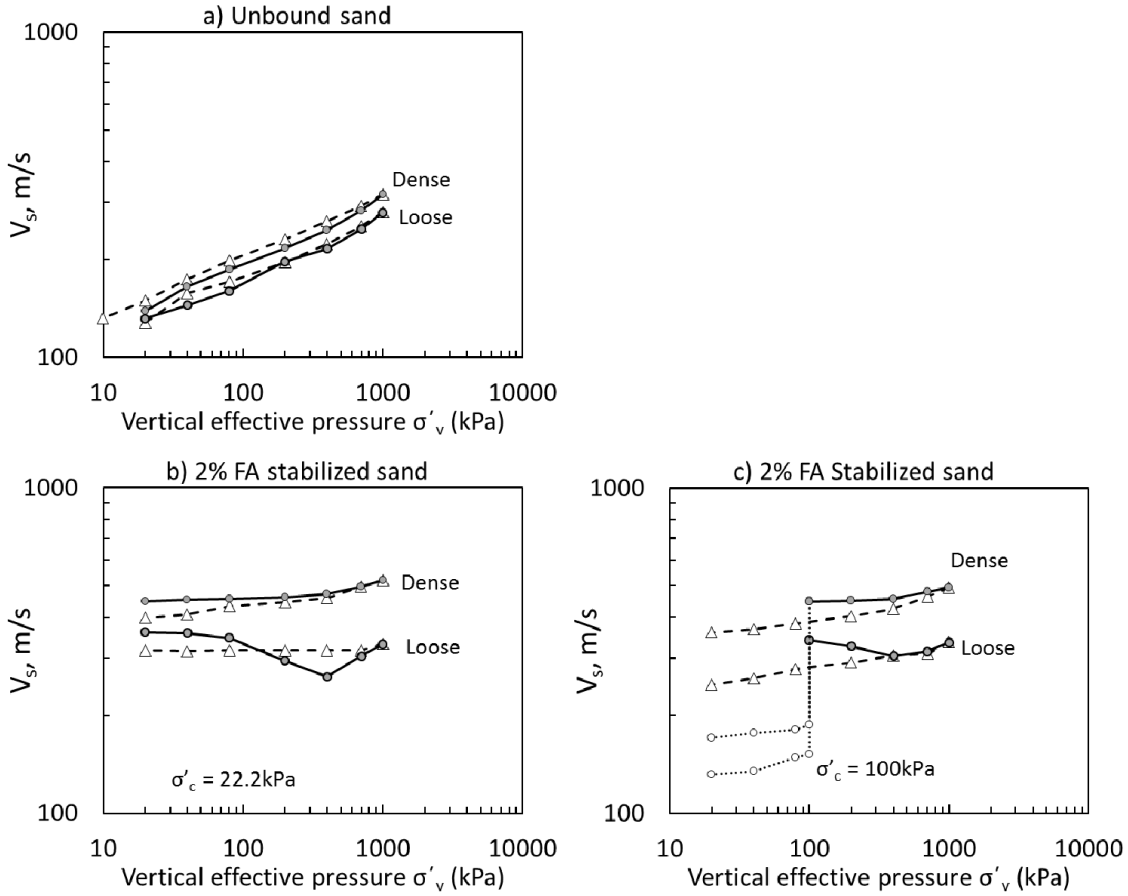


Fig. 7. Variation of shear wave velocity (V_s) with vertical effective stress (σ'_v)

To evaluate the effect of confinement on curing, a set of similar samples were produced and the shear velocity was immediately measured up to 100kPa at which point the sand was cured for 1 day before further loading (Fig. 7.c.). The shear velocity of the samples before curing of the binders is significantly low. An abrupt jump was observed in shear wave velocity under the same 100 kPa of confinement after curing of the specimen. A similar behaviour of decementation was observed by further loading the FA stabilized sand at a higher vertical stress (5 times higher than that of loose FA stabilized sand). Conversely, Portland cement stabilized sample did not experienced decementation under the test loading. However, the unloading plot of both cement and FA stabilized sand drops below their respective loading graph which indicated some level of loss in cementation. The shear wave velocity during unloading reaches much lower values than those observed during loading at similar confinement. All the dense samples show a relative similar trends to relative loose cemented specimens. However, decementation collapse is either absent or less visible in dense specimens. The shear velocity V_s is notably higher in dense specimens compared to that of loose specimens which shows the dominant

effect of packing to inter-particular bond between the aggregates. The shear wave velocity plot during unloading stays constantly below the shear wave values of loading path which shows despite no significant change in shear wave velocity and deformation was observed in the dense specimens, some level of decementation has taken place.

CONCLUSION

Portland cement can potentially be replaced by FA in deep mixing construction. The lower carbon footprint of FA compared to Portland cement along with economic advantages of replacing cement with alkali activated FA encourages studying mechanical and environmental characteristics of alternative binder mixes. Optimization of activator content not only improves the economic aspects of the project, but also develops a better understanding of mechanism of stabilization. In addition, optimization of alkaline activator can result in reducing the FA content to 15% (approximately 300kg/m^3) which is comparable to the typical values used in the deep mixing application with Portland cement.

The amount and type of binder, initial void ratio (i.e. relative density), and the cementation–stress history control the behaviour of cemented soil. Small-strain stiffness, dilative tendency during shear can significantly increase with low levels of cementation. The understanding of behaviour of lightly cemented sand cemented sand can lead to more economical designs. On the other hand, misinterpretation of cementation effects can lead to unsafe design. For instance, the high shear velocity in a soil mass does not necessarily imply a strong soil layer. The lightly stabilized sand often exhibit progressive brittle collapse, and hence a deeper understanding of characterization of cemented sand should be achieved.

The behaviour of cemented soil is gradually moving to the stress-controlled behaviour of unbound soils at very high stresses. The small-strain stiffness is determined by the size of contact areas, i.e., flatness. Hence, even light cementation can have a more pronounced effect than confinement on the small-strain stiffness of hard-grained soils.

ACKNOWLEDGMENT

This research was supported under Australian Research Council's Linkage Projects funding scheme (project number LP 150100043).

REFERENCES

ASTM D1633 (2007). "Standard Test Methods for Compressive Strength of Molded Soil-Cement Cylinders. ASTM Standard D1633." ASTM International, West Conshohocken, PA.

Boehm, D. W. "The utilization of jet grouting and soil mixing methods to repair and support bulkhead structures." *Proc., Ports 2004: Port Development in the Changing World*, ASCE, 1-10.

Bruce, M. E. C., Berg, R. R., Collin, J. G., Filz, G. M., Terashi, M., and Yang, D. S. (2013). "Federal Highway Administration design manual: deep mixing for embankment and foundation support."

Burke, G. K., Brengola, A. F., and Triplett, R. E. (2001). "Soil mixing: A new approach to soft soil stabilization for structural support." *Foundations and Ground Improvement*, ASCE, 190-203.

Consoli, N., and Foppa, D. (2014). "Porosity/cement ratio controlling initial bulk modulus and incremental yield stress of an artificially cemented soil cured under stress." *Geotech. Lett*, 4, 22-26.

Cuccovillo, T., and Coop, M. (1999). "On the mechanics of structured sands." *Géotechnique*, 49(6), 741-760.

Dalla Rosa, F., Consoli, N., and Baudet, B. (2008). "An experimental investigation of the behaviour of artificially cemented soil cured under stress." *Géotechnique*, 58(8), 675-679.

Han, J., Zhou, H.-T., and Ye, F. (2002). "State-of-practice review of deep soil mixing techniques in China." *Transportation Research Record: Journal of the Transportation Research Board*(1808), 49-57.

Lee, J.-S., and Santamarina, J. C. (2005). "Bender elements: performance and signal interpretation." *Journal of geotechnical and geoenvironmental engineering*, 131(9), 1063-1070.

Oliveira, P. J. V., Pinheiro, J. L., and Correia, A. A. (2011). "Numerical analysis of an embankment built on soft soil reinforced with deep mixing columns: Parametric study." *Computers and Geotechnics*, 38(4), 566-576.

Poulos, H. G. (1989). "Pile behaviour—theory and application." *Geotechnique*, 39(3), 365-415.

Provis, J. L., Duxson, P., Lukey, G. C., and van Deventer, J. S. (2005). "Statistical thermodynamic model for Si/Al ordering in amorphous aluminosilicates." *Chemistry of materials*, 17(11), 2976-2986.

Provis, J. L., and van Deventer, J. S. (2014). *Alkali activated materials*, Springer.

Rao, S. M., Sridharan, A., and Ramanath, K. P. (1995). "Collapse behavior of an artificially cemented clayey silt."

Rebata-Landa, V., and Santamarina, J. C. (2006). "Mechanical limits to microbial activity in deep sediments." *Geochemistry, Geophysics, Geosystems*, 7(11).

Ribeiro, D., Néri, R., and Cardoso, R. (2016). "Influence of Water Content in the UCS of Soil-Cement Mixtures for Different Cement Dosages." *Procedia Engineering*, 143, 59-66.

Scrivener, K. L., and Kirkpatrick, R. J. (2008). "Innovation in use and research on cementitious material." *Cement and Concrete Research*, 38(2), 128-136.

Shen, S.-L., Han, J., and Du, Y.-J. (2008). "Deep mixing induced property changes in surrounding sensitive marine clays." *Journal of Geotechnical and Geoenvironmental Engineering*, 134(6), 845-854.

Taki, O. "Strength properties of soil cement produced by deep mixing." *Proc., Grouting and Ground Treatment*, ASCE, 646-657.

Taki, O., and Yang, D. S. "Soil-cement mixed wall technique." *Proc., Geotechnical Engineering Congress—1991*, ASCE, 298-309.

Ye, S., Han, J., and Ye, G. (1994). "Soil Improvement and Underpinning Techniques." *China Architecture and Building Press, Beijing, China*.

Yun, T. S., and Santamarina, J. C. (2005). "Decementation, softening, and collapse: changes in small-strain shear stiffness in k 0 loading." *Journal of Geotechnical and Geoenvironmental engineering*, 131(3), 350-358.

WRIGLEY FIELD – THE 1060 PROJECT

Darren S. Diehm, P.E., GEI Consultants, Inc., Chicago, Illinois, USA
1+312.985.0366, ddiehm@geiconsultants.com

ABSTRACT

Construction for the restoration and expansion of 102-year-old Wrigley Field in Chicago, Illinois began at the conclusion of the 2014 baseball season. This six year project involves structural upgrades to the Stadium, improvements to the facade, infrastructure, restrooms, concourses, suites, press box, and bullpens, as well as the addition of restaurants, patio areas, batting tunnels, video boards, an adjacent Office-retail Tower and a new Hotel. The Bleachers were demolished and replaced, and a new underground Clubhouse was constructed for the Chicago Cubs beneath a new open-air Plaza. The 1060 Project is privately funded, projected at $750 million (US). The work will be completed in phases during consecutive off-seasons, each with a maximum 23-week duration extending through the Chicago winter. Ownership mandated that on-going construction cause no disruption to the Major League Baseball season, have no impact on hosting concerts and other special events, and it should not adversely affect seating capacity, or diminish the fan experience.

The 1060 Project

After purchasing the Chicago Cubs baseball team in 2009 from the Tribune Company, the Ricketts family began planning the renovation and improvement of Wrigley Field and its near neighborhood surroundings in Chicago, Illinois. What came to be known as the 1060 Project was officially announced at the annual Cubs Convention in 2013. Construction began on the $750M privately funded project in October 2014 at the conclusion of the Major League Baseball season. In their vision, the Ricketts committed the 1060 Project to three primary goals. First and foremost as a MLB franchise, the work should provide a meaningful contribution toward winning the World Series and ending the championship drought which stretched to the last win in 1908. Second, the project should be focused on preserving and improving Wrigley Field. Finally, the project should be committed to outcomes that enable the team to be a good neighbor and provide economic and social benefit to the local community.

Constructed as Weeghman Park in 1914 for an estimated total cost of $250,000, the stadium provided seating for 18,000 fans and a home for the Chi-Feds and Whales of the National Federal League. The Chicago Cubs were enticed to move from the West Side Grounds in 1915. In the next 100 years, the Wrigley Field would be sliced apart and expanded, double its seating capacity with the addition of double deck grandstands, be enclosed by bleachers (and an ivy covered wall), and, in 1988, experience its first nighttime baseball game with the addition of lighting.

The 1060 Project has a total budget of $750M, with an expected construction value of $350M. It is projected to add over 2,100 jobs to the economy and be completed before the 2020 baseball season.
The work will be completed in phases during consecutive off-seasons, each with a maximum 23-week duration extending through the Chicago winter. Ownership mandated that on-going construction cause no disruption to the Major League Baseball season, have no impact on hosting concerts and other special events, and it should not adversely affect seating capacity, or diminish the fan experience.

Project Area Geology (Subsurface Conditions)

Wrigley Field is located at 1060 West Addison Street, approximately 0.8 miles west (1.3 km) of Lake Michigan. Historically, the Chicago shoreline consisted of a natural sand edge, with dunes, swales and marshy lowlands backing onto a western ridge which parallels the alignment of modern day North Clark Street. Had it existed prior to the 1830s, Wrigley Field would have been located just over 0.3 miles (0.5 km) from the water's edge.

Subsurface Site Investigation

- 54 Soil Borings
- 66 Vane Shear Tests
- 59 Pressuremeter Tests
- 6 Rock Cores
- 2 Multilevel VW Piezometers
- Downhole Shear Wave Velocity Test
- Surface Wave Microtremor Array Measurement



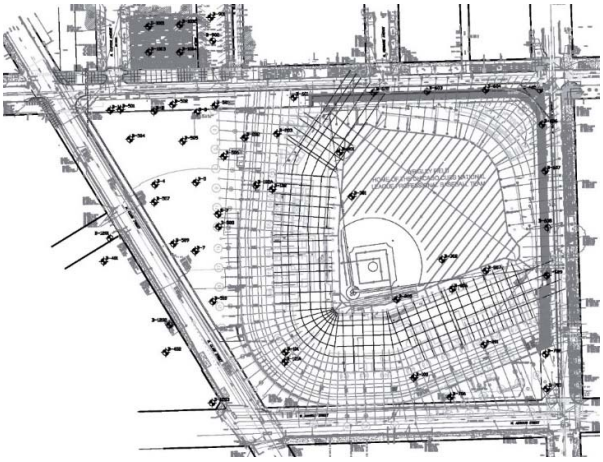


Figure 1: Subsurface investigation at Wrigley Field

The near lakefront Chicago subsoils are predominantly composed of large masses of clay deposited by the advances and retreats of the continental ice sheet during the Wisconsin glacial period. The clays consist of a series of ground moraines (or till sheets) lying one atop another. In section, the till sheets can be visualized as a nested set of half-bowls wrapping the southwest coast of Lake Michigan. Geologically, six separate till sheets, representing six advances and retreats of the ice front, have been identified: (from bottom up typically) the Valparaiso moraine, Tinley moraine, and the Lake Border moraine which is comprised of the Park Ridge, Deerfield, Blodgett and Highland Park. The Chicago bedrock consists of shallow dolomite formations mainly of Silurian age, and deep sandstone and dolomite formations of Cambrian and Ordovician age. The Tinley moraine, and to a lesser extent the Park Ridge till are redeposited Devonian shale scoured by the glaciers to create the Lake Michigan basin.

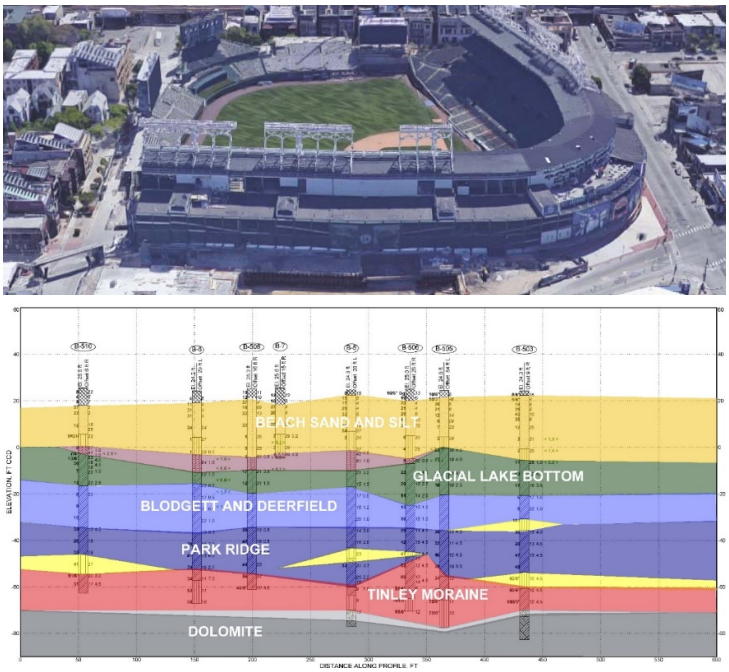


Figure 2: Subsurface profile along west (at Stadium from Waveland to Addison)

Figure 3: Generalized soil profile and strength parameters at Wrigley Field

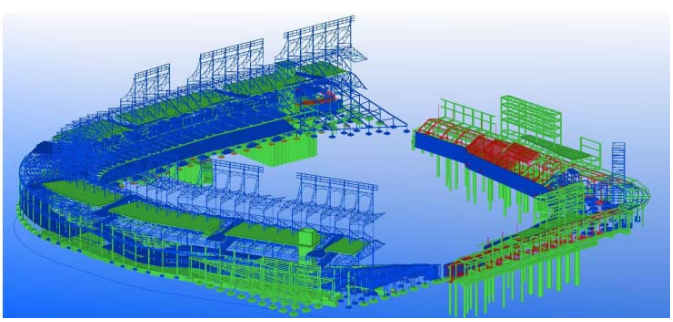
Age	Unit	Log	Name		Description	SPT N-Value	Total Unit Wt, γ	Shear Strength, S_u	Friction Angle, ϕ	Creep Press, P_f
			Fill	I	Man placed material consisting predominantly of sand-size particles with varying inclusions of cinders, brick, and concrete fragments.	4 - 15	110-120 pcf	-	25-30 deg	-
Pleistocene - Wisconsin	Littoral Drift		Beach Sand and Silt	II	Fine to medium sands and silty sands with varying coarse sands and gravels, typically overlying loose to very loose silts and sandy silts.	30 - 49	115–120 pcf	-	30-33 deg	5-10 tsf
						1 - 29	105-115 pcf	-	28-32 deg	-
			Organic Clay	III	Soft to Stiff clay, moderate plasticity with natural moisture content between 40-90%	4 - 5	95-110 pcf	0.4-0.9 ksf	-	-
			Glacial Lake Bottom	IV	Weathered, over-consolidated clays with low to medium PI. Identified by Peck and Reed as "Desiccated Clay Crust."	8 - 15	110-115 pcf	0.6-1 ksf	-	4-6 tsf
	Glacial Drift / Lake Border moraines		Blodgett and Deerfield	V	Compressible, lacustrine clays with low to medium PI. Very soft and soft grey to medium bluish grey.	0 - 4	122-127 pcf	0.3-0.9 ksf	-	-
			Park Ridge	VI	Lacustrine, low plasticity clay with occasional silt and sand seams. Natural moisture content between 18-22%. Transitional zone of variable thickness.	8 - 30	130-135 pcf	3-5 ksf	-	10-18 tsf
			Tinley moraine	VII	Glacially consolidated low plasticity clay, silty clay and clayey silt. Blow counts in excess of 40 bpf and natural moisture contents below 14%. Locally referred to as "Chicago Hardpan."	30 – 50+	130-135 pcf	5-7 ksf	-	25-35 tsf
	Terminal moraine		Valparaiso moraine	VIII	Ex. Dense Sandy Silt, Silty Gravel and Gravelly Sand with Occasional Cobbles and Boulders.	100+	130-135 pcf	-	35-45 deg	40-50 tsf
Age	Unit	Log	Name		Description	Thickness	Total Unit Wt, γ	Uniaxial Strength	RQD	GSI
Silurian	Niagran Series		Dolomite	IXa	Extremely Weathered to Disintegrated Dolomite	2-5 ft	135-140 pcf	-	-	20-25
				IXb	Fresh to moderately weathered, hard to medium, grey to light tan, blocky, slightly to moderately vuggy dolomite and dolomite limestone. Generally near-horizontal bedding with slightly inclined to near-vertical joints.	200-400+ ft	140-145 pcf	9-21 ksi	70-95	50-65

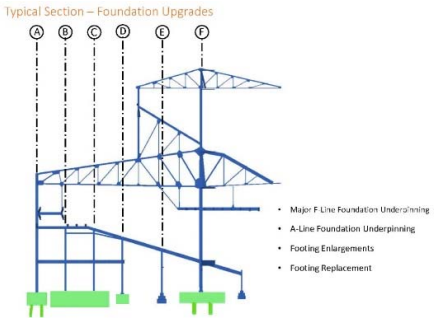
Groundwater in Chicago is contained in three primary aquifer systems. The shallowest aquifer occurs in the fill and upper sand deposits of the glacial drift, and it is directly influenced by the surface levels of the Chicago River and Lake Michigan. The remaining aquifers are contained within the bedrock. The groundwater at Wrigley Field is located 10 to 12 feet (3 to 4 m) below grade, and it generally follows the slope of Waveland Avenue from west to east. The readings from the multi-level vibrating wire piezometers were indicative of vertical drainage of the upper aquifer to the underlying bedrock. Saturation extends through the littoral drift and lacustrine clay of the Park Ridge, then hydrostatic pressures remains constant through the Tinley moraine to the top of bedrock.

Stadium Strengthening and Underpinning

The stadium is a wide flange steel frame structure arranged roughly on rectilinear and radial column lines. In section, the typical frame is comprised of six columns (identified as A through F) which support the stadium seating and mezzanine. Major A and F-Line Columns (every other frame in plan) extend up to a horizontal jack, or main, truss from which the suites are hung. The upper deck seating is supported on the front of the truss and a concessions deck projects off the rear. Media and broadcast facilities are packed around the F-Line which is the only column which projects to the upper grandstand canopy roof. The stadium lighting added in 1988 is mounted on the timber roof. The stadium was constructed on spread-type footing foundations bearing in the beach sands. The concourse level is located 5 to 6 feet (2 m) above the playing field.

Unsurprisingly for a 100 year old structure, as-built drawings were unavailable for the much of the stadium and the majority of foundations. When LIDAR (Light Detection and Ranging) mapping was assembled with the structural survey it revealed that virtually every one of the 59 column line frames within the stadium was unique. It was also revealed that the frame system did not appear to provide a clear load path for lateral restraint.

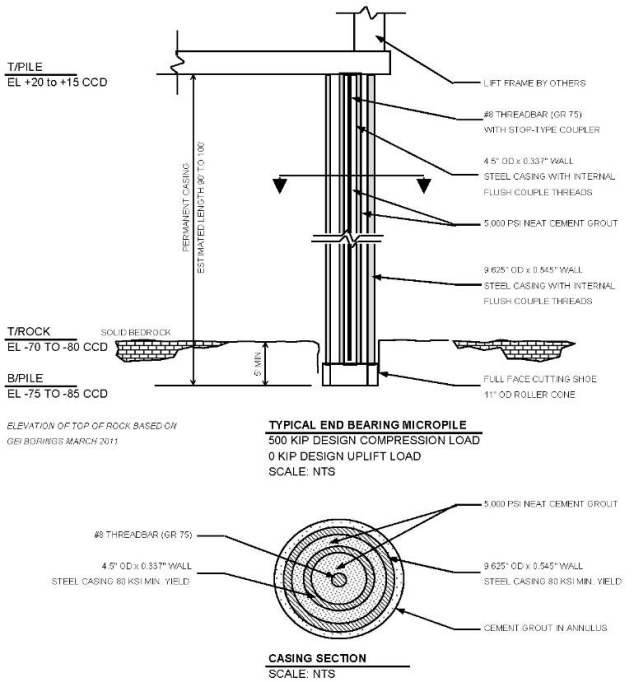


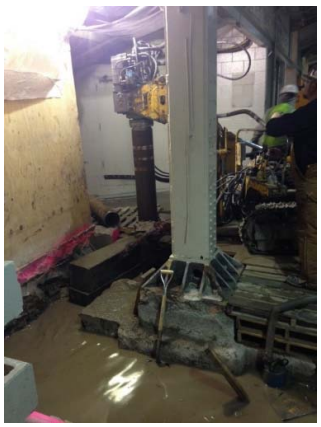


4a: TEKLA model of Stadium (courtesy Thornton Tomasetti) **4b:** Stadium frame

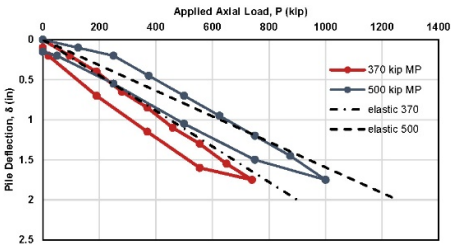
Figure 4: Stadium structure

Because it is the only truly continuous member in the full height of the frame, the structural reaction loads concentrate at the major F-Line column foundations. It was planned as part of the renovation to excavate each column footing and document it during construction. In recognition of their importance in the structure, and more practically their accessibility through the concourse, the F-Line columns were excavated early in the design process. The exposed footings were determined to be applying contact pressures of 2,700 to 11,000 psf (130 to 525 kPa) to the bearing soils under the existing load cases. The load increase resulting from the new permanent loading, and the temporary loading associated with the phased construction required the underpinning of 27 F-Line columns around the stadium. The lateral restraint system and the Plaza and Player's Tunnel excavations required underpinning an additional 48 column locations on the left field (west) side. Several micropiles were designed with axial compression capacities ranging from 95 to 500 kips (420 to 2,225 kN). All the micropiles were rock socketed, and they were installed using low overhead drill rigs inside the existing structure.





5b: Low overhead installation on Concourse

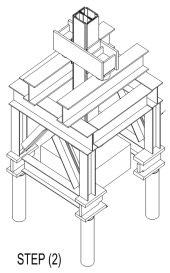


5a: 500 kip Micropile design **5c:** Compression load tests (370 and 500 kip)

Figure 5: Micropile foundations for F-Line Stadium support

Following installation of the micropiles, a reusable jacking frame was mounted over the underpinning piles, and the column was lifted to transfer load from the existing footing. The concrete pedestal and column base casting were then removed after cutting away the lower column. The base assembly of the reaction frame was installed, and the column was spliced to extend it to the new bearing plate. The

elevation of the column was field verified, and the shoring load was transferred back to column. The jacking frame was removed, and the base assembly and micropile foundations were encapsulated in reinforced concrete.

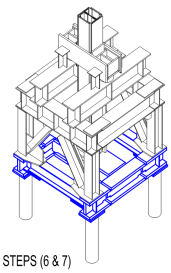




6a: Micopiles completed for new fnd.



6b: Shoring frame being installed





6c: Column load transferred to frame



6d: Final reaction frame encasement

Figure 6: Micropile support and load transfer sequence at F-Line (photos courtesy Thornton Tomasetti)

Caisson Foundations

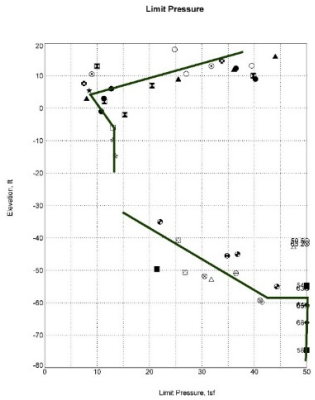
Similar to the stadium, the bleachers were constructed in 1937 on spread-type footing foundations bearing in the sand. However, the change in site elevation resulted in the footings being located only a few feet above the loose saturated silts of the lower beach deposits. The long-term differential settlement from the 1954 bleacher expansion and the 1970s centerfield deck addition combined to produce angular distortion that quite literally tore the cast-in-place diaphragm apart. Due to the extent of the rehabilitation that would have been required to preserve the bleachers in their deteriorated state (and the constraints of the allowable construction schedule), a new steel frame structure with concrete stadia was provided.

Following demolition, belled caisson foundations (drilled shafts with enlarged bases) were installed for the left and right field bleachers. Caisson foundations were also the preferred foundation for the New Office Tower to be constructed in the triangular property west of the stadium. In Chicago, caisson foundations are designed as end bearing elements. The glacially consolidated silty clays and clayey silts of the Tinley moraine provide a suitable bearing material that is within relatively easy reach of conventional drilling equipment. The Chicago Building Code provides a presumptive bearing capacity of 12,000 psf (575 kPa) for this “hardpan” material. With in-situ pressuremeter testing however, the allowable bearing capacity can be increased to as high as 50,000 psf (2,400 kPa). The pressuremeter test consists of lowering an inflatable probe into the borehole to the desired test depth. The probe is expanded against the soils forming the walls of the borehole, and the pressure required to expand the probe and the corresponding volume changes are recorded incrementally. In effect, an in-situ stress-strain load test is performed in the soil. The results of the pressuremeter test are related empirically to both allowable bearing capacity and settlement estimates.

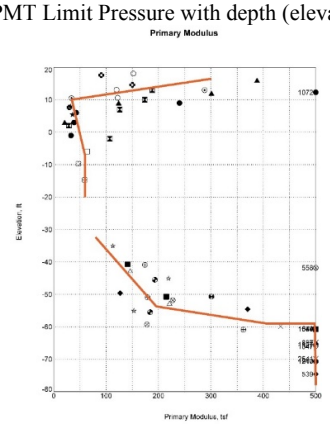
In general, the pressuremeter creep and limit pressures increase with increasing depth through lower Park Ridge and the Tinley moraine. At Wrigley Field, allowable bearing capacities of 25,000 and 35,000 psf (1,200 and 1,675 kPa) were determined from the pressuremeter tests. The economy of the belled (enlarged base) geometry becomes readily apparent at these bearing pressures. Bell diameters as large as 28 feet (8.5 m) have been constructed in Chicago, but for the loading at Wrigley Field, bells

between 9 and 18 feet (2.7 and 5.5 m) were sufficient. In general, bell diameters are restricted to diameters no larger than three times the shaft diameter. At the maximum bearing pressure of 35,000 psf, the pressuremeter moduli indicated settlements slightly greater than 1 inch (25 mm) for bell diameters smaller than about 12 feet. Lower settlements were predicted for bell diameters greater than 15 feet as a result of the bearing pressure bulb extending below the bedrock surface.

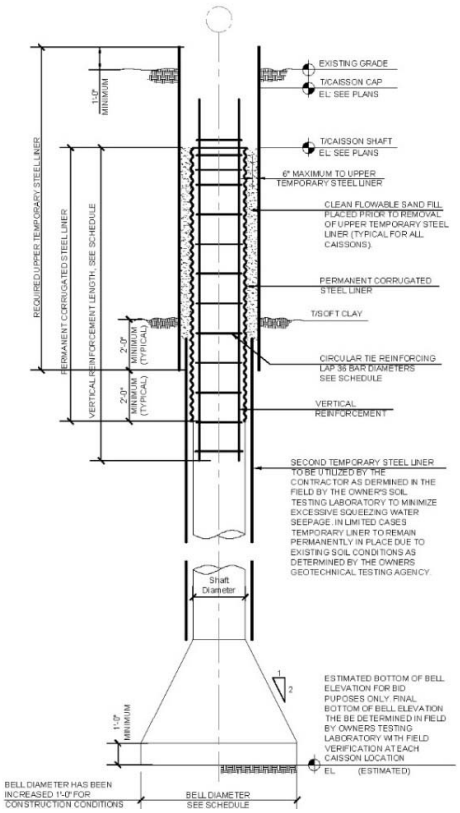
The predominantly cohesive subsurface profile of the Chicago area is conducive to open-hole construction methods. An oversized, temporary top (or starter) casing is provided through the fill and sand of the littoral drift, and it is seated in the weathered clay of the glacial lake bottom to seal off the shallow groundwater table. The caisson shaft is excavated to design depth through repeatedly tripping a soil auger in and out of the shaft. Historically, high torque drilling systems supported on crane platforms were utilized for caisson construction, but as technology has improved, fixed mast drill rig rigs have come to dominate the market for all but the very largest (10-foot, or 3 m) diameter shafts. Once the design bearing elevation is reached, the tooling is swapped from an auger to a belling bucket, and the shaft is enlarged at depth to the design diameter. Cleaning is accomplished by a bottom sweeping "one-eye" bucket. Caisson inspection is performed by downhole camera, or the bell diameter may be increased by 1 foot (0.3 m).



7a: PMT Limit Pressure with depth (elevation)



7a: Pressuremeter Modulus with elevation



7a: Caisson foundation components

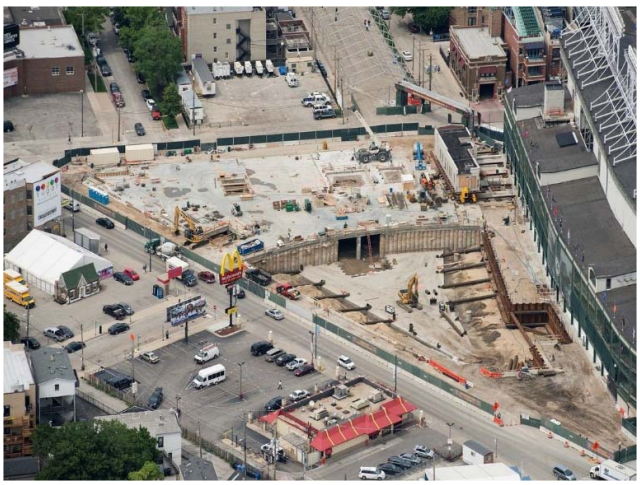
7a: Chicago belled caisson foundation (Bleachers and Office Tower)

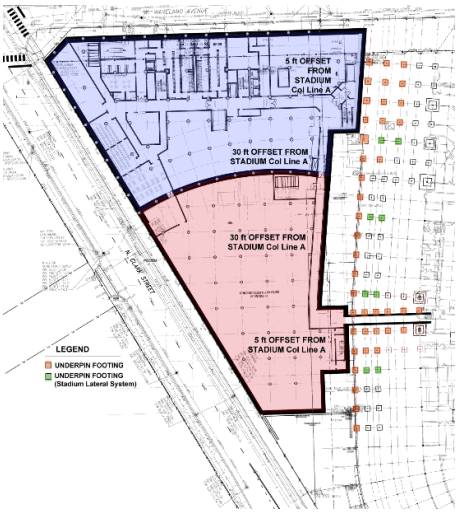
Upon approval of the bearing level, and after belling, a corrugated permanent liner is installed inside the caisson shaft. The soft clays of the Blodgett and Deerfield are prone to squeeze, and vane shear tests are utilized to evaluate the risk of necking while the shaft excavation is open. In lieu of analysis incorporating plastic flow and cavity contraction theory, an empirical relationship for the likelihood of squeeze has been established between the ratio of the total overburden pressure to the shear strength, and the ratio of the depth to shaft diameter. The corrugated liner is extended slightly below the level at which squeeze is indicated, the reinforcing cage is set, and concrete is placed by free-fall methods to

the caisson cutoff level. After the concrete has set, typically the next day, grout is placed in the annular space between the corrugated liner and the temporary casing, and then the casing is pulled.

Top Down Construction

The Chicago Cubs offices were packed into the stadium beneath the seating, and the renovation provided an opportunity to provide a modern space and relocate the catering facilities. The resulting Office/Retail Tower was six stories high, with a mechanical penthouse, and two basement levels extending slightly more than 32 feet (10 m) below grade. Following several programming meetings it was determined that the new Clubhouse would be relocated from beneath the stadium lower bowl to a basement location below the open-air Plaza planned for the area south of the Office Tower. To achieve the desired headroom, and to be consistent with the B1 level of the Office Tower, the single level Clubhouse basement slab was located 17 feet (5 m) below grade. The combined below grade space of the Office Tower and Clubhouse exceed 90,000 square feet (8,400 m^2).





8a: Plaza excavation (looking north) **8b:** Excavation and underpinning plan

Figure 8: Top Down construction for Office Tower basements

Structural analysis limited the settlement and lateral deflection of the stadium foundations to 0.75 inch (20 mm). The angular distortion due to differential settlement between adjacent column lines was restricted to less than 1/300. To limit ground movements associated with the excavation, top down construction was utilized for the Office Tower. Conventionally, top down construction is utilized to accelerate a project schedule. Following foundation construction, the grade level (or first basement level if site pre-excavation was possible) of the structure is installed. The basement excavation is performed as a mining operation, progressively constructing floor levels and excavating underneath each successively to advance to the final subgrade elevation. As the excavation proceeds, the building framing is erected, and construction advances vertically upwards. The top down method effectively compresses the delay between substructure and superstructure construction inherent in traditional bottom up methods. In addition, because the bracing is installed before the underlying excavation, the deflection of the system is generally less than that of conventional methods.

A secant pile wall system with alternating reinforced and unreinforced elements was selected for the Office Tower. The unreinforced piles were installed first using a 48-inch (1200 mm) diameter continuous flight auger. Pile locations were identified by survey, and controlled through the use of a cast-in-place guide wall and a styrofoam template system. The reinforced piles were installed using fixed mast rigs equipped with segmental casing and a 42 inch (1050 mm) diameter central auger. The casing sealed the excavation through the sand and saturated silt and aided in maintaining vertical alignment of the elements. The lead casing section was equipped with a cutting shoe that resulted in an

approximately 48 inch (1200 mm) diameter shaft through the depth of the unreinforced piles. The final secant pile spacing was 38.5 inches (980 mm) center-to-center.

Depending upon the column location, secant piles carrying vertical load were analyzed either as isolated single piles, or as rectangular barrettes comprised of an equivalent two pile spacing. Reinforcement consisted of wide flange beams placed full length in the pile excavations using a service crane after the secant pile excavation. Supplemental wide flange reinforcement was provided where columns landed on unreinforced piles. The use of wide flange beams is preferred over cages because of the greater capacity in bending and the speed and control of construction.

Being shallower, the Clubhouse excavation was determined to provide a smaller foundation settlement and lateral translation risk to the stadium. The excavation was supported by a high modulus sheet pile section. On the stadium side, where wall deflection was critical, the sheet pile was anchored with a row of tiebacks grouted in the sands beneath the stadium, a temporary perimeter berm, and a lower row of rakers braced against the mat foundation. The City of Chicago allows a maximum of 2 inches (50 mm) of top deflection for earth retention systems adjacent to public infrastructure, and temporary berms with a single line of raker bracing was adequate to achieve this performance on the west side (North Clark Street) of the Clubhouse excavation.

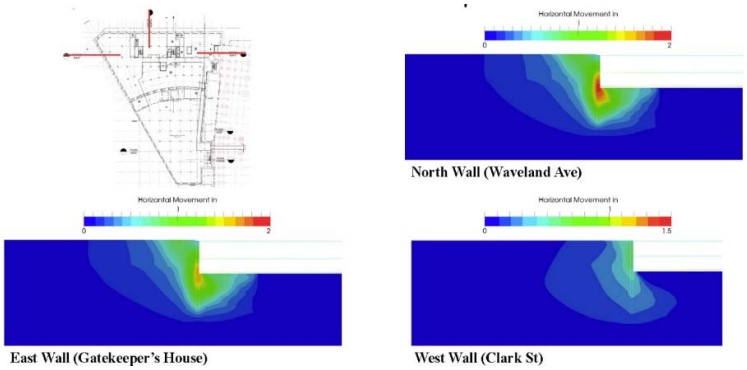
Because the design was performance based, finite element analyses incorporating the time dependent, non-linear behavior of both the soil and structural elements were formulated to reasonably predict the behavior of the retaining walls during excavation. The major steps of the construction (excavation, dewatering, slab or tieback installation, *etc.*) were represented as stages in the numerical analyses. All granular soils including fill, sands and silts, were modelled with the hardening soil (HS) model which is a successor to the well-known Duncan-Chang model. The HS model idealizes soil stiffness as a hyperbolic, stress-dependent relationship between the principal strain and deviatoric stress. All cohesive soils were modeled using the hypoplastic soil model for clays (HC) proposed by Mašín. Hypoplastic models obey a single equation that determines the relationship between stress and strain based on the direction of loading and other state variables.

Although they utilize names familiar to classical soil mechanics, many of the model parameters used in the HS and HC models are mere calibrations factors, and as such they lack a clear physical meaning. To provide a clear depiction of the stiffness and strength of the soil models used in the analysis, finite element simulations of the laboratory drained and undrained triaxial compression and extension triaxial tests were performed as part of the analysis. The simulations used the same model parameters and confining pressures as the analysis of the proposed excavations, and followed typical stress paths as would be performed in commercial laboratories.

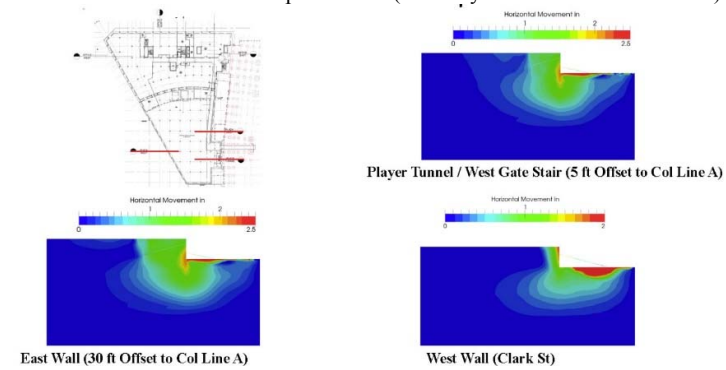
Because the primary and secondary secant piles did not have the same tip elevation, two different material models were used to represent the upper and lower portion of the wall to capture the change in bending stiffness resulting from the design geometry. The application of load to the secant piles causes tensile stresses to accumulate in areas with high bending moments. When the concrete matrix cracks, a localized reduction in bending stiffness is created. Based on a preliminary analysis, it was determined that the magnitude of the forces in the wall during the excavation would likely exceed the cracking moment (concrete cracks in tension), however, the forces were not expected to be sufficient to cause the steel to yield in tension. Based on the shape of the generated moment-curvature diagrams (pre-steel yield), the relationship between bending moment and curvature was simplified into a bilinear function.

Over time and as a result of loading, the permanent basement slabs will experience elastic shortening, creep and shrinkage. Estimated values of these effects for each slab were estimated and incorporated into the derived stiffness of the element by simulating an imposed lateral displacement (equal in magnitude to the slab shrinkage). The sheet pile wall was modelled as a linear-elastic, isoparametric element. It was assigned a stiffness and moment of inertia equivalent to the selected sheet pile wall. The rakers and tiebacks were modelled as preloaded linear-elastic elements. The rakers included a loss of preload over time due to deformation of the sheet pile.

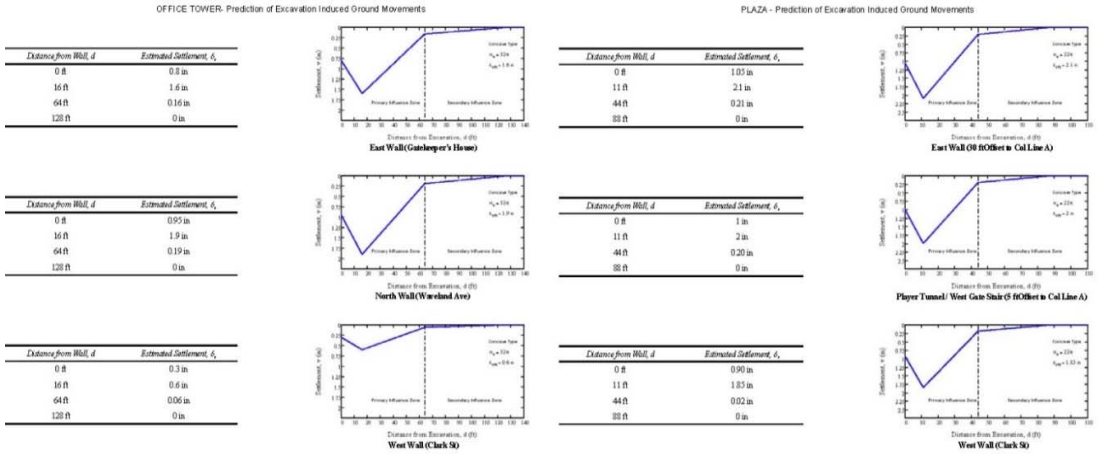
Because of the sensitivity of the stadium structure, the finite element analysis of the excavations for the Office Tower and Clubhouse excavations was developed to provide the most accurate prediction of the wall behavior throughout, and after construction. Empirical correlations were then used to estimate ground surface settlement from the predicted wall deformations.



9a: Secant Pile horizontal displacements (FE analysis for New Office Tower)



9b: Sheet Pile horizontal displacements (FE analysis for Plaza Basement - Clubhouse)



9c: Excavation induced ground movements

Figure 9: Predictive modelling to assess effects of excavation on adjacent Stadium structure

The settlement profile caused by excavation can be broadly divided into two categories: a spandrel type, in which maximum surface settlement occurs very close to the wall, and a concave type, in which maximum surface settlement occurs at a distance away from the supported wall. If the deflection at the first stage of excavation is large and the wall is then restrained (exhibits small deflections at succeeding excavations), or the wall has a cantilever-type deflection, the settlement profile is typically spandrel type. Conversely, if the wall is restrained at the initial stages of excavation (as may occur in top-down construction or high, early tieback installation), the lateral wall deflection would be transferred deeper in the profile resulting in a concave settlement profile.

For the wall types and construction methods proposed at the Office Tower and Plaza basements, a concave settlement profile was anticipated. In most retaining walls, the maximum lateral wall deflection occurs near the final excavation bottom, and the distance behind the wall at which the maximum ground surface settlement occurs is estimated at half the final excavation depth. At a distance equal to twice the excavation depth, the settlement is taken to be 10% of the maximum value. The distance at which buildings would be expected to be essentially unaffected by the range of ground movements extends to four excavation depths behind the retaining wall. The ratio of the maximum horizontal wall movements to vertical ground surface settlements ranges from about 0.5 to 1.0 depending upon the nature of the subgrade material, the wall stiffness, and the type of construction. Observations in Chicago have indicated that top down construction generally corresponds to a ratio of 1.0 between displacement and settlement. Using this method, the wall displacements from the finite element analyses were projected to create settlement trough profiles below the stadium which were then used to evaluate the need for underpinning.

Field monitoring during exaction was provided by vertical inclinometers, manual survey, and via remote sensing that provided vertical and lateral readings of instrumented columns and foundations in real time. The remote sensing was set to trigger alarms at movements of 0.5 and 0.75 inch (15 and 20 mm) to allow re-evaluation of construction procedures and design. The maximum lateral deflection of the secant pile wall was approximately 1.2 inches (30 mm). The sheet pile deflected 2 inches (50 mm) at Clark Street where it was supported with a berm and raker, and less than about 1.6 inches (40 mm) at the stadium. At two isolated locations, the settlement and lateral deflection of stadium foundations reached the 0.75 inch (20 mm) allowable limit. Typical settlement was less than about 0.5 inch (15 mm) at footings without underpinning.

Conclusions

The 1060 Project represents the best efforts, knowledge, and innovation of a wide group of dedicated professionals. Unlike most stadium renovations of this scale, a joint venture or multi-discipline consortium was not the default selection of ownership to achieve the ambitious project goals. Success was the result of collaborative, interactive design involving the architect, the structural and geotechnical engineers, as well the practical construction expertise of the general and specialty contractors. Communication was key to producing design solutions that could reliably be executed in the limited off season construction window, and still respect the owner's imperative to preserve the history and integrity of the landmark structure.

References

Butterfield R (1979) A natural compression law for soils (an advance on e-log p prime).

Duncan J. M. and Chang C.-Y. (1970), "Nonlinear analysis of stress and strain in soils," Journal of the Soil Mechanics and Foundations Division, vol. 96, no. 5, pp. 1629–1653.

Hsieh and Ou (1998), "Shape of ground surface settlement profiles caused by excavation," Canadian Geotechnical Journal, vol. 35, 1998, pp1004-1017.

Mašín, D. (2005). "A hypoplastic constitutive model for clays", International Journal for Numerical and Analytical Methods in Geomechanics 29, No. 4, 311-336.

Niemunis A (2002). "Extended hypoplastic models for soils", PhD thesis, Ruhr-University Bochum.

Matsuoka H. and Nakai T. (1974) "Stress-Deformation and strength characteristics of soil under three different principal stresses". Proc. of JSCE, (232):59-70.

Sarabia, F. (2012). "Hypoplastic constitutive law adapted to simulate excavations in Chicago glacial clays," PhD thesis, Northwestern University, Evanston, IL

A SYSTEM WITH LOCAL STRAIN FOR STUDYING SHEAR MODULUS DEGRADATION OF CEMENT TREATED CLAY WITH FIBERS

Huawen Xiao, Department of Civil and Environmental Engineering, National University of Singapore, Singapore, 6565164566,ceexh@nus.edu.sg
Siang Huat Goh, Department of Civil and Environmental Engineering, National University of Singapore, Singapore, 6565168663, gohsianghuat@nus.edu.sg
Min Sunn Ye, Department of Civil and Environmental Engineering, National University of Singapore, Singapore, 6594370345, a0116412@u.nus.edu.sg
Kai Yao, Department of Civil and Environmental Engineering, National University of Singapore, Singapore, 6590592451,yaokai@u.nus.edu.sg
Fook Hou Lee, Department of Civil and Environmental Engineering, National University of Singapore, Singapore, 6565162274,ceeleefh@nus.edu.sg
Wei Wang, Department of Civil and Environmental Engineering, National University of Singapore, Singapore, 6594214868,ceev88@nus.edu.sg

ABSTRACT

Previous research have shown that introducing fibers to cement soil mixture is effective in improving the ductility as well as maintaining the strength of cement-treated soil. A good knowledge of stiffness of the improved soil at small strain is essential for realistic predictions of ground movements that may affect adjacent buildings or underlying infrastructure. This paper presents a triaxial system with local strain measurement developed for studying shear modulus degradation of cement treated clay with fibers. Cylinder specimens (70mm diameter by 140mm height) with 50% cement, 100% water, 0% to 1% polypropylene fibers by mass, and 7 days of curing period were used. A local strain measurement system with floating type miniature submersible LVDT is introduced in this paper. Configuration of the mounts including the pin size, length and distance are presented and discussed. Based on the experimental results, a reasonable configuration of the mounts is recommended for fiber reinforced cement treated clay. Results showed that the proposed local strain measurement system is effective for testing the shear modulus degradation of cement treated clay with fibers under both unconfined and confined condition. Comparisons with results from resonant column and bender element tests served to verify the reliability of the local strain measurements using the proposed method.

Keywords: fibers, cement-treated clay, local strain, triaxial system, shear modulus degradation

INTRODUCTION

In many geotechnical engineering problems, the operational strain domain ranges from 10^{-3}% to 10^{-1}%. A good knowledge of stiffness at small strains is essential for realistic predictions of the ground movements that may affect adjacent buildings or underlying infrastructure. As such, during the last 3 to 4 decades, the importance of using the small strain stiffness of soils for the design of foundation and underground structures has widely been accepted. Triaxial testing has been widely used to study the stress-strain behavior of soil in the laboratory. However, the stiffness obtained from the conventional triaxial apparatus is usually far smaller than those back-calculated from field measurements. This is mainly attributed to the overestimation of axial strains from the external strain measurements, which usually includes compliance effects of the loading and load measuring system as well as sitting, bedding and alignment errors between sample and system (Baldi et al., 1988). The poor resolution of the external strain measurements is another important contribution. Therefore, conventional procedures are inappropriate for small-strain stiffness evaluation due to low accuracy and resolution.

It is necessary to measure the strains internally and locally with high accuracy (e.g., 10^{-3}%) for accurate small strain stiffness evaluation. The importance of making local strain measurements was highlighted by many researchers (e.g., Jardine et al. 1985; Goto et al. 1991; Hoque et al. 1997). Many

local strain measurement techniques were developed and applied for small strain stiffness study in triaxial testing over the past several decades (e.g., Scholey et al. 1995; Yimsiri and Soga 2002). These include linear variable differential transformer (LVDT), local deformation transducers (LDTs), electro-level inclinometer, Hall effect local strain, and proximity transducers.

LVDTs have been widely used for small strain stiffness study since it was introduced by Brown and Snaith (1974). However, the earlier LVDTs are cumbersome and difficult to fix to the sample in such a way that barreling at large strains can be accommodated without impeding free movement of the armature (Cuccovillo and Coop 1997). To overcome these problems, Cuccovillo and Coop (1997) designed a mount for a submersible miniature LVDT. The new mount can be used in clays and uncemented sands by attaching the specimen and membrane with flexible adhesive and four pins, and in stiffer soils and soft rocks by simply gluing membrane with cyanoacrylate instant cement. However, the details of the mounts including the configurations of the pins and installation of the transducer were not given by Cuccovillo and Coop (1997). Particularly, for stiff soils and soft rocks, simply gluing the mounts to the membrane does not always work. For example, for cement treated clay specimens, the membrane may not always deform together with the specimen as it may detach from the specimen in undrained shearing test (Xiao et al. 2014a). Santagata et al. (1999) reported a customized LVDT and new design of mount for their initial stiffness study for re-sedimented Boston blue clay. The new customized LVDT was mounted on upper and lower yokes, which are clamped onto the specimen with three points. This eliminated the need to insert the pin into the specimen. However, this may introduce the same issues as Cuccovillo and Coop's design (1997) due to the possible detachment of membrane during triaxial testing of the cement treated soil. Ibraim and Benedetto (2005) designed a fixed type non-submersible LVDT to investigate the axial behavior at large strains which can accommodate radial deformation, tilting and barreling of the sand specimen. Both Santagata et al.'s (1999) and Ibraim and Benedetto's (2005) designs are quite complex and may not be easily adopted by other users for their own testing.

Cement-stabilization method has been used widely in ground improvement during the past forty years and is becoming more attractive and efficient method for soil treatment due to its economy, availability and feasibility. Small strain measurement has been widely used to investigate the small strain stiffness for cement treated sand (e.g., Tatsuoka et al. 1997; Schnaid et al. 2001; Onishi et al. 2010; Silva et al. 2013), cement treated gravely soil (e.g., Kongsukprasert et al. 2002; Taheria et al. 2012), and cement treated clay (e.g., Tan et al. 2002; Gomes Correia et al. 2009). Many of these studies used LDT while some studies employed LVDT or Hall effect transducer. As Ibraim and Benedetto (2005) highlighted, problems such as mounting of transducers and ability of local strain system to accommodate radial deformation, tilting and barreling of specimens must be resolved properly. For cement-treated clay with fibers, the main problem will be how to design the mount and install the LVDT transducers.

In this paper, a triaxial system with floating type miniature submersible LVDT is developed for studying the shear modulus degradation of cement treated clay with fibers. As proper installation of local strain transducers on the specimen is critical to the experimental results, the paper will focus on the configuration of the mounts and its influence on the test results, and propose a reasonable configuration of the mounts that can be used for testing fiber reinforced cement treated clay (FRCTC) specimens. To verify the effectiveness and reliability of the local strain measurements, the results obtained from local strain measurement will be compared with those from resonant column and bender element test.

MATERIALS AND TESTING PROGRAM

Materials

The materials used in this study are Singapore upper marine clay, type I Ordinary Portland Cement (OPC) and fibers. The constituents of the clay are 24.13% col-loid, 21.77% clay, 47.71% silt and 6.39%

very fine to medium sand. The plastic and liquid limit of the clay is 31% and 74% respectively. Polypropylene (PP) fibers with 6mm long cut length and 31 μm diameter were used. The density of fibers is 910 kg/m^3. The tensile strength and elastic modulus of fibers are 510MPa and 7GPa respectively.

Specimen preparation

The remoulded marine clay was mixed with cement according to mix proportion in a Hobart Mixer for about 5minutes. The fibers were then added to cement soil mixing and mixed for another 10 minutes before being casted into split PVC mould. The details of preparation can be referred to Xiao et al. (2013, 2014b, 2015). Two holes were drilled along the same vertical line on the PVC mould (70mm diameter by 140mm height) according to the requirement of the LVDT stalling. Different sizes of holes (or pins) are used to the study the effect of mount on the shear modulus degradation of FRCTC specimen. After casting, stainless steel rods were inserted horizontally into the specimen through the premade hole. The rods were smeared with a thin layer of grease. The specimens were then cured under distilled water in a box.

Test Program

After 7 days of curing, the specimens were removed from the moulds and tested by triaxial machine with and without local strain measurement. Two types of tests were conducted in this study: unconfined compression test (UCT) and consolidated undrained shearing test (CIU). The test procedures and strain rates followed those prescribed in ISO/TS 17892 (2004) and can be found in Xiao et al. (2014a). The specimens have dimensions of 70mm diameter by 140mm height. The strain rate used for UCT is 1%/min, while the strain rate for CIU is 0.071%/min. For the CIU test, the effective confining pressure is 300kPa, which is slightly roughly representative of the stress condition of cement improved clay of the site.

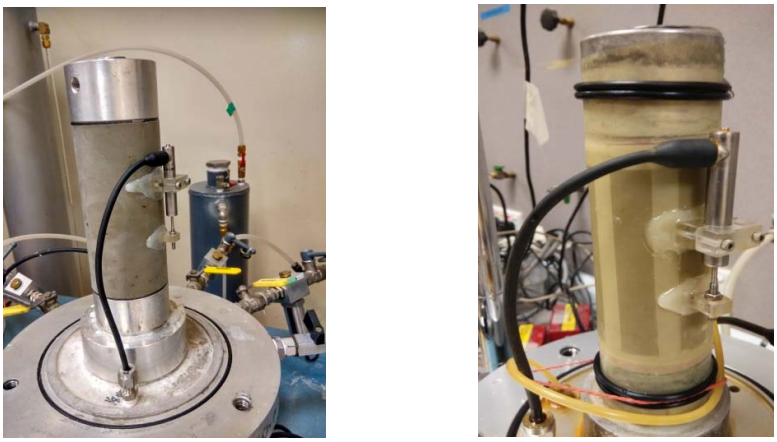
The cement soil mix ratio is expressed in the form S:C:W, where S is mass of soil solids, C the mass of cement and W the mass of water at the point of mixing. The cement content Aw is defined as the ratio of the mass of cement to the mass of soil solids. The water content Cw is defined as the ratio of mass of water to the total mass of soil solids and cement. Following Xiao et al. (2013), the fiber content is defined as the ratio of mass of fibers to the total mass of the cement soil mixture at the point of mixing, and ranges from 0 to 1%.

LOCAL STRAIN MEASUERMENT

The local strain measurement system consists of several components: LVDT transducer with mounts (Fig. 1), transducer amplifier, power supply, data logger and computer. The LVDT transducer is the RDP D5/200WRA/131 type, with a sensitivity of 65.16mv/v/mm, linearity 0.09% and a linear range of ±5mm. It employs an excitation voltage of 5V and frequency 5KHz. A S7AC type transducer amplifier is used to provide AC excitation and synchronous demodulation for the LVDT transducer, which produces a DC output voltage or current. Therefore, the S7AC amplifier is connected with the LVDT transducer on one end and with the power supply/data logger on the other end. The data logger is the MPX 3000 type, with automatic data collection and calibration function controlled by computer software.

To overcome the problem associated with the significant stiffness of the submersible cable, the LVDT has a right-angled cable entry (Fig. 1).The local LVDT was calibrated with a micrometer (0.005mm division) using a commercial software linked to a data logger system. The calibration procedure is basically the same as that for a conventional external LVDT. The resolution of the local LVDT is 1μm and accuracy is 10μm, which is within the range of 0.2μm to14μm and 2μm to 140μm reported by Yimsiri and Soga (2002) for resolution and accuracy of local LVDT respectively.

As Fig. 1 shows, the mount has lower and upper parts, which are made of perspex and connected to the specimen via a stainless steel pin. The lower mount supports the armature or the core of the transducer. The armature can rotate freely as a non-rigid contacting connection. The upper mount supports the body of the transducer. Since the upper mount is designed to be a split holder, it can be easily and conveniently adjusted to hold the transducer. This can minimize any disturbance effects when installing the transducer on the specimen. The new mount system avoids the issue of membrane detachment during undrained triaxial shearing of cement treated clay by connecting the mounts with specimen through pins.



(a) (b)

Fig.1. LVDT transducer with mounts. (a) for UCT test, (b) for CIU test

After the specimen was removed from the curing box, the stainless steel rods were pulled out. Both ends of the specimen were carefully trimmed to achieve smooth and horizontal surfaces so that the specimen could stand vertically. The split PVC mould was then removed carefully. As shown on Fig. 1, for UCT test, the mounts with guide were installed directly on the specimen. For CIU test, the membrane and filter paper, as well as porous stone, were placed on the specimen before installing the mounts. A fast-setting epoxy adhesive (Araldite) was used to install the mount. The specimen set up procedure is exactly the same as the conventional specimen without local strain measurement. The cable was coiled halfway around the sample before passing through the base of the cell to avoid any resistance to vertical movement (Fig. 1). For UCT test, the top cap was simply placed on top of the specimen. To reduce the friction between the specimen and the test system, a thin layer of grease was applied between the specimen and platen as well as specimen and top cap. For CIU test, both ends of the specimen were sealed with plastic O-rings. The specimen was tested after installing the transducer.

CONFIGURATION OF MOUNTS

As the transducer is much lighter than conventional external LVDT and installed properly, the effect of transducer on the specimen can be considered as small. However, the effect of the mounts on the specimen is not clear. To minimize disturbance effects to the structure of cement treated soil arising from mount installation, pre-made holes are introduced to the specimens during specimen preparation. The mount consists of perspex brackets and stainless steel pins. The bracket is lightweight and its size can be quite easily optimized to cater to the dimensions of the transducer. On the other hand, it is worthwhile to investigate the pin dimensions and configurations to minimize the effect of mount installation and ensure good connection between specimen and mounts.

Different pin sizes (1.2mm to 2.4mm in diameter), pin lengths (12mm to 23mm) and pin distances or local strain lengths (46mm to 70mm) were investigated to optimize the mount configuration. The configurations of the pins are summarized in Table 1.

Table 1. Summary of configurations of pins for mount installation effect study.

Configurations	Pin diameter D (mm)	Pin length L(mm)	Pin distance d(mm)
A	1.2	12,15,18,23	46, 70
B	1.6	15, 23	70
C	2.0	15, 23	70
D	2.4	15, 23	70

Fig. 2 presents the effect of pin size, pin length and pin distance on shear modulus degradation for cement admixed clay with fibers. As can be seen from Fig. 2a, shear modulus degradation curves from specimens with different pin sizes and the same pin length of 15mm are quite comparable except for the specimen with pin size of 2.4mm diameter. The shear modulus measured by the specimen with 2.4mm diameter pins is significantly higher than specimens with other pin sizes. Fig. 2b also shows similar trend for specimens with different pin sizes and the same pin length of 23mm. This indicates that pin size should be less than 2.4mm and its reasonable range can be from 1.2mm to 2.0mm. Fig. 2c shows that the shear modulus degradation curves from specimens with different pin lengths and the same pin size of 1.2mm diameter are quite comparable, indicating that the effect of pin length is small and its range can be from 12mm to 23mm. Fig. 2d shows the shear modulus degradation curves from specimens with different pin distances and the same pin size of 1.2mm diameter as well as the same pin length of 12mm. As can be seen from Fig. 2d, the results are very close, indicating that the effect of pin distance or LVDT length is also small and its range can be from be from 46mm to 70mm (one third to one half center height of specimen). Based on the preceding experimental results and performance, an appropriate pin configuration for local strain measurements could be proposed as follows: 1.2 to 1.5mm diameter, 12 to 15mm length and 46mm distance. Fig. 2c also shows that the introduction of fibers increases the shear modulus and reduces the degradation of shear modulus within 0.01% strain.

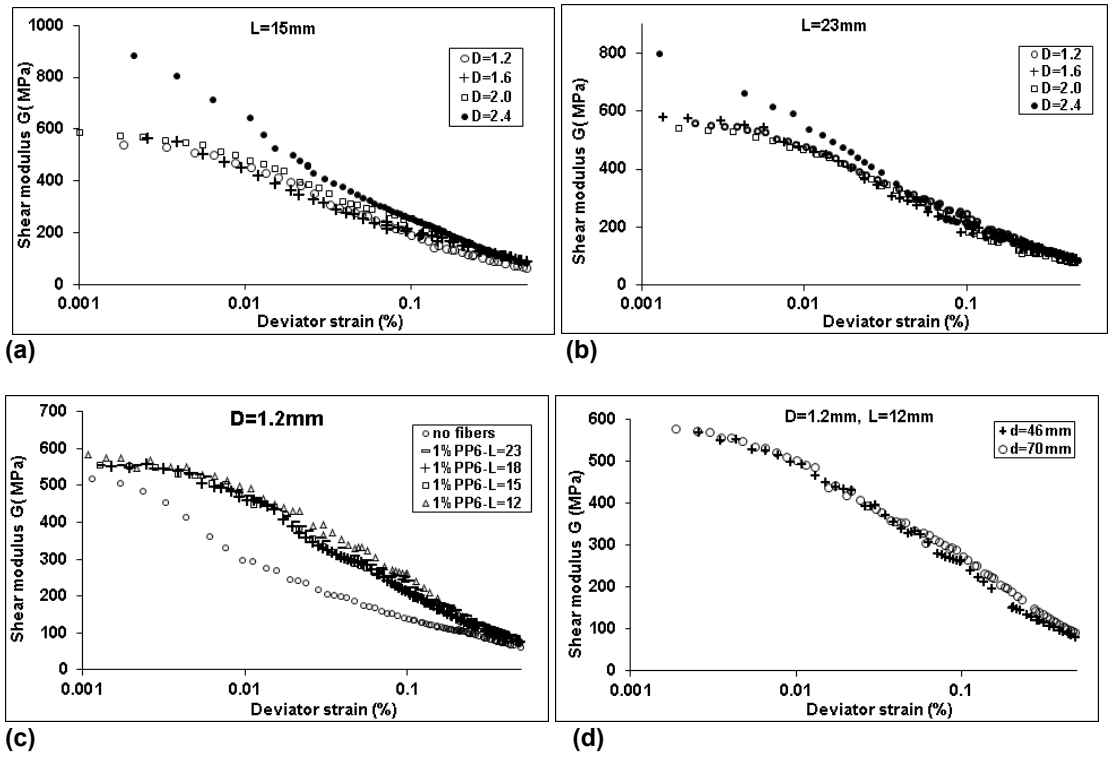
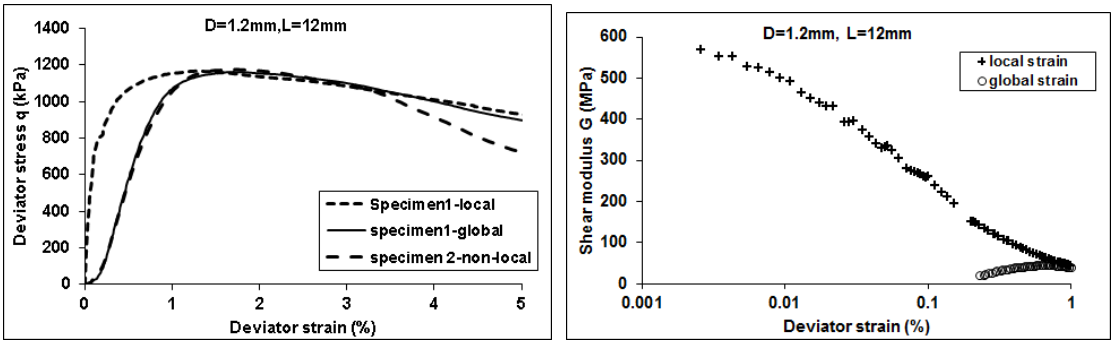


Fig.2. Pin size, length and distance effect study. (a) Pin length L=15mm, pin size D=1.2 to 2.4mm. (b) Pin length L=23mm, pin size D=1.2 to 2.4mm. (c) Pin size D=1.2mm, pin length L=12 to 23mm. (d) Pin size D=1.2mm, pin length L=12mm, pin distance d=46, 70mm.

EFFECTIVENESS OF LOCAL STRAIN MEASUREMENT

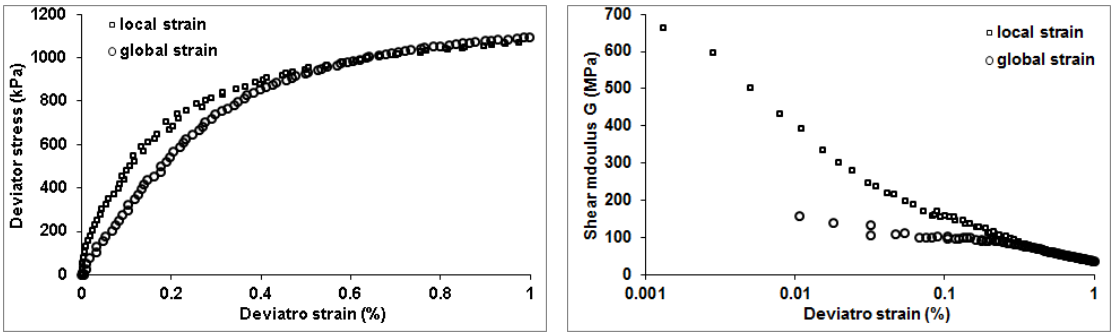
Fig. 3 presents the stress-strain behavior and shear modulus degradation measured by external and local strains on two different specimens under unconfined condition (UCT test). Both local and external strain measurement were performed for specimen 1 while only external strain measurement was carried out for specimen 2. As can be seen from Fig. 3a, the stress-strain relations measured by external strain transducers are very similar for specimens 1 and 2. This indicates the specimens are repeatable and the installation effect of local strain measurement on behavior of specimen is small. Fig. 3a also shows that the deviator stress obtained from local strain is much higher than that from external strain at the same strain level, indicating the effectiveness of local strain measurement. This is consistent with other researches results (e.g., Goto et al. 1991; Cuccovillo and Coop 1997; Tan et al. 2002). Figure 3b shows the corresponding shear modulus degradation up to 1% of strain obtained by local and external strain measurements on specimen 1. As can be seen from Fig. 3b, the shear moduli obtained using external strain measurements are significantly lower than those obtained via local strain measurements. This further indicates the effectiveness of local strain measurement.



(a) **(b)**

Fig.3. Effectiveness of local strain measurement under unconfined condition. (a) Stress-strain relationship. (b) shear modulus degradation versus deviator strain.

Fig. 4 presents the stress-strain behavior and shear modulus degradation obtained by external and local strain measurements from undrained triaxial shearing test (CIU test). The specimen was consolidated under 300kPa of effective confining pressure. As can be seen from Fig. 4a, the deviator stresses obtained from local strain measurements within 0.5% strain are noticeably higher than those obtained from external strain measurements at the same strain level, indicating the effectiveness of local strain measurement. This is consistent with the trend from UCT test shown in Fig. 3a. Similarly, Fig. 4b shows the shear moduli measured by external strain measurements up to about 0.2% strain level are significantly lower than those obtained by local strain measurements. This indicates that local strain measurement is also effective under triaxial testing condition. Comparing the local strain measurement results of Fig. 4b with Fig. 3b shows that the shear modulus under confining pressure is slightly higher than that without confining pressure when deviator strain is lower than 0.004% and the degradation of shear modulus under confining pressure is faster than that without confining pressure. Xiao et al. (2014a) showed that, for cement treated marine clay with 50% cement content, 100% water content and 7 days of curing, the primary isotropic yield stress is about 580kPa. As such, an effective confining pressure 300kPa is likely to condense the specimen and the destructuration due to consolidation should be quite small. Primary studies showed that, for the same cement and water content, introduction of fibers leads to a bit higher primary yield stress. Therefore, the same reason can go for cement treated marine clay specimens with fibers. This explains higher small strain shear modulus and faster degradation of shear modulus for specimen consolidated under 300kPa of effective confining pressure.



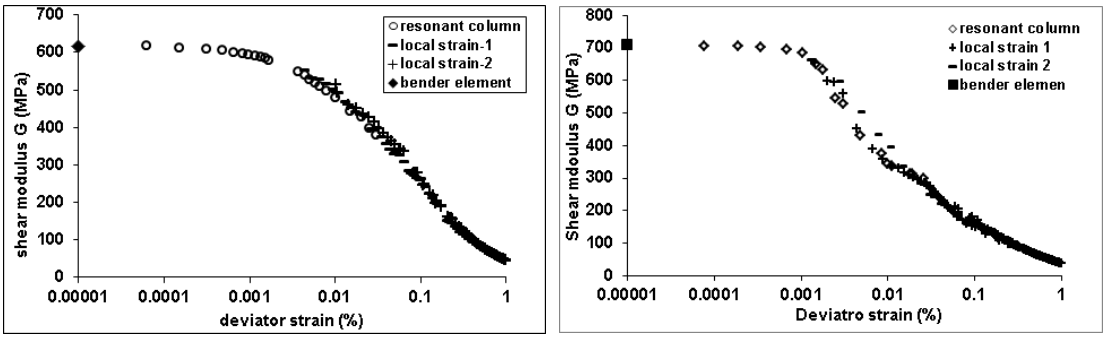
(a) (b)

Fig.4. Effectiveness of local strain measurement under 300kPa of effective confining pressure. (a) Stress-strain relationship. (b) Shear modulus degradation versus deviator strain.

COMPARISON WITH RESONANT COLUMN TEST AND BENDER ELEMENT TEST

Experimental results from resonant column tests and bender element tests were used to verify the small strain shear modulus obtained from local strain measurements. The existing Drnevich Long-Tor Resonant column equipment in the NUS geotechnical laboratory was used to measure the shear modulus of cement treated clayey soil. The Resonant column equipment mainly consists of accelerometer, multimeter, signal conditioner, power amplifier, function generator and oscilloscope. The cylindrical specimen with dimension of 35mm diameter by 70mm height is fixed at the bottom (the passive-end) and a sinusoidal torsional excitation is applied to the top (the active-end). Sinusoidal rotational motion was induced in the active-end platen using a function generator acting through a power amplifier. The specimen can also be tested under confining pressure. The bender element test was conducted using the GDS bender element setup.

Fig. 5 plots the shear moduli obtained by local strain measurements together with those obtained from resonant column tests and bender element tests for FRCTC soil, under both unconfined and confined (300kPa effective confining pressure) condition. As can be seen from Fig. 5, the shear moduli obtained by local strain measurement are comparable to and consistent with the resonant column test results within 0.1% to 0.001% of strain for both unconfined and confined test conditions. Fig. 5 shows that the small strain shear moduli are also comparable and consistent with the results obtained from bender element tests. The good agreements indicate that the results from local strain measurement are reliable.



(a) (b)

Fig.5. Comparison with resonant column test and bender element test. (a) Specimens under unconfined condition, (b) specimens under 300kPa of effective confining pressure.

SUMMARY AND CONCLUSIONS

Miniature submersible LVDT is becoming popular due to its small size, large working range, high

resolution and accuracy. However, the application of LVDT to some test procedures can be quite challenging, and thus require special consideration and configuration in order to obtain reliable results. For the testing of cement treated clayey soils with fibers, the main problem lies in how to design the mount and install the LVDT transducers with minimal disturbance to the specimens. In this study, a local strain measurement system suitable for triaxial testing was introduced for studying shear modulus degradation of cement treated clay with fibers. Cylinder specimens (70mm diameter by 140mm height) with 50% cement, 100% water, 0% to 1% polypropylene fiber by mass, and 7 days of curing period were used. The test results obtained using a mounting system with different configurations of pin sizes, pin lengths and pin distances were presented and discussed. Based on the experimental results analysis and discussions, the main contributions and conclusions can be drawn as follows:

1. A local strain measurement system using a floating type miniature submersible LVDT was introduced for the testing of FRCTC specimens. The designed mount can minimize the effect of transducer installation on the specimen as well as the friction between the transducer body and core. It also avoids the issue of membrane detachment during undrained triaxial shearing by connecting the mounts with specimen through pins.

2. Different configurations of the mounting system were presented. To minimize installation effects on the structure of cement treated soil, premade holes are introduced in the specimens during specimen preparation. The influence of pin sizes and lengths, as well as the distance between the pins, were investigated to minimize effects due to mount installation and ensure good connection between specimen and mounts. Based on the experimental results and performance, an appropriate pin configuration is recommended as 1.2 to 1.5mm diameter, 12 to 15mm length and 46mm distance.

3. The results showed that the local strain measurement is effective for FRCTC specimens tested under both unconfined and confined conditions. The difference in the shear modulus and its degradation between local strain and conventional external strain measurement is significant. The difference in the shear modulus between different specimens with the same mix ratio was small. These confirmed the repeatability of the test and the reliability of the local strain measurement. The results also showed that for specimens subjected to confining pressure, the small strain shear modulus is higher and the degradation of shear modulus is faster than that without confining pressure, indicating confining stress effect on shear modulus for FRCTC soil.

4. Comparison with results from resonant column tests and bender element tests verified the reliability of the local strain measurements. The results showed that the shear moduli obtained by local strain measurement are comparable to and consistent with those obtained by resonant column tests within the strain range of 0.1% to 0.001% for both unconfined and confined test condition.

5. The present experimental results also showed that the introduction of fibers increases the shear modulus and reduces the rate of modulus degradation for the strain range up to 0.01%. This suggests that FRCTC may potentially be useful for underground improvement works such as deep foundations and tunneling where the minimization of soil deformation is desirable.

Factors such as mix ratio, curing period and fiber content may contribute to the shear modulus degradation of FRCRC and are not discussed here due to length constraints. Introducing fibers to cement-treated soil has attracted more and more interest because it is highly effective in improving strength and stiffness, particularly tensile strength, ductility and modulus degradation. It may raise the costs of ground improvement, but will reduce significantly the risk of water leakage due to tensile failure of cement-treated soil and the associated costs to prevent and repair the leakage. It will also increase the useful life span of cement-treated soils and underground structures. All these are critical considerations in the safe construction and operation of underground structures, such as tunnels, as urbanization is becoming more widespread in many parts of the world.

ACKNOWLEDGMENTS

This research is supported by the National Research Foundation Singapore under its Competitive Research Programme (CRP Award No. NRF-CRP 6-2010-03).

REFERENCES

Baldi, G., Hight, D.W., and Thomas, G. E., 1988. A Re-evaluation of Conventional Triaxial Test Methods-a state-of-the-art. Advanced Triaxial Testing of Soil and Rock, ASTM STP 977, Philadelphia, Donaghe, R.T., Chancy, R.C., and Silver, M.L., Eds., American Society for Testing and Materials, pp. 219-263.

Brown, S.E. and Snaith, M.S., 1974. The Measurement of Recoverable and Irrecoverable Deformations in the Repeated Load Triaxial Test. Geotechnique, 24(2), pp. 255-259.

Cuccovillo, T. and Coop, M.R., 1997. The measurement of local axial strains in triaxial tests using LVDTs. Geotechnique, 47(1), pp. 167-171.

Gomes Correia A., Valente, T., Tinoco, J., Falcão, J., Barata, J., Cebola, D. and Coelho, S., 2009. Evaluation of mechanical properties of jet-grouting columns using different test methods. Proceedings, 17th ICSMFE, Alexandria, Egypt, October 5-9, M. Hamza et al. (Eds.), pp2169-2171.

Goto, S., Tatsuoka, E, Shibuya, S, Kim, Y-S., and Sato, T., 1991. A Simple Gage for Local Small Strain Measurements in the Laboratory. Soils and Foundations, 31(1), pp. 169-180.

Hoque, E., Tatsuoka, F. and Sato, T., 1996. Measuring anisotropic elastic properties of sand using a large triaxial specimen. Geotech. Testing J., ASTM 19(4), pp. 411-420.

Ibraim, E. and Benedetto, H.D., 2005. New Local System of Measurement of Axial Strains for Triaxial Apparatus Using LVDT. Geotechnical Testing Journal, 28(5), pp.1-9.

Jardine, R. J., Fourie, A., Maswoswe, J. and Burland, J.B., 1985. Field and laboratory measurements of soil stiffness. Proceedings, 11th ICSMFE, San Francisco, August 12-16,Vol. 2, pp. 511-514.
Kongsukprasert, L., Kuwano, R., Tatsuoka, F., 2002. Ageing Effects on The Stress-Strain Behaviour of Cement-Mixed Granular Materials. Proc. the Thirty-seventh Japan National Conference on Geotechnical Engineering, OSAKA, July, pp. 813-814.

Onishi, K., Tsukamoto, Y., Saito, R., and Chiyoda, T., 2010. Strength and small-strain modulus of lightweight geomaterials: cement-stabilised sand mixed with compressible expanded polystyrene beads. Geosynthetics International, 17(6), pp. 380-388.

Santagata, M.C., Germaine, J.T., and Ladd, C.C., 1999. Initial stiffness of K0-normally consolidated Boston Blue Clay measured in the triaxial apparatus. Proc. Of the 2nd international symposium on pre-failure deformaiton characteristics of geomaterials, IS-Torino-99, Vol.1, pp.27-34.

Schnaid, F., Prietto, P., and Consoli, N., 2001. Characterization of Cemented Sand in Triaxial Compression. J. Geotech. Geoenviron. Eng., ASCE, 127(10), pp.857-868.

Scholey, G. K., Frost, J.D., Lo Presti, D.C. F. and Jamiolkowski, M. ,1995. A review of instrumentation for measuring small strains during triaxial testing of soil specimens. Geotechnical Testing Journal, 18(2), pp. 137-156.

Silva, J., Azenha, M., Correia, A.G. and Feffeira, C., 2013. Continuous stiffness assessment of cement-stabilised soils from early age. Geotechnique, 63(16), pp. 1419–1432.

Taheri, A., Sasaki, Y., Tatsuoka, F., Watanabe, K., 2012. Strength and deformation characteristics of cement-mixed gravelly soil in multiple-step triaxial compression. Soils Found. 52 (1), pp. 126–145.

Tan, T.S., Goh, T.L. & Yong, K.Y. , 2002. Properties of Singapore Marine Clays Improved by Cement Mixing. Geotech. Test. J., 25(4), pp. 422-433.

Tatsuoka, F., Uchida, K., Imai, K., Ouchi, T. and Kohata, Y.., 1997. Properties of cement-treated soils in Trans-Tokyo Bay Highway project. Proceedings of the Institution of Civil Engineers - Ground Improvement, Volume 1, Issue 1, pp. 37-57.

Xiao H. W., Lee F. H., Zhang M. H. and Yeoh S. Y. 2013. Fiber reinforced cement treated clay. Proceedings,18 ICSMFE, Paris, Sept 2-6, Pierre D., Jacques D., Roger F., Alain P., Francois S., eds., pp 2633-2636.

Xiao H.W., Lee F. H. and Chin K. G., 2014a. Yielding of Cement-Treated Marine Clay. Soils and Foundations, 54(3), pp. 488-501.

Xiao H. W., Ng C.H.Y., Lee F.H., Zhang M.H., B.S. Ahmad M.R. , 2014b. Size effect study on fiber-reinforced cement-treated clay. Proceedings of the International Symposium on Geomechanics and Geotechnics: From Micro to Macro (Is-Cambridge 2014), Cambridge, London, 1-3, September 1-3, K. Soga, K. Kumar, G. Biscontin & M. Kuo (Eds) , CRC Pr I Llc, pp1351-1356.

Xiao H.W., Lee F.H. and Goh S.H. ,2015. Fibre distribution effect on behavior of fibre-reinforced cement-treated clay. Proceedings of 15th Asian Regional Conference of Soil Mechanics and Geotechnical Engineering, Fukuoka, Japan, Nov., Vol. 2, No. 60, pp. 2063-2068.

Yimsiri, S. and Soga, K., 2002. A Review of Local Strain Measurement Systems for Triaxial Testing of Soils. Geotechnical Engineering, SEAGS, 33(1), pp.41–52.

MICROSTRUCTURE OF BIO-CEMENTED COARSE SAND

Aamir Mahawish, PhD Student, Department of Civil Engineering, 18 Alliance Lane, Monash University, Victoria, Australia, phone: +61 3 9905 8901, email:aamir.mahawish@monash.edu

Abdelmalek Bouazza, Professor, Department of Civil Engineering, 23 College Walk, Monash University, Victoria, Australia, phone: +61 3 9905 4956, email:malek.bouazza@monash.edu

Will P. Gates, Senior Research Fellow, Australian Centre for Infrastructure Durability, Institute for Frontier Materials, Deakin University, Burwood, Victoria, Australia., phone +61 3 5224 2117; email: will.gates@deakin.edu.au

ABSTRACT

Bio-grouting by means of microbial induced calcite (calcium carbonate) precipitation (MICP) to improve mechanical properties of granular soils has gained much attention in recent years. The bio-grouting process offers an alternative and environmentally friendly approach to conventional soil improvement techniques, such as cement. Bio-grouting by urea hydrolysis has been extensively applied to tackle various geotechnical problems. However, it has yet to be applied to improve engineering properties (compressive strength) of a coarse cohesionless material with the aim using it as sand/stone columns within soft and very soft soils. This paper investigates the effect of using light, moderate and heavy biochemical treatments on the unconfined compressive strength (UCS) of coarse sand columns. In addition, the microstructure of the bio-cemented coarse material has been analysed by X-ray computed tomography (XRCT). The experimental results revealed that the UCS could reach up to 200kPa, 1000kPa and 5500kPa for light, moderate and heavy bio-cemented coarse sand columns, respectively. The microstructure investigations showed that the deposited calcium carbonate can be identified using XRCT imaging and can be associated with the gain in UCS values. Various micro-structure properties, such as void ratio, dry density and porosity were also identified and compared with the laboratory data.

Keyword: Bio-grouting, Bio-cementation, Ground Improvement, Microbial induced calcium carbonate precipitation, stone columns, 3D X-ray CT imaging, Micro-structure

INTRODUCTION

Bio-cementation via MICP method mimics a natural biochemical process that harnesses the metabolism of phenotypic microorganisms to induce insoluble bio-products such as calcium carbonate. When an MICP method is applied within a soil matrix, the engineering properties of soil (strength and stiffness) can be improved (Whiffin 2004, DeJong et al. 2006, Whiffin et al. 2007, Van Paassen 2009, Al Qabany et al. 2012, Mahawish et al. 2016). Most prominent of the MICP process is the urea hydrolysis by urease-producing bacteria such as, *Sporosarcina pasteurii,* which produces the urease enzyme to catalyse the conversion of urea to carbonate. In the presence of supplemental calcium ions, calcium carbonate will be precipitated. Urea hydrolysis provides an ideal environment to induce calcium carbonate crystallization and formation of a bond bio-product.

From an engineering perspective, it is important to quantify the ability of the bio-grouting mechanism to improve engineering properties (compressive strength) of stone/sand columns and the onset of precipitation of calcium carbonate crystals within the pore spaces of granular soils. In this investigation, coarse sand is treated by light, moderate and heavy biochemical treatments using the MICP method. The biochemical treatment process is based on a four-staged treatment strategy. Additionally, the microstructure of the bio-cemented coarse sand columns is investigated by X-ray computed tomography (XRCT) to visualize the precipitation of calcium carbonate.

MATERIALS AND METHODS

Bacterial suspension and cementation solution

The urease producing bacteria used was *Sporosarcina Pasteurii* (ATCC® 11859). An urea hydrolysing bacterium was grown at 30^{o}C in an ammonium-yeast extract medium (20g/L yeast extract, 10g/L $(NH_4)_2SO_4$ and 130 mM tris buffer (pH=9.0). The individual recipes were autoclaved separately and then mixed together post sterilization. A group of 1 litre bottles containing a growth medium were inoculated with two-percent of *S. Pasteurii* stock culture and incubated aerobically at 30^{o}C in a shaking water bath (200rpm). The bacterial cells were harvested at a final optical density (OD_{600}) of 3.0-3.5 using a WPA CO 8000 spectrophotometer (BioChrom Ltd).

An enzyme urease activity of 21.45 mM/min was used in this study. The bacterial cells were harvested at the beginning of the stationary growth phase, in which the size of a population of bacteria remained relatively constant to ensure that no further growth of bacterial cells could occur in the granular columns during the prescribed retention time (incubation time). The reason for this was to ensure that roughly same number of bacterial cells was used in each sand column due to the lack of required nutrient to grow more bacterial cells. The harvested microorganisms were stored at 4^{o}C in the 1 litre bottles for a maximum of two weeks. The ureolytic process was driven by using cementation solutions of urea and-calcium chloride at 1M concentrations.

Sand

The sand used in this study has an average grain size of 1.6 mm. It is classified as poorly graded coarse sand (SP) according to the Unified Soil Classification System (ASTM 2006). Maximum and minimum dry density measurements were conducted in accordance with ASTM D4253 and ASTM D4254, to control compaction of the sand column model. A summary of the sand properties (specific gravity (Gs), coefficient of curvature (Cc), coefficient of uniformity (Cu), the median grain size (D_{50}), maximum and minimum void ratios (e_{max} and e_{min}) are presented in Table 1. The sand particles were typically sub-angular in shape and were deemed to be representative of the stone aggregate used for full scale stone columns (Gniel and Bouazza 2009, 2010). Coarse sand columns were compacted up to 60% relative density.

Table 1. Coarse sand characteristics

Soil Type	Classification	Gs	Cc	Cu	D_{50} (mm)	e_{max}	e_{min}
Grade 8/16	SP	2.64	0.97	1.35	1.60	0.84	0.55

Soil treatment procedures

A percolation method was used for bio-cementation of very coarse sand specimens as described by Mahawish et al. (2016). However, the protocol that was adopted throughout this study was a four-phase percolation protocol. The strategy consisted of the following steps:

i. Percolation of tap water to expel air from the specimens (200% pore water capacity of sand columns (160 ml)). This step was done without retention time.
ii. Percolation of cementation solution (100% pore water capacity of sand columns (80 ml). This process was performed without retention time to promote high ionic strength within pore matrix.
iii. After the cementation solution volume had been drained out from each specimen, the bottom valve was closed, followed by percolating of bacterial suspension alternately with cementation solution for a total of four times to achieve a four-phase percolation protocol. (50% of the pore water capacity of the sand specimens, 40 ml.)
iv. Incubation (retention time) for 24 hours at 20±2 ºC, allowing the percolated liquids to facilitate number of reactions to happen between microorganisms and reagents solutions.
v. Percolation of cementation solution (40 ml) and allowing ureolysis and calcium carbonate deposition to take place for same retention time.
vi. Steps iii-v were considered as two treatments and were repeated until reaching the required number of treatments (*i.e.,* 4, 8, and 16).

Unconfined compressive strength (UCS) tests and calcium carbonate quantification

After completion of the bio-cementation treatments, all specimens were flushed with tap water to remove residual chemical reagents from the pore space of coarse sand columns. Unconfined compressive strength (UCS) tests were conducted on specimens cured over 14-days. The tests were performed on specimens 51mm in diameter with a selected height to diameter ratio of 2:1. The tests were carried out at a constant rate of 1%/min.

An Instron 4204 50kN constant-displacement mode UCS machine and laser extensometer were used in the current study. After completion of the UCS tests, calcium carbonate content was measured using gravimetric acid washing (2M HCl) technique. For this purpose, the specimens were dried in an oven at a temperature of 105^{o}C and their masses were measured before and after acid wash. The quantification of calcium carbonate was done by rinsing dissolved calcium carbonate-HCl several times through sieve No.200 and allowing the dissolved salts to be rinsed out from the specimens. The difference between two masses was taken as the mass of calcium carbonate and the percentage of calcium carbonate was obtained by dividing the mass of calcium carbonated by the mass of soil.

X-Ray computed tomography (XRCT) and image processing

XRCT tests were conducted on three bio-cemented coarse sand columns (4, 8, and 16 biochemical treatments). The coarse sand samples were packed into small tubes up to 60% relative density, each with an internal diameter of 25mm and 50mm high. This coarse sand column were similar in terms of void ratio (e), dry density (ρ) and porosity, which were equal to 0.66, 1.59 g/cm^3 and 0.40, respectively. These sand columns were similar to the ones that were prepared for the UCS tests. In addition, for verification purposes, the amount of calcium carbonate at the middle of the bio-cemented coarse sand columns were also quantified using the gravimetric acid washing technique.

A ZEISS Xradia 520 Versa (Xradia, Pleasanton, CA, USA) X-ray CT-imaging instrument was used in this study to capture changes in the microstructure of the bio-cemented coarse sand. To acquire the image projections, the sample-stage was incrementally rotated 360° around its vertical axis to obtain 1004 image projections with a pixel size of 25 microns. The acquired image projections represented the middle of the bio-cemented coarse sand column (around 25 mm high). The image size of the projections was 1024 x 1024 pixels. The values of XRCT scanning parameters are shown in Table 2.

Table 2: Values of XRCT scanning parameters.

Parameter	Value
Voltage	140.06 keV
Power	10.05 W
Exposure Time	0.5 sec
Camera binning	2
Source Distance	50 mm
Detector Distance	89.994 mm
Pixel Size	25 µm
Optical Magnification	0.39X

The 3D images were processed using the commercially available image processing software Avizo (V9.1. FEI, Hillsboro, OR, USA). The software was used to visualize and analyse the microstructure of the bio-cemented coarse sand specimens. For the purpose of the analysis, 2D tomographs (image projections) were firstly reconstructed to 3D volume using X-ray microscopy (XRM) software (Cone Beam-10, Xradia, Pleasanton, CA, USA) (Al Mahbub and Haque 2016). Next, the assembled 3D images were cropped from top and bottom regions to remove the excessive noises from these regions. 800 tomographs were used for analysis purposes in each bio-cemented coarse sand column. These tomographs were considered to be a candidate for the middle region (equal to 20mm high) of the bio-cemented coarse sand columns. Yet again, different filters were examined to reduce the remaining noises and a suitable filter was selected to be used for all columns. Finally, a segmentation of the voids, soil particles and the precipitated calcium carbonate was conducted and materials statistics were recorded. The operations of image processing were basically done as follows:

- Load reconstructed 3D tomographs (greyscale images) of the coarse sand column.
- Crop the coarse sand column to the height (20mm), where there are no apparent noises.
- Apply different filters for grayscale images to reduce noises (Non-local means filters was seen to be a suitable filter for all columns).
- Apply auto thresholding to get an idea about the intensity ranges, and then interactive thresholding was used for segmentation of voids, coarse sand particles and deposited calcium carbonate.
- Scrutinise and manual adjustments in the interactive thresholding to identify voxels as either voids, particle or calcium carbonate (visual judgment) (Hasan and Alshibli, 2010).
- Perform materials statistics of the segmented 3D images.
- Determine volume void (Vv), dry density (ρ) and porosity of the bio-cemented coarse sand columns based on the materials statistics. Materials statistics provides the volumes of voids, coarse sand particles and the deposited calcium carbonate.

- Quantify the amount of deposited calcium carbonate by dividing the volume of calcium carbonate by the volume of coarse sand particles.

RESULTS AND DISCUSIONS

Unconfined compressive strength (UCS)

Figure 1, shows the relationship between the number of biochemical treatments with the mean of amount of calcium carbonate precipitation in the middle of the bio-cemented coarse sand and the UCS. Because XRCT scanning was done to the middle parts of the bio-cemented coarse sand columns, the UCS results were correlated with the deposited calcium carbonate content at these parts of the columns. As shown in Fig. 1, an increase of the number of biochemical treatments is associated with the increase of the deposited calcium carbonate content. The precipitated calcium carbonate crystals act as bridging points surrounding soil particles and fill the pore spaces of the soil matrix (Martinez and DeJong 2009) leading to increase of the mechanical properties of the bio-cemented sand specimens (Whiffin et al. 2007, Van Paassen 2009, Rong et al. 2012, Mahawish et al. 2016). It can also be seen from Fig. 1 that the UCS of the bio-cemented coarse sand increased with the increase of the deposited calcium carbonate content. The maximum UCS was achieved with 16 biochemical treatments, which induced the highest calcium carbonate precipitation in the middle part of the bio-cemented coarse sand column.

It was postulated that the most critical aspect in calcium carbonate precipitation is the distribution of calcium carbonate crystals within the soil pores. Point to point contact conditions are required to achieve high strength and stiffness (DeJong et al. 2010). However, the amount of inter-particle contacts is practically correlated with the amount of deposited calcium carbonate. It was observed that the failure pattern propagated from the regions with a low bio-mineralisation content (Fig. 2 where it is shown that the failure occurred at the top portion of 16-biochemical treatment columns associated with lower calcium carbonate content (around 12%) compared to the middle and bottom portions). Importantly, the laboratory determined calcium carbonate precipitation correlated with the increasing of UCS as shown in Fig. 1. In other words the more calcium carbonate precipitates, the higher is the UCS. This is consistent with Mahawish et al. (2016), where they found that strength and stiffness was dependent on the overall mass of the bio-cemented materials.

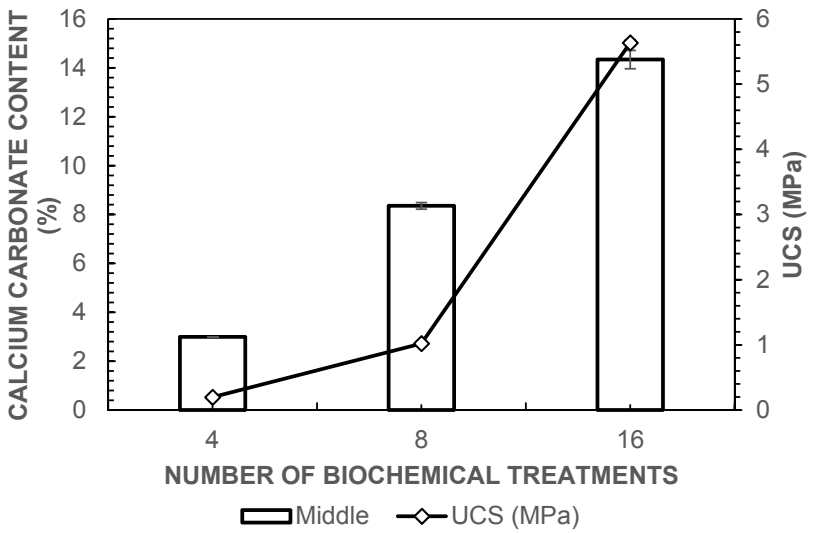


Fig.1. Correlation between calcium carbonate precipitation content and UCS.

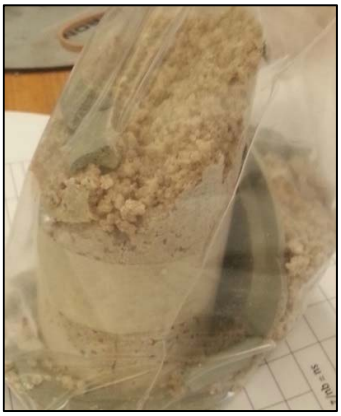


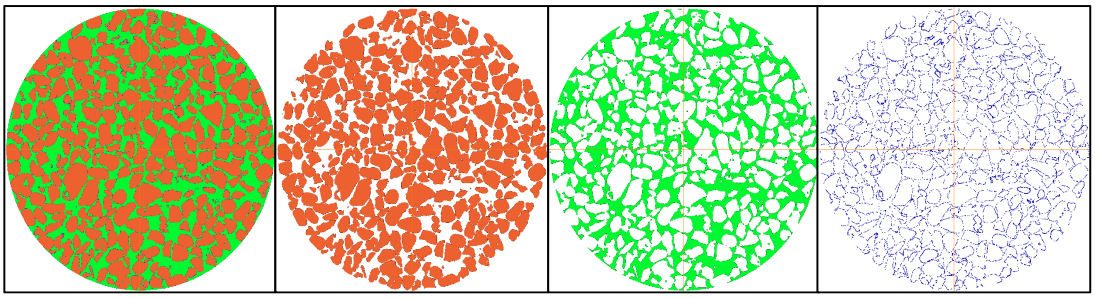
Fig. 2. Failure patterns in 16-biochemcical treatments column.

Microstructure evolution of bio-cemented coarse sand columns

Image analyses

Figure 3 shows the segmentation of the coarse sand specimen which underwent 4-biochemical treatments. Based on the intensity ranges (0-65535 voxels), the inner structure of 4-biochemical treatment specimens was investigated. The inner structure of this specimen was divided into three regions (coarse sand particles, void spaces and deposited calcium carbonate) as shown in Fig. 3, where Fig. 3a represents all segmented regions. The most important feature in Fig. 3 is the distribution of the precipitated calcium carbonate, as shown in Fig. 3d. It is clearly deposited within pores and around coarse sand particles. This is consistent with previous observations (Martinez and DeJong 2009), where they used scanning electron microscopy (SEM) to investigate the microstructure of MICP treated sand. Using the XRCT technique, it was found that the precipitated calcium carbonate in the coarse sand column treated up to 4-biochemical treatments was around 3.1%, whereas the laboratory acid washing technique showed that the deposited calcium carbonate was around 2.9%. The error between XRCT determined calcium carbonate and laboratory determined calcium carbonate was around 7%. Hence, XRCT can be used to identify the amount of calcium carbonate precipitation within the pore matrix of soil with a high level of accuracy.

To ensure the accuracy of the segmentation process, the XRCT determined parameters (void ratio, dry density, and porosity) should be consistent with the laboratory determined parameters. Based on XRCT materials statistics (volume of voids, soil particle volume, and calcium carbonate volume), the initial void ratio, dry density and porosity were computed as 0.67, 1.58 g/cm^3, and 0.40, respectively. These values are in agreement with the laboratory determined data (0.66, 1.59 g/cm^3 and 0.40). Therefore, the light treated coarse sand column was successfully analysed using XRCT images and all initial parameters relatively matched the laboratory parameters. Image analyses could be used as an alternative approach to the acid wash technique to quantify the amount of precipitated calcium carbonate. It can also be adopted to investigate the micro-scale distribution of the deposited calcium carbonate within the pore matrix of the coarse sand columns. This can also be useful when it comes to interpreting the increase in the UCS associated with the increase in the amount of calcium carbonate.



a. Sand Particles, bio-cement materials (blue hue) and pore spaces (green hue)

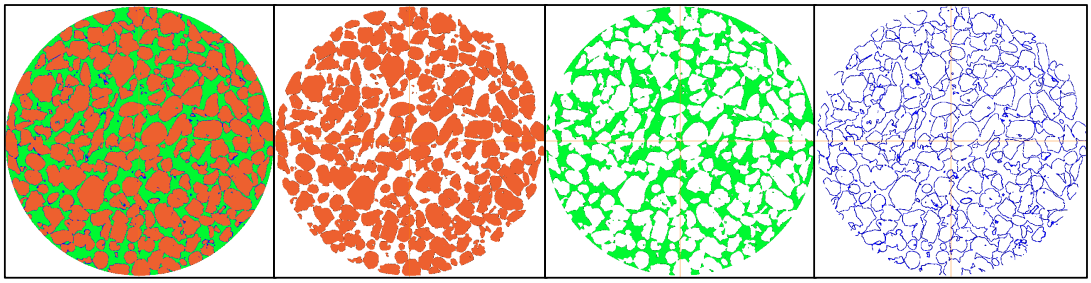
b. Sand Particles

c. Pore Spaces

d. Calcium Carbonate

Figure 3. 2D images of bio-cemented coarse sand samples with 4-biochemical treatments.

Figure 4 displays the inner structure in the bio-cemented coarse sand column which underwent 8-biochemical treatments. The deposited calcium carbonate crystals are clearly evident in Fig. 4d, where it surrounded and connected coarse sand particles. The microstructure of the second column (8-biocchemical treatments) could explain the increase in the UCS as compared with the first column (4-biochemical treatments). The main differences between the first column and second column were the amount and the distribution of calcium carbonate precipitation which filled a part of the pore spaces of the coarse sand columns (Fig. 3a and Fig. 4a). Image analyses of the second column were consistent with laboratory results as the amount of calcium carbonate shown in Fig. 4d is relatively equal to the laboratory result (around 7%). The error estimated for the difference between the amount of calcium carbonate determined via the XRCT technique and the laboratory technique was smaller than 5%. To verify this analysis, the parameters (void ratio, dry density and porosity) of the second coarse sand column should be same as, or close to, their initial counterparts. The error of the XRCT analysis in relation to the laboratory parameters of the second bio-cemented coarse sand varied between around 0.5 to 1%. Thus, it is evident that the image analysis of the second coarse sand column has a high level of accuracy. Image analysis based on XRCT imaging could also be reliable to be used to capture the microstructure changes of the bio- cemented coarse sand samples. The amount and distribution of precipitated calcium carbonate in the second column could explain the increasing of UCS by 5x compared with the first column.



a. Sand Particles, bio-cement materials (blue hue) and pore spaces (green hue)

b. Sand particles

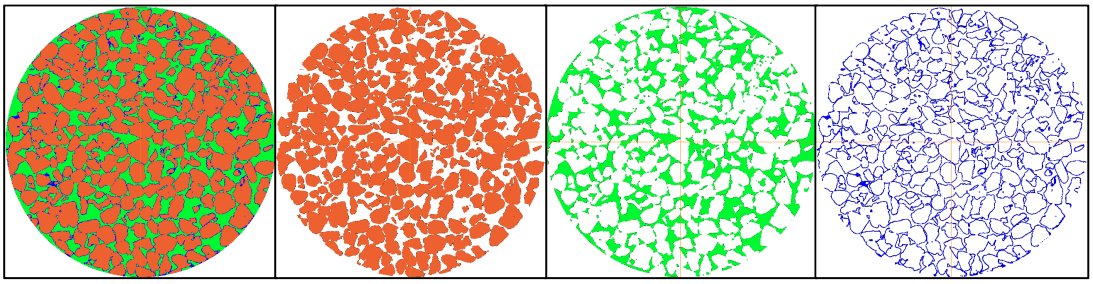
c. Pore spaces

d. Calcium carbonate

Figure 4. 2D images of bio-cemented coarse sand samples with 8-biochemical treatments.

Figure 5 shows a segmentation of heavily bio-improved coarse sand column (16-biochemical treatments). As shown in Fig. 5a, the deposited calcium carbonate is evident in inter-particle and intra-particles of the third bio-cemented coarse sand column. The crystals of precipitated calcium carbonate in this column (Fig. 5d) were thicker than previous coarse sand columns (Fig. 3d and Fig. 4d). It can also be seen from Fig. 5a that the distribution of precipitated calcium carbonate over the diameter of the third column was heterogeneous (some particles were heavily connected by calcium carbonate). This is evidence of microbe augmentation leading to creation of colonies within the pore matrix of the coarse sand columns. It could be seen from Fig. 5c that the pore spaces were substantially reduced as a result of the precipitation of calcium carbonate. The XRCT results of the third coarse sand column indicated that the determined calcium carbonate was around 12%. This is in agreement with the laboratory determined calcium carbonate (around 11%). The XRCT determined calcium carbonate could explain the substantial increase in the UCS of the third column. As the calcium carbonate crystals layer increased, the UCS of the bio-cemented coarse sand column increased.

The other coarse sand column parameters (void ratio, dry density and porosity) were used to verify the segmentation validity. It was found that the void ratio, dry density and porosity were around 0.60, 1.65g/cm^3 and 0.37, respectively. This is reasonable in agreement with the laboratory data and the desired level of segmentation was achieved.



a. Sand Particles, bio-cement materials (blue hue) and pore spaces (green hue)

b. Sand particles

c. Pore spaces

d. Calcium carbonate

Figure 5. 2D images of bio-cemented coarse sand samples with 16-biochemical treatments.

CONCLUSIONS

Three coarse sand columns were prepared and treated with different number of treatments (light, moderate and heavy biochemical treatments). Based on the UCS and the microstructure analysis of the middle regions of the bio-cemented coarse sand columns, the following conclusions can be drawn from the current investigation;

- The laboratory data showed that increasing the number of biochemical treatments leads to an increase of calcium carbonate precipitation. The precipitated calcium carbonate in the middle regions of the bio-cemented coarse sand columns correlated with the UCS of these columns. The UCS increased with the increase in the amount of deposited calcium carbonate, and the maximum UCS (5500kPa) was achieved with around 12% calcium carbonate precipitation.
- The precipitation and the distribution of calcium carbonate in the pore spaces of the bio-cemented coarse sand columns was investigated using imaging analyses. The segmentation of (voids volume, sand particle volume and calcium carbonate volume) of the bio-cemented coarse sand columns was successfully achieved. The calcium carbonate was seen as a thin layer surrounding and connecting coarse sand particles. This layer was getting thicker with the increase in the number of biochemical treatments. It was also shown that the XRCT technique can identify the amount of precipitated calcium carbonate. In addition, there was a reasonable agreement between the XRCT determined calcium carbonate content and the acid quantified calcium carbonate content. The amount and distribution of the precipitated calcium carbonate could be associated with the increasing of the UCS of the bio-cemented coarse sand columns.
- Using non-destructive XRCT imaging technique and image analyses process to investigate the microstructure of bio-cemented soils is believed to provide a significant insight about MICP treated soils. The XRCT technique can also give a high level of accuracy in micro-scale investigations.

REFERENCES

Al Mahbub, A. and Haque, A., 2016. X-ray computed tomography imaging of the microstructure of sand particles subjected to high pressure one-dimensional compression, Materials, **9**(11), pp. 890.

Al Qabany, A., Soga, K. and Santamarina, C., 2012. Factors affecting efficiency of microbially induced calcite precipitation, Journal of Geotechnical and Geoenvironmental Engineering, **138**(8), pp. 992-1001.

ASTM. 2006. Standard practice for classification of soils for engineering purposes (Unified Soil Classification System). ASTM standard D2487. American Society for Testing and Materials. West Conshohocken, Pa. doi:10.1520/ D2487-11.

ASTM. 2014a. Standard test methods for maximum index density and unit weight of soils using a vibratory table. ASTM standard D4253. American Society for Testing and Materials. West Conshohocken, Pa. doi:10.1520/ D4253-14.

ASTM. 2014b. Standard test methods for minimum index density and unit weight of soils and calculation of relative density. ASTM standard D4254. American Society for Testing and Materials. West Conshohocken, Pa. doi:10. 1520/D4254-14.

Cheng, L., and Cord-Ruwisch, R., 2012. *In-situ* soil cementation with ureolytic bacteria by surface percolation, Ecological Engineering, **42**(0), pp. 64-72.

Cord-Ruwisch, R.DeJong, J. T., Mortensen, B. M., Martinez, B. C. and Nelson, D. C. (2010). Bio-mediated soil improvement. Ecological Engineering **36**(2): 197-210.

Dick, J., De Windt, W., De Graef, B., Saveyn, H., Van der Meeren, P., De Belie, N. and Verstraete, W. (2006). Bio-deposition of a calcium carbonate layer on degraded limestone by Bacillus species, Biodegradation **17**(4), pp. 357-367.

Faibish, R.S., Elimelech, M., and Cohen, Y., 1998. Effect of interparticle electrostatic double layer interactions on permeate flux decline in crossflow membrane filtration of colloidal suspensions: an experimental investigation, Journal of Colloid and Interface Science, 204(1), pp. 77–86.

Foppen, J., and Schijven, J., 2006. Evaluation of data from the literature on the transport and survival of Escherichia coli and thermotolerant coliforms in aquifers under saturated conditions, Water Research, **40**(3), pp. 401–426.

Gniel, J. and Bouazza, A., 2009. Improvement of soft soils using geogrid encased stone columns. Geotextiles and Geomembranes, **27**(3), pp. 167-175.

Gniel, J. and Bouazza, A. 2010. Construction of geogrid encased stone columns: A new proposal based on laboratory testing, Geotextiles and Geomembranes, **28**(1), pp. 108-118.

Harkes, M. P., Van Paassen, L. A., Booster, J. L., Whiffin, V. S. and van Loosdrecht, M. 2010. Fixation and distribution of bacterial activity in sand to induce carbonate precipitation for ground reinforcement, Ecological Engineering, **36**(2), pp. 112-117.

Hasan, A. and AlShibli, K. A. 2010. Experimental assessment of 3D particle-to-particle interaction within sheared sand using synchrotron microtomography, Geotechnique, **60**(5), pp. 369-379.

Mahawish, A., Bouazza, A. and Gates, W. P., 2016. Biogrouting coarse materials using soil-lift treatment strategy, Canadian Geotechnical Journal, (999), pp. 1-6.

Martinez, B. C. and DeJong, J. T., 2009. Bio-mediated soil improvement: Load Transfer Mechanisms at the Micro- and Macro- Scales, Advances in Ground Improvement**,** pp. 242-251.

Rong, H., Qian, C.-X. and Li, L. z., 2012. Study on microstructure and properties of sandstone cemented by microbe cement, Construction and Building Materials, **36**(0), pp. 687-694.

Van Paassen, L. A., 2009. Biogrout, ground improvement by microbial induced carbonate precipitation, TU Delft, Delft University of Technology.

Whiffin, V. S., 2004. Microbial CaCO3 precipitation for the production of biocement, Australia, Murdoch University. **PhD**.

Whiffin, V. S., van Paassen, L. A. and Harkes, M. P., 2007. Microbial Carbonate Precipitation as a Soil Improvement Technique Geomicrobiology Journal, **24**(5), pp. 417-423.

PILE FOUNDATION RESPONSE TO GROUND VIBRATION FROM ROCK BLASTING

Laddu B. Jayasinghe, Nanyang Technological University, Singapore, ljayasinghe@ntu.edu.sg
Anthony T.C. Goh, Nanyang Technological University, Singapore, ctcgoh@ntu.edu.sg
Zhiye Zhao, Nanyang Technological University, Singapore
Hongyuan Zhou, Nanyang Technological University, Singapore
Yilin Gui, Nanyang Technological University, Singapore

ABSTRACT

Ground vibrations from blasting are undesirable and they are very short in duration with high principal frequencies and high amplitude. Structural response to that kind of excitations may differ significantly from that generated by lower-frequency earthquake vibrations. In practice, the damage to nearby structures to generated ground vibrations has been controlled by various codes and regulations available. However, the existing vibrations limits are not always applicable, as they depend on the geological conditions of the site and the dynamic characteristics of the structure. This paper investigated the influence of the rock-soil interface on the response of pile foundation to ground-borne vibration from rock blasting, through numerical simulations using finite element software LS-DYNA. It is found that the slope of the rock-soil interface greatly influences the location of damage and the extent of damage on the pile. The bottom of the pile is subjected to a larger blast pressure and stresses are highly concentrated at the pile bottom. Thus, the pile bottom can fail in shear before it reaches its plastic moment capacity.

Keywords: rock blasting, numerical simulation, pile foundation

INTRODUCTION

Drilling and blasting is the widely accepted method to large-scale rock breaking activities in civil engineering constructions due to its cost effectiveness, higher efficiency and ability to break hard rock. However, ground vibrations from blasting are undesirable and it can cause damage to nearby structures. In practice, the damage to nearby structures to generated ground vibrations has been controlled by various codes and regulations available. The existing vibration limits are not always applicable, as they depend on the geological conditions of the site and dynamic characteristics of the structure.

Pile foundations are commonly used as foundations of high-rise buildings and bridges to transfer the heavy loads from the superstructure above through weak compressible soil strata into deeper, competent soil layers which have adequate capacity to carry these loads. In engineering practice, many piles are normally designed to carry mainly vertical loads and very little lateral loads, as typically the vertical loads (the gravity) are significantly larger than the horizontal loads such as wind loading. However, in recent years, there have been a number of reported case studies of translational soil movements that have induced stresses and bending moments that have damaged pile foundations and in some cases resulted in collapse of the superstructure. Typical lateral load include nearby construction activities such as an excavation for a basement or slope, the construction of a road embankment or a tunnel, as well as earthquakes (Abdoun 1997; Goh et al. 1997; 2003; Chen et al. 1999; Dobry et al. 2003; Boulanger et al. 2007; Black et al. 2007).

Short duration, high frequency, high amplitude loads such as rock blasting may also have an impact on the pile foundation system. The ground vibration can induce lateral and bending stresses in the piles and cause significant damage, resulting in differential settlement and tilting of the superstructure, leading to weakening of the structure. Thus, the lateral response of piled foundation is important in the designing of structures that may be subjected to lateral loads. The performance of pile foundations subjected to dynamic lateral loads is a complex research area, as the laterally loaded pile is a three-

dimensional problem, and the soil-pile interaction (SPI) is extremely complex as non-linear and dynamic conditions exist simultaneously and also it plays a significant role in the pile response to ground vibrations (Wu and Finn 1997)

Unfortunately, studies and discussions on the damage and failures of piles under blasting vibration are limited in the literature. Thus, it is necessary to study the performance of piles under blast loading, because of the wide application of blasting and to highlight their impact on the surrounding piled foundation structures.

PROBLEM DESCRIPTION

The present study aims to assess the damage on a pile foundation system subjected to ground vibrations from rock blasting. A pile group of two 600 mm diameter circular reinforced concrete (RC) piles of 8 m length is considered in this study. The distance between the leading pile of the pile group and the blast hole is 7.5 m and blast responses of piles are studied when fully coupled charges are detonated. Moreover, a sloping soil-rock interface is considered in the present study as shown in Fig. 1. Three different slope angles (α) are considered for the purpose of comparison as shown in Table 1.

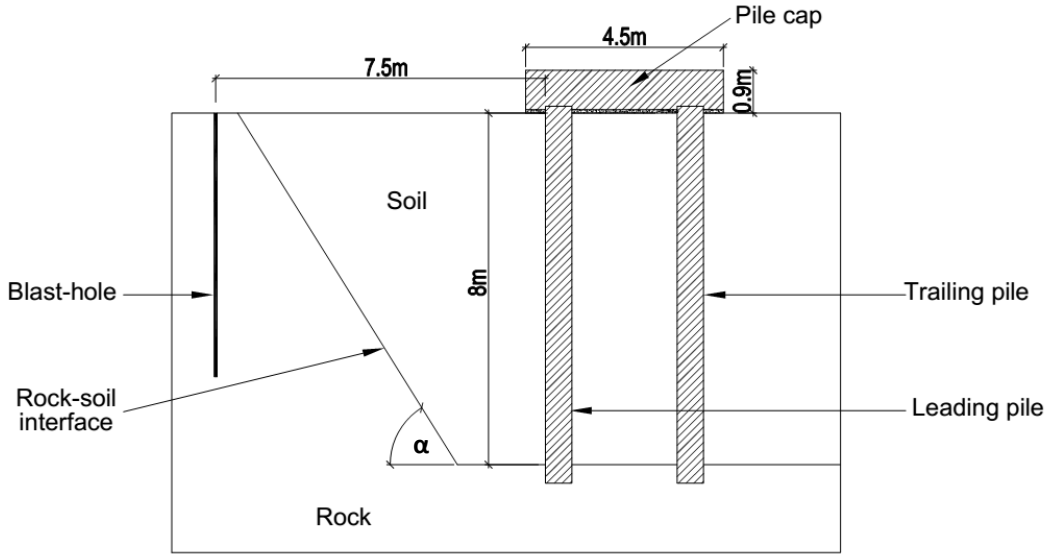


Fig. 1. Cross-section of pile group

Table 1. Analysis cases

Analysis case	Slope angle (α)
1	60°
2	75°
3	90°

NUMERICAL SIMULATION

Currently, a number of Finite element (FE) codes are available that are capable of analyzing challenging engineering problems, but selection of the appropriate numerical technique is dependent on the type of problem and its computational cost. The commercial software package LS-DYNA (LSTC, 2007) which is a non-linear, dynamic analysis software, suitable for modeling large strain problems including blasts and impact was used in this study. The software allows different numerical simulation techniques such as Lagrangian, Eulerian, Arbitrary Lagrangian-Eulerian (ALE) and

Smooth particle hydrodynamics (SPH). This paper uses coupled SPH-FEM technique in LS-DYNA to investigate the response of a pile group of 2 piles subjected to ground vibration from rock blasting.

By making use of the symmetry of the model, only a half symmetry-geometrical FE model was developed to minimise the computational time. Fig. 2 shows the developed 3D FE model to study the the response of piles subjected to ground vibration from rock blasting. The explosive charge, stemming materials and the part of the rock experiencing large deformations were modelled with SPH particles while the rest of the model (rock and soil) was based on Lagrange FEM element. The symmetry face is fixed against translational displacements normal to the symmetry plane. Non-reflecting boundaries are applied to the other surfaces, except the top surface which has the free boundary condition.

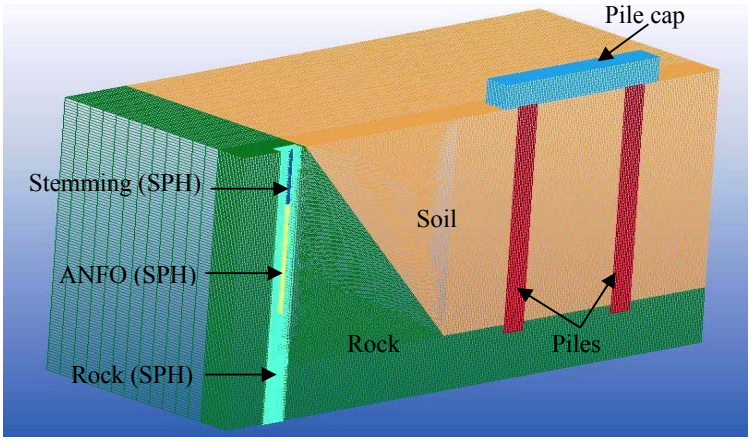


Fig. 2. A half symmetrical model

The 3D FE model was developed for the 8 m long reinforced concrete (RC) piles with 600 mm diameter circular cross section. Both the leading and tailing piles are socketed 1 m into the rock. The piles were reinforced with 8 numbers of 16 mm diameter bars, providing a vertical reinforcement ratio of 0.6% and spiral reinforcement of 10 mm bars at spacing of 200 mm. Except for the reinforcing cage, eight-node solid elements were used for the 3D explicit analysis. Both the vertical reinforcements and the ties were modelled with 25mm long beam elements having 2x2 Gauss integration. The vertical reinforcements were defined as Hughes-Liu beam elements with cross-integration and ties were defined as truss elements. The ANFO explosive, stemming material and part of rock close to the explosive were modelled with SPH particles while Lagrangian meshes were used to model the pile, soil and the rock region away from the explosive charge. The simulations used automatic node to surface contact conditions for the coupling interaction between the SPH particles and Lagrange FEM elements.

Nonlinear effects near the explosive source were considered to accurately model the physical behaviour. There are several material models for rock implemented in LS-DYNA. The plastic kinematic model was used to simulate the constitutive characteristics of rock under blast loading. The physical and mechanical parameters of the Bukit Timah granite are described in Jayasinghe et al. (2017) and were used in the simulations. The constitutive behaviour of the soil model is also an important aspect in wave propagations in soil and SPI analysis. Generally, there are two types of soil models that are used in finite element analyses of soils such as elastic models and elastic-plastic models. Elastic-plastic constitutive models such as Mohr-Coulomb and Drucker-Prager can provide a reasonable representation of a typical wave propagation problem. In this study, the Mohr-Coulomb model in LS-DYNA was used to simulate the soil. This material model requires the main parameters of mass density, elastic shear modulus, Poisson's ratio, friction angle and cohesion. The corresponding parameters for the rock and soil are described in Table 2 and 3, respectively.

Table 2. Material parameters for rock

Density (kg/m^3)	Young's modulus (GPa)	Poisson's ratio	Yield stress (MPa)	Tangent modulus (GPa)	Hardening Parameter (β)
2650	61.41	0.27	154.57	24.56	1

Table 3. Material parameters for soil

Density (kg/m^3)	Elastic shear modulus (MPa)	Poisson's ratio	Friction angle	Cohesion (kPa)
1960	140	0.3	30°	22

Concrete_damage_rel3 material model was used to simulate the concrete behaviour. It is a plasticity-based model with three shear failure surfaces and includes damage and strain rate effects (Malvar et al. 1997). The literature has shown that material concrete_damage_rel3 model can successfully incorporate non-linear concrete properties (Thilakarathna et al. 2010; Jayasinghe et al. 2014). The advantage of this model is that unconfined compressive strength and density of concrete are the only two parameters required in the calibration process. In this study, the concrete density and the compressive strength of concrete were assumed as 2300 kg/m^3 and 35 MPa, respectively. In order to account for the increase in strength under high strain rates, a coefficient called the dynamic increased factor (DIF) is employed in this analysis. The plastic kinematic model was used to model the vertical and lateral reinforcement. It is an elastic-plastic material model with strain rate effect. A strain rate effect is accounted for using the Cowper-Symonds model which scales the yield stress by a strain rate dependent factor. The parameters of concrete and steel used in this study can be found in Jayasinghe et al. (2017) and are listed in Table 4.

Table 4. Material parameters for steel

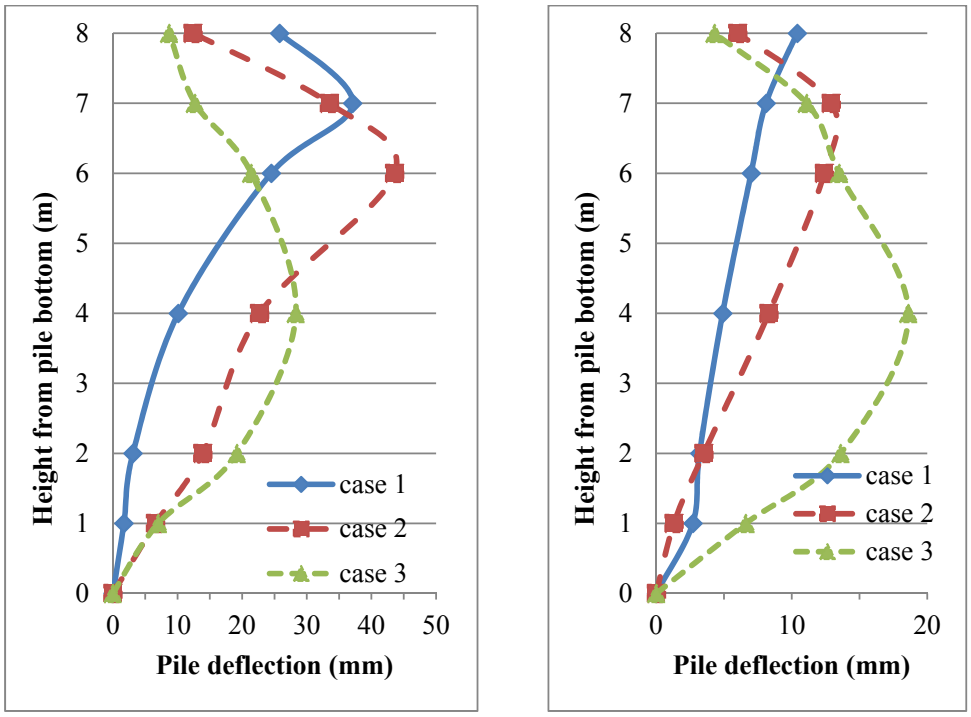
	Density (kg/m^3)	Young's modulus (GPa)	Poisson's ratio	Yield stress (MPa)	Tangent modulus (GPa)	Hardening Parameter (β)	C	P
Vertical R/F	7850	210	0.3	460	2	0	40	5
Ties	7850	210	0.3	250	2	0	40	5

RESULTS AND DISCUSSION

The horizontal deformations of the pile were obtained at 7 monitoring points along the pile at different heights from the pile bottom: 0 m, 1 m , 2 m, 4 m, 6 m, 7 m and 8 m, in each case. Horizontal deforamtions of the piles obtained in each case are compared as shown in Fig. 3. Figure 3(a) shows the horizontal deformation of the leading piles in the pile groups. It is clearly seen that the pile is subjected to a maximum deformation of 37 mm at a height of 7 m above the pile bottom in case 1. However, it was found that the leading pile is subjected to a maximum deformation of 44 mm at a height of 6 m above the pile bottom and 29 mm at the mid-height, in cases 2 and 3, respectively. Figure 3(b) shows that the horizontal deformation of the trailing piles in the pile groups. It can be clearly seen that leading piles of the 2-pile groups are subjected to larger deformation than the trailing piles. They have pile head displacements of 26 mm, 12.5 mm and 8.7 mm in cases, 1, 2 and 3, respectively.

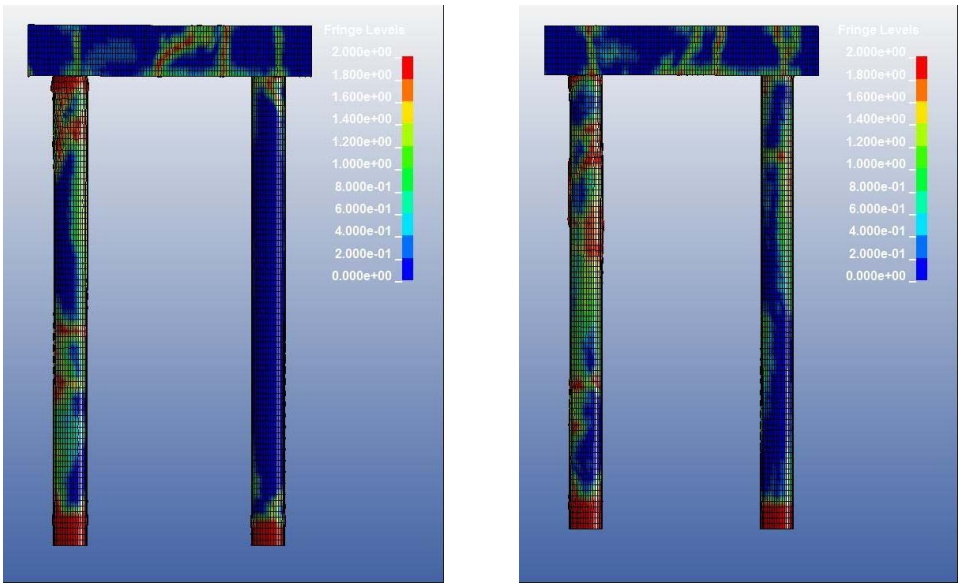
To further study the behavior of each pile, blast damage in each pile in the pile groups were examined using the effective plastic strain diagrams. Fig. 4 depicts the concrete effective plastic strain variation of each individual pile in the pile groups. The effective plastic strain in the concrete_damage_rel3

material model is the damage parameter which ranges between 0 and 2, with fringe levels 0 and 2 indicating no yielding and maximum yielding of the concrete, respectively.

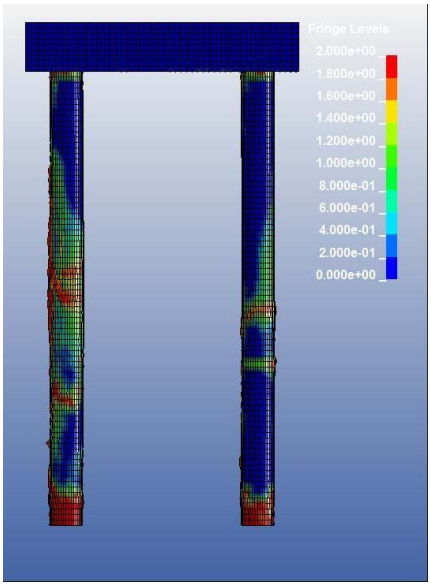


(a) **(b)**

Fig. 3. Comparison of pile deformations obtained in cases 1 to 3 (a) leading pile of pile groups (b) trailing pile of pile groups



(a) **(b)**



(c)

Fig. 4. Results for effective plastic strain diagram of concrete in (a) case 1 (b) case 2 (c) case 3

As can be seen in Fig. 4, a significant portion of each pile has suffered damage and local failure, as the effective plastic strains are greater than 0. It is also clear that the bottom of the piles were significantly damaged in all cases. This is because of the bottom of the pile is subjected to a larger blast pressure and stresses are highly concentrated at the pile bottom. Because of this, the pile bottom can fail in shear before it reaches its plastic moment capacity. Also as expected, the trailing pile has less damage and deformations due to shielding effect from the leading pile.

The formed shapes of the piles are different in each case. It can be noted that the top of the pile suffered the most damage in the analysis case 1 compared to the other two cases while concrete in the middle of the pile suffered most damage in the analysis case 3. Therefore, it is clear that the slope of the rock-soil interface greatly influences the location of damage and the extent of damage on the pile.

CONCLUSION

This paper investigated the influence of the slope angle of the rock-soil interface on the dynamic response of a reinforced concrete pile foundation system to ground-borne vibration from rock blasting using the commercial computer program LS-DYNA. A downslope soil-rock interface was considered in the present simulation. Through the comparison of numerical simulation results, it was demonstrated that the rock-soil interface affects the ground wave propagation significantly and hence the location of damage and the extent of damage on the pile are greatly influenced by the slope of the rock-soil interface. In addition to that, because the wave attanuation in the rock is slower than in soil, the bottom of the pile is subjected to a larger blast pressure and stresses are highly concentrated at the pile bottom. Because of this, the pile bottom can fail in shear before it reaches its plastic moment capacity.

ACKNOWLEDGMENTS

This material is based on research/work supported by the Land and Liveability National Innovation Challenge under L2NIC award Number L2NICCFP1-2013-1. The support from JTC Corporation is also gratefully acknowledged.

REFERENCES

Abdoun T.H., 1997. Modelling of seismically induced lateral spreading of multi-layer soil deposit and its effect on pile foundations, PhD thesis, Department of of Civil Engineering, Rensselaer Polytechnic Institute, Troy, N.Y.

Black D.A., Black J.A., Issarayangyun T., and Samuels S.E., 2007. Aircraft noise exposure and resident's stress and hypertension: A public health perspective for airport environmental management. Journal of Air Transport Management, 13(5), pp. 264-276.

Boulanger R.W., Chang D., Brandenberg S.J., Armstrong R.J., and Kutter B.L., 2007. Seismic design of pile foundations for liquefaction effects, Proceedings, 4th International Conference on Earthquake Geotechnical Engineering, Invited Lectures, K.D. Pitilakis, ed., Springer, The Netherlands, pp. 277-302.

Chen L.T., Poulos H.G., and Loganathan N., 1999. Pile responses caused by tunnelling. Journal of Geotechnical and Geoenvironmental Engineering, 125(3), pp. 207-215.

Dobry R., Abdoun T., O'Rourke T., and Goh S.H., 2003. Single piles in lateral spreads: Field bending moment evaluation. Journal of Geotechnical and Geoenvironmental Engineering, 129(10), pp. 879–889.

Goh A.T.C., Teh C.I., and Wong K.S., 1997. Analysis of piles subjected to embankment induced lateral soil movements. Journal of Geotechnical and Geoenvironmental Engineering ASCE, 123(9), pp. 792-801.

Goh A.T.C, Wong K.S., Teh C.I., and Wen D., 2003. Pile response adjacent to braced excavations. Journal of Geotechnical and Geoenvironmental Engineering, ASCE, 129(4), pp. 383-386.

Jayasinghe L.B., Thambiratnam D.P., Perera N., and Jayasooriya J.H.A.R., 2014. Effect of soil properties on the response of pile to underground explosion, Structural Engineering International, 24(3), pp. 361-370.

Jayasinghe L.B., Zhou H.Y., Goh A.T.C., Zhao Z.Y., and Gui Y.L., 2017. Pile response subjected to rock blasting induced ground vibration near soil-rock interface, Computers and Geotechnics, 82, pp 1-15.

Livermore software technology cooperation, LS-DYNA user's manual, version 971, 2007.

Malvar L.J., Crawford J.E., Wesevich J.W., and Simons D.A., 1997. A plasticity concrete material model for DYNA3D, International Journal of Impact Engineering, 19 (9-10), pp.847-873.

Thilakarathna H.M.I., Thambiratnam D.P., Dhanasekar M., and Perara N.J., 2010. Numerical Simulation of Axially Loaded Concrete Columns under Transverse Impact and Vulnerability Assessment, International Journal of Impact Engineering, 37(11), pp.1100-1112.

Wu G., and Finn W.D.L., 1997. Dynamic Nonlinear Analysis of Pile Foundations using Finite Element Method in the Time Domain, Canadian Geotechnical Journal, 34, pp 44-52.

RISK-BASED APPROACH IN DRILLED SHAFT DESIGN FOR INFRASTRUCTURE PROJECTS

Ramanujachari Kannan, P.E. D.GE., FASCE, US Army Corps of Engineers, Fort Worth, Texas, USA, (817) 996 9057, kannangator@yahoo.com

ABSTRACT

Design of drilled shafts involves a number of constraints that have been improved by advanced analytical design methods and by using input from performance monitoring and instrumentation. The number of variables involved in design require an assessment of the data and assumptions are reliable. Despite improvements in design and monitoring, the variability in soil and subsurface conditions as well as the reliability of models introduce an element of risk, which the designer avoids primarily by incorporating redundancy in design. In the last two decades probabilistic and statistical methods have been introduced in predicting soil properties and behavior, thereby refining the predicted behavior of the designed structure. Design of geotechnical structures using a risk-based approach was recently introduced for the design of levees. This paper builds on the concept of applying risk-based design method to the design of other geotechnical structures, such as retaining structures, and this paper considers such an approach to the design of drilled shafts.

Keywords: Drilled Shafts, design, risk-based analysis, risk-based assessment

INTRODUCTION

Risk is defined in terms of probability of occurrence of an event and its consequences as Risk = Probability x Consequence. In geotechnical engineering design there is always a risk that the soil properties as determined from a representative sample may differ from the conditions at the site, when extrapolated. Unlike many other designed systems, geotechnical design often demands self-sustainability once the system is built. One of the primary requirements of sustainable systems is that they require little or no maintenance, perform as designed and achieve a balance between the natural and the engineered environments. In this context, deep foundations, in particular drilled shafts could use a risk-based design methodology earlier in the design process. Current practice relies on analytical design methods, codes and standards that have evolved over time, and have incorporated better methods of accounting for variability in the determination of the soil properties in the laboratory as well as the design, construction and monitoring of the drilled shafts. However, there are a number of unknowns in the design process that could increase the risk that the installed drilled shafts may not perform as designed. Conventional design process could be improved by the use of risk-based decision making process. This paper illustrates the potential for risk-based design concept, using the design of drilled shafts as an example. The concept could be expanded to any aspect of geotechnical engineering design, as it is essentially a question of asking at every step of the design process, "what if…."

CONVENTIONAL DESIGN PROCESS

An excellent summary of design methods as practiced currently was presented by Bolton (1992) where he identified design as a four-component process. Briefly stated, these four components are: define performance requirements, synthesise a solution, evaluate the design and refine and redesign as necessary. He also quoted the need for the "design as you go" or "the observational method" process, from Peck's 1969 Rankine lecture. Thus, design, observe, redesign has become more or less a standard operating procedure for geotechnical design. In discussing the design of drilled shafts, we therefore start with the loading conditions and performance requirements, use the known geotechnical data, analyse the performance requirements and in some cases, monitor the performance against the design requirements. As drilled shafts which have to be designed as non-redundant members of the engineered system, there is little room for error, or compromising the performance requirements. We resolve these issues by incorporating a higher factor of safety and sometimes monitor the performance by instrumentation. An example of this would be bridge piers, where a single, large-diameter drilled shaft

will carry the critical loads, every risk and its consequence has to be considered in the design. The variables involved in the design of drilled shafts could be understood if we consider the design process recommended by the American Concrete Institute, ACI 336.3R-93 (1993) Design and Construction of Drilled Piers. This guide could be seen as a list of the variables that must be considered and it could be broadly divided in two sections as design and construction aspects. Despite the fact that all of the guidelines apply to the design, including the construction, it should be understood that this is not a linear process and practically everything is interrelated. Figure 1 below is the author's attempt to link some of the obvious inter-related steps in the design process. The intention of showing a limited number of links is not to confuse the illustration but to show the inter-dependence of one factor on another.

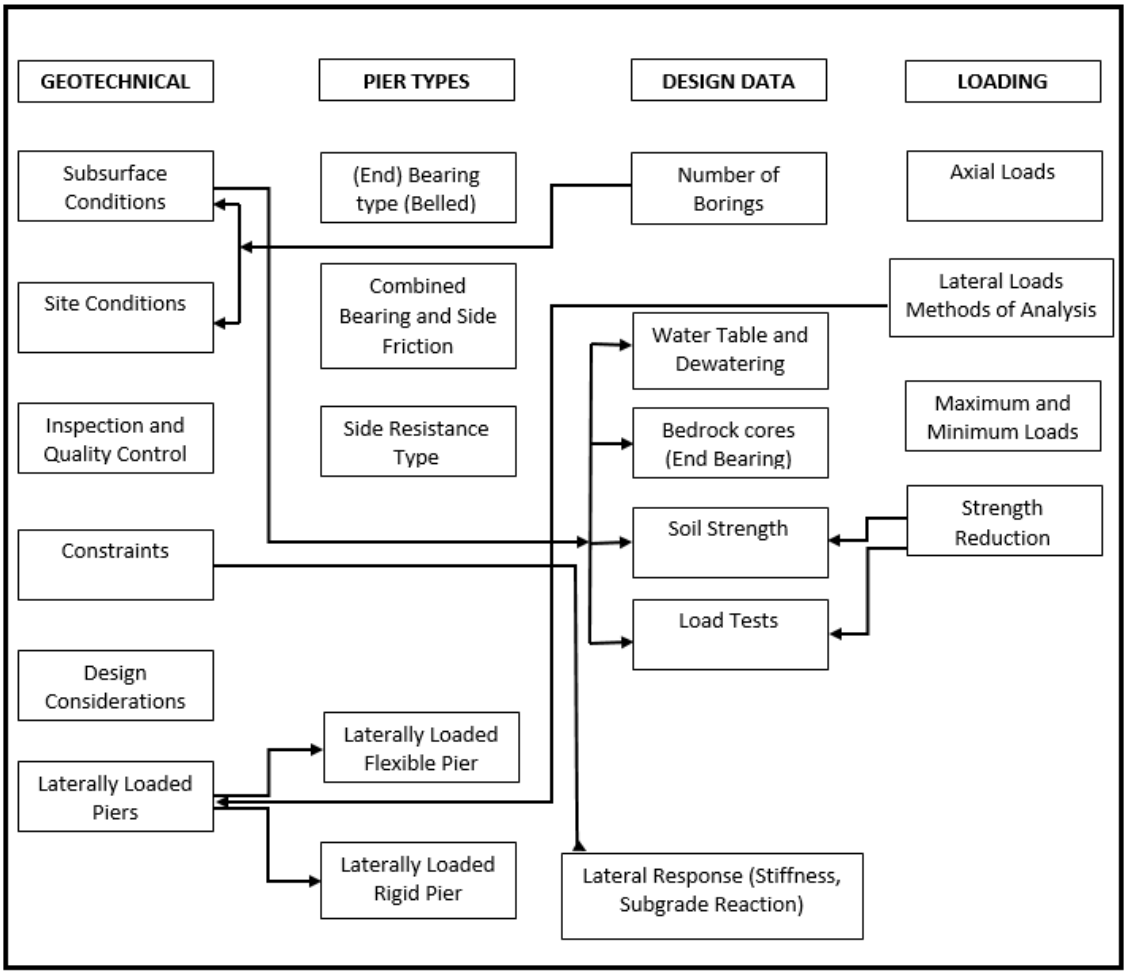


Fig. 1. ACI 336.3(R) lists all the above elements as required components of the design process and construction of drilled shafts. This links shown are some of the inter-dependent associations. ACI guides the design through a sequence of decision steps.

In the design of drilled shafts mathematical models could be built to evaluate the behavior of a single shaft or a group of shafts in a foundation system. Such simulations and behavior models depend on accurate input of soil data, reliable model of the anticipated behavior and material characteristics. For example, computer simulations will use simplified soil stratification, which may be different for each drilled shaft in a large infrastructure project, such as a bridge or highway construction. This leaves the designer with the need to analyse each drilled shaft separately, which could be time consuming. The easier alternative is to choose the worst case and use that design for the rest of the drilled shafts, which would be an expensive overdesign. The design could be optimised by choosing a few different designs

on the project, such as drilled shafts with three or four different diameters and depths, which might increase the construction cost. In fact, this is one of the more common sources of error in placing the wrong sized drilled shaft at a location that may result in design modifications, delays and cost escalation. In the author's experience, when problems were encountered with a 9-foot diameter (2743 mm) drilled shaft, one of the suggestions offered was to over-drill and convert that to a 10-foot diameter (3048 mm) drilled shaft. This proposal was abandoned very quickly because it imposed two problems – change in design and the probability of encountering the same problem with the larger diameter drilled shaft. Construction crews find it especially complicated when a foundation structure involves both vertical and battered drilled shafts, a very common occurrence, where different equipment will have to be mobilised at different times and ensure that all the installed piers perform as designed. The author has also confronted designing and installing drilled shafts in karst terrain, where the presence of cavities could require that soil borings be performed at the location of every drilled shaft to verify that the designed depths could be adhered to. As one could easily appreciate, this is a contractor's nightmare to find that the shaft has sunk a few meters overnight, as it happened on the Crosstown Expressway in Tampa, Florida. (Saint Petersburg Times, 2004.) Thus computer simulation is not an ultimate answer to all unknowns and there will always be some risk, which will require redesign. Based on Bolton's (1992) flow chart of conventional design, Figure 2 shows an adaptation to drilled shaft design.

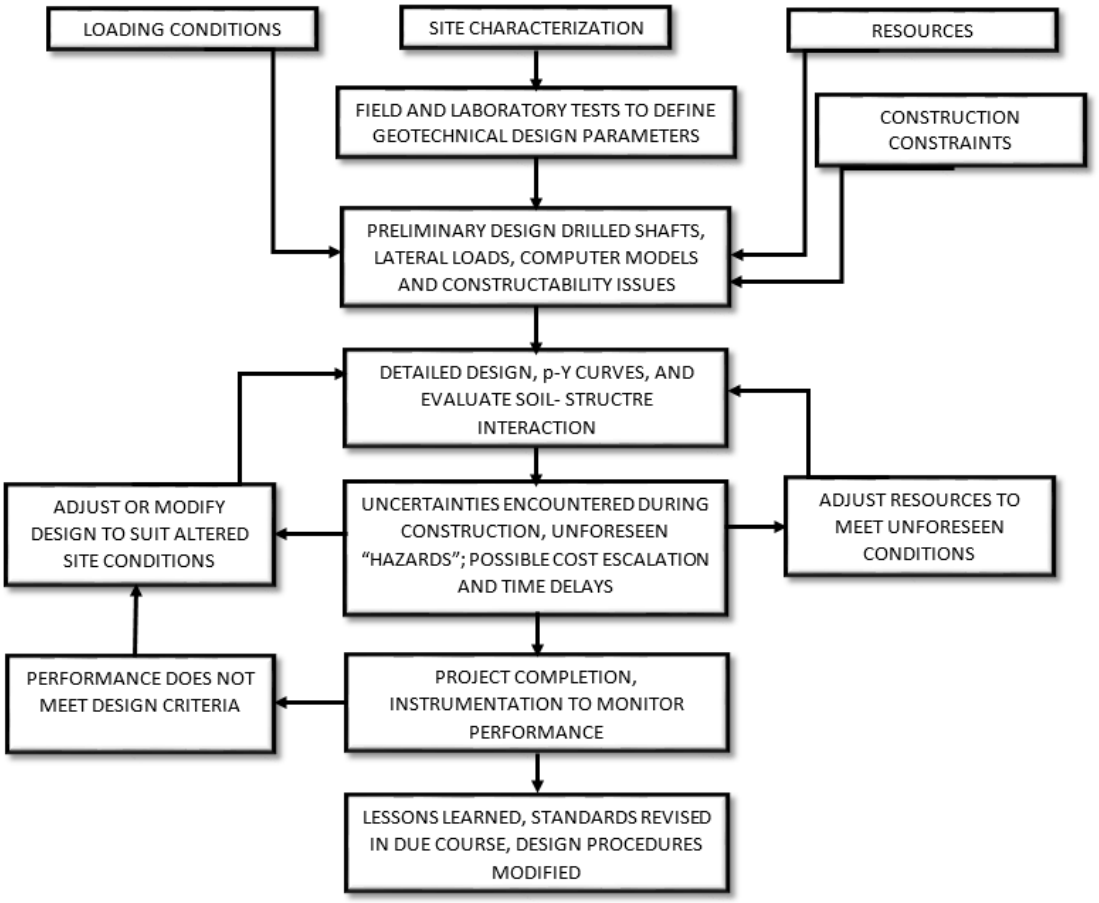


Fig. 2. A typical flow chart for conventional design process for drilled shaft design.

The foregoing discussion leads to the conclusion that there are many interrelated factors in design and uncertainties in construction, resulting in the risk that installed drilled shaft systems may not meet the design goals. Therefore reducing risks at the design stage becomes the first logical step. Risk-based

decision making has been applied to many problems in various aspects of economics and logistics, but rarely in engineering design. Though not incorporated in textbook design concepts, geotechnical design has always attempted to reduce risk in design by other means besides a risk-based approach to design. Some examples of risk reduction are listed below, which is not an exhaustive list:

1. If the risks associated with the selected site are easily identified (e.g., geological features such as faults and sinkholes, archeological or historical sites, contaminated sites, etc.) choose an alternative site.
2. If there is a question on the design parameters or the assumptions, reduce the risk by building a test section (e.g. Test piles)
3. Incorporate instrumentation in the test section to refine the estimated design parameters.
4. Use computer simulation. In many cases three-dimensional modeling of the engineered system is possible, though time consuming and is subject to risks associated with the input data and assumptions (also known as garbage in garbage out.)
5. Introduce redundancy where possible. This might not be possible in cases where the drilled shafts are non-redundant. Examples of non-redundant drilled shafts would be bridge piers and tower foundations where a single drilled shaft may carry the entire load and building in redundancy is not possible. In such cases, the risk is reduced by introducing a resistance factor in design.

RISK-BASED DESIGN CONCEPT

The four-step design process recommended by Bolton (ibid) includes the concept of design-as-you go. A number of infrastructure projects rely on the observational method, which Dr. Ralph Peck emphasized strongly. Chowdhury, R. and Flentje, P., (2007) discuss risk-based methodology as the future of geotechnical engineering design. As our knowledgebase increases, observations and lessons from our failures get incorporated in our assessment of risk in our design. What if we could adopt a way of thinking, whereby we first consider what could go wrong in our design, what its consequences would be and how to avoid them? That is the premise of risk-based design.

Risk analysis is introduced in ISO 31000 Risk Management Process which could be reduced to the following fundamental steps:

1. Identify the risk – Identify the events that could lead to a potential hazard (failure).
2. Analyse the risk – Quantify the risk in terms of the consequences of the risk happening.
3. Evaluate the risk – Evaluate the probability of the risk factor and assess the value of the loss (or gain) of the consequences
4. Mitigate the risk – Take steps to avoid or compensate for the consequences should the event occur.

Following the damage caused by Hurricane Katrina in New Orleans in 2005, numerous investigations conducted to analyse the failure pointed in the direction of design oversights. Two significant factors emerged from the analysis of the failure of the flood walls incorporated in the levee system – compromise to save cost by assuming a less severe catastrophic event and the impact of the weakest link (undermining the flood wall foundation) in the built system. The U. S. Army Corps of Engineers (USACE) and the U. S. Bureau of Reclamation (BUREC) had started the building blocks of risk-based analysis in the mid-1990s. In 2009 both agencies applied the principles of risk-based analysis to understanding the failure mechanism of the levees in New Orleans. An approach to the evaluation of the performance of dams and levees was developed and Scott (2011) published the BUREC's approach to inspecting dams and levees, which eventually developed in to a Dam Safety Classification System and later a similar Levee Safety Classification System. The object of the classification systems was to assess the risk factors, evaluate the consequences in terms of economic loss and loss of life, and thereby prioritize the safety modifications to these dams and levees. In the USA, apart from the USACE and BUREC, the Federal Energy Regulatory Commission (FERC) and a number of private parties also own and or operate dams and levees for various purposes from irrigation, power generation, hazardous waste containment and many other purposes. Recently, the FERC issued a circular to introduce risk-based assessment of its dams, which are primarily used for power generation and hence form a significant link in the critical infrastructure. Building on its experience with Dam and Levee Safety evaluation, USACE is developing risk-based design methodology for levee design.

INTRODUCING RISK IN THE DESIGN PROCESS

While the concept of risk-based design is presented in this paper as a new approach, the development of the process is neither new nor unique to the design of drilled shafts. As one of the key factors in reliability in design is the evaluation of the soil properties, steps have been introduced to reduce the risk that the measured soil parameters are reliable before they are introduced in the design. Development of instruments to simulate actual field behaviour and instruments that measure soil properties in-situ have substantially reduced risk in the selection of design parameters. For example, direct measurement of soil subgrade reaction is possible. Could this be used to design the lateral load behavior of drilled shafts to reduce the risk of unacceptable levels of lateral movement that might lead to loss of functionality, if not the risk of total failure? Precision of the measurement of in-situ soil tests have continually improved with better instrumentation. Probabilistic methods have been introduced in the evaluation of soil properties in the laboratory, which reduce the uncertainty of a single albeit replicable test method. As discussed above, identifying the risk starts with identifying the event that triggers an unacceptable hazardous consequence. Christian and Beacher (2011) discussed the use of "event tree" in assessing risk, by taking an example of internal erosion failure of an earth dam from developed first by Van Thun (1996) and used in an analysis by Fell and Fry (2007.) An event tree is used to assign probabilities to each event that could occur in that event tree and the overall risk could be evaluated. This helps the designer to decide on the best option in terms of an acceptable level of risk.

In the design of drilled shafts, risks could be identified at every stage involved in the design process. However quantifying each risk identified is difficult. Risk, does not always imply loss. In economic analysis, risks are taken for the purposes of potential gain. Economists may therefore define risk as

Risk = Hazard x Potential value of the loss (or gain)

In the design of drilled shafts, we could design using a high factor of safety to derive "gain" associated with risk. However, the concern in the design of drilled shafts is to avoid a hazard that would introduce or enhance the loss of functionality. Such a hazard in the analysis and design of engineered systems could be defined in the terminology recommended by the International Society of Soil Mechanics and Geotechnical Engineering (ISSMGE) Technical Committee TC 304. (http://140.112.12.21/issmge/doc_2010.htm) Briefly paraphrased, "Hazard" would imply the Probability that a particular danger (threat) occurs within a given period of time. We could thus relate risk in terms of probability as:

Risk = Probability of an adverse event occurring x Consequences of that event.

This definition helps us to quantify the probability of an adverse event using statistical methods. For example, the relative frequency of an event could be quantified as the ratio of the number of times the event occurs and the number of possible occurrences of that event. If we apply these concepts to the design of drilled shafts, we could potentially arrive at a number of risk factors at every stage of the design. Starting with the ACI 336.3 design process shown in Fig. 1 above, risk factors could be assigned to each of the steps. As opposed to conventional design process illustrated in Fig. 2, the risk-based design process could be illustrated as shown in Fig. 3 below.

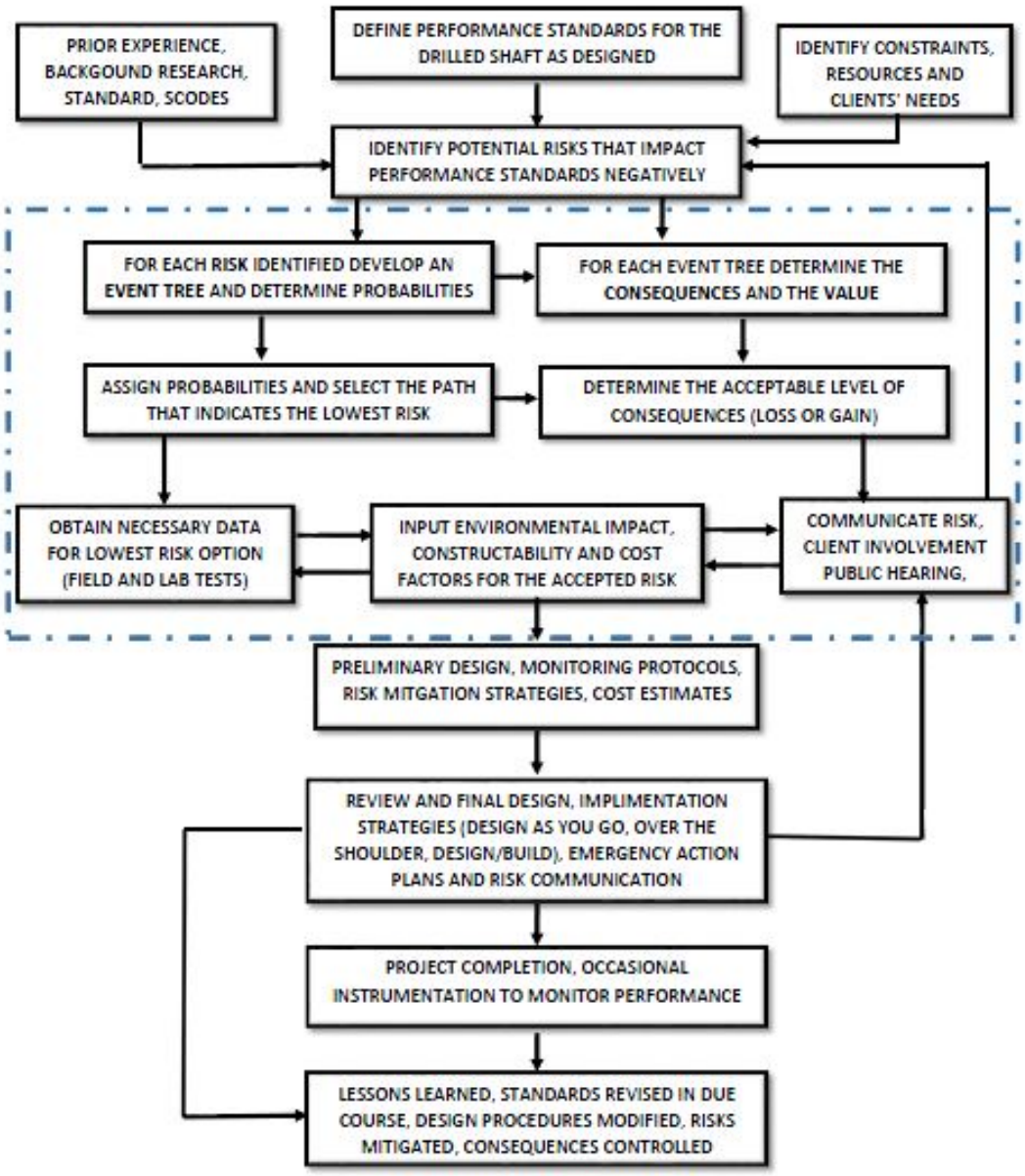


Fig. 3. A typical flow chart for risk-based design process for drilled shaft design. The items inside the dashed box represent the risk-based decision process, as discussed in detail below.

In the conceptual risk-based design process shown in Fig. 3 two concepts re introduced, which are not involved in the conventional design process, which are the "Event Tree" and "Value of Consequences." Risk, as defined, is assessed in terms of these two terms. An Event Tree is a listing of events that may trigger a hazard and assigning a probability for each of the estimated outcomes for that event. This can be best illustrated by an example in the drilled shaft design process. In fact, if one proceeds in the steps outlined in the ACI 336.3 design process shown in Fig. 1, each one of the steps (or boxes) could have its own event tree and some of those event trees may overlap and have interrelated consequences.

For the purposes of illustrating the use of an event tree, let us consider subsurface conditions. As seen in Fig. 1, subsurface conditions impact design data. An event tree could be developed as shown below.

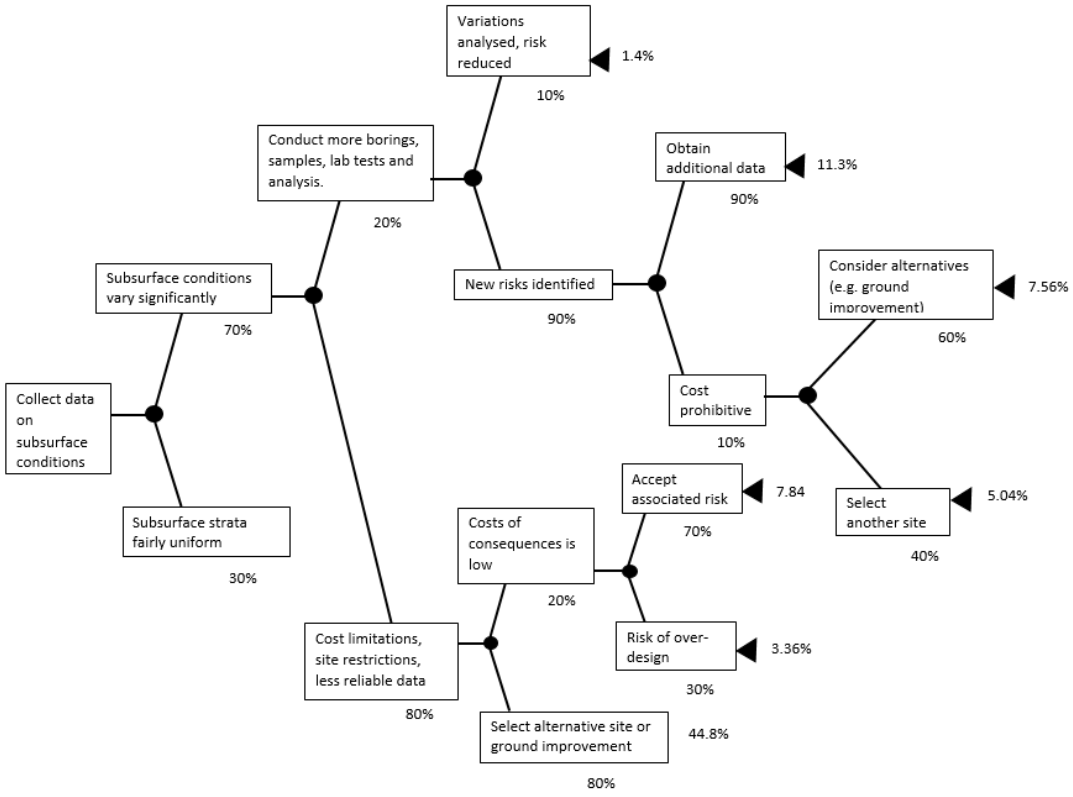


Fig. 4. Typical Event Tree for risks related to Subsurface conditions.

Though the probabilities shown in the event tree are hypothetical, the resulting probabilities are indicative of the risks associated with each event in the tree. For example, if we find that the cost of obtaining additional data by increasing the number of borings, samples or testing is a limiting factor, we can choose to weigh the risks associated with proceeding with the design, knowing that site conditions vary dramatically. When would one consider the cost of consequences to be low or at an acceptable level? Let us say, the uncertainty in this case is that the depth of rock varies by $\pm$ 5m from one boring to another. The cost of this consequence is that some shafts may be longer, some shorter. If there is a possibility that the increases and decreases balance out, the risk of proceeding with the design with the limited data on varying depth to rock, would result in a probability over-design by 3.36%. If, on the contrary, we assume that the probability of selecting an alternative site or considering ground improvement is 80% when we determine that the cost of additional investigation is prohibitive (which is unlikely in the current example), then we arrive at a 44.8% probability that we would choose that alternative. Logically, it is quite easy to see that if the cost of varying length of the drilled shafts is marginal and we have a very low probability that our design carries an unacceptable risk (7.8% is an acceptable risk.) If we choose to over-design we reduce the risk further to 3.36% probability that we need to over-design. On the other hand, if we do obtain additional data at an additional cost, we reduce the probability of introducing risk in our design is down to 1.4%. Thus the risk-based decision gives us two options – do with the data we have and take a risk that we will over-design the drill shaft or spend the extra money in getting additional data and reduce the risk in the designed product, without increasing the cost by over-designing the drilled shaft.

This is just one aspect of the design where risk-based decision could give us a choice based on outcome. We could then take another aspect of our design process, such as Lateral Response of the drilled shaft shown in Fig. 1. In this case, we would associate the risk with the allowable lateral movement, uncertainties in estimating the subgrade reaction, bending stresses in concrete, possible use of battered drilled shaft, etc. We would perhaps make the same choices in the conventional design

method as well, but without the benefit of asking "what if?" Risk-based design process therefore gives us the option to evaluate the options using quantifiable risks as the design process proceeds. One of the first steps in developing an event tree is to identify the risks. Fig. 4 was just an illustration of how the decision making process works. It was based however on well documented principles of risk management, where the probabilities are assigned on basis of evaluating the potential risk and the consequences.

That brings the discussion to the second part of the risk-based design process, that of the value of consequences. In the simplistic example above, the cost of additional investigation was considered as the consequence of the risk of not having sufficient data. But the value of perceived consequences could be based on a number of factors, essentially associated with loss of economic value and loss of life. In risk-based design methods applied to large infrastructure projects such as dams and levees, the consequences of failure may include both economic losses and loss of life. While there is no way of assigning a "value" to lives lost, the decision making process does take in to account the probability of loss of life. In these cases, the decision is to arrive at a cutoff point where the design will consider loss of life as one of the potential consequences. For example, event trees have been developed to associate internal erosion in a levee to catastrophic failure of the levee, Von Thun (ibid). The designer is now left with options to design a means of erosion control, which may vary from sand bags to cutoff wall. Each option has an associated construction cost and an associated loss of life and economic loss if the designed measure fails. In some cases, even with the choice of the best option at the highest cost, the analysis may indicate that loss of life is inevitable. At this point there is a need to communicate the risk to the affected population.

Fortunately, in infrastructure projects associated with drilled shaft design, such levels of loss of life are rare. Most happen due to unforeseen natural events such as earthquakes and floods, but some could be attributed to design deficiencies. One such example is the Crosstown Expressway in Tampa, Florida. The area is a known karst terrane and sinkholes are common. The expressway was an elevated structure over an existing road and many of the supporting columns were placed in the existing median, many designed as non-redundant drilled shafts. During construction, one of the supporting columns sunk overnight by about 4.5 m (15 feet) due to the supporting drilled shaft collapsing the roof of a large cavity in the limestone. The resulting settlement dragged down with it two adjacent spans, crushing four cars under the bridge partially and two people were hospitalized with minor injuries. Apart from that, the cost of repair by adding sister columns, re-evaluating every drilled shaft design along the 22 km stretch of the expressway and redesigning many of the supporting columns were required. The $350 million project finally resulted in a $92 million cost escalation. The cost of drilling one boring at each of the drilled shaft locations would have probably added $6 million to the geotechnical exploration cost. Knowing the karst terrane, that would have been money well spent, if a risk-based decision had been taken at the design stage.



Fig. 5. Crosstown Expressway collapse due to sinkhole on April 14, 2004. Photo taken from St. Petersburg Times website.
http://www.sptimes.com/2004/04/14/news_pf/Tampabay/Unseen_sinkhole_downs.shtml)

CONCLUSION

Risk-based design is a new approach in geotechnical design process. While risk-based decision making is not a new concept, it is making inroads in the design of levees and may be expended to the design of dams as well. The International Levee Handbook lists the concept of introducing risk-based decisions in the design of levees. This paper is the author's attempt to encourage risk-based design process in different aspects of geotechnical design, with an example of drilled shafts. The idea of introducing a risk-based design in the accepted ACI 336.3 design process is illustrated. This concept needs more modifications and amplification before it could be considered a viable process of design. However, the introduction of risk-based decision making introduced at the early stages of design in infrastructure projects, which utilise a large number of non-redundant drilled shafts makes obvious sense.

REFERENCES

American Concrete Institute (1993) ACI Committee Report, Reapproved 2006.

Bolton, M.D., "Design Methods," (1992). *Wroth Memorial Symposium, Cambridge, U.K.*

Christian, John T., and Beacher, Gregory, B., "Unresolved Problems in Geotechnical Risk and Reliability," *Proc. Georisk 2011, American Society of Civil Engineers,* 130(8), 50-63.

Chowdhury, R. and Flentje, P., (2007). "Perspectives for the Future of Geotechnical Engineering," *Proc. Intl. Conf. on Civil Engineering for the New Millennium,* Shibpur, India. 130(8), 50-63.

Fell, R. and J. J. Fry (2007). *Internal erosion of dams and their foundations*. London and New York, Taylor & Francis.

International Levee handbook (2013) Construction Industry Research and Information Association (CIRIA), London, UK

Kannan, R. (2015) "Risk-based Design and Evaluation of Earth Structures" XV Pan American Conference on Soil Mechanics and Geotechnical Engineering, Buenos Aires, Argentina.

Saint Petersburg Times, (2004)
http://www.sptimes.com/2004/04/14/news_pf/Tampabay/Unseen_sinkhole_downs.shtml

Scott, Gerg A., (2011). "The Practical Application of Risk Assessment to Dam safety." *Proc. Georisk 2011,* ASCE Press. ASCE, Reston, VA.

Von Thun, J. L. (1996). "Understanding seepage and piping failures – the No.1 dam safety problem in the west." ASDSO Western Regional Conference. Lake Tahoe, Nevada, Association of State Dam Safety Officials.